

Siri | Glimstad

200 Park Avenue, Seventeenth Floor, New York, NY 10166
sirillp.com | P: (212) 532-1091 | F: (646) 417-5967

VIA ELECTRONIC FILING

May 6, 2021

Division of Dockets Management
Department of Health and Human Services
Food and Drug Administration
Commissioner Stephen M. Hahn, M.D.
5630 Fishers Lane, Rm. 1061
Rockville, MD 20852

**UNITED STATES DEPARTMENT OF HEALTH AND HUMAN SERVICES
AND THE FOOD AND DRUG ADMINISTRATION**

**PETITION FOR ADMINISTRATIVE :
ACTION TO ENSURE ACCURATELY :
REPORTED AND CONSISTENT :
LEVELS OF ALUMINUM IN ALL :
VACCINES : Docket No. _____**

CITIZEN PETITION

This petition for administrative action is submitted on behalf of the Informed Consent Action Network and a large number of its members, including parents deciding whether to vaccinate their child/children, (“**Petitioner**”) pursuant to 21 C.F.R. § 10.30 and related and relevant provisions of law (including the Federal Food, Drug, and Cosmetic Act or the Public Health Service Act) to request that the Commissioner of Food and Drugs (the “**Commissioner**”) take the actions listed below to assure accurately reported and consistent levels of aluminum in Adacel, Boostrix, Engerix-B, Havrix, Infanrix, Infanrix hexa, Kinrix, Pediarix, Pedvax-HIB, Pentacel, Prevnar-13, Synflorix, and Vaqta (the “**Subject Vaccines**”).

A. ACTION REQUESTED

1. The Food & Drug Administration (“FDA”) forthwith publicly release documentation sufficient to establish that the aluminum content in each Subject Vaccine is consistent with amount provided in its labeling.¹

2. If the FDA is unable to forthwith comply with the foregoing request, the FDA forthwith pause distribution of each Subject Vaccine until it has confirmed and publicly released documentation sufficient to establish that the aluminum content in each Subject Vaccine is consistent with the amount provided in its labeling.

B. STATEMENT OF GROUNDS

3. On April 15, 2021, Dr. Christopher Exley along with four other researchers have published a study after reviewing the aluminum content of thirteen childhood vaccines. Dr. Exley has authored over 200 published peer reviewed articles regarding aluminum, has been a Professor of Bioinorganic Chemistry at Keele University for the last 29 years, and has otherwise spent almost his entire 37-year career studying aluminum and its biological effects.

4. This study found that only three vaccines of the thirteen tested contained the amount of aluminum indicated on its labeling approved by the FDA. Six vaccines (Pentacel, Havrix, Adacel, Pedvax, Prevnar 13, and Vaqta) contained a statistically significant greater quantity while four vaccines (Infanrix, Kinrix, Pediarix, and Synflorix) contained a statistically significant lower quantity. A copy of this peer-reviewed study with these findings are appended hereto as Exhibit A and is available at <https://www.sciencedirect.com/science/article/pii/S0946672X21000523>.

5. These deviations from each product’s labeling render the product adulterated and misbranded and violates various federal statutes and regulations, and therefore requires immediate action from the FDA to either provide proof the study’s results are incorrect or otherwise cease distribution of these vaccines until this issue has been corrected. *See, e.g.*, 21 U.S.C. § 351; 21 U.S.C. § 352; 21 C.F.R. § 56; 21 C.F.R. § 57.

6. The finding in this study is extremely concerning because doses with less than the approved amount of aluminum adjuvant will not have the same efficacy, and doses with more than the approved amount of aluminum adjuvant raise safety concerns. Indeed, aluminum adjuvant is

¹ The term “labeling” as used herein shall include all documentation from the manufacturer and the FDA with regard to a given product, including its package insert, product label, patient information sheet, and approval documents, and any other documents that list its ingredients.

a known cytotoxic and neurotoxic substance used to induce autoimmunity in lab animals, and which numerous peer-reviewed publications implicate in various autoimmune conditions.²

7. The FDA must ensure that vaccines in current use and those that will be on the market in the future are accurately labeled. Vaccine recipients and their caregivers must be able to rely on the FDA-approved labeling for these products, especially considering that they are given to babies and children.

8. Petitioner and its constituent members, and the parents seeking to decide whether to vaccinate their children, are entitled to know if the aluminum adjuvant content in the FDA approved childhood vaccines they are being asked to inject their children with are not adulterated or mislabeled, and otherwise contain the amount of aluminum adjuvant actually listed on their label.

C. ENVIRONMENTAL IMPACT

9. The undersigned hereby states that the relief requested in this petition will have no environmental impact and therefore an environmental assessment is not required under 21 C.F.R. Sections 25.30 and 25.31.

D. ECONOMIC IMPACT

10. Economic impact information will be submitted upon request of the commissioner.

E. CERTIFICATION

11. The undersigned certifies that, to the best knowledge and belief of the undersigned, this petition includes all information and views on which the petition relies, and that it includes representative data and information known to the petitioner which are unfavorable to the petition.

² <https://www.simonandschuster.com/books/Imagine-You-Are-An-Aluminum-Atom/Christopher-Exley/9781510762534>; <https://www.wiley.com/en-us/Vaccines+and+Autoimmunity-p-9781118663431>; <https://www.ncbi.nlm.nih.gov/pubmed/25923134>; <http://icandecide.org/white-papers/ICAN-Aluminum-Adjuvant-Autism.pdf>; Macrophages phagocytize (ingest) aluminum adjuvant (AA): <https://www.ncbi.nlm.nih.gov/pubmed/15297065>; <https://www.ncbi.nlm.nih.gov/pubmed/18496530>. Macrophages transport material into the brain: <https://www.ncbi.nlm.nih.gov/pubmed/27213597>; <https://www.ncbi.nlm.nih.gov/pubmed/21348773>; <https://www.ncbi.nlm.nih.gov/pubmed/27115998>; <https://www.ncbi.nlm.nih.gov/pubmed/27213597>. AA transport to brain: <https://www.ncbi.nlm.nih.gov/pubmed/26384437>; <https://www.ncbi.nlm.nih.gov/pubmed/27908630>; <https://www.ncbi.nlm.nih.gov/pubmed/23557144>. AA causes neuro impairment: <https://www.ncbi.nlm.nih.gov/pubmed/27908630>; <https://www.ncbi.nlm.nih.gov/pubmed/19740540>; <https://www.ncbi.nlm.nih.gov/pubmed/23932735>. Macrophages infiltrate the brain : <https://www.ncbi.nlm.nih.gov/pubmed/16401547>; <https://www.ncbi.nlm.nih.gov/pubmed/15546155>; <https://www.ncbi.nlm.nih.gov/pubmed/28167942>; <https://www.ncbi.nlm.nih.gov/pubmed/24951035>.

12. The Petitioner therefore respectfully urges that this request be granted forthwith.

Respectfully submitted,

/s/ Aaron Siri

Aaron Siri

Elizabeth Brehm

Jessica Wallace

SIRI & GLIMSTAD LLP

200 Park Avenue

17th Floor

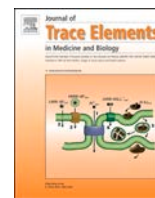
New York, NY 10166

Telephone: (212) 532-1091

Facsimile: (646) 417-5967

Email: aaron@sirillp.com

Exhibit A



The measurement and full statistical analysis including Bayesian methods of the aluminium content of infant vaccines

Emma Shardlow^a, Caroline Linhart^a, Sameerah Connor^b, Erin Softely^b, Christopher Exley^{a,*}

^a The Birchall Centre, Lennard-Jones Laboratories, Keele University, Staffordshire, United Kingdom

^b Life Sciences, The Huxley Building, Keele University, Staffordshire, United Kingdom

ARTICLE INFO

Keywords:

Human exposure to aluminium
Aluminium adjuvants
Aluminium content of infant vaccines
Vaccine safety and efficacy

ABSTRACT

Background: Aluminium salts are the most common adjuvants in infant vaccines. The aluminium content of a vaccine is provided by the manufacturer and is indicated on the patient information leaflet. There is no independent verification, for example by the European Medicines Agency, of the aluminium content of infant vaccines.

Methods: We have measured the aluminium content of thirteen infant vaccines using microwave-assisted acid and peroxide digestion followed by transversely heated graphite furnace atomic absorption spectrometry. Our data are compared with manufacturer's data using full statistical analyses including Bayesian methods.

Results: We found that only three vaccines contained the amount of aluminium indicated by the manufacturer. Six vaccines contained a statistically significant ($P < 0.05$) greater quantity while four vaccines contained a statistically significant ($P < 0.05$) lower quantity. The range of content for any single vaccine varied considerably, for example, from 0.172 to 0.602 mg/vaccine for Havrix.

Conclusions: The data have raised specific questions about the significance of the aluminium content of vaccines and identified areas of extremely limited information. Since aluminium is a known toxin in humans and specifically a neurotoxin, its content in vaccines should be accurate and independently monitored to ensure both efficacy and safety.

1. Introduction

Aluminium salts are the adjuvants of choice in the majority of inactivated paediatric vaccines. Their presence at injection sites following vaccination results in the activation of humoral immunity. This pathway is characterised by the differentiation of naive CD4⁺ T cells into Th2 effector subsets and the subsequent enhancement of antigen-specific antibody titres [1–5]. T cell priming post-vaccination occurs following the cross-presentation of antigen-MHC complexes by immunocompetent phagocytes and occurs exclusively within draining lymph nodes [6] at locations often distant from the injection site. Aluminium adjuvants have been shown to facilitate this process by; i) actively increasing levels of antigen recognition and uptake by antigen-presenting cells [7–9], ii) acting in a protective capacity to prevent antigen degradation within intracellular compartments [9,10] and (iii) amplifying and sustaining antigen-MHC II expression by antigen-presenting cells [9,11,12]. Other suggested mechanisms underlying the immunostimulatory effects of aluminium adjuvants include

the secretion of pro-inflammatory cytokines by activated antigen-presenting cells [13–17] and the formation of an 'antigen depot' at the vaccine injection site [18,19]. While the latter is regarded by some as superfluous to the mechanism of action of aluminium adjuvants, recent evidence has demonstrated that extracellular traps formed by neutrophils following immunization make a significant contribution to their immunological activity *in vivo* [20]. However, the modus operandi of aluminium adjuvants remains to be fully elucidated [21,22].

Three aluminium salts are currently used as adjuvants in human vaccines. Two of these, aluminium oxyhydroxide (available commercially as Alhydrogel®) and aluminium hydroxyphosphate (available commercially as AdjuPhos®) have been widely studied while the third, aluminium hydroxyphosphate sulphate, is proprietary to Merck and has not been available for independent scrutiny [22,23]. The type and amount of aluminium adjuvant used in paediatric vaccines is made available through patient information leaflets, see the manufacturer's information summarised in Table 1. The information given is, at best, vague. Descriptions of aluminium salts are often inaccurate, for

* Corresponding author at: The Birchall Centre, Lennard-Jones Laboratories, Keele University, Staffordshire, ST5 5BG, United Kingdom.

E-mail address: c.exley@keele.ac.uk (C. Exley).

<https://doi.org/10.1016/j.jtemb.2021.126762>

Received 16 February 2021; Received in revised form 23 March 2021; Accepted 12 April 2021

Available online 15 April 2021

0946-672X/© 2021 The Author(s).

Published by Elsevier GmbH. This is an open access article under the CC BY-NC-ND license

(<http://creativecommons.org/licenses/by-nc-nd/4.0/>).

example, the use of the term aluminium hydroxide when the form of aluminium included is aluminium oxyhydroxide. Quantitative data describing the content of aluminium in a vaccine is often presented in a number of different formats. For example, all do present these data as total aluminium but some additionally present the data in respect of the weight of aluminium salt. This practice is confusing for anyone reading the patient information leaflet. The manufacturers' stated content of aluminium in vaccines listed in Table 1 varies from 0.125 (Pevnar 13) to 0.85 (PEDIARIX) mg per 0.5 mL dose of vaccine though little or no information is available as to why the content is so varied. Why does one vaccine require more aluminium adjuvant to be effective than another? There exists a non-regulatory limit of 1.25 mg aluminium per dose of vaccine based upon maximum titres of antibodies produced. However, even this may be exceeded under certain circumstances. The European Medicines Agency (EMA) and the Food and Drug Administration (FDA) are charged with the responsibility of verifying the information provided by vaccine manufacturers in their patient information leaflets. When questioned repeatedly on this subject (for example, EMA request reference ASK-56123) neither organisation was able to confirm that they routinely measure the aluminium content of vaccines. They indicated that they relied upon data provided to them by manufacturers, though no such data were forthcoming following requests including freedom of information act requests to the FDA (For example, FOIA Requests 2019-11150 to 2019-11156 & 2019-11158). When the EMA was asked, which analytical methods were used by either their organisation or vaccine manufacturers to measure the aluminium content of vaccines, they replied that this was proprietary information and could not be provided (EMA request reference ASK-56707). It would appear that the aluminium content of a vaccine is only measured by the manufacturer, using an unspecified method, and that these data are not made publicly available.

One piece of important information about the aluminium content of a vaccine is that it is clearly critical. Why else would there be such a wide range of contents used across the paediatric vaccine schedule. Since

those charged with ensuring that the information provided by vaccine manufacturers is correct are seemingly choosing to neglect this responsibility, herein we have measured the aluminium content of thirteen paediatric vaccines. We find that the measured content of aluminium is only similar to that given by the manufacturer in three out of thirteen vaccines.

2. Materials and methods

2.1. Vaccines

Whole vaccines were provided under license by a state registered paediatrician. All vaccines were in their original packaging and remained pristine and refrigerated at 4 °C until use.

2.2. Digestion of vaccines

Each whole vaccine was added to an acid-washed, dried and labelled 20 mL PFA Teflon MARSXpress digestion vessel closed with a venting plug and screw cap (CEM Technology, UK). The idea being that the whole vaccine was 'injected' into the digestion vessel in the identical manner as it would be used in human vaccination. In each case, it was assumed, though it was unlikely to be the case, that the whole vaccine volume of 0.5 mL was transferred to the digestion tube. To each whole vaccine, 1 mL of concentrated HNO₃ (Analar, 15.8 M Fisher Scientific, UK) and 1 mL 30 % w/v H₂O₂ (Aristar, BDH, UK) were added and the mixture subjected to microwave-assisted digestion (MARS6 CEM, One Touch Technology, UK). The resulting digests were further diluted by the addition of 2.5 mL of pure water (conductivity <0.067µS/cm) and stored appropriately for subsequent analyses. Method blanks were prepared where 0.5 mL of pure water was substituted for the whole vaccine. Full information pertaining to this method of sample digestion including microwave parameters are available elsewhere [24].

Table 1

Information relating to each of the thirteen infant vaccines taken directly from their patient information leaflets respectively.

Trade name of vaccine	Pharmaceutical company [Country of manufacture]	Paediatric dose (mL)	Manufacturer's stated aluminium content per paediatric dose (mg)	Infant age range	Manufacturer's description of vaccine
PEDIARIX	GlaxoSmithKline (GSK) [Belgium]	0.5	"not more than 0.85 mg aluminium"	from 2 to 6 months	Vaccine for the active immunization against diphtheria, tetanus, pertussis, hepatitis B virus infection and poliomyelitis.
Pentacel	Sanofi Pasteur [Canada]	0.5	0.33 mg of aluminium as 1.5 mg aluminium phosphate	from 6 weeks to 4 years	Vaccine for the active immunization against diphtheria, tetanus, pertussis, poliomyelitis and disease caused by <i>Haemophilus influenzae</i> type b.
ENGERIX-B	GlaxoSmithKline (GSK) [Belgium]	0.5	0.25 mg of aluminium as aluminium hydroxide	from 1 to 6 months	Vaccine for immunization against infection caused by hepatitis B virus.
Pevnar 13	Pfizer [United States]	0.5	0.125 mg of aluminium (as aluminium phosphate)	from 6 weeks to 5 years	Vaccine for active immunization against disease caused by <i>Streptococcus pneumoniae</i> .
PedvaxHIB	Merck & Co., Inc [United States]	0.5	0.225 mg of aluminium as amorphous aluminium hydroxyphosphate sulphate	from 6 to 11 months	Vaccine for immunization against infection caused by <i>Haemophilus influenzae</i> type b.
KINRIX	GlaxoSmithKline (GSK) [Belgium]	0.5	"not more than 0.6 mg aluminium by assay"	from 4 up to 6 years	Vaccine for immunization against diphtheria, tetanus, pertussis and poliomyelitis.
INFANRIX	GlaxoSmithKline (GSK) [Belgium]	0.5	"not more than 0.625 mg aluminium by assay"	from 6 weeks up to 6 years	Vaccine for active immunization against diphtheria, tetanus and pertussis.
BOOSTRIX	GlaxoSmithKline (GSK) [Belgium]	0.5	"not more than 0.39 mg aluminium by assay"	from 10 years	Vaccine for active immunization against tetanus, diphtheria and pertussis.
VAQTA	Merck & Co., Inc [United States]	0.5	0.225 mg of aluminium as amorphous aluminium hydroxyphosphate sulphate	from 12 months (up to 18 years)	Vaccine for immunization against disease caused by hepatitis A virus
Adacel	Sanofi Pasteur [Canada]	0.5	1.5 mg aluminium phosphate (0.33 mg aluminium)	from 10 years	Vaccine for active immunization against tetanus, diphtheria and pertussis.
HAVRIX	GlaxoSmithKline (GSK) [Belgium]	0.5	0.25 mg of aluminium as aluminium hydroxide	from 12 to 24 months	Vaccine for immunisation against disease caused by hepatitis A virus.
Infanrix hexa	GlaxoSmithKline (GSK) [Belgium]	0.5	0.82 mg of aluminium (as aluminium salts)	from 2 to 18 months	Vaccine for immunization against diphtheria, tetanus, pertussis, hepatitis B, poliomyelitis and <i>Haemophilus influenzae</i> type b.
Synflorix	GlaxoSmithKline (GSK) [Belgium]	0.5	0.5 mg of aluminium as aluminium phosphate	from 6 weeks up to 5 years	Vaccine for immunization against infections caused by <i>Streptococcus pneumoniae</i> .

2.3. Determination of aluminium

The total aluminium content of each vaccine digest and each method blank was measured by transversely heated graphite furnace atomic absorption spectrometry (TH GFAAS) using a fully established method including matrix-matched standards and commensurate quality assurance criteria [24]. Method blank data equating to 54 ngAl/5 mL digest were subtracted from each vaccine sample. Data are presented as mgAl/0.5 mL vaccine volume.

2.4. Statistics

Data on the measured concentrations of aluminium, stratified by brand, were tested for normality. Depending on whether the data were normally distributed or not, means and medians were calculated and tested two- and one-sided against the manufacturer's content of aluminium (see Table 1) using one-sample *t*-test and Wilcoxon signed rank test respectively.

Differences in aluminium content between lots were analysed for those vaccines with two lots and sufficient sample numbers.

To determine the probability, expressed as a percentage, that the measured content of aluminium in a vaccine was less than, the same as or greater than the amount given by the vaccine manufacturer, Bayesian methodology was used [25].

The hypotheses tested were as follows:

H0. Declared content of aluminium is equal to or less than the measured concentrations of aluminium. (The difference in means is zero.)

The alternative hypothesis is that the difference in means is not zero:

Ha1. Measured concentration of aluminium is not the same.

Ha2. Measured concentration of aluminium is greater.

Ha3. Measured concentration of aluminium is less.

Tests were repeated one-sided in both directions. For two-sided tests, a *p*-value < 0.05 was considered as statistically significant and for one-sided tests a *p*-value < 0.025.

Analyses were performed using R-Studio version 1.1.1093 [26] including packages ggplot2 [27], doBy [28], BEST [29], BayesianFirstAid [30] and bayesWilcoxTest [31]. The last three packages provide Bayesian alternatives to the classical hypothesis tests in R. Bayesian methods were used to calculate the percentage probability that measured aluminium concentrations were randomly the same or greater/less than amounts stated by the manufacturer. Bayes factors can complement *p*-values by providing additional information for hypothesis testing by quantifying the relative evidence for both alternative and null hypotheses. Moreover, the magnitude of this evidence can be presented as percentages [25,32–36].

The following code was used to produce random data sets of aluminium values for each vaccine with the stated manufacturers mean and 10 % RSD. The latter to reflect 'expected' manufacturing error.

```
rnorm2 <- function(n,mean,sd) {mean + sd*scale(rnorm(n))}
```

The Bayesian approach was repeated with the random data sets including the 10 % variation.

3. Results

3.1. Pentacel

The data for Pentacel were normally distributed. Ten individual vaccines were investigated across two lots. The aluminium content differed significantly between lots ($P < 0.030$). The highest content of aluminium measured was 0.440 mg/vaccine. The lowest content of

aluminium measured was 0.343 mg/vaccine. The mean content of ten vaccines was 0.379 mg/vaccine (Table 2). The aluminium content of Pentacel was significantly higher for both lots combined ($P < 0.001$) (Fig. 1), lot 1 only ($P = 0.005$) and lot 2 only ($P = 0.004$) than the amount stated by the manufacturer (0.330 mg/vaccine) on the patient information leaflet (Table 3).

3.2. Havrix

The data for Havrix were not normally distributed. Twenty individual vaccines were investigated across two lots. The aluminium content differed significantly between lots ($P < 0.001$). The highest content of aluminium measured was 0.602 mg/vaccine. The lowest content of aluminium measured was 0.172 mg/vaccine. The median content of twenty vaccines was 0.307 mg/vaccine (Table 2). The aluminium content of Havrix was significantly higher for both lots combined ($P = 0.003$) (Fig. 1) and lot 2 only ($P = 0.003$) than the amount stated by the manufacturer (0.250 mg/vaccine) on the patient information leaflet (Table 3).

3.3. Adacel

The data for Adacel were not normally distributed. Nine individual vaccines were investigated across two lots. The aluminium content was not significantly different between lots ($P > 0.05$). The highest content of aluminium measured was 0.445 mg/vaccine. The lowest content of aluminium measured was 0.302 mg/vaccine. The median content of nine vaccines was 0.397 mg/vaccine (Table 2). The aluminium content of Adacel was significantly higher ($P = 0.006$) (Fig. 1) than the amount stated by the manufacturer (0.330 mg/vaccine) on the patient information leaflet (Table 3).

3.4. Boostrix

The data for Boostrix were normally distributed. Twenty individual vaccines were investigated from a single lot. The highest content of aluminium measured was 0.525 mg/vaccine. The lowest content of aluminium measured was 0.345 mg/vaccine. The mean content of twenty vaccines was 0.407 mg/vaccine (Table 2). The aluminium content of Boostrix was not significantly different ($P = 0.101$) (Fig. 1) to the amount stated by the manufacturer (0.390 mg/vaccine) on the patient information leaflet (Table 3).

3.5. EngerixB

The data for EngerixB were normally distributed. Twenty individual

Table 2

Descriptive statistics for each of the thirteen infant vaccines including normal distribution (N.D.), number of replicates (N), minimum (Min.), maximum (Max.), mean/median values (mg/0.5 mL dose) and indication of variance (SD, RSD). Vaccines ordered according to their mean/median Al contents.

Vaccine	N.D.	N	Min.	Max.	Mean/ Median	SD	RSD
Prevnar 13	Y	6	0.127	0.141	0.136	0.006	0.04
EngerixB	Y	20	0.187	0.287	0.249	0.027	0.11
Pedvax	Y	20	0.192	0.334	0.287	0.040	0.14
Havrix	N	20	0.172	0.602	0.307	0.084	0.28
Vaqa	N	20	0.270	0.796	0.340	0.109	0.32
Pentacel	Y	10	0.343	0.440	0.379	0.032	0.09
Adacel	N	9	0.302	0.445	0.397	0.041	0.10
Synflorix	Y	3	0.396	0.399	0.398	0.002	0.00
Boostrix	Y	20	0.345	0.525	0.407	0.043	0.11
Kinrix	N	20	0.464	0.635	0.511	0.062	0.12
Infanrix	Y	20	0.415	0.662	0.546	0.069	0.13
Pediarix	Y	20	0.575	0.743	0.661	0.039	0.06
Infanrix Hexa	Y	6	0.766	0.851	0.806	0.028	0.04

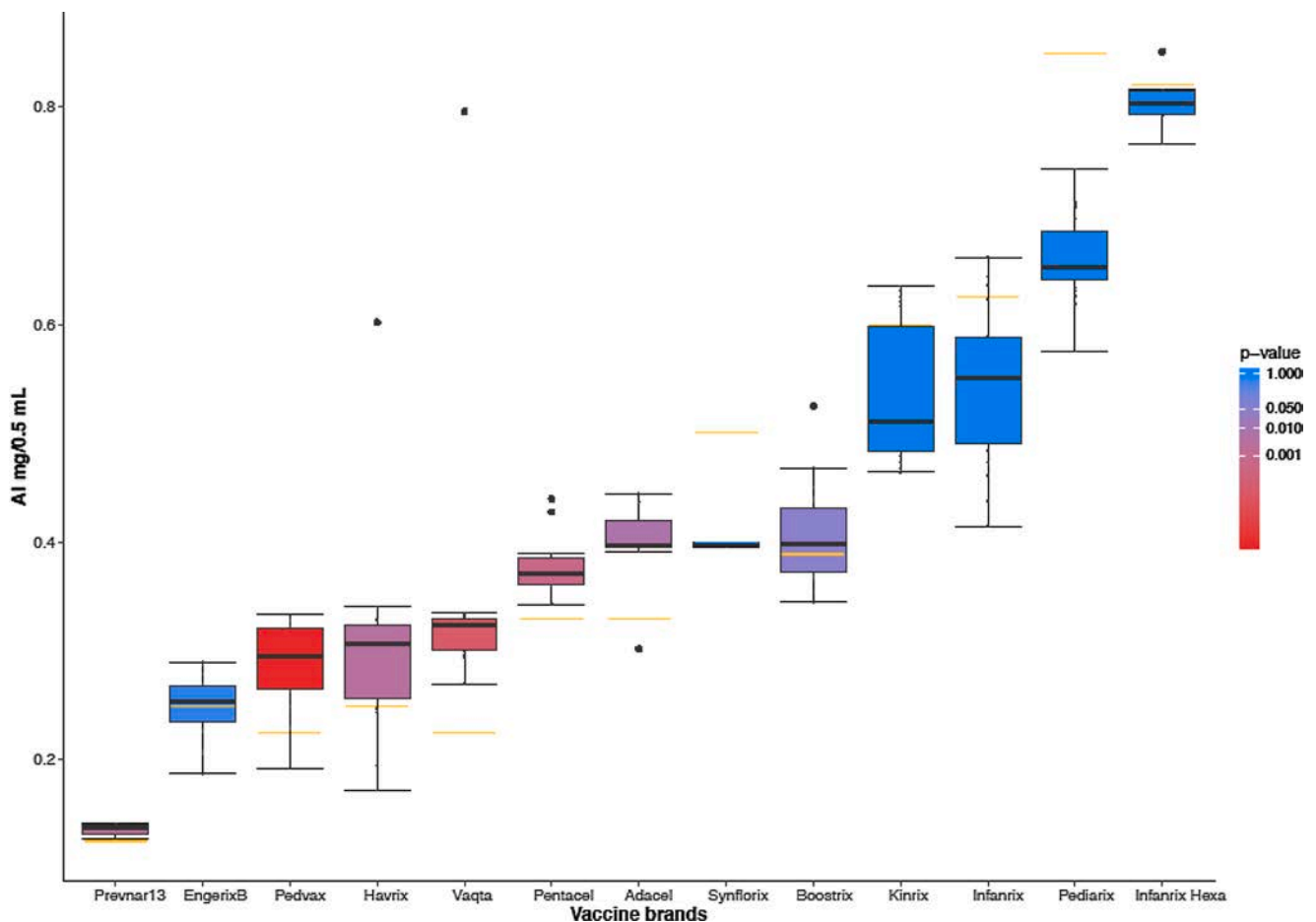


Fig. 1. Boxplots of measured aluminium concentrations (mg/0.5 mL dose) stratified per vaccine brand and compared to the manufacturers' stated amounts (yellow line). The colour gradient represents p-values of one-sided t-tests or Mann-Whitney U tests of the measured Al against the manufacturers' stated amounts. The red boxplots indicate vaccines with significantly more aluminium than that stated by the manufacturer. Boxplots in violet and blue represent data for vaccines where the measured content is either not significantly to or significantly less than the manufacturers' stated amounts. (For interpretation of the references to colour in this figure legend, the reader is referred to the web version of this article).

vaccines were investigated from a single lot. The highest content of aluminium measured was 0.287 mg/vaccine. The lowest content of aluminium measured was 0.187 mg/vaccine. The mean content of twenty vaccines was 0.249 mg/vaccine (Table 2). The aluminium content of EngerixB was not significantly different ($P = 0.897$) (Fig. 1) to the amount stated by the manufacturer (0.250 mg/vaccine) on the patient information leaflet (Table 3).

3.6. Infanrix

The data for Infanrix were normally distributed. Twenty individual vaccines were investigated from a single lot. The highest content of aluminium measured was 0.662 mg/vaccine. The lowest content of aluminium measured was 0.415 mg/vaccine. The mean content of twenty vaccines was 0.546 mg/vaccine (Table 2). The aluminium content of Infanrix was significantly lower ($P < 0.001$) (Fig. 1) than the amount stated by the manufacturer (0.625 mg/vaccine) on the patient information leaflet (Table 3).

3.7. Infanrix Hexa

The data for Infanrix Hexa were normally distributed. Six individual vaccines were investigated from a single lot. The highest content of aluminium measured was 0.851 mg/vaccine. The lowest content of aluminium measured was 0.766 mg/vaccine. The mean content of six vaccines was 0.806 mg/vaccine (Table 2). The aluminium content of

Infanrix Hexa was not significantly different ($P = 0.268$) (Fig. 1) to the amount stated by the manufacturer (0.820 mg/vaccine) on the patient information leaflet (Table 3).

3.8. Kinrix

The data for Kinrix were not normally distributed. Twenty individual vaccines were investigated across two lots. The aluminium content was not significantly different between lots ($P > 0.05$). The highest content of aluminium measured was 0.635 mg/vaccine. The lowest content of aluminium measured was 0.464 mg/vaccine. The median content of twenty vaccines was 0.511 mg/vaccine (Table 2). The aluminium content of Kinrix was significantly less ($P = 0.001$) (Fig. 1) than the amount stated by the manufacturer (0.600 mg/vaccine) on the patient information leaflet (Table 3).

3.9. Pediarix

The data for Pediarix were normally distributed. Twenty individual vaccines were investigated across two lots. The aluminium content was not significantly different between lots ($P > 0.05$). The highest content of aluminium measured was 0.743 mg/vaccine. The lowest content of aluminium measured was 0.575 mg/vaccine. The mean content of twenty vaccines was 0.661 mg/vaccine (Table 2). The aluminium content of Pediarix was significantly lower ($P < 0.001$) (Fig. 1) than the amount stated by the manufacturer (0.850 mg/vaccine) on the patient

Table 3

Summary statistics of results including statistical test used (T test or Mann Whitney U), two- and one-sided p-values of statistical tests, difference in means (stated Al amount – measured amount) and percentage of evidence for the outcome according to Bayesian methodology. Vaccines ordered according to their mean/median Al content.

Vaccine	Test	p-value 2-sided	p-value 1-sided	Diff. in Means	Outcome (H ₁)	Probability of Outcome
Prevnar 13	T	0.005	0.003	−0.01	Greater	0.993
EngerixB	T	0.897	0.551	0.00	Same or Less	0.513
Pedvax	T	< 0.001	< 0.001	−0.06	Greater	> 0.999
Havrix	MWU	0.006	0.003	−0.06	Greater	0.872
Havrix Lot 1	T	0.710	0.355	−0.01	Greater	0.661
Havrix Lot 2	MWU	0.006	0.003	−0.08	Greater	0.988
Vaqtā	MWU	< 0.001	< 0.001	−0.11	Greater	0.995
Pentacel	T	0.001	< 0.001	−0.05	Greater	0.999
Pentacel Lot 1	T	0.010	0.005	−0.03	Greater	0.986
Pentacel Lot 2	T	0.008	0.004	−0.07	Greater	0.991
Adacel	MWU	0.013	0.006	−0.07	Greater	0.938
Synflorix	T	< 0.001	1.000	0.10	Same or Less	0.998
Boostrix	T	0.101	0.051	−0.02	Greater	0.924
Kinrix	MWU	0.001	0.999	0.09	Same or Less	0.878
Infanrix	T	< 0.001	1.000	0.08	Same or Less	> 0.999
Pediarix	T	< 0.001	1.000	0.19	Same or Less	> 0.999
Infanrix Hexa	T	0.268	0.866	0.01	Same or Less	0.846

information leaflet (Table 3).

3.10. Pedvax

The data for Pedvax were normally distributed. Twenty individual vaccines were investigated across two lots. The aluminium content was not significantly different between lots ($P > 0.05$). The highest content of aluminium measured was 0.334 mg/vaccine. The lowest content of aluminium measured was 0.192 mg/vaccine. The mean content of twenty vaccines was 0.287 mg/vaccine (Table 2). The aluminium content of Pedvax was significantly higher ($P < 0.001$) (Fig. 1) than the amount stated by the manufacturer (0.225 mg/vaccine) on the patient information leaflet (Table 3).

3.11. Prevnar13

The data for Prevnar13 were normally distributed. Six individual vaccines were investigated in a single lot. The highest content of aluminium measured was 0.141 mg/vaccine. The lowest content of aluminium measured was 0.127 mg/vaccine. The mean content of six vaccines was 0.136 mg/vaccine (Table 2). The aluminium content of Prevnar13 was significantly higher ($P = 0.003$) (Fig. 1) than the amount stated by the manufacturer (0.125 mg/vaccine) on the patient information leaflet (Table 3).

3.12. Synflorix

The data for Synflorix were normally distributed. Three individual vaccines were investigated from a single lot. The highest content of aluminium measured was 0.399 mg/vaccine. The lowest content of aluminium measured was 0.396 mg/vaccine. The mean content of three

vaccines was 0.398 mg/vaccine (Table 2). The aluminium content of Synflorix was significantly less ($P < 0.001$) (Fig. 1) than the amount stated by the manufacturer (0.500 mg/vaccine) on the patient information leaflet (Table 3).

3.13. Vaqtā

The data for Vaqtā were not normally distributed. Twenty individual vaccines were investigated across two lots. The aluminium content was not significantly different between lots ($P > 0.05$). The highest content of aluminium measured was 0.796 mg/vaccine. The lowest content of aluminium measured was 0.270 mg/vaccine. The median content of twenty vaccines was 0.340 mg/vaccine (Table 2). The aluminium content of Vaqtā was significantly higher ($P < 0.001$) (Fig. 1) than the amount stated by the manufacturer (0.225 mg/vaccine) on the patient information leaflet (Table 3).

4. Discussion

We present the aluminium content of 13 paediatric vaccines (Supplementary Table 1). We have compared our raw data with values given by manufacturers on patient information leaflets. In addition, we have applied a generous $\pm 10\%$ margin of manufacturing error to the latter published values when applying Bayesian methods (see Supplementary Table 2). Using a level of statistical significance of $P = 0.05$, 3 vaccines contained the amount of aluminium stated by the manufacturer on the patient information leaflet (Boostrix, Engerix B, Infanrix Hexa). Six vaccines contained significantly more aluminium (Pentacel, Havrix, Adacel, Pedvax, Prevnar 13, Vaqtā) while 4 vaccines contained significantly less (Infanrix, Pediarix, Kinrix, Synflorix). Statistical significance, of course, does not tell the only story. For example, while the aluminium content of Boostrix is not significantly different to that stated by the manufacturer ($P > 0.05$) there remains a 92 % chance that the aluminium content of a Boostrix vaccine will exceed the official content (Table 3). In addition, the content of aluminium is extremely variable with many vaccines showing %RSD in excess of 10 % even within the same lot (Table 2). For example, an infant receiving Havrix could receive anything between 0.172 and 0.602 mg of aluminium per vaccine. The data presented herein will be an underestimate of the actual content of aluminium as it is inevitable that some aluminium adjuvant will remain within the syringe system following injection. This will also be true when vaccines are injected *in vivo*. Vaccines that include an aluminium adjuvant are cloudy suspensions and manufacturers recommend that they are shaken prior to injection. For a few vaccines we were unable to obtain ten or more individual products and so data are limited, especially Synflorix. However, we present the first robust data obtained using state-of-the-art methods on the aluminium content of vaccines currently being administered in infants. The data are not reassuring. They suggest that vaccine manufacturers have limited control over the aluminium content of their vaccines. The aluminium content of individual vaccines within vaccine lots vary significantly. The amount of aluminium an infant receives in a vaccine is, it would appear, akin to a lottery. The true significance of this lottery is unknown. Vaccine manufacturers do not provide experimental protocols or rationales to support the amount of aluminium used in vaccines. If the amount used relates to a vaccine's potency in eliciting antibody titres then this should be explained in complementary information including, for example, that provided with the vaccine. Equally, how this potency is affected by the quantity of aluminium should also be a matter of public record. For example, using the data previously noted for Havrix, does it matter for the vaccine's efficacy if the content of aluminium received by an infant is 0.172 or 0.602 mg/vaccine. The natural assumption is that it does matter, otherwise why state specific amounts of aluminium on patient information leaflets. If the vaccine manufacturers stated content of aluminium is significant then it is concerning that six of the thirteen vaccines measured had statistically higher contents of aluminium. In

practice, this would mean that many infants are receiving significantly more aluminium than recommended by the manufacturer. How is this additional aluminium affecting the efficacy and safety of the vaccine? Similarly, four out of the thirteen vaccines contained statistically significantly less aluminium than recommended by the manufacturer. Is the lower than prescribed amount of aluminium in these vaccines affecting their efficacy?

The data raise many open questions about the significance of the amount of aluminium included in vaccines. They demonstrate if nothing else that further clarity and transparency is required from vaccine manufacturers as well as regulatory organisations such as the EMA and FDA. The aluminium content of a vaccine is never trivial [37]. There is a long history of testing the efficacy of childhood vaccines against false placebos and warnings against this practice continue to go unheeded [38]. It should be a matter of concern that a recent freedom of information act request (FOIA Case Number 50882, and HHS Appeal No.; 19-0083-AA) revealed that the NIH were unable to provide a single study relied upon by them in relation to the safety of injection of aluminium adjuvants in infants. Human exposure to aluminium is an unequivocal consequence of everyday living [39]. Aluminium adjuvants in infant vaccines contribute towards the body burden of aluminium [37]. Aluminium in the body has the potential to be toxic and significantly neurotoxic [40]. Where aluminium is being used for apparent human benefit, as in vaccines, we cannot simply ignore the other side of the coin, its known toxicity. We cannot afford to be complacent about its injection into infants [22].

Aluminium adjuvants are critical to the efficacy of vaccines and are far from being benign components [22]. Information on their content, activity and safety is severely lacking and this void requires urgent attention. Until such information is forthcoming, aluminium adjuvants remain prime suspects in widely documented vaccination-related adverse events.

Author contributions

ES: Analytical support and contributed to writing of the manuscript. CL: Carried out all statistics and contributed to writing of the manuscript. SC and ES: Carried out the majority of measurements and contributed to writing of the manuscript. CE: Design of study, analytical support and contributed to writing the manuscript.

Declaration of Competing Interest

The authors report no declarations of interest.

Acknowledgements

ES is a Children's Medical Safety Research Institute research fellow. Additional funding came from independent donations to CE via Keele University.

Appendix A. Supplementary data

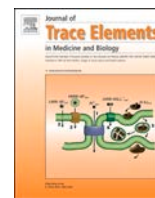
Supplementary material related to this article can be found, in the online version, at doi:<https://doi.org/10.1016/j.jtemb.2021.126762>.

References

- J.L. Grun, P.H. Maurer, Different T helper cell subsets elicited in mice utilizing two different adjuvant vehicles: the role of endogenous interleukin-1 in proliferative responses, *Cell. Immunol.* 121 (1989) 134–145.
- M.B. Jordan, D.M. Mills, J. Kappler, P. Marrack, J.C. Cambier, Promotion of B cell immune responses via an alum-induced myeloid cell population, *Science* 304 (2004) 1808–1810.
- J.M. Brewer, M. Conacher, A. Satoskar, H. Bluethmann, J. Alexander, In interleukin-4-deficient mice, alum not only generates T helper 1 responses equivalent to Freund's complete adjuvant, but continues to induce T helper 2 cytokine production, *Eur. J. Immunol.* 26 (1996) 2062–2066.
- J.M. Brewer, M. Conacher, M. Gaffney, M. Douglas, H. Bluethmann, J. Alexander, Neither interleukin-6 nor signalling via tumour necrosis factor receptor-1 contribute to the adjuvant activity of Alum and Freund's adjuvant, *Immunology* 93 (1998) 41–48.
- J.M. Brewer, M. Conacher, C.A. Hunter, M. Mohrs, F. Brombacher, J. Alexander, Aluminium hydroxide adjuvant initiates strong antigen-specific Th2 responses in the absence of IL-4- or IL-13-mediated signaling, *J. Immunol.* 163 (1999) 6448–6454.
- F. Liang, G. Lindgren, K.J. Sandgren, E.A. Thompson, J.R. Francica, A. Seubert, E. De Gregorio, S. Barnett, D.T. O'Hagan, N.J. Sullivan, R.A. Koup, R.A. Seder, K. Loré, Vaccine priming is restricted to draining lymph nodes and controlled by adjuvant-mediated antigen uptake, *Sci. Transl. Med.* 9 (2017) eaal2094.
- G.L. Morefield, A. Sokolovska, D. Jiang, H. HogenEsch, J.P. Robinson, S.L. Hem, Role of aluminum-containing adjuvants in antigen internalization by dendritic cells in vitro, *Vaccine* 23 (2005) 1588–1595.
- J.W. Mannhalter, H.O. Neychev, G.J. Zlabinger, R. Ahmad, M.M. Eibl, Modulation of the human immune response by the non-toxic and non-pyrogenic adjuvant aluminium hydroxide: effect on antigen uptake and antigen presentation, *Clin. Exp. Immunol.* 61 (1985) 143–151.
- T.R. Ghimire, R.A. Benson, P. Garside, J.M. Brewer, Alum increases antigen uptake, reduces antigen degradation and sustains antigen presentation by DCs in vitro, *Immunol. Lett.* 147 (2012) 55–62.
- L. Delamarre, R. Couture, I. Mellman, E.S. Trombetta, Enhancing immunogenicity by limiting susceptibility to lysosomal proteolysis, *J. Exp. Med.* 203 (2006) 2049–2055.
- A. Sokolovska, S.L. Hem, H. HogenEsch, Activation of dendritic cells and induction of CD4(+) T cell differentiation by aluminum-containing adjuvants, *Vaccine* 25 (2007) 4575–4585.
- A.C. Rimaniol, G. Gras, F. Verdier, F. Capel, V.B. Grigoriev, F. Porcheray, E. Sauzeat, J.G. Fournier, P. Clayette, C.A. Siegrist, D. Dormont, Aluminium hydroxide adjuvant induces macrophage differentiation towards a specialized antigen-presenting cell type, *Vaccine* 22 (2004) 3127–3135.
- H. Li, S. Nookala, F. Re, Aluminium hydroxide adjuvants activate caspase-1 and induce IL-1beta and IL-18 release, *J. Immunol.* 178 (2007) 5271–5276.
- S.C. Eisenbarth, O.R. Colegio, W. O'Connor, F.S. Sutterwala, R.A. Flavell, Crucial role for the Nalp3 inflammasome in the immunostimulatory properties of aluminium adjuvants, *Nature* 453 (2008) 1122–1126.
- H. Li, S.B. Willingham, J.P. Ting, F. Re, Cutting edge: inflammasome activation by alum and alum's adjuvant effect are mediated by NLRP3, *J. Immunol.* 181 (2008) 17–21.
- F.A. Sharp, D. Ruane, B. Claass, E. Creagh, J. Harris, P. Malyala, M. Singh, D. T. O'Hagan, V. Pétrilli, J. Tschopp, L.A. O'Neill, E.C. Lavelle, Uptake of particulate vaccine adjuvants by dendritic cells activates the NALP3 inflammasome, *Proc. Natl. Acad. Sci. U. S. A.* 106 (2009) 870–875.
- M. Kool, V. Pétrilli, T. De Smedt, A. Rolaz, H. Hammad, M. van Nimwegen, I. M. Bergen, R. Castillo, B.N. Lambrecht, J. Tschopp, Cutting edge: alum adjuvant stimulates inflammatory dendritic cells through activation of the NALP3 inflammasome, *J. Immunol.* 181 (2009) 3755–3759.
- A.T. Glenn, G.A.H. Buttle, M.F. Stevens, Rate of disappearance of diphtheria toxoid injected into rabbits and guinea-pigs: toxoid precipitated with alum, *J. Pathol. Bacteriol.* 34 (1931) 267–275.
- L.B. Holt, Developments in Diphtheria Prophylaxis, Heinemann Ltd, London, UK, 1950.
- J. Stephen, H.E. Scales, R.A. Benson, D. Erben, P. Garside, J.M. Brewer, Neutrophil swarming and extracellular trap formation play a significant role in alum adjuvant activity, *Npj Vaccines* 2 (2017) 1.
- C. Exley, P. Siesjö, H. Eriksson, The immunobiology of aluminium adjuvants: how do they really work? *Trends Immunol.* 31 (2010) 103–109.
- E. Shardlow, M. Mold, C. Exley, Unravelling the enigma: elucidating the relationship between the physicochemical properties of aluminium-based adjuvants and their immunological mechanisms of action, *Allergy Asthma Clin. Immunol.* 14 (2018) 80.
- M.J. Caulfield, L. Shi, S. Wang, B. Wang, T.W. Tobery, H. Mach, P.L. Ahl, J. L. Cannon, J.C. Cook, J.H. Heinrichs, R.D. Sitrin, Effect of alternative aluminum adjuvants on the absorption and immunogenicity of HPV16 L1 VLPs in mice, *Hum. Vaccin. Immunother.* 3 (2007) 139–145.
- E. House, M. Esiri, G. Forster, P.G. Ince, C. Exley, Aluminium, iron and copper in human brain tissues donated to the medical research council's cognitive function and ageing study, *Metallomics* 4 (2012) 56–65.
- S.N. Goodman, Introduction to Bayesian methods I: measuring the strength of evidence, *Clin. Trials* 2 (2005) 282–290, discussion 301–304, 364–378.
- R Core Team, R: A Language and Environment for Statistical Computing, R Foundation for Statistical Computing, Vienna, Austria, 2020. <https://www.R-project.org/>.
- H. Wickham, W. Chang, L. Henry, T.L. Pedersen, K. Takahashi, C. Wilke, K. Woo, H. Yutani, D. Dunnington, ggplot2: Create Elegant Data Visualisations Using the Grammar of Graphics, 2020. <https://CRAN.R-project.org/package=ggplot2>.
- S. Højsgaard, U. Halekoh, doBy: Groupwise Statistics, LSmeans, Linear Contrasts, Utilities, 2020. <https://CRAN.R-project.org/package=doBy>.
- J.K.K. Meredith, J. Kruschke, BEST: Bayesian Estimation Supersedes the t-Test, 2020. <https://CRAN.R-project.org/package=BEST>.
- R. Bååth, Bayesian first aid: a package that implements Bayesian alternatives to the classical *.Test functions in R, Proceedings of User! the International R User Conference (2014). <https://www.rdocumentation.org/packages/BayesianFirstAid/versions/0.1>.

- [31] R. Joachim. `bayesWilcoxTest`: A Bayesian Alternative to the Wilcoxon Signed Rank Test. 20210. R package version 0.1.0. <https://rdrr.io/github/joereinhardt/BayesianFirstAid-Wilcoxon/>.
- [32] C. Keyzers, V. Gazzola, E.J. Wagenmakers, Using Bayes factor hypothesis testing in neuroscience to establish evidence of absence, *Nat. Neurosci.* 23 (2020) 788–799.
- [33] D.S. Quintana, D.R. Williams, Bayesian alternatives for common null-hypothesis significance tests in psychiatry: a non-technical guide using JASP, *BMC Psychiatry* 18 (2018) 178.
- [34] S.N. Goodman, Toward evidence-based medical statistics. 1: the P value fallacy, *Ann. Intern. Med.* 130 (1999) 995–1004.
- [35] J. Skinner, Statistics for immunologists, *Curr. Protoc. Immunol.* 122 (2018) 5436.
- [36] S. Goodman, A dirty dozen: twelve P-value misconceptions, *Sem. Hematol.* 45 (2008) 135–140.
- [37] C. Exley, An aluminium adjuvant in a vaccine is an acute exposure to aluminium, *J. Trace Elem. Med. Biol.* 57 (2020) 57–59.
- [38] C. Exley, Aluminium-based adjuvants should not be used as placebos in clinical trials, *Vaccine* 29 (2011) 9289.
- [39] C. Exley, Human exposure to aluminium, *Environ. Sci. Process. Impacts* 15 (2013) 1807–1816.
- [40] C. Exley, What is the risk of aluminium as a neurotoxin? *Expert Rev. Neurother.* 14 (2014) 589–591.

Footnote 1



The measurement and full statistical analysis including Bayesian methods of the aluminium content of infant vaccines

Emma Shardlow^a, Caroline Linhart^a, Sameerah Connor^b, Erin Softely^b, Christopher Exley^{a,*}

^a The Birchall Centre, Lennard-Jones Laboratories, Keele University, Staffordshire, United Kingdom

^b Life Sciences, The Huxley Building, Keele University, Staffordshire, United Kingdom

ARTICLE INFO

Keywords:

Human exposure to aluminium
Aluminium adjuvants
Aluminium content of infant vaccines
Vaccine safety and efficacy

ABSTRACT

Background: Aluminium salts are the most common adjuvants in infant vaccines. The aluminium content of a vaccine is provided by the manufacturer and is indicated on the patient information leaflet. There is no independent verification, for example by the European Medicines Agency, of the aluminium content of infant vaccines.

Methods: We have measured the aluminium content of thirteen infant vaccines using microwave-assisted acid and peroxide digestion followed by transversely heated graphite furnace atomic absorption spectrometry. Our data are compared with manufacturer's data using full statistical analyses including Bayesian methods.

Results: We found that only three vaccines contained the amount of aluminium indicated by the manufacturer. Six vaccines contained a statistically significant ($P < 0.05$) greater quantity while four vaccines contained a statistically significant ($P < 0.05$) lower quantity. The range of content for any single vaccine varied considerably, for example, from 0.172 to 0.602 mg/vaccine for Havrix.

Conclusions: The data have raised specific questions about the significance of the aluminium content of vaccines and identified areas of extremely limited information. Since aluminium is a known toxin in humans and specifically a neurotoxin, its content in vaccines should be accurate and independently monitored to ensure both efficacy and safety.

1. Introduction

Aluminium salts are the adjuvants of choice in the majority of inactivated paediatric vaccines. Their presence at injection sites following vaccination results in the activation of humoral immunity. This pathway is characterised by the differentiation of naive CD4⁺ T cells into Th2 effector subsets and the subsequent enhancement of antigen-specific antibody titres [1–5]. T cell priming post-vaccination occurs following the cross-presentation of antigen-MHC complexes by immunocompetent phagocytes and occurs exclusively within draining lymph nodes [6] at locations often distant from the injection site. Aluminium adjuvants have been shown to facilitate this process by; i) actively increasing levels of antigen recognition and uptake by antigen-presenting cells [7–9], ii) acting in a protective capacity to prevent antigen degradation within intracellular compartments [9,10] and (iii) amplifying and sustaining antigen-MHC II expression by antigen-presenting cells [9,11,12]. Other suggested mechanisms underlying the immunostimulatory effects of aluminium adjuvants include

the secretion of pro-inflammatory cytokines by activated antigen-presenting cells [13–17] and the formation of an 'antigen depot' at the vaccine injection site [18,19]. While the latter is regarded by some as superfluous to the mechanism of action of aluminium adjuvants, recent evidence has demonstrated that extracellular traps formed by neutrophils following immunization make a significant contribution to their immunological activity *in vivo* [20]. However, the *modus operandi* of aluminium adjuvants remains to be fully elucidated [21,22].

Three aluminium salts are currently used as adjuvants in human vaccines. Two of these, aluminium oxyhydroxide (available commercially as Alhydrogel®) and aluminium hydroxyphosphate (available commercially as AdjuPhos®) have been widely studied while the third, aluminium hydroxyphosphate sulphate, is proprietary to Merck and has not been available for independent scrutiny [22,23]. The type and amount of aluminium adjuvant used in paediatric vaccines is made available through patient information leaflets, see the manufacturer's information summarised in Table 1. The information given is, at best, vague. Descriptions of aluminium salts are often inaccurate, for

* Corresponding author at: The Birchall Centre, Lennard-Jones Laboratories, Keele University, Staffordshire, ST5 5BG, United Kingdom.

E-mail address: c.exley@keele.ac.uk (C. Exley).

<https://doi.org/10.1016/j.jtemb.2021.126762>

Received 16 February 2021; Received in revised form 23 March 2021; Accepted 12 April 2021

Available online 15 April 2021

0946-672X/© 2021 The Author(s).

Published by Elsevier GmbH. This is an open access article under the CC BY-NC-ND license

(<http://creativecommons.org/licenses/by-nc-nd/4.0/>).

example, the use of the term aluminium hydroxide when the form of aluminium included is aluminium oxyhydroxide. Quantitative data describing the content of aluminium in a vaccine is often presented in a number of different formats. For example, all do present these data as total aluminium but some additionally present the data in respect of the weight of aluminium salt. This practice is confusing for anyone reading the patient information leaflet. The manufacturers' stated content of aluminium in vaccines listed in Table 1 varies from 0.125 (Pevnar 13) to 0.85 (PEDIARIX) mg per 0.5 mL dose of vaccine though little or no information is available as to why the content is so varied. Why does one vaccine require more aluminium adjuvant to be effective than another? There exists a non-regulatory limit of 1.25 mg aluminium per dose of vaccine based upon maximum titres of antibodies produced. However, even this may be exceeded under certain circumstances. The European Medicines Agency (EMA) and the Food and Drug Administration (FDA) are charged with the responsibility of verifying the information provided by vaccine manufacturers in their patient information leaflets. When questioned repeatedly on this subject (for example, EMA request reference ASK-56123) neither organisation was able to confirm that they routinely measure the aluminium content of vaccines. They indicated that they relied upon data provided to them by manufacturers, though no such data were forthcoming following requests including freedom of information act requests to the FDA (For example, FOIA Requests 2019-11150 to 2019-11156 & 2019-11158). When the EMA was asked, which analytical methods were used by either their organisation or vaccine manufacturers to measure the aluminium content of vaccines, they replied that this was proprietary information and could not be provided (EMA request reference ASK-56707). It would appear that the aluminium content of a vaccine is only measured by the manufacturer, using an unspecified method, and that these data are not made publicly available.

One piece of important information about the aluminium content of a vaccine is that it is clearly critical. Why else would there be such a wide range of contents used across the paediatric vaccine schedule. Since

those charged with ensuring that the information provided by vaccine manufacturers is correct are seemingly choosing to neglect this responsibility, herein we have measured the aluminium content of thirteen paediatric vaccines. We find that the measured content of aluminium is only similar to that given by the manufacturer in three out of thirteen vaccines.

2. Materials and methods

2.1. Vaccines

Whole vaccines were provided under license by a state registered paediatrician. All vaccines were in their original packaging and remained pristine and refrigerated at 4 °C until use.

2.2. Digestion of vaccines

Each whole vaccine was added to an acid-washed, dried and labelled 20 mL PFA Teflon MARSXpress digestion vessel closed with a venting plug and screw cap (CEM Technology, UK). The idea being that the whole vaccine was 'injected' into the digestion vessel in the identical manner as it would be used in human vaccination. In each case, it was assumed, though it was unlikely to be the case, that the whole vaccine volume of 0.5 mL was transferred to the digestion tube. To each whole vaccine, 1 mL of concentrated HNO₃ (Analar, 15.8 M Fisher Scientific, UK) and 1 mL 30 % w/v H₂O₂ (Aristar, BDH, UK) were added and the mixture subjected to microwave-assisted digestion (MARS6 CEM, One Touch Technology, UK). The resulting digests were further diluted by the addition of 2.5 mL of pure water (conductivity <0.067µS/cm) and stored appropriately for subsequent analyses. Method blanks were prepared where 0.5 mL of pure water was substituted for the whole vaccine. Full information pertaining to this method of sample digestion including microwave parameters are available elsewhere [24].

Table 1

Information relating to each of the thirteen infant vaccines taken directly from their patient information leaflets respectively.

Trade name of vaccine	Pharmaceutical company [Country of manufacture]	Paediatric dose (mL)	Manufacturer's stated aluminium content per paediatric dose (mg)	Infant age range	Manufacturer's description of vaccine
PEDIARIX	GlaxoSmithKline (GSK) [Belgium]	0.5	"not more than 0.85 mg aluminium"	from 2 to 6 months	Vaccine for the active immunization against diphtheria, tetanus, pertussis, hepatitis B virus infection and poliomyelitis.
Pentacel	Sanofi Pasteur [Canada]	0.5	0.33 mg of aluminium as 1.5 mg aluminium phosphate	from 6 weeks to 4 years	Vaccine for the active immunization against diphtheria, tetanus, pertussis, poliomyelitis and disease caused by <i>Haemophilus influenzae</i> type b.
ENGERIX-B	GlaxoSmithKline (GSK) [Belgium]	0.5	0.25 mg of aluminium as aluminium hydroxide	from 1 to 6 months	Vaccine for immunization against infection caused by hepatitis B virus.
Pevnar 13	Pfizer [United States]	0.5	0.125 mg of aluminium (as aluminium phosphate)	from 6 weeks to 5 years	Vaccine for active immunization against disease caused by <i>Streptococcus pneumoniae</i> .
PedvaxHIB	Merck & Co., Inc [United States]	0.5	0.225 mg of aluminium as amorphous aluminium hydroxyphosphate sulphate	from 6 to 11 months	Vaccine for immunization against infection caused by <i>Haemophilus influenzae</i> type b.
KINRIX	GlaxoSmithKline (GSK) [Belgium]	0.5	"not more than 0.6 mg aluminium by assay"	from 4 up to 6 years	Vaccine for immunization against diphtheria, tetanus, pertussis and poliomyelitis.
INFANRIX	GlaxoSmithKline (GSK) [Belgium]	0.5	"not more than 0.625 mg aluminium by assay"	from 6 weeks up to 6 years	Vaccine for active immunization against diphtheria, tetanus and pertussis.
BOOSTRIX	GlaxoSmithKline (GSK) [Belgium]	0.5	"not more than 0.39 mg aluminium by assay"	from 10 years	Vaccine for active immunization against tetanus, diphtheria and pertussis.
VAQTA	Merck & Co., Inc [United States]	0.5	0.225 mg of aluminium as amorphous aluminium hydroxyphosphate sulphate	from 12 months (up to 18 years)	Vaccine for immunization against disease caused by hepatitis A virus
Adacel	Sanofi Pasteur [Canada]	0.5	1.5 mg aluminium phosphate (0.33 mg aluminium)	from 10 years	Vaccine for active immunization against tetanus, diphtheria and pertussis.
HAVRIX	GlaxoSmithKline (GSK) [Belgium]	0.5	0.25 mg of aluminium as aluminium hydroxide	from 12 to 24 months	Vaccine for immunisation against disease caused by hepatitis A virus.
Infanrix hexa	GlaxoSmithKline (GSK) [Belgium]	0.5	0.82 mg of aluminium (as aluminium salts)	from 2 to 18 months	Vaccine for immunization against diphtheria, tetanus, pertussis, hepatitis B, poliomyelitis and <i>Haemophilus influenzae</i> type b.
Synflorix	GlaxoSmithKline (GSK) [Belgium]	0.5	0.5 mg of aluminium as aluminium phosphate	from 6 weeks up to 5 years	Vaccine for immunization against infections caused by <i>Streptococcus pneumoniae</i> .

2.3. Determination of aluminium

The total aluminium content of each vaccine digest and each method blank was measured by transversely heated graphite furnace atomic absorption spectrometry (TH GFAAS) using a fully established method including matrix-matched standards and commensurate quality assurance criteria [24]. Method blank data equating to 54 ngAl/5 mL digest were subtracted from each vaccine sample. Data are presented as mgAl/0.5 mL vaccine volume.

2.4. Statistics

Data on the measured concentrations of aluminium, stratified by brand, were tested for normality. Depending on whether the data were normally distributed or not, means and medians were calculated and tested two- and one-sided against the manufacturer's content of aluminium (see Table 1) using one-sample *t*-test and Wilcoxon signed rank test respectively.

Differences in aluminium content between lots were analysed for those vaccines with two lots and sufficient sample numbers.

To determine the probability, expressed as a percentage, that the measured content of aluminium in a vaccine was less than, the same as or greater than the amount given by the vaccine manufacturer, Bayesian methodology was used [25].

The hypotheses tested were as follows:

H0. Declared content of aluminium is equal to or less than the measured concentrations of aluminium. (The difference in means is zero.)

The alternative hypothesis is that the difference in means is not zero:

Ha1. Measured concentration of aluminium is not the same.

Ha2. Measured concentration of aluminium is greater.

Ha3. Measured concentration of aluminium is less.

Tests were repeated one-sided in both directions. For two-sided tests, a *p*-value < 0.05 was considered as statistically significant and for one-sided tests a *p*-value < 0.025.

Analyses were performed using R-Studio version 1.1.1093 [26] including packages ggplot2 [27], doBy [28], BEST [29], BayesianFirstAid [30] and bayesWilcoxTest [31]. The last three packages provide Bayesian alternatives to the classical hypothesis tests in R. Bayesian methods were used to calculate the percentage probability that measured aluminium concentrations were randomly the same or greater/less than amounts stated by the manufacturer. Bayes factors can complement *p*-values by providing additional information for hypothesis testing by quantifying the relative evidence for both alternative and null hypotheses. Moreover, the magnitude of this evidence can be presented as percentages [25,32–36].

The following code was used to produce random data sets of aluminium values for each vaccine with the stated manufacturers mean and 10 % RSD. The latter to reflect 'expected' manufacturing error.

```
rnorm2 <- function(n,mean,sd) {mean + sd*scale(rnorm(n))}
```

The Bayesian approach was repeated with the random data sets including the 10 % variation.

3. Results

3.1. Pentacel

The data for Pentacel were normally distributed. Ten individual vaccines were investigated across two lots. The aluminium content differed significantly between lots ($P < 0.030$). The highest content of aluminium measured was 0.440 mg/vaccine. The lowest content of

aluminium measured was 0.343 mg/vaccine. The mean content of ten vaccines was 0.379 mg/vaccine (Table 2). The aluminium content of Pentacel was significantly higher for both lots combined ($P < 0.001$) (Fig. 1), lot 1 only ($P = 0.005$) and lot 2 only ($P = 0.004$) than the amount stated by the manufacturer (0.330 mg/vaccine) on the patient information leaflet (Table 3).

3.2. Havrix

The data for Havrix were not normally distributed. Twenty individual vaccines were investigated across two lots. The aluminium content differed significantly between lots ($P < 0.001$). The highest content of aluminium measured was 0.602 mg/vaccine. The lowest content of aluminium measured was 0.172 mg/vaccine. The median content of twenty vaccines was 0.307 mg/vaccine (Table 2). The aluminium content of Havrix was significantly higher for both lots combined ($P = 0.003$) (Fig. 1) and lot 2 only ($P = 0.003$) than the amount stated by the manufacturer (0.250 mg/vaccine) on the patient information leaflet (Table 3).

3.3. Adacel

The data for Adacel were not normally distributed. Nine individual vaccines were investigated across two lots. The aluminium content was not significantly different between lots ($P > 0.05$). The highest content of aluminium measured was 0.445 mg/vaccine. The lowest content of aluminium measured was 0.302 mg/vaccine. The median content of nine vaccines was 0.397 mg/vaccine (Table 2). The aluminium content of Adacel was significantly higher ($P = 0.006$) (Fig. 1) than the amount stated by the manufacturer (0.330 mg/vaccine) on the patient information leaflet (Table 3).

3.4. Boostrix

The data for Boostrix were normally distributed. Twenty individual vaccines were investigated from a single lot. The highest content of aluminium measured was 0.525 mg/vaccine. The lowest content of aluminium measured was 0.345 mg/vaccine. The mean content of twenty vaccines was 0.407 mg/vaccine (Table 2). The aluminium content of Boostrix was not significantly different ($P = 0.101$) (Fig. 1) to the amount stated by the manufacturer (0.390 mg/vaccine) on the patient information leaflet (Table 3).

3.5. EngerixB

The data for EngerixB were normally distributed. Twenty individual

Table 2

Descriptive statistics for each of the thirteen infant vaccines including normal distribution (N.D.), number of replicates (N), minimum (Min.), maximum (Max.), mean/median values (mg/0.5 mL dose) and indication of variance (SD, RSD). Vaccines ordered according to their mean/median Al contents.

Vaccine	N.D.	N	Min.	Max.	Mean/ Median	SD	RSD
Prevnar 13	Y	6	0.127	0.141	0.136	0.006	0.04
EngerixB	Y	20	0.187	0.287	0.249	0.027	0.11
Pedvax	Y	20	0.192	0.334	0.287	0.040	0.14
Havrix	N	20	0.172	0.602	0.307	0.084	0.28
Vaqa	N	20	0.270	0.796	0.340	0.109	0.32
Pentacel	Y	10	0.343	0.440	0.379	0.032	0.09
Adacel	N	9	0.302	0.445	0.397	0.041	0.10
Synflorix	Y	3	0.396	0.399	0.398	0.002	0.00
Boostrix	Y	20	0.345	0.525	0.407	0.043	0.11
Kinrix	N	20	0.464	0.635	0.511	0.062	0.12
Infanrix	Y	20	0.415	0.662	0.546	0.069	0.13
Pediarix	Y	20	0.575	0.743	0.661	0.039	0.06
Infanrix Hexa	Y	6	0.766	0.851	0.806	0.028	0.04

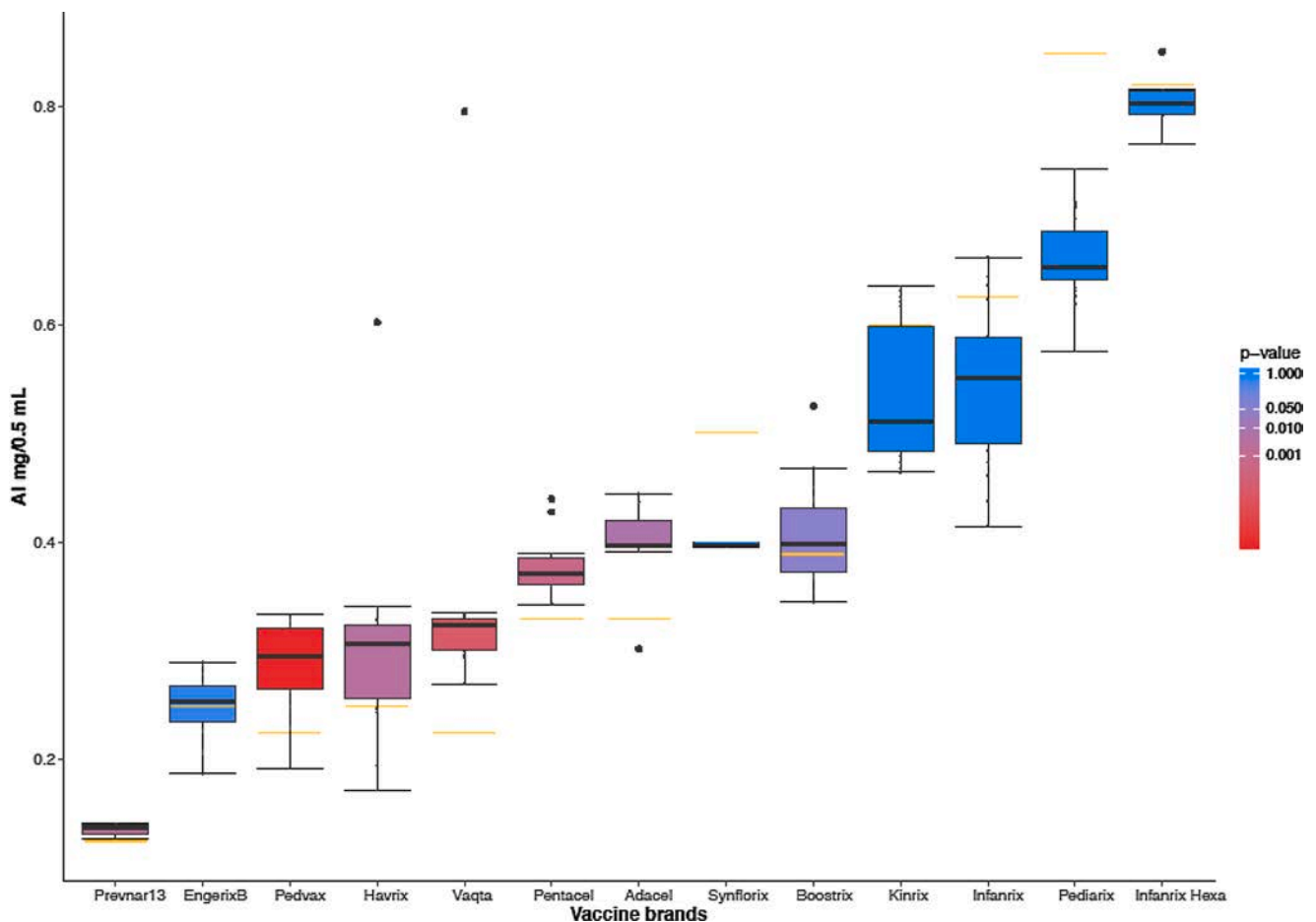


Fig. 1. Boxplots of measured aluminium concentrations (mg/0.5 mL dose) stratified per vaccine brand and compared to the manufacturers' stated amounts (yellow line). The colour gradient represents p-values of one-sided t-tests or Mann-Whitney U tests of the measured Al against the manufacturers' stated amounts. The red boxplots indicate vaccines with significantly more aluminium than that stated by the manufacturer. Boxplots in violet and blue represent data for vaccines where the measured content is either not significantly to or significantly less than the manufacturers' stated amounts. (For interpretation of the references to colour in this figure legend, the reader is referred to the web version of this article).

vaccines were investigated from a single lot. The highest content of aluminium measured was 0.287 mg/vaccine. The lowest content of aluminium measured was 0.187 mg/vaccine. The mean content of twenty vaccines was 0.249 mg/vaccine (Table 2). The aluminium content of EngerixB was not significantly different ($P = 0.897$) (Fig. 1) to the amount stated by the manufacturer (0.250 mg/vaccine) on the patient information leaflet (Table 3).

3.6. Infanrix

The data for Infanrix were normally distributed. Twenty individual vaccines were investigated from a single lot. The highest content of aluminium measured was 0.662 mg/vaccine. The lowest content of aluminium measured was 0.415 mg/vaccine. The mean content of twenty vaccines was 0.546 mg/vaccine (Table 2). The aluminium content of Infanrix was significantly lower ($P < 0.001$) (Fig. 1) than the amount stated by the manufacturer (0.625 mg/vaccine) on the patient information leaflet (Table 3).

3.7. Infanrix Hexa

The data for Infanrix Hexa were normally distributed. Six individual vaccines were investigated from a single lot. The highest content of aluminium measured was 0.851 mg/vaccine. The lowest content of aluminium measured was 0.766 mg/vaccine. The mean content of six vaccines was 0.806 mg/vaccine (Table 2). The aluminium content of

Infanrix Hexa was not significantly different ($P = 0.268$) (Fig. 1) to the amount stated by the manufacturer (0.820 mg/vaccine) on the patient information leaflet (Table 3).

3.8. Kinrix

The data for Kinrix were not normally distributed. Twenty individual vaccines were investigated across two lots. The aluminium content was not significantly different between lots ($P > 0.05$). The highest content of aluminium measured was 0.635 mg/vaccine. The lowest content of aluminium measured was 0.464 mg/vaccine. The median content of twenty vaccines was 0.511 mg/vaccine (Table 2). The aluminium content of Kinrix was significantly less ($P = 0.001$) (Fig. 1) than the amount stated by the manufacturer (0.600 mg/vaccine) on the patient information leaflet (Table 3).

3.9. Pediarix

The data for Pediarix were normally distributed. Twenty individual vaccines were investigated across two lots. The aluminium content was not significantly different between lots ($P > 0.05$). The highest content of aluminium measured was 0.743 mg/vaccine. The lowest content of aluminium measured was 0.575 mg/vaccine. The mean content of twenty vaccines was 0.661 mg/vaccine (Table 2). The aluminium content of Pediarix was significantly lower ($P < 0.001$) (Fig. 1) than the amount stated by the manufacturer (0.850 mg/vaccine) on the patient

Table 3

Summary statistics of results including statistical test used (T test or Mann Whitney U), two- and one-sided p-values of statistical tests, difference in means (stated Al amount – measured amount) and percentage of evidence for the outcome according to Bayesian methodology. Vaccines ordered according to their mean/median Al content.

Vaccine	Test	p-value 2-sided	p-value 1-sided	Diff. in Means	Outcome (H ₁)	Probability of Outcome
Prevnar 13	T	0.005	0.003	−0.01	Greater	0.993
EngerixB	T	0.897	0.551	0.00	Same or Less	0.513
Pedvax	T	< 0.001	< 0.001	−0.06	Greater	> 0.999
Havrix	MWU	0.006	0.003	−0.06	Greater	0.872
Havrix Lot 1	T	0.710	0.355	−0.01	Greater	0.661
Havrix Lot 2	MWU	0.006	0.003	−0.08	Greater	0.988
Vaqtā	MWU	< 0.001	< 0.001	−0.11	Greater	0.995
Pentacel	T	0.001	< 0.001	−0.05	Greater	0.999
Pentacel Lot 1	T	0.010	0.005	−0.03	Greater	0.986
Pentacel Lot 2	T	0.008	0.004	−0.07	Greater	0.991
Adacel	MWU	0.013	0.006	−0.07	Greater	0.938
Synflorix	T	< 0.001	1.000	0.10	Same or Less	0.998
Boostrix	T	0.101	0.051	−0.02	Greater	0.924
Kinrix	MWU	0.001	0.999	0.09	Same or Less	0.878
Infanrix	T	< 0.001	1.000	0.08	Same or Less	> 0.999
Pediarix	T	< 0.001	1.000	0.19	Same or Less	> 0.999
Infanrix Hexa	T	0.268	0.866	0.01	Same or Less	0.846

information leaflet (Table 3).

3.10. Pedvax

The data for Pedvax were normally distributed. Twenty individual vaccines were investigated across two lots. The aluminium content was not significantly different between lots ($P > 0.05$). The highest content of aluminium measured was 0.334 mg/vaccine. The lowest content of aluminium measured was 0.192 mg/vaccine. The mean content of twenty vaccines was 0.287 mg/vaccine (Table 2). The aluminium content of Pedvax was significantly higher ($P < 0.001$) (Fig. 1) than the amount stated by the manufacturer (0.225 mg/vaccine) on the patient information leaflet (Table 3).

3.11. Prevnar13

The data for Prevnar13 were normally distributed. Six individual vaccines were investigated in a single lot. The highest content of aluminium measured was 0.141 mg/vaccine. The lowest content of aluminium measured was 0.127 mg/vaccine. The mean content of six vaccines was 0.136 mg/vaccine (Table 2). The aluminium content of Prevnar13 was significantly higher ($P = 0.003$) (Fig. 1) than the amount stated by the manufacturer (0.125 mg/vaccine) on the patient information leaflet (Table 3).

3.12. Synflorix

The data for Synflorix were normally distributed. Three individual vaccines were investigated from a single lot. The highest content of aluminium measured was 0.399 mg/vaccine. The lowest content of aluminium measured was 0.396 mg/vaccine. The mean content of three

vaccines was 0.398 mg/vaccine (Table 2). The aluminium content of Synflorix was significantly less ($P < 0.001$) (Fig. 1) than the amount stated by the manufacturer (0.500 mg/vaccine) on the patient information leaflet (Table 3).

3.13. Vaqtā

The data for Vaqtā were not normally distributed. Twenty individual vaccines were investigated across two lots. The aluminium content was not significantly different between lots ($P > 0.05$). The highest content of aluminium measured was 0.796 mg/vaccine. The lowest content of aluminium measured was 0.270 mg/vaccine. The median content of twenty vaccines was 0.340 mg/vaccine (Table 2). The aluminium content of Vaqtā was significantly higher ($P < 0.001$) (Fig. 1) than the amount stated by the manufacturer (0.225 mg/vaccine) on the patient information leaflet (Table 3).

4. Discussion

We present the aluminium content of 13 paediatric vaccines (Supplementary Table 1). We have compared our raw data with values given by manufacturers on patient information leaflets. In addition, we have applied a generous $\pm 10\%$ margin of manufacturing error to the latter published values when applying Bayesian methods (see Supplementary Table 2). Using a level of statistical significance of $P = 0.05$, 3 vaccines contained the amount of aluminium stated by the manufacturer on the patient information leaflet (Boostrix, Engerix B, Infanrix Hexa). Six vaccines contained significantly more aluminium (Pentacel, Havrix, Adacel, Pedvax, Prevnar 13, Vaqtā) while 4 vaccines contained significantly less (Infanrix, Pediarix, Kinrix, Synflorix). Statistical significance, of course, does not tell the only story. For example, while the aluminium content of Boostrix is not significantly different to that stated by the manufacturer ($P > 0.05$) there remains a 92 % chance that the aluminium content of a Boostrix vaccine will exceed the official content (Table 3). In addition, the content of aluminium is extremely variable with many vaccines showing %RSD in excess of 10 % even within the same lot (Table 2). For example, an infant receiving Havrix could receive anything between 0.172 and 0.602 mg of aluminium per vaccine. The data presented herein will be an underestimate of the actual content of aluminium as it is inevitable that some aluminium adjuvant will remain within the syringe system following injection. This will also be true when vaccines are injected *in vivo*. Vaccines that include an aluminium adjuvant are cloudy suspensions and manufacturers recommend that they are shaken prior to injection. For a few vaccines we were unable to obtain ten or more individual products and so data are limited, especially Synflorix. However, we present the first robust data obtained using state-of-the-art methods on the aluminium content of vaccines currently being administered in infants. The data are not reassuring. They suggest that vaccine manufacturers have limited control over the aluminium content of their vaccines. The aluminium content of individual vaccines within vaccine lots vary significantly. The amount of aluminium an infant receives in a vaccine is, it would appear, akin to a lottery. The true significance of this lottery is unknown. Vaccine manufacturers do not provide experimental protocols or rationales to support the amount of aluminium used in vaccines. If the amount used relates to a vaccine's potency in eliciting antibody titres then this should be explained in complementary information including, for example, that provided with the vaccine. Equally, how this potency is affected by the quantity of aluminium should also be a matter of public record. For example, using the data previously noted for Havrix, does it matter for the vaccine's efficacy if the content of aluminium received by an infant is 0.172 or 0.602 mg/vaccine. The natural assumption is that it does matter, otherwise why state specific amounts of aluminium on patient information leaflets. If the vaccine manufacturers stated content of aluminium is significant then it is concerning that six of the thirteen vaccines measured had statistically higher contents of aluminium. In

practice, this would mean that many infants are receiving significantly more aluminium than recommended by the manufacturer. How is this additional aluminium affecting the efficacy and safety of the vaccine? Similarly, four out of the thirteen vaccines contained statistically significantly less aluminium than recommended by the manufacturer. Is the lower than prescribed amount of aluminium in these vaccines affecting their efficacy?

The data raise many open questions about the significance of the amount of aluminium included in vaccines. They demonstrate if nothing else that further clarity and transparency is required from vaccine manufacturers as well as regulatory organisations such as the EMA and FDA. The aluminium content of a vaccine is never trivial [37]. There is a long history of testing the efficacy of childhood vaccines against false placebos and warnings against this practice continue to go unheeded [38]. It should be a matter of concern that a recent freedom of information act request (FOIA Case Number 50882, and HHS Appeal No.; 19-0083-AA) revealed that the NIH were unable to provide a single study relied upon by them in relation to the safety of injection of aluminium adjuvants in infants. Human exposure to aluminium is an unequivocal consequence of everyday living [39]. Aluminium adjuvants in infant vaccines contribute towards the body burden of aluminium [37]. Aluminium in the body has the potential to be toxic and significantly neurotoxic [40]. Where aluminium is being used for apparent human benefit, as in vaccines, we cannot simply ignore the other side of the coin, its known toxicity. We cannot afford to be complacent about its injection into infants [22].

Aluminium adjuvants are critical to the efficacy of vaccines and are far from being benign components [22]. Information on their content, activity and safety is severely lacking and this void requires urgent attention. Until such information is forthcoming, aluminium adjuvants remain prime suspects in widely documented vaccination-related adverse events.

Author contributions

ES: Analytical support and contributed to writing of the manuscript. CL: Carried out all statistics and contributed to writing of the manuscript. SC and ES: Carried out the majority of measurements and contributed to writing of the manuscript. CE: Design of study, analytical support and contributed to writing the manuscript.

Declaration of Competing Interest

The authors report no declarations of interest.

Acknowledgements

ES is a Children's Medical Safety Research Institute research fellow. Additional funding came from independent donations to CE via Keele University.

Appendix A. Supplementary data

Supplementary material related to this article can be found, in the online version, at doi:<https://doi.org/10.1016/j.jtemb.2021.126762>.

References

- J.L. Grun, P.H. Maurer, Different T helper cell subsets elicited in mice utilizing two different adjuvant vehicles: the role of endogenous interleukin-1 in proliferative responses, *Cell. Immunol.* 121 (1989) 134–145.
- M.B. Jordan, D.M. Mills, J. Kappler, P. Marrack, J.C. Cambier, Promotion of B cell immune responses via an alum-induced myeloid cell population, *Science* 304 (2004) 1808–1810.
- J.M. Brewer, M. Conacher, A. Satoskar, H. Bluethmann, J. Alexander, In interleukin-4-deficient mice, alum not only generates T helper 1 responses equivalent to Freund's complete adjuvant, but continues to induce T helper 2 cytokine production, *Eur. J. Immunol.* 26 (1996) 2062–2066.
- J.M. Brewer, M. Conacher, M. Gaffney, M. Douglas, H. Bluethmann, J. Alexander, Neither interleukin-6 nor signalling via tumour necrosis factor receptor-1 contribute to the adjuvant activity of Alum and Freund's adjuvant, *Immunology* 93 (1998) 41–48.
- J.M. Brewer, M. Conacher, C.A. Hunter, M. Mohrs, F. Brombacher, J. Alexander, Aluminium hydroxide adjuvant initiates strong antigen-specific Th2 responses in the absence of IL-4- or IL-13-mediated signaling, *J. Immunol.* 163 (1999) 6448–6454.
- F. Liang, G. Lindgren, K.J. Sandgren, E.A. Thompson, J.R. Francica, A. Seubert, E. De Gregorio, S. Barnett, D.T. O'Hagan, N.J. Sullivan, R.A. Koup, R.A. Seder, K. Loré, Vaccine priming is restricted to draining lymph nodes and controlled by adjuvant-mediated antigen uptake, *Sci. Transl. Med.* 9 (2017) eaal2094.
- G.L. Morefield, A. Sokolovska, D. Jiang, H. HogenEsch, J.P. Robinson, S.L. Hem, Role of aluminum-containing adjuvants in antigen internalization by dendritic cells in vitro, *Vaccine* 23 (2005) 1588–1595.
- J.W. Mannhalter, H.O. Neychev, G.J. Zlabinger, R. Ahmad, M.M. Eibl, Modulation of the human immune response by the non-toxic and non-pyrogenic adjuvant aluminium hydroxide: effect on antigen uptake and antigen presentation, *Clin. Exp. Immunol.* 61 (1985) 143–151.
- T.R. Ghimire, R.A. Benson, P. Garside, J.M. Brewer, Alum increases antigen uptake, reduces antigen degradation and sustains antigen presentation by DCs in vitro, *Immunol. Lett.* 147 (2012) 55–62.
- L. Delamarre, R. Couture, I. Mellman, E.S. Trombetta, Enhancing immunogenicity by limiting susceptibility to lysosomal proteolysis, *J. Exp. Med.* 203 (2006) 2049–2055.
- A. Sokolovska, S.L. Hem, H. HogenEsch, Activation of dendritic cells and induction of CD4(+) T cell differentiation by aluminum-containing adjuvants, *Vaccine* 25 (2007) 4575–4585.
- A.C. Rimaniol, G. Gras, F. Verdier, F. Capel, V.B. Grigoriev, F. Porcheray, E. Sauzeat, J.G. Fournier, P. Clayette, C.A. Siegrist, D. Dormont, Aluminium hydroxide adjuvant induces macrophage differentiation towards a specialized antigen-presenting cell type, *Vaccine* 22 (2004) 3127–3135.
- H. Li, S. Nookala, F. Re, Aluminium hydroxide adjuvants activate caspase-1 and induce IL-1beta and IL-18 release, *J. Immunol.* 178 (2007) 5271–5276.
- S.C. Eisenbarth, O.R. Colegio, W. O'Connor, F.S. Sutterwala, R.A. Flavell, Crucial role for the Nalp3 inflammasome in the immunostimulatory properties of aluminium adjuvants, *Nature* 453 (2008) 1122–1126.
- H. Li, S.B. Willingham, J.P. Ting, F. Re, Cutting edge: inflammasome activation by alum and alum's adjuvant effect are mediated by NLRP3, *J. Immunol.* 181 (2008) 17–21.
- F.A. Sharp, D. Ruane, B. Claass, E. Creagh, J. Harris, P. Malyala, M. Singh, D. T. O'Hagan, V. Pétrilli, J. Tschopp, L.A. O'Neill, E.C. Lavelle, Uptake of particulate vaccine adjuvants by dendritic cells activates the NALP3 inflammasome, *Proc. Natl. Acad. Sci. U. S. A.* 106 (2009) 870–875.
- M. Kool, V. Pétrilli, T. De Smedt, A. Rolaz, H. Hammad, M. van Nimwegen, I. M. Bergen, R. Castillo, B.N. Lambrecht, J. Tschopp, Cutting edge: alum adjuvant stimulates inflammatory dendritic cells through activation of the NALP3 inflammasome, *J. Immunol.* 181 (2009) 3755–3759.
- A.T. Glenn, G.A.H. Buttle, M.F. Stevens, Rate of disappearance of diphtheria toxoid injected into rabbits and guinea-pigs: toxoid precipitated with alum, *J. Pathol. Bacteriol.* 34 (1931) 267–275.
- L.B. Holt, Developments in Diphtheria Prophylaxis, Heinemann Ltd, London, UK, 1950.
- J. Stephen, H.E. Scales, R.A. Benson, D. Erben, P. Garside, J.M. Brewer, Neutrophil swarming and extracellular trap formation play a significant role in alum adjuvant activity, *Npj Vaccines* 2 (2017) 1.
- C. Exley, P. Siesjö, H. Eriksson, The immunobiology of aluminium adjuvants: how do they really work? *Trends Immunol.* 31 (2010) 103–109.
- E. Shardlow, M. Mold, C. Exley, Unravelling the enigma: elucidating the relationship between the physicochemical properties of aluminium-based adjuvants and their immunological mechanisms of action, *Allergy Asthma Clin. Immunol.* 14 (2018) 80.
- M.J. Caulfield, L. Shi, S. Wang, B. Wang, T.W. Tobery, H. Mach, P.L. Ahl, J. L. Cannon, J.C. Cook, J.H. Heinrichs, R.D. Sitrin, Effect of alternative aluminum adjuvants on the absorption and immunogenicity of HPV16 L1 VLPs in mice, *Hum. Vaccin. Immunother.* 3 (2007) 139–145.
- E. House, M. Esiri, G. Forster, P.G. Ince, C. Exley, Aluminium, iron and copper in human brain tissues donated to the medical research council's cognitive function and ageing study, *Metallomics* 4 (2012) 56–65.
- S.N. Goodman, Introduction to Bayesian methods I: measuring the strength of evidence, *Clin. Trials* 2 (2005) 282–290, discussion 301–304, 364–378.
- R Core Team, R: A Language and Environment for Statistical Computing, R Foundation for Statistical Computing, Vienna, Austria, 2020. <https://www.R-project.org/>.
- H. Wickham, W. Chang, L. Henry, T.L. Pedersen, K. Takahashi, C. Wilke, K. Woo, H. Yutani, D. Dunnington, ggplot2: Create Elegant Data Visualisations Using the Grammar of Graphics, 2020. <https://CRAN.R-project.org/package=ggplot2>.
- S. Højsgaard, U. Halekoh, doBy: Groupwise Statistics, LSmeans, Linear Contrasts, Utilities, 2020. <https://CRAN.R-project.org/package=doBy>.
- J.K.K. Meredith, J. Kruschke, BEST: Bayesian Estimation Supersedes the t-Test, 2020. <https://CRAN.R-project.org/package=BEST>.
- R. Bååth, Bayesian first aid: a package that implements Bayesian alternatives to the classical *.Test functions in R, Proceedings of User! the International R User Conference (2014). <https://www.rdocumentation.org/packages/BayesianFirstAid/versions/0.1>.

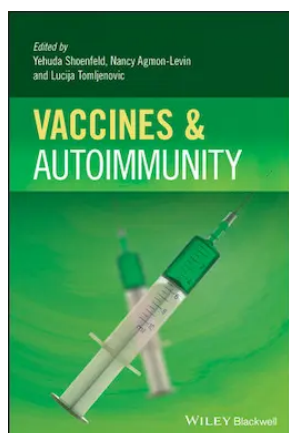
- [31] R. Joachim. `bayesWilcoxTest`: A Bayesian Alternative to the Wilcoxon Signed Rank Test. 20210. R package version 0.1.0. <https://rdrr.io/github/joereinhardt/BayesianFirstAid-Wilcoxon/>.
- [32] C. Keyzers, V. Gazzola, E.J. Wagenmakers, Using Bayes factor hypothesis testing in neuroscience to establish evidence of absence, *Nat. Neurosci.* 23 (2020) 788–799.
- [33] D.S. Quintana, D.R. Williams, Bayesian alternatives for common null-hypothesis significance tests in psychiatry: a non-technical guide using JASP, *BMC Psychiatry* 18 (2018) 178.
- [34] S.N. Goodman, Toward evidence-based medical statistics. 1: the P value fallacy, *Ann. Intern. Med.* 130 (1999) 995–1004.
- [35] J. Skinner, Statistics for immunologists, *Curr. Protoc. Immunol.* 122 (2018) 5436.
- [36] S. Goodman, A dirty dozen: twelve P-value misconceptions, *Sem. Hematol.* 45 (2008) 135–140.
- [37] C. Exley, An aluminium adjuvant in a vaccine is an acute exposure to aluminium, *J. Trace Elem. Med. Biol.* 57 (2020) 57–59.
- [38] C. Exley, Aluminium-based adjuvants should not be used as placebos in clinical trials, *Vaccine* 29 (2011) 9289.
- [39] C. Exley, Human exposure to aluminium, *Environ. Sci. Process. Impacts* 15 (2013) 1807–1816.
- [40] C. Exley, What is the risk of aluminium as a neurotoxin? *Expert Rev. Neurother.* 14 (2014) 589–591.

Footnote 2

WILEY

To Purchase this product, please visit

<https://www.wiley.com/en-us/Vaccines+and+Autoimmunity-p-9781118663493>



Vaccines and Autoimmunity

Nicola Luigi Bragazzi, Nancy Agmon-Levin, Lucija Tomljenovic

E-Book	978-1-118-66349-3	May 2015	\$146.00
Hardcover	978-1-118-66343-1	July 2015	\$182.95
O-Book	978-1-118-66372-1	May 2015	Available on Wiley Online Library

Description

In light of the discovery of Autoimmune Syndrome Induced by Adjuvants, or ASIA, *Vaccines and Autoimmunity* explores the role of adjuvants – specifically aluminum in different vaccines – and how they can induce diverse autoimmune clinical manifestations in genetically prone individuals.

Vaccines and Autoimmunity is divided into three sections; the first contextualizes the role of adjuvants in the framework of autoimmunity, covering the mechanism of action of adjuvants, experimental models of adjuvant induced autoimmune diseases, infections as adjuvants, the Gulf War Syndrome, sick-building syndrome (SBS), safe vaccines, toll-like receptors, TLRs in vaccines, pesticides as adjuvants, oil as adjuvant, mercury, aluminum and autoimmunity. The following section reviews literature on vaccines that have induced autoimmune conditions such as MMR and HBV, among others. The final section covers diseases in which vaccines were known to be the solicitor – for instance, systemic lupus erythematosus – and whether it can be induced by vaccines for MMR, HBV, HCV, and others.

Edited by leaders in the field, *Vaccines and Autoimmunity* is an invaluable resource for advanced students and researchers working in pathogenic and epidemiological studies.

About the Author

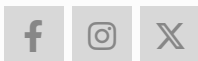
Yehuda Shoenfeld is the Incumbent of the Laura Schwarz-Kipp Chair of Research of Autoimmune Diseases, Sackler Faculty of Medicine, Tel Aviv University in Tel Aviv, Israel. He is also Founder of the Center for Autoimmune Diseases, both at the Sheba Medical Center in Tel Hashomer, Israel.

Nancy Agmon-Levin is a specialist in Clinical Immunology and Allergology, and serves as Deputy Head of the Zabudowicz Center for Autoimmune Diseases, Sheba Medical Center in Tel Hashomer, Israel. She is also President of the Israel Association for Allergy and Clinical Immunology (IAACI).

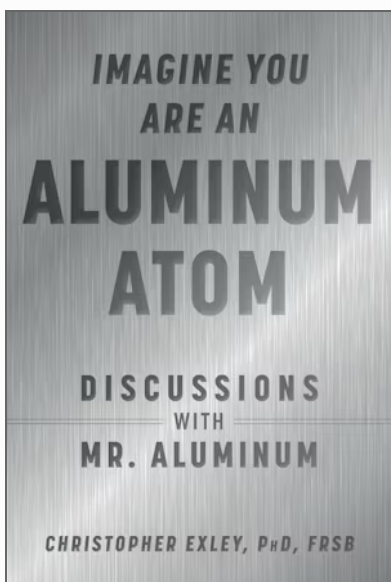
Lucija Tomljenovic is a Senior Postdoctoral Fellow in the Neural Dynamics Research Group at the University of British Columbia in Vancouver, BC, Canada.

To Purchase this product, please visit

<https://www.wiley.com/en-us/Vaccines+and+Autoimmunity-p-9781118663493>



search



Imagine You Are An Aluminum Atom

Discussions With Mr. Aluminum

Christopher Exley

176 Pages

November 24, 2020

ISBN: 9781510762534

Imprint: Skyhorse Publishing

Trim Size: 6in x 9in x 0in

FORMAT: \$22.99

DESCRIPTION

Join "Mr. Aluminum," a scientist who has made the study of aluminum his life's work, on a journey of discovery, reflection, and the science of aluminum.

Professor Christopher Exley is a firm believer that science is only useful when it is properly communicated. Scientific papers are

difficult vehicles for the wider communication of science and thus he has always endeavored to tell the story of his scientific research as widely as possible through myriad blogs, presentations, and interviews. Through a series of easy-reading entries written for non-scientists, Exley will educate readers about his lifelong scientific passion: aluminum. In scientific circles, aluminum—in relation to human health specifically—has gone the way of the dinosaurs (though, unlike dinosaurs, there has not yet been a popular revival!). Yet aluminum is also the greatest untold story of science.

But why do we all need to know a little bit more about aluminum? Do we need a self-help guide for living in what Exley has coined "The Aluminum Age"? What is it about aluminum that makes it different? What about iron, copper, or any of the so-called "heavy metals," like mercury, cadmium, or lead? Why must we pay particular attention to aluminum? Because its bio-geochemistry, its natural history, raises two red flags immediately and simultaneously.

These two danger signals are easily missed by all of us and easily dismissed by those whose interests are conflicted by aluminum's omnipresence in human life and consequently, are purposely blind to its danger signals. First, aluminum, in all of its myriad forms, is super abundant; it is the third most abundant element (after oxygen and silicon) of the Earth's crust. Second, aluminum is super reactive; it is both chemically and biologically reactive. However, these two red flags identify a paradox, as the abundant and biologically reactive aluminum has no biological function either in any organism today nor in any extinct biota from the evolutionary past. This means in practical terms that when we encounter aluminum in our everyday lives, our bodies only see aluminum as an impostor, something foreign, and something for which we have not been prepared through biochemical evolution. This in turn means that all of our encounters with aluminium are adventitious, random, and chaotic. And potentially dangerous.

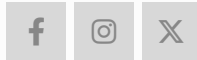
Imagine You Are An Aluminum Atom: Discussions With "Mr. Aluminum" examines the science of aluminum and human health and makes them understandable to all. Within the science you will find personal recollections of events, as well as opinions and reflections upon how the politics of aluminum have influenced and interfered with doing and reporting the science. It is at once both a personal recollection of Exley's life in aluminum research

and a guide on the dangers of the constant exposure to aluminum we as humans face during this "Aluminum Age." It will inform, it will provide the means to question the science, and it will, if the reader is prepared to participate, answer those frequently asked questions on aluminum and human health.

AUTHORS



© 2024 Skyhorse Publishing. All Rights Reserved



Created by Supadu

RESEARCH ARTICLE

Development and Characterization of an Effective Food Allergy Model in Brown Norway Rats

Mar Abril-Gil^{1,2*}, Alba Garcia-Just^{1,2*}, Francisco J. Pérez-Cano^{1,2*}, Àngels Franch^{1,2*}, Margarida Castell^{1,2*}

1 Departament de Fisiologia, Facultat de Farmàcia, Universitat de Barcelona, Barcelona, Spain, **2** Institut de Recerca en Nutrició i Seguretat Alimentària, Universitat de Barcelona (INSA-UB), Barcelona, Spain

* Current address: *Department de Fisiologia, Facultat de Farmàcia, Universitat de Barcelona, Barcelona, Spain*

* margaridacastell@ub.edu



OPEN ACCESS

Citation: Abril-Gil M, Garcia-Just A, Pérez-Cano FJ, Franch À, Castell M (2015) Development and Characterization of an Effective Food Allergy Model in Brown Norway Rats. PLoS ONE 10(4): e0125314. doi:10.1371/journal.pone.0125314

Academic Editor: Lucienne Chatenoud, Université Paris Descartes, FRANCE

Received: November 12, 2014

Accepted: March 17, 2015

Published: April 29, 2015

Copyright: © 2015 Abril-Gil et al. This is an open access article distributed under the terms of the [Creative Commons Attribution License](https://creativecommons.org/licenses/by/4.0/), which permits unrestricted use, distribution, and reproduction in any medium, provided the original author and source are credited.

Data Availability Statement: All figure files are available from the figshare database (accession number <http://dx.doi.org/10.6084/m9.figshare.1297737>).

Funding: This study was supported by grants from the Spanish Ministries of Science and Innovation (AGL2008-02790) and Economy and Competitiveness (AGL2011-24279). The funders had no role in study design, data collection and analysis, decision to publish, or preparation of the manuscript.

Competing Interests: The authors have declared that no competing interests exist.

Abstract

Background

Food allergy (FA) is an adverse health effect produced by the exposure to a given food. Currently, there is no optimal animal model of FA for the screening of immunotherapies or for testing the allergenicity of new foods.

Objective

The aim of the present study was to develop an effective and rapid model of FA in Brown Norway rats. In order to establish biomarkers of FA in rat, we compared the immune response and the anaphylactic shock obtained in this model with those achieved with only intraperitoneal immunization.

Methods

Rats received an intraperitoneal injection of ovalbumin (OVA) with alum and toxin from *Bordetella pertussis*, and 14 days later, OVA by oral route daily for three weeks (FA group). A group of rats receiving only the i.p. injection (IP group) were also tested. Serum anti-OVA IgE, IgG1, IgG2a, IgG2b and IgA antibodies were quantified throughout the study. After an oral challenge, body temperature, intestinal permeability, motor activity, and mast cell protease II (RMCP-II) levels were determined. At the end of the study, anti-OVA intestinal IgA, spleen cytokine production, lymphocyte composition of Peyer's patches and mesenteric lymph nodes, and gene expression in the small intestine were quantified.

Results

Serum OVA-specific IgG1, IgG2a and IgG2b concentrations rose with the i.p. immunization but were highly augmented after the oral OVA administration. Anti-OVA IgE increased two-fold during the first week of oral OVA gavage. The anaphylaxis in both IP and FA groups

decreased body temperature and motor activity, whereas intestinal permeability increased. Interestingly, the FA group showed a much higher RMCP II serum protein and intestinal mRNA expression.

Conclusions

These results show both an effective and relatively rapid model of FA assessed by means of specific antibody titres and the high production of RMCP-II and its intestinal gene expression.

Introduction

Food allergy (FA) is 'an adverse health effect arising from a specific immune response that occurs reproducibly on exposure to a given food' [1]. Nowadays it is a major public health problem and the only therapy available consists of avoiding the causative foods [2]. An American retrospective study showed that the economic burden of FA reactions and anaphylaxis treatments is near to \$300 million [3]. Despite the fact that more than 170 foods have been reported to cause IgE-mediated hypersensitivity [4], most of the allergic reactions are attributed to a limited number of foods, cow's milk, egg, nuts and seafood being the most common in Europe [5], whereas they share prominence with wheat, soy and peanut in the USA [6]. Although the exact prevalence of FA remains uncertain, data supports that its prevalence is increasing with current rates around 5% in adults and approaching 8% in the child population [7].

In healthy conditions, the intestinal barrier, constituted by the epithelium covered with mucus, enzymes and bile salts together with extreme pH, acts as a physical barrier preventing the passage of harmful pathogens, as well as a selective filter, allowing essential dietary nutrients to pass into the circulation [8,9]. In general, food ingestion results in oral tolerance: when dendritic cells, the professional antigen-presenting cells, capture food antigen in the lamina propria (LP) and Peyer's patches (PP), they carry them to the mesenteric lymph nodes (MLN) where they induce regulatory T (Treg) cells that migrate back to the LP. The resident macrophages in the LP can expand Treg cells, suppressing Th2 cytokines and IgE as well as the effector functions of mast cells and basophils, thus inhibiting allergic inflammation and food hypersensitivity [8,10]. In contrast, patients with FA have lost the immune mechanisms responsible for oral tolerance, and recognize some food antigens as harmful molecules. In this population, alterations in Treg cell function and environmental factors, such as microbiota, have been suggested to be important contributors to food sensitization and allergy [11].

Animal models, such as those described in dogs, swine, guinea pigs, mice and rats, have been used for assessment of allergenicity of foods, although the optimal model has not been reached [12–18]. In the case of dogs, the gut anatomy, physiology and nutritional requirements are similar to humans and in swine the anatomy, physiology and immunology of skin and gastrointestinal tract are also comparable to humans [19], but in both animal species there are some disadvantages in comparison with rodents, such as the expense incurred by animal maintenance, the limited availability of strains, the lack of commercially available immunological reagents, and the long process to sensitization (18 months for dogs) [20]. Studies related to cow's milk allergy commonly use guinea pigs for oral sensitization [21,22]. However, it is not an appropriate model for the assessment of allergenicity of novel proteins because the immunological reactions to proteins differ from those in humans [22], there are a lack of available tools to

study the guinea pig immune system and, for FA research, there are significant differences in the immunophysiology in comparison with other species [19].

Regarding the use of mice in allergy research, the transcriptional analysis approach has shown remarkable consistency between murine and human samples, and studies in atopic dermatitis showed a high degree of homology in the gene expression profile [23]. In addition, their small size, short breeding cycle and well-characterized immunology are certainly key factors. Several allergy models performed in mice differ in the strain, the sensitization route, the type of allergen, the dosage, or the use of an adjuvant [16,24–27]. Nevertheless, the natural complexity of the allergic reactions makes it difficult to find a single reliable marker to quantify the sensitization potential of a protein [28]. Finally, the use of rats has a number of advantages compared with other animal models, particularly with respect to being one of the most commonly used species in toxicity testing [29]. Brown Norway (BN) rats have been widely studied because this strain is a high IgE responder, similar to atopic humans. BN rats have been used as a model of FA in the presence or absence of an adjuvant. In this latter condition, Knippels et al. have demonstrated oral sensitization and have evaluated the influence of rat strain [30] and dosage [31,32]. However, the model of oral sensitization without an adjuvant requires a long process of sensitization (six weeks) and, although it has been used in several studies [33–36], success after oral sensitization was not always achieved in a high percentage of rats [37] and/or the sensitization does not always induce the synthesis of IgE antibodies [20,30,38,39]. This limitation makes it difficult to use this model for the screening of new therapies or allergenicity studies. Regarding the use of other sensitization routes and an adjuvant to induce FA in BN rats, the administration of two to three intraperitoneal (i.p.) injections of allergen and, in some cases, the oral gavage of the same allergen has been applied [40–42]. The present study aimed to develop an effective and more rapid model of FA in BN rats based on that reported by Ogawa et al. [43] with only one i.p. injection of the allergen with alum together with toxin from *Bordetella pertussis* (tBp) to promote IgE synthesis [44], and two weeks later the oral administration of soluble allergen. In order to establish biomarkers of FA in rat, we compared the specific immune and the anaphylactic responses obtained in this model with those achieved with only an i.p. immunization.

Material and Methods

Animals and experimental design

Three-week-old female BN rats obtained from Janvier (Saint-Berthevin, France) were maintained on an OVA-free diet and water *ad libitum*. The parent rats had followed the SSNIFF S8189-S105 diet, free of egg proteins. The rats were housed in cages under conditions of controlled temperature and humidity in a 12:12 h light-dark cycle. After an acclimatization period of one week, the rats were randomized into three groups: reference (RF) group, intraperitoneal (IP) group and food allergy (FA) group (n = 8 per group). The FA induction was carried out by combining an i.p. immunization with OVA mixed with alum and tBp followed, 14 days later, by oral OVA administration for three weeks; five days later, an oral challenge was given to cause an anaphylactic response (AR). The AR was evaluated by means of body temperature, protease release of mast cells, intestinal permeability and also by motor activity assessment [45]. Finally, rats were sacrificed on day 42, two days after the oral challenge, to collect tissue samples. During the study, the body weight was registered and blood samples were collected weekly to determine specific antibodies production.

Experimental design was repeated twice in order to get representative results of an enough number of animals per group.

Experimental procedures in rats were reviewed and approved by the Ethical Committee for Animal Experimentation at the University of Barcelona (ref.359/12).

Food allergy induction

An emulsion of OVA (grade V, Sigma-Aldrich, Madrid, Spain) as allergen, in alum (Imject, Pierce, IL, USA) as an adjuvant and tBp (Sigma-Aldrich) was prepared. Each rat from the IP group received by i.p. route 0.5 mL of the emulsion containing 50 µg of OVA, 2.5 mg of Imject and 50 ng of tBp. In the FA group, in addition to the i.p. injection as administered in the case of the IP group, the animals received, starting 14 days later, 1 mL of OVA solution in sodium bicarbonate (1 mg per rat) by oral gavage five days/week for three weeks. As a control, the IP and RF groups received 1 mL of sodium bicarbonate by oral gavage for the same period.

Anaphylaxis induction

Forty days after OVA i.p. immunization, the animals were deprived of food overnight and then received 2 mL of OVA (200 mg per rat) orally. Blood was collected every 30 min up to 2 h post-AR induction from the saphenous vein. During this period rectal temperature was measured using a digital thermometer (OMRON Healthcare Europe, the Netherlands).

In order to determine the intestinal barrier integrity, 30 min after the challenge each rat received 100 mg/mL of β-lactoglobuline (βLG, Sigma-Aldrich) by oral gavage [31], details are described in the “Quantification of intestinal permeability” section

Motor activity measurement

Motor activity was assessed for 21 min using individual cages in an isolated room, with an activity meter that included two perpendicular infrared beams, which crossed the cage 6 cm above the floor. These facilities have been commonly used to study rat motor activity in different conditions [46,47]. Two motor activity measures were performed: the first was measured 24 h before anaphylaxis induction to determine the basal movements, and the second immediately after the oral challenge to establish the changes produced by anaphylaxis induction. Activity counts were recorded using time frames of 1 min for 21 min. To stimulate rat movements, 8 min after the beginning of the measurement, the lights were turned off for 5 min and then turned on until the end of the measurement. The results refer to the movements in three time phases (pre-darkness, darkness and post-darkness) as well as the entire period. The area under the curve (AUC) for the 21-min period and the percentage of decrease in motor activity after AS induction with respect to the basal measurement in each studied phase as well as in the whole period were also calculated.

Sacrifice and sample processing

Two days after AR the rats were anaesthetized with ketamine (90 mg/kg) (Merial Laboratories S.A, Barcelona, Spain) and xylazine (10 mg/kg) (Bayer A.G, Leverkusen, Germany). Blood was obtained by heart puncture. MLN and spleen were also dissected for immediate lymphocyte isolation. From the middle of the small intestine (SI), a small piece (0.5 cm) was excised and kept in RNA later (Ambion, Life Technologies, Austin, USA) until gene expression analysis by real-time PCR, the procedure is detailed in the “Quantification of gene expression in small intestine” section. From the distal part of the SI, visible PP were collected for immediate lymphocyte isolation, and gut washes were obtained for quantification of specific IgA.

Peyer's patches lymphocyte isolation and gut wash obtention

The processing of these samples was performed as previously described [48,49]. Briefly, PP were incubated with complete culture medium containing Roswell Park Memorial Institute (RPMI 1640, Sigma-Aldrich), 10% fetal bovine serum (FBS), 100 IU/mL streptomycin-penicillin, 2 mM L-glutamine (Sigma-Aldrich), and 0.05 mM 2- β -mercaptoethanol (Merck, Darmstadt, Germany) with 1 mM of dithiothreitol (Sigma-Aldrich) (5 min, 37°C). Thereafter, PP were washed with RPMI medium and passed through a cell strainer (40 μ m, BD Biosciences, Madrid, Spain).

The remaining distal SI tissue (without PP) was cut into 5 mm pieces, weighed and used to obtain the gut wash by shaking in phosphate-buffered saline (PBS) (37°C, 10 min). Gut washes were conserved at -20°C for anti-OVA IgA determination.

Ovalbumin-specific stimulation of mesenteric lymph nodes and spleen lymphocytes

MLN and spleen cell suspensions were obtained as previously described [48] by passing the tissue through a cell strainer (40 μ m, BD Biosciences). Erythrocytes from the spleen were eliminated by osmotic lysis. MLN and spleen cells were cultured at 5×10^6 cells in 1 mL of medium with or without OVA (50 μ g/mL) for 96 h. Supernatants from spleen cultures were collected to assess cytokine concentrations. MLN cells were used to establish changes in lymphocyte composition after specific stimulation.

Assessment of lymphocyte composition in Peyer's patches and mesenteric lymph nodes

Peyer's patches and MLN lymphocytes were stained with the following mouse anti-rat monoclonal antibodies (mAb) conjugated to fluorescein isothiocyanate, phycoerythrin or allophycocyanin: anti-TCR $\alpha\beta$ (R73), anti-CD4 (OX-35), anti-CD8 α (OX-8), anti-CD45RA (OX-33), anti-NKR-P1A (10/78), anti-CD25 (OX-39) (BD Biosciences) and anti-IgA (Abcam, Cambridge, UK). Cells were labeled with saturating concentrations of conjugated mAb in PBS containing 1% FBS and 0.09% Na₃N as previously described [50]. Negative control staining using isotype-matched mAb was included for each sample.

Analyses were performed using a FC 500 Series Flow Cytometer (Beckman Coulter, FL, USA), and data were assessed by the FlowJo v7.6.5 software (Tree Star Inc., Ashland, OR, USA). Lymphocyte populations were defined as: B (CD45RA⁺CD4⁻), B expressing IgA (IgA⁺CD45RA⁺), T (TCR $\alpha\beta$ ⁺), Th (TCR $\alpha\beta$ ⁺CD4⁺), Tc (TCR $\alpha\beta$ ⁺CD8⁺) and activated Th (TCR $\alpha\beta$ ⁺CD4⁺CD25⁺) cells. Results are expressed as percentages of positive cells in the lymphocyte population previously selected according to their forward scatter and side scatter characteristics.

Quantification of serum mast cell protease II

In serum samples obtained during the AR, rat mast cell protease II (RMCP-II) concentration was quantified using a commercial ELISA set (Moredun Animal Health, Edinburgh, UK) with slight modifications. In brief, 96-well ELISA plates (Nunc Maxisorp, Wiesbaden, Germany) were coated with anti-rat RMCP-II antibody (overnight, 4°C). After blocking and washing, appropriately diluted serum samples were incubated for 3 h. Peroxidase-conjugated anti-rat RMCP-II antibody was incubated for 2 h and, finally, a 3,3',5,5'-tetramethylbenzidine solution with H₂O₂ was added, and optical density (OD) was measured on a microtiter plate photometer

(Labsystems Multiskan, Helsinki, Finland). Data were interpolated by means of Ascent v.2.6 software (Thermo Fisher Scientific, S.I.U., Barcelona, Spain).

Quantification of intestinal permeability

To assess intestinal permeability, a method previously described in BN rats was used [30,51]. In this method, β LG was orally given 30 min after the OVA challenge and then were quantified by ELISA in serum obtained every 30 min during anaphylaxis. In brief, ELISA plates were coated with rabbit anti-bovine β LG antibody (A10-125A, Bethyl, Montgomery, USA) and incubated overnight at room temperature. The plates were then blocked with bovine serum albumin (Sigma-Aldrich) in TRIS-buffered saline containing 0.05% Tween 20, and after washing, appropriate diluted samples and standard dilutions were added. Finally, an adequate dilution of peroxidase-conjugate anti-bovine β LG antibody (A10-125P, Bethyl) was incubated and an *o*-phenylenediamine dihydrochloride solution was added for detection of β LG from samples. OD was measured as detailed above.

Determination of cytokines released from spleen lymphocytes

IL-2, IL-4, IL-10 and IFN- γ cytokines released from spleen cell cultures were measured using the BD Cytometric Beads Assay Rat Soluble Protein Flex Set (BD Biosciences). Briefly, samples and standards were incubated with a mix of specific fluorescent beads for each cytokine. Then, a mix containing the detection antibodies conjugated with phycoerythrin was incubated and, after that, samples were washed. Analysis was carried out by a BD FACSAria (BD Biosciences) cytometer and the FCAP Array Software (BD Biosciences). The limits of detection were 0.46 pg/mL for IL-2, 3.4 pg/mL for IL-4, 19.4 pg/mL for IL-10 and 6.8 pg/mL for IFN- γ .

Quantification of gene expression in small intestine

For RNA isolation, samples from the SI were processed as previously described [52]. Tissue samples were homogenized in a FastPrep (MP Biomedicals, Illkirch, France) for 30 s. Total RNA was isolated with the RNeasy Mini Kit (Qiagen, Madrid, Spain) following the manufacturer's recommendations. The quality of the RNA was assessed by the Agilent 2100 Bioanalyzer with the RNA 6000 LabChip kit (Agilent Technologies, Madrid, Spain). Two micrograms of total RNA were converted to cDNA using random hexamers (Life Technologies). The specific PCR TaqMan primers and probes (Applied Biosystems, Weiterstadt, Germany) used were: *Iga* (331943, made to order), *Fcer1a* (Rn00562369_m1, inventoried (I)), *Il2* (Rn00587673_m1, I), *Il4* (Rn01456866_m1, I), *Il10* (Rn00563409_m1, I), *Ifng* (Rn00594078_m1, I) and *Mcpt2* (Rn00756479_g1, I). Quantification of the genes of interest was normalized to the endogenous control *Hprt1* (Rn01527840_m1, I). Real-time PCR assays were performed in duplicate using an ABI Prism 7900HT sequence detection system (Applied Biosystems). The SDS software (version 2.4) was used to analyze the expression data.

The amount of target mRNA relative to HPRT expression and relative to values from the RF group was calculated using the $2^{-\Delta\Delta C_t}$ method, as previously described [53]. C_t is the cycle number at which the fluorescence signal of the PCR product crosses an arbitrary threshold set within the exponential phase of the PCR. Results are expressed considering gene expression in the RF group as 100%.

Anti-OVA antibody quantification

Anti-OVA IgG1, IgG2a, IgG2b and IgA antibody concentrations were quantified using an indirect ELISA, and OVA-specific IgE concentration by an antibody-capture ELISA as previously

described [54]. The relative concentration of each anti-OVA Ig isotype was calculated by comparison with a pool of OVA-immunized rat sera to which arbitrary units (AU) were assigned according to the dilution of the serum samples used for each isotype determination. The AU/mL assigned were 100000 AU/mL for IgG1 and IgG2a, 10000 AU/mL for IgG2b, 50 AU/mL for IgA, and 10 AU/mL for IgE.

Statistical analysis

The software package IBM SPSS Statistics 20 (SPSS Inc., USA) was used. The Levene and the Kolmogorov-Smirnov tests were applied to assess variance equality and normal distribution, respectively. Two-way ANOVA tests were used to study the effect of group and group x time interaction. The motor activity data were analyzed by two-way ANOVA for repeated measures considering the group (FA vs. IP vs. RF group) and time as the interacting factor, followed by Bonferroni's *post hoc* test. To evaluate the correlation among studied variables, Pearson's coefficient (ρ) was applied. To analyze the results from anti-OVA antibodies, RMCP-II, β LG and cytokine concentrations, body temperature, relative gene expression, AUC of motor activity, and lymphocyte composition, non-parametric tests (Kruskal-Wallis and Mann-Whitney U) were used due to non-variance homogeneity. Differences were considered statistically significant for p values < 0.05 .

Results

Body weight and mortality

Rats weighed 66.6 ± 3.68 g (mean \pm S.E.M.) at the beginning of the study. Rat growth was monitored throughout the study and was similar among groups. At the end of the study, body weight was 137.1 ± 6.88 g [127.2–146.2], 136.7 ± 4.49 g [130.5–141.6], and 138.4 ± 3.22 g [135.1–143.7] in the RF, IP and FA groups, respectively. No death was produced after the oral challenge in any of the experimental groups.

Serum and intestinal anti-OVA antibodies

Sera from the RF group did not contain anti-OVA antibodies of any isotype (data not shown). The i.p. immunization caused the synthesis of anti-OVA IgG1, IgG2a and IgG2b antibodies in the IP and FA groups that were already detectable 14 days after OVA immunization (Fig 1A–1C). The oral administration of the allergen boosted the synthesis of anti-OVA IgG isotypes, which increased in the FA group more than tenfold for IgG1 and IgG2a, remaining elevated until the end of the study (Fig 1A and 1B; $p < 0.05$). This increase was also produced in anti-OVA IgG2b, but to a lower degree (Fig 1C; $p < 0.05$).

Regarding serum anti-OVA IgE antibodies (Fig 1D) the OVA immunization also induced their synthesis in both the IP and FA groups. Nevertheless, the oral administration of OVA for a week magnified the production of this antibody in the FA group, increasing almost twofold the levels of specific IgE with respect to the IP group ($p < 0.05$). Afterwards, however, anti-OVA IgE underwent a progressive decrease in both the IP and FA groups.

With regards to the anti-OVA IgA concentrations measured in serum and gut wash samples, the i.p. immunization did not induce the synthesis of this antibody in either compartment (Fig 1E and 1F). In contrast, the oral OVA administration in the FA group induced the synthesis of anti-OVA IgA antibodies (Fig 1E) and they were also found in gut washes at the end of the study (Fig 1F).

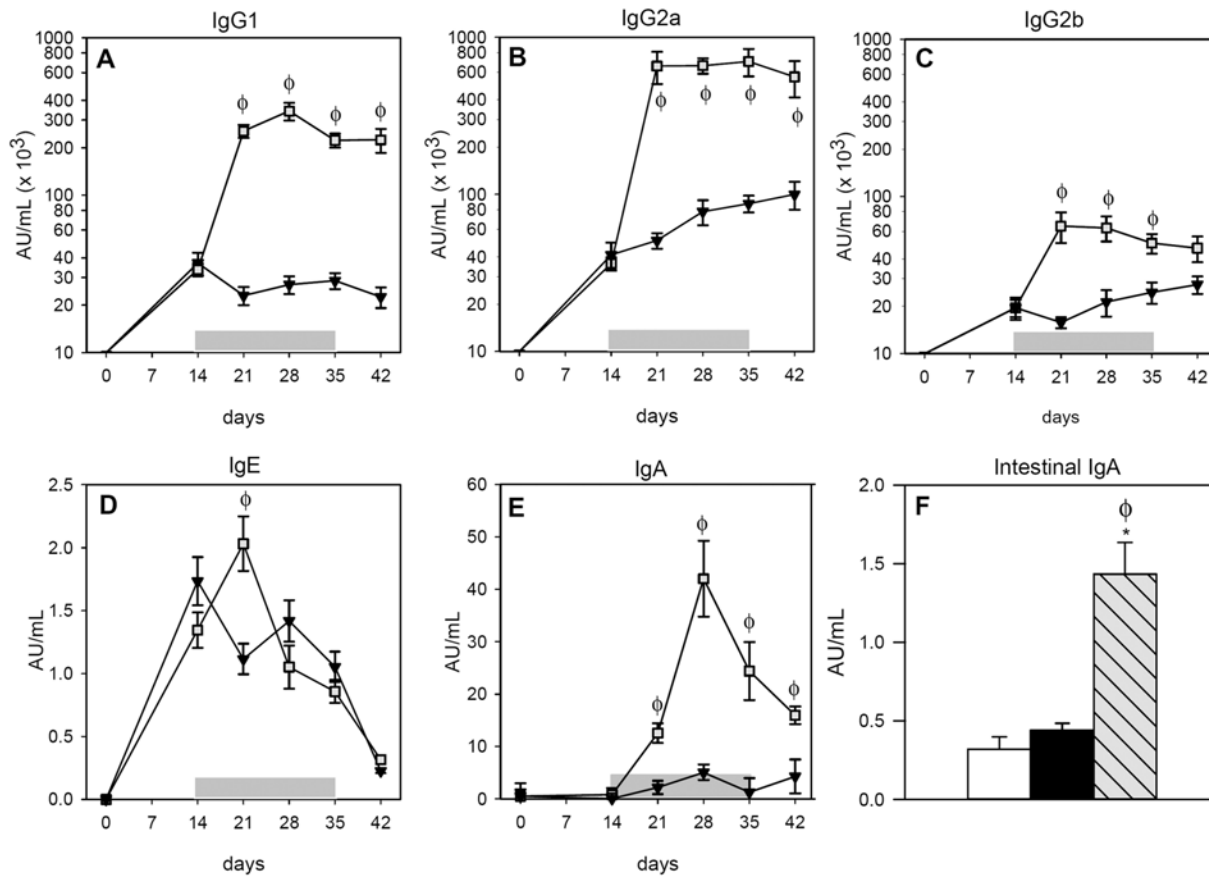


Fig 1. Concentrations of OVA-specific antibodies during post-immunization period. A) serum IgG1, B) serum IgG2a, C) serum IgG2b, D) serum IgE, E) serum IgA and F) intestinal IgA. White bars represent RF group, ▼ or black bars represent IP group and ■ or grey-striped bars represent FA group. Shadow period corresponds to oral administration of OVA in FA group. Results are expressed as mean \pm S.E.M. (n = 8). * $p < 0.05$ vs. RF group and $\phi p < 0.05$ vs. IP group.

doi:10.1371/journal.pone.0125314.g001

Assessment of anaphylaxis

Body temperature, RMCP-II concentration and intestinal permeability, together motor activity, allowed to quantify anaphylaxis in rats after oral OVA challenge.

The body temperature, registered during the 2 h after oral challenge in intervals of 30 min, revealed that there was a decrease of about 2°C in both the IP and FA groups compared to the RF group throughout the whole studied period (Fig 2A; $p < 0.05$). No significant differences were observed between the IP and FA groups.

After AR induction, the IP group showed about a threefold increase in serum RMCP-II concentration compared to that in RF animals (Fig 2B; $p < 0.01$). However, in the FA group the increase was much higher. The FA animals underwent a rise about 18 times ($p < 0.01$) higher than that of the RF animals and six times higher compared with the IP group ($p < 0.01$). This effect lasted for at least 2 h post-challenge.

β LG given orally 30 min after AR induction, quantified in sera as a measure of intestinal permeability, increased significantly at 30 min from oral protein administration (60 min after AR induction) in both IP and FA groups (Fig 2C; $p < 0.05$). Later, IP rats kept the serum β LG concentration whereas the FA rats showed a faster decrease, although at the end of the studied period, both groups had significantly higher levels compared to RF animals ($p < 0.05$).

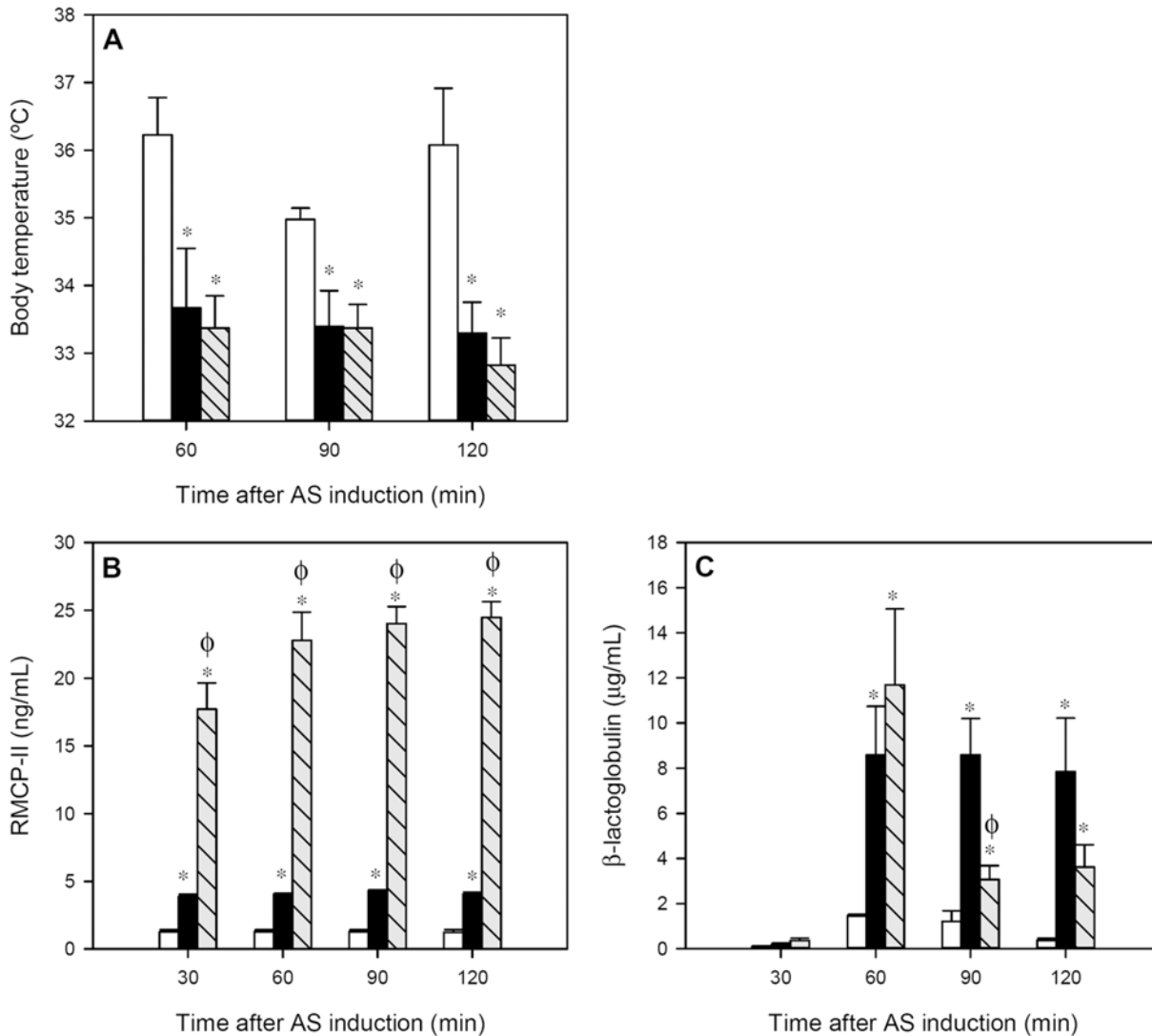


Fig 2. Variables measured during 2 h after anaphylactic shock induction: A) body temperature, B) serum RMCP-II concentration and C) serum βLG concentration. White bars represent RF group, black bars represent IP group and grey-striped bars represent FA group. Results are expressed as mean ± S.E.M. (n = 8). **p* < 0.05 vs. RF group and ϕ *p* < 0.05 vs. IP group.

doi:10.1371/journal.pone.0125314.g002

Motor activity

Rat motor activity was measured for 21 min at 24 h before (Fig 3A) and immediately after (Fig 3C) AR induction to obtain basal values and data representative of AR-induced behavioral changes, respectively. With regards to basal motor activity, the pattern of movements during the time showed that the three groups became quieter over the 21 min period (Fig 3A; *p* < 0.05 for time) although motor activity increased when the lights were turned off (*p* < 0.05 for RF and FA groups). The motor activity of the IP group was lower than that of the RF group, looking at the whole period and the three established phases (pre-darkness, darkness and post-darkness) (*p* < 0.05). Similarly, in the basal pattern, FA rats also made a lower number of movements than RF animals, taking into account the whole period (*p* < 0.001) and also the pre- and post-darkness phases (*p* < 0.05). The differences among basal groups' movements in

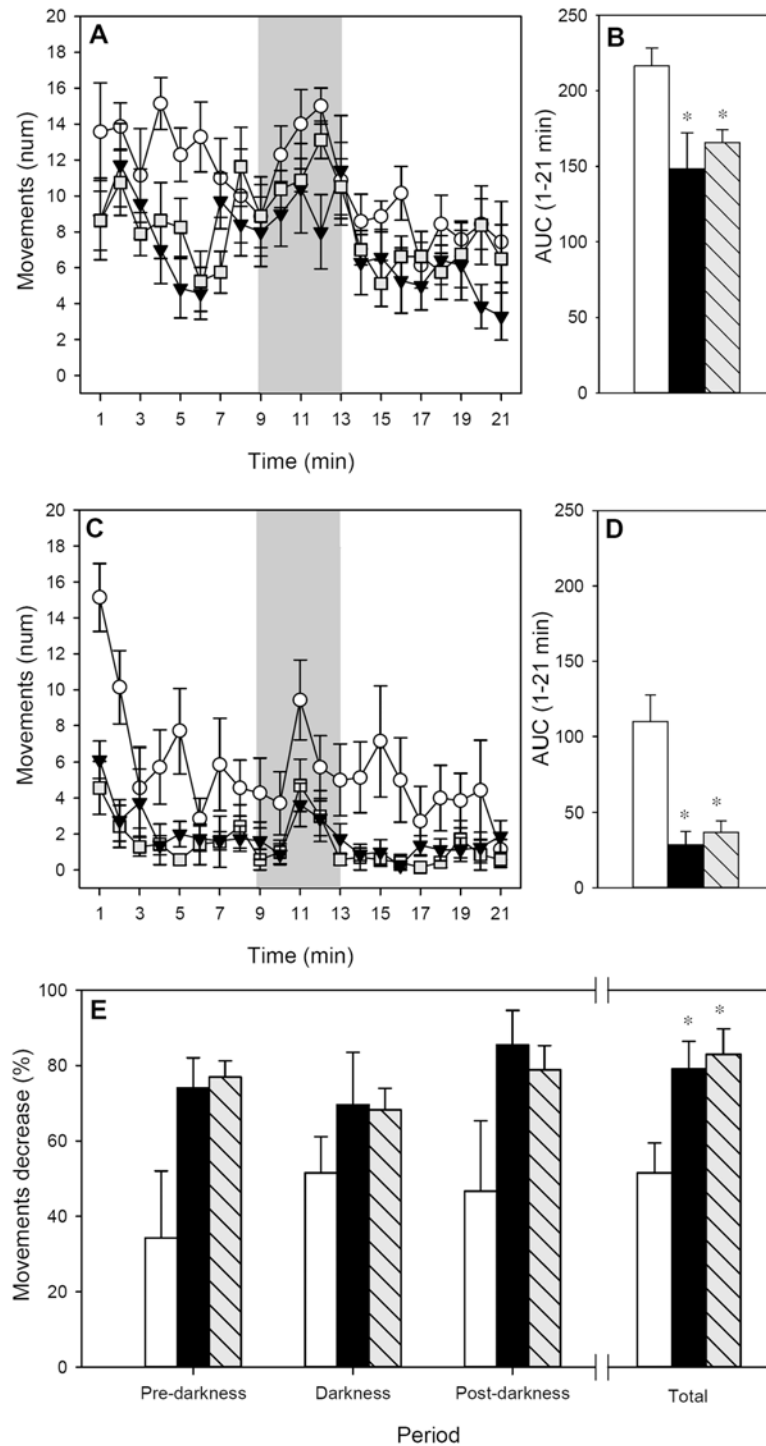


Fig 3. Motor activity for 21-min period. **A)** Basal motor activity assessed 24 h before the AR induction; **B)** area under the curve from the whole studied period before AR induction; **C)** motor activity assessed immediately after AR induction; **D)** area under the curve from the whole studied period after AR induction; **E)** percentage of motor activity decrease after AR induction referring to pre-darkness, darkness, post-darkness and the whole period. ○ or white bars represent RF group, ▼ or black bars represent IP group and ■ or grey-striped bars represent FA group. In A and C, shadow period corresponds to darkness. Results are expressed as mean ± S.E.M. (n = 8). *p < 0.05 vs. RF group.

doi:10.1371/journal.pone.0125314.g003

the whole studied period can also be observed when AUC was calculated (Fig 3B; $p < 0.05$ IP and FA groups vs. RF).

The motor activity registered after AR induction showed a similar pattern to the basal one, the animals being quieter during the pre-darkness phases and more active in the darkness period (Fig 3C; $p < 0.05$). However, the three studied groups showed a lower number of movements than those observed in basal conditions. Interestingly, for those animals belonging to the IP and FA groups, the AR induction produced a more noticeable decrease in the motor activity than in the RF group ($p < 0.001$), which can also be observed when considering the AUC of the whole period (Fig 3D; $p < 0.05$ IP and FA groups vs. RF).

The reduction in motor activity resulting from AR induction was also calculated as the percentage of motor activity decrease between basal and post-AR induction in each phase (Fig 3E). RF animals reduced by about 35–50% their number of movements; however, both IP and FA groups underwent a 70–85% reduction of motor activity ($p < 0.05$ in the whole studied period).

There was a correlation between the percentage of decrease in motor activity and the body temperature after AR ($\rho = -0.615$, $p < 0.05$ at 90 min; $\rho = -0.601$, $p < 0.05$ at 120 min) meaning that the higher the percentage of decrease, the lower the animal's body temperature.

Lymphocyte composition in Peyer's patches and mesenteric lymph nodes

The percentage of TCR $\alpha\beta$ cells, Tc and Th subsets, activated Th cells, B cells and B IgA⁺ subset from PP and MLN lymphocytes in the three studied groups is summarized in Fig 4. No differences between the groups were observed either in PP or MLN (Fig 4A and 4B), showing that both i.p. immunization and FA induction did not produce significant changes in the considered cell populations in either intestinal compartments.

After 96 h of OVA stimulation, the composition of MLN cells from RF animals did not significantly change (Fig 4C). Interestingly, in the IP group there was an increase in the TCR $\alpha\beta$ cell proportion after OVA stimulation ($p < 0.05$). This increase corresponded to Tc and activated Th cells ($p < 0.05$). In cells from the FA group, no significant variations were observed in any of the studied MLN subsets after OVA stimulation.

Cytokine production by spleen cells

The cytokine quantification of supernatants obtained from spleen cells isolated after two days of AR induction and cultured for four days with or without OVA was carried out. Those samples that had concentrations below the cutoff received a value corresponding to one-half the cutoff value, as previously described [55]. Spleen cells from RF animals did not produce detectable amounts of the studied cytokines (Table 1). After OVA stimulation, cells from the IP group increased their IL-2, IL-4 and IL-10 production with respect to that in the RF group ($p < 0.05$). On the contrary, the concentrations of cytokines from cells obtained from FA animals did not significantly differ from that of RF group, which could be due to the fact that IL-2 and IL-4 cytokines were only detected in 25% of FA animals, and IL-10 and IFN- γ in 50% and 75% of these animals, respectively. In comparison with the IP group, FA rats produced significantly lower amounts of IL-10 ($p < 0.05$).

Small intestine gene expression

The gene expression of IFN- γ , IL-2, IL-4, IL-10, IgA, RMCP-II and Fc ϵ RI was analyzed in the SI at the end of the study (Fig 5). In both the IP and FA groups, IFN- γ and IL-10 gene expression was down-regulated whereas IgA mRNA levels increased but these changes did not

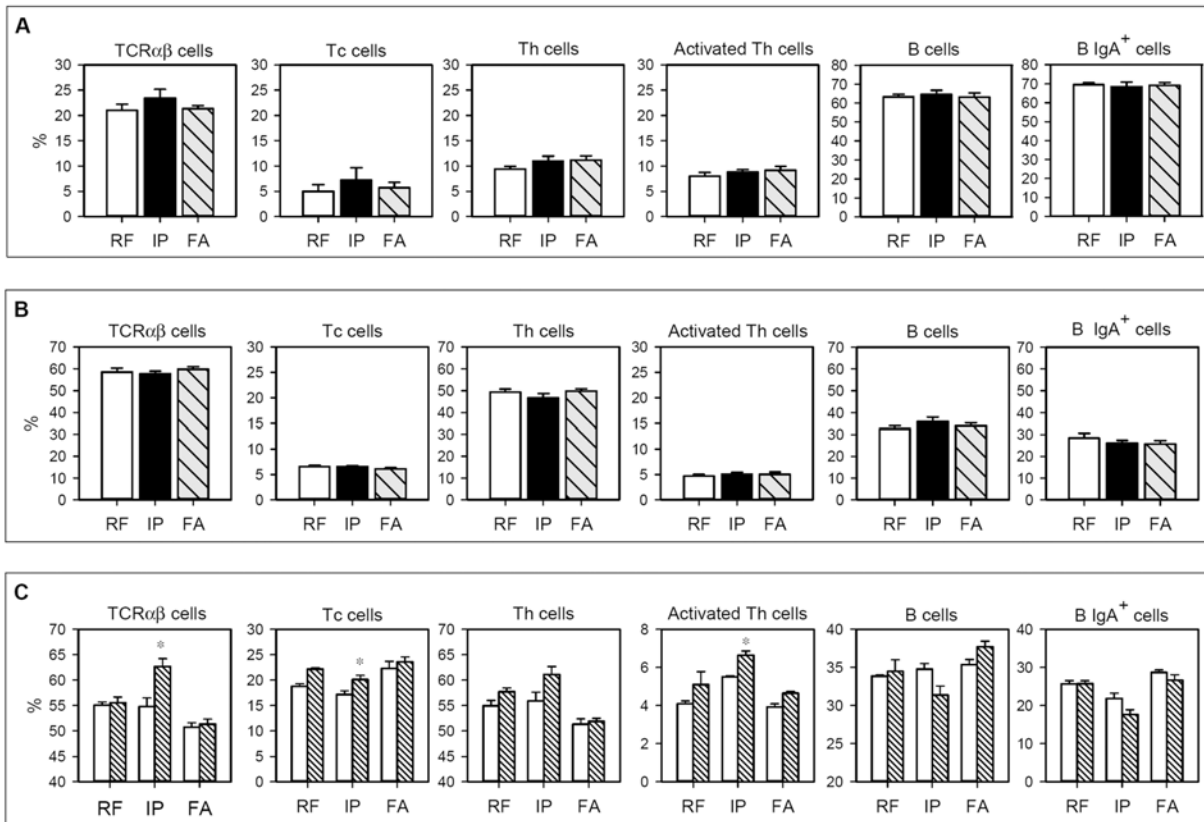


Fig 4. Lymphocyte composition isolated from A) Peyer's patches, B) mesenteric lymph nodes, and C) mesenteric lymph nodes after culturing for 96 h in the presence or absence of OVA. In A and B, white bars represent RF group, black bars represent IP group and grey-striped bars represent FA group. In C, white bars summarize values without stimulus and striped bars represent values after OVA stimulation. Results are expressed as mean \pm S.E.M. (n = 8). * $p < 0.05$ vs. non stimulated condition.

doi:10.1371/journal.pone.0125314.g004

achieve statistical significance. In the IP group a significant up-regulation of FcεRI gene expression was found in comparison with RF animals ($p < 0.05$) and RMCP-II mRNA levels also increased but not significantly. Regarding the FA group, the gene expression of RMCP-II increased about fourfold with respect to RF animals ($p < 0.05$), but no changes were detected in FcεRI. No significant amounts of mRNA of IL-2 and IL-4 were expressed in the small intestine wall from either the reference or immunized animals.

Table 1. Cytokine production by spleen cells after stimulation with OVA.

Groups	IL-2 (pg/mL)	IL-4 (pg/mL)	IL-10 (pg/mL)	IFN-γ (pg/mL)
Reference	0.23	1.70	9.70	3.40
Intraperitoneal	54.18 \pm 9.94*	104.34 \pm 40.93*	803.3 \pm 300.5*	26.94 \pm 10.08
Food allergy	68.17 \pm 25.32	38.97 \pm 15.25	61.25 \pm 33.54 ^φ	7.55 \pm 4.15

Results are expressed as mean \pm S.E.M.

* $p < 0.05$ vs. RF group,

^φ $p < 0.05$ vs. IP group.

doi:10.1371/journal.pone.0125314.t001

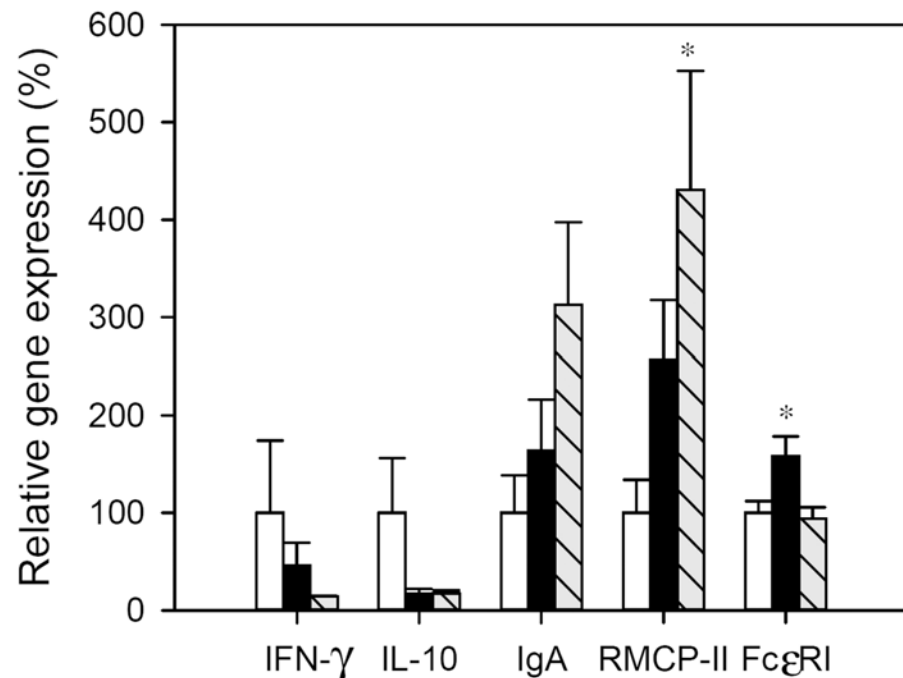


Fig 5. Relative gene expression in small intestine. Expression levels were normalized using HPRT as the endogenous housekeeping gene and were expressed as percentage in comparison with the RF group, which was considered as 100% gene expression. White bars represent RF group, black bars represent IP group and grey-striped bars represent FA group. Results are expressed as mean \pm S.E.M. ($n = 8$). * $p < 0.05$ vs. RF group.

doi:10.1371/journal.pone.0125314.g005

Discussion

The present study provides the set-up and characterization of a FA model in BN rats, including the induction of an AR, carried out following the previous i.p. immunization with the allergen, OVA, together with alum and tBp and a subsequent daily oral administration of OVA for a period of three weeks. In order to establish specific biomarkers of FA, we compared the anti-allergen immune response and the AR obtained in this model with those achieved with only the i.p. immunization.

For the screening of drugs, nutritional interventions or immunotherapies to fight against allergies or for testing the allergenicity of new foods, many rat models of FA have been described, including those that only use the oral route [30–32], those that only use the i.p. route without adjuvant [40,56] and those that combine i.p. and oral administration [42]. Although BN rats are high IgE responders, similar to atopic humans, experimental procedures in this rat strain to induce oral sensitization without adjuvant are time-consuming and are not always able to generate a reproducible and effective FA model [20,30,37–39]. In fact, we previously tested a model in BN rats administered only by oral route and the result was that a few animals were sensitized and none produced specific IgE [39]. In contrast, other studies using several i.p. immunization protocols, with or without adjuvant, reported a successful production of specific IgE [40,56,57]. It is for this reason that we applied here an i.p. immunization with alum and tBp previous to the oral allergen administration.

As described in previous studies [54], the i.p. immunization of BN rats with OVA, alum and tBp induces the synthesis of specific antibodies in 100% of the animals, especially those isotypes related to Th2 immune response in rat, such as IgE, IgG1 and IgG2a [18,36,58]. The anti-OVA

antibody profile, including specific IgE, is not surprising and can be attributed to both alum adjuvant and tBp which favor IgE synthesis [59,60]. Interestingly, when two weeks later a daily OVA solution was given orally, the specific antibody response was strengthened. This pattern was observed for serum IgG isotypes, which rose steeply during the first week of oral gavage, demonstrating that anti-OVA immune response was rapidly boosted by oral OVA administration. Similarly, OVA-specific IgE antibodies increased nearly twofold after one week of oral gavage but, however, when longer oral OVA administration was carried out, IgE serum concentrations decreased, following the same pattern as those that only received i.p. immunization. These results regarding serum anti-OVA antibody kinetics agree with those reported by Golias et al. [61] in a mouse model of FA obtained by two i.p. immunizations (two weeks apart) and oral feeding 14 days later every two days. In particular, this last study found that specific IgE response was already present before oral OVA administration, peaked during the first week after oral gavage and decreased later. Therefore, from the overall results concerning specific IgE, it could be suggested that only the first doses of the allergen administered are responsible for an exacerbation of the IgE synthesis and this response is lost with time. Overall, from the results concerning anti-OVA antibodies, it could be concluded that an effective FA model had been achieved because it produced the synthesis of specific antibodies in 100% of the animals and was relatively rapid since the highest specific IgE and IgG levels were reached one week after oral allergen administration, which was sooner than other reported models [34,37].

The FA model proposed here produced the synthesis of serum and intestinal anti-OVA IgA antibodies, which were not found when only i.p. immunization was carried out, thus demonstrating the stimulation of gut-associated lymphoid tissue. Although intestinal IgA is thought to contribute to gut homeostasis by limiting the uptake of oral antigens and it has been considered to have a protective role against oral sensitization [62], its role in food allergy is still controversial. In human FA, it has been reported that specific IgA2 levels (isotype mainly found in mucosa surfaces such as those of the intestine) increased when children became tolerant [63]. However, other authors reported that increased specific IgA was associated with a later FA [64] and that serum allergen-specific IgA seems not to be associated with food tolerance [65]. From our results, although oral challenge was performed with a high dose of oral OVA, the protective effect of intestinal IgA antibodies in the FA group was not observed because the measurement of AR provided similar results in both the FA and IP groups.

After AR induction, the FA model was characterized by a high increase in serum RMCP-II concentration, which again might reflect the stimulation of gut-associated lymphoid tissue because this protease is typical of activated mucosal mast cells [66]. In addition, other mediators released from mast cells produce vasodilatation and are responsible for the decrease in body temperature [67,68]. Animals immunized with only OVA by i.p. route and those immunized by i.p. route and subsequent oral OVA administration underwent a similar drop in body temperature after AR induction. There was no correlation between body temperature and the serum RMCP-II concentration, suggesting that other mast cells different from those in the intestinal mucosa could contribute to AR-induced hypothermia. On the other hand, AR caused an increase in intestinal permeability in both IP and FA groups, which must reflect the disrupted intestinal barrier after OVA immunization. It has been demonstrated that repeated OVA oral gavage produces an accumulation of RMCP-II in the intestine leading to altered motor responses in both the small intestine and the colon [69,70]. Nevertheless, it has been reported that an i.p. immunization produced a higher increase in intestinal permeability than an oral sensitization without an adjuvant, and this was attributed to the release of RMCP-II, among other mediators, which could increase the absorption by paracellular route [31]. From the results obtained here, rats with FA (i.p. and oral sensitization) seem to absorb β LG faster

than the IP group because serum protein concentration tended to be higher at 30 min after β LG oral administration (60 min after AR induction) and disappeared faster. The collection of samples earlier than 30 min should confirm this suggestion and can shed some light as to whether there is any difference in intestinal permeability when OVA is given orally after the i.p. immunization. AR-induced behavioral changes were quantified by the decrease in motor activity as performed in a previous study [45], instead of using the classical score systems which require the subjective validation by the investigator [71,72]. The results after AR induction revealed a clear decrease of movements in comparison with the basal ones. However, when comparing the motor activity between the IP and FA groups, it could be observed that the decrease in motor activity induced by AR was similar in both groups. Therefore, from the results obtained after AR induction, it could be concluded that only the serum concentrations of RMCP-II, which were highly increased by oral OVA, clearly indicated the development of an FA model. Further studies on intestinal permeability should be directed to elucidate changes induced by oral allergen administration in this FA model. However, the decrease in body temperature and also in motor activity did not differ between IP and FA rats, which could be attributed to the similar serum IgE levels present at the end of the study.

Tissue samples obtained two days after AR induction allowed the detailed characterization of the FA process in comparison with the i.p. immunization. The study of lymphocyte composition in PP and MLN shows that neither the i.p. immunization nor the oral OVA administration changed the proportion of the main lymphocyte subsets in these intestinal compartments, at least at the moment when these samples were collected. These results did not agree with those of Ogawa et al. [43], which reported the accumulation of T lymphocytes in PP in a model of FA. Further studies carried out at different times could help to clarify this controversy, but from our results, it could be suggested that the characterization of lymphocyte phenotype in PP and MLN did not constitute a biomarker of FA induction. On the other hand, we observed that the proportion of T cells increased when MLN lymphocytes isolated from the IP group were specifically stimulated *in vitro*, but these results were not found in the FA group. These data could suggest the lymphocyte responsiveness in the IP group in contrast to the lymphocyte unresponsiveness after oral gavage of OVA for three weeks. This suggestion agrees with the cytokine results obtained from OVA-stimulated spleen cells, which show that only in the IP group was the amount of IL-4 and IL-10 released from spleen cells higher than that observed in the RF group, whereas the concentration of cytokines released by the FA group did not differ from reference values. In this sense, although some authors describe an increase of IL-4 and IL-10 in supernatants of spleen cultures of FA animals [34,73,74], other authors do not [42], and none of them compare the changes between i.p. immunization alone and i.p. together with an oral allergen administration. From these results it could be suggested that cytokines released from spleen cells collected after three weeks of allergen gavage did not reflect the oral sensitization process present in FA. Studies carried out in a previous phase of FA induction could better represent this response. In addition, other conditions of spleen cell incubation, such as a shorter stimulation and higher stimulus concentration, among others, could be better conditions for releasing representative cytokines. Nevertheless, it could be speculated that, at the end of the study, the continuous oral OVA administration produced a certain tolerance. This lack of response would not be reflected in the great synthesis of antibodies that occurred throughout the process, but would be only observed in the specific stimulation of cells collected at the end of the study.

Finally, the study of gene expression on intestinal tissue could reflect changes induced locally by oral OVA administration. We found that the gene expression of RMCP-II was significantly increased in FA animals, and these results agree with serum concentrations of this mediator and also with changes reported concerning the gene expression of this molecule in mice and

rats with food allergies [33,35,43]. However, surprisingly the gene expression of FcεRI did not change with FA induction, although it did after i.p. immunization alone. It has been reported in mouse mast cells that the internalization of FcεRI is a mechanism of antigen-specific desensitization [75]. Therefore, the comparison of the results obtained in the FcεRI gene expression in IP and FA groups could endorse the idea that the FA group developed a certain tolerance from the continuous oral allergen administration.

In conclusion, by means of the combination of i.p. immunization followed by the oral gavage of the food allergen, we have established a rat model of FA that is effective because it was able to induce the synthesis of specific Th2-related antibodies, especially IgE, and consequently an AR after oral challenge in all animals. This fact represents a great advantage with respect to FA models only induced by oral route, which did not provide effective and reproducible results in all experiments. In addition, the allergic response development is faster than in other FA models described because one week after the oral administration of allergen i.e., three weeks after i.p. immunization, high levels of specific IgE were produced. In comparison with only i.p. immunization, the developed model provides much higher levels of specific IgG antibodies, achieving high amounts of Th2-related antibodies in rat (IgG1 and IgG2a), and also anti-OVA IgE, although the anaphylactic response after five weeks was similar in both groups. In addition, the levels of RMCP-II released after the anaphylaxis induction and the intestinal gene expression of this protease with respect to those of the i.p. immunization are the best biomarkers of the FA process. The results from *in vitro* antigen-specific activation of lymphocytes from spleen and mesenteric lymph nodes suggest a certain unresponsiveness state of these cells possibly induced by repeated oral doses of the allergen. Nevertheless, although further studies must confirm this hypothesis, the specific antibody response kinetics suggest that the best FA model could be obtained after only a week of oral OVA administration.

Acknowledgments

The authors would like to thank Dr. Antoni Díez-Noguera and Dra. Trinitat Cambras for lending us the activity metres and Malén Massot-Cladera for her technical assistance.

Author Contributions

Conceived and designed the experiments: FPC AF MC. Performed the experiments: MAG AGJ. Analyzed the data: MAG AGJ FPC AF MC. Contributed reagents/materials/analysis tools: MAG FPC AF MC. Wrote the paper: MAG AF MC.

References

1. Boyce JA, Assa'ad A, Burks AW, Jones SM, Sampson HA, Wood RA, et al. Guidelines for the diagnosis and management of food allergy in the United States: summary of the NIAID-Sponsored Expert Panel report. *J Am Acad Dermatol* 2011; 64:175–192. doi: [10.1016/j.jaad.2010.11.020](https://doi.org/10.1016/j.jaad.2010.11.020) PMID: [21167411](https://pubmed.ncbi.nlm.nih.gov/21167411/)
2. Fox M, Mugford M, Voordouw J, Cornelisse-Vermaat J, Antonides G, de la Hoz Caballer B, et al. Health sector costs of self-reported food allergy in Europe: a patient-based cost of illness study. *Eur J Public Health* 2013; 23:757–762. doi: [10.1093/eurpub/ckt010](https://doi.org/10.1093/eurpub/ckt010) PMID: [23402805](https://pubmed.ncbi.nlm.nih.gov/23402805/)
3. Patel D, Holdford D, Edwards E, Carroll N V. Estimating the economic burden of food-induced allergic reactions and anaphylaxis in the United States. *J Allergy Clin Immunol* 2011; 128:110–115. doi: [10.1016/j.jaci.2011.03.013](https://doi.org/10.1016/j.jaci.2011.03.013) PMID: [21489610](https://pubmed.ncbi.nlm.nih.gov/21489610/)
4. Burks WA, Tang M, Sicherer S, Muraro A, Eigenmann PA, Ebisawa M, et al. ICON: food allergy. *J Allergy Clin Immunol* 2012; 129:906–920. doi: [10.1016/j.jaci.2012.02.001](https://doi.org/10.1016/j.jaci.2012.02.001) PMID: [22365653](https://pubmed.ncbi.nlm.nih.gov/22365653/)
5. Nwaru BI, Hickstein L, Panesar SS, Roberts G, Muraro A, Sheikh A, et al. Prevalence of common food allergies in Europe: a systematic review and meta-analysis. *Allergy* 2014; 69:992–1007. doi: [10.1111/all.12423](https://doi.org/10.1111/all.12423) PMID: [24816523](https://pubmed.ncbi.nlm.nih.gov/24816523/)
6. Sicherer SH, Sampson HA. Food allergy. *J Allergy Clin Immunol* 2006; 117:S470–475. PMID: [16455349](https://pubmed.ncbi.nlm.nih.gov/16455349/)

7. Sicherer SH, Sampson HA. Food allergy: Epidemiology, pathogenesis, diagnosis, and treatment. *J Allergy Clin Immunol* 2014; 133:291–307; quiz 308. doi: [10.1016/j.jaci.2013.11.020](https://doi.org/10.1016/j.jaci.2013.11.020) PMID: [24388012](https://pubmed.ncbi.nlm.nih.gov/24388012/)
8. Ruiters B, Shreffler WG. The role of dendritic cells in food allergy. *J Allergy Clin Immunol* 2012; 129:921–928. doi: [10.1016/j.jaci.2012.01.080](https://doi.org/10.1016/j.jaci.2012.01.080) PMID: [22464669](https://pubmed.ncbi.nlm.nih.gov/22464669/)
9. Blikslager AT, Moeser AJ, Gookin JL, Jones SL, Odle J. Restoration of barrier function in injured intestinal mucosa. *Physiol Rev* 2007; 87:545–564. PMID: [17429041](https://pubmed.ncbi.nlm.nih.gov/17429041/)
10. Pabst O, Mowat AM. Oral tolerance to food protein. *Mucosal Immunol* 2012; 5:232–239. doi: [10.1038/mi.2012.4](https://doi.org/10.1038/mi.2012.4) PMID: [22318493](https://pubmed.ncbi.nlm.nih.gov/22318493/)
11. Oyoshi MK, Oettgen HC, Chatila TA, Geha RS, Bryce PJ. Food allergy: Insights into etiology, prevention, and treatment provided by murine models. *J Allergy Clin Immunol* 2014; 133:309–317. doi: [10.1016/j.jaci.2013.12.1045](https://doi.org/10.1016/j.jaci.2013.12.1045) PMID: [24636470](https://pubmed.ncbi.nlm.nih.gov/24636470/)
12. Buchanan BB, Frick OL. The dog as a model for food allergy. *Ann N Y Acad Sci* 2002; 964:173–183. PMID: [12023204](https://pubmed.ncbi.nlm.nih.gov/12023204/)
13. Helm RM, Furuta GT, Stanley JS, Ye J, Cockrell G, Connaughton C, et al. A neonatal swine model for peanut allergy. *J Allergy Clin Immunol* 2002; 109:136–142. PMID: [11799380](https://pubmed.ncbi.nlm.nih.gov/11799380/)
14. Teuber SS, del Val G, Morigasaki S, Jung HR, Eisele PH, Frick OL, et al. The atopic dog as a model of peanut and tree nut food allergy. *J Allergy Clin Immunol* 2002; 110:921–927. PMID: [12464960](https://pubmed.ncbi.nlm.nih.gov/12464960/)
15. Piacentini GL, Vicentini L, Bodini A, Mazzi P, Peroni DG, Maffei C, et al. Allergenicity of a hydrolyzed rice infant formula in a guinea pig model. *Ann Allergy Asthma Immunol* 2003; 91:61–64. PMID: [12877451](https://pubmed.ncbi.nlm.nih.gov/12877451/)
16. Ganeshan K, Neilsen C V, Hadsaitong A, Schleimer RP, Luo X, Bryce PJ. Impairing oral tolerance promotes allergy and anaphylaxis: a new murine food allergy model. *J Allergy Clin Immunol* 2009; 123:231–238. doi: [10.1016/j.jaci.2008.10.011](https://doi.org/10.1016/j.jaci.2008.10.011) PMID: [19022495](https://pubmed.ncbi.nlm.nih.gov/19022495/)
17. Vinje NE, Larsen S, Løvik M. A mouse model of lupin allergy. *Clin Exp Allergy* 2009; 39:1255–1266. doi: [10.1111/j.1365-2222.2009.03269.x](https://doi.org/10.1111/j.1365-2222.2009.03269.x) PMID: [19438583](https://pubmed.ncbi.nlm.nih.gov/19438583/)
18. Sun N, Zhou C, Pu Q, Wang J, Huang K, Che H. Allergic reactions compared between BN and Wistar rats after oral exposure to ovalbumin. *J Immunotoxicol* 2013; 10:67–74. doi: [10.3109/1547691X.2012.693546](https://doi.org/10.3109/1547691X.2012.693546) PMID: [23110332](https://pubmed.ncbi.nlm.nih.gov/23110332/)
19. Ahuja V, Quatchadze M, Ahuja V, Stelter D, Albrecht A, Stahlmann R. Evaluation of biotechnology-derived novel proteins for the risk of food-allergic potential: advances in the development of animal models and future challenges. *Arch Toxicol* 2010; 84:909–917. doi: [10.1007/s00204-010-0582-0](https://doi.org/10.1007/s00204-010-0582-0) PMID: [20842347](https://pubmed.ncbi.nlm.nih.gov/20842347/)
20. Kimber I, Dearman RJ, Penninks AH, Knippels LMJ, Buchanan RB, Hammerberg B, et al. Assessment of protein allergenicity on the basis of immune reactivity: animal models. *Environ Health Perspect* 2002; 111:1125–1130.
21. Kitagawa S, Zhang S, Harari Y, Castro GA. Relative allergenicity of cow's milk and cow's milk-based formulas in an animal model. *Am J Med Sci* 1995; 310:183–187. PMID: [7485221](https://pubmed.ncbi.nlm.nih.gov/7485221/)
22. Fritsché R. Animal models in food allergy: assessment of allergenicity and preventive activity of infant formulas. *Toxicol Lett* 2003; 140–141:303–309.
23. Ando T, Matsumoto K, Namiranian S, Yamashita H, Glatthorn H, Kimura M, et al. Mast cells are required for full expression of allergen/SEB-induced skin inflammation. *J Invest Dermatol* 2013; 133:2695–2705. doi: [10.1038/jid.2013.250](https://doi.org/10.1038/jid.2013.250) PMID: [23752044](https://pubmed.ncbi.nlm.nih.gov/23752044/)
24. Fattouh R, Pouladi MA, Alvarez D, Johnson JR, Walker TD, Goncharova S, et al. House dust mite facilitates ovalbumin-specific allergic sensitization and airway inflammation. *Am J Respir Crit Care Med* 2005; 172:314–321. PMID: [15879422](https://pubmed.ncbi.nlm.nih.gov/15879422/)
25. Li X-M, Schofield BH, Huang C, Kleiner GI, Sampson HA. A murine model of IgE-mediated cow's milk hypersensitivity. *J Allergy Clin Immunol* 1999; 103:206–214. PMID: [9949309](https://pubmed.ncbi.nlm.nih.gov/9949309/)
26. Bailón E, Cueto-Sola M, Utrilla P, Rodríguez-Ruiz J, Garrido-Mesa N, Zarzuelo A, et al. A shorter and more specific oral sensitization-based experimental model of food allergy in mice. *J Immunol Methods* 2012; 381:41–49. doi: [10.1016/j.jim.2012.04.007](https://doi.org/10.1016/j.jim.2012.04.007) PMID: [22542400](https://pubmed.ncbi.nlm.nih.gov/22542400/)
27. Sun J, Arias K, Alvarez D, Fattouh R, Walker T, Goncharova S, et al. Impact of CD40 ligand, B cells, and mast cells in peanut-induced anaphylactic responses. *J Immunol* 2007; 179:6696–6703. PMID: [17982059](https://pubmed.ncbi.nlm.nih.gov/17982059/)
28. Aldemir H, Bars R, Herouet-Guicheney C. Murine models for evaluating the allergenicity of novel proteins and foods. *Regul Toxicol Pharmacol* 2009; 54:S52–57. doi: [10.1016/j.yrtph.2008.11.004](https://doi.org/10.1016/j.yrtph.2008.11.004) PMID: [19100305](https://pubmed.ncbi.nlm.nih.gov/19100305/)
29. Penninks AH, Knippels LM. Determination of protein allergenicity: studies in rats. *Toxicol Lett* 2001; 120:171–180. PMID: [11323175](https://pubmed.ncbi.nlm.nih.gov/11323175/)

30. Knippels LM, Penninks AH, van Meeteren M, Houben GF. Humoral and cellular immune responses in different rat strains on oral exposure to ovalbumin. *Food Chem Toxicol* 1999; 37:881–888. PMID: [10506012](#)
31. Knippels LMJ, Penninks AH, Smit JJ, Houben GF. Immune-mediated effects upon oral challenge of ovalbumin-sensitized Brown Norway rats: further characterization of a rat food allergy model. *Toxicol Appl Pharmacol* 1999; 156:161–169. PMID: [10222308](#)
32. Knippels LM, Penninks AH, Houben GF. Continued expression of anti-soy protein antibodies in rats bred on a soy protein-free diet for one generation: the importance of dietary control in oral sensitization research. *J Allergy Clin Immunol* 1998; 101:815–820. PMID: [9648709](#)
33. Zhong Y, Huang J, Tang W, Chen B, Cai W. Effects of probiotics, probiotic DNA and the CpG oligodeoxynucleotides on ovalbumin-sensitized Brown-Norway rats via TLR9/NF-κB pathway. *FEMS Immunol Med Microbiol* 2012; 66:71–82. doi: [10.1111/j.1574-695X.2012.00991.x](#) PMID: [22612777](#)
34. Huang J, Zhong Y, Cai W, Zhang H, Tang W, Chen B. The effects of probiotics supplementation timing on an ovalbumin-sensitized rat model. *FEMS Immunol Med Microbiol* 2010; 60:132–141. doi: [10.1111/j.1574-695X.2010.00727.x](#) PMID: [20846358](#)
35. Cao S, He X, Xu W, Luo Y, Ran W, Liang L, et al. Potential allergenicity research of Cry1C protein from genetically modified rice. *Regul Toxicol Pharmacol* 2012; 63:181–187. doi: [10.1016/j.yrtph.2012.03.017](#) PMID: [22504668](#)
36. De Jonge JD, Baken KA, Konings J, Pennings JL, Ezendam J, Van Loveren H. Gene expression changes in the mesenteric lymph nodes of rats after oral peanut extract exposure. *J Immunotoxicol* 2008; 5:385–394. doi: [10.1080/15476910802586126](#) PMID: [19404872](#)
37. Pilegaard K, Madsen C. An oral Brown Norway rat model for food allergy: comparison of age, sex, dosing volume, and allergen preparation. *Toxicology* 2004; 196:247–257. PMID: [15036751](#)
38. Dearman RJ, Caddick H, Stone S, Basketter DA, Kimber I. Characterization of antibody responses induced in rodents by exposure to food proteins: influence of route of exposure. *Toxicology* 2001; 167:217–231. PMID: [11578801](#)
39. Camps-Bossacoma M, Abril-Gil M, Franch À, Pérez-Cano FJ, Castell M. Induction of a model of oral sensitization in rat. *Clin Immunol Endocr Metab Drugs* 2015; in press.
40. Bøgh KL, Kroghsbo S, Dahl L, Rigby NM, Barkholt V, Mills ENC, et al. Digested Ara h 1 has sensitizing capacity in Brown Norway rats. *Clin Exp Allergy* 2009; 39:1611–1621. doi: [10.1111/j.1365-2222.2009.03333.x](#) PMID: [19689460](#)
41. Kroghsbo S, Bøgh KL, Rigby NM, Mills ENC, Rogers A, Madsen CB. Sensitization with 7S globulins from peanut, hazelnut, soy or pea induces IgE with different biological activities which are modified by soy tolerance. *Int Arch Allergy Immunol* 2011; 155:212–224. doi: [10.1159/000321200](#) PMID: [21282960](#)
42. Ahrens B, Quarcoo D, Buhner S, Reese G, Vieths S, Hamelmann E. Development of an animal model to evaluate the allergenicity of food allergens. *Int Arch Allergy Immunol* 2014; 164:89–96. doi: [10.1159/000363109](#) PMID: [24903216](#)
43. Ogawa T, Miura S, Tsuzuki Y, Ogino T, Teramoto K, Inamura T, et al. Chronic allergy to dietary ovalbumin induces lymphocyte migration to rat small intestinal mucosa that is inhibited by MAdCAM-1. *Am J Physiol Gastrointest Liver Physiol* 2004; 286:G702–710. PMID: [14670821](#)
44. Dong W, Selgrade MK, Gilmour MI. Systemic administration of Bordetella pertussis enhances pulmonary sensitization to house dust mite in juvenile rats. *Toxicol Sci* 2003; 72:113–121. PMID: [12604840](#)
45. Abril-Gil M, Garcia-Just A, Cambras T, Pérez-Cano FJ, Cristina C, Franch À, et al. Motor activity as unbiased variable to assess anaphylactic shock in allergic rats. *Exp Biol Med (Maywood)* 2015; 1535370215573393, first published on February 25.
46. Chiesa JJ, Cambras T, Carpentieri AR, Díez-Noguera A. Arrhythmic rats after SCN lesions and constant light differ in short time scale regulation of locomotor activity. *J Biol Rhythms* 2010; 25:37–46. doi: [10.1177/0748730409352843](#) PMID: [20075299](#)
47. Albert N, da Silva C, Díez-Noguera A, Cambras T. Different adaptation of the motor activity rhythm to chronic phase shifts between adolescent and adult rats. *Behav Brain Res* 2013; 252:347–355. doi: [10.1016/j.bbr.2013.06.025](#) PMID: [23792134](#)
48. Ramiro-Puig E, Pérez-Cano FJ, Ramos-Romero S, Pérez-Berezo T, Castellote C, Permanyer J, et al. Intestinal immune system of young rats influenced by cocoa-enriched diet. *J Nutr Biochem* 2008; 19:555–565. PMID: [18061430](#)
49. Pérez-Berezo T, Franch A, Ramos-Romero S, Castellote C, Pérez-Cano FJ, Castell M. Cocoa-enriched diets modulate intestinal and systemic humoral immune response in young adult rats. *Mol Nutr Food Res* 2011; 55:S56–66. doi: [10.1002/mnfr.201000588](#) PMID: [21462334](#)
50. Pérez-Berezo T, Ramírez-Santana C, Franch A, Ramos-Romero S, Castellote C, Pérez-Cano FJ, et al. Effects of a cocoa diet on an intestinal inflammation model in rats. *Exp Biol Med* 2012; 237:1181–1188. doi: [10.1258/ebm.2012.012083](#) PMID: [23104506](#)

51. Sakamoto Y, Ohtsuka T, Yoshida H, Ohto K, Onobori M, Matsumoto T, et al. Time course of changes in the intestinal permeability of food-sensitized rats after oral allergen challenge. *Pediatr Allergy Immunol* 1998; 9:20–24. PMID: [9560838](#)
52. Massot-Cladera M, Pérez-Berezo T, Franch A, Castell M, Pérez-Cano FJ. Cocoa modulatory effect on rat faecal microbiota and colonic crosstalk. *Arch Biochem Biophys* 2012; 527:105–112. doi: [10.1016/j.abb.2012.05.015](#) PMID: [22663919](#)
53. Livak KJ, Schmittgen TD. Analysis of relative gene expression data using real-time quantitative PCR and the 2⁻(Delta Delta C(T)) Method. *Methods* 2001; 25:402–408. PMID: [11846609](#)
54. Abril-Gil M, Massot-Cladera M, Pérez-Cano FJ, Castellote C, Franch À, Castell M. A diet enriched with cocoa prevents IgE synthesis in a rat allergy model. *Pharmacol Res* 2012; 65:603–608. doi: [10.1016/j.phrs.2012.02.001](#) PMID: [22342543](#)
55. Zanardo V, Golin R, Amato M, Trevisanuto D, Favaro F, Faggian D, et al. Cytokines in human colostrum and neonatal jaundice. *Pediatr Res* 2007; 62:191–194. PMID: [17597660](#)
56. Bøgh KL, Barkholt V, Madsen CB. The sensitising capacity of intact β -lactoglobulin is reduced by co-administration with digested β -lactoglobulin. *Int Arch Allergy Immunol* 2013; 161:21–36. doi: [10.1159/000351238](#) PMID: [23689241](#)
57. Bellou A, Saint-Laudy J, Knippels L, Montémont C, Vauthier E, Gerard P, et al. Brown Norway rat ovalbumin-specific immunoglobulin E antibodies increase the human basophil expression of CD63 marker. *Scand J Immunol* 2003; 57:271–278. PMID: [12641656](#)
58. Gracie JA, Bradley JA. Interleukin-12 induces interferon- γ -dependent switching of IgG alloantibody subclass. *Eur J Immunol* 1996; 8:1217–1221.
59. Terhune TD, Deth RC. How aluminum adjuvants could promote and enhance non-target IgE synthesis in a genetically-vulnerable sub-population. *J Immunotoxicol* 2013; 10:210–222. doi: [10.3109/1547691X.2012.708366](#) PMID: [22967010](#)
60. Saavedra Y, Vergara P. Hypersensitivity to ovalbumin induces chronic intestinal dysmotility and increases the number of intestinal mast cells. *Neurogastroenterol Motil* 2005; 17:112–122. PMID: [15670271](#)
61. Golias J, Schwarzer M, Wallner M, Kverka M, Kozakova H, Srutkova D, et al. Heat-induced structural changes affect OVA-antigen processing and reduce allergic response in mouse model of food allergy. *PLoS One* 2012; 7: e37156. doi: [10.1371/journal.pone.0037156](#) PMID: [22629361](#)
62. Berin MC, Mayer L. Immunophysiology of experimental food allergy. *Mucosal Immunol* 2009; 2:24–32. doi: [10.1038/mi.2008.72](#) PMID: [19079331](#)
63. Konstantinou GN, Nowak-Węgrzyn A, Bencharitwong R, Bardina L, Sicherer SH, Sampson HA. Egg-white-specific IgA and IgA2 antibodies in egg-allergic children: is there a role in tolerance induction? *Pediatr Allergy Immunol* 2014; 25:64–70. doi: [10.1111/pai.12143](#) PMID: [24118158](#)
64. Orivuori L, Mustonen K, Roduit C, Braun-Fahrlander C, Dalphin J-C, Genuneit J, et al. Immunoglobulin A and immunoglobulin G antibodies against β -lactoglobulin and gliadin at age 1 associate with immunoglobulin E sensitization at age 6. *Pediatr Allergy Immunol* 2014; 25:329–337. doi: [10.1111/pai.12246](#) PMID: [24953294](#)
65. Vazquez-Ortiz M, Pascal M, Juan M, Alsina L, Martín-Mateos MA, Plaza AM. Serum allergen-specific IgA is not associated with natural or induced tolerance to egg in children. *Allergy* 2013; 68:1327–1332. doi: [10.1111/all.12217](#) PMID: [24004369](#)
66. Gibson S, Mackeller A, Newlands G, Miller H. Phenotypic expression of mast cell granule proteinases. Distribution of mast cell proteinases I and II in the rat digestive system. *Immunology* 1987; 62:621–627. PMID: [3323033](#)
67. Makabe-Kobayashi Y, Hori Y, Adachi T, Ishigaki-Suzuki S, Kikuchi Y, Kagaya Y, et al. The control effect of histamine on body temperature and respiratory function in IgE-dependent systemic anaphylaxis. *J Allergy Clin Immunol* 2002; 110:298–303. PMID: [12170272](#)
68. Khodoun M, Strait R, Orekov T, Hogan S, Karasuyama H, Herbert DR, et al. Peanuts can contribute to anaphylactic shock by activating complement. *J Allergy Clin Immunol* 2009; 123:342–351. doi: [10.1016/j.jaci.2008.11.004](#) PMID: [19121857](#)
69. Traver E, Torres R, de Mora F, Vergara P. Mucosal mast cells mediate motor response induced by chronic oral exposure to ovalbumin in the rat gastrointestinal tract. *Neurogastroenterol Motil* 2010; 22: e34–43. doi: [10.1111/j.1365-2982.2009.01377.x](#) PMID: [19682267](#)
70. Jardí F, Martínez V, Vergara P. NGF is involved in oral ovalbumin-induced altered colonic contractility in rats: evidence from the blockade of TrkA receptors with K252a. *Neurogastroenterol Motil* 2012; 24: e580–590. doi: [10.1111/nmo.12027](#) PMID: [23072452](#)
71. Leonard SA, Martos G, Wang W, Nowak-Węgrzyn A, Berin MC. Oral immunotherapy induces local protective mechanisms in the gastrointestinal mucosa. *J Allergy Clin Immunol* 2012; 129:1579–1587. doi: [10.1016/j.jaci.2012.04.009](#) PMID: [22554705](#)

72. Shindo T, Kanazawa Y, Saito Y, Kojima K, Ohsawa M, Teshima R. Effective induction of oral anaphylaxis to ovalbumin in mice sensitized by feeding of the antigen with aid of oil emulsion and salicylate. *J Toxicol Sci* 2012; 37:307–315. PMID: [22467021](#)
73. Duncker SC, Philippe D, Martin-Paschoud C, Moser M, Mercenier A, Nutten S. *Nigella sativa* (black cumin) seed extract alleviates symptoms of allergic diarrhea in mice, involving opioid receptors. *PLoS One* 2012; 7:e39841. doi: [10.1371/journal.pone.0039841](#) PMID: [22768141](#)
74. Okada Y, Oh-oka K, Nakamura Y, Ishimaru K, Matsuoka S, Okumura K, et al. Dietary resveratrol prevents the development of food allergy in mice. *PLoS One* 2012; 7:e44338. doi: [10.1371/journal.pone.0044338](#) PMID: [22962611](#)
75. Oka T, Rios EJ, Tsai M, Kalesnikoff J, Galli SJ. Rapid desensitization induces internalization of antigen-specific IgE on mouse mast cells. *J Allergy Clin Immunol* 2013; 132:922–32. doi: [10.1016/j.jaci.2013.05.004](#) PMID: [23810240](#)

AUTISM & ALUMINUM ADJUVANTS IN VACCINES

How Aluminum Adjuvants in Vaccines Can Cause Autism



Published: August 18, 2017 (Version 1.0)

The Centers for Disease Control (CDC) asserts that vaccines and vaccine ingredients have been disproven as potential causes of autism. Statements by the CDC are generic and encompass all vaccines and vaccine ingredients. For example, the CDC states:

*“Vaccines Do Not Cause Autism”
“There is no link between vaccines and autism.” “...no links have been found between any vaccine ingredients and autism spectrum disorder.” (CDC website, August 2017)*

These statements are not supported by available science. The CDC’s evidence supporting these statements is limited to the MMR vaccine (Taylor 2014), thimerosal preservative (Taylor 2014) and vaccine antigen exposure (DeStefano 2013).

Dr. Frank DeStefano of the CDC’s Immunization Safety Office is co-author of a paper (Glanz 2015) which states:

“To date, there have been no population-based studies specifically designed to evaluate associations between clinically meaningful outcomes and non-antigen ingredients, other than thimerosal.”

This statement applies to, among other vaccine ingredients, aluminum adjuvant. Studies of MMR vaccine cannot be used as evidence of safety for other vaccines, for example vaccines that contain aluminum adjuvant. The overly-broad, generic

assertions that no vaccines and no ingredients cause autism are thus not supported by scientific evidence. In fact, the CDC statements are contradicted by a large, consistent and growing body of scientific evidence, including:

1) studies showing neurotoxic and neuroinflammatory effects (e.g. microglial activation) from dosages of aluminum adjuvants lower than or approximately equal to dosages received by infants according to the CDC vaccine schedule (Crepeaux 2017, Petrik 2007, Shaw 2013, Shaw 2009);

2) studies linking vaccines to immune activation brain injury (Zerbo 2016, Li 2015);

3) studies showing that early-life immune activation is a causal factor in autism and other neurodevelopmental disorders and mental illnesses (e.g. schizophrenia) (Meyer 2009, Deverman 2009, Estes 2016, Kneusel 2014, Careaga 2017, Meyer 2014).

The accumulating evidence indicates that vaccine-induced immune activation, and aluminum adjuvants in particular, may cause mental illnesses and neurodevelopmental disorders, including autism.

In this paper, we present scientific evidence that aluminum adjuvants can cause autism and other brain injuries. Also, we explain why the studies allegedly supporting the safety of aluminum adjuvants do not show safety for adverse neurological outcomes.

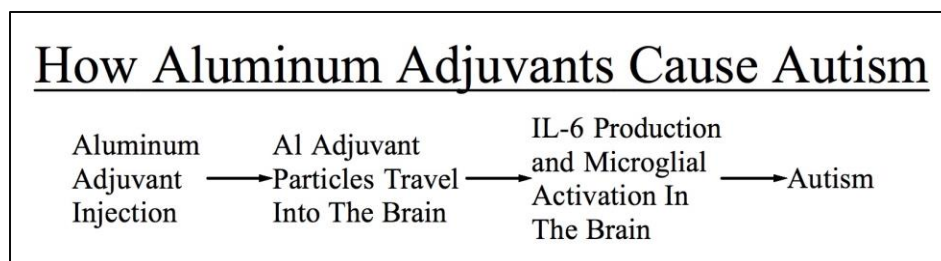


Fig 1: Proposed mechanism for how aluminum adjuvants cause autism. Each step is supported by replicated scientific studies.

Immune Activation: A Cause of Autism and Mental Illness

The term “immune activation” describes the activation of the cellular components of the immune system. The developing brain can be injured by immune activation, with life-long consequences (Meyer 2009, Deverman 2009, Estes 2016, Kneusel 2014, Careaga 2017, Meyer 2014). Immune activation injury is linked to autism, schizophrenia, depression and other mental illnesses or neurodevelopmental disorders. Immune activation effects on the brain are mediated by immune system signaling molecules, especially cytokines (Estes 2016, Meyer 2014, Smith 2007, Choi 2016, Pineda 2013).

It is generally accepted that immune activation (e.g., from infection) during pregnancy is a risk factor for autism and schizophrenia in the offspring (Ciaranello 1995, Atladottir 2010, Brown 2012). The intensity and duration of immune activation and cytokine expression appear to be important factors influencing autism risk (Meyer 2014). Intense immune activation is associated with greater risk of autism (Careaga 2017, Atladottir 2010). Chronic inflammation is associated with greater risk of autism (Jones 2016, Zerbo 2014). However, there is no evidence that short-duration, low-intensity

immune activation resulting from common childhood illnesses increase autism risk. Timing of immune activation in relation to stages of brain development is also an important factor (Meyer 2006, Meyer 2009).

Animal experiments have tested the effects of immune activation during pregnancy and postnatally on the development of offspring (Meyer 2009, Deverman 2009, Estes 2016, Kneusel 2014, Careaga 2017, Meyer 2014). In these experiments, pregnant animals (mice, rats and monkeys) or neonates are injected with a non-infectious immune activating substance such as “poly-IC” (which mimics a viral infection) or lipopolysaccharide (LPS, which mimics a bacterial infection). These substances cause immune system activation without infection. They induce fever and cytokine production and can have substantial effects on brain development if activation is sufficiently intense or prolonged and if exposure occurs during vulnerable developmental stages.

Immune activation has been demonstrated in mice to cause the three core behavioral symptoms of autism: decreased socialization and communication, and increased repetitive behaviors (Malkova 2012). Immune activation has also been shown to cause neuropathology (Weir 2015) and behavioral abnormalities in monkeys that resemble behaviors in human schizophrenia and autism (Bauman 2014, Machado 2015). See Fig. 2.

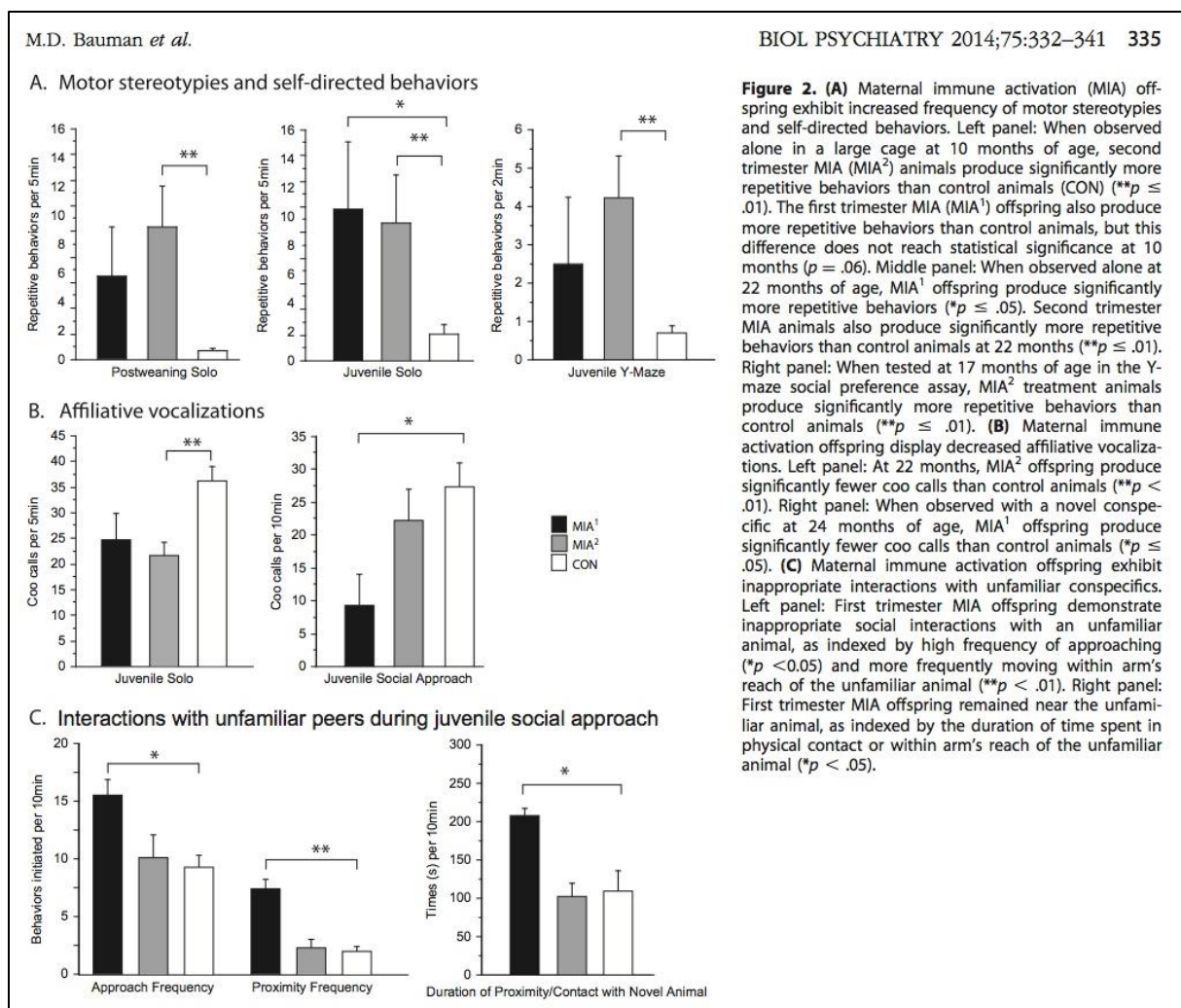


Fig 2: Maternal immune activation in monkeys caused behavioral abnormalities in juvenile offspring resembling behaviors in both autism and schizophrenia. MIA₁ (Black)= first trimester immune activation; MIA₂ (grey) 2nd trimester immune activation; CON (white) saline control. From Bauman et al. 2014

Immune activation also causes non-behavioral effects associated with human autism (citations here link immune activation with these effects):

- 1) reduction in Purkinje cells (Shi 2009);
- 2) mitochondrial dysfunction (Giulivi 2013);
- 3) increase in brain volume (from IL-6 exposure, Wei 2012(b)) and neuron density in the brain (Smith 2012);
- 4) long term chronic brain inflammation (Garay 2012); and
- 5) microbiome disruption (dysbiosis) (Hsiao 2013).

These non-behavioral similarities further support the relevance of the immune activation models to human autism. The non-behavioral (e.g., physiological) effects of immune activation have been reviewed (Labouesse 2015).

The cytokines interleukin-6 (IL-6) and interleukin-17a (IL-17) have been identified as mediating the behavioral effects of immune activation (Smith 2007, Malkova 2012, Choi 2016, Pineda 2013, Wei 2012(a), Wei 2013, Parker-Athill 2010, Wei 2016). The IL-6 findings have been replicated by different researchers using a variety of experimental methods. For example, in an experiment with

poly-IC, abnormal behavior is almost completely prevented by simultaneous administration of IL-6-blocking antibody (Smith 2007, Pineda 2013). Injection of IL-6 by itself causes abnormal behavior that closely matches behavior resulting from poly-IC immune activation (Smith 2007). Inhibition of IL-6 signaling in a genetic autism model (BTBR mice) normalized social and repetitive behavior (Wei 2016). These results demonstrate that IL-6 is responsible for causing abnormal autism-like behavior.

The Patterson laboratory at CalTech was the first to report that IL-6 is responsible for causing the autism-like behavioral effects of immune activation (Smith 2007). Two papers from this research group state:

“IL-6 is central to the process by which maternal immune activation causes long-term behavioral alterations in the offspring.” (Smith 2007)

“...blocking IL-6 prevents >90% of the changes seen in offspring of poly(I:C)-injected females, showing that gene expression changes, as well as behavioral changes, are normalized by eliminating IL-6 from the maternal immune response.” (Smith 2007)

“IL-6 is necessary and sufficient to mediate these effects since the effects...are prevented by injection of pregnant mice with poly-IC combined with an anti-IL-6 antibody, and are mimicked by a single maternal injection of IL-6.” (Garay 2013)

Brain exposure to elevated IL-6 by engineered virus showed that IL-6 exposure, initiated after birth, caused autism-like behaviors (Wei 2012(a)). The Wei 2012(a) paper states:

“We demonstrated that IL-6 is an important mediator of autism-like behaviors. Mice with an elevated IL-6 in brain developed autism-like behaviors, including impaired cognition ability, deficits in learning,

abnormal anxiety-like trait and habituation, as well as a decreased social interaction initiated at later stages. These findings suggest that an IL-6 elevation in the brain could modulate certain pathological alterations and contribute to the development of autism.” (Wei 2012(a))

More recent evidence shows that IL-17 acts downstream of IL-6 to cause autism-like behavioral abnormalities and atypical cortical development in mice (Choi 2016). Blocking either IL-6 or IL-17 prevents the autism-like behavior; an injection of IL-17 by itself causes the autism-like behavior (Choi 2016). IL-6 is known to induce IL-17 by promoting the development of Th17 cells which produce IL-17.

Immune activation animal models appear to be valid models for human neurological/psychiatric disorders, including autism (Estes 2016, Careaga 2017, Meyer 2014). The Estes 2016 review argues for the validity of the immune activation models to humans:

“These MIA (maternal immune activation) animal models meet all of the criteria required for validity for a disease model: They mimic a known disease-related risk factor (construct validity), they exhibit a wide range of disease-related symptoms (face validity), and they can be used to predict the efficacy of treatments (predictive validity).” (Estes 2016)

Evidence suggests a mediating role for IL-6 and IL-17 in human autism. For example, IL-6 is significantly elevated in the cerebellum in human autism (Wei 2011) and is highly elevated in some brain regions of some autistic individuals (Vargas 2005). Treatment of human autistics with the anti-inflammatory flavonoid luteolin improves autistic behaviors in the individuals that also experience a decline in IL-6 blood levels (Tsiloni 2015). This result is consistent with a causal role for IL-6 in human autism. Also, IL-17 is elevated in human autism (Akintunde 2015, Al-Ayadhi

2012, Suzuki 2011). Vitamin D reduces IL-17 production (Bruce 2011, Wobke 2014, Drozdenko 2014) and improves autistic behaviors in humans (Saad 2016, Jia 2015). The vitamin D findings are consistent with a causal role for IL-17 in human autism.

IL-6 functioning appears to be similar or identical in mice and humans. No mouse-human differences in IL-6 functioning are described in a 2004 review (Mestas 2004). IL-6 functioning is quite conserved across species (Brown 2014). Central nervous system development in rodents and humans is governed by the same principles (Brown 2014). Hence, the fact that IL-6 causes autism-like behavioral abnormalities in animal models deserves a presumption of validity to humans.

Immune activation is a risk factor for autism, schizophrenia and other neurological/psychiatric disorders. The cytokines IL-6 and IL-17 are responsible for mediating the autism-like behavioral effects of immune activation in the animal models. The available evidence supports a causal role for IL-6 and IL-17 in human autism.

Maternal vs. Postnatal Immune Activation

The timing of immune activation is an important factor influencing effects on the brain. The developing brain is vulnerable to immune activation injury; the mature, adult brain is apparently not nearly as vulnerable. Sensitivity to immune activation likely declines as the brain matures (Meyer 2014, Meyer 2007).

In most immune activation experiments, the offspring are exposed to immune activation during gestation (by stimulating the maternal immune system). In

contrast, most vaccines are administered postnatally. This raises the question of whether postnatal immune activation can have similar effects on the brain as maternal immune activation. Diverse evidence indicates that the brain can be adversely affected by postnatal immune activation. Postnatal immune activation experiments, human case reports, and consideration of brain development timelines suggest that the human brain is vulnerable to immune activation injury for years after birth.

In the maternal immune activation experiments, inflammatory signaling and some cytokines (e.g. IL-6) traverse the placenta into the fetus. Consequently, immune activation in the mother causes immune activation and elevated cytokines in the fetus, and in the fetal brain (Oskvig 2012, Ghiani 2011).

Postnatal immune activation can have adverse neurological effects, including increased seizure susceptibility (Chen 2013, Galic 2008), learning and memory deficits (Harre 2008), and an increase in excitatory synapse formation (Shen 2016). Seizure disorders, learning and memory dysfunction, and elevated excitatory signaling are associated with autism.

Elevated IL-6 in the brain in the postnatal period causes neuronal circuitry imbalance and mediates autism-like behaviors in mice (Wei 2012(a)). The circuitry imbalance observed in Wei 2012(a) was an excess of excitatory synapses and a deficit of inhibitory synapses. See Fig. 3. Excessive excitatory signaling is observed in human autism (Robertson 2016, Freyberg 2015). In fact, an imbalance between excitatory and inhibitory signaling (towards excess excitation) has been posited as a central characteristic of autism (Robertson 2016, Freyberg 2015).

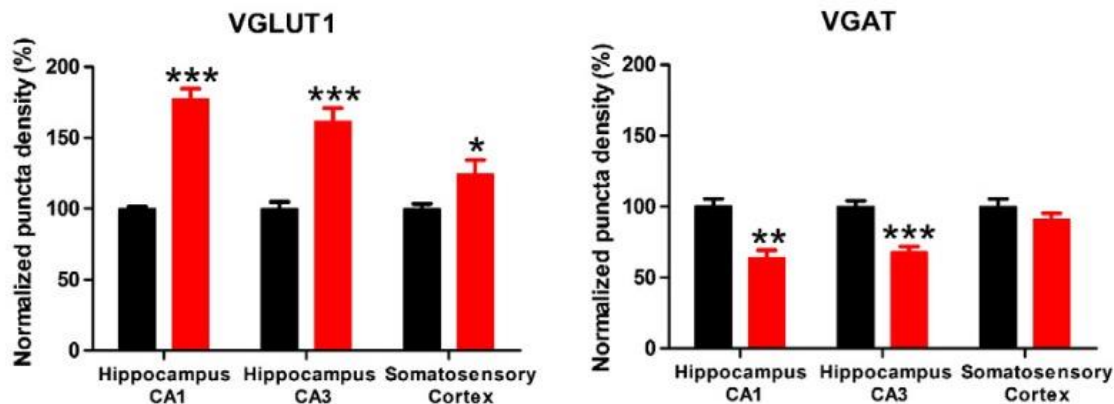


Fig 3: Elevation of IL-6 in the brains of mice (initiated shortly after birth) caused an increase in excitatory synapses (VGLUT1) and a decrease in inhibitory synapses (VGAT). Excessive excitatory signaling is observed in human autism. Red=Elevated IL-6; Black=Control. VGLUT1=excitatory synapses; VGAT=inhibitory synapses. *P<0.05, **P<0.01 and *P<0.001. Adapted from Wei et al 2012(a).**

In a maternal immune activation experiment with mice (Coiro 2015), autism-relevant behavior and dendritic spine abnormalities (relevant to autism and schizophrenia) were ameliorated by administering an anti-inflammatory drug postnatally. The drug was started at birth and continued for 2 weeks, which roughly corresponds to age 2 in humans (Semple 2013). This result indicates that brain development is affected by postnatal inflammation, at times corresponding to when vaccines are given to humans.

Several case reports describe previously-healthy children that displayed sudden-onset autistic behavior during or subsequent to infection in the brain. All the cases had signs of intense brain inflammation. Here are brief descriptions:

Delong 1981: describes 3 children, ages 5, 7 and 11 with full-blown autistic behavior associated with brain inflammation. Brain inflammation was presumed in two cases and confirmed in one. The 5 and 7 year olds recovered completely, and the 11-year recovered partially.

Marques 2014: describes a previously healthy 32-month-old girl that

suffered autistic regression from a viral central nervous system infection with associated brain inflammation.

Ghaziuddin 2002: describes a previously healthy 11-year-old boy that suffered permanent autistic regression after sudden onset herpes brain infection with associated brain inflammation.

Gillberg 1986: describes a previously healthy 14-year-old girl with permanent autistic regression from herpes brain infection with associated brain inflammation.

The most parsimonious explanation for these cases is that autistic behavior resulted from intense inflammation and cytokine production in the brain. Accordingly, these cases indicate that the human brain remains vulnerable to immune activation injury well into childhood, though the vulnerability almost certainly decreases with maturation. The susceptibility of older children to inflammation-induced autistic behavior strongly suggests that younger infants, of 0-2 years of age, are also vulnerable. It is not reasonable to claim, and there is no evidence to suggest, that the age range of 0-2 years (when most vaccines are given) is uniquely resistant to immune activation

injury. All the available evidence indicates the opposite.

The immune activation experiments and case reports are consistent and indicate that immune activation and elevated cytokines in the postnatal period can cause brain injury.

The next critical question to consider is whether vaccines can cause immune activation and elevated cytokines in the brain.

Postnatal Vaccination Affects Brain Development in Animal Model

The first study to test the effect of postnatal vaccination on brain development was published in 2015 (Li 2015). In this

experiment, neonatal rats were administered bacillus calmette-guerin (BCG) vaccine, hepatitis B (HBV) vaccine or a combination (BCG+HBV) timed to imitate human infant vaccination schedules. BCG and HBV vaccines produced opposite effects on the brain. Specifically, BCG enhanced synaptic plasticity and long-term potentiation (LTP, the basis for learning and memory); HBV inhibited synaptic plasticity and LTP. BCG and HBV vaccines also caused opposite changes in some synapse protein levels.

HBV vaccine (but not BCG vaccine) increased IL-6 gene expression in the brain; increased gene expression likely indicates an elevation in brain IL-6. The HBV vaccine contains aluminum adjuvant, and the BCG does not contain aluminum adjuvant. Hence, the aluminum adjuvant may be the ingredient responsible for the elevated IL-6 gene expression. See Fig. 4.

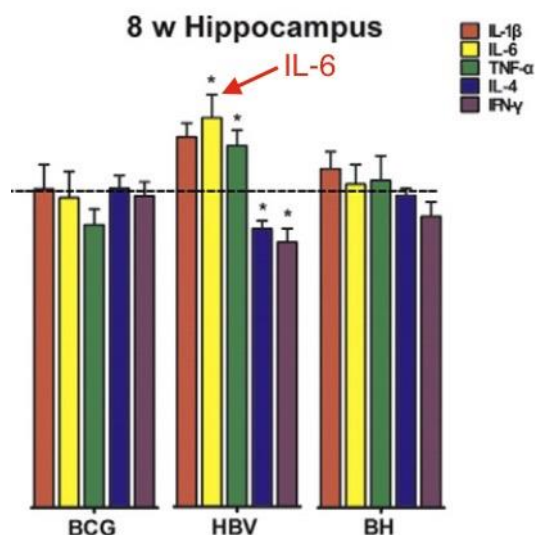


Fig. 4: Hepatitis B vaccine, but not BCG vaccine, increased IL-6 gene expression in the brain at 8 weeks after neonatal vaccination. Hepatitis B vaccine contains aluminum adjuvant; BCG vaccine does not. Elevated IL-6 causes autism-like behaviors in animal models. *P<0.05 Adapted from Li et al 2015.

The Li et al study showed that the vaccines caused other changes in the brain, including 1) changes in long-term potentiation (LTP) (Hep B decreased LTP), 2) changes in dendritic spines, and 3) changes in synapse protein expression. Changes in synapse

proteins and dendritic spines have been observed in human brain disorders.

Li et al. attribute the brain effects to changes in cytokine levels and immune polarization (Th1/Th2 polarization) induced by the vaccines. Aluminum adjuvants cause

Th2 polarization. Li et al. state that the results suggest vaccines can interact by way of immune activation effects:

“...our data suggested that combinations of different vaccines can mutually interact (enhance or counteract). The mechanism of synaptic plasticity modulation through neonatal BCG/HBV vaccination may be via systemic Th1/Th2 bias accompanied by a specific profile of cytokines and neurotrophins in the brain.” (Li 2015)

Li 2015 demonstrates that vaccines affect brain development by an immune activation mechanism. Further, since aluminum adjuvants induce Th2 activation and long term Th2 polarization, the Li 2015 results suggest that all aluminum-adjuvanted vaccines may cause adverse effects similar to the HBV vaccine. Accordingly, the Li 2015 results suggest that studies showing that immune activation causes neurological/psychiatric disorders are relevant to vaccine adverse effects.

Vaccines Are Given During Synaptogenesis

Another way to answer the question of brain vulnerability to immune activation is to consider the types of brain development processes occurring when vaccines are administered. Vaccines are given primarily in the first 18 months after birth. The human brain undergoes intense and rapid development during this period. Synaptogenesis (formation of synapse connections between neurons) is especially intense in this period.

The vulnerability of the developing brain to immune activation is apparently related to the specific types of brain development processes occurring (Tau 2010, Meyer 2006, Meyer 2007). Such processes include migration (movement of neurons to

final locations in the brain), adhesion (formation of chemical-mechanical attachments between brain cells), and synaptogenesis (formation of synapse connections between neurons), among others (neurogenesis, gliogenesis, myelination etc).

Cytokines affect brain development processes. For example, elevated IL-6 affects migration, adhesion and synaptogenesis (Wei 2011). Elevated IL-6 in the postnatal period promotes an excess of excitatory synapses and a deficit of inhibitory synapses, and mediates autism-like behaviors (Wei 2012(a)).

In humans, a dramatic increase in synaptogenesis begins around the time of birth, and continues until about age 3 (Huttenlocher 1997, Tau 2010, Stiles 2010, Semple 2013). Vaccines are administered during this intense synaptogenesis. See Figs. 5-6. Elevated brain IL-6 induced by vaccination during synaptogenesis may cause an excitatory-inhibitory imbalance, towards excitation. An excitatory imbalance has been observed in human autism (Robertson 2016, Freyberg 2015).

Synaptogenesis tapers off through childhood and adolescence. This fact may explain why some older children and teens can suffer autistic regression after intense brain inflammation, but apparently become less vulnerable to immune activation brain injury with age.

Intense synaptogenesis occurs at ages 0-18 months, when many vaccines are administered. Consequently, vaccines may adversely impact synaptogenesis if they induce inflammation or IL-6 in the brain.

The timing of brain development processes in humans supports the idea that the human brain is vulnerable to immune activation and cytokines in the first few years after birth, when vaccines are administered. Disruption of synaptogenesis by vaccine-induced immune activation is a particular concern.

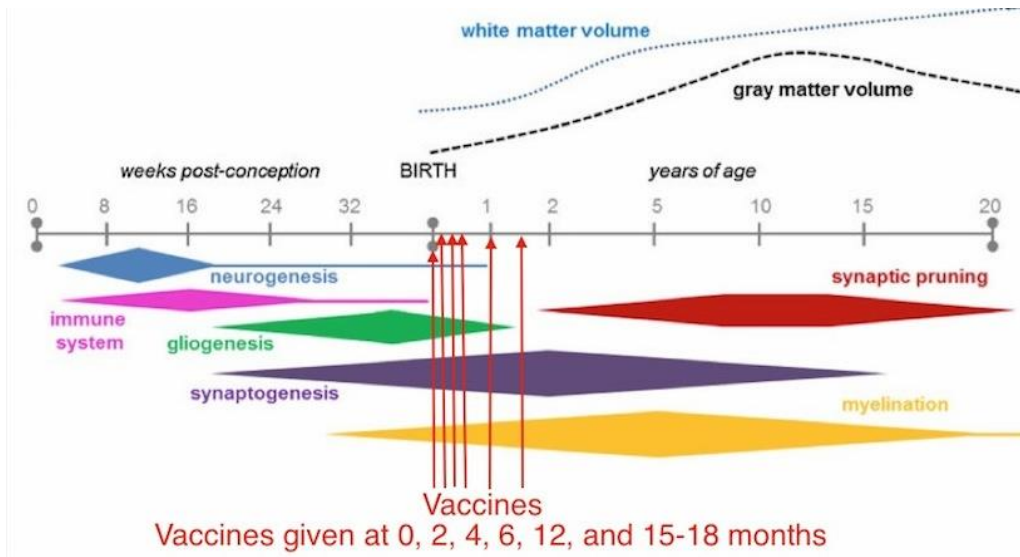


Fig. 5: Timeline of specific brain developmental processes in humans. Synaptogenesis is most intense during the first couple years of life, when vaccines are administered. Timing of vaccination according to the CDC vaccine schedule is shown. Elevated IL-6 during synaptogenesis may cause an excitatory-inhibitory synapse imbalance, towards excitation. Adapted from Semple 2013.

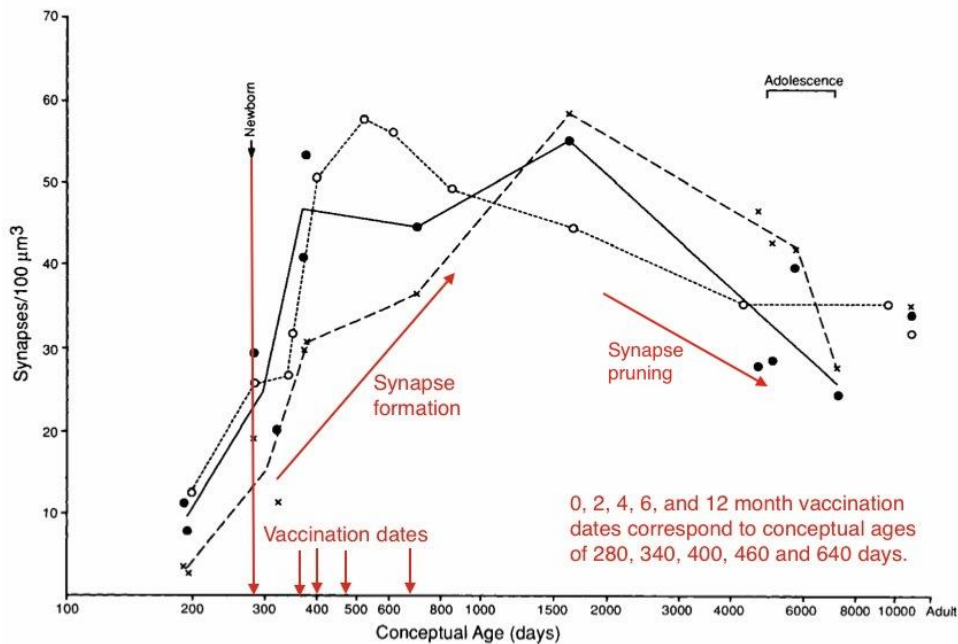


Fig. 2. Mean synaptic density in synapses/100 μm³ in auditory, calcarine, and prefrontal cortex at various ages. Open circles, visual cortex (area 17); filled circles, auditory cortex; x, prefrontal cortex (middle frontal gyrus).

Fig. 6: Measurements of synapse density in human cadavers of various ages indicate a dramatic increase in synapses in the first few years of life. Vaccines are administered during intense synapse formation. Elevated IL-6 during synaptogenesis may cause an excitatory-inhibitory synapse imbalance, towards excitation. Image adapted from Huttenlocher and Dabholkar 1997.

Aluminum Adjuvants: Neurotoxic At Vaccine Dosages

Aluminum (Al) adjuvants have an essential role in many vaccines: to stimulate immune activation. Without Al adjuvants, these vaccines would have greatly reduced efficacy.

Aluminum adjuvants comprise sub-micron particles (primary particles) of aluminum compounds, typically $\text{Al}(\text{OH})_3$, AlPO_4 , Al_2SO_4 or mixtures. The primary particles are typically agglomerated into larger particles with sizes of about 2-20 microns (Harris 2012). The Al adjuvant materials have low solubility in water and body fluids. Al adjuvant particles are biopersistent and can remain in the body for months or years (Flarend 1997, Khan 2013, Gherardi 2001).

Aluminum ingested in the diet has low oral absorption (about 0.3%), is rapidly excreted by the kidneys, is (mostly) excluded from the brain by the blood-brain barrier, and is in a solubilized, Al^{3+} ionic form (not particulate). These defenses are adequate for protecting the brain from natural levels of aluminum exposure. These protective mechanisms are unable to protect the brain from injected aluminum adjuvant particles. Al adjuvant particles are too large to be removed by the kidneys, and are carried across the blood-brain barrier by macrophages.

Dosages of aluminum adjuvants received by infants according to the CDC vaccination schedule are:

Birth (Hep B):

74 mcg/kg (250 mcg for 3.4 kg infant)

2 month:

245 mcg/kg (1225 mcg for 5 kg infant)

4 month:

150 mcg/kg (975 mcg for 6.5 kg infant)

6 month:

153 mcg/kg (1225 mcg for 8 kg infant)

These are maximum-possible dosages (because different vaccine products have different amounts) for average-weight infants.

Accumulating evidence shows that aluminum adjuvants have adverse neurological effects at dosages lower than or approximately equal to dosages infants receive from vaccines. These effects appear to depend on the particulate nature and biopersistence of the aluminum adjuvant. Injected Al adjuvant has adverse effects that are apparently mediated by the particles and independent of solubilized Al^{3+} ions released by the slowly dissolving particles (Crepeaux 2017).

Al adjuvant injections in mice cause adverse effects at vaccine-relevant dosages of 100, 200, 300 and 550 mcg/Kg body weight (Crepeaux 2017, Shaw 2009, Petrik 2007, Shaw 2013). These include deficits in learning and memory (Shaw 2009), deficits in neuromuscular strength/function (Petrik 2007), and changes in locomotor activity and/or gait (Shaw 2009, Shaw 2013). Autism is associated with gait and movement abnormalities (Kindregan 2015) and memory dysfunction (Williams 2006).

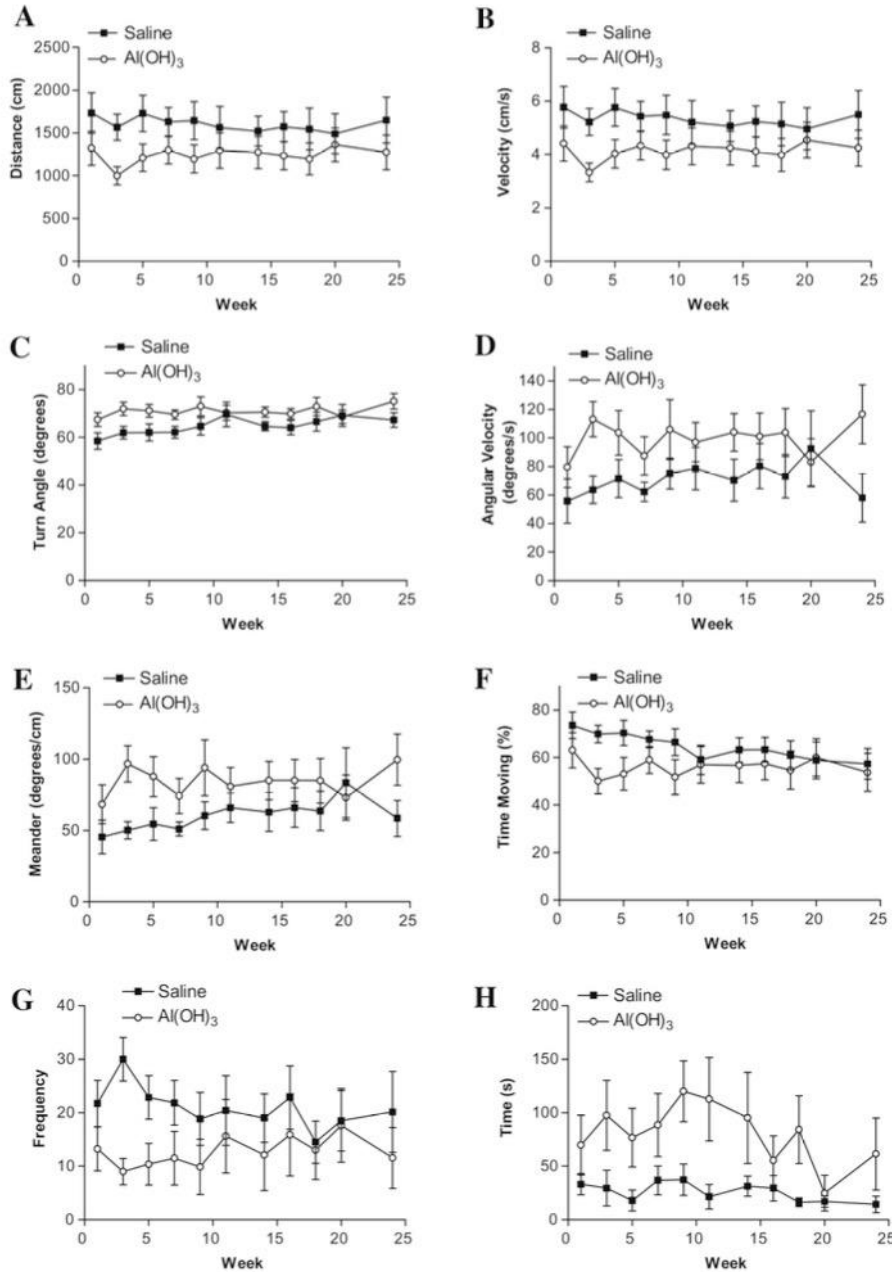


Fig. 4. Open field movement analysis as an assessment of spontaneous activity and anxiety in control mice vs. mice injected six times with aluminum hydroxide. Aluminum hydroxide injected mice showed the following behavioural changes: (A) Shorter distances moved ($***p < 0.0001$). (B) Slower movement ($***p < 0.0001$). (C) Greater mean turn angle ($***p < 0.0001$). (D) More rapid turning ($***p < 0.0001$). (E) Greater meander ($***p < 0.0001$). (F) Smaller percentage of time in overall movement ($**p = 0.0030$). (G) Fewer entries into the centre of the open field ($***p < 0.001$). Late entry into centre ($***p < 0.0001$). (All measures, two-way ANOVA).

Fig. 7: Dosage of 300mcg/Kg ALOH adjuvant caused large and persistent changes in exploratory behavior and movement in open field tests. This is an indicator of neurotoxicity. Human autistics also display abnormal movement and exploratory behavior. Adapted from Shaw and Petrik 2009.

Al adjuvant dosages of 200mcg/Kg (as 3 x 66mcg/Kg) (Crepeaux 2017) and 300mcg/Kg (as 6 x 50mcg/Kg) (Shaw 2009) increased microglial activation in the ventral forebrain and lumbar spinal cord, respectively. The elevated microglial activation was measured about 6 months after Al adjuvant injection, which suggests that the

microglial activation is chronic. Activated microglia indicate an ongoing inflammatory process and suggest the presence of elevated cytokines. Human autistics have activated microglia and elevated cytokines throughout the brain (Vargas 2005, Suzuki 2013, Li 2009).

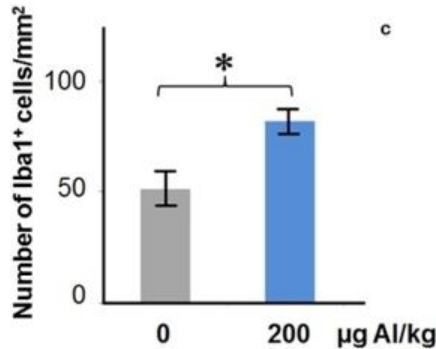


Fig. 8: Al adjuvant (200mcg/Kg) caused an increase in microglial activation in the brain of mice. The protein iba1 indicates activated microglia. Measurements were performed 6 months after Al adjuvant injection, indicating that the microglial activation is a chronic condition. * P<0.05. From Crepeaux et al., 2017.

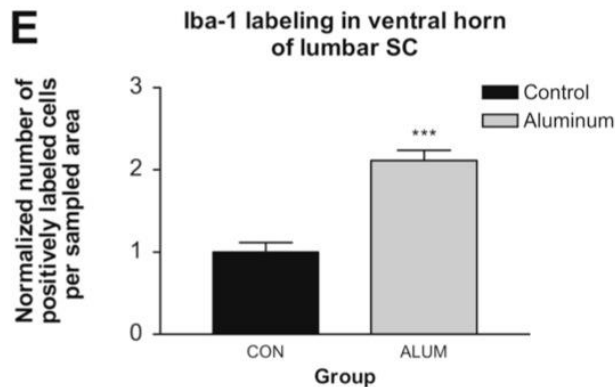


Fig. 9: Al adjuvant (300mcg/Kg) caused an increase in microglial activation in the lumbar spinal cord of mice. The protein iba1 indicates activated microglia. Measurements were performed 6 months after Al adjuvant injection, indicating that the microglial activation is a chronic condition. *p < 0.001, one-way ANOVA. From Shaw and Petrik 2009.**

Activated microglia are implicated as a causal factor in autism, because microglia mediate inflammation in the brain. Microglia can produce IL-6 when in an activated state. A recent review on microglia and autism (Takano 2015) states:

“...any factors that alter the number or activation state of microglia either in utero or during the early postnatal period can profoundly affect neural development, thus resulting in neurodevelopmental disorders, including autism.” (Takano 2015)

Microglia appear to play an important role in the causation of autism (Takano 2015, Kneusel 2014). Hence, the microglial activation caused by aluminum adjuvants suggests a role in autism.

Several studies show that Al adjuvants increase brain aluminum content (Crepeaux 2017, Flarend 1997, Shaw 2009, Khan 2013, Crepeaux 2015). A dosage of 200 mcg/Kg Al adjuvant caused a 50-fold increase in brain aluminum content in mice, from 0.02 ug/g to 1.00 ug/g dry weight of brain (Crepeaux 2017). These measurements were performed 6

months after the final injection, indicating that the Al persists in the brain long-term (Crepeaux 2017). See Fig. 10. Al adjuvants have been found to accumulate in the brain of mice up to one year after injection (Khan 2013). Crepeaux 2015 demonstrated persistence and increasing accumulation of Al adjuvant particles up to 270 days in spleen and lymph nodes of mice. Increasing accumulation of Al in distant organs over time suggests that toxic effects may increase with time, and may be delayed by months or years after exposure.

The 400 and 800 mcg/Kg doses used in the Crepeaux 2017 study did not cause adverse effects or elevated brain aluminum. The authors attribute this surprising inverted dose-response relationship to granulomas induced by the higher dosages. Granulomas trap the Al adjuvant at the injection site, thereby preventing its transport into the brain and other sensitive tissues. Granulomas occur after about 1% of vaccinations (Bergfors 2014). This is cause for concern because it indicates that, for 99% of vaccinations, the Al adjuvant can be transported around the body. It is not confined to a granuloma. See Fig. 11.

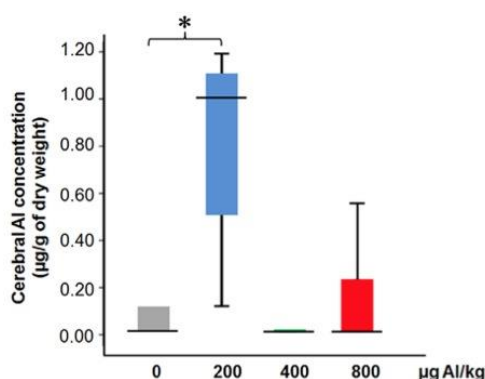


Fig. 10: Dosage of 200 mcg/Kg Al adjuvant caused a 50-fold increase in brain aluminum content, from 0.02 to 1.00 ug/g dry weight, in mice. Higher dosages (400 and 800 mcg/Kg) did not increase brain Al content, presumably because the higher dosages caused a granuloma at the injection site. A granuloma traps the Al adjuvant at the injection site, thereby preventing systemic dispersal and transport into the brain. These measurements were performed 6 months after the final injection, indicating that the Al persists in the brain long-term. *P<0.05. From Crepeaux et al., 2017.

Proposed Mechanism For Inverse Dose-Toxicity Relationship:

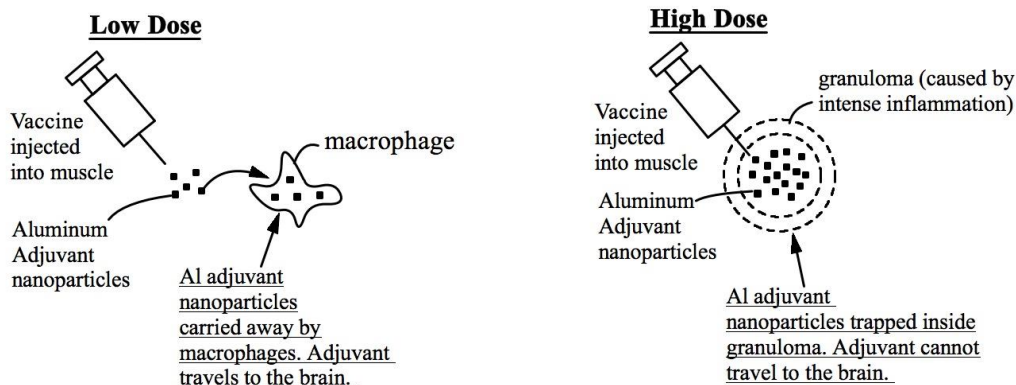


Fig. 11: High dose Al adjuvant injection into the muscle causes a granuloma, which traps the Al adjuvant and prevents it from traveling into the brain. Low dose does not form a granuloma. Hence, the lower dose is free to travel to the brain. Consequently, the lower dose is more toxic than the higher dose. This mechanism explains the surprising inverted dose-toxicity results of Crepeaux et al. 2017.

Particle Transport and Macrophage Chemotactic Protein (MCP-1)

Aluminum adjuvants travel into the brain (Khan 2013, Crepeaux 2015, Crepeaux 2017, Shaw 2009, Flarend 1997). Al adjuvant particles are carried through the blood-brain barrier and into the brain by macrophages (Khan 2013). Transport is promoted by macrophage chemotactic protein-1 (MCP-1) (Khan 2013). MCP-1 causes macrophages to travel around the body and into the brain. Particle transport into the brain by macrophages is well-established and has been investigated for therapeutic applications (Choi 2012, Pang 2016).

MCP-1 is elevated in the brains of human autistics (Vargas 2005) and is elevated in the blood of neonates later diagnosed with autism (Zerbo 2014). This suggests that neonates with high MCP-1 will experience elevated Al adjuvant transport into the brain when injected with Al adjuvanted vaccines. This is consistent with Al adjuvants causing autism by inducing immune activation and elevated cytokines in the brain.

Aluminum Induces IL-6 Expression In The Brain

Water-soluble aluminum salts (e.g. AlCl_3 , Al lactate) induce elevated IL-6 in the brain and other tissues. In fact, aluminum appears to selectively induce IL-6 (Viezeliene 2013). Studies of aluminum exposure and IL-6 expression in the brain include:

Cao 2016: Ingestion of 30 or 90 mg/kg/day aluminum (as AlCl_3) for 90 days significantly increased gene expression of IL-6 and other cytokines in the brain (hippocampus).

Alawdi 2016: Ingestion of 3.4 mg/kg/day aluminum (as AlCl_3) for 6 weeks caused a 4-fold increase in IL-6 in the brain (hippocampus). This dosage is far lower than the outdated “no observed adverse effects level” (NOAEL) oral dosages (26 and 62 mg/kg/day) used as benchmarks for toxicity threshold (Mitkus 2011, Offit 2003).

In fact, other experiments show that oral dosages of 3.4, 4, 5.6, 6, and 20.2

mg/Kg/day aluminum cause numerous adverse effects in mice or rats and hence the NOAEL for orally ingested Al is currently unknown (Alawdi 2016, Dera 2016, Sethi 2008, Sethi 2009, Bilkei-Gorzo 1993).

The induction of IL-6 may occur because aluminum strongly induces oxidative stress (Exley 2003). Oxidative stress induces IL-6 expression (Viezeliene 2013).

CDC Website Cites Fatally Flawed Study Of Al Adjuvants (Mitkus 2011)

Dosages of Al adjuvants received by infants increased dramatically as the vaccine schedule was expanded in the 1980s and 1990s. However, as the vaccine schedule expanded, the increasing dosages of Al adjuvants were not tested for safety. Government agencies (HHS, NIH, CDC, FDA) have not pursued any new experimental work on Al adjuvant toxicity.

To support the safety of Al adjuvants at today's higher dosages, the CDC cites a 2011 FDA study of aluminum exposure from vaccines (Mitkus 2011). This study is the only scientific evidence cited by the CDC and FDA websites to support the safety of Al adjuvants.

The Mitkus 2011 study is a theoretical modeling study of Al adjuvant kinetics; it contains no new data concerning Al adjuvant toxicity (from animal models or epidemiology). Mitkus 2011 calculates a body burden of aluminum resulting from the slow dissolution of Al adjuvant particles, and compares the dissolved-aluminum body burden to a "minimal risk level" (MRL). The MRL is derived from a study of ingested Al toxicity in mice (Golub 2001). The Golub 2001 study provides the NOAEL (26 mg/kg/day ingested), which is converted into the MRL for human infants (based on 1mg/kg/day ingested) by using a safety factor of about 30.

The Mitkus study is fatally flawed for these reasons:

1) MITKUS ASSUMES AL ADJUVANT PARTICLES ARE HARMLESS

Mitkus makes an unstated assumption that Al adjuvants have zero toxicity while in particulate form. Mitkus only considers the potential toxicity of aluminum ions (Al³⁺) released by the slowly-dissolving Al adjuvant particles.

Al adjuvants comprise low-solubility and biologically-persistent microscopic particles. The Mitkus analysis assumes that the particles are absolutely nontoxic and perfectly harmless, even when present in the brain and other organs. Mitkus provides no justification for this unstated assumption. Further, the assumption is contradicted by recent findings on Al adjuvant toxicity (Crepeaux 2017) and particulate toxicity generally. Particles can have toxic effects mediated by surface chemistry (e.g. surface charge and surface catalytic activity) and particle shape, among other characteristics of solid particles (Sharifi 2012, Podila 2013).

Several studies show injected Al adjuvants cause behavioral abnormalities, abnormal weight gain, learning and memory impairment, motor neuron death/apoptosis, neuromuscular strength deficits, chronic microglial activation/brain inflammation, and large (e.g. 50X) increases in brain and spinal cord aluminum content (Petrik 2007, Shaw 2009, Shaw 2013, Crepeaux 2017). These adverse effects occur at dosages less than or approximately equal to dosages received by infants according to the CDC vaccine schedule.

2) NEW RESEARCH SHOWS INGESTED AL HARMFUL AT DOSAGES LOWER THAN 26 MG/KG/DAY

Mitkus assumes that Al adjuvant toxicity is mediated exclusively by solubilized Al (Al³⁺ ions) released by the slowly-dissolving Al adjuvant particles. To establish a threshold toxicity level from the solubilized Al, Mitkus relies on a mouse feeding study (Golub 2001) reporting a "no-observed adverse effects level" (NOAEL) oral dosage of 26 mg/Kg/day ingested aluminum. Mitkus

used a 30X safety factor for applying this dosage to humans, which is reasonable.

However, other experiments show that much lower oral dosages of 3.4, 4, 5.6, 6, and 20.2 mg/Kg/day aluminum cause adverse effects in mice or rats (Alawdi 2016, Dera 2016, Sethi 2008, Sethi 2009, Bilkei-Gorzo 1993). The adverse effects include chronic brain inflammation, learning and memory impairment, and kidney inflammation. So, the Mitkus analysis is wrong because 26 mg/kg/day is not a NOAEL. The “minimal risk level” (MRL) determined by Mitkus is too high by a factor of at least $26/3.4 = 7.6$. Using

a corrected NOAEL of 3.4 mg/Kg/day (based on Alawdi 2016) results in vaccine aluminum exposure exceeding the MRL for AlPO₄ adjuvant, and approximately matching the MRL for AlOH adjuvant. The new, corrected MRL lines indicate that Al phosphate adjuvant (Fig. 12) and Al hydroxide adjuvant (Fig. 13) from the CDC vaccine schedule may cause toxicity from the solubilized Al per se.

Since 3.4mg/Kg/day is not a NOAEL (adverse effects were observed at this dosage) the true NOAEL is less than 3.4/mg/Kg/day. See Figs. 12-13.

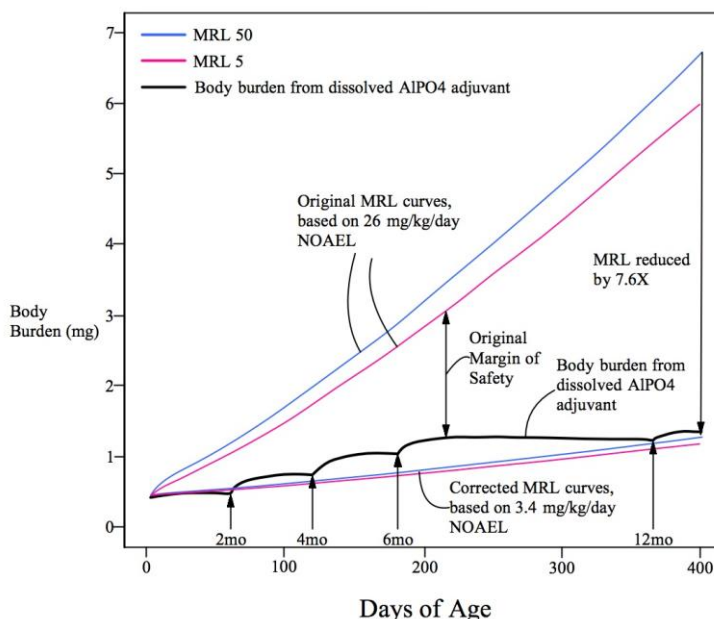


Fig. 12: Body burden vs. MRL comparison chart for Al phosphate adjuvant (AlPO₄) corrected in accordance with the new discovery (Alawdi 2016) that ingestion of 3.4 mg/kg/day Al causes adverse effects. The body burden exceeds the corrected MRL curve for almost the entire first year of life, indicating toxicity. The toxicity of Al adjuvant particles is a separate, additional issue. MRL 50 and MRL 5 refer to two different infant growth rates. Adapted from Mitkus et al., 2011.

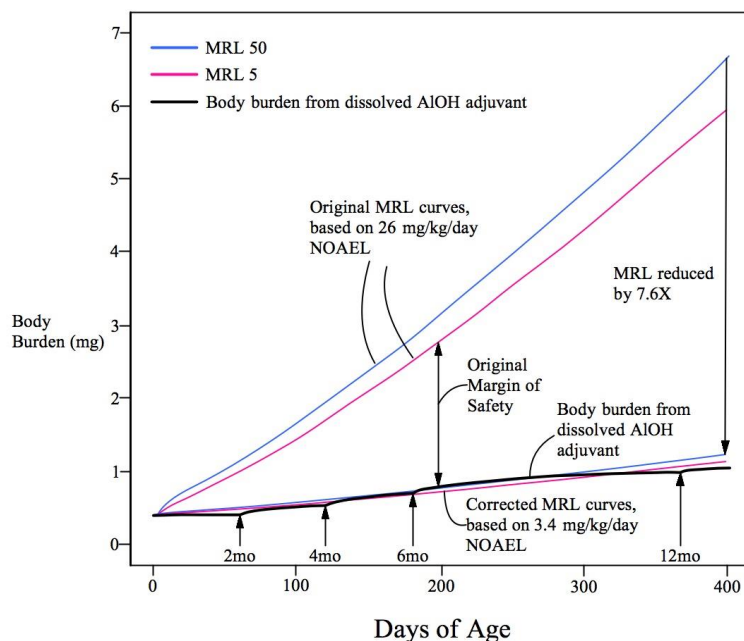


Fig. 13: Body burden vs. MRL comparison chart for Al hydroxide adjuvant (AlOH), corrected in accordance with the new discovery (Alawdi 2016) that ingestion of 3.4 mg/kg/day Al causes adverse effects. The body burden overlaps the new, corrected MRL, indicating borderline toxicity. The margin of safety is gone. MRL 50 and MRL 5 refer to two different infant growth rates. The toxicity of Al adjuvant particles is a separate, additional issue. Adapted from Mitkus et al., 2011.

3) NO AL ADJUVANT TOXICITY DATA CITED, DESPITE AVAILABILITY

Mitkus does not cite any toxicity data for injected Al adjuvants. Mitkus instead uses toxicity data for ingested, non-particulate, water-soluble Al (Golub 2001, which used Al lactate) to derive the MRL. This data comes from a single study (Golub 2001).

So, remarkably, Mitkus claims a safe level of injected Al adjuvant exposure, without citing any Al adjuvant toxicity data. The error is unnecessary and neglectful because at least two animal studies of injected Al adjuvant toxicity were available prior to the Mitkus publication in 2011 (Petrik 2007, Shaw 2009). These papers were not cited or mentioned by Mitkus 2011.

Each of these three flaws is fatal for the validity of the Mitkus study in establishing the safety of aluminum adjuvants. Hence, the CDC is completely lacking valid evidence for the

safety of Al adjuvants. This is especially true for safety regarding neurological and long-term outcomes, because other available studies of Al adjuvant safety (e.g., Jefferson 2004) do not consider (or are incapable of detecting) these outcomes.

CDC Fails To Investigate Toxicity of Al Adjuvants

The CDC has conducted no epidemiological studies on long term safety (e.g. considering neurological outcomes) of Al adjuvants. There is one ecological study of country-level data, which reported an association between Al adjuvant exposure and autism (Tomljenovic 2011). However, being an ecological study, it is highly susceptible to confounding and biases.

Dr Frank DeStefano of the CDC's Immunization Safety Office is co-author of a

feasibility study (Glanz 2015) on using the Vaccine Safety Datalink (VSD) to investigate the safety of individual vaccine ingredients. The paper focuses on Al adjuvants. It acknowledges that thimerosal is the only vaccine ingredient studied for autism or neurological safety, and that a possible association between Al adjuvants and autism has not been explored in epidemiological studies. Glanz 2015 states:

“To date, there have been no population-based studies specifically designed to evaluate associations between clinically meaningful outcomes and non-antigen ingredients, other than thimerosal.”

The CDC has not investigated Al adjuvant safety concerns, despite the accumulating scientific evidence of harm and evidence linking Al adjuvants to immune activation mechanisms of brain injury.¹

Conclusion

The science reviewed here tells a consistent and compelling story: that vaccines may cause autism by stimulating immune activation and elevated cytokines in the brain. Al adjuvants are implicated as a cause of autism because they can be transported into the brain, because they cause microglial activation at vaccine-relevant dosages, and because aluminum induces IL-6 in the brain.

In statements asserting no vaccine-autism link, the CDC cites scientific evidence that is not relevant to Al adjuvant safety or is incapable of disproving an Al adjuvant-autism link (Taylor 2014, DeStefano 2013, Mitkus 2011). In support of claims for Al adjuvant safety, the CDC relies on a profoundly flawed theoretical modelling study (Mitkus 2011). There is little scientific evidence supporting the safety of Al adjuvants, especially in relation to autism and other long term neurological outcomes.

¹ However, the Glanz paper notes that studies of aluminum adjuvants are problematic because of expected small differences in exposures in the low and high exposure groups. Glanz 2015 concludes: “...children below the 10th percentile would be exposed to between 0 mg and 3.1mg, while children above the 90th percentile would be exposed to between 4.8 mg and 5.3 mg of aluminum from vaccines. It is unclear if such differences in aluminum exposure would be biologically meaningful.” (Glanz 2015). So, epidemiological studies may not provide reliable evidence for safety or harm. Controlled, prospective human trials of aluminum adjuvant exposure from vaccines will likely be prohibited for ethical reasons. Also, Al adjuvants are essential ingredients for Al adjuvanted vaccines. Consequently, it will be

challenging to design studies of long term adverse effects of Al adjuvants in humans. Experiments in animal models can provide valuable information. Al adjuvants should be tested for effects on: 1) excitatory/inhibitory imbalance; 2) core symptoms of autism (social, communicative and repetitive/stereotyped behaviors); 3) IL-6, IL-17, and other cytokine levels in the brain; 4) other physiological abnormalities associated with autism (e.g. mitochondrial dysfunction, microbiome dysbiosis, Purkinje cell loss, cerebellum abnormalities etc); and 5) microglial activation and immune activity in the brain. Investigating these outcomes can provide valuable information concerning the safety of Al adjuvants.

References

Akintunde et al., 2015 Increased production of IL-17 in children with autism spectrum disorders and co-morbid asthma, *Journal of Neuroimmunology* 286 (2015) 33-41.

Al-Ayadhi et al., 2012 Elevated serum levels of interleukin-17A in children with autism, *Journal of Neuroinflammation* 2012, 9:158.

Alawdi et al., Neuroprotective Effect of Nanodiamond in Alzheimer's Disease Rat Model: a Pivotal Role for Modulating NF- κ B and STAT3 Signaling, *Molecular Neurobiology*, 54 (3):1906-1918.

Atladdottir et al., Maternal infection requiring hospitalization during pregnancy and autism spectrum disorders, *Journal of Autism and Developmental Disorders*, 2010 Dec;40(12):1423-1430.

Bauman et al., 2014 Activation of the Maternal Immune System During Pregnancy Alters Behavioral Development of Rhesus Monkey Offspring, *Biological Psychiatry*, 2014;75: 332–341

Bergfors et al., 2014 How common are long-lasting, intensely itching vaccination granulomas and contact allergy to aluminium induced by currently used pediatric vaccines? A prospective cohort study, *European Journal of Pediatrics*, 173:1297–1307.

Bilkei-Gorzo, 1993, Neurotoxic effect of enteral aluminum, *Food and Chemical Toxicology*, 31(5):357-361.

Brown et al., 2014 Metabolic consequences of interleukin-6 challenge in developing neurons and astroglia, *Journal of Neuroinflammation*, 11:183.

Brown et al., Epidemiologic studies of exposure to prenatal infection and risk of schizophrenia and autism, *Developmental Neurobiology*, 2012 October ; 72(10): 1272–1276.

Bruce et al., 2011 Converging pathways lead to overproduction of IL-17 in the absence of vitamin D signaling, 2011 Aug; 23(8): 519–528.

Careaga et al 2017 Maternal Immune Activation and Autism Spectrum Disorder: From Rodents to Nonhuman and Human Primates, *Biological Psychiatry*, March 1, 2017; 81:391–401.

Chen et al., Postnatal systemic inflammation exacerbates impairment of hippocampal synaptic plasticity in an animal seizure model, *Neuroimmunomodulation*, 2013;20(4):223-32.

Choi et al., 2012, Delivery of nanoparticles to brain metastases of breast cancer using a cellular Trojan horse, *Cancer Nanotechnology*, 3:47–54.

Choi et al., 2016 The maternal interleukin-17a pathway in mice promotes autismlike phenotypes in offspring, *Science*, 2016 Feb 26; 351(6276): 933–939.

Ciaranello et al. The Neurobiology of Infantile Autism, *The Neuroscientist*, 1:361-367

Coiro et al., Impaired synaptic development in a maternal immune activation mouse model of neurodevelopmental disorders, *Brain, Behavior, and Immunity*, Nov;50:249-258.

Crepeaux et al., 2015 Highly delayed systemic translocation of aluminum-based adjuvant in CD1 mice following intramuscular injections, *Journal of Inorganic Biochemistry*, 152:199-205.

Crepeaux et al., 2017 Non-linear dose-response of aluminium hydroxide adjuvant particles: Selective low dose neurotoxicity, *Toxicology*, 375 (2017) 48–57.

DeLong et al., 1981 Acquired reversible autistic syndrome in acute encephalopathic illness in children, *Archives of Neurology*, 36:191-194.

Dera 2016, Protective effect of resveratrol against aluminum chloride induced nephrotoxicity in rats, *Saudi Medical Journal*, 37 (4).

DeStefano et al., 2013 Increasing Exposure to Antibody-Stimulating Proteins and Polysaccharides in Vaccines Is Not Associated with Risk of Autism, *The Journal of Pediatrics*, 163 (2).

Deverman and Patterson, 2009 Cytokines and CNS Development, *Neuron* 64:61-78.

Drozdenko et al., 2014 Oral vitamin D increases the frequencies of CD38+ human B cells and ameliorates IL-17-producing T cells, *Experimental Dermatology*, 23: 107-112.

- Estes and McAllister, 2016 Maternal immune activation: implications for neuropsychiatric disorders, *Science*, 353 (6301) 772-777.
- Exley, 2003 The Pro-Oxidant Activity of Aluminum, *Free Radical Biology and Medicine*, 36(3): 380-387.
- Flarend et al., 1997 In vivo absorption of aluminum-containing vaccine adjuvants using 26 Al, *Vaccine*, 15(12/13):1314-1318.
- Freyberg et al., 2015 Reduced perceptual exclusivity during object and grating rivalry in autism, *Journal of Vision*, 15(13):11, 1–12.
- Galic et al., 2008 Postnatal Inflammation Increases Seizure Susceptibility in Adult Rats, *The Journal of Neuroscience*, 2008, 28 (27) 6904-6913.
- Garay et al., 2013 Maternal immune activation causes age- and region-specific changes in brain cytokines in offspring throughout development, *Brain, Behavior, and Immunity*, 31: 54-68.
- Ghaziuddin et al., 2002 Autistic symptoms following herpes encephalitis, *European Child and Adolescent Psychiatry*, Vol. 11, No. 3:142-146.
- Gherardi et al., 2001 Macrophagic myofasciitis lesions assess long-term persistence of vaccine-derived aluminium hydroxide in muscle, *Brain*, 124:1821-1831.
- Ghiani et al., 2011 Early effects of lipopolysaccharide induced inflammation on foetal brain development in rat, *ASN Neuro*, 3 (4): 233-245.
- Gillberg 1986 Brief Report: Onset at Age 14 of a Typical Autistic Syndrome. A Case Report of a Girl with Herpes Simplex Encephalitis, *Journal of Autism and Developmental Disorders*, Vol 16, No. 3:369-375.
- Giulivi et al 2013 Gestational Exposure to a Viral Mimetic Poly(I:C) Results in Long-Lasting Changes in Mitochondrial Function by Leucocytes in the Adult Offspring, *Mediators of Inflammation*, Vol 2013:609602.
- Glanz et al., 2015, Cumulative and episodic vaccine aluminum exposure in a population-based cohort of young children, *Vaccine* 33:6736–6744.
- Golub et al., 2001 Long-term consequences of developmental exposure to aluminum in a suboptimal diet for growth and behavior of Swiss Webster mice, *Neurotoxicology and Teratology* 23 (2001) 365–372.
- Gupta et al., 1998 Th1- and Th2-like cytokines in CD4+ and CD8+ T cells in autism, *Journal of Neuroimmunology*, 85:106-109.
- Harre et al., 2008 Neonatal inflammation produces selective behavioural deficits and alters *N*-methyl-D-aspartate receptor subunit mRNA in the adult rat brain, *European Journal of Neuroscience*, 2008 Feb; 27(3): 644–653.
- Harris et al., 2012 Alhydrogel® adjuvant, ultrasonic dispersion and protein binding: A TEM and analytical study, *Micron*, 43:192-200.
- Hsiao et al., 2013 The microbiota modulates gut physiology and behavioral abnormalities associated with autism, *Cell*, 155(7): 1451-1463.
- Huttenlocher and Dabholkar, 1997 Regional Differences in Synaptogenesis in Human Cerebral Cortex, *Journal of Comparative Neurology*, 387:167–178 (1997).
- Jefferson 2004 Adverse events after immunisation with aluminium-containing DTP vaccines: systematic review of the evidence, *The Lancet* 4:84-90.
- Jones et al., 2016 Autism with Intellectual Disability is Associated with Increased Levels of Maternal Cytokines and Chemokines During Gestation, *Molecular Psychiatry*, 22(2):273-279.
- Khan et al., 2013 Slow CCL2-dependent translocation of biopersistent particles from muscle to brain, *BMC Medicine*, 11:99.
- Kindregan et al., 2015 Gait Deviations in Children with Autism Spectrum Disorders: A Review, *Autism Research and Treatment*, ID:741480.
- Knuesel et al., 2014, Maternal immune activation and abnormal brain development across CNS disorders, *Nature Reviews* 10:643-660.
- Labouesse et al., 2015, Long-term pathological consequences of prenatal infection: beyond brain disorders, *American Journal of Physiology*, 309:1.

Li et al. 2009 Elevated Immune Response in the Brain of Autistic Patients, *Journal of Neuroimmunology*, 207(1-2): 111–116.

Li et al., 2015 Neonatal vaccination with bacillus Calmette–Guérin and hepatitis B vaccines modulates hippocampal synaptic plasticity in rats, *Journal of Neuroimmunology*, 288 (2015) 1-12.

Machado et al., 2015 Maternal Immune Activation in Nonhuman Primates Alters Social Attention in Juvenile Offspring, *Biological Psychiatry*, 2015 May 1;77(9):823-32.

Malkova et al., 2012 Maternal immune activation yields offspring displaying mouse versions of the three core symptoms of autism, *Brain Behavior and Immunity*, 2012 May ; 26(4): 607–616.

Marques et al., 2014 Autism Spectrum Disorder Secondary to Enterovirus Encephalitis, *Journal of Child Neurology*, 2014, Vol. 29(5) 708-714.

Mestas et al., 2004 Of Mice and Not Men: Differences between Mouse and Human Immunology, *Journal of Immunology*, 0022-1767:2731-2738.

Meyer et al., 2006 The Time of Prenatal Immune Challenge Determines the Specificity of Inflammation-Mediated Brain and Behavioral Pathology, *The Journal of Neuroscience*, 26(18):4752– 4762.

Meyer et al., 2007 The neurodevelopmental impact of prenatal infections at different times of pregnancy: the earlier the worse?, *Neuroscientist*, Jun;13(3):241-56.

Meyer et al., 2009 In-vivo rodent models for the experimental investigation of prenatal immune activation effects in neurodevelopmental brain disorders, *Neuroscience and Biobehavioral Reviews*, 33 (2009) 1061–1079.

Meyer 2014, Prenatal Poly(I:C) Exposure and Other Developmental Immune Activation Models in Rodent Systems, *Biological Psychiatry*, 75:307-315.

Mitkus et al., 2011 Updated aluminum pharmacokinetics following infant exposures through diet and vaccination, *Vaccine* 29 (2011) 9538–9543.

Offit et al., 2003 Addressing Parents’ Concerns: Do Vaccines Contain Harmful Preservatives, Adjuvants, Additives, or Residuals? *Pediatrics*, 112(6): 1394-1401.

Oskvig et al., 2012 Maternal immune activation by LPS selectively alters specific gene expression profiles of interneuron migration and oxidative stress in the fetus without triggering a fetal immune response, *Brain Behavior and Immunity*, 2012 May ; 26(4): 623–634.

Pang et al., 2016 Exploiting macrophages as targeted carrier to guide nanoparticles into glioma, *Oncotarget* 7(24):37081.

Parker-Athill and Tan, 2010 Maternal Immune Activation and Autism Spectrum Disorder: Interleukin-6 Signaling as a Key Mechanistic Pathway, *NeuroSignals*, 2010;18:113–128.

Petrik et al., 2007 Aluminum Adjuvant Linked to Gulf War Illness Induces Motor Neuron Death in Mice, *NeuroMolecular Medicine*, Vol. 9, 83-100.

Pineda et al., 2013 Maternal immune activation promotes hippocampal kindling epileptogenesis in mice, *Annals of Neurology*, 2013 July ; 74(1): 11–19.

Podila et al., 2013 Toxicity of Engineered Nanomaterials: A Physicochemical Perspective, *Journal of Biochemical and Molecular Toxicology*, 2013 January ; 27(1): 50–55.

Robertson et al., 2016 Reduced GABAergic Action in the Autistic Brain, *Current Biology*, 26, 1-6.

Saad et al., 2016 Vitamin D status in autism spectrum disorders and the efficacy of vitamin D supplementation in autistic children, *Nutritional Neuroscience*, 19 (8) 346-351.

Semple et al., 2013 Brain development in rodents and humans: Identifying benchmarks of maturation and vulnerability to injury across species, *Progress in Neurobiology*, Jul-Aug;106-107:1-16.

Sethi et al., 2008 Aluminium-induced electrophysiological, biochemical and cognitive modifications in the hippocampus of aging rats, *Neurotoxicology* 29, 1069-1079.

Sethi et al., 2009 Curcumin attenuates aluminium-induced functional neurotoxicity in rats, *Pharmacology, Biochemisatry, and Behavior* 93:31-39.

- Shen et al., 2016 Postnatal activation of TLR4 in astrocytes promotes excitatory synaptogenesis in hippocampal neurons, *Journal of Cell Biology*, 215(5):719-734.
- Sharifi et al., 2012 Toxicity of Nanomaterials, *Chemical Society Reviews*, 2012 Mar 21; 41(6): 2323–2343.
- Shaw and Petrik, 2009 Aluminum hydroxide injections lead to motor deficits and motor neuron degeneration, *Journal of Inorganic Biochemistry* 103 (11).
- Shaw and Tomljenovic, 2013 Administration of aluminium to neonatal mice in vaccine-relevant amounts is associated with adverse long term neurological outcomes, *Journal of Inorganic Biochemistry*, 128 (2013) 237–244.
- Shi et al., 2009 Activation of the Maternal Immune System Alters Cerebellar Development in the Offspring, *Brain, Behavior, and Immunity*, January, 23(1): 116–123.
- Smith et al., 2007 Maternal Immune Activation Alters Fetal Brain Development through Interleukin-6, *Journal of Neuroscience*, 2007 October 3; 27(40).
- Smith et al., 2012, Maternal Immune Activation Increases Neonatal Mouse Cortex Thickness and Cell Density, *Journal of Neuroimmune Pharmacology*, 7(3):529-532.
- Stiles et al., 2010 The Basics of Brain Development, *Neuropsychology Reviews* (2010) 20:327–348.
- Suzuki et al., 2011 Plasma Cytokine Profiles in Subjects with High-Functioning Autism Spectrum Disorders, *PloS ONE* 6(5).
- Suzuki et al., 2013 Microglial Activation in Young Adults With Autism Spectrum Disorder, *JAMA Psychiatry* 70(1): 49-58.
- Takano 2015 Role of Microglia in Autism: Recent Advances, *Developmental Neuroscience*, 37:195-202.
- Tau and Peterson, 2010 Normal Development of Brain Circuits, *Neuropsychopharmacology*, (2010) 35:147–168.
- Taylor et al., 2014 Vaccines are not associated with autism: An evidence-based meta-analysis of case-control and cohort studies, *Vaccine*, 32:3623-3629.
- Tomljenovic and Shaw, 2011 Do aluminum vaccine adjuvants contribute to the rising prevalence of autism? *Journal of Inorganic Biochemistry* 105.
- Tsilioni et al., 2015 Children with autism spectrum disorders, who improved with a luteolin-containing dietary formulation, show reduced serum levels of TNF and IL-6, *Translational Psychiatry*, 5, 647.
- Vargas et al., 2005 Neuroglial Activation and Neuroinflammation in the Brain of Patients with Autism, *Annals of Neurology*, 2005;57:67–81.
- Viezeliene et al., 2013 Selective induction of IL-6 by aluminum-induced oxidative stress can be prevented by selenium, *Journal of Trace Elements in Medicine and Biology*, 27:226-229.
- Wei et al., 2011 IL-6 is increased in the cerebellum of autistic brain and alters neural cell adhesion, migration and synaptic formation, *Journal of Neuroinflammation* 2011, 8:52.
- Wei et al., 2012 (a) Brain IL-6 elevation causes neuronal circuitry imbalances and mediates autism-like behaviors, *Biochimica et Biophysica Acta*, 1822 (2012) 831–842.
- Wei et al. 2012 (b) Alteration of brain volume in IL-6 overexpressing mice related to autism, *International Journal of Developmental Neuroscience*, 30:554-559.
- Wei et al., 2013 Brain IL-6 and autism, *Neuroscience* 252 (2013): 320–325.
- Wei et al., 2016 Inhibition of IL-6 trans-signaling in the brain increases sociability in the BTBR mouse model of autism, *Biochimica et Biophysica Acta*, 1862(10):1918-1925.
- Weir et al., 2015 Preliminary evidence of neuropathology in nonhuman primates prenatally exposed to maternal immune activation, *Brain, Behavior, and Immunity*, 48,139–146.
- Williams et al., 2006 The Profile of Memory Function in Children With Autism, *Neuropsychology*, 20(1): 21-29.
- Wobke et al., 2014 Vitamin D in inflammatory diseases, *Frontiers in Physiology*, 5: 244.
- Zerbo et al., 2014 Neonatal cytokines and chemokines and risk of Autism Spectrum Disorder: the Early Markers for Autism (EMA) study: a case-control study, *Journal of Neuroinflammation*, 11:113.



Zerbo et al., 2017 Association Between Influenza Infection and Vaccination During Pregnancy and Risk of Autism Spectrum Disorder, *JAMA Pediatrics*, 171(1).



Vaccine

Volume 22, Issues 23–24, 13 August 2004, Pages 3127–3135

Aluminum hydroxide adjuvant induces macrophage differentiation towards a specialized antigen-presenting cell type

Anne-Cécile Rimaniol ^a, Gabriel Gras ^b  , François Verdier ^c, Francis Capel ^d, Vladimir B Grigoriev ^e, Fabrice Porcheray ^b, Elisabeth Sauzeat ^c, Jean-Guy Fournier ^b, Pascal Clayette ^a, Claire-Anne Siegrist ^f, Dominique Dormont ^b

Show more 

 Share  Cite

<https://doi.org/10.1016/j.vaccine.2004.01.061> 

[Get rights and content](#) 

Abstract

Aluminum hydroxide (AIOOH) has been used for many years as a vaccine adjuvant, but little is known about its mechanism of action. We investigated in this study the in vitro effect of aluminum hydroxide adjuvant on isolated macrophages. We showed that AIOOH-stimulated macrophages contain large and persistent intracellular crystalline inclusions, a characteristic property of muscle infiltrated macrophages described in animal models of vaccine injection, as well as in the recently described macrophagic myofasciitis (MMF) histological reaction in humans. AIOOH-loaded macrophages exhibited phenotypical and functional modifications, as they expressed the classical markers of myeloid dendritic cells (HLA-DR^{high}/CD86^{high}/CD83⁺/CD1a⁻/CD14⁻) and displayed potent ability to induce MHC-II-restricted antigen specific memory responses, but kept a macrophage morphology. This suggests a key role of macrophages, in the reaction to AIOOH-adjuvanted vaccines and these mature antigen-presenting macrophages may therefore be of particular importance in the

establishment of memory responses and in vaccination mechanisms leading to long-lasting protection.

Introduction

Vaccine adjuvants have been used for many years to induce strong and sustained humoral immune responses, but little is known about their mechanisms of action. The most frequently used adjuvant in commercial vaccines is aluminum hydroxide (Al(OH)₃). The adjuvant activity of these molecules seems to result partly from a deposition effect and from antigen adsorption, as they can retain small amounts of antigen at the injection site for a prolonged period [1]. Al(OH)₃ immunoadjuvant property is also associated with the induction of Th2-type responses in animal models [2]. Aluminum salts also exert immunomodulatory activities on isolated cells, especially those of the monocyte-macrophage lineage. Indeed, the adsorption of tetanus toxoid onto aluminum hydroxide leads to a significant increase of in vitro antigen-induced T-cell proliferation, correlated with an increase in tetanus toxoid uptake and IL-1 secretion by monocytes [3]. Exposure of human peripheral blood mononuclear cells (PBMC) to aluminum hydroxide induces monocyte differentiation into mature CD83⁺ dendritic cells (DC), with a typical DC morphology, which strictly requires paracrine secretion of IL-4 by helper T lymphocytes [4]. Aluminum hydroxide also increases the survival and proliferation of murine bone marrow-derived macrophages in vitro [5].

Intramuscular injection of aluminum adjuvants causes tissue reactions and may lead to the local secretion of cell recruitment and differentiation factors. Several studies have been performed in laboratory animals to evaluate the safety of vaccines containing aluminum hydroxide adjuvants, as required by the EMEA guidelines (EMEA (1997); note for guidance on preclinical pharmacological and toxicological testing of vaccines; CPMP/SWP/465/95) [8]. These studies included the histological examination of the injection site after intramuscular administration, which showed a homogeneous pattern of macrophage infiltration within 1–2 weeks of vaccine injection (EMEA (2002); Hexavac: European Public Assessment Report (EPAR), scientific discussion). Follow-up study of the histological reaction has also been carried out in rabbits and cynomolgus monkeys after the intramuscular injection of diphtheria, tetanus, pertussis, and polio and the combined polio and diphtheria vaccines, respectively (Verdier et al., manuscript in preparation). Both studies showed that aggregates of macrophages persisted for several months between muscle fibers. These observations are consistent with those of Gherardi et al., obtained after intramuscular injection of aluminum hydroxide-containing Hepatitis B vaccine in the rat [6]. There was a clear predominance of macrophages following the injection of aluminum hydroxide-containing vaccines in

animals, and the data obtained illustrate the key role of this cell type in the physiological reaction to aluminum hydroxide containing vaccines.

Muscle reaction to vaccine injection thus consists in a granuloma with striking muscle fascia infiltration by aluminum-loaded macrophage, a histological entity called macrophagic myofasciitis (MMF) that is also found in some human vaccinees. Altogether, these results strongly suggest that macrophages may play a critical role in vaccine-induced immune responses.

This led us to investigate the effect of aluminum adjuvants on isolated macrophages. As reported here, we found that aluminum-loaded macrophages differentiate into mature, specialized antigen-presenting cells different from monocyte-derived DC.

Access through your organization

Check access to the full text by signing in through your organization.

 Access through your organization

Section snippets

Human monocyte isolation and differentiation

PBMC were isolated from the blood of healthy HIV-seronegative donors by Ficoll-hypaque density gradient centrifugation. Monocytes were separated from PBMC by incubation for 1 h in 75 cm² culture flasks to allow adhesion. They were cultured in DMEM-glutamax medium (Life Technologies, Grand Island, NY, USA) supplemented with 10% heat-inactivated (+56°C for 30 min) FCS (Roche Diagnostics, Mannheim, Germany), 1% antibiotic mixture (penicillin, streptomycin, neomycin, Life Technologies) and 15 ng/ml ...

Morphological and phenotypic changes induced by ALOOH

We first assessed the toxicity of ALOOH by the MTT assay, by incubating macrophages cultures for 3 days with ALOOH concentrations ranging from 0.1 to 100 µg/ml. The dose of ALOOH used for vaccination is about 0.8 mg per dose of vaccine. The ALOOH concentration resulting in 50% mortality was 11 ± 1.7 µg/ml (*n*=13) (data not shown). ALOOH concentrations ranging from 1 to 5 µg/ml did not induce more than 30% toxicity. Treatment with 2 µg/ml ALOOH for 2 days induced morphological changes in macrophages: ...

Discussion

Overall, data from animal models have shown that *in vivo*, macrophage recruitment is a normal response to the intramuscular injection of ALOOH-containing vaccines [6]. However, it has also been suggested that the presence of a MMF in muscle would be associated with a diffuse arthromyalgia and fatigue syndrome [6], [7], [9], [10], raising questions about the physiological or pathophysiological role of macrophages infiltrating muscle fascia. Although the interaction between cell types that can ...

Acknowledgements

We thank Pr. Pierre Galanaud, Pr. Serge Herson, Dr. Olivier Benveniste and Pr. Romain Gherardi for helpful scientific discussion. ...

[Recommended articles](#)

References (20)

R.K Gherardi *et al.*

[Macrophagic myofasciitis: an emerging entity. Groupe d'Etudes et Recherche sur les Maladies Musculaires Acquisées et Dysimmunitaires \(GERMMAD\) de l'Association Française contre les Myopathies \(AFM\)](#)

Lancet (1998)

S.J Seeber *et al.*

[Predicting the adsorption of proteins by aluminium-containing adjuvants](#)

Vaccine (1991)

R.K Gupta *et al.*

[Adjuvant properties of aluminum and calcium compounds](#)

Pharm. Biotechnol. (1995)

J.M Brewer *et al.*

[In interleukin-4-deficient mice, alum not only generates T helper 1 responses equivalent to Freund's complete adjuvant, but continues to induce T helper 2 cytokine production](#)

Eur. J. Immunol. (1996)

J.W Mannhalter *et al.*

Modulation of the human immune response by the non-toxic and non-pyrogenic adjuvant aluminum hydroxide: effect on antigen uptake and antigen presentation

Clin. Exp. Immunol. (1985)

M Ulanova *et al.*

The common vaccine adjuvant aluminum hydroxide up-regulates accessory properties of human monocytes via an interleukin-4-dependent mechanism

Infect. Immun. (2001)

J.A Hamilton *et al.*

Particulate adjuvants can induce macrophage survival, DNA synthesis, and a synergistic proliferative response to GM-CSF and CSF-1

J. Leukoc. Biol. (2000)

R.K Gherardi *et al.*

Macrophagic myofasciitis lesions assess long-term persistence of vaccine-derived aluminium hydroxide in muscle

Brain (2001)

Vaccine safety. Vaccine Safety Advisory Committee. Wkly Epidemiol Rec...

FJ Authier *et al.*

Central nervous system disease in patients with macrophagic myofasciitis

Brain (2001)

There are more references available in the full text version of this article.

Cited by (148)

[Enhanced humoral and memory B cellular immunity using HPV16/18 L1 VLP vaccine formulated with the MPL/aluminium salt combination \(AS04\) compared to aluminium salt only](#)

2006, Vaccine

[Show abstract](#) ✓

[Mechanisms of action of adjuvants](#) ↗

2013, Frontiers in Immunology

[Crucial role for the Nalp3 inflammasome in the immunostimulatory properties of aluminium adjuvants ↗](#)

2008, Nature

[The adjuvants aluminum hydroxide and MF59 induce monocyte and granulocyte chemoattractants and enhance monocyte differentiation toward dendritic cells1 ↗](#)

2008, Journal of Immunology

[The perfect mix: Recent progress in adjuvant research ↗](#)

2007, Nature Reviews Microbiology

[Human health risk assessment for aluminium, aluminium oxide, and aluminium hydroxide ↗](#)

2007, Journal of Toxicology and Environmental Health - Part B: Critical Reviews



[View all citing articles on Scopus ↗](#)

[View full text](#)

Copyright © 2004 Elsevier Ltd. All rights reserved.



All content on this site: Copyright © 2024 Elsevier B.V., its licensors, and contributors. All rights are reserved, including those for text and data mining, AI training, and similar technologies. For all open access content, the Creative Commons licensing terms apply.

As a library, NLM provides access to scientific literature. Inclusion in an NLM database does not imply endorsement of, or agreement with, the contents by NLM or the National Institutes of Health.


Learn more: [PMC Disclaimer](#) | [PMC Copyright Notice](#)

Author Manuscript

Peer reviewed and accepted for publication by a journal



[Nature](#). Author manuscript; available in PMC: 2016 Mar 23.

Published in final edited form as: [Nature](#). 2008 May 21;453(7198):1122–1126. doi: [10.1038/nature06939](https://doi.org/10.1038/nature06939) 




Crucial role for the Nalp3 inflammasome in the immunostimulatory properties of aluminium adjuvants

[Stephanie C Eisenbarth](#)^{1,2}, [Oscar R Colegio](#)^{1,3}, [William O'Connor Jr](#)¹, [Fayyaz S Sutterwala](#)^{1,5}, [Richard A Flavell](#)^{1,4}

[Author information](#) [Article notes](#) [Copyright and License information](#)

PMCID: PMC4804622 NIHMSID: NIHMS488129 PMID: [18496530](#)

The publisher's version of this article is available at [Nature](#) 

Abstract

Aluminium adjuvants, typically referred to as ‘alum’, are the most commonly used adjuvants in human and animal vaccines worldwide, yet the mechanism underlying the stimulation of the immune system by alum remains unknown. Toll-like receptors are critical in sensing infections and are therefore common targets of various adjuvants used in immunological studies. Although alum is known to induce the production of proinflammatory cytokines *in vitro*, it has been repeatedly demonstrated that alum does not require intact Toll-like receptor signalling to activate the immune system^{1,2}. Here we show that aluminium adjuvants activate an intracellular innate immune response system called the Nalp3 (also known as cryopyrin, CIAS1 or NLRP3) inflammasome. Production of the pro-inflammatory cytokines interleukin-1 β and interleukin-18 by macrophages in response to alum *in vitro* required intact

inflammasome signalling. Furthermore, *in vivo*, mice deficient in Nalp3, ASC (apoptosis-associated speck-like protein containing a caspase recruitment domain) or caspase-1 failed to mount a significant antibody response to an antigen administered with aluminium adjuvants, whereas the response to complete Freund's adjuvant remained intact. We identify the Nalp3 inflammasome as a crucial element in the adjuvant effect of aluminium adjuvants; in addition, we show that the innate inflammasome pathway can direct a humoral adaptive immune response. This is likely to affect how we design effective, but safe, adjuvants in the future.

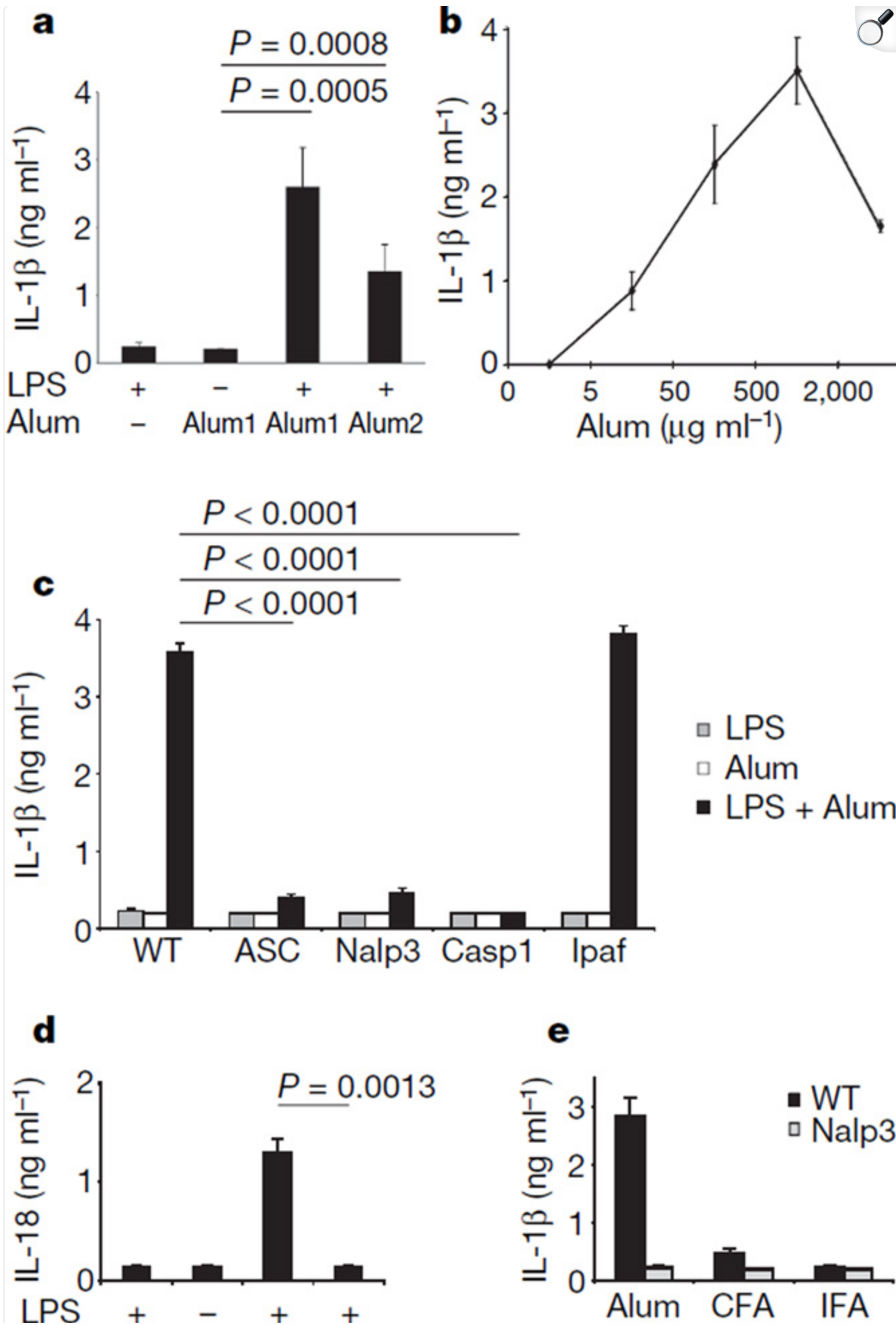
Shortly after the discovery that alum could be used as an adjuvant in the 1920s (ref. [3](#)), a hypothesis was put forth that alum stimulated an immune response by acting as a 'depot'; antigens were proposed to be slowly released in a particulate form that was favourable for uptake by antigen-presenting cells (APCs), thereby enhancing the immune response to the antigen (reviewed in ref. [4](#)). Since then, many of the signals used by APCs to initiate T-cell responses have been identified along with the immune stimuli (for example, Toll-like receptor (TLR) ligands) required to enhance interactions between APCs and T cells. However, the cellular signalling pathways triggered by alum that induce effective immunity against antigens have remained elusive.

The initiation of adaptive immune responses is controlled by innate immune signals. Regulation of these immune signals relies on a large group of intracellular and extracellular receptors called pattern recognition receptors⁵. The best-described class of these receptors is the TLRs, which sense conserved molecular patterns from a wide range of microbes. Whereas TLRs sense non-self motifs of infectious organisms, another class of intracellular pattern recognition receptors, the NOD-like receptors (NLRs), can sense stimuli of microbial origin as well as endogenous markers of cellular damage (for example ATP or uric acid crystals)^{6,7}. Nalp3, a member of the NLR family, along with ASC (also known as Pycard) and caspase-1, forms a molecular platform called the inflammasome, which regulates the cleavage and release of the potent pro-inflammatory cytokines interleukin (IL)-1 β , IL-18 and IL-33 (ref. [8](#)). One recently described endogenous molecule that activates the Nalp3 inflammasome is crystalline (but not soluble) uric acid (monosodium urate; MSU)⁹⁻¹¹.

Aluminium particles of various aluminium adjuvants form insoluble particles that can aggregate, are readily phagocytosed by macrophages and have been shown to stimulate IL-1 β and IL-18 production *in vitro*¹²⁻¹⁵. We formed the hypothesis that the particulate nature of alum might be recognized by NLRs, much like crystalline MSU. To test whether alum activates the Nalp3 inflammasome, we used primary peritoneal macrophages from mice deficient in critical signalling components of the Nalp3 inflammasome. Because inflammasome activation requires two signals for the production of mature IL-1 β , we first primed macrophages with lipopolysaccharide (LPS) and then exposed them to aluminium

adjuvants. Consistent with previous reports¹³⁻¹⁵, aluminium adjuvants induced the production of IL-1 β and IL-18 from wild-type (C57BL/6; WT) primary murine macrophages ([Fig. 1a,d](#)), bone-marrow-derived macrophages ([Supplementary Fig. 1a](#)) and bone-marrow-derived dendritic cells ([Supplementary Fig. 1b](#)) *in vitro*. IL-1 β secretion was dependent on the dose of alum ([Fig. 1b](#)) and peaked between 8 and 10 h of stimulation with alum in WT macrophages, but continued out to 48 h ([Fig. 2c](#) and data not shown).

Figure 1. Aluminium-containing adjuvants stimulate macrophages to produce the pro-inflammatory cytokines IL-1 β and IL-18 in a Nalp3 inflammasome-dependent manner.



Alum	-	+	+	+
	WT		Nalp3	

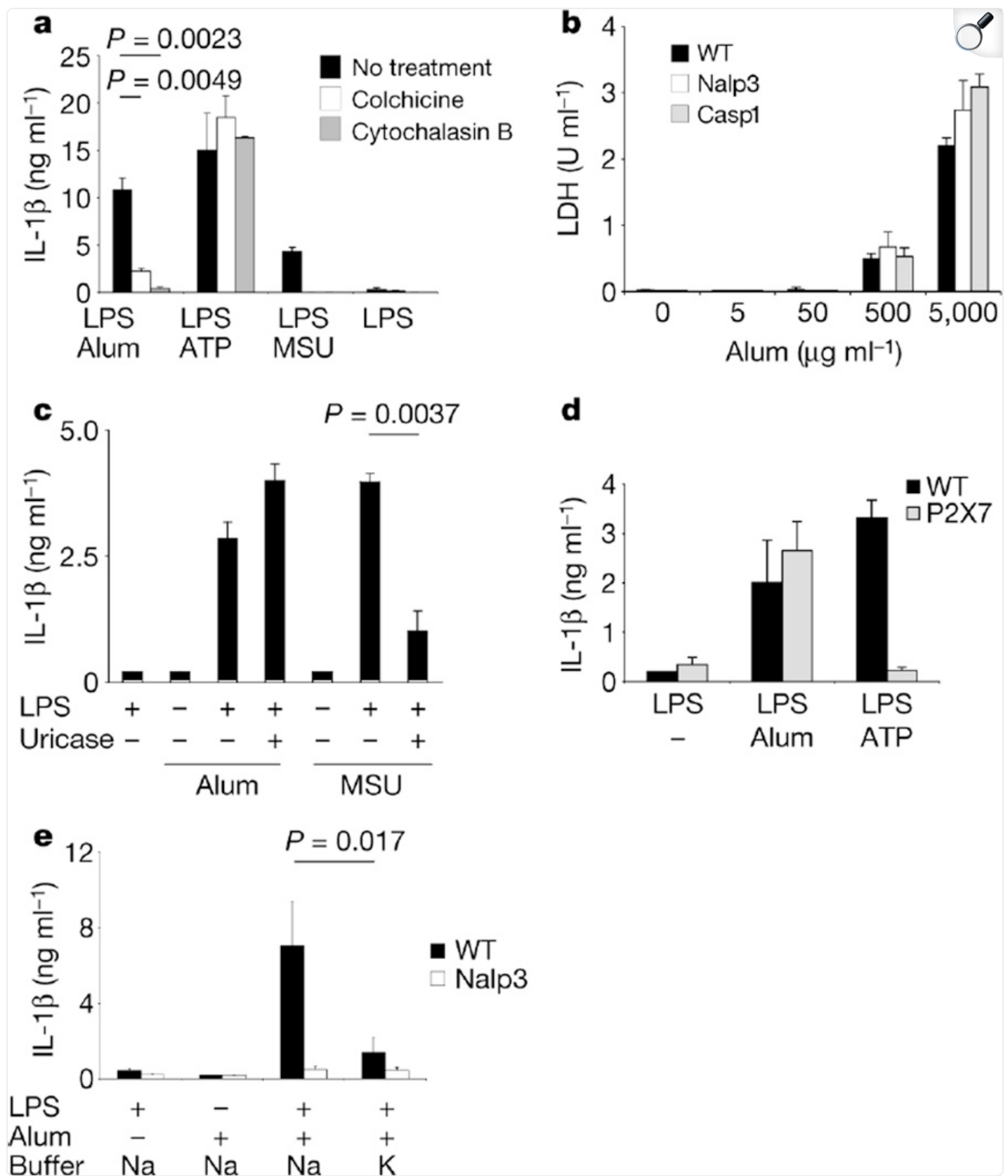
[Open in a new tab](#)

a, Macrophages were stimulated with 50 ng ml^{-1} LPS for 18 h and then $500 \text{ } \mu\text{g ml}^{-1}$ Imject alum ('Alum1') or aluminium hydroxide gel ('Alum2') for 8 h. IL-1 β released into culture supernatants was measured by ELISA with a minimum detection level of 200 pg ml^{-1} . **b**, LPS-primed macrophages were stimulated with the indicated amount of Imject alum for 8 h and analysed as in **a**. **c**, Unprimed or LPS-primed WT, ASC-deficient, Nalp3-deficient, caspase-1-deficient (Casp1) and Ipaf-deficient macrophages were stimulated with Imject alum ($500 \text{ } \mu\text{g ml}^{-1}$) for 8 h, and the IL-1 β released into the culture supernatants was measured by ELISA. **d**, WT or Nalp3-deficient macrophages were stimulated as in **c**, and the IL-18 released was measured by ELISA. **e**, WT or Nalp3-deficient LPS-primed macrophages were stimulated with either Imject alum, CFA ($120 \text{ } \mu\text{g ml}^{-1}$) or IFA ($30 \text{ } \mu\text{l ml}^{-1}$) for 8 h and analysed as in **a**. Determinations were performed in triplicate and are expressed as means and s.d.; data are from one of at least three independent experiments.

Caspase-1 activation involves autocatalytic processing of the 45-kDa pro-caspase-1 to generate two subunits, p20 and p10. Caspase-1 activation in LPS-primed WT macrophages stimulated with alum was detected by western blotting by the appearance of the p10 cleavage product 4 h after the addition of alum ([Fig. 2a](#)). Consistent with the lack of IL-1 β production, caspase-1 activation was absent in macrophages deficient in Nalp3 and ASC that were exposed to LPS and alum ([Fig. 2a, b](#)). Nalp3 knockout macrophages did not show caspase-1 activation or IL-1 β production even at later time points, arguing against delayed caspase-1 activation by alum in the absence of Nalp3 ([Fig. 2a, c](#)). These data demonstrate that alum activates macrophages *in vitro* to secrete mature IL-1 β in a manner dependent on the Nalp3 inflammasome.

To understand how alum might stimulate the inflammasome pathway, we first tested whether the endocytic ability of macrophages was required for the alum-stimulated production of IL-1 β . Inhibiting actin or tubulin polymerization with either cytochalasin B or colchicine, respectively, inhibited IL-1 β production by LPS and alum ([Fig. 3a](#)) but did not affect secretion of the inflammasome-independent cytokines TNF- α or IL-6 ([Supplementary Fig. 2a, b](#)). Neither cytochalasin B nor colchicine decreased IL-1 β production in response to stimulation with ATP, which uses the P2X7 receptor (P2X7R) to activate the Nalp3 inflammasome^{18,19}, confirming that macrophages were still viable and capable of secreting inflammasome-dependent IL-1 β ([Fig. 3a](#)).

Figure 3. Alum requires intact endocytic macrophage machinery and causes potassium-gradient-dependent IL-1 β secretion without causing significant cell death.



[Open in a new tab](#)

a, LPS-primed peritoneal macrophages were treated with either colchicine ($28 \mu\text{g ml}^{-1}$) or cytochalasin B ($10 \mu\text{M}$) for 1 h before the addition of Imject alum ($500 \mu\text{g ml}^{-1}$), ATP (5 mM) or MSU ($200 \mu\text{g ml}^{-1}$). **b**, Lactate dehydrogenase (LDH) release was measured from LPS-primed WT, Nalp3-deficient and caspase-1-deficient (Casp1) macrophage culture supernatants stimulated with the indicated amounts of Imject alum. **c**, Unprimed or LPS-primed WT macrophages were stimulated for 8 h with either Imject alum ($500 \mu\text{g ml}^{-1}$) or MSU ($200 \mu\text{g ml}^{-1}$) in the presence or absence of 2 U ml^{-1} uricase. **d**, LPS-primed macrophages from WT or P2X7R-deficient (P2X7) mice were stimulated with Imject alum ($500 \mu\text{g ml}^{-1}$) or ATP (5 mM) and samples were analysed as in **a**. **e**, Unprimed or LPS-primed WT or Nalp3-deficient macrophages were stimulated with Imject alum in serum-free buffer with either 150 mM NaCl or 150 mM KCl and analysed as in **a**. Determinations were performed in triplicate and are expressed as means and s.d.; data are from one of at least three independent experiments.

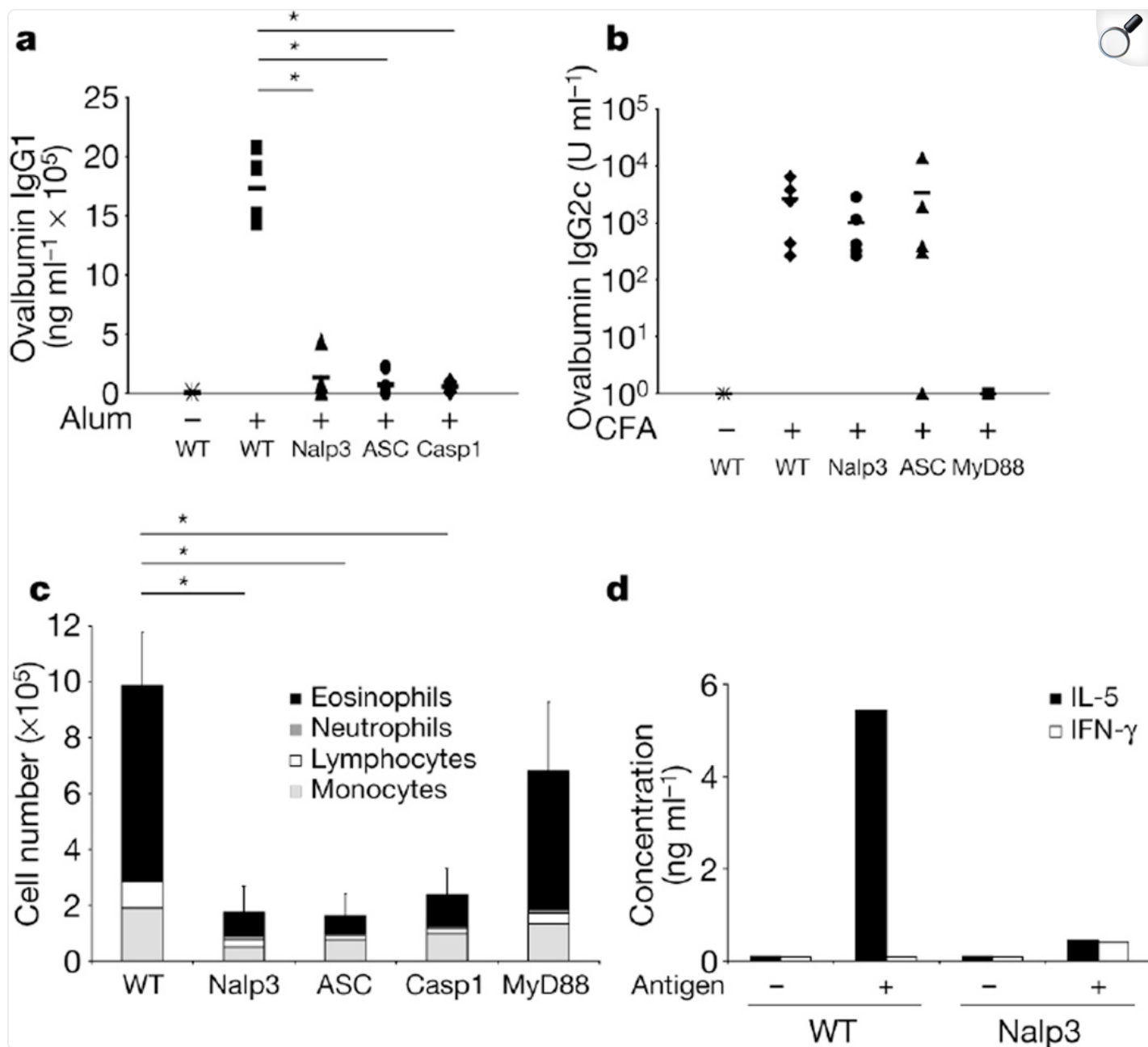
ATP and MSU released from dying and injured cells into the extracellular milieu may activate the Nalp3 inflammasome^{8,9,19}. *In vitro*, alum induced cell death at very high doses (that did not induce significant IL-1 β) in WT macrophages and in macrophages deficient in Nalp3 and Caspase-1 (Fig. 3b); however, the induction of IL-1 β by alum did not depend on the presence of MSU because the addition of uricase, which degrades MSU crystals and prevents the induction of IL-1 β (ref. 10), had no effect on IL-1 β production in response to LPS and alum (Fig. 3c). To exclude the possibility that Nalp3 inflammasome activation was in response to ATP release caused by alum-induced cellular damage, we used macrophages from P2X7R knockout mice. P2X7R-deficient macrophages showed no defect in IL-1 β production after stimulation with LPS and alum (Fig. 3d). Taken together, these data support a model of active endocytosis of alum by viable macrophages leading to Nalp3 inflammasome activation with the resultant secretion of pro-inflammatory cytokines.

Although several diverse stimuli activate the Nalp3 inflammasome, the efflux of cellular potassium seems to be a common step shared by these stimuli and is required for Nalp3-dependent caspase-1 activation; it has therefore been suggested that the inflammasome acts as a sensor of cellular membrane disruption⁷. Preventing this potassium efflux by increasing extracellular potassium inhibits inflammasome activation with a variety of Nalp3 triggers²⁰. Indeed, increased extracellular potassium significantly inhibited alum-induced IL-1 β production from macrophages (Fig. 3e) but not the LPS-dependent production of TNF- α or IL-6 (data not shown). Pannexin pores are thought to have a function in inflammasome activation induced by ATP, nigericin or maitotoxin, possibly by facilitating potassium efflux²¹. We did not detect a significant difference in IL-1 β secretion between macrophages exposed to a

pannexin-pore-blocking peptide and those exposed to a scrambled peptide. Therefore we do not currently have evidence that pannexin pores mediate alum-induced inflammasome activation. Alum is therefore a new Nalp3 trigger and, like other triggers, may induce inflammasome activation through membrane disruption with resultant potassium efflux.

Aluminium adjuvants are used in human vaccines to induce a potent humoral response; alum is also used as a potent adjuvant to induce T helper type 2 (T_H2)-mediated inflammation in murine allergy/asthma models. Given the Nalp3-dependent activation of macrophages that we observed *in vitro*, we tested whether immunity in mice against a model protein antigen, ovalbumin, required a functional Nalp3 inflammasome. Ovalbumin-specific IgG1 antibody induction was significantly decreased in Nalp3-deficient, ASC-deficient and caspase-1-deficient mice primed intraperitoneally with ovalbumin and alum ([Fig. 4a](#)) or subcutaneously with another protein antigen, human serum albumin (HSA) in alum ([Supplementary Fig. 3](#)), but was not affected in MyD88 knockout mice ([Supplementary Fig. 4](#); ref. [2](#)). We tested whether Nalp3 and ASC knockout mice have a general antibody-production defect by immunizing them with the adjuvant CFA. Ovalbumin-specific IgG2c ([Fig. 4b](#)) and IgG1 (not shown) in Nalp3 and ASC knockout mice were equivalent to levels in WT mice but, as expected, CFA-induced ovalbumin-specific IgG2c was completely dependent on MyD88 ([Fig. 4b](#)).

Figure 4. Antibody production and T_H2-dependent inflammation induced by aluminium adjuvants are decreased in the absence of Nalp3, ASC and caspase-1.



[Open in a new tab](#)

a, WT, Nalp3-deficient, ASC-deficient or caspase-1-deficient (Casp1) mice (three to five mice per group) 6–8 weeks old were injected intraperitoneally with ovalbumin adsorbed on Imject alum on day 0 and again on day 10. Mice were challenged intranasally with ovalbumin on days 21, 22 and 23. Sera were collected from mice on day 25 and analysed for ovalbumin-specific IgG1 by ELISA as described previously². Asterisk, $P < 0.03$; nonparametric Mann–Whitney U -test. **b**, WT,

Nalp3-deficient, ASC-deficient or MyD88-deficient mice (three to five mice per group) were primed subcutaneously with ovalbumin in CFA on day 0 and on day 10 in IFA. Sera were collected on day 21 and analysed for ovalbumin-specific IgG2c by ELISA. **c**, Three to five mice per group were primed and challenged as in **a**; bronchoalveolar lavage was collected on day 25 and analysed as described previously² (see Methods) (total cell number; means and s.d. are shown). Asterisk, $P < 0.03$; nonparametric Mann-Whitney U -test. **d**, Lung draining (hilar) lymph nodes were collected from WT and Nalp3-deficient mice primed and challenged as in **a** and pooled within each group for restimulation; cells were restimulated *in vitro* with (+) or without (-) $200 \mu\text{g ml}^{-1}$ ovalbumin and mitomycin-C-treated splenocytes for 48 h. Supernatants were analysed for IL-5 (filled bars) or IFN- γ (open bars).

T_H2 cell priming was also impaired in Nalp3, ASC and caspase-1 knockout mice as demonstrated by decreased airway eosinophilia and hilar lymph-node IL-5 production in an alum-dependent model of asthma ([Fig. 4c, d](#)). The overall inflammation was decreased in these knockout mice without evidence of a switch to a T_H1 response (typically characterized by airway neutrophilia and IgG2c induction). Consistent with previous reports, alum-induced T_H2 responses are not affected in mice lacking MyD88 (ref. [2](#)) or lacking both MyD88 and TRIF (ref. [1](#); [Fig. 4c](#) and [Supplementary Fig. 4](#)). Previous studies have suggested that antigen must be physically associated with (although not necessarily adsorbed on) alum for it to have an adjuvant effect²². Indeed, we saw a significantly impaired antibody response ([Supplementary Fig. 5a](#)) and an absence of T_H2 inflammation in the airways when alum and ovalbumin were injected separately into the peritoneum ([Supplementary Fig. 5b](#)). In mouse cells, but not in human cells, there is a clear requirement *in vitro* for two signals to activate the inflammasome and to produce pro-IL-1 β (LPS and alum), yet it is not clear what is providing the first signal for alum *in vivo* (or other Nalp3 stimuli including MSU). We have preliminary evidence from *in vitro* studies that IL-1 β itself can prime macrophages for alum-induced inflammasome activation (data not shown); these results are consistent with previous reports that IL-1 β can act in an autocrine manner to induce its own gene expression²³. Other groups have similarly seen macrophage priming with cytokines (for example TNF- α) instead of LPS¹³. Combining the above information with the fact that alum must be encountered simultaneously with antigen *in vivo* for efficient priming suggests that the antigen might provide the first signal either directly, or indirectly by inciting the production of local pro-inflammatory cytokines from resident monocytes or specialized cells recruited by alum²⁴. Once the first signal has primed the cell, alum provides the second signal for activation of the Nalp3 inflammasome. These two stimuli must be sensed by the same cell for effective immune activation, thereby increasing the specificity of an immune response and perhaps explaining why alum (which readily adsorbs antigens) is such an effective adjuvant.

Thus, by eliminating signalling through the Nalp3 inflammasome, we have eliminated one critical pathway used by alum to initiate humoral and cellular immunity. In doing so, aluminium hydroxide adjuvants ‘hijack’ an innate immune pathway that is exquisitely sensitive to cellular damage, perhaps as a result of the similarity to MSU in its physical structure. Although intraperitoneal MSU induces peritonitis⁹ and subcutaneous MSU in concert with antigen injection has been used *in vivo* to initiate CD8 T-cell responses¹⁰, we predicted, on the basis of our findings, that this Nalp3 stimulant would also induce a significant antibody response to a protein antigen. Indeed, MSU injected intraperitoneally with antigen induces an IgG1-type antibody response similar in nature to that induced by alum in WT mice but not in Nalp3-deficient mice ([Supplementary Fig. 6](#)). These mice did not develop a significant T_H1-type antibody response (IgG2c) under these immunization conditions (data not shown), suggesting that MSU and alum induce a similar pattern of inflammation when injected at similar doses in the same location.

A critical question regarding the mechanism by which alum influences immunity is how alum initiates lymphocyte activation and how it favours T_H2 differentiation over T_H1 differentiation. Inflammasome-dependent cytokines have been implicated in various aspects of T_H2 responses: IL-1 has classically been thought to promote T_H2 cell proliferation^{25,26}, IL-33 is a potent pro-T_H2 stimulus²⁶ and IL-18 has been shown to augment IgE antibody production (although it primarily potentiates T_H1 responses)²⁷. On the basis of our *in vitro* findings, we would predict that local production of IL-1 β , IL-18 and/or IL-33 could induce the requisite signals for activation of the adaptive immune system. Indeed, we found a lower expression of *Il1b* mRNA from peritoneal cells of Nalp3-deficient mice immunized with ovalbumin and alum than in WT mice ([Supplementary Fig. 7](#)). In further support of an IL-1-dependent model, the antibody response in another immunization model has been shown to be defective in IL-1 α /IL-1 β knockout mice as the result of a defect in the induction of CD40L on T cells by activated APCs²⁸. However, there is no antibody production or T_H2 defect after alum priming in MyD88 knockout mice. MyD88 is critical in the IL-1 receptor signalling cascade²⁹, although one recent study has identified a MyD88-independent IL-1 pathway³⁰. It will therefore be of interest to study the relative roles of IL-1 family members in alum-dependent priming in future work. In addition, as new functions of caspase-1 and the inflammasome are uncovered, we will further understand how stimulation of this potent pro-inflammatory machinery results in activation of the adaptive immune response.

METHODS SUMMARY

Mice

The generation of mice deficient in Nalp3, ASC, Ipaf, caspase-1 and P2X7R has been reported previously^{8,16,18}. Nalp3-deficient, Caspase-1-deficient and ASC-deficient mice were backcrossed nine

generations, and Ipaf-deficient mice were backcrossed six generations onto a C57BL/6 background. Age-matched and sex-matched C57BL/6 mice from the National Cancer Institute were used as all WT controls. All protocols used in this study were approved by the Yale Institutional Animal Care and Use Committee.

Macrophages

The generation of thioglycollate-elicited peritoneal and bone-marrow-derived macrophages and bone-marrow-derived dendritic cells has been described previously^{2,8}. Unless indicated, macrophages were primed by stimulating with 50 ng ml⁻¹ LPS from *Escherichia coli* serotype 0111:B4 (Invivogen) for 16–18 h before stimulation with Imject alum (unless otherwise indicated), MSU or ATP. For ATP-stimulated cells, the medium was changed at 20 min and all stimulants were replaced. Macrophage cell death was measured by the release of lactate dehydrogenase with a cytotoxicity detection kit (Promega).

Sensitizations

For intraperitoneal sensitization, 6–8-week-old mice were injected intraperitoneally on day 0 with 50 µg of ovalbumin (Grade V; Sigma) adsorbed on 4 mg of Imject alum and again on day 10 with 25 µg of ovalbumin adsorbed on 4 mg of Imject alum. Mice were challenged intranasally with 25 µg of ovalbumin in PBS on days 21, 22 and 23. Mice were killed for analysis on day 25. For subcutaneous sensitization, mice were injected subcutaneously on day 0 with 50 µg of ovalbumin in 400 µg (180 µl) of CFA and again on day 10 with 25 µg of ovalbumin in 180 µl of IFA.

Full Methods and any associated references are available in the online version of the paper at www.nature.com/nature [↗](#).

Supplementary Material

Supplemental Files

[NIHMS488129-supplement-Supplemental Files.pdf](#) (195.2KB, pdf)

Acknowledgments

We thank L. Zenewicz, Y. Ogura, A. Williams and Y. Wan for discussion and review of this manuscript; A. Coyle, E. Grant and J. Bertin for providing ASC-deficient, Nalp3-deficient and Ipaf-deficient mice; and J. Genzen for providing the P2X7R-deficient mice. This work was supported by the Ellison Foundation, the Bill and Melinda Gates Foundation through the Grand Challenges in Global Health Initiative, and National Institutes of Health grant K08 (F.S.S.). R.A.F. is an Investigator of the Howard Hughes Medical Institute.

Footnotes

Supplementary Information is linked to the online version of the paper at www.nature.com/nature [↗](#).

References

1. Gavin AL, et al. Adjuvant-enhanced antibody responses in the absence of toll-like receptor signaling. *Science*. 2006;314:1936–1938. doi: 10.1126/science.1135299. [[DOI ↗](#)] [[PMC free article](#)] [[PubMed](#)] [[Google Scholar ↗](#)]
2. Piggott DA, et al. MyD88-dependent induction of allergic Th2 responses to intranasal antigen. *J. Clin. Invest.* 2005;115:459–467. doi: 10.1172/JCI22462. [[DOI ↗](#)] [[PMC free article](#)] [[PubMed](#)] [[Google Scholar ↗](#)]
3. Glenny AT, Pope CG, Waddington H, Wallace U. The antigenic value of toxoid precipitated by potassium alum. *J. Pathol. Bacteriol.* 1926;29:31–40. [[Google Scholar ↗](#)]
4. Lindblad EB. Aluminium compounds for use in vaccines. *Immunol. Cell Biol.* 2004;82:497–505. doi: 10.1111/j.0818-9641.2004.01286.x. [[DOI ↗](#)] [[PubMed](#)] [[Google Scholar ↗](#)]
5. Medzhitov R. Recognition of microorganisms and activation of the immune response. *Nature*. 2007;449:819–826. doi: 10.1038/nature06246. [[DOI ↗](#)] [[PubMed](#)] [[Google Scholar ↗](#)]
6. Mariathasan S, Monack DM. Inflammasome adaptors and sensors: intracellular regulators of infection and inflammation. *Nature Rev. Immunol.* 2007;7:31–40. doi: 10.1038/nri1997. [[DOI ↗](#)] [[PubMed](#)] [[Google Scholar ↗](#)]
7. Sutterwala FS, Ogura Y, Flavell RA. The inflammasome in pathogen recognition and inflammation. *J. Leukoc. Biol.* 2007;82:259–264. doi: 10.1189/jlb.1206755. [[DOI ↗](#)] [[PubMed](#)] [[Google Scholar ↗](#)]

8. Sutterwala FS, et al. Critical role for NALP3/CIAS1/Cryopyrin in innate and adaptive immunity through its regulation of caspase-1. *Immunity*. 2006;24:317–327. doi: 10.1016/j.immuni.2006.02.004. [[DOI](#)] [[PubMed](#)] [[Google Scholar](#)]
9. Martinon F, Petrilli V, Mayor A, Tardivel A, Tschopp J. Gout-associated uric acid crystals activate the NALP3 inflammasome. *Nature*. 2006;440:237–241. doi: 10.1038/nature04516. [[DOI](#)] [[PubMed](#)] [[Google Scholar](#)]
10. Shi Y, Evans JE, Rock KL. Molecular identification of a danger signal that alerts the immune system to dying cells. *Nature*. 2003;425:516–521. doi: 10.1038/nature01991. [[DOI](#)] [[PubMed](#)] [[Google Scholar](#)]
11. Chen CJ, et al. Identification of a key pathway required for the sterile inflammatory response triggered by dying cells. *Nature Med*. 2007;13:851–856. doi: 10.1038/nm1603. [[DOI](#)] [[PubMed](#)] [[Google Scholar](#)]
12. Rimaniol AC, et al. Aluminum hydroxide adjuvant induces macrophage differentiation towards a specialized antigen-presenting cell type. *Vaccine*. 2004;22:3127–3135. doi: 10.1016/j.vaccine.2004.01.061. [[DOI](#)] [[PubMed](#)] [[Google Scholar](#)]
13. Li H, Nookala S, Re F. Aluminum hydroxide adjuvants activate caspase-1 and induce IL-1 β and IL-18 release. *J. Immunol*. 2007;178:5271–5276. doi: 10.4049/jimmunol.178.8.5271. [[DOI](#)] [[PubMed](#)] [[Google Scholar](#)]
14. Mannhalter JW, Neychev HO, Zlabinger GJ, Ahmad R, Eibl MM. Modulation of the human immune response by the non-toxic and non-pyrogenic adjuvant aluminium hydroxide: effect on antigen uptake and antigen presentation. *Clin. Exp. Immunol*. 1985;61:143–151. [[PMC free article](#)] [[PubMed](#)] [[Google Scholar](#)]
15. Sokolovska A, Hem SL, HogenEsch H. Activation of dendritic cells and induction of CD4+ T cell differentiation by aluminum-containing adjuvants. *Vaccine*. 2007;25:4575–4585. doi: 10.1016/j.vaccine.2007.03.045. [[DOI](#)] [[PubMed](#)] [[Google Scholar](#)]
16. Sutterwala FS, et al. Immune recognition of *Pseudomonas aeruginosa* mediated by the IPAF/NLRC4 inflammasome. *J. Exp. Med*. 2007;204:3235–3245. doi: 10.1084/jem.20071239. [[DOI](#)] [[PMC free article](#)] [[PubMed](#)] [[Google Scholar](#)]
17. Mariathasan S, et al. Differential activation of the inflammasome by caspase-1 adaptors ASC and Ipaf. *Nature*. 2004;430:213–218. doi: 10.1038/nature02664. [[DOI](#)] [[PubMed](#)] [[Google Scholar](#)]

18. Solle M, et al. Altered cytokine production in mice lacking P2X7 receptors. *J. Biol. Chem.* 2001;276:125–132. doi: 10.1074/jbc.M006781200. [[DOI](#)] [[PubMed](#)] [[Google Scholar](#)]
19. Mariathasan S, et al. Cryopyrin activates the inflammasome in response to toxins and ATP. *Nature.* 2006;440:228–232. doi: 10.1038/nature04515. [[DOI](#)] [[PubMed](#)] [[Google Scholar](#)]
20. Petrilli V, et al. Activation of the NALP3 inflammasome is triggered by low intracellular potassium concentration. *Cell Death Differ.* 2007;14:1583–1589. doi: 10.1038/sj.cdd.4402195. [[DOI](#)] [[PubMed](#)] [[Google Scholar](#)]
21. Pelegrin P, Surprenant A. Pannexin-1 couples to maitotoxin- and nigericin-induced interleukin-1 β release through a dye uptake-independent pathway. *J. Biol. Chem.* 2007;282:2386–2394. doi: 10.1074/jbc.M610351200. [[DOI](#)] [[PubMed](#)] [[Google Scholar](#)]
22. Chang M, et al. Degree of antigen adsorption in the vaccine or interstitial fluid and its effect on the antibody response in rabbits. *Vaccine.* 2001;19:2884–2889. doi: 10.1016/s0264-410x(00)00559-4. [[DOI](#)] [[PubMed](#)] [[Google Scholar](#)]
23. Toda Y, et al. Autocrine induction of the human pro-IL-1 β gene promoter by IL-1 β in monocytes. *J. Immunol.* 2002;168:1984–1991. doi: 10.4049/jimmunol.168.4.1984. [[DOI](#)] [[PubMed](#)] [[Google Scholar](#)]
24. Jordan MB, Mills DM, Kappler J, Marrack P, Cambier JC. Promotion of B cell immune responses via an alum-induced myeloid cell population. *Science.* 2004;304:1808–1810. doi: 10.1126/science.1089926. [[DOI](#)] [[PubMed](#)] [[Google Scholar](#)]
25. Kaye J, et al. Growth of a cloned helper T cell line induced by a monoclonal antibody specific for the antigen receptor: interleukin 1 is required for the expression of receptors for interleukin 2. *J. Immunol.* 1984;133:1339–1345. [[PubMed](#)] [[Google Scholar](#)]
26. Dunne A, O'Neill LA. The interleukin-1 receptor/Toll-like receptor superfamily: signal transduction during inflammation and host defense. *Sci. STKE.* 2003;2003:re3. doi: 10.1126/stke.2003.171.re3. [[DOI](#)] [[PubMed](#)] [[Google Scholar](#)]
27. Yoshimoto T, et al. IL-18 induction of IgE: dependence on CD4+ T cells, IL-4 and STAT6. *Nature Immunol.* 2000;1:132–137. doi: 10.1038/77811. [[DOI](#)] [[PubMed](#)] [[Google Scholar](#)]
28. Nakae S, Asano M, Horai R, Sakaguchi N, Iwakura Y. IL-1 enhances T cell-dependent antibody production through induction of CD40 ligand and OX40 on T cells. *J. Immunol.* 2001;167:90–97. doi: 10.4049/jimmunol.167.1.90. [[DOI](#)] [[PubMed](#)] [[Google Scholar](#)]

29. Adachi O, et al. Targeted disruption of the MyD88 gene results in loss of IL-1- and IL-18-mediated function. *Immunity*. 1998;9:143–150. doi: 10.1016/s1074-7613(00)80596-8. [[DOI](#)] [[PubMed](#)] [[Google Scholar](#)]

30. Davis CN, et al. MyD88-dependent and -independent signaling by IL-1 in neurons probed by bifunctional Toll/IL-1 receptor domain/BB-loop mimetics. *Proc. Natl Acad. Sci. USA*. 2006;103:2953–2958. doi: 10.1073/pnas.0510802103. [[DOI](#)] [[PMC free article](#)] [[PubMed](#)] [[Google Scholar](#)]

Associated Data

This section collects any data citations, data availability statements, or supplementary materials included in this article.

Supplementary Materials

Supplemental Files

[NIHMS488129-supplement-Supplemental Files.pdf](#) (195.2KB, pdf)

Exploiting macrophages as targeted carrier to guide nanoparticles into glioma

Liang Pang¹, Jing Qin¹, Limei Han¹, Wenjie Zhao², Jianming Liang¹, Zhongyi Xie¹, Pei Yang¹, Jianxin Wang¹

¹Key Laboratory of Smart Drug Delivery, Ministry of Education, Department of Pharmaceutics, School of Pharmacy, Fudan University, Shanghai, 201203, China

²Shanghai Institute of Pharmaceutical Industry, Shanghai, 201203, China

Correspondence to: Jianxin Wang, **email:** jxwang@fudan.edu.cn

Keywords: macrophages, glioma, inflammation, hypoxic, nanoparticles

Received: October 18, 2015

Accepted: April 24, 2016

Published: May 18, 2016

ABSTRACT

The restriction of anti-cancer drugs entry to tumor sites in the brain is a major impediment to the development of new strategies for the treatment of glioma. Based on the finding that macrophages possess an intrinsic homing property enabling them to migrate to tumor sites across the endothelial barriers in response to the excretion of cytokines/chemokines in the diseased tissues, we exploited macrophages as 'Trojan horses' to carry drug-loading nanoparticles (NPs), pass through barriers, and offload them into brain tumor sites. Anticancer drugs were encapsulated in nanoparticles to avoid their damage to the cells. Drug loading NPs was then incubated with RAW264.7 cells *in vitro* to prepare macrophage-NPs (M-NPs). The release of NPs from M-NPs was very slow in medium of DMEM and 10% FBS and significantly accelerated when LPS and IFN- γ were added to mimic tumor inflammation microenvironment. The viability of macrophages was not affected when the concentration of doxorubicin lower than 25 $\mu\text{g}/\text{ml}$. The improvement of cellular uptake and penetration into the core of glioma spheroids of M-NPs compared with NPs was verified in *in vitro* studies. The tumor-targeting efficiency of NPs was also significantly enhanced after loading into macrophages in nude mice bearing intracranial U87 glioma. Our results provided great potential of macrophages as an active biocarrier to deliver anticancer drugs to the tumor sites in the brain and improve therapeutic effects of glioma.

INTRODUCTION

The treatment of glioma is one of the greatest challenges in cancer therapy [1]. Despite the substantial progress of current treatment strategies in recent decades, the prolongation of glioma patients' survival has not been efficiently achieved [2]. Since infiltrative growth of glioma leads to incomplete surgical excision [3], radiotherapy and chemotherapy are necessary following surgery. Therefore, how to deliver drugs into tumor site represents one of the most important obstacles during the treatment of glioma.

In the early stage of glioma, an endothelial cell monolayer associated with pericytes and astrocytes constitutes the blood-brain barrier (BBB), which protects brain tissue from harmful substances in blood circulation [4–6]. Meanwhile, it prevents therapeutic drugs from entering the brain to treat various diseases. With the

progression of glioma into later stage, the integrity of BBB is compromised due to enhanced permeability and retention (EPR) effect [7]. However, the increased interstitial fluid pressure (IFP) inside the tumor and the blood tumor barrier (BTB) still impede therapeutic agents into tumor [8, 9]. Only by overcoming these barriers, the drug could be successfully delivered into the diseased site. Recently, multifunctional nano-drug delivery systems have been developed to improve therapeutic effect of different drugs [10], but rapid clearance from blood, limited targeting to diseased tissues and serious immunogenicity seriously restricted their application in tumor therapy.

To our knowledge, when inflammation happens, leukocyte will be mobilized from bone marrow into circulation and move into inflammatory site. Some studies have exploited this pathological property to design cell-based drug delivery system. For

instance, monocytes were used as drug carrier to treat atherosclerosis with high efficiency [11]. As with other inflammatory responses, inflammation in the brain is also characterized by extensive leukocytes infiltration into brain tissue by cell diapedesis and chemotaxis [12–14]. Brynskikh et al. utilized macrophage as a drug vehicle to improve the delivery of redox enzymes into the brain for neuroprotection of dopaminergic neurons in a mouse model of Parkinson's disease. Therapeutic efficacy of macrophages loaded with nanozyme was confirmed by twofold reductions in microgliosis and twofold increase in tyrosine hydroxylase-expressing dopaminergic neurons [15].

Rudolf Virchow identified the presence of leukocytes within tumors for the first time in the 19th century, which indicated a possible link between inflammation and cancer [16]. Inflammation is a critical component in the progression of tumor, including initiation, promotion, invasion and metastasis [16, 17]. A larger number of immune cells, mainly macrophages and T cells, are recruited into tumor microenvironments. It has been reported that macrophages constitute up to a third of the whole tumor mass in glioma [18]. Additionally, hypoxia is the hallmark feature of most solid tumors due to their rapid growth and poorly organized vasculature. Such hypoxic pressure impedes the penetration of anticancer drugs into tumor tissues. Therefore, the hypoxic regions in tumor are usually resistant to radio- and chemotherapy [19, 20]. Interestingly, the chemoattractant released by tumor cells in response to hypoxia attract macrophages infiltration into tumor tissues [21, 22]. Huang et al. employed bone marrow-derived monocytes to deliver polymer bubbles and vesicles for chemotherapy of tumor hypoxia [23]. Inspired by these understandings, a novel strategy utilizing macrophage as a carrier to migrate across the BBB, BBTB and home into tumor sites is conceived. Importantly, macrophages are able to carry drugs into brain tumor throughout the whole progress.

In this manuscript, RAW264.7, a kind of mouse macrophage-like cell line with similar functions to primary macrophage cells, were used here to demonstrate the feasibility of macrophage as vehicle to deliver drug into glioma. Figure 1 illustrates schematic strategy adopted in this work for the construction of M-NPs and *in vivo* fate. A fluorescent dye, coumarin-6, and a near infrared dye, DiR, were respectively encapsulated to quantitatively or qualitatively track the behavior of a macrophage based drug delivery system. The stability of this system and its release kinetics in a simulated inflammatory environment was studied. Avascular U87 glioma spheroids were employed to explore the penetration ability of M-NPs system. The tumor targeting capacity of this system was validated in orthotopic U87 glioma bearing mice model by *in vivo* imaging system, and the brain distribution was evaluated by confocal microscopy in frozen brain slices.

RESULTS

Characterization of nanoparticles

In order to study the effect of particle size on the uptake efficiency of macrophages, nanoparticles in three sizes (50–100 nm, 100–200 nm, 200–300 nm) were prepared by emulsion-solvent evaporation method. The particle size, Zeta potential and polydispersity index (PDI) of the nanoparticles were listed in Table 1. Encapsulation of coumarin-6, DiR did not significantly influence the characteristics of nanoparticles. Owing to the water solubility of doxorubicin hydrochloride, the DOX-NPs were prepared by double-emulsion method. The size, zeta potential and PDI of DOX-NPs is 141.6 nm, -31.7mv and 0.086, respectively.

Effect of particle size on macrophages uptake

Macrophages itself could efficiently phagocytize nanoparticles by endocytosis. The size of NPs influences the phagocytosis capacity of macrophages greatly. Coumarin-6 was used as fluorescent probe to investigate the cellular uptake characteristics. As illustrated in Figure 2, qualitative fluorescent images showed that macrophages incubated with 100–200 nm NPs exhibited the highest fluorescence intensity among three types of NPs under the same incubation conditions. Quantitatively, the cellular uptake of 100–200 nm NPs was 1.56 and 2.0 fold of the uptake efficiency of 50–100 nm and 200–300 nm NPs, respectively.

Effect of DOX-NPs loading on macrophages viability

The function of macrophage as carrier is strongly correlated with its viability after the loading of DOX-NPs. Macrophages showed reduced viability after incubation with 10, 25, and 50 µg/ml free DOX. Whereas, incubation with DOX-NPs resulted in higher viability than that of free DOX under the same concentration (Figure 3). Hence, in a certain concentration range of DOX, DOX-NPs was successfully loaded with low toxicity into macrophages, leading us to conclude that macrophages would be a useful candidate as a biocarrier to deliver nanodrugs. It is worthwhile to note that the incubation concentration of NPs and cell viability should be carefully balanced because high drug concentration may cause toxicity to macrophages.

Release profile of NPs from macrophages

DiR was used to track the release profile of NPs from macrophages. The cells were pre-loaded with nanoparticles for 2 hours, then washed with phosphate buffered saline (PBS) and incubated in fresh media for different time intervals (0 h, 2 h, 4 h, 8 h, 12 h, 24 h).

The media was collected and the fluorescence intensity was measured by fluorospectro photometer. Sustained release of DiR-NPs from macrophages was observed and achieved cumulative release of 42% after 24 h incubation in Dulbecco's Modified Eagle Medium (DMEM) containing 10% fetal bovine serum (FBS). Meanwhile, a faster release pattern was obtained (71%) in DMEM containing 10% FBS with addition of LPS and IFN- γ (Figure 4), which indicated that drug release would be accelerated in tumor microenvironment.

***In vitro* glioma spheroid penetration of M-NPs**

In vitro U87 glioma spheroids model was established to evaluate the penetration ability of M-NPs. After 12 h incubation, M-NPs showed more extensive infiltration into tumor spheroids than NPs. M-NPs could reach about 56.42 μm away from the rim of the spheroids, and was 1.56 fold deeper than that of NPs which penetrated only 36.07 μm into glioma spheroids (Figure 5A, 5C). Multi-level scanning from the top of the glioma spheroid with an interval 20 μm into the core showed that the fluorescence intensity of M-NPs treatment is higher than that of NPs (Figure 5B, 5D). Therefore, nanoparticles loaded in macrophage could not only facilitate the uptake by tumor cells, but also enhance their penetration into tumor spheroids.

Tumor targeting of M-NPs

To determine the biodistribution of NPs and M-NPs, *in vivo* imaging was conducted to track the particles in nude mice bearing intracranial U87 glioma. Both the NPs and M-NPs could apparently accumulate in the tumor tissues from 0.5 h after injection (data not shown). However, the fluorescence intensity of M-NPs treated mice was much higher than that of NPs treated mice at all-time points from 2 to 24 h (Figure 6), indicating that macrophage as cell carrier significantly improved the tumor-targeting efficiency of NPs. Correspondingly, the conclusion was further confirmed by *ex vivo* imaging of the brains.

***In vivo* tumor localization of M-NPs**

Three weeks after glioma cell inoculation, *in vivo* brain distribution of coumarin 6-labeled NPs and M-NPs was measured 12 h after intravenous administration into mice. As shown in Figure 7, there was only a little green fluorescence distributed in glioma tissues in NPs group. but in the case of the M-NPs group, an obvious stronger fluorescent signal was detected and a much deeper permeation was observed at the glioma parenchyma. The results indicated that macrophage as carrier can increase the accumulation of NPs in brain tumor.

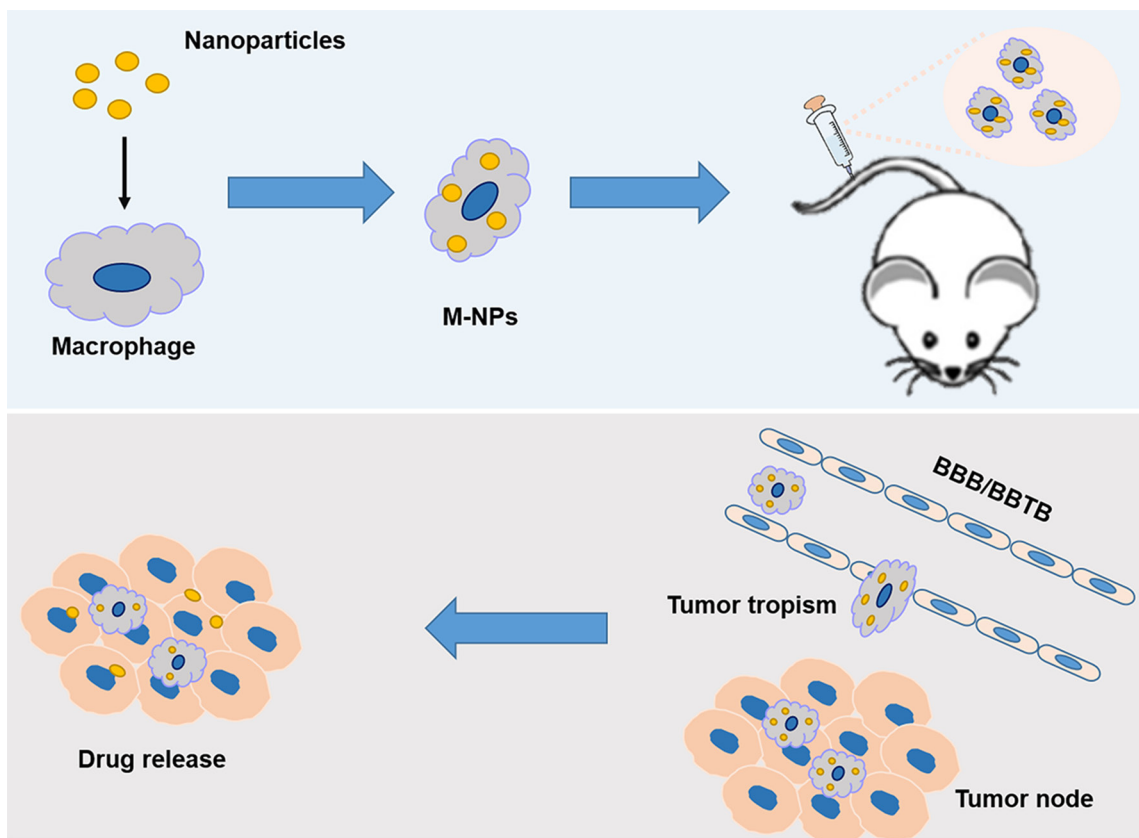


Figure 1: Schematic illustration of the construction of 'Macrophage-NPs' and their targeting delivery into brain tumor.

Table 1: Characterization of nanoparticles

Nanoparticles	Mean Size (nm)	Polydispersity (PDI)	Zeta potential (mV)
NP-Small	69.90 ± 3.730	0.29 ± 0.034	- 41.33 ± 3.092
NP-Middle	138.13 ± 2.205	0.10 ± 0.007	- 42.93 ± 1.305
NP-Large	236.67 ± 9.730	0.20 ± 0.029	- 43.90 ± 0.436

DISCUSSION

During the progression of glioma, tumor tissues are protected by BBB, BBTB and high IFP, which make the parenchyma inaccessible to therapeutic drugs [4, 7, 8]. Nanoparticle drug delivery systems with active targeting capabilities have been explored for enhancing drug delivery to glioma by conjugating target moiety onto the surface of nanoparticles [24, 25]. In recent decades, cell based drug delivery systems take advantage of circulatory cell (red blood cell, T cell, macrophage, antigen presenting cell, etc.) to improve the therapeutic effect of anti-cancer drugs [15, 26, 27]. Using cells as carriers for drug delivery offers several advantages over free drug, including improved drug efficacy, extended half-lives, sustained drug release, and limited immunogenicity and cytotoxicity.

When tumor occurs, the tumor inflammation environment could induce the overexpression of the cell adhesion molecules (CAMs) on the surface of endothelial cell monolayer, which mediate interaction between macrophages and endothelial cells, facilitate the initial process of macrophage rolling, firm attachment to endothelium and transmigration [28, 29]. Meanwhile, there are accumulating evidences showing that a larger number of macrophages are attracted and retained in hypoxia regions by local synthesis of chemoattractant in tumor cells undergoing hypoxia due to rapid tumor growth [20, 21]. We compared the chemotactic ability of unactivated RAW264.7 and activated RAW264.7 by boyden chamber method. The migration rate of unactivated and activated RAW264.7 is $9.28 \pm 0.54\%$ and $11.06 \pm 0.53\%$, respectively. No significant difference was

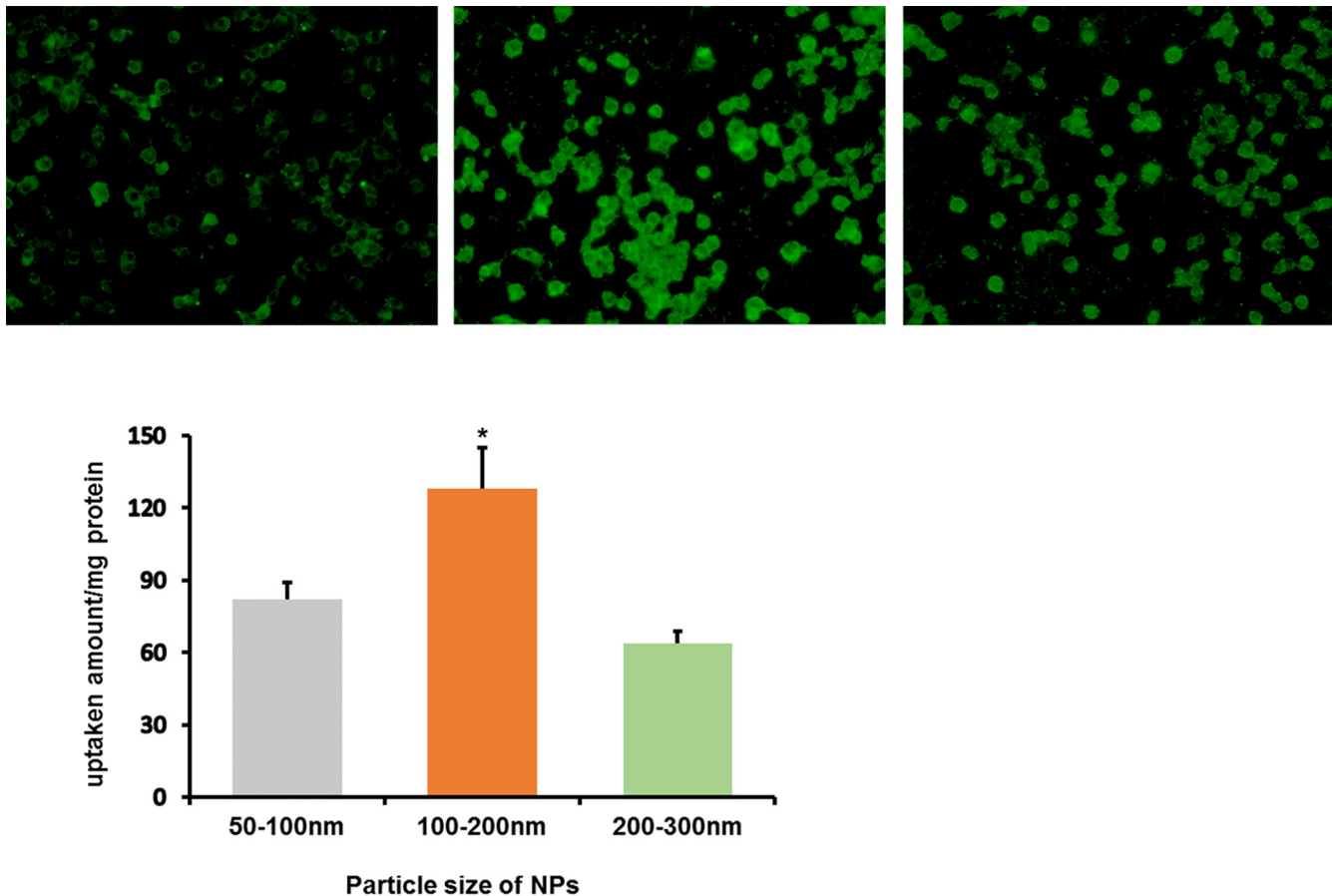


Figure 2: *In vitro* cellular uptake of coumarin-6-labeled NPs in three sizes by RAW264.7 after incubation for 2 h. (A) Left: 50–100 nm; Middle: 100–200 nm; Right: 200–300 nm. (B) The quantitative results of cellular uptake for RAW264.7, * $P < 0.05$, compared with other two groups.

found between them. Therefore, unactivated RAW264.7 cell line was chosen in this manuscript.

If free anticancer drugs are encapsulated into cells, it may cause damage to the carrier itself before arriving at tumor sites and suppress the functions of cells as transporter. Therefore, we encapsulated anticancer drugs into nanoparticles with the purpose to reduce the damage of the drug to the cell carriers [30]. As illustrated in Figure 2, CCK8 assay showed that the viability of macrophages incubated with NPs-DOX was higher than those incubated with free DOX. By blocking direct contact between the cell and the drug, DOX-NPs efficiently reduced drug-induced cellular toxicity. The properties of nanoparticles, such as size, shape, chemical functionality and surface charge, are closely related to the uptake capacity of macrophages [31]. Nanoparticles in three sizes were prepared by the same method using the same materials. Under identical conditions, 100–200 nm nanoparticles are easily internalized by macrophages compared with other two particles of different size, and the loading of NPs did not affect the migration of macrophages into tumor tissues [32].

Experiments performed on 3D glioma spheroids investigated the migratory potential of macrophages

loaded with nanoparticles. Tumor cells in spheroids display higher resistance to radio- and chemotherapy than monolayer tumor cells, and are thought to mimic tumor nodes well prior to vascularization *in vivo* [33, 34]. As illustrated in Figure 5, NPs loaded macrophages infiltration toward spheroids was observed to be 1.5-fold deeper penetration into the spheroids than free NPs. These results demonstrated that macrophage as an anticancer agent transporter could enhance drug delivery in inaccessible tumor hypoxic region effectively.

In vivo imaging experiments were performed to evaluate the behavior of M-NPs in nude mice bearing intracranial U87 glioma. The accumulation of NPs in tumors via passive EPR effect was limited, while M-NPs exhibited a significant superiority in glioma targeting with high fluorescent intensity at all-time points. Consistently, in frozen brain sections, the accumulation of NPs was low and located on the border of glioma. However, M-NPs showed an extensive distribution and deep penetration into glioma parenchyma, indicating circulating macrophages could overcome the barriers (BBB, BBTB, IFP) and penetrate into the tumor tissue. The major organs, including heart, liver, spleen, lung, kidney, and brain, were harvested 24 hours after the administration of M-NPs and

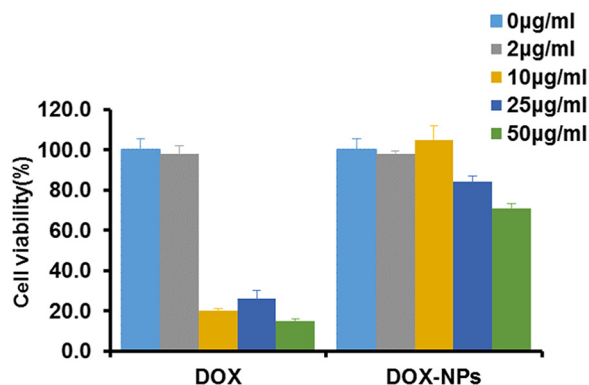


Figure 3: Macrophages viability after incubation with DOX or DOX-NPs for 12 h at 37°C.

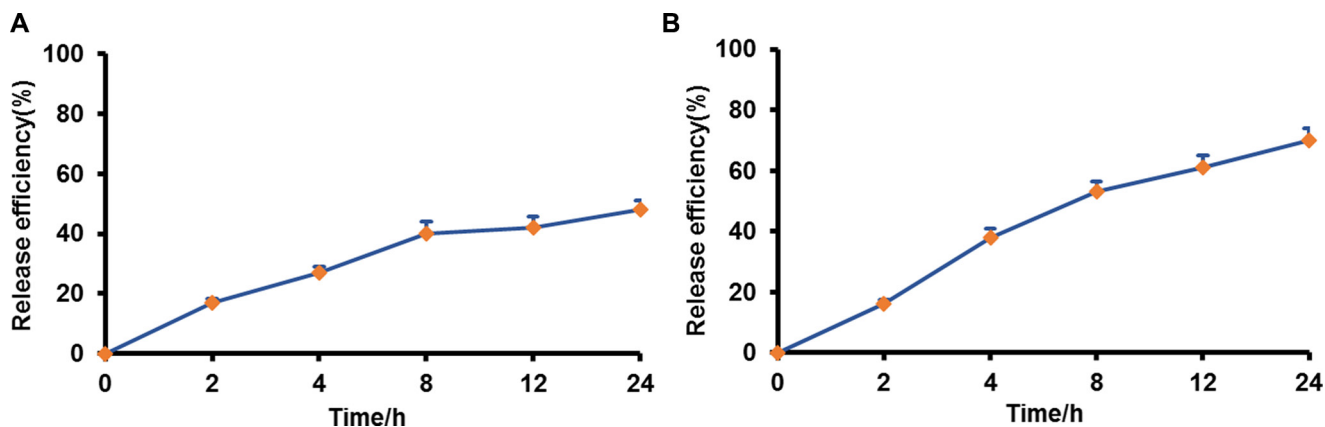


Figure 4: Drug release from pre-loaded macrophages in different medium. (A) DMEM, 10% FBS; (B) DMEM, 10% FBS, LPS and IFN- γ .

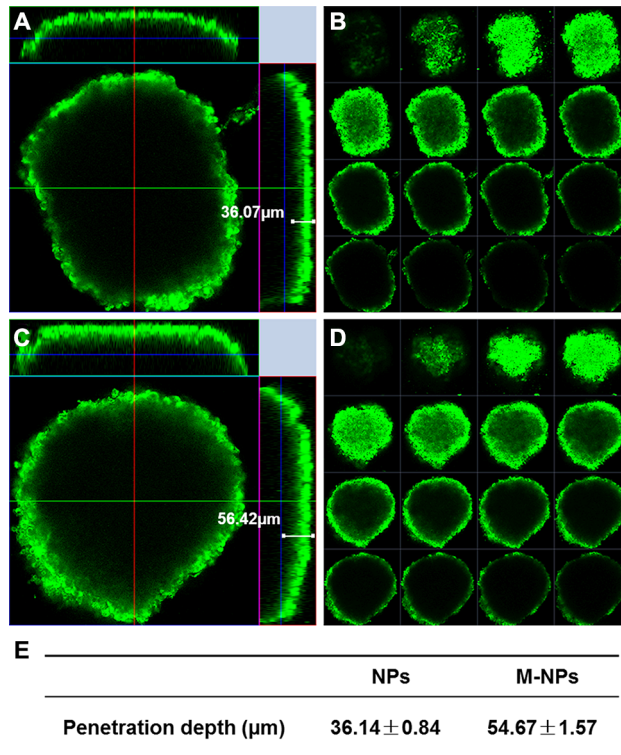


Figure 5: Penetration of coumarin-6-labeled NPs (A, B) and M-NPs (C, D) into U87 glioma spheroids after incubation for 12 h. (A and C) penetration depth of NPs and M-NPs ; (B and D) multi-level scan of the penetration of NPs and M-NPs with intervals of 20 μm; (E) the value of penetration depth were expressed as mean ± standard deviation ($n = 3$), $P < 0.05$.

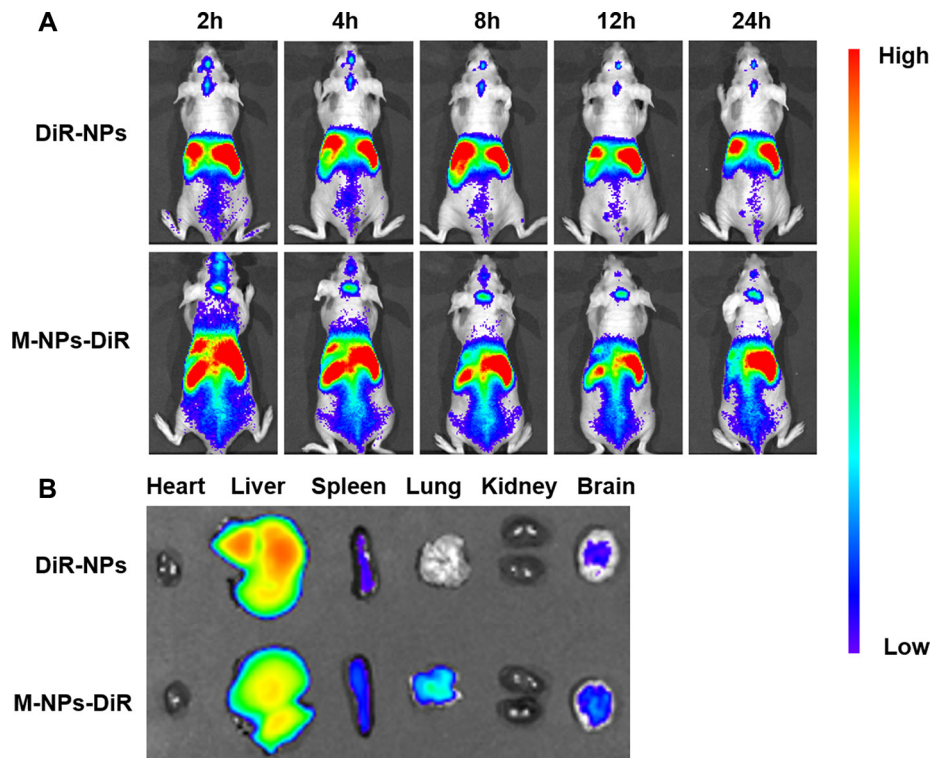


Figure 6: *In vivo* imaging of brain glioma-bearing nude mice administrated with DiR-labeled NPs and M-NPs at different time points (A), *Ex vivo* imaging of major organs collected at 24 h after dosing (B).

imaged under *ex vivo* fluorescence. The results illustrated in Figure 6B showed that there were some differences in tissues distribution between NPs and M-NPs, especially in the lung, which might due to pulmonary capillaries retention of macrophages.

It was reported that therapeutically meaningful amount of free DOX could be loaded into the RAW264.7 cells by short time incubation, About 65% of the drug were released from the cells in the first 2 h [35]. Less than 20% and only 42% NPs were released from preloaded macrophages after 2 h and 24 h incubation respectively, indicating the sustained release of NPs from macrophages. The release of drug from macrophages is a complicated process. Based on the results of our study and literature [13, 35, 36], we speculated that the drug could be released from macrophages in two ways. Firstly, NPs was excreted from macrophages by exocytosis, and the free drug diffused from NPs into extracellular medium subsequently. Secondly, the free drug might be released from NPs within cells, and then diffuse into the surroundings via passive driving force caused by concentration gradient between cells and surroundings, or the multi-drug resistant proteins P-gp expressed in the macrophage could pump the drug out of the cells. The former plays a dominant role in the process. Once NPs loading macrophages enter into the

tumor sites, tumor inflammation environment will activate macrophages and result in significant increase in drug release from macrophages. It was found that when the cell carrier enters into diseased site in Parkinson's disease, the direct contact between cell carrier and endothelial, neuronal and glial cells promote drug transfer through endocytosis-independent mechanism, which mainly involve fusion of cell membranes, bridging conduits and nanoparticle lipid coating [37]. Therefore, it is supposed that the increased nanoparticles transfer might be occurred in a similar way after macrophage being attracted into tumor tissue. The inner of tumor tissue is filled with inflammatory cytokines [16, 17]. In order to mimic the inflammatory microenvironment in tumor tissue, LPS and IFN- γ were added to the medium according to previous reports [42, 43]. When LPS and IFN- γ were added, they would bind with Toll-like receptor 4 and IFN- γ receptor expressed on macrophage respectively, activate RAW264.7 and finally promote drug release by exocytosis.

The study demonstrated the feasibility of using macrophages as carriers for targeting anticancer drug into glioma. Considering that the M2 phenotype macrophage in tumor promotes tumor growth and contributes to tumor angiogenesis, its migration into tumor would weaken the effect of anticancer agents [38], the M1 type macrophage

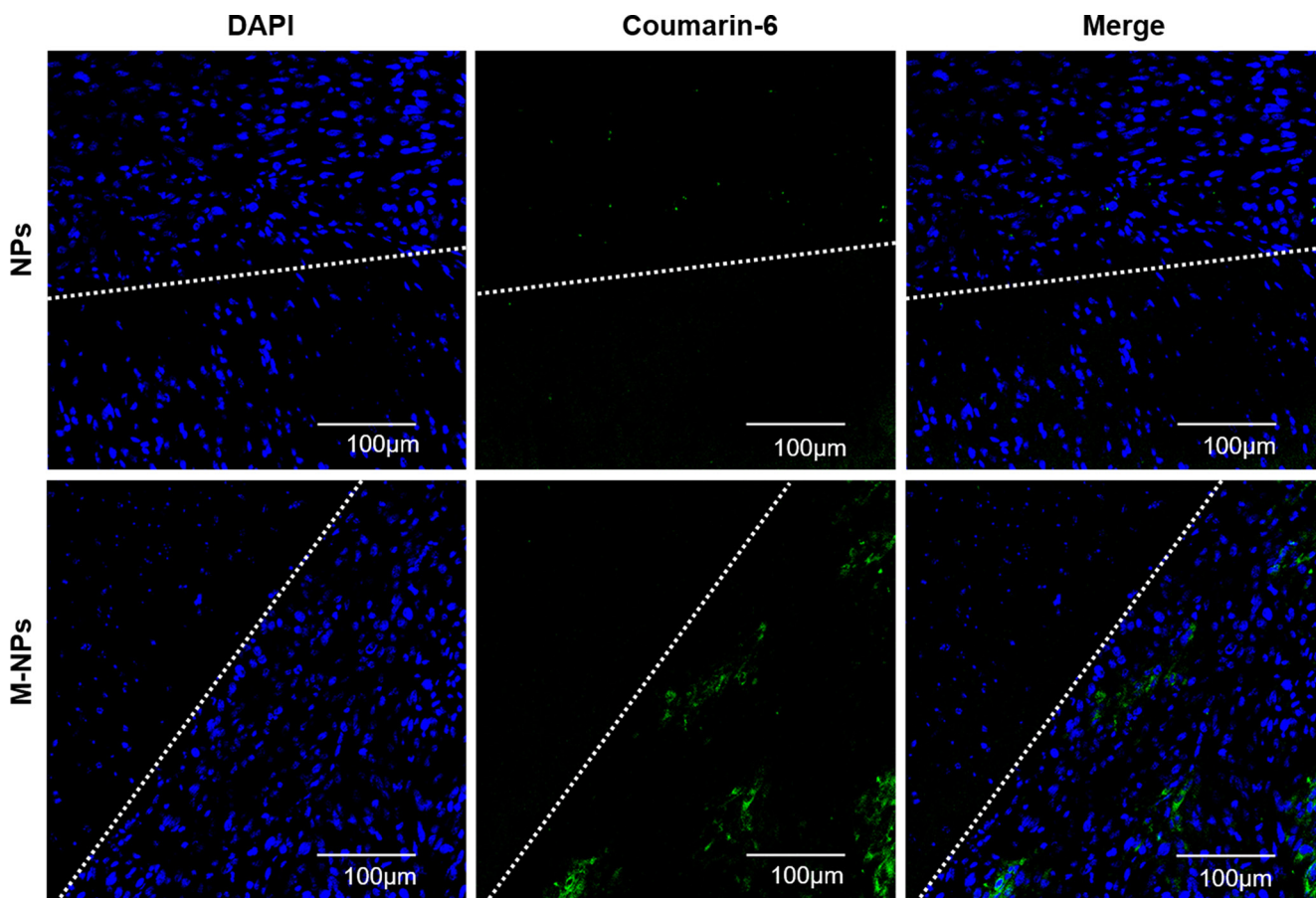


Figure 7: *In vivo* glioma distribution of coumarin-6-labeled NPs and M-NPs 12 h after administration. Blue: DAPI stained cell nuclei, Green: Coumarin-6-labeled NPs, White line: border of the glioma, Dense area: glioma tissue, Sparse area: brain tissue.

maybe the best candidate as a cell carrier since it resist tumor progression. Our ultimate goal is to encapsulate nanodrugs into patient derived M1 type macrophage, then transfer the macrophage-NPs back into the patient to achieve improved efficacy and to reduce immune responses.

MATERIALS AND METHODS

Reagents

PLGA (LA: GA = 75:25, Mw: 12,000 Da) was kindly provided by Evonik (Germany). Emprove exp poly (vinyl alcohol) (PVA) 4–88 was given as a present from Merck (Darmstadt, Germany). DiR (1, 1'-dioctadecyl-3, 3, 3', 3'-tetramethyl indotricarbocyanine Iodide), Coumarin-6 was purchased from Caliper (USA), Aladdin (Shanghai, China) respectively. DAPI (4, 6-diamidino-2-phenylindole) was purchased from Beyotime (Haimen, China). Doxorubicin hydrochloride (DOX·HCL) was obtained from Melonapharma (Dalian, China). Lipopolysaccharide (LPS) from Sigma (St. Louis, MO, USA) and IFN- γ from Peprotech (Rokey Hill, USA) were used. All cell culture reagents were purchased from Corning, Inc. (VA, USA) except Gibco fetal bovine serum.

Cell culture

RAW264.7 cell lines, obtained from the Chinese Academy of Sciences Cells Bank (Shanghai, China), were cultured in Dulbecco's Modified Eagle Medium (DMEM) supplemented with 10% FBS, 1% L-glutamine, 1% antibiotics and 1% nonessential amino acids at 37°C, 5% CO₂, and 95% humidity in a CO₂ incubator.

Animals

Balb/c nude mice (Female, 4–5 weeks, 20–22 g) were obtained from the Shanghai B&K Lab Animal Ltd. (Shanghai, China) and housed under standard conditions with free access to food and water. The protocol of animal study was approved by the Animal Experimentation Ethics Committee of Fudan University.

Preparation of NPs

PLGA nanoparticles in three sizes loaded with fluorescent dye were prepared by emulsion/solvent evaporation method according to the procedure reported previously [39]. The particle size could be controlled by adjusting PLGA amount, emulsifier concentration, ultrasonic time. Briefly, 5 mg, 20 mg, 150 mg PLGA and 100 μ l coumarin 6 (1 mg/ml) or 10 μ l DiR (5 mg/ml) were dissolved in 1 ml dichloromethane respectively, to which 2 ml of different concentration (0.05%, 0.5%, 2.0% respectively) of sodium cholate aqueous solution was added, with the mixture sonicated on ice using a probe sonicator (Scientz Biotechnology Co., Ltd., China). Then

the emulsion was dispersed into 18 ml of corresponding concentration of sodium cholate aqueous solution under rapid magnetic stirring for 60 min. After evaporating dichloromethane with a ZX-98 rotary evaporator (LOOYE, China) at 40°C, the suspensions were centrifuged using a TJ-25 centrifuge (Beckman Counter, USA). After discarding the supernatant, the obtained nanoparticles were re-suspended with 0.1 M PBS buffer (pH 7.4) and stored at 4°C for further use.

DOX·HCL loaded nanoparticles were prepared by the double/emulsion method as previously reported [40, 41]. 20 mg PLGA was dissolved in 1 ml of ethyl acetate followed by addition of 100 μ l of DOX·HCL (10 mg/ml), the first emulsion was formed by tip sonication in ice bath, to which 2 ml of 2% PVA was added immediately followed by sonication in ice bath to finally form double emulsion. The emulsion was dispersed into 9 ml of 2%PVA with magnetic stirring in room temperature (600 rpm) for 2 hours. The organic solvent was removed by vacuum evaporation at 40°C for 20min. The residues were concentrated by centrifugation using a TJ-25 centrifuge.

The physiochemical parameters of NPs, including particle size, zeta potential, polydispersity were measured using a dynamic light scattering detector (Zetasizer, Nano-ZS, Malvern, UK).

Preload of NPs in macrophages

RAW264.7 were seeded into 12-well plates at a density of 2×10^4 cells/ml. 24 h later, the cells were incubated with 200 ng/mL coumarin-6-loaded NPs in three particle sizes (50–100 nm, 100–200 nm, 200–300 nm) respectively in the absence of FBS for 2 h ($n = 3$). After being rinsed with PBS three times, the cells were harvested and probe sonicated in ice bath, then centrifuged at 8000 rpm for 10min. The supernatant is collected. One half was measured for protein concentration, the other for fluorescence intensity. The fluorescence intensity was normalized for protein content and expressed in fluorescence intensity per mg of protein. Meanwhile, the pre-loaded cells were washed three times with PBS and observed under fluorescent microscopy (Leica, DMI4000D, Germany) immediately.

Cell viability assay

5×10^3 RAW264.7 in 100 μ l medium were cultured into each well of a 96-well plate. Free DOX·HCL or DOX-NPs were then added at concentrations 2, 10, 25 and 50 μ g/ml. Macrophages were incubated with DOX or DOX-NPs for 12 h. At the end of incubation, the culture medium was discarded and the cells were washed with PBS. Cell counting kit-8 (CCK-8) (Beyotime, Nantong, China) was used to test viability of macrophages by incubating with 100 μ l of fresh medium containing 10 μ l of CCK8 solution for 3 h at 37°C in 5% CO₂. The absorbance of medium was measured at 450 nm using a multimode reader (Bio-tek).

***In vitro* release study**

RAW264.7 were seeded into 12-well plates at a density of 2×10^4 cells/ml. After 24 h, cells were pre-loaded with DiR-labeled NPs for 2 h, washed three times with ice-cold PBS, The NPs loaded macrophages were incubated with two different fresh release media, DMEM (no phenol red) and 10% FBS, DMEM (no phenol red) and 10% FBS with 500 ng/ml LPS and 200 ng/ml IFN- γ , respectively ($n = 3$). LPS and IFN- γ were added to mimic tumor inflammation microenvironment to activate RAW264.7 [42, 43]. The media was collected at various time intervals. The levels of fluorescence were measured on a Shimadzu RF5000 fluorescent spectrophotometer.

Avascular glioma spheroids penetration of M-NPs

Three-dimensional spheroids of U87 cells were prepared by a lipid overlay method as reported previously [44]. Briefly, a 48-well plate was pretreated with 200 μ l 2% (w/v) agarose gel to prevent cell adhesion, U87 cells were seeded into each well at the density of 2×10^3 cells/well, then the plates were gently agitated for 5 min and cultured at 37°C in the presence of 5% CO₂ for 7 days. Glioma spheroids were incubated with coumarin-6 labeled NPs and M-NPs respectively for 12 hours, with the final coumarin-6 concentration at 100 ng/ml in each well. After that, glioma spheroids were rinsed with PBS for three times, fixed with 4% paraformaldehyde, transferred to a chambered covered slip, and analyzed by confocal microscopy (LSM710, Leica, Germany).

***In vivo* imaging of M-NPs in orthotopic U87 glioma mice**

The orthotopic U87 glioma bearing mice model was established by slowly injecting U87 cells (5×10^5 cells/5 μ l in pH 7.4 PBS) into right corpus striata of nude mice with the help of a stereotaxic apparatus. Three weeks later, six nude mice bearing intracranial U87 glioma were divided into two groups randomly ($n = 3$), the mice in two groups were intravenously administrated with 200 μ l DiR-NPs and M-NPs-DiR via the tail vein. The distribution of fluorescence was observed at predetermined time points (2, 4, 8, 12, 24 h) via an *in vivo* imaging system (IVIS Spectrum, Caliper, USA). Twenty-four hours after administration, the mice were sacrificed and the brains were harvested and imaged.

Brain distribution of M-NPs in orthotopic U87 glioma mice

Coumarin-6-loaded NPs and M-NPs were injected to the orthotopic U87 glioma bearing mice respectively ($n = 3$) by tail vein. The mice were anesthetized 12 hours later, and their hearts were perfused with saline followed

by 4% paraformaldehyde. The brains were collected, fixed with 4% paraformaldehyde overnight, and dehydrated using 15% glucose in PBS followed by 30% glucose in PBS. Then the tumors were embedded in Tissue Tek O.C.T. compound, frozen at -80°C and sectioned as slides at 5 μ m thicknesses. The slides were subjected to confocal microscopy analysis after stained with DAPI for 10 min and rinsed with PBS.

Statistical analysis

All the data were presented as mean \pm standard deviation. Unpaired student's *t* test was used for between two-group comparisons. Statistical significance was defined as $p < 0.05$.

ACKNOWLEDGMENTS AND FUNDING

We thank for the financial support from National Basin Research Program of China (No. 2013CB 932500), National Natural Science Foundation of China (No.81361140344), and the Development Project of Shanghai Peak Disciplines – Integrated Chinese and Western Medicine.

CONFLICTS OF INTEREST

There is no conflicts of interest.

REFERENCES

1. Behin A, Hoang-Xuan K, Carpentier AF, Delattre JY. Primary brain tumours in adults. *Lancet*. 2003; 361: 323–331.
2. Madsen SJ, Baek SK, Makkouk AR, Krasieva T, Hirschberg H. Macrophages as Cell-Based Delivery Systems for Nanoshells in Photothermal Therapy. *Ann Biomed Eng*. 2012; 40:507–515.
3. Newton HB. Advances in strategies to improve drug delivery to brain tumors. *Expert Rev Neurother*. 2006; 6:1495–1509.
4. Zhan C, Lu W. The blood-brain/tumor barriers: challenges and chances for malignant gliomas targeted drug delivery. *Curr Pharm Biotechnol*. 2012; 13:2380–2387.
5. Hawkins BT, Egleton RD. Pathophysiology of the blood-brain barrier: animal models and methods. *Curr Top Dev Biol*. 2008; 80:277–309.
6. Wolburg H, Lippoldt A. Tight junctions of the blood-brain barrier: development, composition and regulation. *Vascul Pharmacol*. 2002; 38:323–337.
7. Liu Y, Lu W. Recent advances in brain tumor-targeted nano-drug delivery systems. *Expert Opin Drug Deliv*. 2012; 9:671–686.
8. Heldin CH, Rubin K, Pietras K, Ostman A. High interstitial fluid pressure - an obstacle in cancer therapy. *Nat Rev Cancer*. 2004; 4:806–813.

9. Gao X, Li C. Nanoprobes visualizing gliomas by crossing the blood brain tumor barrier. *Small*. 2014; 10:426–440.
10. Garg T, Bhandari S, Rath G, Goyal AK. Current strategies for targeted delivery of bio-active drug molecules in the treatment of brain tumor. *J Drug Target*. 2015:1–23.
11. Lee S. Monocytes: a novel drug delivery system targeting atherosclerosis. *Journal of Drug Targeting*. 2014; 22:138–145.
12. Batrakova EV, Gendelman HE, Kabanov AV. Cell-mediated drug delivery. *Expert Opin Drug Del*. 2011; 8:415–433.
13. Tao Y, Ning M, Dou H. A novel therapeutic system for malignant glioma: nanoformulation, pharmacokinetic, and anticancer properties of cell-nano-drug delivery. *Nanomedicine: Nanotechnology, Biology and Medicine*. 2013; 9:222–232.
14. Baek SK, Makkouk AR, Krasieva T, Sun CH, Madsen SJ, Hirschberg H. Photothermal treatment of glioma; an *in vitro* study of macrophage-mediated delivery of gold nanoshells. *J Neuro-Oncol*. 2011; 104:439–448.
15. Brynskikh AM, Zhao Y, Mosley RL, Li S, Boska MD, Klyachko NL, Kabanov AV, Gendelman HE, Batrakova EV. Macrophage delivery of therapeutic nanozymes in a murine model of Parkinson's disease. *Nanomedicine (Lond)*. 2010; 5:379–396.
16. Grivennikov SI, Greten FR, Karin M. Immunity, Inflammation, and Cancer. *Cell*. 2010; 140:883–899.
17. Coussens LM, Werb Z. Inflammation and cancer. *Nature*. 2002; 420:860–867.
18. Fleige G, Nolte C, Synowitz M, Seeberger F, Kettenmann H, Zimmer C. Magnetic labeling of activated microglia in experimental gliomas. *Neoplasia*. 2001; 3:489–499.
19. Murdoch C, Lewis CE. Macrophage migration and gene expression in response to tumor hypoxia. *Int J Cancer*. 2005; 117:701–708.
20. Wilson WR, Hay MP. Targeting hypoxia in cancer therapy. *Nat Rev Cancer*. 2011; 11:393–410.
21. Choi MR, Stanton-Maxey KJ, Stanley JK, Levin CS, Bardhan R, Akin D, Badve S, Sturgis J, Robinson JP, Bashir R, Halas NJ, Clare SE. A cellular Trojan horse for delivery of therapeutic nanoparticles into tumors. *Nano Letters*. 2007; 7:3759–3765.
22. Lewis CE, Pollard JW. Distinct role of macrophages in different tumor microenvironments. *Cancer Res*. 2006; 66:605–612.
23. Huang WC, Chiang WH, Cheng YH, Lin WC, Yu CF, Yen CY, Yeh CK, Chern CS, Chiang CS, Chiu HC. Tumortropic monocyte-mediated delivery of echogenic polymer bubbles and therapeutic vesicles for chemotherapy of tumor hypoxia. *Biomaterials*. 2015; 71:71–83.
24. Chen Y, Liu L. Modern methods for delivery of drugs across the blood-brain barrier. *Adv Drug Deliv Rev*. 2012; 64:640–665.
25. Huang Y, Jiang Y, Wang H, Wang J, Shin MC, Byun Y, He H, Liang Y, Yang VC. Curb challenges of the “Trojan Horse” approach: smart strategies in achieving effective yet safe cell-penetrating peptide-based drug delivery. *Adv Drug Deliv Rev*. 2013; 65:1299–1315.
26. He H, Ye J, Wang Y, Liu Q, Chung HS, Kwon YM, Shin MC, Lee K, Yang VC. Cell-penetrating peptides mediated encapsulation of protein therapeutics into intact red blood cells and its application. *Journal of Controlled Release*. 2014; 176:123–132.
27. Stephan MT, Stephan SB, Bak P, Chen JZ, Irvine DJ. Synapse-directed delivery of immunomodulators using T-cell-conjugated nanoparticles. *Biomaterials*. 2012; 33:5776–5787.
28. Wong D, Prameya R, Dorovini-Zis K. Adhesion and migration of polymorphonuclear leukocytes across human brain microvessel endothelial cells are differentially regulated by endothelial cell adhesion molecules and modulate monolayer permeability. *J Neuroimmunol*. 2007; 184:136–148.
29. Penberthy TW, Jiang Y, Graves DT. Leukocyte adhesion molecules. *Crit Rev Oral Biol Med*. 1997; 8:380–388.
30. Choi J, Kim HY, Ju EJ, Jung J, Park J, Chung HK, Lee JS, Park HJ, Song SY, Jeong SY, Choi EK. Use of macrophages to deliver therapeutic and imaging contrast agents to tumors. *Biomaterials*. 2012; 33:4195–4203.
31. Dobrovolskaia MA, Aggarwal P, Hall JB, McNeil SE. Preclinical studies to understand nanoparticle interaction with the immune system and its potential effects on nanoparticle biodistribution. *Mol Pharm*. 2008; 5:487–95.
32. Chang Y-N, Guo H, Li J, Song Y, Zhang M, Jin J, Xing G, Zhao Y. Adjusting the Balance between Effective Loading and Vector Migration of Macrophage Vehicles to Deliver Nanoparticles. *PLoS ONE*. 2013; 8: e76024.
33. Baek SK, Makkouk AR, Krasieva T, Sun CH, Madsen SJ, Hirschberg H. Photothermal treatment of glioma; an *in vitro* study of macrophage-mediated delivery of gold nanoshells. *J Neurooncol*. 2011; 104:439–448.
34. Hirschhaeuser F, Menne H, Dittfeld C, West J, Mueller-Klieser W, Kunz-Schughart LA. Multicellular tumor spheroids: An underestimated tool is catching up again. *J Biotechnol*. 2010; 148:3–15.
35. Fu J, Wang D, Mei D, Zhang H, Wang Z, He B, Dai W, Wang X, Zhang Q. Macrophage mediated biomimetic delivery system for the treatment of lung metastasis of breast cancer. *J Control Release*. 2015; 204:11–19.
36. Klyachko NL, Haney MJ, Zhao Y, Manickam DS, Mahajan V, Suresh P, Hingtgen SD, Mosley RL, Gendelman HE, Kabanov AV, Batrakova EV. Macrophages offer a paradigm switch for CNS delivery of therapeutic proteins. *Nanomedicine (Lond)*. 2014; 9:1403–1422.
37. Haney MJ, Zhao Y, Li S, Higginbotham SM, Booth SL, Han HY, Vetro JA, Mosley RL, Kabanov AV, Gendelman HE, Batrakova EV. Cell-mediated transfer of catalase nanoparticles from macrophages to brain endothelial, glial and neuronal cells. *Nanomedicine (Lond)*. 2011; 6:1215–1230.

38. Hao NB, Lu MH, Fan YH, Cao YL, Zhang ZR, Yang SM. Macrophages in tumor microenvironments and the progression of tumors. *Clin Dev Immunol.* 2012; 2012:948098.
39. Zhang L, Han L, Qin J, Lu W, Wang J. The use of borneol as an enhancer for targeting aprotinin-conjugated PEG-PLGA nanoparticles to the brain. *Pharm Res.* 2013; 30:2560–2572.
40. Tewes F, Munnier E, Antoon B, Ngaboni Okassa L, Cohen-Jonathan S, Marchais H, Douziech-Eyrolles L, Souce M, Dubois P, Chourpa I. Comparative study of doxorubicin-loaded poly(lactide-co-glycolide) nanoparticles prepared by single and double emulsion methods. *Eur J Pharm Biopharm.* 2007; 66:488–492.
41. Sheng J, Han L, Qin J, Ru G, Li R, Wu L, Cui D, Yang P, He Y, Wang J. N-Trimethyl Chitosan Chloride-Coated PLGA Nanoparticles Overcoming Multiple Barriers to Oral Insulin Absorption. *ACS Appl Mater Interfaces.* 2015; 7:15430–15441.
42. Glass CK, Natoli G. Molecular control of activation and priming in macrophages. *Nat Immunol.* 2015; 17:26–33.
43. Hambardzumyan D, Gutmann DH, Kettenmann H. The role of microglia and macrophages in glioma maintenance and progression. *Nat Neurosci.* 2015; 19:20–27.
44. Gao H, Yang Z, Zhang S, Cao S, Pang Z, Yang X, Jiang X. Glioma-homing peptide with a cell-penetrating effect for targeting delivery with enhanced glioma localization, penetration and suppression of glioma growth. *J Control Release.* 2013; 172:921–928.

Published in final edited form as:

Expert Opin Drug Deliv. 2011 April ; 8(4): 415–433. doi:10.1517/17425247.2011.559457.

Cell-Mediated Drugs Delivery

Elena V. Batrakova^{1,2,*}, Howard E. Gendelman^{1,2,3,4}, and Alexander V. Kabanov^{1,2,4,5}

¹Center for Drug Delivery and Nanomedicine, University of Nebraska Medical Center, Omaha, Nebraska, USA

²Department of Pharmaceutical Sciences, University of Nebraska Medical Center, Omaha, Nebraska, USA

³Center for Neurodegenerative Disorders, University of Nebraska Medical Center, Omaha, Nebraska, USA

⁴Department of Pharmacology and Experimental Neuroscience, University of Nebraska Medical Center, Omaha, Nebraska, USA

⁵Department of Chemistry, M.V. Lomonosov Moscow State University, Moscow, Russia.

Abstract

INTRODUCTION—Drug targeting to sites of tissue injury, tumor or infection with limited toxicity is the goal for successful pharmaceuticals. Immunocytes (including mononuclear phagocytes (dendritic cells, monocytes and macrophages), neutrophils, and lymphocytes) are highly mobile; they can migrate across impermeable barriers and release their drug cargo at sites of infection or tissue injury. Thus immune cells can be exploited as trojan horses for drug delivery.

AREAS COVERED IN THIS REVIEW—This paper reviews how immunocytes laden with drugs can cross the blood brain or blood tumor barriers, to facilitate treatments for infectious diseases, injury, cancer, or inflammatory diseases. The promises and perils of cell-mediated drug delivery are reviewed, with examples of how immunocytes can be harnessed to improve therapeutic end points.

EXPERT OPINION—Using cells as delivery vehicles enables targeted drug transport, and prolonged circulation times, along with reductions in cell and tissue toxicities. Such systems for drug carriage and targeted release represent a novel disease combating strategy being applied to a spectrum of human disorders. The design of nanocarriers for cell-mediated drug delivery may

*Correspondence: Elena V. Batrakova, Center for Drug Delivery and Nanomedicine, 985830 Nebraska Medical Center, Omaha, NE 68198-5830; Tel: (402) 559-9364 ; Fax (402) 559-9365, ebatrako@unmc.edu.

Article Highlights

- Using cell-mediated drug delivery systems offers several advantages including: a) targeted drug transport to disease sites; b) prolonged drug half-lives; c) time-controlled release of loaded drugs; and d) diminished drug immunogenicity and cytotoxicity profiles.
- The goals need to be achieved for successful cell-mediated drug delivery include: a) high drug loading into cell-carriers; b) efficient preservation of entrapped therapeutic agents against disintegration and clearance in the host cells; c) drug triggered release at the site of action; d) efficient homing of cell-carriers to a disease site; e) safety of cell-based drug formulations for the whole organism.
- Two different approaches are utilized in cell-mediated drug delivery: genetically modified cell-carriers producing therapeutically active molecules; and drug loaded cell-carriers used as “Trojan horses” to deliver the drug to the disease side.
- Living cells for drug carriage and release represent a novel disease combating strategy that can be applied to a spectrum of human infectious, cancerous, and degenerative disorders.

differ from those used for conventional drug delivery systems; nevertheless, engaging different defense mechanisms into drug delivery may open new perspectives for the active delivery of drugs.

Keywords

cell-carriers; drug delivery; immunocytes; nanoparticles; targeted drug transport

Introduction

The development of targeted drug delivery is amongst the most important goals of pharmaceutical research. Its realization can lead to improved therapeutic efficacy, reductions in drug dosing intervals, and decreased toxicities. However, this is not a simple task as drug homing to pathologically relevant disease sites has only recently been investigated. Obstacles are substantial and include sustained time-based plasma concentrations and local blood flow.

1. Promise and Perils of Cell-Mediated Drug Delivery

Using immunocytes, mononuclear phagocytes (MP; monocytes, macrophages, and dendritic cells) lymphocytes, and neutrophils and stem cells as drug carrier systems offers several advantages over common drug administration regimens. These include targeted drug transport to disease sites; prolonged drug half-lives; time-controlled drug release; and diminished drug immunogenicity and cytotoxicity profiles. Immunocytes and stem cells exhibit an intrinsic homing property enabling them to migrate to sites of injury, inflammation, and tumor. In addition, they can act as Trojan horses carrying concealed drug cargoes while migrating across impermeable barriers (for example, the blood brain or blood tumor barriers) to sites of disease.

Despite such advantages, there is as yet limited success for several reasons. *First*, drug loading in cell carriers is low. *Second*, there are limitations due to the ability of immunocytes and stem cells to efficiently disintegrate and clear entrapped therapeutic agents. *Third*, the loaded drug should not be prematurely released, but unloaded, in continuous action, upon the cell's arrival to the site of action or disease. *Fourth*, the cell carriers should migrate to the disease site in substantial quantities. This should not be compromised during drug loading. *Finally*, all used formulations must be safe for both the cell carrier and the organism.

Many of these limitations can be addressed by incorporation of drugs into protective polymeric nanocarriers (liposomes and lipid nanoparticles¹⁻⁴, micelles⁵⁻⁸, nanogels^{9, 10}, nanospheres and nanocapsules^{11, 12}, solid nanoparticles and nanosuspensions¹³⁻¹⁶, block ionomer complexes^{17, 18} or nanofibers and nanotubes^{19, 20}) that preserve drugs inside subcellular organelles (Figure 1). The ideal drug carrier for cell-mediated delivery should have optimal size, shape and surface characteristics; multivalent attachment; controlled drug release; and biocompatibility. All these characteristics are essential for translating cell-mediated drug delivery systems for human use.

Drug loading into cell-carriers—Nanocarriers commonly have a core-shell structure. Their central part (such as aqueous pool of nanospheres, hydrophobic core of micelles, or polyelectrolyte core of nanogels) permits drug entrapment. It is surrounded with a polymer shell (or lipids in liposomes and lipid nanoparticles), which defines the nanocarrier dispersion stability, circulation time and cell interactions^{1-8, 10, 11, 13, 14, 17, 18}. Both the core and shell are crucial for successful cell-mediated delivery. For example, the surface coating affects the ability of particles to internalize into the cells and therefore, affects the

loading of cell-carriers. In general, charged nanocarriers are rapidly taken up by MP and other immunocytes or stem cells compared to neutral nanoparticles^{1, 21-25}. The recognition occurs by receptors located on the cell plasma membranes, in particular, mannose, complement, and Fc receptors (MR, CR and FcR)²⁶⁻²⁸. In general, MR recognize mannans, as well as integrins (for example CD11b/CD18), CR interact with particles after nonspecific complement opsonization, and FcR recognize particles after specific antibody opsonization²⁸. Furthermore, positively charged nanoparticles accumulate in MP to a greater extent than negatively charged particles. Thus, positively charged nanoparticles prepared by high pressure homogenization with antiretroviral drugs, indinavir (IDV), ritonavir (RTV), and efavirenz (EFV) accumulate in MP at about two-fold greater than the same size negatively charged carriers¹⁴. Similar effect was reported for nanoparticles (“nanozymes”) comprising of redox enzyme, catalase, and variant synthetic polyelectrolyte block copolymers²⁹. Loading capacity of nanozymes comprising of positively-charged mono-polymers (polyethyleneimine-(PEI) and poly-L-lysine- (PL) based) is greater than the nanozyme prepared with negatively-charged block poly-L-glutamic acid (PGLU)-based copolymer, This likely occurs due to the greater absorption and internalization of positively-charged nanoparticles to negatively-charged outside plasma membrane of cell-carriers.

An electrostatically neutral and hydrophilic poly(ethylene glycol) (PEG) is perhaps the most common shell-forming polymer currently used in injectable nanocarriers³⁰⁻³². Particularly, commercial PEGylated liposome-encapsulated Dox, Doxil, is approved for use in the treatment of recurrent ovarian cancer, AIDS-related Kaposi's sarcoma³³ and metastatic breast cancer³⁴. However, PEG is by far not the only polymer that should be considered in the context of the cell-mediated delivery, as it can limit cellular uptake as was demonstrated for microspheres bearing high-density surface PEG chains that were resistant to phagocytosis³⁵. Similar results were obtained with nanoparticles comprised of catalase and positively charged polymers based on PEI²⁹. Thus, loading capacity of nanozymes without PEG corona in MP was significantly greater than those with PEG. To this end, modification of nanocarrier shell with specific vector moieties can provide for targeted cell delivery of nanocarriers^{1, 26, 36-38}. In particular, modification of PEG shell of a poly(amidoamine) nanoparticles (PAMAM) with streptavidin facilitates targeting to biotinylated T-cell markers such as anti-CD3 or peptide/ major histocompatibility (MHC) complexes³⁹ (Figure 2).

Size and shape of nanocarriers are also of importance for cell uptake, although the phagosome may have different sizes depending of the size of the particles, which can range from as little as few hundred nanometers^{35, 40, 41} to several of microns⁴². For example, murine bone marrow-derived macrophages accumulate IgG-opsonized latex beads greater than 20 μm in diameter⁴³. Furthermore, particles with the size about 1 μm were accumulated at greater extent (2.56 fold) than smaller drug carriers at 500 μm ¹⁴.

A recent study by Champion et al. reported striking effects of shape of particles on phagocytosis in alveolar rat macrophages⁴⁴. Polystyrene-based particles of more than twenty shapes including spheres, rectangles, rods, worms, oblate ellipses, elliptical disks and UFO-like particles were manufactured. The local particle shape at the point where it was attached to the cell played the crucial role in phagocytosis. For example, a macrophage attached to a sharper side of the ellipse would internalize the particle in a few minutes. In contrast, a macrophage attached to a dull side would not internalize the same ellipse for hours. Although, particle size played a reduced role in the initiation of the phagocytosis it could of course affect its completion especially when the particle volume exceeded that of a cell.

Drug preservation inside cells—The stability of the drug loaded into cell carriers among other factors can depend on the intracellular trafficking of the nanocarriers. In

general, drug-loaded nanocarriers need to avoid lysosomes to reduce drug disintegration inside cells¹⁴. In this regard, it is noteworthy that cationic and anionic nanoparticles show divergent fates inside MP³⁸. For example, phagocytosis of cationic polyamine-coated nanoparticles leads to the diminished phagosomal acidification when compared to anionic protein-coated particles. Such cationic nanoparticles protect the incorporated drug against lysosomal degradation^{29, 38}. Furthermore, loading of “nanozymes” containing positively-charged block copolymers (PEI-PEG and PL-PEG) protected the enzyme in macrophages. Increasing the amount of the block copolymer in the nanozyme formulation improved the stability of the enzyme. In contrast, catalase loaded in a polyion complex with a negatively charged block copolymer (PGLU-PEG) was degraded in macrophages to an even greater extent than catalase loaded alone. Protection of the enzymatic activity inside carrier cells may be, in part, due to a “proton sponge” effect of block copolymers⁴⁵, when an excess of amino groups on the surface of the nanoparticles buffers acidification of the cell's endocytic compartments. This serves to inhibit protease activity and decrease drug degradation³⁸. In other words, a positively charged block-copolymer prevents phagosome-lysosomal clearance functions and as a result, enzyme degradation.

In extreme case, intracellular drug degradation can be avoided by attaching the drug to the surface of cell-carriers. This “back pack” approach would still provide targeted transport and increased blood circulation along with the preserved drug activity. Thus, attaching avidin-coated nanoparticles to the biotinylated plasma membrane can be achieved through the avidin-biotin complex⁴⁶. Another possibility is red blood cells (RBCs) with attached drugs on their surface⁴⁷. Specifically, glycoprotein A covalently conjugated to the surface of the RBCs may provide extended half-life, controlled volume of distribution, and multivalent therapeutic interactions. However, general limitations of the “back pack” approach may include decreased loading of cell carriers, impeded drug release at the disease site, as well as increased immunogenicity and toxicity.

Drug release from cell-carriers—Mechanism of nanoparticle unloading at the site of action remains an active area of investigation. Controlled release of drugs from the cell-carriers modulates the rate of drug appearance, dose and duration of exposure at the diseased sites. To this end, utilizing cellular responses to various conditions could provide desired triggered release. Obviously, targeting of cell-carriers and their prolonged residence at the disease site should provide opportunities for drug unloading. In addition, MP, in particular, are known to produce and store various compounds in intracellular vesicles, and liberate them *via* exocytosis at the site of the disease. A similar mechanism can trigger release of drug-loaded nanocarriers, when macrophages serve as drug delivery vehicles⁴⁸. Furthermore, the drug release can be also triggered by the increase of intracellular concentration of Ca²⁺⁴⁹. Finally, mild hypothermia was shown to facilitate controlled release of drug-loaded liposomes from macrophages in anti-cancer therapy⁵⁰.

Overall the structure and composition of protective nanocontainers play a crucial role in the effectiveness of formulations for cell-based drug delivery systems. For example, our recent studies indicate that structure of block copolymer used for catalase nanoformulation, nanozyme, affect its cytotoxicity, loading and release capacities, as well as preservation of catalase enzymatic activity inside cell-carriers²⁹. Thus, nanozymes containing a negatively-charged block copolymer (PGLU-PEG/catalase) demonstrated low toxicity, high loading capacity and effective release from macrophages. However, the polymer provided limited protection of the enzyme against cell-associated protease degradation. In contrast, nanozymes based on positively charged block copolymers, especially the PLs, showed increased cytotoxicity and low loading and release rates, but were protective of the catalase. Increasing the amount of positively-charged block-copolymer in nanozyme led to protection of catalase enzymatic activity but substantially reduced loadings and release.

Importantly, nanozymes with PEG corona show water stability, limited cytotoxicity and efficient catalase protection. Nonetheless, these formulations also demonstrated decreased loading capacity and release rates. In addition, nanozymes based on mono-polymer (without PEG corona) have higher loading and release levels, but did not protect catalase inside the cell-carriers. Taken together, the most optimal nanozyme formulation was the one based on positively charged block copolymers (PEI-PEG/catalase and PL-PEG/catalase) that demonstrate the most efficient protection of catalase enzymatic activity along with relatively high loading and release rates with limited cytotoxicity (Figure 3).

Homing of drug-loaded cell-carriers at disease sites—The numbers of cell-carriers that can reach the disease site is especially crucial in the case of CNS disorders when drug-loaded cells need to penetrate the blood brain barrier (BBB) to mediate therapeutic effect. Many neurological diseases, such as Alzheimer's and Parkinson's diseases (AD and PD), Prion disease, meningitis, encephalitis and HIV-associated neurocognitive disorders (HAND), have in common an inflammatory component⁵¹. The process of inflammation is characterized by extensive MP recruitment. Notably, MP migrate toward the inflammation site *via* the processes known as diapedesis and chemotaxis⁵². Such cells efficiently cross the BBB due to their margination and extravasation properties causing barrier breakdown as a consequence of brain inflammation⁵³⁻⁵⁷. Many reports in the literature indicate that blood borne monocytes traffic primarily between adjacent endothelial cells, *i.e.* paracellularly through the junctional complexes^{58, 59}. Therefore, these cells can be loaded with a required drug and administered intravenously to reach the brain. For example in an experimental model of PD, considerable levels of catalase loaded into BMM were reported in 1-methyl-4-phenyl-1,2,3,6-tetrahydropyridine (MPTP)-intoxicated brains⁴⁸. Approximately 2.1% of the injected catalase dose was delivered to the brain during MPTP-associated inflammation. Furthermore, several studies confirmed the migration of inflammatory-response cells, in particular, bone-marrow-derived mesenchymal stromal cells toward injury sites such as infarcted myocardium^{60, 61}, spinal cord injury⁶², and cerebral ischemia⁶³.

Neural stem cells (NSCs) were also suggested as drug delivery vehicles for gene therapy in the CNS⁶⁴⁻⁶⁶. Indeed, these cells are highly migratory and migrate to areas of brain pathology including ischemic and neoplastic brain lesions that are commonly present in AD, PD, brain cancer, stroke, and multiple sclerosis. How the mobility of stem cells are directed is not understood, although NSCs express a wide variety of receptors that should enable them to respond to many chemotactic signals present in brain pathologies (Figure 4)⁶⁶. In particular, activated microglia induced NSCs migration to the brain. Delivery of various neurotropic factors is in the focus of cell-mediated strategies for neurological diseases treatment.

In regards to cell-mediated drug delivery of antineoplastic agents, MP are known to accumulate in large numbers in vascular, hypoxic sites in cancer tumors, for example, in breast and prostate carcinomas^{67, 68}. Hypoxia is widespread in malignant human tumors due to their poorly organized vasculature. The cytokines released by tumor cells in response to hypoxia and other physiological stresses usually attract macrophages and monocytes, which should facilitate anticancer drug delivery using these cells as vehicles, avoiding indiscriminate drug distribution and decreasing severe toxicity.

Finally, targeting to disease sites can be improved by drug-incorporated magnetic nanoparticles loaded into the cell-carriers and followed by application of local magnetic fields³⁷. Thus, albino rats with brain inflammation (induced by intrastriatal microinjection of human recombinant IL-1 β) received intravenous injections of RGD-coated magnetic liposomes and non-magnetic liposomes as a control. RGD peptide (*i.e.* small peptide domane Arg-Gly-Asp) was used for selective binding by monocytes and neutrophils that

express integrin receptors on their surface. Magnetic liposomes demonstrated about a ten-fold increase in brain levels compared with non-magnetic controlled carriers when local magnetic field was applied. In addition, magnetic neutrophils prepared *in vitro* target lungs under magnetic guidance following intravenous injection⁶⁹. Moreover, drug loaded magnetic liposomes can be targeted for selective and preferential presentation to blood monocytes/neutrophils that result in both drug and magnetic incorporation into these cells and can be guided to target tissue sites.

Safety of cell-mediated drug delivery systems—An obvious concern for inflammatory-response cell based drug delivery relates to possible cytotoxic effects of cell-carriers. MP attracted to the site of pathology by cytokines release reactive oxygen species (ROS) that cause cell damage. Moreover, a number of therapeutic strategies for CNS neurodegenerative disorders are based on the prevention of monocyte-macrophage infiltration⁷⁰. Therefore, precluding cytotoxicities for cell-based drug formulations is a requirement for formulation developments. Furthermore, genetically-modified and immortalized cell-carriers show atypical characteristics, such as higher degree of multipotency, which may increase the probability of tumor formation. Nevertheless, studies so far report no cytotoxic effects after macrophage-mediated drug delivery in the brain of healthy C57BL/6 mice adoptively transferred with macrophages carrying nanoformulated catalase⁷¹. In addition, propagation and expansion of immortalized and genetically-modified cell-carriers should allow improve quality controls⁶⁶.

Cell-mediated drug delivery systems in clinical settings—Finally, developing such methods in a clinical setting may be successful when cell-carriers are harvested from peripheral blood by apheresis, then loaded with particles and re-infused into the patient. An alternative approach may be harvesting stem cells from bone marrow, propagation them in culture to obtain monocytes, and then loading the cells with a drug and adoptively transferring them. This procedure will allow for expansion of the cell population, although this would require a more invasive procedure. To this end, immortalization of cell-carriers can allow propagation of cells with definable properties so that clonal populations with particular traits can be established. Furthermore, drug loading into cell-carriers can be achieved directly in the patient's peripheral blood, when nanoformulated drugs would be injected and selectively taken up by circulating cell carriers. Targeting of such nanocarriers could be achieved by coating the nanocarrier surface with the receptor-specific moieties (e.g., folate, gelatin, fibronectin, A-protein, mannose, or RGD peptide), which is recognized by specific MP surface receptors. Overall, chronic diseases are more suitable for this type of drug delivery than pathologies that require acute intervention. Based on such considerations, we now present some successful investigations using living cells as drug delivery vehicles for therapeutics (Table 1).

2. Neurodegenerative disorders and cell-based carriage of therapeutic nanoparticles

AD and PD—The progressive impairment of short-term memory and emotional disturbances that typify AD results from synaptic dysfunction and neuronal death in the hippocampus and linked regions in the cerebral cortex and limbic system. Because of the increasing numbers of affected people, there is an urgent need to develop strategies able to interfere with disease progression and protect neurons. In this respect, delivery of neurotrophic factors (NTFs) including nerve growth factor (NGF)⁶⁵, brain-derived neurotrophic factor (BDNF)⁶⁴, and choline acetyltransferase (ChAT)⁷² is of urgent need. To overcome limited drug transport across the BBB, direct brain implantation of cells engineered to produce NTFs was developed⁷³. In particular, ciliary neurotrophic factor delivered in cells implanted in the brain prevents A β oligomer-induced neuronal damage and neurobehavioral impairments in mouse models of AD. In another study NSCs

overexpressing ChAT cDNA targeted acetylcholine deficits⁷⁴. The ability cell-carriers, placed by cortical transplants, to improve cognition was tested after induced cholinergic lesions in rats. Significant improvements were recorded in Water maze acquisition as well as in the retention and spatial probe trials⁷⁴. A robust enhancement of hippocampal synaptic density, mediated by BDNF and delivered by NSCs was seen⁷⁵. NSCs ameliorated complex behavioral deficits associated with AD pathology by BDNF. In these experiments the intracranial transplantation of the cell-carriers were utilized.

Due to specific nigrostriatal degeneration, PD was one of the first targets for cell therapy transplants. Fetal dopamine neurons were inoculated into the putamen, where the cells worked as dopamine pumps as seen during systemic administration of L-DOPA⁷⁶. It was suggested that the transplanted cells were gene therapy vehicles for dopamine delivery rather than replacement neurons⁷⁶. Delivery of neurotrophic factors such as glial cell-line derived neurotrophic factor (GDNF) or vascular endothelial growth factor (VEGF) in neural stem cell transplants were tested in PD mouse models⁷⁷⁻⁷⁹. GDNF was delivered in bone marrow-derived macrophages to the effected brain⁸⁰. The cells were transduced *ex vivo* with lentivirus expressing a GDNF gene driven by a synthetic macrophage-specific promoter and then transplanted into recipient mice. Eight weeks after transplantation, the mice were injected with MPTP for seven days to induce nigrostriatal neurodegeneration. Macrophage GDNF treatments dramatically ameliorated MPTP-induced degeneration of tyrosine hydroxylase (TH)-positive neurons seen in the substantia nigra and TH(+) terminals in the striatum. This resulted in axon regeneration and reversed hypoactivity in the open field test.

Development of novel CNS drug delivery using macrophages carriers for delivery of the antioxidant enzyme, catalase, in MPTP mice was reported by our laboratories^{48, 71}. In this system, nanoformulated catalase (nanozyme) was obtained by coupling the enzyme to a cationic block copolymer, PEI-PEG, leading to a polyion complex micelle. Bone marrow-derived macrophages (BMM) carried significant amounts of catalase then slowly released the active enzyme over several days⁴⁸. The enzyme released upon stimulation of nanozyme-loaded cell-carriers decomposed microglial hydrogen peroxide produced upon nitrated alpha-synuclein (N- α -syn) or tumor necrosis factor alpha (TNF- α) induced activation *in vitro*. Subsequent studies examined relationships between the composition of catalase nanozyme, their physicochemical characteristics (morphology, size, and ξ -potential), and cell loadings, release, and enzymatic activities for macrophage carriage²⁹.

Significant amount of catalase was detected in brains of mice after transfer of BMM loaded with nanoformulated catalase following MPTP intoxication. It was demonstrated that such nanozyme-loaded BMM injected into MPTP-intoxicated mice reduce neuroinflammation and attenuate nigrostriatal degeneration⁷¹. In particular, MPTP intoxication decreased the number of TH-positive nigral dopaminergic neurons (32 % survival) compared to saline-treated controls (Figure 5). In contrast, the number of surviving dopaminergic neurons in MPTP-intoxicated mice treated with nanozyme-loaded BMM was greater than the total number of neurons in MPTP-treated mice (62.4 % survival). Furthermore, treatment with nanozyme alone (without cell carriers) also produced some neuroprotection effect, although with fewer neurons (41.3 % survival) compared to the mice treated with cell/nanozyme formulation. Finally, treatment with empty monocytes did not preserve neurons in MPTP-intoxicated animals (31.1 % survival). This signified a neuroprotective effect of nanozyme-loaded monocytes in MPTP-induced neurodegeneration.

The possible means by which BMM-mediated therapeutic effects of the nanozymes were suggested (Figure 6) : 1) nanozyme-loaded BMM cross the BBB and release catalase at the site of inflammation (particularly, in the substantia nigra pars compacta, *SNpc*); 2) a “depot”

was established such that nanozyme is slowly released from BMM to the blood stream and bypasses the BBB independently of cell-carriers; and 3) catalase nanozyme released from BMM in the liver and spleen suppresses peripheral leukocyte activation that results in significant protection of SNpc neurons against MPTP-induced neurodegeneration⁷¹. Overall, as few therapeutic modalities exist which affect progression of PD and aimed at neuroregenerative therapies, the cell-mediated delivery of catalase and GDNF may represent efficacious strategies that attenuate neuroinflammation and provide neuroprotection for disease.

HIV-1 infections and neuroAIDS—NeuroAIDS is a clinical disorder that encompasses neurologic disorders seen primarily as a consequence of damage to the central nervous system by HIV. The clinical syndromes include cognitive, motor and behavioral disorders of varying severity. Such syndromes affect 30 to 40% of adults and children with AIDS and, despite the advent of potent combination antiretroviral therapy (cART), incidence rates remain constant although disease severity is less. MP carriage has been utilized as a delivery system for antiretroviral therapy of HIV in mice^{14, 57, 81-83}. To protect the drug against degradation, as well as the cell-carriers against the drug, it was incorporated into nanosized drug crystals (termed nano antiretroviral therapy or nanoART, Figure 7). NanoART were made by high-pressure homogenization of crystalline drug with various poloxamer and/or phospholipid surfactants, or by wet-milling homogenization, which produced nanoformulations with high loading capacities (over 80%) and relatively small particle sizes (200 to 350 nm). Scanning electron microscopy analysis revealed particles of various sizes and morphologies, which were either polygonal, rod, cuboidal, or spherical in shape with smooth-surfaces.

Simultaneous uptake of nanoformulated cART into the cell-carriers was shown⁸³. It was also demonstrated that size, charge, coating, and shape of the nanoparticles are crucial for efficient MP uptake, drug release, and cell migration¹⁴. Coating of nanoART greatly affected drug accumulation in cell-carriers. Positively-charged nanoART are taken up better than negatively charged ones. To determine whether any of the wet-milled nanoformulations could induce long-term antiretroviral effects, macrophages were pretreated with individual nanoART preparations and then challenged with HIV-1_{ADA} up to 15 days after drug treatment. Nanoparticles loaded with atazanavir, ritonavir and indinavir were released from macrophages and demonstrated >85, 80 and 40% inhibition, respectively, of progeny virion production and HIV-1p24 antigen through challenge day 15. All formulations of EFV showed almost complete suppression of viral infection⁸³. These results supported the continued development of macrophage-mediated nanoART carriage for treating HIV-1 disease. In addition, delivery of antisense oligodeoxynucleotides, ribozymes, incorporated into liposomes to HIV-1-infected cells was reported in human monocyte-derived macrophages⁸⁴. Thus, in addition to nanoART a ribozyme complementary to HIV-1 5'-long terminal repeat delivered in pH-sensitive liposomes inhibited virus production by 90%, while the free ribozyme caused limited viral inhibitions.

3. Cancer

Cell-mediated delivery is also a potential therapeutic and diagnostic strategy for cancer^{46, 50, 85-93}. The advantage herein is that cytotoxic activity of the cell-carriers can be used in tandem with site-specific delivery of antineoplastic agents. In addition, antineoplastic agents are safely packaged into cell-carriers to reduce secondary cytotoxicities. However, adverse effects of the cytotoxic drugs on the cell-carriers themselves need be considered. For example, when nanoparticles coated with cytotoxic antibiotic, doxorubicin, were loaded into T-cells, the release of drug inside the cell-carrier caused cell damage⁹⁴. As a result over 60% T cells loaded with the nanoparticles were dead over 15 hours after the loading.

To overcome these limitations, mesenchymal stem cells (MSCs) were genetically engineered to produce antitumor proteins^{86, 90-93, 95}. MSCs possess a set of several unique properties, which make them ideally suited for both cellular therapies in regenerative medicine and as vehicles for gene and drug delivery to treat cancer. These properties include: 1) relative ease of isolation; 2) the ability to differentiate into a wide variety of functional cell types of both mesenchymal and non-mesenchymal origin; 3) the ability to be extensively expanded in culture without loss of differentiative capacity; 4) the hypoimmunogenicity and even ability to produce immunosuppression upon transplantation; 5) the pronounced anti-inflammatory properties; and last but not the least, 6) the ability to home to damaged tissues, tumors, and metastases following *in vivo* administration. Thus, MSCs of human origins were genetically modified to express TNF related apoptosis-inducing ligand (TRAIL) at the glioma tumor site. First, the retention of tumor tropic ability of hMSC S-TRAIL cells by *in vitro* and *in vivo* migration assays was clearly demonstrated⁹³. Next, for the *in vivo* assessment of therapeutic efficacy, hMSCs were injected ipsilateral to an established intracranial glioma tumor in a mouse xenograft model. Genetically engineered hMSC S-TRAIL cells were effective in inhibiting intracranial U87 glioma tumor growth (81.6%) *in vivo* and resulted in significantly longer animal survival. Immunohistochemical studies demonstrated a significant, 8-fold greater tumor cell apoptosis in the hMSC S-TRAIL-treated group compared to controls. Overall, the study demonstrated the therapeutic efficacy of hMSC S-TRAIL cells and confirmed that hMSCs can serve as a powerful cell-based delivery vehicle for the site-specific release of therapeutic proteins. Furthermore, reduction of tumor growth by genetically-modified hMSCs expressing interferon- β was reported in models of metastatic breast cancer, melanoma^{86, 90}, and gliomas⁹⁵. The hMSC were also used as carriers for conditionally replicating adenoviruses in a breast cancer metastasis model⁹¹ and in a model of intracranial malignant glioma⁹².

Attachment of nanoparticles with cytotoxic agent to the cell surface allowed cell carriers to remain intact. Thus, NeutrAvidin-coated nanoparticles were anchored on biotinylated plasma membrane of hMSC where they remained attached for up to two days⁴⁶. The hMSC with such nanoparticulate patches retained their inherent tumortropic properties in a tumor model with a 3D-extracellular matrix. These results provide a novel strategy to actively deliver nanostructures and therapeutics to tumors utilizing stem cells as carriers.

Besides MSCs, erythrocytes, MP, and bacterially-derived minicells were also evaluated as carriers for delivery of antineoplastic agents. In particular, erythrocytes were used as carriers for anticancer agent, 5-fluorouracil (5-FU), to treat malignant ascites⁹⁶. Intravenous injections of the cell-carriers loaded with 5-FU resulted in significant regression of the quantity of malignant ascites and the increase of survival time in mice. Notably, MP can serve as "Trojan Horses" for nanoparticle transport into tumor regions^{85, 89}. Thus, infiltration of monocytes and active delivery of Au-containing nanoparticles to the center of tumor spheroids (which contain hypoxic centers) was reported⁸⁹. Following the delivery the tumor spheroids were destroyed by irradiation with near-infrared light, which actuated the delivered Au-containing nanoparticles. In another study, macrophages acted as a cellular vehicle for 5-FU encapsulated in oligomannose-coated liposomes (OMLs)⁵⁰. The successful decrease of tumor growth by co-administration of OML-encased 5-FU and OML-encased magnetic nanoparticles, followed by treatment with an alternating magnetic field was reported in a mice. These OMLs were injected into the peritoneal cavity, and then gradually accumulated in the omentum and the other lymphoid tissues within 24 hours. Treatment of macrophages at 39 °C for 30 min. led to the release of 5-FU from the macrophages, suggesting that controlled release from macrophages could be achieved by mild hyperthermia. The encased magnetic nanoparticles, which are known to convert electromagnetic energy to heat in the OMLs allowed achieving *in vivo* hyperthermia. Finally, MP were utilized for delivery of therapeutic DNA constructs into tumors⁸⁵.

Bacterially-derived minicells with diameters of 400 nm were suggested for targeted delivery of different chemotherapeutics and small interfering RNA (siRNA) duplexes that cause stabilization and regression of tumor size in human cancer xenografts in mice^{97, 98}. The cell-carriers were specifically targeted to tumor cell-surface proteins with biospecific antibodies (BsAb). About 80% efficiency of packing minicells with siRNA was reported. Thus, minicells carrying at least 12,000 siRNA molecules and 100 copies of short hairpin RNA (shRNA)-encoding plasmid can specifically and sequentially deliver to tumor xenografts these therapeutics and compromise drug resistance by knocking down a drug resistance protein. This cell-mediated drug delivery system enables to use several thousand-fold less drug than needed for conventional systemic administration of cancer therapies. Evaluation of uptake and intracellular kinetics of minicell-delivered siRNA indicates that after endocytosis, the minicells traverse the well-established early and late endosomal pathways, terminating into acidified organelles, the lysosomes, where mini-cells are degraded and release their cargo⁹⁸. In addition, several methods of packaging in minicells of a range of anticancer chemotherapeutic drugs, such as doxorubicin, paclitaxel, irinotecan, 5-FLU, cisplatin, carboplatin, monastrol, and vinblastine despite their disparate structure, charge, hydrophobicity, and solubility were developed⁹⁹⁻¹⁰¹.

Antibody-producing hybridoma cells were used for delivery of anti-CD137 and anti-OX40 mAb¹⁰². Microcapsules containing viable cells that secrete antibody were implanted by injection into the subcutaneous tissue of Balb/C mice bearing CT26 colon carcinomas. CD137 and OX40 are members of the TNF receptor family that provide costimulatory effect on T lymphocytes. The treatment resulted in complete tumor eradication in an elevated fraction of cases and strong tumor-specific cytotoxic T lymphocyte responses with either anti-CD137 or anti-OX40 producing hybridomas.

Besides cytotoxic agents, delivery of imaging agents is of importance for cancer therapy. MP-mediated delivery of quantum dots to brain tumors was explored for this purpose¹⁰³. Thus, the surgical management of brain tumors requires the precise localization of tumor tissues within normal brain parenchyma in order to achieve accurate diagnostic biopsy and complete surgical resection. To this end, quantum dots are optical semiconductor nanocrystals that exhibit stable, bright fluorescence. It was demonstrated that the intravenous injection of quantum dots is accompanied by reticuloendothelial system and macrophage sequestration. Macrophages infiltrate brain tumors and phagocytize intravenously injected quantum dots, optically labeling the tumors.

Another class of imaging agents, *N*-(2-hydroxypropyl)methacrylamide (HPMA) copolymer-gadolinium (Gd) chelates, were used for enhanced magnetic resonance imaging (MRI) of macrophage-mediated malignancies¹⁰⁴. To increase the nanoparticles uptake in macrophages, copolymers were vectorized with mannosamine, which was shown to increase mannose receptor mediated uptake in human MP. It was suggested that intravenously administered GD-nanoparticles will be accumulated in macrophages and then transported to the pathological sites (e.g., solid tumor). Overall, the tumor recruitment of inflammatory-response cells may be exploited for cell-mediated delivery of antineoplastic and imaging agents.

4. Lung Injury

Drug delivery to small airways, terminal bronchioles and alveoli is complicated due to the methodological limitations in targeting the deep lung with high efficiency drug distribution to the site of pathology. To overcome these limitations, chitosan nanoparticles with entrapped curcumin (an anti-inflammatory compound) was loaded into Testis-derived Sertoli cells and then injected intravenously into mice with bronchial or alveolar injuries¹⁰⁵. By 24-hours post-injection, most of the curcumin load (~90%) delivered in the injected

Sertoli cells was present and distributed throughout the lungs including the perialveolar sac area in the lower lungs. These results identify a novel and efficient method for targeted delivery of drugs for treatment of bronchitis and alveolitis. In addition, lungs are suitable for both local and systemic drug delivery, therefore this route may be used broadly for other diseases.

5. Microbial Infections

The efficiency of antifungal agents has been diminished by their severe side effects and poor pharmacokinetics. To this end, erythrocytes were suggested as delivery vehicles for antifungal agent, amphotericin B (AmB). In order to avoid toxic effects and achieve efficient drug loading, AmB was encapsulated in nanosuspension (AmB-NS) by high-pressure homogenization¹⁰⁶. AmB-NS was loaded into RBC by using hypotonic hemolysis, leading to intracellular AmB amounts of 3.81 +/- 0.47 pg RBC⁻¹ and an entrapment efficacy of 15-18%. Hence, RBC served as primary carriers. Then, the uptake of RBC loaded with AmB-NS by leucocytes was studied by flow cytometry. More than 98% of the phagocyte population (granulocytes and peripheral monocytes accumulated AmB-NS after four hours of incubation, and then showed a slow AmB release over ten days without any alteration in cell viability. This results in an immediate, permanent inhibition of intra- and extracellular fungal activity. AmBNS-RBC-leukocyte-mediated delivery of AmB was efficient in amounts 1000 times lower than the toxic dose.

Another antifungal agent, chloroquine, loaded into phosphatidylserine-containing negatively charged liposomes was used in MP-mediated delivery against *C. neoformans* infection in the mouse brain¹⁰⁷. Administration of chloroquine-loaded liposomes accumulated inside macrophage phagolysosomes resulted in a remarkable reduction in fungal load in the brain even in low doses compared to free drug in high doses thus increasing antifungal activity of macrophages. Therefore, this drug-delivery method is effective for the transport of water-insoluble substances, such as AmB, and this warrants consideration for further testing.

6. Epilepsy

Relatively straightforward method of engineered adenosine-releasing cells was developed for treatment of epilepsy¹⁰⁸. Lack of adenosine, a modulator of neuronal activity with anticonvulsant and neuroprotective properties, was found to contribute to ictogenesis. Therefore, focal reconstitution of adenosine within an epileptogenic brain region constitutes a rational therapeutic approach, whereas systemic augmentation of adenosine is precluded by side effects. To this end, human mesenchymal stem cells and human embryonic stem cells were embedded in a cell-encapsulation device to release adenosine and reduce acute injury and seizures, as well as chronic seizures¹⁰⁸. Human embryonic stem cells (hESCs) have a high proliferative capacity and can be subjected to specific cellular differentiation pathways. hESCs, differentiated *in vitro* into neuroepithelial cells and grafted into the mouse brain, displayed intrahippocampal location and neuronal morphology. Overall, this therapeutic approach demonstrated antiepileptic and neuroprotective properties when grafted into the mouse hippocampus. The therapeutic potential of this approach suggests the feasibility to engineer autologous adenosine-releasing stem cells derived from a patient¹⁰⁹.

7. Expert Opinion

The concept of using cells as drug delivery vehicles is under development. Challenges include sufficient loading capacity and triggered drug release, preservation of therapeutic agents against degradation inside the cells, protection of cell-carriers from drug cytotoxic effects, and efficient homing of cells to the disease site. In addition, harvesting of cells sufficient quantities or their expansion is also important issue.

Two different approaches are utilized in cell-mediated drug delivery. *First*, cell-carriers (predominantly MP) are genetically modified to produce therapeutically active molecules. *Second*, host cells are loaded with a drug usually incorporated into protective container, and then used as “Trojan horses” to deliver the drug to the disease site (Figure 8). Most of cell-based delivery systems suggest the unloading the therapeutic agent at the disease site. However, a few utilized another approach, when the targeted cells accumulate the carrier along with the drug (mini-cells with anticancer agents and red blood cells with antifungal agents).

Regarding the first approach, the ideal cell delivery vehicle would be stable in tissue culture and capable of sustained, preferably regulated expression of therapeutic molecules. The cells should have appropriate and predictable differentiation pattern and survive long time *in vivo* after transplantation. Obviously, for both approaches, the cell carriers should demonstrate responsiveness to the chemotactic signals produced by the type of pathology that they are used to treat. Regarding the second approach, loading cell-carriers with drug in the blood stream by injecting nanoparticulate drug targeted to these cells is the most attractive strategy. To this end, it is important to note that these cells are moving targets. Nanosystems that bind to these targets are potentially a powerful approach for imaging their movement and delivering a therapeutic drug dose to the disease site. Clearly, a multifunctional molecular scaffold that is aimed at delivery of drug specifically to the cell-carrier, but in addition could be engineered for imaging purposes would offer substantial benefits over current approaches.

Such strategy is opposite to the common approach when drug-loaded nanoparticles are designed to minimize their entrapment in reticulo-endothelial system and avoid drug decomposition and clearance. Consequently, design of nanocarriers for cell-mediated drug delivery (size, shape, surface charge, etc.) may differ from those used for conventional drug delivery systems. Nevertheless, engaging different defense mechanisms into drug delivery may open a new perspective of active delivery of drugs for treatment of various devastating diseases.

Acknowledgments

Declaration of interest

This work was supported by the United States National Institutes of Health grants 1R01 NS057748 (to EVB); 2R01 NS034239, 2R37 NS36126, P01 NS31492, P20RR 15635, P01 MH64570, 5 P01 DA026146, 1P01 DA028555 and P01 NS43985 (to HEG); RO1 NS051334, 2RO1 CA89225, 1 R01 CA116591, U01 CA151806, 1P20 RR021937, the United States Department of Defense grants W81XWH-09-1-0386 and DoD USAMRMC 06108004, and the Government of Russian Federation grants 02.740.11.523 and 11.G4.31.0004 (to AVK).

REFERENCES

1. Fujiwara M, Baldeschwieler JD, Grubbs RH. Receptor-mediated endocytosis of poly(acrylic acid)-conjugated liposomes by macrophages. *Biochim Biophys Acta*. Jan 12; 1996 1278(1):59–67. [PubMed: 8611608]
2. Torchilin VP. Drug targeting. *Eur J Pharm Sci*. Oct; 2000 11(Suppl 2):S81–91. [PubMed: 11033430]
3. Mora M, Sagrista ML, Trombetta D, et al. Design and characterization of liposomes containing long-chain N-acylPEs for brain delivery: penetration of liposomes incorporating GM1 into the rat brain. *Pharm Res*. Oct; 2002 19(10):1430–8. [PubMed: 12425459]
4. Aoki H, Kakinuma K, Morita K, et al. Therapeutic efficacy of targeting chemotherapy using local hyperthermia and thermosensitive liposome: evaluation of drug distribution in a rat glioma model. *Int J Hyperthermia*. Sep; 2004 20(6):595–605. [PubMed: 15370816]

5. Kabanov AV, Chekhonin VP, Alakhov V, et al. The neuroleptic activity of haloperidol increases after its solubilization in surfactant micelles. Micelles as microcontainers for drug targeting. *FEBS Lett.* Dec 4; 1989 258(2):343–5. [PubMed: 2599097]
6. Kabanov AV, Vinogradov SV, Suzdaltseva YG, et al. Water-soluble block polycations as carriers for oligonucleotide delivery. *Bioconjug Chem.* Nov-Dec; 1995 6(6):639–43. [PubMed: 8608176]
7. Kabanov A, Alakhov V. Pluronic block copolymers in drug delivery: from micellar nanocontainers to biological response modifiers. *Crit Rev Ther Drug Carrier Syst.* 2002; 19(1):1–72. [PubMed: 12046891]
8. Kwon GS. Polymeric micelles for delivery of poorly water-soluble compounds. *Crit Rev Ther Drug Carrier Syst.* 2003; 20(5):357–403. [PubMed: 14959789]
9. Vinogradov S, Batrakova E, Kabanov A. Poly(ethylene glycol)-polyethyleneimine NanoGel (TM) particles: novel drug delivery systems for antisense oligonucleotides. *Colloids and Surfaces B-Biointerfaces.* Nov; 1999 16(1-4):291–304.
10. Vinogradov SV, Batrakova EV, Kabanov AV. Nanogels for oligonucleotide delivery to the brain. *Bioconjug Chem.* Jan-Feb; 2004 15(1):50–60. [PubMed: 14733583]
11. Gref R, Minamitake Y, Peracchia M, et al. Biodegradable long-circulating polymeric nanospheres. *Science.* Mar 18; 1994 263(5153):1600–3. [PubMed: 8128245]
12. Hyuk IS, Jeong U, Xia Y. Polymer hollow particles with controllable holes in their surfaces. *Nat Mater.* Sep; 2005 4(9):671–5. [PubMed: 16086022]
13. Calvo P, Gouritin B, Chacun H, et al. Long-circulating PEGylated polycyanoacrylate nanoparticles as new drug carrier for brain delivery. *Pharm Res.* Aug; 2001 18(8):1157–66. [PubMed: 11587488]
- 14**. Nowacek AS, Miller RL, McMillan J, et al. NanoART synthesis, characterization, uptake, release and toxicology for human monocyte-macrophage drug delivery. *Nanomed.* Dec; 2009 4(8):903–17. [This study described characterization of nanoformulated antiretroviral drugs for HIV-1 infection and its application for human cell-mediated drug delivery.]
15. Muller RH, Jacobs C, Kayser O. Nanosuspensions as particulate drug formulations in therapy. Rationale for development and what we can expect for the future. *Adv Drug Deliv Rev.* Mar 23; 2001 47(1):3–19. [PubMed: 11251242]
16. Friedrich I, Reichl S, Muller-Goymann CC. Drug release and permeation studies of nanosuspensions based on solidified reverse micellar solutions (SRMS). *Int J Pharm.* Nov 23; 2005 305(1-2):167–75. [PubMed: 16242276]
17. Harada A, Kataoka K. Chain length recognition: core-shell supramolecular assembly from oppositely charged block copolymers. *Science.* Jan 1; 1999 283(5398):65–7. [PubMed: 9872741]
18. Jaturanpinyo M, Harada A, Yuan X, et al. Preparation of bionanoreactor based on core-shell structured polyion complex micelles entrapping trypsin in the core cross-linked with glutaraldehyde. *Bioconjug Chem.* Mar-Apr; 2004 15(2):344–8. [PubMed: 15025530]
19. Bull SR, Guler MO, Bras RE, et al. Self-assembled peptide amphiphile nanofibers conjugated to MRI contrast agents. *Nano Lett.* Jan; 2005 5(1):1–4. [PubMed: 15792402]
20. Guler MO, Pokorski JK, Appella DH, et al. Enhanced oligonucleotide binding to self-assembled nanofibers. *Bioconjug Chem.* May-Jun; 2005 16(3):501–3. [PubMed: 15898715]
21. Juliano R, Stamp D. The effect of particle size and charge on the clearance rates of liposomes and liposome encapsulated drugs. *Biochem Biophys Res Commun.* 1975; 63:651–8. [PubMed: 1131256]
22. Lee KD, Hong K, Papahadjopoulos D. Recognition of liposomes by cells: in vitro binding and endocytosis mediated by specific lipid headgroups and surface charge density. *Biochim Biophys Acta.* Jan 31; 1992 1103(2):185–97. [PubMed: 1543703]
23. Nishikawa K, Arai H, Inoue K. Scavenger receptor-mediated uptake and metabolism of lipid vesicles containing acidic phospholipids by mouse peritoneal macrophages. *J Biol Chem.* Mar 25; 1990 265(9):5226–31. [PubMed: 2318890]
24. Miller CR, Bondurant B, McLean SD, et al. Liposome-cell interactions in vitro: effect of liposome surface charge on the binding and endocytosis of conventional and sterically stabilized liposomes. *Biochemistry.* Sep 15; 1998 37(37):12875–83. [PubMed: 9737866]

25. Ishihara T, Izumo N, Higaki M, et al. Role of zinc in formulation of PLGA/PLA nanoparticles encapsulating betamethasone phosphate and its release profile. *J Control Release*. Jun 20; 2005 105(1-2):68–76. [PubMed: 15955367]
26. Tempone AG, Perez D, Rath S, et al. Targeting Leishmania (L.) chagasi amastigotes through macrophage scavenger receptors: the use of drugs entrapped in liposomes containing phosphatidylserine. *J Antimicrob Chemother*. Jul; 2004 54(1):60–8. [PubMed: 15163652]
27. Krieger M. Molecular flypaper and atherosclerosis: structure of the macrophage scavenger receptor. *Trends Biochem Sci*. Apr; 1992 17(4):141–6. [PubMed: 1585457]
28. Aderem A, Underhill DM. Mechanisms of phagocytosis in macrophages. *Annu Rev Immunol*. 1999; 17:593–623. [PubMed: 10358769]
29. Zhao Y, Haney MJ, Klyachko NL, et al. Polyelectrolyte complex optimization for macrophage delivery of redox enzyme nanoparticles. *Nanomedicine (Lond)*. Jan; 2011 6(1):25–42. [PubMed: 21182416]
30. Harada A, Kataoka K. Pronounced activity of enzymes through the incorporation into the core of polyion complex micelles made from charged block copolymers. *J Control Release*. May 14; 2001 72(1-3):85–91. [PubMed: 11389987]
31. Harada A, Kataoka K. Switching by pulse electric field of the elevated enzymatic reaction in the core of polyion complex micelles. *J Am Chem Soc*. Dec 17; 2003 125(50):15306–7. [PubMed: 14664571]
32. Knop K, Hoogenboom R, Fischer D, et al. Poly(ethylene glycol) in drug delivery: pros and cons as well as potential alternatives. *Angew Chem Int Ed Engl*. Aug 23; 49(36):6288–308. [PubMed: 20648499]
33. Gabizon A, Shmeeda H, Barenholz Y. Pharmacokinetics of pegylated liposomal Doxorubicin: review of animal and human studies. *Clin Pharmacokinet*. 2003; 42(5):419–36. [PubMed: 12739982]
34. Papaldo P, Fabi A, Ferretti G, et al. A phase II study on metastatic breast cancer patients treated with weekly vinorelbine with or without trastuzumab according to HER2 expression: changing the natural history of HER2-positive disease. *Ann Oncol*. Apr; 2006 17(4):630–6. [PubMed: 16410363]
35. Gbadamosi JK, Hunter AC, Moghimi SM. PEGylation of microspheres generates a heterogeneous population of particles with differential surface characteristics and biological performance. *FEBS Lett*. Dec 18; 2002 532(3):338–44. [PubMed: 12482589]
36. Daleke DL, Hong K, Papahadjopoulos D. Endocytosis of liposomes by macrophages: binding, acidification and leakage of liposomes monitored by a new fluorescence assay. *Biochim Biophys Acta*. May 24; 1990 1024(2):352–66. [PubMed: 2162207]
37. Jain S, Mishra V, Singh P, et al. RGD-anchored magnetic liposomes for monocytes/neutrophils-mediated brain targeting. *Int J Pharm*. Aug 11; 2003 261(1-2):43–55. [PubMed: 12878394]
38. Thiele L, Merkle HP, Walter E. Phagocytosis and phagosomal fate of surface-modified microparticles in dendritic cells and macrophages. *Pharm Res*. Feb; 2003 20(2):221–8. [PubMed: 12636160]
39. Fahmy TM, Schneck JP, Saltzman WM. A nanoscopic multivalent antigen-presenting carrier for sensitive detection and drug delivery to T cells. *Nanomedicine*. Mar; 2007 3(1):75–85. [PubMed: 17379171]
40. Tabata Y, Ikada Y. Effect of the size and surface charge of polymer microspheres on their phagocytosis by macrophage. *Biomaterials*. Jul; 1988 9(4):356–62. [PubMed: 3214660]
41. Mizushima Y, Hamano T, Yokoyama K. Tissue distribution and anti-inflammatory activity of corticosteroids incorporated in lipid emulsion. *Ann Rheum Dis*. Jun; 1982 41(3):263–7. [PubMed: 6896429]
42. Hillaireau H, Couvreur P. Nanocarriers' entry into the cell: relevance to drug delivery. *Cell Mol Life Sci*. Sep; 2009 66(17):2873–96. [PubMed: 19499185]
43. Cannon GJ, Swanson JA. The macrophage capacity for phagocytosis. *J Cell Sci*. Apr; 1992 101(Pt 4):907–13. [PubMed: 1527185]
44. Champion JA, Katare YK, Mitragotri S. Making polymeric micro- and nanoparticles of complex shapes. *Proc Natl Acad Sci U S A*. Jul 17; 2007 104(29):11901–4. [PubMed: 17620615]

45. Behr J-P. The Proton Sponge: a Trick to Enter Cells the Viruses Did Not Exploit CHIMIA. International Journal for Chemistry. 1997; 51(1):34–6.
46. Cheng H, Kastrop CJ, Ramanathan R, et al. Nanoparticulate cellular patches for cell-mediated tumorotropic delivery. ACS Nano. Feb 23; 2010 4(2):625–31. [PubMed: 20121215]
47. Krantz A. Red cell-mediated therapy: opportunities and challenges. Blood Cells Mol Dis. 1997; 23(1):58–68. [PubMed: 9215751]
- 48*. Batrakova EV, Li S, Reynolds AD, et al. A macrophage-nanozyme delivery system for Parkinson's disease. Bioconjug Chem. Sep-Oct; 2007 18(5):1498–506. [PubMed: 17760417] [This manuscript reported development and characterization of cell-mediated delivery system of antioxidant enzyme, catalase. Loading, release, and protection of enzymatic activity of catalase in bone marrow-derived monocytes (BMM) are evaluated in *in vitro* model of PD.]
49. Sollner T, Bennett MK, Whiteheart SW, et al. A protein assembly-disassembly pathway *in vitro* that may correspond to sequential steps of synaptic vesicle docking, activation, and fusion. Cell. Nov 5; 1993 75(3):409–18. [PubMed: 8221884]
50. Ikehara Y, Niwa T, Biao L, et al. A carbohydrate recognition-based drug delivery and controlled release system using intraperitoneal macrophages as a cellular vehicle. Cancer Res. Sep 1; 2006 66(17):8740–8. [PubMed: 16951190]
51. Perry VH, Bell MD, Brown HC, et al. Inflammation in the nervous system. Curr Opin Neurobiol. Oct; 1995 5(5):636–41. [PubMed: 8580715]
52. Kuby, J. Immunology. Freeman, WH. and Co.; New York: 1994.
53. Anthony DC, Bolton SJ, Fearn S, et al. Age-related effects of interleukin-1 beta on polymorphonuclear neutrophil-dependent increases in blood-brain barrier permeability in rats. Brain. Mar; 1997 120(Pt 3):435–44. [PubMed: 9126055]
54. Anthony DC, Blond D, Dempster R, et al. Chemokine targets in acute brain injury and disease. Prog Brain Res. 2001; 132:507–24. [PubMed: 11545015]
55. Blamire AM, Anthony DC, Rajagopalan B, et al. Interleukin-1beta -induced changes in blood-brain barrier permeability, apparent diffusion coefficient, and cerebral blood volume in the rat brain: a magnetic resonance study. J Neurosci. Nov 1; 2000 20(21):8153–9. [PubMed: 11050138]
56. Persidsky Y, Ghorpade A, Rasmussen J, et al. Microglial and astrocyte chemokines regulate monocyte migration through the blood-brain barrier in human immunodeficiency virus-1 encephalitis. Am J Pathol. Nov; 1999 155(5):1599–611. [PubMed: 10550317]
57. Dou H, Destache CJ, Morehead JR, et al. Development of a macrophage-based nanoparticle platform for antiretroviral drug delivery. Blood. Oct 15; 2006 108(8):2827–35. [PubMed: 16809617]
58. Pawlowski NA, Kaplan G, Abraham E, et al. The selective binding and transmigration of monocytes through the junctional complexes of human endothelium. J Exp Med. Nov 1; 1988 168(5):1865–82. [PubMed: 3183575]
59. Lossinsky AS, Shivers RR. Structural pathways for macromolecular and cellular transport across the blood-brain barrier during inflammatory conditions. Review. Histol Histopathol. Apr; 2004 19(2):535–64. [PubMed: 15024715]
60. Orlic D, Kajstura J, Chimenti S, et al. Bone marrow cells regenerate infarcted myocardium. Nature. Apr 5; 2001 410(6829):701–5. [PubMed: 11287958]
61. Orlic D, Kajstura J, Chimenti S, et al. Mobilized bone marrow cells repair the infarcted heart, improving function and survival. Proc Natl Acad Sci U S A. Aug 28; 2001 98(18):10344–9. [PubMed: 11504914]
62. Hofstetter CP, Schwarz EJ, Hess D, et al. Marrow stromal cells form guiding strands in the injured spinal cord and promote recovery. Proc Natl Acad Sci U S A. Feb 19; 2002 99(4):2199–204. [PubMed: 11854516]
63. Mahmood A, Lu D, Lu M, et al. Treatment of traumatic brain injury in adult rats with intravenous administration of human bone marrow stromal cells. Neurosurgery. Sep; 2003 53(3):697–702. discussion -3. [PubMed: 12943585]
64. Martinez-Serrano A, Hantzopoulos PA, Bjorklund A. Ex vivo gene transfer of brain-derived neurotrophic factor to the intact rat forebrain: neurotrophic effects on cholinergic neurons. Eur J Neurosci. Apr; 1996 8(4):727–35. [PubMed: 9081624]

65. Martinez-Serrano A, Bjorklund A. Ex vivo nerve growth factor gene transfer to the basal forebrain in presymptomatic middle-aged rats prevents the development of cholinergic neuron atrophy and cognitive impairment during aging. *Proc Natl Acad Sci U S A*. Feb 17; 1998 95(4):1858–63. [PubMed: 9465107]
66. Muller FJ, Snyder EY, Loring JF. Gene therapy: can neural stem cells deliver? *Nat Rev Neurosci*. Jan; 2006 7(1):75–84. [PubMed: 16371952]
67. Leek RD, Lewis CE, Whitehouse R, et al. Association of macrophage infiltration with angiogenesis and prognosis in invasive breast carcinoma. *Cancer Res*. Oct 15; 1996 56(20):4625–9. [PubMed: 8840975]
68. Lewis JS, Landers RJ, Underwood JC, et al. Expression of vascular endothelial growth factor by macrophages is up-regulated in poorly vascularized areas of breast carcinomas. *J Pathol*. Oct; 2000 192(2):150–8. [PubMed: 11004690]
69. Ranney DF, Huffaker HH. Magnetic microspheres for the targeted controlled release of drugs and diagnostic agents. *Ann N Y Acad Sci*. 1987; 507:104–19. [PubMed: 3327407]
70. Hendriks JJ, Teunissen CE, de Vries HE, et al. Macrophages and neurodegeneration. *Brain Res Brain Res Rev*. Apr; 2005 48(2):185–95. [PubMed: 15850657]
- 71*. Brynskikh AM, Zhao Y, Mosley RL, et al. Macrophage delivery of therapeutic nanozymes in a murine model of Parkinson's disease. *Nanomedicine (Lond)*. Apr; 2010 5(3):379–96. [PubMed: 20394532] [This study supports the feasibility of cell-mediated drug delivery to the brain by examining i) the nanozyme loading capacity for cell carriers; ii) the effect of nanozymes on cell viability and function; and iii) the neuroprotective activities of BMM-carried nanozyme against MPTP intoxication in *in vivo* model of PD.]
72. Low WC, Lewis PR, Bunch ST, et al. Function recovery following neural transplantation of embryonic septal nuclei in adult rats with septohippocampal lesions. *Nature*. Nov 18; 1982 300(5889):260–2. [PubMed: 7144881]
73. Garcia P, Youssef I, Utvik JK, et al. Ciliary neurotrophic factor cell-based delivery prevents synaptic impairment and improves memory in mouse models of Alzheimer's disease. *J Neurosci*. Jun 2; 2010 30(22):7516–27. [PubMed: 20519526]
74. Pizzo DP, Coufal NG, Lortie MJ, et al. Regulatable acetylcholine-producing fibroblasts enhance cognitive performance. *Mol Ther*. Jan; 2006 13(1):175–82. [PubMed: 16185935]
75. Blurton-Jones M, Kitazawa M, Martinez-Coria H, et al. Neural stem cells improve cognition via BDNF in a transgenic model of Alzheimer disease. *Proc Natl Acad Sci U S A*. Aug 11; 2009 106(32):13594–9. [PubMed: 19633196]
76. Zurn AD, Tseng J, Aebischer P. Treatment of Parkinson's disease. Symptomatic cell therapies: cells as biological minipumps. *Eur Neurol*. 1996; 36(6):405–8. [PubMed: 8954314]
77. Akerud P, Canals JM, Snyder EY, et al. Neuroprotection through delivery of glial cell line-derived neurotrophic factor by neural stem cells in a mouse model of Parkinson's disease. *J Neurosci*. Oct 15; 2001 21(20):8108–18. [PubMed: 11588183]
78. Casper D, Engstrom SJ, Mirchandani GR, et al. Enhanced vascularization and survival of neural transplants with ex vivo angiogenic gene transfer. *Cell Transplant*. 2002; 11(4):331–49. [PubMed: 12162374]
79. Yasuhara T, Shingo T, Muraoka K, et al. Neurorescue effects of VEGF on a rat model of Parkinson's disease. *Brain Res*. Aug 16; 2005 1053(1-2):10–8. [PubMed: 16045899]
80. Biju K, Zhou Q, Li G, et al. Macrophage-mediated GDNF delivery protects against dopaminergic neurodegeneration: a therapeutic strategy for Parkinson's disease. *Mol Ther*. Aug; 2010 18(8):1536–44. [PubMed: 20531393]
81. Dou H, Morehead JR, Destache C, et al. Laboratory investigations for the morphologic, pharmacokinetic, and anti-retroviral properties of indinavir nanoparticles in human monocyte-derived macrophages. *Virology*. Feb; 2007 358(1):148–58. [PubMed: 16997345]
82. Dou H, Grotepas CB, McMillan JM, et al. Macrophage delivery of nanoformulated antiretroviral drug to the brain in a murine model of neuroAIDS. *J Immunol*. Jul 1; 2009 183(1):661–9. [PubMed: 19535632]

83. Nowacek AS, McMillan J, Miller R, et al. Nanoformulated Antiretroviral Drug Combinations Extend Drug Release and Antiretroviral Responses in HIV-1-Infected Macrophages: Implications for NeuroAIDS Therapeutics. *J Neuroimmune Pharmacol.* Mar 17.2010
84. Duzgunes N, Pretzer E, Simoes S, et al. Liposome-mediated delivery of antiviral agents to human immunodeficiency virus-infected cells. *Mol Membr Biol.* Jan-Mar; 1999 16(1):111–8. [PubMed: 10332745]
85. Chokri M, Lopez M, Oleron C, et al. Production of human macrophages with potent antitumor properties (MAK) by culture of monocytes in the presence of GM-CSF and 1,25-dihydroxy vitamin D3. *Anticancer Res.* Nov-Dec; 1992 12(6B):2257–60. [PubMed: 1295473]
86. Studeny M, Marini FC, Champlin RE, et al. Bone marrow-derived mesenchymal stem cells as vehicles for interferon-beta delivery into tumors. *Cancer Res.* Jul 1; 2002 62(13):3603–8. [PubMed: 12097260]
87. Stagg J, Lejeune L, Paquin A, et al. Marrow stromal cells for interleukin-2 delivery in cancer immunotherapy. *Hum Gene Ther.* Jun; 2004 15(6):597–608. [PubMed: 15212718]
88. Nakamura K, Ito Y, Kawano Y, Kurozumi K, et al. Antitumor effect of genetically engineered mesenchymal stem cells in a rat glioma model. *Gene Ther.* Jul; 2004 11(14):1155–64. [PubMed: 15141157]
89. Choi MR, Stanton-Maxey KJ, Stanley JK, et al. A cellular Trojan Horse for delivery of therapeutic nanoparticles into tumors. *Nano Lett.* Dec; 2007 7(12):3759–65. [PubMed: 17979310]
90. Studeny M, Marini FC, Dembinski JL, et al. Mesenchymal stem cells: potential precursors for tumor stroma and targeted-delivery vehicles for anticancer agents. *J Natl Cancer Inst.* Nov 3; 2004 96(21):1593–603. [PubMed: 15523088]
91. Stoff-Khalili MA, Rivera AA, Mathis JM, et al. Mesenchymal stem cells as a vehicle for targeted delivery of CRAbs to lung metastases of breast carcinoma. *Breast Cancer Res Treat.* Oct; 2007 105(2):157–67. [PubMed: 17221158]
92. Sonabend AM, Ulasov IV, Tyler MA, et al. Mesenchymal stem cells effectively deliver an oncolytic adenovirus to intracranial glioma. *Stem Cells.* Mar; 2008 26(3):831–41. [PubMed: 18192232]
93. Menon LG, Kelly K, Yang HW, et al. Human bone marrow-derived mesenchymal stromal cells expressing S-TRAIL as a cellular delivery vehicle for human glioma therapy. *Stem Cells.* Sep; 2009 27(9):2320–30. [PubMed: 19544410]
94. Steinfeld U, Pauli C, Kaltz N, et al. T lymphocytes as potential therapeutic drug carrier for cancer treatment. *Int J Pharm.* Mar 27; 2006 311(1-2):229–36. [PubMed: 16460895]
95. Nakamizo A, Marini F, Amano T, et al. Human bone marrow-derived mesenchymal stem cells in the treatment of gliomas. *Cancer Res.* Apr 15; 2005 65(8):3307–18. [PubMed: 15833864]
96. Wang GP, Guan YS, Jin XR, et al. Development of novel 5-fluorouracil carrier erythrocyte with pharmacokinetics and potent antitumor activity in mice bearing malignant ascites. *J Gastroenterol Hepatol.* May; 2010 25(5):985–90. [PubMed: 20546454]
97. MacDiarmid JA, Mugridge NB, Weiss JC, et al. Bacterially derived 400 nm particles for encapsulation and cancer cell targeting of chemotherapeutics. *Cancer Cell.* May; 2007 11(5):431–45. [PubMed: 17482133]
98. MacDiarmid JA, Amaro-Mugridge NB, Madrid-Weiss J, et al. Sequential treatment of drug-resistant tumors with targeted minicells containing siRNA or a cytotoxic drug. *Nat Biotechnol.* Jul; 2009 27(7):643–51. [PubMed: 19561595]
99. Nikaido H. Multidrug efflux pumps of gram-negative bacteria. *J Bacteriol.* Oct; 1996 178(20):5853–9. [PubMed: 8830678]
100. Nikaido H. Molecular basis of bacterial outer membrane permeability revisited. *Microbiol Mol Biol Rev.* Dec; 2003 67(4):593–656. [PubMed: 14665678]
101. Poole K. Outer membranes and efflux: the path to multidrug resistance in Gram-negative bacteria. *Curr Pharm Biotechnol.* Jun; 2002 3(2):77–98. [PubMed: 12022261]
102. Dubrot J, Portero A, Orive G, et al. Delivery of immunostimulatory monoclonal antibodies by encapsulated hybridoma cells. *Cancer Immunol Immunother.* Nov; 2010 59(11):1621–31. [PubMed: 20607237]

103. Popescu MA, Toms SA. In vivo optical imaging using quantum dots for the management of brain tumors. *Expert Rev Mol Diagn.* Nov; 2006 6(6):879–90. [PubMed: 17140375]
104. Zarabi B, Nan A, Zhuo J, et al. Macrophage targeted N-(2-hydroxypropyl)methacrylamide conjugates for magnetic resonance imaging. *Mol Pharm.* Sep-Oct; 2006 3(5):550–7. [PubMed: 17009854]
105. Kumar A, El-Badri N, Glaum M, et al. Initial Observations of Cell Mediated Drug Delivery to the Deep Lung. *Cell Transplant.* Nov 5.2010 Nov 5, (Epub ahead of print).
106. Staedtke V, Braehler M, Muller A, et al. In vitro inhibition of fungal activity by macrophage-mediated sequestration and release of encapsulated amphotericin B nanosuspension in red blood cells. *Small.* Jan; 2010 6(1):96–103. [PubMed: 19882684]
107. Khan MA, Jabeen R, Nasti TH, et al. Enhanced anticryptococcal activity of chloroquine in phosphatidylserine-containing liposomes in a murine model. *J Antimicrob Chemother.* Feb; 2005 55(2):223–8. [PubMed: 15590713]
108. Boison D. Engineered adenosine-releasing cells for epilepsy therapy: human mesenchymal stem cells and human embryonic stem cells. *Neurotherapeutics.* Apr; 2009 6(2):278–83. [PubMed: 19332320]
109. Boison D. Adenosine augmentation therapies (AATs) for epilepsy: prospect of cell and gene therapies. *Epilepsy Res.* Aug; 2009 85(2-3):131–41. [PubMed: 19428218]
110. Kabanov, AV.; Batrakova, EV. Polymer nanomaterials.. In: Gendelman, HE.; Ikezu, T., editors. *Neuroimmune Pharmacology.* Springer; Omaha: 2008. p. 691-707.
111. Nowacek A, Gendelman HE. NanoART, neuroAIDS and CNS drug delivery. *Nanomedicine (Lond).* Jul; 2009 4(5):557–74. [PubMed: 19572821]

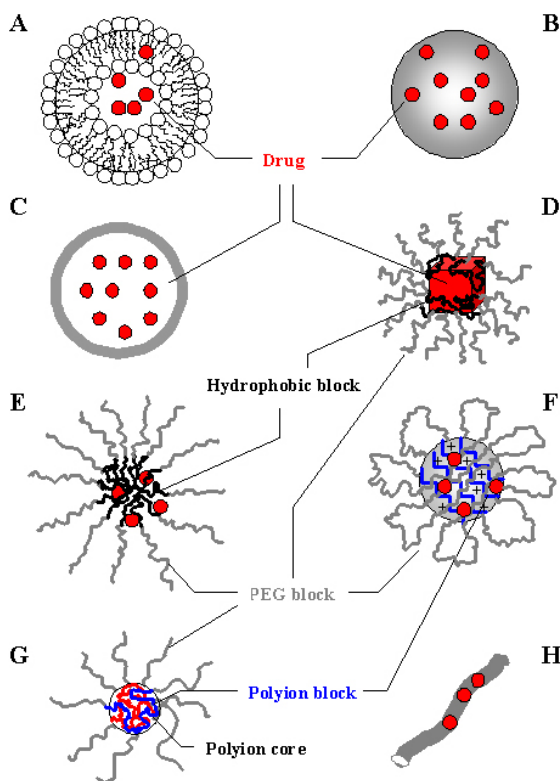


Figure 1. Types of nanocarriers for drug delivery. **A:** liposomes; **B:** polymer and lipid nanoparticles; **C:** nanospheres and nanocapsules; **D:** nanosuspensions; **E:** polymer micelles; **F:** nanogels; **G:** block ionomer complexes; **H:** nanofibers and nanotubes. Used with permission ¹¹⁰.

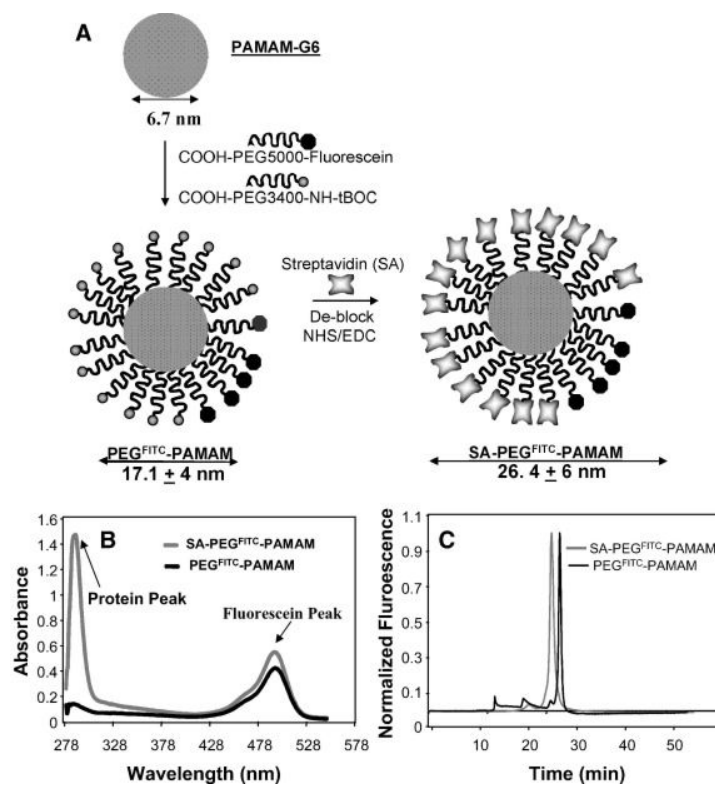


Figure 2. Schematic representation of SA-PEG^{FITC}/PAMAM construction
A. The construction of streptavidin-PEG^{FITC}/PAMAM. **B.** Absorbance profiles of streptavidin-PEG^{FITC}/PAMAM and PEG^{FITC}/PAMAM. **C.** Reverse-phase HPLC of SAPEG^{FITC}/PAMAM and PEG^{FITC}/PAMAM. Used with permission ³⁹.

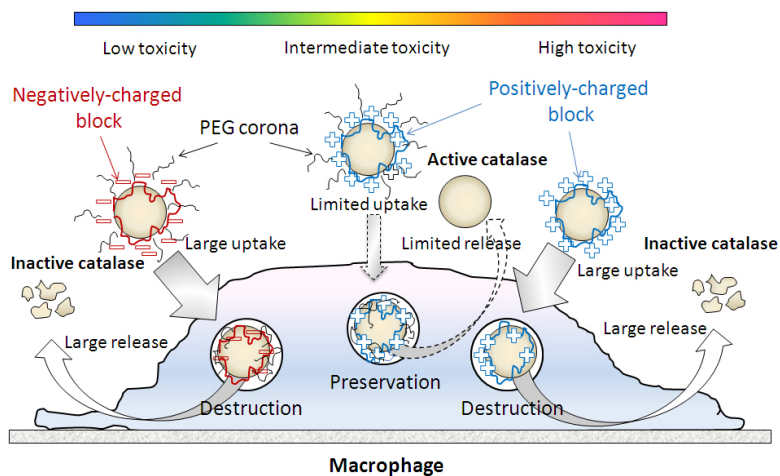


Figure 3. Optimization of nanocarriers structure for catalase delivery in macrophages
 Nanozymes consisting of catalase and a negatively charged block copolymer demonstrate low toxicity, high loading capacity and release from BMM, however provide limited protection of the enzyme against protease degradation inside the cell-carriers. Nanozymes based on positively charged block copolymers, especially the PLs, showed increased cytotoxicity and low loading and release rates, but were highly protective of catalase. Furthermore, nanozymes with PEG corona show good stability in water, limited cytotoxicity and efficient protection of catalase, but decreased loading capacity and cell release. The optimal nanozyme formulation is one based on positively charged block copolymers (PEI-PEG/catalase and PL-PEG/catalase). Used with permission ²⁹.

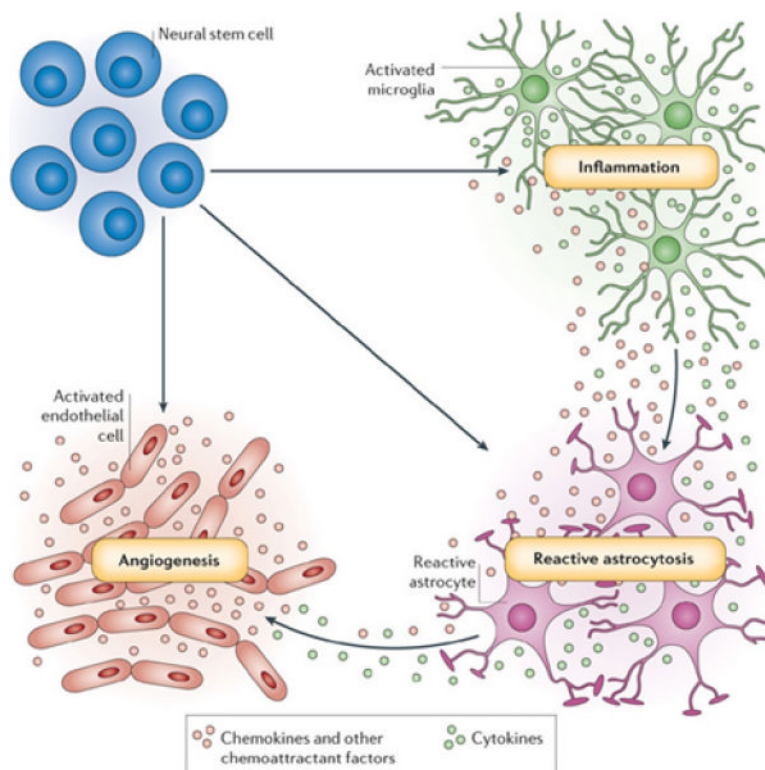


Figure 4. Using neural stem cells for drug delivery to CNS

Neural stem cells are attracted by at least three physiological processes that are common to many brain pathologies: inflammation, reactive astrocytosis and angiogenesis. Pathology-induced CNS inflammation is mediated by activated microglia that release cytokines and chemokines, which, in turn, increases the inflammatory reaction. The brain lesion and subsequent inflammation trigger reactive astrocytosis. The lesion-induced angiogenesis and inflammation-activated endothelial cells enhance neural stem cell homing to brain pathology by secreting chemoattractant factors, and also offer an atypical, perivascular niche for support of immigrating neural stem cells. Used with permission ⁶⁶.

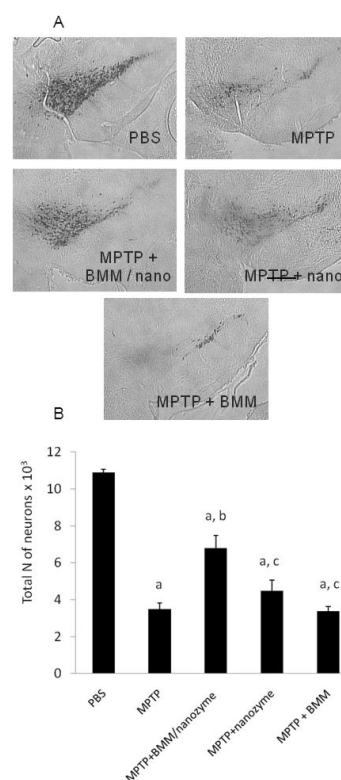


Figure 5. Neuroprotective effect of nanozyme-loaded BMM in an MPTP model of PD MPTP-intoxicated C57Bl/6 mice (18 mg/kg) were intravenously injected with saline (second bar), nanozyme alone (third bar), macrophages loaded with nanozyme (5×10^6 cells/mouse/100 μ l) (fourth bar), or empty macrophages (fifth bar). Healthy non-intoxicated animals were used as control group (first bar). Seven days after treatment the animals were sacrificed; brain slices were stained for tyrosine hydroxylase-positive nigral dopaminergic neurons (A). Results from $N = 5$ animals per group demonstrate a significant loss of nigrostriatal neurons in MPTP treated mice, which is prevented by adoptive transfer of macrophages loaded with nanozyme (B). No significant neuroprotective effect was detected after treatment with nanozyme alone, or empty macrophages. Values are means \pm SEM, and $P < 0.05$ compared with ^asaline; ^bMPTP; ^cMPTP+macrophage/nanozyme. Used with permission ⁷¹.

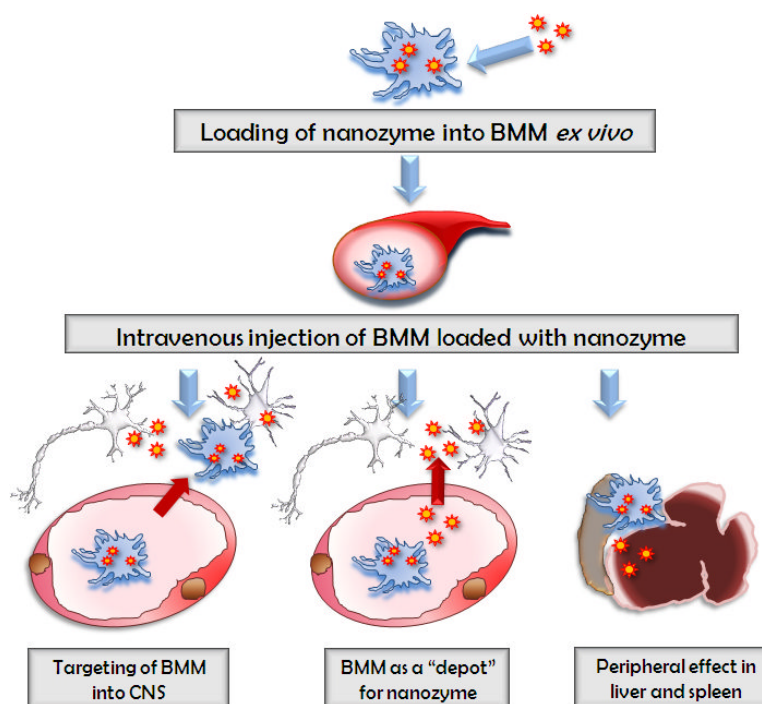


Figure 6. A pictorial scheme for cell-based nanoformulated drug delivery

Three possible ways of BMM-mediated therapeutic effects of catalase nanozyme in PD mouse model: **Pathway I:** BMM loaded with nanozyme cross the BBB and release catalase in the SNpc; **Pathway II:** nanozyme is released from BMM to the blood stream and bypasses the BBB independently of cell-carriers; **Pathway III:** catalase nanozyme released from BMM in the liver and spleen suppresses peripheral leukocyte activation that results in significant protection of nigrostriatal neurons against MPTP-induced neurodegeneration. Used with permission ⁷¹.

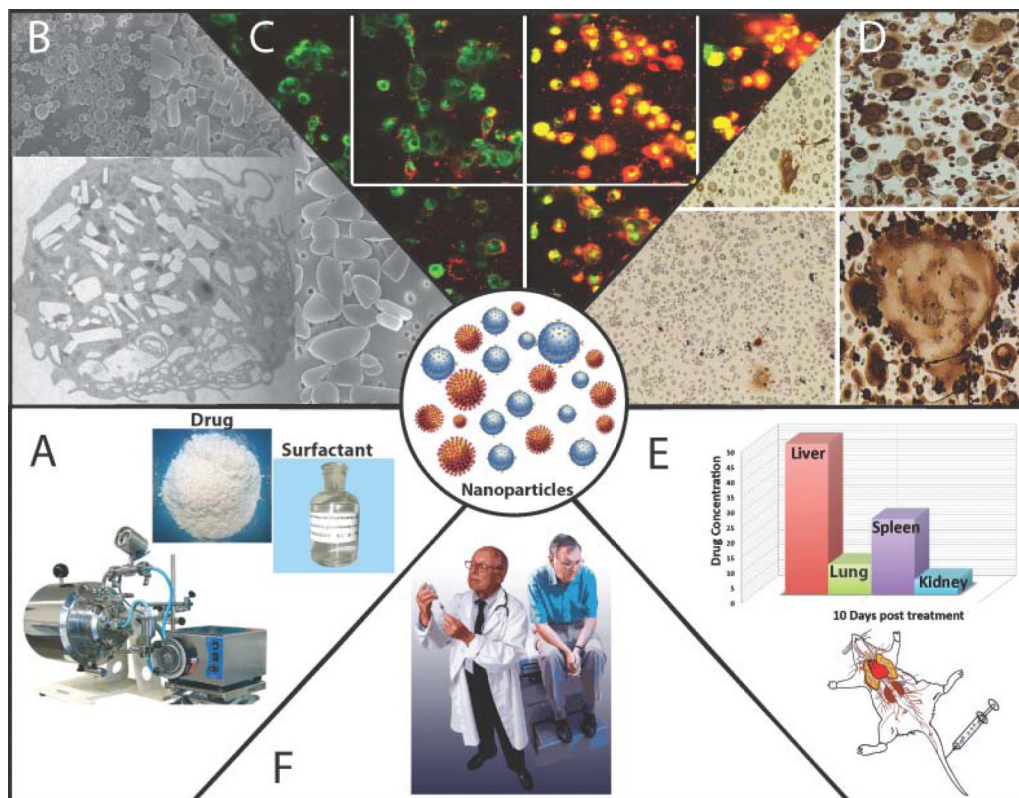


Figure 7. NanoART

(A) NanoART of antiretroviral agents were prepared by high-pressure homogenization using an AvestinC-5 homogenizer; (B) scanning-electron microscopy demonstrated different nanoparticle morphology; (C) uptake of drug-loaded nanoART (red) in monocyte-derived macrophages (green); (D) cells treated with nanoART showed complete or near complete suppression of HIV1 p24 antigen production; (E) biodistribution of nanoART in mice following intravenous injections; (F) patient treatment with nanoART in clinical settings. Used with permission ¹¹¹.

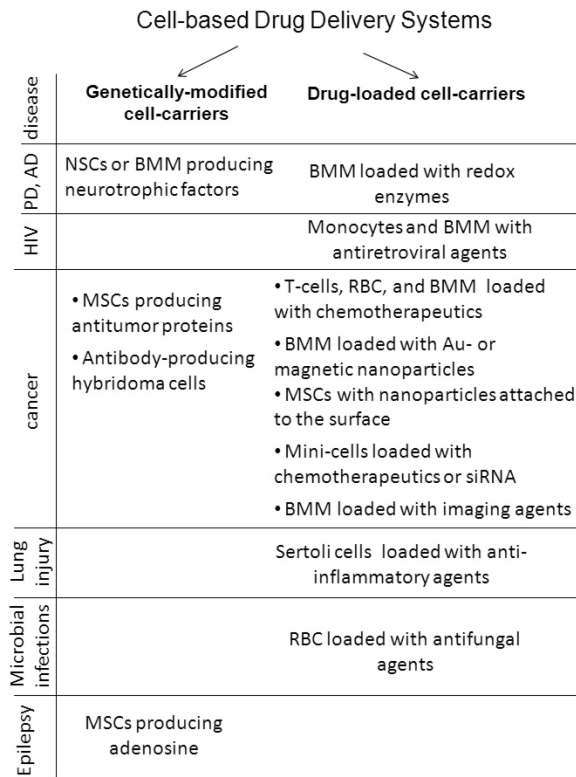


Figure 8.
Cell-based Drug Delivery Systems.

Table 1

Examples of cell-mediated drug delivery systems

Type of cell-carrier	Therapeutic agent	Route of administration ¹	References
Alzheimer's disease			
Neural stem cells (NSCs)	ciliary neurotrophic factor (NTFs)	<i>i.c.</i>	73
NSCs	nerve growth factor (NGF)	<i>i.c.</i>	65
NSCs	brain-derived neurotrophic factor (BDNF)	<i>i.c.</i>	64, 75
NSCs	choline acetyltransferase (ChAT)	<i>i.c.</i>	72, 74
Parkinson's disease			
Monocytes, macrophages	catalase	<i>i.v.</i>	29, 48, 71
Fetal dopamine neurons	dopamine	<i>i.c.</i>	76
NSCs	glial cell-line derived neurotrophic factor (GDNF)	<i>i.c.</i>	77, 80
NSCs	vascular endothelial growth factor (VEGF)	<i>i.c.</i>	78, 79
HIV-1 infection and neuroAIDS			
Monocytes, macrophages	atazanavir, ritonavir, indinavir	<i>i.v.</i>	14, 81-83
Cancer			
T-cells	doxorubicin	<i>In vitro</i>	94
Mesenchymal stem cells (MSCs)	tumor necrosis factor-related apoptosis-inducing ligand (TRAIL)	<i>ipsilateral</i>	93
MSCs	interferon- β	<i>i.v.</i>	86, 90, 95
MSCs	oncolytic adenovirus	<i>i.v.</i>	91, 92
MSCs	antineoplastic agent	<i>In vitro, in 3D collagen gels</i>	46
Erythrocytes	5-fluorouracil	<i>i.v.</i>	96
Monocytes and macrophages	Au-containing nanoparticles	<i>In vitro, in spheroids</i>	85, 89
Interoitoneal macrophages	5-fluorouracil	<i>i.p.</i>	50
Bacterially-derived mini-cells	small interfering RNA (siRNA), cytotoxic drugs	<i>i.v., i.t.</i>	97, 98
Bacterially-derived mini-cells	doxorubicin	<i>i.v., i.t.</i>	98
Macrophages	imaging agents, quantum dots	<i>i.v.</i>	103
Macrophages	<i>N</i> -(2-hydroxypropyl)methacrylamide (HPMA) copolymer-gadolinium (Gd) chelates	<i>i.v.</i>	104
Hybridoma cell lines 2A and OX86	anti-CD137 and anti-OX40 mAb	<i>s.c.</i>	102
Inflammation			
Macrophages	betamethasone phosphate	<i>in situ</i>	25
Erythrocytes	glycoprotein A		25
Sertoli cells	anti-inflammatory agent, curcumin	<i>i.v.</i>	105
Microbial Infections			
Erythrocytes	antifungal agent, amphotericin B	<i>in viro</i>	106
Macrophages	chloroquine	<i>i.v.</i>	107

Type of cell-carrier	Therapeutic agent	Route of administration ¹	References
<i>Epilepsy</i>			
Human MSCs and human embryonic stem cells	adenosine	<i>i.c. in</i> cell-encapsulation device	108, 109

¹ *i.c.*, intracranial; *i.v.*, intravenous; *i.p.*, intraperitoneal; *i.t.*, intratumoral; *s.c.*, subcutaneous injections.

RESEARCH ARTICLE

Monocyte Trafficking, Engraftment, and Delivery of Nanoparticles and an Exogenous Gene into the Acutely Inflamed Brain Tissue – Evaluations on Monocyte-Based Delivery System for the Central Nervous System

Hsin-I Tong^{1,2}, Wen Kang^{1#a}, Philip M. C. Davy³, Yingli Shi^{1#b}, Si Sun¹, Richard C. Allsopp³, Yuanan Lu^{1*}

1 Office of Public Health Studies, University of Hawaii at Manoa, Honolulu, Hawaii, United States of America, **2** Department of Microbiology, University of Hawaii at Manoa, Honolulu, Hawaii, United States of America, **3** Institute for Biogenesis Research, University of Hawaii at Manoa, Honolulu, Hawaii, United States of America

#a Current address: Department of Infectious Diseases, Tangdu Hospital, the Fourth Military Medical University, Xi'an, Shaanxi, China

#b Current address: Institute of Oceanology, Chinese Academy of Science, Qingdao, Shandong, China
* yuanan@hawaii.edu



CrossMark
click for updates

OPEN ACCESS

Citation: Tong H-I, Kang W, Davy PMC, Shi Y, Sun S, Allsopp RC, et al. (2016) Monocyte Trafficking, Engraftment, and Delivery of Nanoparticles and an Exogenous Gene into the Acutely Inflamed Brain Tissue – Evaluations on Monocyte-Based Delivery System for the Central Nervous System. PLoS ONE 11(4): e0154022. doi:10.1371/journal.pone.0154022

Editor: Mária A. Deli, Hungarian Academy of Sciences, HUNGARY

Received: December 16, 2015

Accepted: April 7, 2016

Published: April 26, 2016

Copyright: © 2016 Tong et al. This is an open access article distributed under the terms of the [Creative Commons Attribution License](https://creativecommons.org/licenses/by/4.0/), which permits unrestricted use, distribution, and reproduction in any medium, provided the original author and source are credited.

Data Availability Statement: All relevant data are within the paper and its Supporting Information files.

Funding: This study was funded by the National Institute of Mental Health of National Institutes of Health (R01 MH079717). <https://www.nimh.nih.gov/index.shtml>. The funders had no role in study design, data collection and analysis, decision to publish, or preparation of the manuscript.

Competing Interests: The authors have declared that no competing interests exist.

Abstract

The ability of monocytes and monocyte-derived macrophages (MDM) to travel towards chemotactic gradient, traverse tissue barriers, and accumulate precisely at diseased sites makes them attractive candidates as drug carriers and therapeutic gene delivery vehicles targeting the brain, where treatments are often hampered by the blockade of the blood brain barrier (BBB). This study was designed to fully establish an optimized cell-based delivery system using monocytes and MDM, by evaluating their homing efficiency, engraftment potential, as well as carriage and delivery ability to transport nano-scaled particles and exogenous genes into the brain, following the non-invasive intravenous (IV) cell adoptive transfer in an acute neuroinflammation mouse model induced by intracranial injection of *Escherichia coli* lipopolysaccharides. We demonstrated that freshly isolated monocytes had superior inflamed-brain homing ability over MDM cultured in the presence of macrophage colony stimulating factor. In addition, brain trafficking of IV infused monocytes was positively correlated with the number of adoptive transferred cells, and could be further enhanced by transient disruption of the BBB with IV administration of Mannitol, Bradykinin or Serotonin right before cell infusion. A small portion of transmigrated cells was detected to differentiate into IBA-1 positive cells with microglia morphology in the brain. Finally, with the use of superparamagnetic iron oxide nanoparticles SHP30, the ability of nanoscale agent-carriage monocytes to enter the inflamed brain region was validated. In addition, lentiviral vector DHIV-101 was used to introduce green fluorescent protein (GFP) gene into monocytes, and the exogenous

GFP gene was detected in the brain at 48 hours following IV infusion of the transduced monocytes. All together, our study has set up the optimized conditions for the more-in-depth tests and development of monocyte-mediated delivery, and our data supported the notion to use monocytes as a non-invasive cell-based delivery system for the brain.

Introduction

Monocytes and monocyte-derived macrophages (MDM) possess broad homeostatic, immune sensing and surveillance functions [1, 2]. Their ability to traffic through circulation and accumulate precisely at the diseased sites makes them an attractive tool for drug carriage and gene delivery [3–7]. The need for cell-based delivery systems is immediate in order to combat central nervous system (CNS) diseases, because many therapeutic compounds and biologics are known to have limited capability to penetrate the blood-brain barrier (BBB) or to reach sites further from their administration points effectively [8].

Early studies using hematopoietic stem cell (HSC) transplanted into lethally irradiated animals demonstrated that blood circulating monocytes were recruited to the CNS and differentiated into resident macrophages and microglia cells once reaching their destinations [9–11]; whereas recent studies have suggested the use of lethal irradiation induced additional damages to the CNS, hence overestimated the true ability of monocyte to infiltrate and differentiate into resident microglia cells [12, 13]. Nevertheless, recruitments of circulating monocytes to the diseased sites within the CNS were evident in numerous neurological disorders [6, 14–17]. Therefore, the use of monocytes and MDM for precise therapeutics delivery still holds great promises for combating many CNS disorders, including Parkinson's and Alzheimer's Diseases, Multiple Sclerosis, and HIV-associated neurocognitive disorders [3, 5–7].

Comparing to bone marrow transplants (BMT) using precursor cells, adoptive transfer of differentiated cells avoids the involvement of lethal irradiation, and is a relatively risk free procedure with minimum side effects [18–20]. Thus, by exploring the migration property of IV transferred monocytes and MDM to regions of interests, it is possible to selectively transport disease combating genes or medicines to inflamed or damaged sites in the brain in a non-invasive fashion. Thus far, a number of studies have been conducted to test monocytes- and MDM-mediated delivery of nano-formulated medicines and therapeutic genes into the CNS [3, 5–7], but the optimum conditions for such delivery system has not been fully established. In order to carry out effective treatment functions, therapeutics-carriage cells need to be present at target sites in high numbers. Therefore, identifying suitable cellular sources to be used as transporting vehicles, and developing methods to increase cell vehicle target site concentration are essential for establishment of a cell-based delivery system [21]. Both freshly isolated monocytes and culture-expanded MDM (cMDM) were tested for their capability to reach the CNS following adoptive transfer [3, 5–7, 22], but no quantitative comparison have been performed to evaluate the suitable cellular source for transporting therapeutic agents to the brain. Hence, this study was aimed to establish the optimized conditions for the non-invasive cell-based delivery system, including testing and determining the homing efficiency of freshly isolated monocytes and cMDM to the inflamed brain regions, establishing conditions that could enhance the cell vehicle concentration at the target sites, assessing the potential of these recruited cells to engraft and differentiate in the brain, and validating the ability of the cell vehicles to carry "cargos" into the brain following systemic IV adoptive transfer.

Using a mouse model of acute brain subregional inflammation induced by intracranial (IC) injection of *Escherichia coli* (*E. coli*) Lipopolysaccharide (LPS), we have demonstrated that

freshly isolated monocytes have high inflamed-brain homing efficiency following IV adoptive transfer, and have established the conditions for enhanced cell transmigration and increased cell vehicle concentrations in brain target sites by increasing IV infusion cell amount and transiently disrupting the BBB using chemical agents including Mannitol, Bradykinin, and Serotonin. In addition, we have observed that a small portion of the recruited monocytes were able to differentiate into IBA-1 positive cells with microglia morphology in the brain. Furthermore, with the use of superparamagnetic iron oxide nanoparticle (SPION) SHP30, the ability of nanoscaled agent-carriage monocytes to enter the inflamed brain region was validated. In addition, lentiviral vector (LV) DHIV-101 (D101) was utilized to mediate the transfer of green fluorescent protein (GFP) gene into monocytes in this study, and the presence of GFP gene was detected in the brain of affected animals 2 days after IV infusion of the LV-transduced monocytes.

All together, our study has set up the optimized conditions for the more-in-depth study of monocyte-mediated delivery system, and our new data supports the notion of using monocyte migration as a means of therapeutics delivery into the brain—with the ultimate goal of affecting neuronal disease outcomes.

Materials and Methods

Animals

Six- to 10-week old male and female C57BL/6 mice (Obtained from Animal and veterinarian services, University of Hawaii at Manoa) and male green fluorescent protein (GFP) transgenic male C57BL/6-Tg (UBC-GFP) 30Scha/J mice (The Jackson Laboratory, stock #004353) were acquired for this study. C57BL/6 mice were used in all experiments except for immunohistochemical (IHC) and immunofluorescent studies, which GFP transgenic mice were used as cell donors and C57BL/6 mice as recipients. In all studies, male mice were used as cell donors, and female mice as recipients. All mice were bred and maintained in the animal facility at University of Hawaii at Manoa campus by following the institutional guidelines for the humane care and investigation of laboratory animals, and all animal studies were reviewed and approved by the Institutional Animal Care and Use Committee (IACUC) of University of Hawaii at Manoa (Protocol # 09–767). In all experiments, mice were monitored twice daily throughout the experimental periods. A humane endpoints protocol was included in this study, and experimental animals were to be euthanized if they displayed inability to reach food or water for more than 24 hours, and if more than 20% decrease in body weight was detected. No early death was observed in any animal prior to the experimental endpoints in this study.

Isolation and Cultivation of Mouse Monocytes and cMDM

Eight- to 10-week old male mice were used as cell donors. Mouse cMDM were prepared as described previously [5]. In brief, bone marrow cells (BMC) were isolated from donor mice femur and tibia of the hind limbs. Erythrocytes were removed by lysis with ACK lysis buffer (Quality Biological, Inc.), and a single cell suspension was obtained by passing through 40- μ m cell strainers (BD Falcon, #352340), and was either resuspended in PBS and used for cell IV infusion, or cultured in suspension with complete growth medium composed of RPMI1640 medium supplemented with 10% FBS and 1,000 U/ml M-CSF (obtained from 5/9 m alpha3-18 cell media, ATCC#CRL-10154. M-CSF in condition media was quantified using Human M-CSF quantikine ELISA kit, R&D system cat#DMC00B), at 37°C with 5% CO₂ for 2, 5, 7, 9, 12, 15, 21 and 28 days prior to flow cytometry analysis or adoptive transfer study.

In studies using freshly isolated monocytes (Enriched monocytes, EnMo), monocytes were enriched from the freshly isolated BMC suspension using EasySep mouse monocyte enrichment kit (Stem Cell Technologies, #19761) according to manufacturer's instructions.

Flow Cytometry

In vitro monocyte to macrophage differentiation was assessed in cMDM at 0, 2, 5, 7, 9, 12, 15 and 21 days post isolation by fluorescence-activated cell sorting (FACS) with a FACSAria III, and cytometry data were analyzed using FACSDiva v. 6.1 (BD Biosciences). Cells were collected from suspension culture flask, washed with PBS, and incubated with antibodies (details below) for 30 minutes on ice. Unbound antibodies were removed by washing cells with PBS. Recovered cell pellets were resuspended in 1% PFA in PBS and stored at 4°C until analysis. Cell samples were stained with the following dye and antibodies for FACS analysis according to the manufacturers recommendations: Zombie Green (1:500, BioLegend cat#423111) for viability assessment, rat anti-CD11b (1:500, PE-Dazzle594 conjugated, BioLegend cat#101255), rat anti-Ly6c (1:200, PerCP conjugated, BioLegend cat#128027), monoclonal rat anti-CCR2 (1:20, APC conjugated, R&D Systems cat#FAB5538A), and rat anti-F4/80 (1:40, APC-Cy7 conjugated, BioLegend cat#123117).

Freshly isolated BMC were used in single stain controls to create spectral compensation, and in fluorescence minus one (FMO) controls to establish appropriate gating strategies. Forward and side scatter properties were applied in gating to exclude doublets and cell debris, and the single cell population was assessed for their viability in the FITC channel (Zombie Green viability assessment). CD11b+ cells (Zombie Green^{neg}) were then divided into three populations based on combined assessment of their expression of F4/80 and Ly6c. The F4/80^{high}Ly6C^{neg}, F4/80^{low}Ly6C^{low}, and F4/80^{med}Ly6C^{high} populations in this plot were labeled as macrophages, Ly6C^{low} monocytes, and Ly6C^{high} monocytes, respectively. CCR2 expression was assessed for each of these three populations separately, Ly6C^{high} monocytes were positive, Ly6C^{low} monocytes and macrophages were low to negative. The relative percentages of each cell population within the samples were generated from statistical analysis of the F4/80 –Ly6c plots.

EnMO was further analyzed for their expression of CD115 (rat anti-CD115, APC conjugate, 1:100, BioLegend #135509), CD11b+, F4/80, and Ly6C to confirm the purity of the enriched cells.

E. coli LPS-Induced Acute Brain Inflammation and Cell IV Adoptive Transfer

Six- to 8-week old female mice were anesthetized with Avertin (2,2,2-Tribromoethanol, 250 mg/kg, IP) and positioned on a stereotaxic apparatus (Stoelting co.). *E. coli* LPS (Serotype O111:B4, S-form. Enzo Life Sciences, ALX-581-M005) was administered into the right hemisphere (AP 0.0 mm, ML +2.5 mm, DV -4.0 mm from bregma) to induce acute subregional neuroinflammation in the brain. Each animal received 5 µg of *E. coli* LPS in 5 µL solution or 5 µL of PBS (Sham) over a period of 5 minutes. PBS-injected animals and the un-injected contralateral hemisphere were used as controls. At 24 hrs following ICI delivery of LPS, 100–150 µL cell suspension containing cells (5×10^6 if not otherwise indicated) or PBS (Sham) were injected into the lateral tail vein of recipient mice. Mice were sacrificed at day 1, 2, 3, 5, 7 or 14 after cell infusion for analysis.

LV-Mediated GFP Gene Transfer into Monocytes

The HIV-1-based defective LV system D101 was used for transduction of monocytes [23–26]. The vector was produced by transient transfection in HEK293T cells by calcium phosphate precipitation method with a packaging construct pCMV-ΔR8.2, an envelop construct pCMV-VSV-g, and a transfer construct pD101 which contained the reporter gene GFP, as described previously [24]. Transduction of monocytes was done by spin-infection. 2×10^7

transducing units (as titrated on HEK293T cells) D101 vectors were incubated with polybrene (final concentration 8 $\mu\text{g}/\text{mL}$) at RT for 10 minutes before combined with 1×10^6 freshly isolated, enriched monocytes (MOI = 20) in serum free medium. The cell/vector/polybrene mix is then transferred to a 5mL round-bottom polystyrene tube, and transduction was carried out by centrifuging the culture at 1,500 $\times g$ for 90 minutes at 32°C. Cells were then washed three times by centrifugation with PBS to remove excess vector and polybrene, and immediately injected IV into recipient animals. A small portion of the transduced cells were maintained *in vitro* for 7 additional days following in complete culture medium, and the efficiency of monocyte transduction was determined by counting the number of GFP-positive cells at random fluorescent microscope fields.

Monocyte Uptake of SHP30

Commercially available SPIO nanoparticle (NP) SHP-30 (Ocean NanoTech) was used in this study. SHP30 is 30 nm in core diameter (38–40 in hydrodynamic diameter), has oleic acid and amphiphilic polymer coating with carboxylic acid reactive group, and with a Zeta potential range from -30mV to -50mV. Immediately following isolation and enrichment, monocytes were transferred to 5mL round-bottom PS tubes, and cultured in suspension with complete culture medium containing 50 $\mu\text{g}/\text{mL}$ SHP30, for 12 to 14 hours. The cells were then washed 3 times with PBS by centrifugation to remove extracellular SHP30, and injected IV into recipient animals. The SHP30 uptake efficiency was 100% as determined by Prussian blue staining.

Trypan Blue Exclusion Assay

Following LV transduction or SHP30 uptake, the cell viability of control and carrier monocytes was measured with Trypan blue exclusion assay, by mixing equal volume of cells and 0.4% trypan blue solution (Sigma, Cat#T8154). Cells stained blue were considered dead, and unstained cells were considered viable. The final cell viability was presented in percentage, as comparing to the viability of control monocytes (no gene or SHP30 carriage) set as 100%.

Real-Time qPCR

Genomic DNA was isolated from brain regions ± 1.0 mm from the LPS injection site (average tissues weight ranged from 50–60 mg) using QIAamp DNA mini kit (Qiagen) following the manufacturer's instructions. The amount of donor-derived cell DNA was quantitatively determined by real-time qPCR with primers and probe specific to male murine Y chromosome [27]. Real-time qPCR was performed on an iQ5 optical system (BioRad) using forward primer 5' - TTTTGCCCTCCCATAGTAGTATTTTCCT-3' , reverse primer 3' -TGTACCGCTCTGCCAACCA-3' and the TaqMan probe 5' - /56-FAM/AGGGATGCC/ZEN/CACCTCGCCAGA-/3 IABkFQ/-3' (Integrated DNA Technologies). Standard curves were generated by serially diluting DNA from male mouse brain. DNA isolated from female mouse brain was included as a negative control in every assay. The average DNA content in a diploid mouse cell range from 5 to 7 pg [28], therefore a parameter of 6 pg gDNA per cell was applied to convert DNA to cell numbers presented in all results.

PCR

The presence of GFP gene delivered by D101 transduced monocytes to the brain were detected with conventional PCR method using forward primer F-GFPreal: 5' -GGTGAGC AAGGGCGAGGAG-3' , and reverse primer R-GFPreal: 5' -GCCGGTGGTGCAGATGAACT-3' . PCR was performed with a MasterCycler Gradient (Eppendorf, Germany). Five

Table 1. Real-time RT-PCR primer sequences for cytokine transcription profile.

Gene name	GeneBank Accession #	Oligonucleotide sequences	Reference
GAPDH	NM_008084	forward: 5' -CTCCACTCACGGCAAATTCAA-3' reverse: 5' -GATGACAAGCTTCCCATTCTCG-3'	[7]
TNF α	NM_013693	forward: 5' -CCGTCAGCCGATTTGCTATCT-3' reverse: 5' -ACGGCAGAGAGGAGGTTGACTT-3'	[7]
IL-1 β	NM_008361	forward: 5' -ACAACAAAAAGCCTCGTGCTG-3' reverse: 5' -CCATTGAGGTGGAGAGCTTTCA-3'	[7]
IFN γ	NM_008337	forward: 5' -ACAGGTCCAGCGCCAAGCAT-3' reverse: 5' -ACCCCGAATCAGCAGCGACT -3'	This study
TGF β 1	NM_011577	forward: 5' -AGGACCTGGGTTGGAAGTGG-3' reverse: 5' -AGTTGGCATGGTAGCCCTTG-3'	[7]
IL-10	NM_010548	forward: 5' -AGGCGCTGTCATCGATTCTC-3' reverse: 5' -TGCTCCACTGCCTTGCTCTTA-3'	[7]
NOS2	NM_010927	forward: 5' -GGCAAACCCAAGGTCTACGTTTC-3' reverse: 5' -TACCTCATTGGCCAGCTGCTT-3'	[7]
IL-2	NM_008366	forward: 5' -GCATGCAGCTCGCATCCTGT-3' reverse: 5' -TGCTGCTGTGCTTCCGCTGT-3'	This study
IL-4	NM_021283	forward: 5' -CACGGATGCGACAAAAATCA-3' reverse: 5' -CTCGTTCAAAATGCCGATGA-3'	[7]
IL-12p35	NM_008351	forward: 5' -AAATGAAGCTCTGCATCCTGC-3' reverse: 5' -TCACCCGTGTTGATGGTCACG-3'	[7]
IL-12p40	NM_008352	forward: 5' -ACCAGGCGACTCGCAGCAAA-3' reverse: 5' -ACACATCCCACTCCCACGCT-3'	This study
BDNF	NM_007540	forward: 5' -AGGCACCTGGAAGTTCGCAATG-3' reverse: 5' -AAGGGCCCGAACATACGATT-3'	[7]
GDNF	NM_010275	forward: 5' -GGGTGCGTTTTAACTGCCAT-3' reverse: 5' -GCCCAAACCCAAGTCAGTGA-3'	[7]

doi:10.1371/journal.pone.0154022.t001

microliter of inflamed brain tissue DNA was combined with 20 μ L of a mixture containing 1X Taq (Mg^{2+} free) reaction buffer (New England Biolabs, NEB, MA), 1.5 mM $MgCl_2$ solution (NEB, MA), 200 nM of each dNTPs (Sigma-Aldrich, MO), 400 nM of each primer (Integrated DNA technologies, IA), and 2 units of Taq polymerase (provided by Dr. Huang, University of Hawaii at Manoa). The Amplification started with an initial denaturation at 94°C for 5 min, followed by 30 cycles of denaturation at 94°C for 30 sec, annealing at 56°C for 30 sec, extension at 72°C for 30 sec, and a final extension at 72°C for 5 min. PCR products were subjected to 2% agarose gel electrophoresis, alongside a 50 bp DNA marker (NEB, MA), stained with ethidium bromide (EtBr) and viewed with the Molecular Imager Gel Doc XR+ system (BioRad Laboratories, Inc., CA).

Analysis of Cytokine Transcripts by Real-Time RT-PCR

Tissue RNA was isolated from the inflamed and control brain region by TRIZOL reagent (Life technology) at 72 hrs post ICI of LPS or PBS (48 hrs post cell IVI). Reverse transcription (RT) was performed with iScript Reverse Transcription Supermix for RT-qPCR (Bio-Rad laboratories), followed by quantitative real-time PCR with specific primer sets (Table 1) using iQ SYBR Green Supermix (Bio-Rad laboratories) through an iQ5 optical system (Bio-Rad). Results were analyzed for relative gene expression using the 2-delta-delta CT method.

Transient Disruption of the BBB by Chemical Agents

Twenty-four hours after LPS injection (5 μ g, IC), female recipient mice were anesthetized with Avertin (125 mg/kg, IP), and different transient BBB disrupting (BBBD) agents were administered prior to IVI of 5×10^6 monocytes (see below). Dosages and injection time points of the BBB disrupting agents were selected from previously published methods, with some modifications [22, 29–32]. Detailed descriptions for each BBB disrupting agent usage are as follows: 1) D-Mannitol (Sigma, cat#M9546): 200 μ L of 25% (w/v), IV, with IV delivery of donor cells 8 minutes later; 2) L(+)Arabinose (Calbiochem, cat#78680): 200 μ L of 1.8M, IV, with IV delivery of donor cells immediately thereafter; 3) Bradykinin (Sigma #B3259): 200 μ L of 1g/L, IV, with IV delivery of donor cells 20 minutes later; 4) 5-Hydroxytryptamine creatinine sulfate monohydrate (Serotonin creatinine sulfate) (MP Biomedicals, 151315): 200 μ L of 1g/L, IV, with IV delivery of donor cells immediately thereafter. 5) Cyclosporin A (Enzo Life Sciences, 380–002):

50 mg/kg, Subcutaneous (SQ), injected right after LPS ICI, followed by IV delivery of donor 24 hrs later. For the BBB disrupting agents administered by IV injection, monocytes were infused into the alternative tail vein at indicated time points as described above. Animals that received cells only (with no BBB disrupting reagents) at 24 hrs post ICI delivery of LPS were used as controls (value set at 100%), and the relative amount of recruited donor cells from the test groups was quantified and comparatively analyzed with the control groups using unpaired student t-test, and one-way ANOVA among all test groups.

IHC and immunofluorescent Analyses

Twenty-four hours post ICI of 5 μ L LPS (1 μ g/ μ L) or sham (PBS), female C57BL/6 recipient mice received IVI of 5×10^6 GFP-positive enriched monocytes from male donor C57BL/6-tg (UBC-GFP) 30Scha/J mice. At days 2, 5, 7 and 14 post cell infusion, recipient mice were sacrificed by intracardiac perfusion with PBS followed by 4% paraformaldehyde (PFA) in PBS. Brain tissues were collected and post-fixed in 4% PFA overnight at 4°C prior to dehydration in gradient sucrose solutions. Brain tissues were then embedded in OCT compound and frozen in 2-methylbutane cooled on dry ice. Serial coronal brain sections of 25- μ m were prepared from sample tissue ± 1.0 mm of the injection point. Donor-derived GFP-positive cells were detected with goat anti-GFP antibody (1:200, Rockland #600-101-215). Polyclonal antibody to ionized calcium-binding adaptor molecule 1 (Iba-1, 1:400, Wako Pure Chemical Industries, Ltd. Japan. Stock#01919741) was used to identify mice brain microglial cells. Astrocytes were detected with Rabbit polyclonal Abs against glial fibrillary acidic protein (GFAP, 1:1,000, DaKo Cytomation #Z0334). Secondary antibody conjugated with Rhodamine was used for fluorescent imaging (Goat anti-Rabbit IgG with Rhodamine conjugate, 1:200, Jackson Immuno Research; Donkey anti-Goat IgG with Rhodamine conjugate, 1:200, Rockland #605-700-002). For IHC detection of GFP expressing cells, Donkey anti-Goat IgG with Biotin conjugate was used (1:200, Rockland). In addition to IHC, the presence of SHP30 within the cytoplasm of recruited donor cells in the brain was detected by Prussian blue staining, and counter stained with Nuclear Fast Red solution (Sigma). All microscope images were viewed with a Nikon eclipse TE2000-U epi-fluorescence microscope (with 4x, 10x, and 20x objective lenses, total magnifications of 40x, 100x, and 200x, respectively), which was equipped with a CoolSNAP ES2 CCD camera (for fluorescent image acquisition), and with a QIClick™ CCD Camera (for bright-field color image acquisition). All microscope image were captured at room temperature (25°C) using NIS-elements BR2.30 software, images were further processed with Adobe Photoshop CS3 (version 10.0.1) and Image J (1.48V).

Statistic Analysis

For all experiments, final data presented were obtained from 3 to 6 animal for each test group, and were represented as mean values \pm SD. Analysis of variance (ANOVA) was used to analyze studies with three or more experimental groups. Unpaired t test was used to analyze studies between two experimental groups. Pearson correlation coefficient was used to calculate correlation (R) and coefficient (R²). Results with *p-value* < 0.05 were considered significant.

Results

Migration Efficiency of IV Adoptive Transferred Monocytes and cMDM to Acutely Inflamed Brain Tissues

In all tests, male mice were used as cell donors, and female mice as recipients. This sex-mismatched system allowed tracking and quantifying of recruited donor cells in the brain by

detecting the amount of y-chromosome DNA [27]. Our initial experiments demonstrated that the amount of accumulated donor cells in the inflamed brain region was the highest when cells were introduced to recipient animals at 24 hrs following LPS ICI, and when brain tissues were collected at 48 hrs post cell IV infusion (S1 Fig). These test conditions were used in all experiments of this study unless otherwise indicated.

Both freshly isolated monocytes and cMDM have been tested in adoptive transfer studies to reach target tissues with various degree of success [3, 5–7, 22, 33, 34]. To determine the more suitable cellular sources as delivery vehicles for the brain, MDM were cultivated *in vitro* in the presence of M-CSF for 0 to 28 days prior to their IV infusion. As the results, freshly isolated cells (BMC) showed the highest migratory efficiency, even though only ~10% of the total cell population was monocytes in origin (Fig 1A and 1B) [35]. The cell transmigration efficiency decreased with the cultivation time—the efficiency dropped almost by half when 2-day's cultures were used, and continued to drop until a plateau was reached with cells cultured for 9 days and thereafter (Fig 1A).

To explain the decreased brain homing efficiency *in vivo*, cMDM population was analyzed for cell types at corresponding cultivation time points. The frequency of macrophages (CD11b⁺ F4/80^{high} Ly6C^{neg} CCR2^{neg}) and monocytes (including Ly6C^{hi} monocytes as CD11b⁺ F4/80^{med} Ly6C^{high} CCR2⁺, and Ly6C^{lo} monocytes as CD11b⁺ F4/80^{low} Ly6C^{low} CCR2^{low to neg}) was measured with flow cytometry (Fig 1B). Freshly isolated BMC was composed of 10% monocytes and less than 0.4% macrophages (Fig 1C). During *in vitro* cultivation, macrophage numbers increased quickly at day 5, and maintained at a consistent 80% of the total cell population (including all cells present in culture flask), or at > 90% among the CD11b⁺ cell population, from day 9 and thereafter. Conversely, total number of monocytes only showed a brief increase that peaked at day 2, followed by rapid decrease and fell below 0.5% by day 12 and thereafter.

Nevertheless, even with the presence of a much higher percentage of total monocytes, *in vivo* transmigration of day 2- and day 5- cMDM into the brain was not as efficient as the freshly isolated BMC (d0) (Fig 1A). Further analysis revealed that majority of the monocyte population at these later time points was composed of Ly6C^{lo} monocytes (Ly6C^{low} CCR2^{low to neg}); whereas the portion of Ly6C^{hi} monocytes (Ly6C^{high} CCR2⁺) decreased over time (Fig 1D). Previous studies have reported that Ly6C^{high}, but not Ly6C^{low} monocyte, are actively recruited to inflammatory sites [34, 36, 37], and Ly6C^{hi} monocytes are known to appear in circulation in large quantities during both acute and chronic inflammation [38]. Hence, this subtype of the donor cells was likely to be the primary ones entering the acutely inflamed brain following IV administration. Thus, the rapid decline of this cell population during *in vitro* cultivation would explain why the efficiency of cell transmigration into the inflamed brain tissue declines with prolonged culture time.

A previous study has demonstrated that infiltrating neutrophils quickly appeared in the inflamed brain regions but died within 18 hours following LPS IC inoculation, and monocytes were the major infiltrating CD11b⁺ cells detected in the brain after 24 hours [39]. Nevertheless, in this study, the recruited donor-derived cells in the brain might come from cell types other than monocytes and macrophages, since freshly isolated BMC contains mixed cell populations, and cMDM was only partially purified by *in vitro* cultivation with the use of M-CSF. To ensure the cell purity in subsequent studies, monocytes were further enriched from the freshly isolated BMC using a negative selection method. Results from flow analysis have confirmed that over 91% of EnMO (SSC^{low}) were positive for CD11b, and over 90% were positive for the monocyte-macrophage lineage marker, CD115 (Fig 1E). In addition, over 99% of CD11b⁺ cells were found to be F4/80^{med-low}, and over 93% of the CD11b⁺F4/80^{med-low} population were CD115⁺ (Fig 1D). Furthermore, animals received five million of EnMo showed a significant increase in

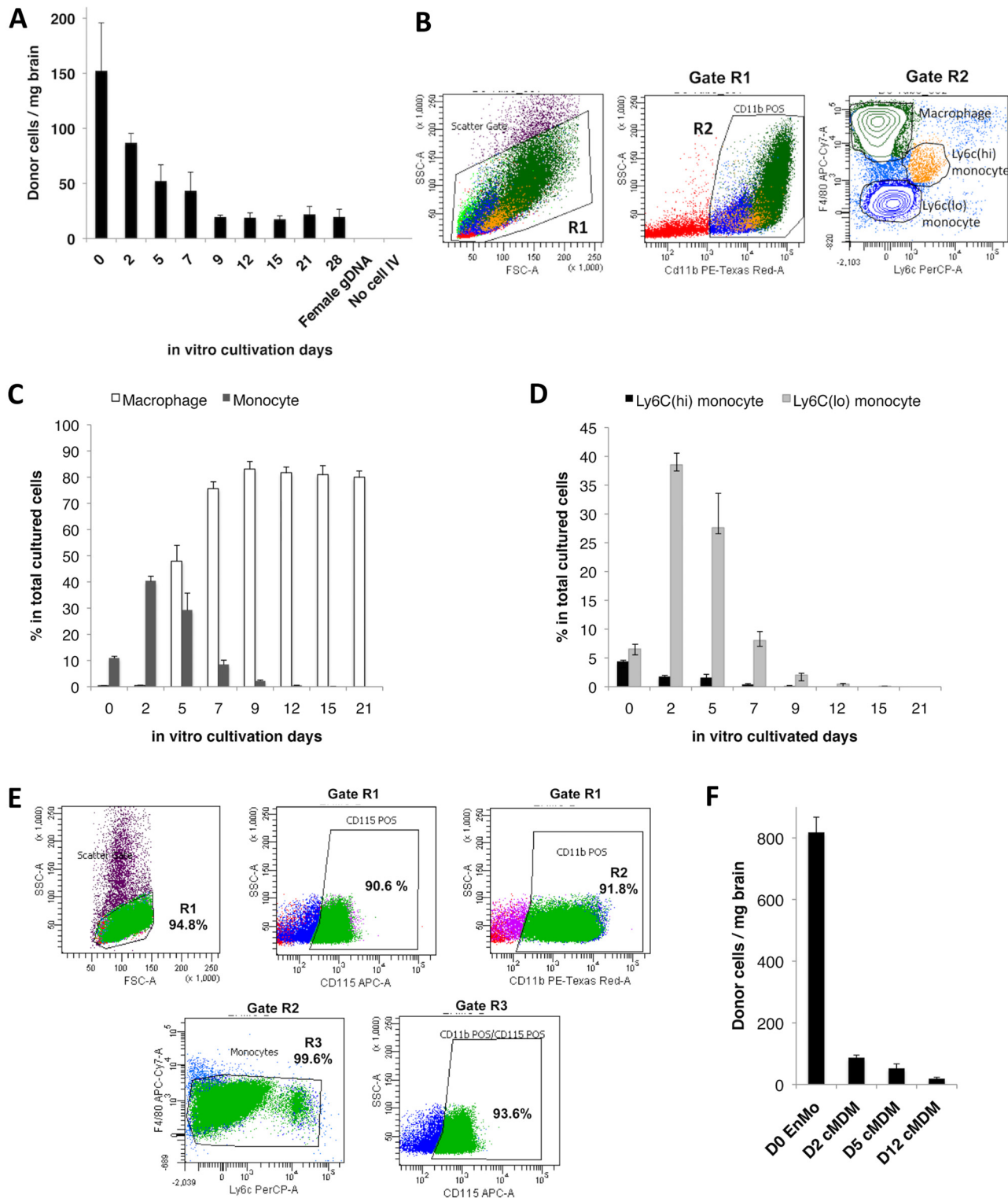


Fig 1. Migration efficiency of IV transferred monocytes and cMDM to acutely inflamed brain tissue is linked to monocyte-to-macrophage differentiation. (A) MDM cultured from day 0 to day 28 were introduced IV (5×10^6 cells) into recipient mice bearing LPS-induced acute neuroinflammation, and cMDM *in vivo* brain homing efficiency decreased as the *in vitro* cultivation time went up. Female gDNA = female mouse brain tissue genomic DNA (negative control). No cell IV = LPS injected control animal that received no cell IV transplant. Final data presented here represents mean values \pm SD. Data was analyzed by one-way ANOVA, with resulting p-value < 0.05 . (B–D) Flow cytometry analysis on cMDM cell populations at different time points post *in vitro*

cultivation. (B) Example of phenotype identification of cMDM using D5 cMDM. The green cluster reflects macrophage phenotype (CD11b⁺ F4/80^{hi} Ly6C^{low to neg}), blue cluster reflects Ly6C^{low} monocytes (CD11b⁺ F4/80^{low to med} Ly6C^{low to neg}), and yellow cluster reflects Ly6C^{hi} monocytes (CD11b⁺ F4/80^{low to med} Ly6C^{high}). (C) The ratio of macrophages (CD11b⁺ F4/80^{high} Ly6C^{neg}) and total monocytes (CD11b⁺ F4/80^{low to med} Ly6C^{low to high}), and (C) the ratio of Ly6C^{hi} monocytes (CD11b⁺ F4/80^{med} Ly6C^{high} CCR2⁺) and Ly6C^{lo} monocytes (CD11b⁺ F4/80^{low} Ly6C^{low} CCR2^{low to neg}) in culture were evaluated. (E) Phenotyping of freshly isolated EnMO by flow cytometry analysis. Expression level of CD115, CD11b, F4/80, and Ly6c were measured to determine the purity of the enriched cells. (F) Freshly isolated EnMO showed superior brain homing efficiency over cMDM. 5x10⁶ of EnMO (D0 EnMO), or MDM cultured for 2-, 5-, or 12-days (D2 cMDM, D5 cMDM, D12 cMDM, respectively) were infused IV to animals with acute neuroinflammation, and the number of donor cells present in the LPS-injected brain hemisphere was quantified at 48 hour following cell IVI. Final data presented here represents mean values ± SD. Data was analyzed by one-way ANOVA, with resulting p-value all < 0.05.

doi:10.1371/journal.pone.0154022.g001

numbers of transmigrated cells in the brain: a 9.4-fold, 15.6-fold and 43-fold increase was observed as compared to animals that received the same amount of d2-, d5- and d12- cMDM (Fig 1F). Confirmed with its superior inflamed-brain homing efficiency, freshly isolated monocyte was deemed to be the better candidate as cellular vehicles for the brain, and was used in all subsequent tests.

IV Adoptive Transferred Monocyte Ingression in the Inflamed Brain Did Not Aggravate Neuroinflammation

Histological results revealed that distributions of recruited monocytes in the brain altered at different time points following the induction of neuroinflammation. At 2 days post cell IV infusion, a large amount of recruited GFP-positive cells were detected in the injected hemisphere, in a broad and widely-distributed fashion (Fig 2A). There were also some GFP-positive cells detected in the contralateral (un-injected) hemisphere, mostly within the motor cortex at

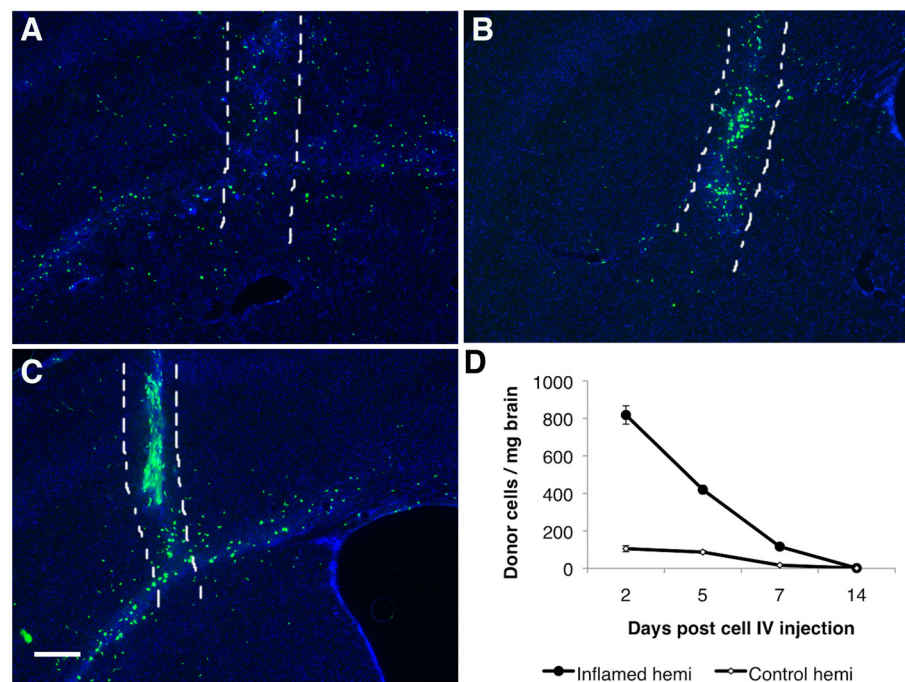


Fig 2. IV transferred monocytes ingress in brain. (A-C) Representative sections show the distribution of GFP positive donor-derived monocytes in the LPS injected brain at day 2(A), day 5(B), and day 7(C) post monocytes IV transfer. The area between the two white dash lines indicated the physical needle insertion site. For panel A-C, bar represent 200 μm, original magnification ×40. (D) Number of donor cells detected in the LPS injected hemisphere (ipsi hemi = ipsilateral hemi) and in the other hemisphere (contral hemi = contralateral) decreased over time post monocyte IV transfer.

doi:10.1371/journal.pone.0154022.g002

regions close to the injected hemisphere (data not shown). This distribution pattern strongly suggested that recruited monocytes were attracted to the CNS sites with inflammatory responses in a controlled fashion, and weren't just passively leaked in from the physical trauma on the BBB created by the microinjection needle, as the CNS responses would be confined to only the needle injection tract in such case [40]. By day 5, most GFP-positive cells appeared to be in close association to the needle insertion site (physical trauma site) (Fig 2B). By day 7, majority of the transmigrated cells were found along the needle tract (at a lower amount as compared to day 5), and within the corpus callosum of the LPS-injected hemisphere (Fig 2C). Quantification results showed that recruited donor cells in brain decreased over time as the animals recovered from LPS-induced acute neuroinflammation (Fig 2D).

The amount of monocytes recruited to the damaged CNS tissues is tightly correlated to the degree of inflammation [14, 40]. Nevertheless, infiltrating monocytes has been related to several CNS disease progressions, including multiple sclerosis and HIV-associated neurocognitive disorders [14, 16]. Whether or not the presence of additional monocytes introduced by adoptive transfer to circulation would aggravate neuroinflammation was unclear. Therefore, quantitative RT-PCR analysis was conducted at 72 hrs following ICI delivery of LPS (48 hrs post cell IV infusion). As compared to control animals that received ICI delivery of PBS, significant increase of gene transcription was detected in the brains of animals received LPS, including tumor necrosis factor alpha (TNF- α), interleukin 1 beta (IL-1 β), transforming growth factor beta (TGF β), interleukin 10 (IL-10), nitric oxide synthase 2 (NOS₂), and interleukin 12 subunit beta (IL-12p40) (Fig 3). However, no significant difference in cytokine gene transcription was observed between animals that received no cells and those received exogenous monocytes IV transfers at 24 hrs post ICI delivery of LPS (Fig 3), suggesting the transient presence of additional IV-transferred monocytes in circulation did not subsequently aggravate LPS-induced neuroinflammation.

Enhancement of Monocyte Entry into Inflamed Brain Tissue

One limitation of conducting cell adoptive transfer without preconditioning by lethal irradiation is that upon their entry into the circulation, these cells are diluted with endogenous cells; and as stated above, the amount of immune cells recruited to the target sites is fixed by the degree of inflammation. Therefore, we hypothesized that by rising exogenous to endogenous monocyte ratio, more transferred monocytes might be able to reach the affected brain regions. To test this, different numbers of monocytes ranged from 1×10^4 to 5×10^6 were infused into recipient mice that had received a fixed dose of LPS ICI (5 μ g) 24 hrs earlier. As the result, the number of donor-derived cells reaching the inflamed brain region was found to be positively correlated with the initial number of cells injected IV ($R = 0.9922$, $R^2 = 0.9845$; Pearson Correlation Coefficient) (Fig 4A). Hence by increasing the number of initial IV transferred cells, it is possible to bring up vehicle concentrations at the target site for more effective treatments.

The permeability of the BBB can be transiently increased through the use of chemical agents to disrupt the barrier [22, 29–32]. Our previous study demonstrated enhanced entry of blood circulating monocytes (infused via common carotid artery, CCA) into the brain in steady physiological state, following transient disruption of the BBB using Mannitol and Bradykinin [22], suggesting the possibility of increasing brain entry of the cell vehicles by transiently modulating BBB permeability. To further optimize BBB agent-facilitated enhancement of IV-infused cell vehicles entry into the CNS under inflammatory conditions, Bradykinin, Mannitol, and several other BBB agents that could temporarily increase the permeability of the BBB via different mechanisms were tested and compared. As shown in Fig 4B, Mannitol, Bradykinin and Serotonin all showed statistically significant enhancement in the amount of recruited donor cells in

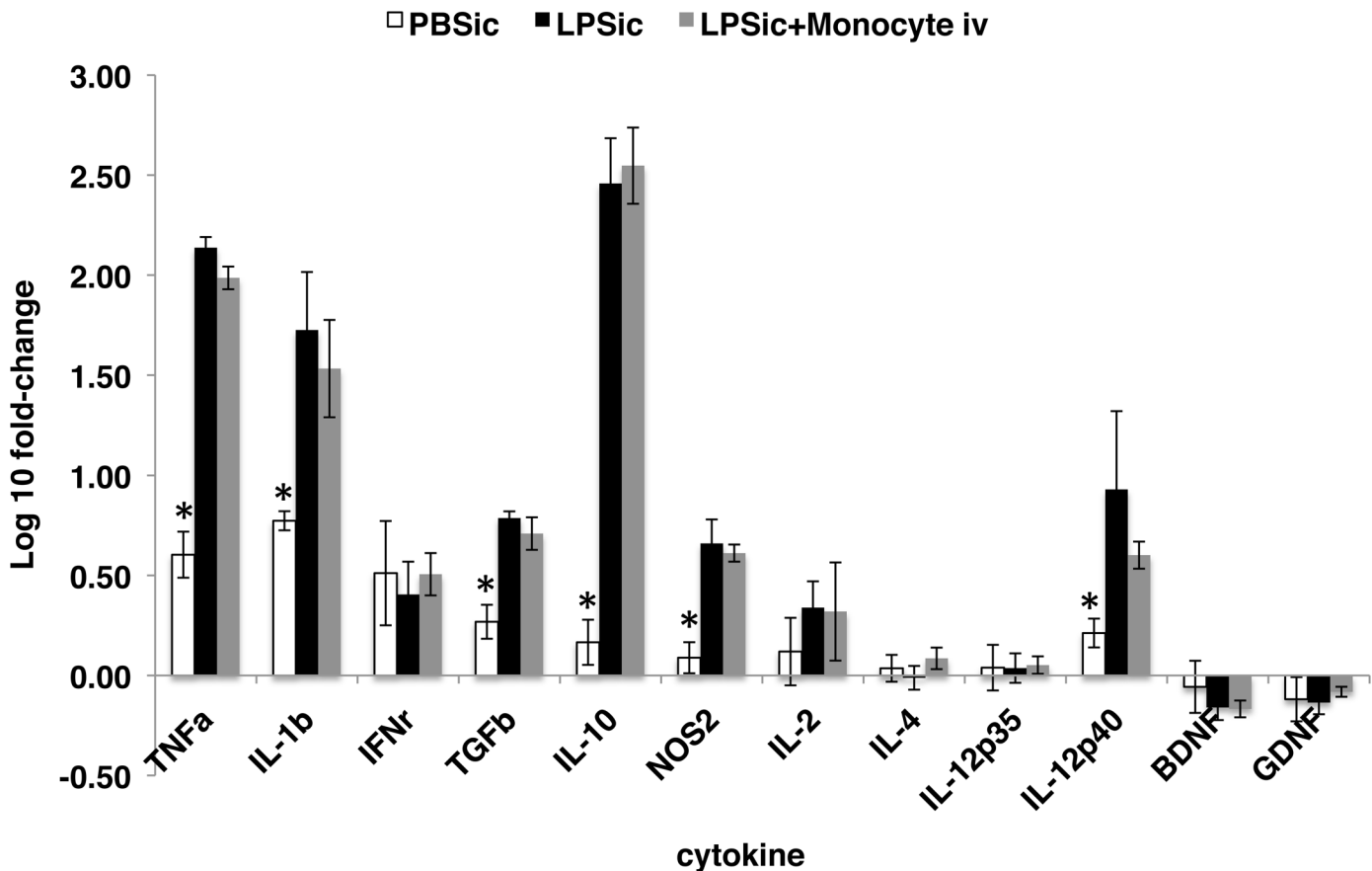


Fig 3. Expression analysis of selected cytokine genes in inflamed brain region. Transcription of TNF α , IL-1 β , TGF β , IL-10, IL-12p40 and NOS2 were significantly different in group PBSic compared to group LPSic and group LPSic+Monocytes iv (p-value < 0.05), but no difference was observed between group LPSic and group LPSic+Monocyte iv, indicating the presence of additional IV infused monocytes in circulation did not aggravate neuroinflammation. PBSic = sham control in which animals received PBS ICI. LPSic = inflammation control in which animals received LPS ICI. LPSic + Monocyte iv = animals received LPS ICI 24 hours prior to monocytes IV transfer. Cytokine gene transcription levels were measured at 72 hours post ICI. * = p-value < 0.05, unpaired *t* test. Final data presented here represents mean values \pm SD.

doi:10.1371/journal.pone.0154022.g003

the inflamed brain region at 48 hrs following cell IV infusion (p<0.05). Interestingly, the two calcium-channel modulating agents, Bradykinin and Serotonin, showed the highest enhancement in facilitating monocytes transmigration into the inflamed brains (176% \pm 51% and 168% \pm 59%), followed by the osmotic agent Mannitol (134% \pm 29%) (Fig 4B).

Recruited Monocyte Differentiated into IBA-1 Positive Cells with Microglia Morphology in the Brain

Histological analysis revealed that at 48 hours post cell infusion, GFP-positive cells recruited to the inflamed brain had a relatively homogeneous morphology, with majority of them being round (Fig 5A), and a few just slightly branched (Fig 5B). By day 5, most of donor-derived cells around the needle tract had a large and round appearance (Fig 5C), whereas cells in the cortex region started to show a more elongated and branched morphology (Fig 5D). By day 7, large and round cells were still detected around the needle tract (Fig 5E), and a small number of highly branched donor cells were also detected, mostly in the cortex regions (Fig 5F). Immunofluorescent analysis further revealed that a small portion of the donor cells had become Iba-1 positive by day 5 and day 7 post cell injection (Fig 6A and 6B), with all of them showing

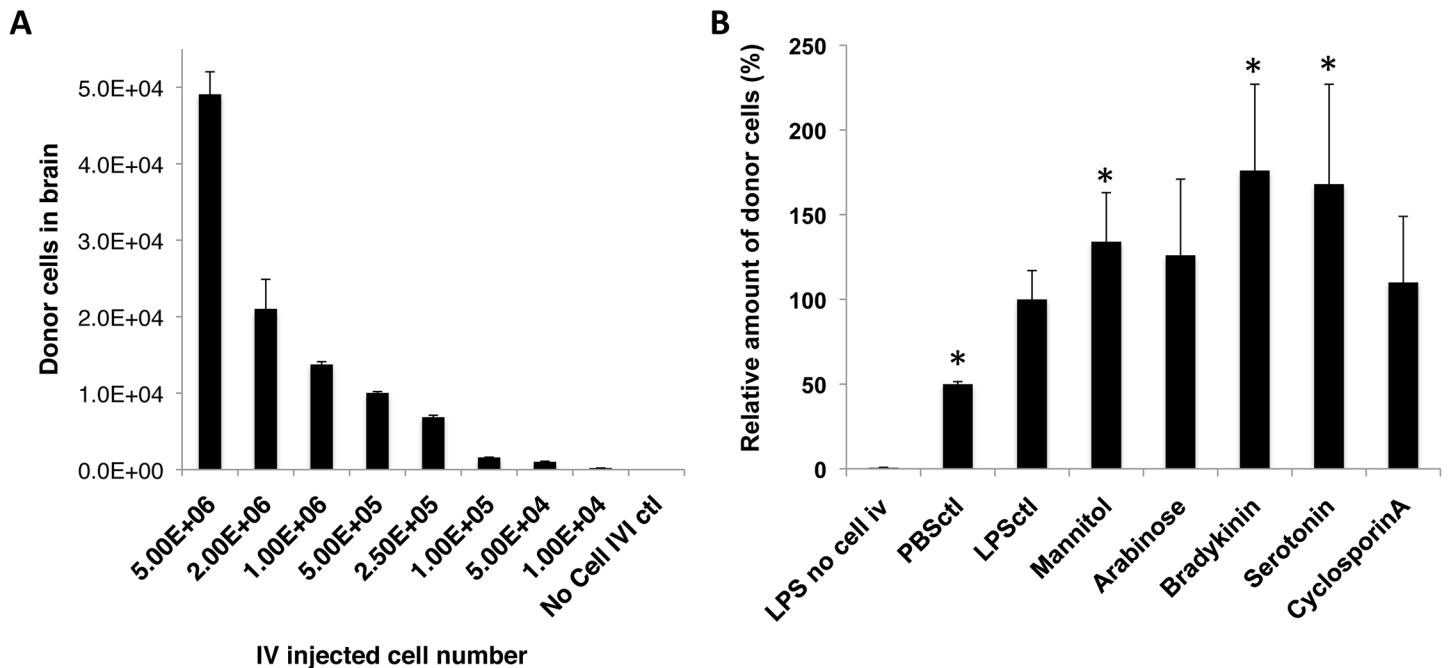


Fig 4. Enhanced monocytes entry into the inflamed brain. The amount of IV infused monocytes recruited to the inflamed brain regions could be enhanced by (A) increasing IV transferred monocyte amounts, and (B) transiently disrupting BBB by chemical agents. (A) The number of recruited donor-derived monocytes in the brain was positively correlated to the number of IV infused cells, as analyzed by Pearson correlation coefficient, with $R = 0.9932$, and $R^2 = 0.9864$. No Cell IVI control = Control animal that received LPS ICI but no monocyte IV. (B) Mannitol, Bradykinin, and Serotonin enhanced entry of IV transferred monocytes into LPS-inflamed brain tissue by $134\% \pm 29\%$, $176\% \pm 51\%$, and $168\% \pm 59\%$ compared to the group that received no BBBB reagents (LPsctl, p value < 0.05 , unpaired t test). Two additional control groups were included: LPS no cell i.v. = mice that received LPS ICI but no cells, and PBSctl = mice that received PBS ICI, followed by monocyte IV transfer. Data was analyzed by unpaired t test (to LPS no cell i.v. control) and one-way ANOVA (among all test groups), with resulting p -value < 0.05 (*) deemed as significant. No difference was found in groups treated with Arabinose and Cyclosporin A (p value > 0.05 , unpaired t test). Final data presented here represents mean values \pm SD.

doi:10.1371/journal.pone.0154022.g004

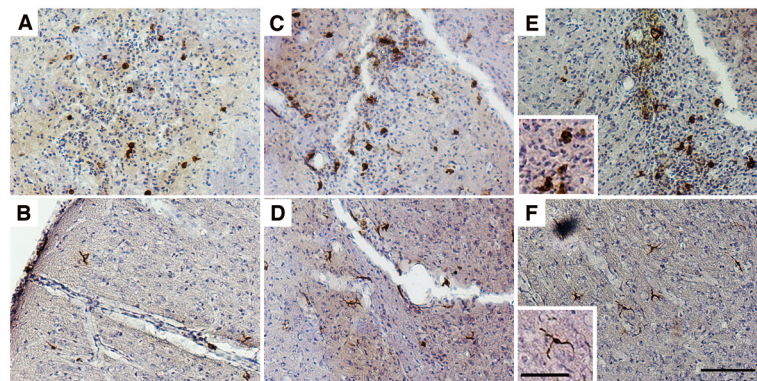


Fig 5. Recruited monocytes matured into cells with two distinguish morphologies in the brain. Two types of GFP positive donor-derived monocytes with very distinct morphologies were identified in the inflamed brain at day 2 (A& B), day 5 (C& D), and day 7 (E& F) post monocytes IVI. Panels A, C, and E show cells with big and round morphology that were often detected along the LPS injection tract, while panels B, D, and F show microglia-like, highly branched cells that were usually found in the cortical regions, further away from the needle tract. GFP positive cells were visualized by IHC staining with a GFP-specific primary antibody and a biotin-conjugated secondary antibody; Bars represent 100 μ m (A-F) and 25 μ m (insets). Original magnification $\times 100$ for panel A-F.

doi:10.1371/journal.pone.0154022.g005

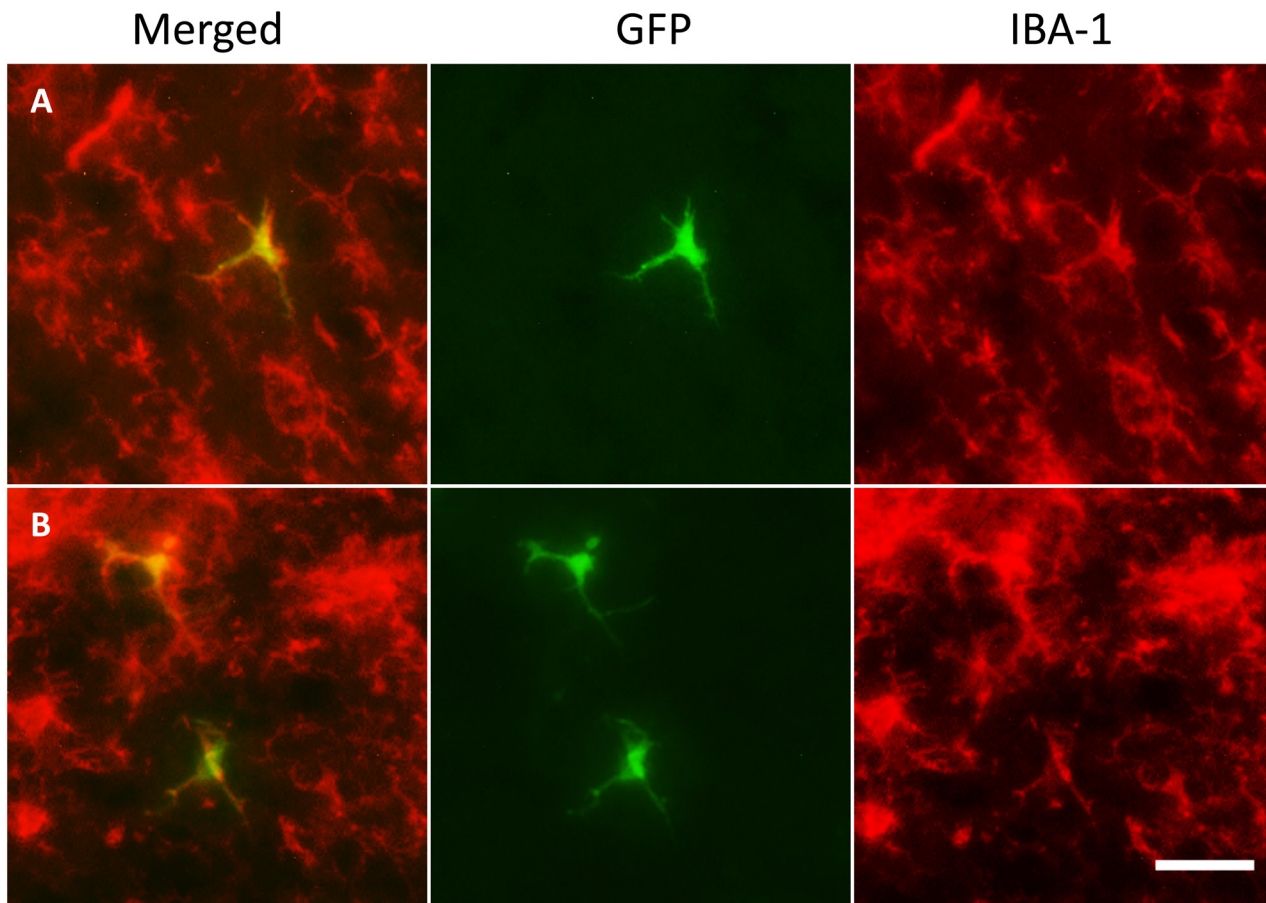


Fig 6. Recruited monocytes differentiated into IBA-1 positive cells with microglia morphology in the brain. GFP positive donor-derived cells (green) with a highly branched, microglia-like morphology located throughout the cortical region were Iba-1 positive (red) by day 5 (A) and day 7 (B) following IV adoptive transfer of monocytes. Bar represent 25 μ m for all panel. Original magnification \times 200 for panel A-F.

doi:10.1371/journal.pone.0154022.g006

branched morphology, and were detected mostly in the cortex region further away from the microinjection site. Differentiation of recruited donor cells into GFAP positive astrocytes in brain was not detected under the described conditions (S2 Fig). qPCR results indicated the presence of a low amount of recruited donor cells in the LPS injected hemisphere at day 14 (Fig 2D), whereas no donor cell was detectable in the peripheral tissues including liver, lungs and spleen (data not show), suggesting that a small population of recruited donor cells were able to last in the brain after animals were recovered from acute neuroinflammation.

Monocyte-Mediated Delivery of Nanoparticle SHP30 and Exogenous GFP Gene into the Inflamed Brain Tissues

Finally, we set out to determine the ability of “cargo” carriage monocytes to enter the brain. Two types of “cargos” were tested in this part of the study: SHP30 and GFP gene. SHP30 is a SPIO nanoparticle (SPION) that is 30nm in diameter. It was used to test the ability of monocytes to carry and transport nano-scaled agents (e.g. nano-formulated medicines or drug carriers) into the brain. On the other hand, GFP reporter gene was transferred into monocyte by an HIV-1-based vector D101, which allows gene integration into cell chromosome for permanent expression.

Overnight incubation of monocytes in SHP30 containing media resulted in 100% particle uptake efficiency, as determined by the presence of the particle accumulates (brown granules) (Fig 7A), and by Prussian blue positive pigments present in cell cytoplasm following Prussian blue staining (Fig 7B). LV-mediated GFP gene transfer, on the other hand, resulted in 36% of GFP-expressing monocytes (GFP-positive), as evaluated by fluorescent microscopy at 7 days post transduction (Fig 7C). After overnight SHP30 uptake, up to 96% SHP30-monocytes remained viable, as determined by Trypan blue exclusion assay (Fig 7D). Conversely, the 90 minutes LV transduction procedure resulted in nearly 30% cell death, with only 70% of transduced monocytes remained viable (Fig 7D). Immediately following the described *ex vivo* modifications, these male-donor derived monocytes were injected IV to female recipient animals bearing acute neuroinflammation induced by LPS IC the day before cell transfer. 48 hours following cell IV transfer, around 400 donor cells/mg brain for SHP30-monocytes, and 200 cells/mg brain for D101 LV transduced monocytes were detected in the inflamed brain tissues (Fig 7E), as determined by real-time qPCR measuring the amount of male-derived cells in the brain. In addition, cytoplasmic SHP30 carriage remained detectable in donor-derived monocytes following trafficking into the brain, as confirmed by IHC and Prussian blue staining (Fig 7E). Furthermore, the presence of the exogenous GFP gene in the inflamed brain region was confirmed by PCR at days 2 and 5 following IV infusion of the transduced cells (Fig 7G).

Discussion

This study was designed to fully characterize the IV adoptive transferred monocytes for their migration into the brain using an acute neuroinflammation mouse model, and thus to establish the optimized conditions to facilitate the cell-based therapeutic delivery system for the CNS. We investigated infused monocytes and MDM for their inflamed-brain homing efficiency, and established conditions that could enhance monocyte brain entry, followed by evaluating the transmigrated donor cell engraftment and differentiation in the brain, and finally, validated the ability of nano-scaled agents- and exogenous genes-carriage monocytes to enter the brain by testing with SHP30 and the GFP reporter gene.

To begin with, cells within the mononuclear phagocyte (MP) family vary largely in their degree of maturation and cellular functions, thus it is important to first identify the cell types that are more suitable as delivery vehicles, which should have the ability to accumulate in the brain target sites with high efficiency following adoptive transfer. Bone marrow is a preferred source of monocytes and MDM for many studies in mice, since it allows generating large quantities of mouse MDM through *in vitro* cultivation [3, 5, 7, 35]. However, it is not clear how the duration of *in vitro* cultivation affects MDM migratory efficiency *in vivo*. MDM have been reported to successfully deliver anti-viral drugs and therapeutic gene products into diseased CNS tissue after 10–14 days of *in vitro* cultivation in the presence of granulocyte macrophage colony stimulating factor (GM-CSF) or M-CSF [5, 7]. Freshly isolated bone marrow CD11b + cells have also been used to deliver therapeutic gene products for Alzheimer's disease in a mouse model [6]. A previous study of IV transferred monocytes in irradiated recipient animals concluded that the relative mature *ex vivo* manipulated monocytes migrated and engrafted with better efficiency in tissues [33]; whereas Xu *et al* reported that only freshly isolated CD11b + monocytic cells could circulate freely and traffic efficiently to the inflamed retina, but not MDM cultured *in vitro* for 6 days [34]. Nevertheless, few studies have provided a clear, quantitative comparison of the transmigratory efficiency of these transferred cells into the inflamed brain. Therefore, this study was first conducted to determine the relationship between the duration of *in vitro* cultivation and the *in vivo* trafficking efficiency of cMDM to inflamed CNS tissue in recipient mice. Our results indicated that freshly isolated monocytes and cMDM with

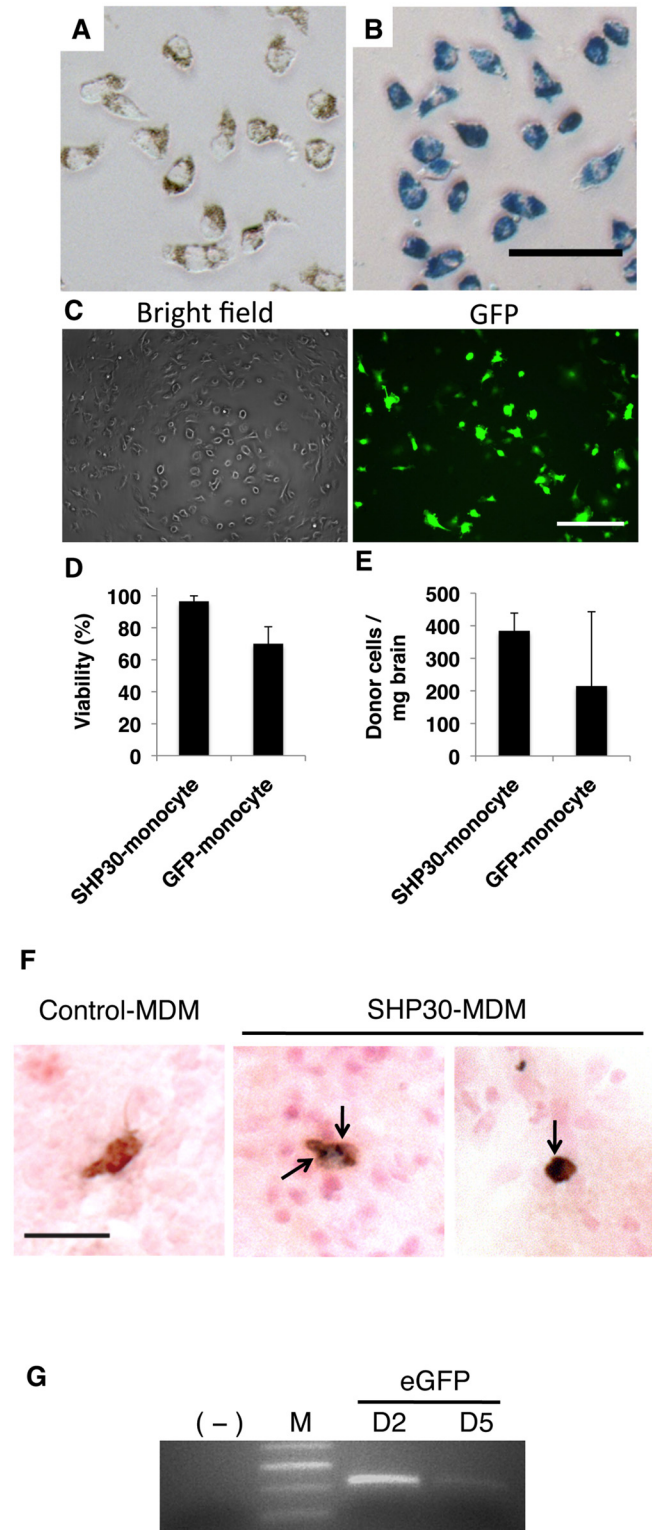


Fig 7. Monocyte-mediated delivery of SHP30 and GFP gene to the brain. (A&B) Overnight incubation of SHP30 with monocytes resulted in 100% SHP30 uptake efficiency, as observed by (A) the presence of brown SHP30 accumulates under the light microscopic fields, and by (B) the presence of Prussian blue pigments at monocytes cytoplasm following Prussian blue staining. (C) D101 LV-mediated GFP gene transfer resulted in around 36% transduction efficiency. (D) Viability of *ex vivo* modified monocytes following overnight incubation with 25 μ g/mL SHP30 (SHP30-monocyte), and 90-minute transduction with D101 LV (GFP-monocyte). (E)

SHP30-laden monocytes (SHP30-monocyte) or monocytes underwent D101 LV transduction (GFP-monocyte) were detected in the inflamed brain regions at 48 hours following cell IV infusion. (F) The presence of SHP30 (Dark blue, Prussian blue positive) was detected in the cytoplasm of the recruited donor-derived cells (Brown, GFP positive) in the brain. The arrow showed the presence of SHP30. (G) The presence of the exogenous GFP gene was detected in the inflamed brain by PCR at day 2 and day 5 following cell IV transfer. For Panel A & B, bar represents 50 μm , at original magnifications $\times 200$. For panel C, bar represents 200 μm , at original magnification $\times 200$. For panel F, bar represents 25 μm , at original magnification $\times 400$.

doi:10.1371/journal.pone.0154022.g007

shorter cultivation times migrated into the inflamed brain with much higher efficiency compared to cells that had undergone prolonged cultivation in the presence of M-CSF. These findings suggested that the relatively immature MP population were more suitable to be used as cell vehicles targeting the brain through the non-invasive IV administration.

Infiltrating monocytes have been reported to play critical roles in several CNS disease progression involving inflammation and tissue damages [14, 16]. Therefore, safety evaluation on conducting monocyte-based therapy is essential. After adoptive transfer, IV infused cells entered the circulation and mix with endogenous monocytes. Under normal physiological condition, there is about one million monocytes in mice peripheral blood, and the number increases during inflammation and pathological conditions [41]. When exogenous monocytes were introduced, there were considerably more monocytes in circulation for a transient period. Quantitative assessment of the mRNA expression level of several pro- and anti-inflammatory cytokine in brain revealed that this transient increase of monocytes in circulation did not aggravate the degree of neuroinflammation.

One important aspect when developing a successful cell-based delivery system is to establish conditions that can increase the number of cell vehicles present at the target sites. Unlike BMT procedure in which the endogenous immune cells and their precursors are largely destroyed by lethal irradiation, monocytes introduced by IV adoptive transfer were diluted with the endogenous cell pool upon entering circulation. As reported, the number for recruited cells into the brain was tightly controlled by the degree of neuroinflammation [14, 40], therefore, we increased the amount of IV transferred monocytes to bring up the exogenous to endogenous cell ratio, and confirmed that by increasing the number of IV infused cells, more donor cells were recruited to the inflamed brain region. In addition, we have further established the conditions in this study to transiently disrupt the BBB using chemical agents Mannitol, Bradykinin, and Serotonin to increase transmigration of donor cells into inflamed brain tissue (1.3–1.8 fold increase on average, $p < 0.05$, unpaired student t-test). The underlying mechanisms of this BBBD reagent-facilitated enhancement is presently not clear, and additional tests as well as further condition optimizations are necessary in the future. Nevertheless, this data supported the notion to increase IV-infused cell vehicle concentration at target brain tissues by increasing initial amount of transferred cells, as well as transiently disrupting the BBB using chemical agents.

Recent parabiosis-studies suggested that blood circulating monocytes were not able to differentiate into brain resident microglia, as demonstrated in both the mouse facial axotomy and experimental autoimmune encephalitis models [12, 14]. However, another study applying LPS IC injection into the brain reported local microglia death within 6 hours around the injection site, followed by replenish of regional IBA-1 positive cells derived from infiltrating monocytes [39]. Based on our observation, IBA-1 positive donor-derived cells started to appear at day 2 following cell IV infusion, and more IBA-1 positive cells with microglia-like morphology were detected at later time points, with majority of them located at the cortex region. To which extent can these IBA-1 positive cells last beyond the test period (14 day) requires further investigations. Nevertheless, the ability of IV transferred monocytes to enter the brain and differentiate into functional CNS tissue cells was indeed validated in this study.

Finally, the ability of monocytes to carry “cargos” into the brain was tested. SHP30 and GFP gene were selected as representative nano-scaled agent and exogenous gene, respectively. The numbers of the cargo-laden monocytes detected in the brains were in fact lower than monocytes without *ex vivo* modification. This decreased in homing efficiency was somewhat expected. The “loading” system we applied required overnight incubation of monocyte culture with the nanoparticles SHP30, and LV-mediated gene transfer involved a 90-minute transduction procedure using centrifugation. As observed in the study, elongated *in vitro* cultivation time has an adverse effect on the homing efficiency of cMDM, hence the overnight incubation with SHP30 was expected to decrease the brain migration level of the carrier monocytes. On the other hand, LV-mediated gene transfer using the spin-infection method involving centrifugation have caused certain degree of physical damages to the cells, which subsequently decreased carrier cells’ *in vivo* brain-migration efficiency. It should be noticed that we have confirmed the presence of SHP30-carriage monocytes in the brain by using histological method. However, it has been very challenging when the same approach was applied to validate the physical presence of GFP gene-carriage monocytes in the brain. As observed *in vitro*, the GFP signal expressed by carrier monocytes at 48 hours post transduction were very weak. Together with only 36% transduction efficiency and the fact of limited number of transduced-cells to enter the brain, detection of GFP-monocytes by IHC method was difficult. Nevertheless, current finding from PCR analysis has clearly demonstrated the presence of the GFP gene in the brain. These results together emphasized the importance of further method optimizations on the “loading” of therapeutic agents, especially therapeutic genes, into monocytes, and warrant for more in-depth study to confirm the viability and biological functionality of these recruited carrier cells in target tissues in the future.

In total, we have established an optimized monocyte-based delivery system, and validated the ability of IV adoptively transferred SHP30-carriage monocytes to enter the brain. The findings from this study support the notion of using monocyte-based delivery system as an alternative therapeutic approach towards neurological disorders, and argue for more in-depth tests and developments of such systems in the future.

Supporting Information

S1 Fig. Condition optimization for exogenous MDM delivery into acutely inflamed brain tissue. (A) The number of donor-derived MDM detected in the inflamed brain region at 24 hours following cell IV injection. Cells were introduced into the recipient animals at indicated time points post LPS-induced acute neuroinflammation. (B) The persistence of the recruited IV-infused donor cells in the inflamed brain of the recipient animals. Each experiment was independently performed 3 times, with 1 animal/group/experiment. Final data presented mean values \pm SD. Results were analyzed by one-way ANOVA, with resulting p-value <0.05 . (TIF)

S2 Fig. Distribution of IV infused monocytes and brain resident astrocytes in the inflamed brain. Distribution of recruited IV-infused GFP positive donor monocytes (Green) and GFAP positive brain resident astrocytes (Red). (A&B) Brain tissue was analyzed at day 5 (A) and day 7 (B) post monocyte IV transfer. Recruited donor-monocytes were found to be in close association to the site in which astrocyte reactivity developed the most along the needle injection tract. (C) No GFAP expression was observed on the recruited IV-infused monocytes, indicating that recruited donor-monocytes do not differentiate into astrocytes after entering the inflamed brain. For panel A and B, scale bar = 100 μ m, original magnification x100. For panel C, scale bar = 50 μ m, original magnification x200. (TIF)

S1 Text. Condition optimization for exogenous MDM delivery into acutely inflamed brain tissues. Initial experiments were conducted with MDM cultured for 5 days with M-CSF; this is reflective of prior works suggesting that the ratio of monocytes to mature macrophage reached its' highest at that time point [35]. Five million D5-cMDM from male donor C57BL6 mice were injected IV at 6, 18, 24, 48 and 72h, as well as 5 and 7 days after IC injection of LPS into female recipient C57BL6 mice. Brain tissues were first collected at 24 hours after cell injection. Quantification analysis was performed with real-time qPCR to determine the amount of male donor-derived cell genomic DNA (gDNA) in each test group. The amount of gDNA within the brain peaked when cells were introduced at 24 hours following LPS treatment (S1A Fig). We then examined the persistence of the donor-derived MDM after the cells entered the inflamed brain. Brain tissues were collected at 1, 2, 3 and 7 days following MDM transfers into LPS ICI treated mice. The number of recruited donor-derived cells peaked at 48h and decreased afterwards (S1B Fig). (DOCX)

Acknowledgments

This study was supported by National Institute of Mental Health (R01 MH079717). We thank Mary Margaret Byron for her invaluable inputs on designing the flow cytometry panel. We are grateful to Dr. Stephen Dewhurst of University of Rochester and Dr. Howard E. Gendelman of University of Nebraska for their assistance in revising this manuscript.

Author Contributions

Conceived and designed the experiments: YL HT. Performed the experiments: HT WK YS PMCD. Analyzed the data: HT WK PMCD YS SS. Contributed reagents/materials/analysis tools: YL RCA. Wrote the paper: HT YL PMCD.

References



1. Burke B, Lewis CE. *The macrophage*. 2nd ed. Oxford: Oxford University Press; 2002. xxvii, 647 p. p.
2. Lech M, Grobmayr R, Weidenbusch M, Anders HJ. Tissues use resident dendritic cells and macrophages to maintain homeostasis and to regain homeostasis upon tissue injury: the immunoregulatory role of changing tissue environments. *Mediators Inflamm*. 2012; 2012:951390. Epub 2012/12/20. doi: [10.1155/2012/951390](https://doi.org/10.1155/2012/951390) PMID: [23251037](https://pubmed.ncbi.nlm.nih.gov/23251037/); PubMed Central PMCID: PMC3518145.
3. Brynskikh AM, Zhao Y, Mosley RL, Li S, Boska MD, Klyachko NL, et al. Macrophage delivery of therapeutic nanozymes in a murine model of Parkinson's disease. *Nanomedicine (Lond)*. 2010; 5(3):379–96. Epub 2010/04/17. doi: [10.2217/nnm.10.7](https://doi.org/10.2217/nnm.10.7) PMID: [20394532](https://pubmed.ncbi.nlm.nih.gov/20394532/); PubMed Central PMCID: PMC2880389.
4. Dou H, Destache CJ, Morehead JR, Mosley RL, Boska MD, Kingsley J, et al. Development of a macrophage-based nanoparticle platform for antiretroviral drug delivery. *Blood*. 2006; 108(8):2827–35. Epub 2006/07/01. doi: [10.1182/blood-2006-03-012534](https://doi.org/10.1182/blood-2006-03-012534) PMID: [16809617](https://pubmed.ncbi.nlm.nih.gov/16809617/); PubMed Central PMCID: PMC1895582.
5. Dou H, Grotepas CB, McMillan JM, Destache CJ, Chaubal M, Werling J, et al. Macrophage delivery of nanoformulated antiretroviral drug to the brain in a murine model of neuroAIDS. *J Immunol*. 2009; 183(1):661–9. Epub 2009/06/19. doi: [10.4049/jimmunol.0900274](https://doi.org/10.4049/jimmunol.0900274) PMID: [19535632](https://pubmed.ncbi.nlm.nih.gov/19535632/); PubMed Central PMCID: PMC2765254.
6. Lebson L, Nash K, Kamath S, Herber D, Carty N, Lee DC, et al. Trafficking CD11b-positive blood cells deliver therapeutic genes to the brain of amyloid-depositing transgenic mice. *J Neurosci*. 2010; 30(29):9651–8. Epub 2010/07/28. doi: [10.1523/JNEUROSCI.0329-10.2010](https://doi.org/10.1523/JNEUROSCI.0329-10.2010) PMID: [20660248](https://pubmed.ncbi.nlm.nih.gov/20660248/); PubMed Central PMCID: PMC2929651.
7. Takahashi K, Prinz M, Stagi M, Chechneva O, Neumann H. TREM2-transduced myeloid precursors mediate nervous tissue debris clearance and facilitate recovery in an animal model of multiple sclerosis. *PLoS Med*. 2007; 4(4):e124. Epub 2007/04/12. doi: [10.1371/journal.pmed.0040124](https://doi.org/10.1371/journal.pmed.0040124) PMID: [17425404](https://pubmed.ncbi.nlm.nih.gov/17425404/); PubMed Central PMCID: PMC1851623.

8. Pardridge WM. The blood-brain barrier: bottleneck in brain drug development. *NeuroRx*. 2005; 2(1):3–14. Epub 2005/02/18. doi: [10.1602/neurorx.2.1.3](https://doi.org/10.1602/neurorx.2.1.3) PMID: [15717053](https://pubmed.ncbi.nlm.nih.gov/15717053/); PubMed Central PMCID: PMC539316.
9. Priller J, Flugel A, Wehner T, Boentert M, Haas CA, Prinz M, et al. Targeting gene-modified hematopoietic cells to the central nervous system: use of green fluorescent protein uncovers microglial engraftment. *Nat Med*. 2001; 7(12):1356–61. Epub 2001/12/01. doi: [10.1038/nm1201-1356](https://doi.org/10.1038/nm1201-1356) PMID: [11726978](https://pubmed.ncbi.nlm.nih.gov/11726978/).
10. Bechmann I, Goldmann J, Kovac AD, Kwidzinski E, Simburger E, Naftolin F, et al. Circulating monocyte cells infiltrate layers of anterograde axonal degeneration where they transform into microglia. *Faseb J*. 2005; 19(6):647–9. Epub 2005/01/27. doi: [10.1096/fj.04-2599fje](https://doi.org/10.1096/fj.04-2599fje) PMID: [15671154](https://pubmed.ncbi.nlm.nih.gov/15671154/).
11. Simard AR, Rivest S. Bone marrow stem cells have the ability to populate the entire central nervous system into fully differentiated parenchymal microglia. *Faseb J*. 2004; 18(9):998–1000. Epub 2004/04/16. doi: [10.1096/fj.04-1517fje](https://doi.org/10.1096/fj.04-1517fje) PMID: [15084516](https://pubmed.ncbi.nlm.nih.gov/15084516/).
12. Ajami B, Bennett JL, Krieger C, Tetzlaff W, Rossi FM. Local self-renewal can sustain CNS microglia maintenance and function throughout adult life. *Nat Neurosci*. 2007; 10(12):1538–43. Epub 2007/11/21. doi: [10.1038/nn2014](https://doi.org/10.1038/nn2014) PMID: [18026097](https://pubmed.ncbi.nlm.nih.gov/18026097/).
13. Mildner A, Schmidt H, Nitsche M, Merkler D, Hanisch UK, Mack M, et al. Microglia in the adult brain arise from Ly-6ChiCCR2+ monocytes only under defined host conditions. *Nat Neurosci*. 2007; 10(12):1544–53. Epub 2007/11/21. doi: [10.1038/nn2015](https://doi.org/10.1038/nn2015) PMID: [18026096](https://pubmed.ncbi.nlm.nih.gov/18026096/).
14. Ajami B, Bennett JL, Krieger C, McNagny KM, Rossi FM. Infiltrating monocytes trigger EAE progression, but do not contribute to the resident microglia pool. *Nat Neurosci*. 2011; 14(9):1142–9. Epub 2011/08/02. doi: [10.1038/nn.2887](https://doi.org/10.1038/nn.2887) PMID: [21804537](https://pubmed.ncbi.nlm.nih.gov/21804537/).
15. Fiala M, Zhang L, Gan X, Sherry B, Taub D, Graves MC, et al. Amyloid-beta induces chemokine secretion and monocyte migration across a human blood–brain barrier model. *Mol Med*. 1998; 4(7):480–9. Epub 1998/08/26. PMID: [9713826](https://pubmed.ncbi.nlm.nih.gov/9713826/); PubMed Central PMCID: PMC2230332.
16. Gonzalez E, Rovin BH, Sen L, Cooke G, Dhanda R, Mummidi S, et al. HIV-1 infection and AIDS dementia are influenced by a mutant MCP-1 allele linked to increased monocyte infiltration of tissues and MCP-1 levels. *Proc Natl Acad Sci U S A*. 2002; 99(21):13795–800. Epub 2002/10/11. doi: [10.1073/pnas.202357499](https://doi.org/10.1073/pnas.202357499) PMID: [12374865](https://pubmed.ncbi.nlm.nih.gov/12374865/); PubMed Central PMCID: PMC129777.
17. Persidsky Y, Ghorpade A, Rasmussen J, Limoges J, Liu XJ, Stins M, et al. Microglial and astrocyte chemokines regulate monocyte migration through the blood-brain barrier in human immunodeficiency virus-1 encephalitis. *Am J Pathol*. 1999; 155(5):1599–611. Epub 1999/11/07. doi: [10.1016/S0002-9440\(10\)65476-4](https://doi.org/10.1016/S0002-9440(10)65476-4) PMID: [10550317](https://pubmed.ncbi.nlm.nih.gov/10550317/); PubMed Central PMCID: PMC1866982.
18. Andreesen R, Hennemann B, Krause SW. Adoptive immunotherapy of cancer using monocyte-derived macrophages: rationale, current status, and perspectives. *J Leukoc Biol*. 1998; 64(4):419–26. Epub 1998/10/10. PMID: [9766621](https://pubmed.ncbi.nlm.nih.gov/9766621/).
19. Burke B. Macrophages as novel cellular vehicles for gene therapy. *Expert Opin Biol Ther*. 2003; 3(6):919–24. Epub 2003/08/29. doi: [10.1517/14712598.3.6.919](https://doi.org/10.1517/14712598.3.6.919) PMID: [12943451](https://pubmed.ncbi.nlm.nih.gov/12943451/).
20. Fidler IJ. Therapy of cancer metastasis by systemic activation of macrophages. *Adv Pharmacol*. 1994; 30:271–326. Epub 1994/01/01. PMID: [7833294](https://pubmed.ncbi.nlm.nih.gov/7833294/).
21. Roth JC, Curiel DT, Pereboeva L. Cell vehicle targeting strategies. *Gene Ther*. 2008; 15(10):716–29. Epub 2008/03/29. doi: [10.1038/gt.2008.38](https://doi.org/10.1038/gt.2008.38) PMID: [18369326](https://pubmed.ncbi.nlm.nih.gov/18369326/).
22. Wu J, Yang S, Luo H, Zeng L, Ye L, Lu Y. Quantitative evaluation of monocyte transmigration into the brain following chemical opening of the blood-brain barrier in mice. *Brain Res*. 2006; 1098(1):79–85. Epub 2006/08/16. doi: [10.1016/j.brainres.2006.04.074](https://doi.org/10.1016/j.brainres.2006.04.074) PMID: [16908012](https://pubmed.ncbi.nlm.nih.gov/16908012/); PubMed Central PMCID: PMC2830797.
23. Klimatcheva E, Planelles V, Day SL, Fulreader F, Renda MJ, Rosenblatt J. Defective lentiviral vectors are efficiently trafficked by HIV-1 and inhibit its replication. *Mol Ther*. 2001; 3(6):928–39. Epub 2001/06/16. doi: [10.1006/mthe.2001.0344](https://doi.org/10.1006/mthe.2001.0344) PMID: [11407907](https://pubmed.ncbi.nlm.nih.gov/11407907/).
24. Wu C, Lu Y. Inclusion of high molecular weight dextran in calcium phosphate-mediated transfection significantly improves gene transfer efficiency. *Cell Mol Biol (Noisy-le-grand)*. 2007; 53(4):67–74. Epub 2007/05/29. PMID: [17531163](https://pubmed.ncbi.nlm.nih.gov/17531163/); PubMed Central PMCID: PMC2830788.
25. Zeng L, Planelles V, Sui Z, Gartner S, Maggirwar SB, Dewhurst S, et al. HIV-1-based defective lentiviral vectors efficiently transduce human monocytes-derived macrophages and suppress replication of wild-type HIV-1. *J Gene Med*. 2006; 8(1):18–28. Epub 2005/09/06. doi: [10.1002/jgm.825](https://doi.org/10.1002/jgm.825) PMID: [16142830](https://pubmed.ncbi.nlm.nih.gov/16142830/); PubMed Central PMCID: PMC2825118.
26. Zeng L, Yang S, Wu C, Ye L, Lu Y. Effective transduction of primary mouse blood- and bone marrow-derived monocytes/macrophages by HIV-based defective lentiviral vectors. *J Virol Methods*. 2006; 134(1–2):66–73. Epub 2006/01/25. doi: [10.1016/j.jviromet.2005.12.006](https://doi.org/10.1016/j.jviromet.2005.12.006) PMID: [16430973](https://pubmed.ncbi.nlm.nih.gov/16430973/); PubMed Central PMCID: PMC2825312.

27. McBride C, Gaupp D, Phinney DG. Quantifying levels of transplanted murine and human mesenchymal stem cells in vivo by real-time PCR. *Cytherapy*. 2003; 5(1):7–18. Epub 2003/05/15. doi: [10.1080/14653240310000038](https://doi.org/10.1080/14653240310000038) PMID: [12745583](https://pubmed.ncbi.nlm.nih.gov/12745583/).
28. dos Anjos Pires M, Palmeira C, Rodrigues P, Lopes C, Oliveira-Torres F. Establishment of a diploid reference value for DNA ploidy analysis by image cytometry in mouse cells. *Anal Quant Cytol Histol*. 2001; 23(6):427–32. Epub 2002/01/05. PMID: [11777278](https://pubmed.ncbi.nlm.nih.gov/11777278/).
29. McCarty DM, DiRosario J, Gulaid K, Muenzer J, Fu H. Mannitol-facilitated CNS entry of rAAV2 vector significantly delayed the neurological disease progression in MPS IIIB mice. *Gene Ther*. 2009; 16(11):1340–52. Epub 2009/07/10. doi: [10.1038/gt.2009.85](https://doi.org/10.1038/gt.2009.85) PMID: [19587708](https://pubmed.ncbi.nlm.nih.gov/19587708/).
30. Liu R, Martuza RL, Rabkin SD. Intracarotid delivery of oncolytic HSV vector G47Delta to metastatic breast cancer in the brain. *Gene Ther*. 2005; 12(8):647–54. Epub 2005/01/14. doi: [10.1038/sj.gt.3302445](https://doi.org/10.1038/sj.gt.3302445) PMID: [15647762](https://pubmed.ncbi.nlm.nih.gov/15647762/).
31. Colgan J, Asmal M, Yu B, Luban J. Cyclophilin A-deficient mice are resistant to immunosuppression by cyclosporine. *J Immunol*. 2005; 174(10):6030–8. Epub 2005/05/10. PMID: [15879096](https://pubmed.ncbi.nlm.nih.gov/15879096/).
32. Winkler T, Sharma HS, Stalberg E, Olsson Y, Dey PK. Impairment of blood-brain barrier function by serotonin induces desynchronization of spontaneous cerebral cortical activity: experimental observations in the anaesthetized rat. *Neuroscience*. 1995; 68(4):1097–104. Epub 1995/10/01. PMID: [8544985](https://pubmed.ncbi.nlm.nih.gov/8544985/).
33. Kennedy DW, Abkowitz JL. Mature monocytic cells enter tissues and engraft. *Proc Natl Acad Sci U S A*. 1998; 95(25):14944–9. Epub 1998/12/09. PMID: [9843995](https://pubmed.ncbi.nlm.nih.gov/9843995/); PubMed Central PMCID: PMC24555.
34. Xu H, Manivannan A, Dawson R, Crane IJ, Mack M, Sharp P, et al. Differentiation to the CCR2+ inflammatory phenotype in vivo is a constitutive, time-limited property of blood monocytes and is independent of local inflammatory mediators. *J Immunol*. 2005; 175(10):6915–23. Epub 2005/11/08. PMID: [16272351](https://pubmed.ncbi.nlm.nih.gov/16272351/); PubMed Central PMCID: PMC2496954.
35. Francke A, Herold J, Weinert S, Strasser RH, Braun-Dullaeus RC. Generation of mature murine monocytes from heterogeneous bone marrow and description of their properties. *J Histochem Cytochem*. 2011; 59(9):813–25. Epub 2011/06/28. doi: [10.1369/0022155411416007](https://doi.org/10.1369/0022155411416007) PMID: [21705645](https://pubmed.ncbi.nlm.nih.gov/21705645/); PubMed Central PMCID: PMC3201167.
36. Geissmann F, Jung S, Littman DR. Blood monocytes consist of two principal subsets with distinct migratory properties. *Immunity*. 2003; 19(1):71–82. Epub 2003/07/23. PMID: [12871640](https://pubmed.ncbi.nlm.nih.gov/12871640/).
37. Tacke F, Randolph GJ. Migratory fate and differentiation of blood monocyte subsets. *Immunobiology*. 2006; 211(6–8):609–18. Epub 2006/08/22. doi: [10.1016/j.imbio.2006.05.025](https://doi.org/10.1016/j.imbio.2006.05.025) PMID: [16920499](https://pubmed.ncbi.nlm.nih.gov/16920499/).
38. Sunderkotter C, Nikolic T, Dillon MJ, Van Rooijen N, Stehling M, Drevets DA, et al. Subpopulations of mouse blood monocytes differ in maturation stage and inflammatory response. *J Immunol*. 2004; 172(7):4410–7. Epub 2004/03/23. PMID: [15034056](https://pubmed.ncbi.nlm.nih.gov/15034056/).
39. Ji KA, Yang MS, Jeong HK, Min KJ, Kang SH, Jou I, et al. Resident microglia die and infiltrated neutrophils and monocytes become major inflammatory cells in lipopolysaccharide-injected brain. *Glia*. 2007; 55(15):1577–88. Epub 2007/09/08. doi: [10.1002/glia.20571](https://doi.org/10.1002/glia.20571) PMID: [17823975](https://pubmed.ncbi.nlm.nih.gov/17823975/).
40. Andersson PB, Perry VH, Gordon S. The acute inflammatory response to lipopolysaccharide in CNS parenchyma differs from that in other body tissues. *Neuroscience*. 1992; 48(1):169–86. Epub 1992/01/01. PMID: [1584421](https://pubmed.ncbi.nlm.nih.gov/1584421/).
41. Van Furth R, Diesselhoff-den Dulk MC, Mattie H. Quantitative study on the production and kinetics of mononuclear phagocytes during an acute inflammatory reaction. *J Exp Med*. 1973; 138(6):1314–30. Epub 1973/12/01. PMID: [4762549](https://pubmed.ncbi.nlm.nih.gov/4762549/); PubMed Central PMCID: PMC2139470.



Highly delayed systemic translocation of aluminum-based adjuvant in CD1 mice following intramuscular injections

Guillemette Crépeaux ^a  , Housam Eidi ^{a b}, Marie-Odile David ^b, Eleni Tzavara ^c, Bruno Giros ^c, Christopher Exley ^d, Patrick A. Curmi ^b, Christopher A. Shaw ^e, Romain K. Gherardi ^{a 1}, Josette Cadusseau ^{a f 1}



Show more 

 Share  Cite

<https://doi.org/10.1016/j.jinorgbio.2015.07.004> ↗

[Get rights and content](#) ↗

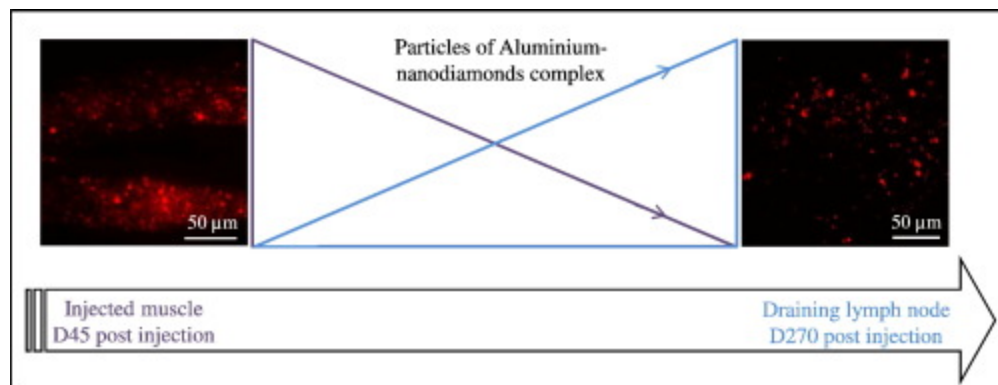
Highlights

- Vaccine safety is a key question due to the reported adverse events in humans & animals.
- Results showed a highly delayed systemic translocation of adjuvant particles.
- This study suggests the importance of mouse strain, route of exposure & doses.
- This study confirms the striking biopersistence of alum.

Abstract

Concerns regarding vaccine safety have emerged following reports of potential adverse events in both humans and animals. In the present study, alum, alum-containing vaccine and alum adjuvant tagged with fluorescent nanodiamonds were used to evaluate i) the persistence time at the injection site, ii) the translocation of alum from the injection site to lymphoid organs, and iii) the behavior of adult CD1 mice following intramuscular injection of alum (400 μ gAl/kg). Results showed for the first time a strikingly delayed systemic translocation of adjuvant particles. Alum-induced granuloma remained for a very long time in the injected muscle despite progressive shrinkage from day 45 to day 270. Concomitantly, a markedly delayed translocation of alum to the draining lymph nodes, major at day 270 endpoint, was observed. Translocation to the spleen was similarly delayed (highest number of particles at day 270). In contrast to C57BL/6J mice, no brain translocation of alum was observed by day 270 in CD1 mice. Consistently neither increase of Al cerebral content, nor behavioral changes were observed. On the basis of previous reports showing alum neurotoxic effects in CD1 mice, an additional experiment was done, and showed early brain translocation at day 45 of alum injected subcutaneously at 200 μ gAl/kg. This study confirms the striking biopersistence of alum. It points out an unexpectedly delayed diffusion of the adjuvant in lymph nodes and spleen of CD1 mice, and suggests the importance of mouse strain, route of administration, and doses, for future studies focusing on the potential toxic effects of aluminum-based adjuvants.

Graphical abstract



[Download: Download full-size image](#)

Introduction

Aluminum (Al) is the third most abundant element in the Earth's crust and it is ubiquitously present in our everyday life in a great variety of objects (cooking utensils, food packaging, housing materials, pharmaceutical products, cosmetics, etc.). Al is found in all body fluids (blood, cerebral spinal fluid, interstitial fluid of the brain, lymph, sweat, seminal fluids and urine) [1]. Despite the widespread use of Al in our environment leading to this increase of its bioavailability, Al has no known biological role [2].

Furthermore, it is widely accepted that Al and Al compounds are neurotoxic for animals and humans [3], [4]. For instance, Al exposure has been implicated in the pathology of several neurodegenerative diseases associated with cognitive impairments, as Alzheimer's disease [5], [6], [7]. The molecular mechanisms by which it causes neuronal damage are not fully understood [8], but it is generally accepted that the nervous system is particularly sensitive to oxidant-mediated damage [9], and that the neurotoxicity of Al is caused by its ability to increase oxidative damage in the brain [10].

Finally, the bioavailability of Al, its ability to cross the blood–brain barrier, and the relatively slow rate of elimination from the brain contribute to progressive accumulation of Al into the brain [11], [12], [13], and enhance neurotoxicological risk [14].

Many severe infectious diseases can be prevented by vaccine and some of them have been eradicated. Furthermore novel vaccine strategies are now being developed as promising therapies to overcome diseases such as cancer. However, though vaccines are commonly and safely used, and are generally well tolerated by most people, they occasionally cause adverse effects, such as ill-defined conditions usually manifesting as symptoms such as myalgia, arthralgia, chronic fatigue and development of autoantibodies [15]. No consensus exists so far on a cause-to-effect relationship, but vaccine adjuvants have been suspected to be associated with several inflammatory/neurodegenerative or autoimmune conditions impacting the central nervous system such as multiple sclerosis [16], amyotrophic lateral sclerosis [17] and autism [6]. A new syndrome has thus been identified by Shoenfeld in 2011, the autoimmune/auto-inflammatory syndrome induced by adjuvants (ASIA) [18].

Several papers from the literature suggest that vaccines containing aluminum adjuvants may be insidiously unsafe over the long-term. This is in line with the role of environmental aluminum that is continuously suspected to represent a possible co-factor of several chronic diseases [19], [20], [21], [1].

Among unusual reactions to aluminum hydroxide (alum) containing vaccines, macrophagic myofasciitis (MMF) is an inflammatory lesion described in 1998 [22], and recognized as a

“distinctive histopathological entity that may be caused by intramuscular injection of Al-containing vaccines” [23].

MMF affects mainly women (>70% of total known cases), and is characterized by highly specific myopathological alterations observed in patients suffering from a combination of diffuse myalgias, arthralgia, chronic fatigue and cognitive impairment such as alterations affecting working memory and attention [22], [24], [25], [26], [27].

Alum-adjuvanted vaccines are usually administered in France through intramuscular injection into the deltoid muscle in adults [28]. In MMF patients deltoid muscle biopsies showed crystalline cytoplasmic inclusions in macrophages corresponding to alum agglomerates of vaccine origin [29]. The constant detection of these agglomerates in MMF assesses the unusually long persistence time of alum in affected individuals [30].

Both Al oxyhydroxide and Al hydroxyphosphate are used as vaccine adjuvants [31], [32]. Indeed, Al has been added to vaccines since the early part of the twentieth century to enhance the primary immunization [33]. The role of Al adjuvants was believed to prolong the retention of adsorbed antigens at the injection site, thus reducing the amount of antigen needed per dose and the number of required doses [34], [35]. However, the “depot” theory has been challenged by early ablation of the injected site [36] and mechanisms of alum immunopotentiality only begin to be progressively understood [31].

Al containing vaccines are commonly used, such as vaccines against tetanus, hepatitis A, hepatitis B, human papillomavirus, haemophilus influenzae B, pneumococcal and meningococcal infections, and anthrax [37]. FDA regulations limit the Al content of an individual vaccinal dose to 0.85 mg of elemental Al [38].

Previous results have shown that Al particles, as other poorly degradable particles, do not stay localized in the injected muscle tissue, but can rather disseminate within phagocyte cells to lymph nodes and distant sites including the spleen and brain [39]. A previous study of our group looked at aluminum translocation after intramuscular injection of alum-containing vaccine in C57BL/6J mice. Aluminum was detected in the injected muscle, but also in distant organs such as the spleen, a few days after injection, and then in the brain where it was still detected one year later. Using surrogate labeled particles containing precipitated alum, a rapid phagocytosis of injected particles by muscle monocyte lineage cells and their translocation via lymph and blood vessels were confirmed. Particles reached the brain as soon as 3 weeks post-injection and were shown to accumulate albeit very slowly and in small numbers [39]. Recently, we developed a new tool allowing tracing of Al(OH)₃ particles in the tissues at very low levels and over the long-term [40]. This method

consists of tagging Al adjuvant itself (Alhydrogel®) with fluorescent nanodiamonds (fNDs) functionalized with hyperbranched polyglycerol (HPG). The complex alum-nanodiamonds (AluDia) had physico-chemical properties similar to HBV vaccine [40]. When injected in the *tibialis anterior* (TA) muscle of C57BL/6J mice, it allowed the monitoring of lymphatic and systemic biodistribution of AluDia particles and their presence in the brain tissue, 3 weeks after the intramuscular injection.

The potential impact of aluminum adjuvant on the nervous system has been studied in mouse models. Aluminum adjuvant, dosed at 100 µgAl/kg and subcutaneously injected in CD1 mice, induced motor deficits and anxiety increases associated with motor neuron death and astrogliosis [17]. Although no motoneuron death was observed when the dose was increased 3-fold, Shaw and Petrik [41] observed a microglial and astrocytic reactivity in the spinal cord of CD1 mice that present with an increase in anxiety, significant impairments in a number of motor functions and diminished spatial memory capacity. A neuroinflammatory syndrome has been described in sheep after the repetitive administration of Al-containing vaccines [42]. Recently, impairment of neurocognitive functions and brain gliosis was reported in a murine model of systemic lupus erythematosus-like disease following intramuscular injection of Al hydroxide or vaccine against the hepatitis B virus (HBV) (200 µg/mouse) [43].

Although progressive shrinkage of the local granuloma [44], [45] and rapid translocation of alum from the injected site to draining lymph nodes (dLNs) and spleen have been repeatedly demonstrated [39], [40], long-term biodisposition of alum particles trapped in the local granuloma remains unexplored. To examine this point we designed a longitudinal study in which alum, alum-containing vaccine and alum tagged with fluorescent nanodiamonds were used in adult CD1 mice to evaluate i) the persistence time at the injection site, ii) the long-term translocation of alum from the injection site to the lymphoid organs, and iii) the behavior and motricity of animals following intramuscular injection of alum.

Access through your organization

Check access to the full text by signing in through your organization.

 Access through your organization

Section snippets

Dose of exposure

The dose of 400 μ gAl/kg was chosen to model a plurivaccination with the HBV ENGERIX® vaccine. Medical histories of MMF patients revealed that 100% (50/50 patients) of them received 1–9 (median 4) doses of an Al-containing vaccine within 10 years prior to their diagnosis [29]. A 60-kg woman injected with 1 dose of HBV ENGERIX® vaccine receives 500 μ g of Al, i.e. 8.3 μ gAl/kg of body weight. The allometric conversion from human to mouse (FDA guidance 5541) gives a final amount of approximately 100 μ g ...

Muscle granuloma size at the injection site

Serial sections of the injected muscle 45, 135, 180 and 270 days after Alhydrogel® (400 μ gAl/kg) or HBV vaccine (400 μ gAl/kg) injection showed progressive shrinkage of muscle granuloma (Table 1). At D45 all animals had granuloma with a majority of sections showing a granuloma (93% for Alhydrogel®, 67% for HBV vaccine). At D270, in contrast to previous time points, one animal was free of granuloma and a majority of overall muscle sections showed no granuloma (65% for Alhydrogel®, 69% for HBV ...

Discussion

This longitudinal study showed that alum (Alhydrogel® or HBV vaccine) injected into the muscle constantly induces a granuloma similar to MMF that shrinks with time with marked clearance of granulomatous lesions observed from D180 to D270. This is similar to what was previously observed with the AluDia complex [40]. Granuloma shrinkage in the muscle was associated with concurrent replenishment of inguinal dLNs (100 fold increase of AluDia particles from D45 to D270). Similar translocation of ...

Conclusion

We observed a strikingly delayed, previously unknown, systemic translocation of alum particles injected into the muscle, with conspicuous alum accumulations in the lymphatic system and spleen 9 months after injection. In addition to the crucial “t” factor, our results strongly suggest the influence of the mouse strain, the dose and the route of administration on alum biodisposition. All these parameters should be taken into account in the design of future alum toxicological studies. ...

List of abbreviations

AluDia

complex alum-nanodiamonds ...

ASIA

autoimmune/auto-inflammatory syndrome induced by adjuvants ...

dLNs

draining lymph nodes ...

FDA

Food and Drug Administration ...

HBV

hepatitis B virus ...

HPG

hyperbranched polyglycerol ...

HPHT

High Pressure High Temperature ...

im

intramuscular ...

fNDs

fluorescent nanodiamonds ...

MMF

macrophagic myofasciitis ...

MCP-1/CCL2

monocyte chemoattractant protein 1/chemokine ligand 2 ...

PBS

phosphate buffer saline ...

TA

tibialis anterior ...

THGA

spectrometer with a transversely heated graphite atomizer ...

TH GFAAS

graphite furnace ...

...

Conflicts of interest

The authors declare that there are no conflicts of interest. ...

Acknowledgments

The authors thank Marina Bermudez de Castro Rubio, Anthony Deust and Frédéric Ros for their technical help, and Marie De Antonio for her statistical explanations. This study was supported by the University of British Columbia in Vancouver (UBC PG#20R17162), Dwoskin Family Foundation (UBC PG#20R65375), ANSM, and Région Ile-de-France DIM NeRF (“Nano-in-brain” project). ...

[Recommended articles](#)

References (67)

C. Exley *et al.*

[A role for the body burden of aluminium in vaccine-associated macrophagic myofasciitis and chronic fatigue syndrome](#)

Med. Hypotheses (2009)

S. Bondy

[The neurotoxicity of environmental aluminum is still an issue](#)

Neurotoxicology (2010)

S. Kumar

[Biphasic effect of aluminium on cholinergic enzyme of rat brain](#)

Neurosci. Lett. (1998)

L. Tomljenovic *et al.*

[Do aluminum vaccine adjuvants contribute to the rising prevalence of autism?](#)

J. Inorg. Biochem. (2011)

P. Zatta *et al.*

[In vivo and in vitro effects of aluminum on the activity of mouse brain acetylcholinesterase](#)

Brain Res. Bull. (2002)

R. Moumen *et al.*

[Aluminium increases xanthine oxidase activity and disturbs antioxidant status in the rat](#)

J. Trace Elem. Med. Biol. Organ Soc. Miner. Trace Elem. GMS. (2001)

P. Nayak

[Aluminum: impacts and disease](#)

Environ. Res. (2002)

C. Exley

[When an aluminium adjuvant is not an aluminium adjuvant used in human vaccination programmes](#)

Vaccine (2012)

S. Sánchez-Iglesias *et al.*

[Analysis of brain regional distribution of aluminium in rats via oral and intraperitoneal administration](#)

J. Trace Elem. Med. Biol. Organ Soc. Miner. Trace Elem. GMS. (2007)

H. Rosenblum *et al.*

[The common immunogenic etiology of chronic fatigue syndrome: from infections to vaccines via adjuvants to the ASIA syndrome](#)

Infect. Dis. Clin. North Am. (2011)



[View more references](#)

Cited by (36)

[Myalgia and chronic fatigue syndrome following immunization: macrophagic myofasciitis and animal studies support linkage to aluminum adjuvant persistency and diffusion in the immune system](#)

2019, Autoimmunity Reviews



[Show abstract](#)



Toxicology

Volume 375, 15 January 2017, Pages 48-57

Non-linear dose-response of aluminium hydroxide adjuvant particles: Selective low dose neurotoxicity

Guillemette Crépeaux ^{a b 2}  , Housam Eidi ^{a c}, Marie-Odile David ^c, Yasmine Baba-Amer ^a, Eleni Tzavara ^d, Bruno Giros ^d, François-Jérôme Authier ^a, Christopher Exley ^e, Christopher A. Shaw ^f, Josette Cadusseau ^{a g 1}, Romain K. Gherardi ^{a 1}

Show more 

 Share  Cite

<https://doi.org/10.1016/j.tox.2016.11.018> 

[Get rights and content](#) 

Abstract

Aluminium (Al) oxyhydroxide (Alhydrogel[®]), the main adjuvant licensed for human and animal vaccines, consists of primary nanoparticles that spontaneously agglomerate. Concerns about its safety emerged following recognition of its unexpectedly long-lasting biopersistence within immune cells in some individuals, and reports of chronic fatigue syndrome, cognitive dysfunction, myalgia, dysautonomia and autoimmune/inflammatory features temporally linked to multiple Al-containing vaccine administrations. Mouse experiments have documented its capture and slow transportation by monocyte-lineage cells from the injected muscle to lymphoid organs and eventually the brain. The present study aimed at evaluating mouse brain function and Al concentration 180 days after injection of various doses of Alhydrogel[®] (200, 400 and 800 µg Al/kg of body weight) in the *tibialis anterior* muscle in adult female CD1 mice. Cognitive and motor performances were

assessed by 8 validated tests, microglial activation by Iba-1 immunohistochemistry, and Al level by graphite furnace atomic absorption spectroscopy.

An unusual neuro-toxicological pattern limited to a low dose of Alhydrogel[®] was observed. Neurobehavioural changes, including decreased activity levels and altered anxiety-like behaviour, were observed compared to controls in animals exposed to 200µg Al/kg but not at 400 and 800µg Al/kg. Consistently, microglial number appeared increased in the ventral forebrain of the 200µg Al/kg group. Cerebral Al levels were selectively increased in animals exposed to the lowest dose, while muscle granulomas had almost completely disappeared at 6 months in these animals.

We conclude that Alhydrogel[®] injected at low dose in mouse muscle may selectively induce long-term Al cerebral accumulation and neurotoxic effects. To explain this unexpected result, an avenue that could be explored in the future relates to the adjuvant size since the injected suspensions corresponding to the lowest dose, but not to the highest doses, exclusively contained small agglomerates in the bacteria-size range known to favour capture and, presumably, transportation by monocyte-lineage cells. In any event, the view that Alhydrogel[®] neurotoxicity obeys “the dose makes the poison” rule of classical chemical toxicity appears overly simplistic.

Introduction

Many severe infectious diseases can be prevented and some of them have been eradicated by vaccines. Commonly used vaccines are generally well tolerated and considered safe by regulatory agencies. However, as other effective medical compounds, vaccines may occasionally cause adverse effects. In particular, a condition manifesting by the combination of myalgia, arthralgia, chronic fatigue, cognitive dysfunction, dysautonomia and autoimmunity has been temporally linked to aluminium adjuvant-containing vaccine administration, called Macrophagic Myofasciitis (MMF) (Gherardi and Authier, 2003, Authier et al., 2003, Exley et al., 2009, Rosenblum et al., 2011, Santiago et al., 2014, Brinthe et al., 2015, Palmieri et al., 2016).

Although no consensus has been reached so far on a cause-to-effect relationship, environmental aluminium has long been suspected to act as a co-factor of several chronic neurological diseases (Van Rensburg et al., 2001, De Sole et al., 2013, Exley, 2013, Exley, 2014) and the idea has emerged that aluminium adjuvants may be insidiously unsafe over the long-term in some predisposed individuals (reviewed in Tomljenovic and Shaw, 2011, Gherardi et al., 2015). Among aluminium salts used in vaccines, crystalline Al hydroxide or

oxyhydroxide (Alhydrogel®) is the more widely used and is found in vaccines against tetanus, hepatitis A, hepatitis B, *Haemophilus influenzae* B, pneumococcal and meningococcal infections, and anthrax (Gherardi et al., 2015). This adjuvant consists of primary particles in the nano-sized range spontaneously forming micron-sized agglomerates (Eidi et al., 2015).

Although aluminium salts have been added to vaccines since 1926 (Glenny et al., 1926), exact mechanisms underlying their immuno-potentiating effects remain incompletely understood (Exley et al., 2010). Previous studies from our laboratory have shown that alum particles, as other poorly degradable particles, may not stay entirely localized in the injected tissue in mice, but can disseminate within phagocytic cells to regional lymph nodes and then to more distant sites and to the brain (Khan et al., 2013, Crépeaux et al., 2015, Eidi et al., 2015). In contrast to a previous belief, alum is characterized by striking biopersistence within immune cells in both the injected muscle, and the draining lymph nodes (dLNs) and spleen, where it may be found in conspicuous quantities 9 months after injection (Crépeaux et al., 2015). In humans, long term biopersistence of aluminium hydroxide within innate immune cells causes a specific lesion at site of previous immunization, called MMF, that may be detected up to >12 years after the last vaccine injection (Gherardi et al., 2001) in patients with a clinical condition now designated as ASIA 'Autoimmune/inflammatory syndrome induced by adjuvants' (Shoenfeld and Agmon-Levin, 2011).

The potential impact of aluminium adjuvant on the nervous system has been studied in mouse models. Alhydrogel® adjuvant, dosed at 100 µg Al/kg and subcutaneously injected in CD1 mice induced motor deficits and cognitive alterations associated with motor neuron death and a significant increase (350%) of reactive astrocytes indicative of an inflammatory process (Petrik et al., 2007). Although no motor neuron death was observed at the dose of 300 µg Al/kg, both microglial and astroglial reactions were observed in the spinal cord and were associated with altered motor and cognitive functions in CD1 mice (Shaw and Petrik, 2009).

In the same way, a neuro-inflammatory/degenerative syndrome has been described in sheep after repeated administrations of alum-containing vaccines (Luján et al., 2013), and impairment of neurocognitive functions and brain gliosis were reported in a murine model of systemic lupus erythematosus-like disease following intramuscular injection of Al hydroxide or vaccine against the hepatitis B virus (Agmon-Levin et al., 2014).

Previous in vivo aluminium adjuvant neurotoxicological studies did not include dose-response analyses. However, several reports studying neurotoxicity of soluble aluminium compounds administered by the oral route (Al chloride, Al nitrate, Al ammonium sulfate) to

rodents showed a non-linear biphasic response on acetyl-cholinesterase activity (Kumar, 1998), dopamine turnover (Tsunoda and Sharma, 1999), nitric oxide synthase expression (Kim, 2003), and behavioural performances (Roig et al., 2006). Poorly understood biphasic Al effects were also observed in vitro: cell cultures showing increased cell growth at low concentrations and diminished cell growth at high concentrations (Exley and Birchall, 1992). Similar unusual observations were made in studies of hippocampal long-term potentiation (Platt et al., 1995), and neuronal cell death in NSC-34 neuron-like cells (Eidi et al., 2015).

The present dose-response study was designed to evaluate long-term aluminium hydroxide neurotoxicity by assessing mouse behaviour, aluminium cerebral concentrations and microglial changes in CD1 mice 180 days after intramuscular injections of Alhydrogel[®]. Strikingly, the lower dose selectively induced neurobehavioural changes, cerebral aluminium level increases and microglial activation.

Access through your organization

Check access to the full text by signing in through your organization.



Access through your organization

Section snippets

Alhydrogel[®] doses

Animals were injected with Alhydrogel[®] adjuvant (InvivoGen), the characteristics of which have been previously determined in terms of size and positive zeta potential (Eidi et al., 2015). Doses were calculated by reference to medical histories of MMF patients who received a median of 4 doses of an Al-containing vaccine within the 10 years prior to their diagnosis (Gherardi et al., 2001). A 60-kg woman (MMF affects mainly women) injected with 1 dose of HBV ENGERIX[®] vaccine (GSK laboratories, ...

Body weight

The initial body weight was 30g. Animals were weighed once a week during the whole procedure. No effects of treatment were observed on body weight (data not shown). ...

Open-field

In the open-field (Table 1), a one-way ANOVA showed a significant difference of the total distance walked ($p=0.012$), the distance in peripheral area ($p=0.002$), and time spent in both central ($p=0.013$) and peripheral ($p=0.003$) areas (Fig. 1a–d). Bonferroni's post hoc analysis showed that mice from the group Alhydrogel[®] 200 μ g Al/kg ...

Discussion

In the present study, 8 widely used behavioural tests performed 180 days after im injections of 200, 400, or 800 μ g Al/kg in form of Alhydrogel[®], in adult female CD1 mice, showed significant effects restricted to animals exposed to the lowest dose. Animals injected with 200 μ g Al/kg showed decreased locomotor activity levels assessed by lower total distance crossed in the open-field, as reported previously after subcutaneous injection of 100 and 300 μ g Al/kg of Alhydrogel[®] (Petrik et al., 2007, ...

Competing interests

The authors declare that there are no conflicts of interest. ...

Acknowledgements

This study was supported by grants from ANSM, CMSRI and University of British Columbia in Vancouver (Luther Allyn Dean Shourds Estate). ...

[Recommended articles](#)

References (73)

N. Agmon-Levin *et al.*

[Immunization with hepatitis B vaccine accelerates SLE-like disease in a murine model](#)

J. Autoimmun. (2014)

F.J. Authier *et al.*

[AlOH₃-adjuvanted vaccine-induced macrophagic myofasciitis in rats is influenced by the genetic background](#)

Neuromuscul. Disord. (2006)

G. Crépeaux *et al.*

[Highly delayed systemic translocation of aluminum-based adjuvant in CD1 mice following intramuscular injections](#)

J. Inorg. Biochem. (2015)

P. De Sole *et al.*

[Possible relationship between Al/ferritin complex and Alzheimer's disease](#)

Clin. Biochem. (2013)

P.A. Dudchenko

[An overview of the tasks used to test working memory in rodents](#)

Neurosci. Biobehav. Rev. (2004)

A. Ennaceur *et al.*

[A new one-trial test for neurobiological studies of memory in rats. 1: behavioural data](#)

Behav. Brain Res. (1988)

A. Ennaceur

[One-trial object recognition in rats and mice: methodological and theoretical issues](#)

Behav. Brain Res. (2010)

E.F. Espejo *et al.*

[Structure of the rat's behaviour in the hot plate test](#)

Behav. Brain Res. (1993)

C. Exley *et al.*

[The cellular toxicity of aluminium](#)

J. Theor. Biol. (1992)

C. Exley *et al.*

[A role for the body burden of aluminium in vaccine-associated macrophagic myofasciitis and chronic fatigue syndrome](#)

Med. Hypotheses (2009)

[View more references](#)

Cited by (82)

[Autism spectrum disorder: Trace elements imbalances and the pathogenesis and severity of autistic symptoms](#)

2021, Neuroscience and Biobehavioral Reviews

[Show abstract](#)

[Myalgia and chronic fatigue syndrome following immunization: macrophagic myofasciitis and animal studies support linkage to aluminum adjuvant persistency and diffusion in the immune system](#)

2019, Autoimmunity Reviews

[Show abstract](#)

[Effects of aluminium and cadmium on hatching and swimming ability in developing zebrafish](#)

2019, Chemosphere

[Show abstract](#)

[Aluminum exposure at human dietary levels promotes vascular dysfunction and increases blood pressure in rats: A concerted action of NAD\(P\)H oxidase and COX-2](#)

2017, Toxicology

Citation Excerpt :

...Therefore, the burgeoning increase in human exposure to Al has been concomitant with an increased development of Al-related adverse effects (Exley 2012; Klein et al., 2014). The accumulation of Al compounds in the human body has been associated with several conditions such as neurological disorders (Crépeaux et al., 2017; Mirza et al., 2016), macrophagic myofasciitis (Gherardi et al., 2016), microcytic anemia (Barata et al., 1996) and osteopenia (Li et al., 2011). Previous studies have payed attention to the relationship between Al exposure and cardiovascular risk (Korchazhkina et al., 1999; Lind et al., 2012; Subrahmanyam et al., 2016)....

[Show abstract](#) 

[Rubella virus infection, the congenital rubella syndrome, and the link to autism](#) ↗

2019, International Journal of Environmental Research and Public Health

[Unraveling the enigma: Elucidating the relationship between the physicochemical properties of aluminium-based adjuvants and their immunological mechanisms of action](#) ↗

2018, Allergy, Asthma and Clinical Immunology



[View all citing articles on Scopus](#) ↗

1 These authors contributed equally to this work.

2 www.imrb.inserm.fr/en/ ↗.

[View full text](#)

© 2016 Elsevier Ireland Ltd. All rights reserved.



All content on this site: Copyright © 2024 Elsevier B.V., its licensors, and contributors. All rights are reserved, including those for text and data mining, AI training, and similar technologies. For all open access content, the Creative Commons licensing terms apply.





RESEARCH ARTICLE

Open Access

Slow CCL2-dependent translocation of biopersistent particles from muscle to brain

Zakir Khan^{1,2}, Christophe Combadière^{3,4,5}, François-Jérôme Authier^{1,2,6}, Valérie Itier^{1,2,11}, François Lux^{7,8}, Christopher Exley⁹, Meriem Mahrouf-Yorgov^{1,2,11}, Xavier Decrouy^{1,2}, Philippe Moretto¹⁰, Olivier Tillement^{7,8}, Romain K Gherardi^{1,2,6,12*†} and Josette Cadusseau^{1,2,11,12*†}

Abstract

Background: Long-term biodistribution of nanomaterials used in medicine is largely unknown. This is the case for alum, the most widely used vaccine adjuvant, which is a nanocrystalline compound spontaneously forming micron/submicron-sized agglomerates. Although generally well tolerated, alum is occasionally detected within monocyte-lineage cells long after immunization in presumably susceptible individuals with systemic/neurologic manifestations or autoimmune (inflammatory) syndrome induced by adjuvants (ASIA).

Methods: On the grounds of preliminary investigations in 252 patients with alum-associated ASIA showing both a selective increase of circulating CCL2, the major monocyte chemoattractant, and a variation in the *CCL2* gene, we designed mouse experiments to assess biodistribution of vaccine-derived aluminum and of alum-particle fluorescent surrogates injected in muscle. Aluminum was detected in tissues by Morin stain and particle induced X-ray emission (PIXE). Both 500 nm fluorescent latex beads and vaccine alum agglomerates-sized nanohybrids (Al-Rho) were used.

Results: Intramuscular injection of alum-containing vaccine was associated with the appearance of aluminum deposits in distant organs, such as spleen and brain where they were still detected one year after injection. Both fluorescent materials injected into muscle translocated to draining lymph nodes (DLNs) and thereafter were detected associated with phagocytes in blood and spleen. Particles linearly accumulated in the brain up to the six-month endpoint; they were first found in perivascular CD11b⁺ cells and then in microglia and other neural cells. DLN ablation dramatically reduced the biodistribution. Cerebral translocation was not observed after direct intravenous injection, but significantly increased in mice with chronically altered blood-brain-barrier. Loss/gain-of-function experiments consistently implicated CCL2 in systemic diffusion of Al-Rho particles captured by monocyte-lineage cells and in their subsequent neurodelivery. Stereotactic particle injection pointed out brain retention as a factor of progressive particle accumulation.

Conclusion: Nanomaterials can be transported by monocyte-lineage cells to DLNs, blood and spleen, and, similarly to HIV, may use CCL2-dependent mechanisms to penetrate the brain. This occurs at a very low rate in normal conditions explaining good overall tolerance of alum despite its strong neurotoxic potential. However, continuously escalating doses of this poorly biodegradable adjuvant in the population may become insidiously unsafe, especially in the case of overimmunization or immature/alterd blood brain barrier or high constitutive CCL-2 production.

Keywords: Alum, Vaccine adverse effect, Vaccine adjuvant, Nanomaterial biodistribution, Nanomaterial neurodelivery, Macrophages, Macrophagic myofasciitis, CCL-2, Single nucleotide polymorphisms (SNPs)

* Correspondence: romain.gherardi@hmn.aphp.fr; josette.cadusseau@inserm.fr

†Equal contributors

¹Inserm, U955, 8 rue du Général Sarrail, Créteil 94010, France

²Université Paris Est, Faculté de Médecine, 8 rue du Général Sarrail, Créteil 94010, France

Full list of author information is available at the end of the article

Background

Nanomaterials have various innovative medical applications including drug and gene delivery, imaging contrast fluids, topical antimicrobials, surgery tools and vaccines [1]. Due to the growing number of novel compounds and formulations, data on their specific biodistribution, persistence and toxicity are generally lacking [1], and clarification regarding how the body handles small particles, especially those which interact with immune cells [2], is urgently needed. Once defined, these basic mechanisms which govern host-particle interactions should be integrated with specific properties of nanomaterials (size, shape, surface, and solubility) to enable predictions of their beneficial or adverse effects.

The use of nanomaterials in humans is not as contemporary as is recently portrayed. For decades, alum, a nanocrystalline compound formed of aluminum oxyhydroxide, has been the most commonly used adjuvant in vaccines. The mechanism by which it stimulates the immune response is incompletely understood [3]. While alum is generally well tolerated, it is occasionally reported as the cause of disabling health problems in individuals with ill-defined susceptibility factors [4-6]. Clinical manifestations attributed to alum are paradigmatic of the so-called auto-immune/inflammatory syndrome induced by adjuvants (ASIA), a syndrome also observed in patients exposed to silicone gel [7]. They include delayed onset of diffuse myalgia [4], chronic fatigue [8] and stereotyped cognitive dysfunction [9]. The persistence of alum-loaded macrophages is typically detected at sites of previous injections (up to >12 years later), resulting in a specific granuloma called macrophagic myofasciitis or MMF [4]. Although the biopersistence of adjuvants is *a priori* undesirable, the exact significance of this remains the subject of some debate since the biodistribution of slowly biodegradable particles following injection into muscle is currently unknown.

There appears to be a fine balance between the efficacy of alum adjuvant and its potential toxicity, and there is good evidence that these may be one and the same effect [3]. Both the efficacy and the potential toxicity of alum will be influenced by whether the bioactive nanomaterial remains localized at injection points or rather scatters and accumulates in distant organs and tissues. A reference study based on isotopic ^{26}Al showed poor (6%) ^{26}Al clearance in the urine at the day 28 (d28) endpoint after i.m. injection of isotopic alum to rabbits, and detected ^{26}Al , in an unknown form, in lymph nodes, spleen, liver, and brain [10]. Aluminum oxyhydroxide is composed of micron/submicron-sized aggregates of nano-sized (about 13 nm) particles and these aggregates were initially believed to remain extracellular until their complete solubilization in interstitial fluids [10]. We now know that quite the reverse is the case and that antigen presenting cells (APCs) avidly take up alum particles [11], and, in so doing, become

long-lived cells [12] and impede alum solubilization [4,13,14]. Inflammatory monocytes (MOs) are attracted into muscle by danger signals through a monocyte chemoattractant protein-1 (MCP-1)/chemokine (C-C motif) ligand 2 (CCL2) driven-mechanism, becoming macrophages (MPs) and MO-derived dendritic cells (DCs), before migrating to the draining lymph nodes (DLNs) [15]. One function of migratory DCs is to transfer antigenic material to a large network of distant resident APCs [16]. Moreover, injections of alum alone induce significant changes linked to activation of the innate immune system in distant organs [17,18]. Therefore, we examined whether nanomaterials injected into muscle could translocate to distant organs as part of a general mechanism linked to phagocytosis and CCL2/MCP-1 signaling.

Methods

Mice models

All animal experiments were conducted in accordance with the European guidelines for animal care. To facilitate mechanistic investigation of particle biodistribution, mice of the B57/B6 genetic background, that are used to generate genetically-manipulated models, were preferred to more toxic-sensitive mouse strains. Male eight- to ten-week-old C57BL/6, *mdx* (with leaky blood brain barrier (BBB)), *CX3CR1^{GFP/+}* (with GFP reporter gene insertion allowing visualization of microglia), and *CCL2^{-/-}* mice were used (Jackson, West Grove, PA, USA). Mice were protected from Al-containing materials, fed with manufactured animal food and water *ad libitum*, and exposed to 12:12 light/dark cycles. Experiments using fluorescent particles were extremely labor intensive and expensive to perform. All of them were done in triplicate. Homogeneity of results made it unnecessary to use more than three mice per point.

Alum administration

The dose of alum-containing vaccine administered to mice was calibrated to mimic the mean number of doses received by MMF patients. One dose of commercially available anti-hepatitis B vaccine contains 0.5 mg Al according to the product data sheet. Based on an average of human body weight of 60 kg (most patients being women), the amount received for each immunization is 8.33 $\mu\text{g}/\text{kg}$. The allometric conversion from human to mouse (FDA Guidance 5541) gives a final amount of approximately 100 $\mu\text{g}/\text{kg}$. A dose of 36 μL vaccine, which corresponds to 18 μg Al, was injected to mimic the cumulative effect induced by 5.2 human doses to 35 g mice (the mean weight at the d180 midtime of brain analysis). This dose represents an equivalent 6.8 human doses in the youngest animal (27 g body weight, 11 weeks of age at sacrifice) and 4.3 in the oldest one (42 g at 62 weeks).

Furnace atomic absorption spectrometry

Al concentrations were determined in whole tibialis anterior (TA) muscles and brains dried at 37°C and digested with concentrated HNO₃ (14 mol/L). Digests were allowed to cool before dilution to 10% HNO₃ with ultra-pure water. The total aluminum in each digest was measured by transversely heated graphite atomizer graphite furnace atomic absorption spectrometry (TH GFAAS) and results were expressed as Al mg/g tissue dry weight.

PIXE

As in normal conditions Al may be detected with marked interindividual variations in tissues, *de novo* incorporation of aluminum in too low doses does not cause easily detectable changes when global conventional approaches are used [10]. Here we used particle induced X-ray emission (PIXE), a procedure analyzing radiation emitted from the interaction of a proton beam with the matter [19], to detect areas enclosing small Al spots. Sections (20 μm-thick) carefully protected from environmental Al were mounted on fresh formvar films, kept in the cryostat for 6 hours and stored under Al-free silica gel. Mineral and metal ions were detected using the nuclear microprobe of the Centre d'Etudes Nucléaires de Bordeaux-Gradignan. A 1 MeV proton beam focused down to a 2 μm spot was randomly scanned over multiple 500 × 500 μm fields of tissue sections. In the case of an Al signal, a re-test of 100 × 100 μm areas of interest was performed. PIXE and Rutherford backscattering spectrometry analyses were employed simultaneously and quantitative results were computed, as previously described [19]. Al spots were considered eligible on three criteria: a size of more than 3 pixels (that is, above the background noise), a depot not colocalized with Si, and a depot surrounded by a rounded halo of decreased intensity (both characteristics limiting confusion with contamination by external dust overcoming the protection procedures).

Synthesis of Al-Rho particles

Gadolinium oxide nanohybrids with Al(OH)₃ coating were obtained in three steps: (i) gadolinium oxide nanoparticles were first synthesized; (ii) polysiloxane shell growth was then induced by hydrolysis-condensation of convenient silane precursors in the presence of the nanoparticles; and (iii) the nanohybrids were coated by the addition of aluminum nitrate and soda in stoichiometric conditions.

Chemicals

Gadolinium chloride hexahydrate ((GdCl₃, 6H₂O) 99.99%), sodium hydroxide (NaOH, 99.99%), tetraethyl orthosilicate (Si(OC₂H₅)₄, TEOS, 98%), (3-aminopropyl) triethoxysilane (H₂N(CH₂)₃-Si(OC₂H₅)₃, APTES, 99%), triethylamine (TEA, 99.5%), rhodamine B isothiocyanate (RBITC),

aluminum nitrate nonahydrate (Al(NO₃)₃·9H₂O, ACS reagent ≥ 98%) and dimethyl sulfoxide (DMSO, 99.5%) were purchased from Sigma-Aldrich (St Louis, MO, USA). Diethylene glycol (DEG, 99%) was purchased from SDS Carlo Erba, Val de Reuil (France).

Preparation of gadolinium oxide core

A first solution was prepared by dissolving GdCl₃·6H₂O (0.56 g) in 50 mL DEG at room temperature. A second solution was prepared by adding a NaOH solution (0.49 mL, 10 M) in 50 mL DEG. The second solution was progressively added to the first one, at room temperature, for 15 hours. A transparent colloid of gadolinium oxide nanoparticles in DEG was obtained.

Encapsulation of Gd₂O₃ cores by polysiloxane shell

A total of 105 μL of APTES and 67 μL of TEOS was added to 100 mL of the gadolinium oxide nanoparticle solution under stirring at 40°C. A total of 5 μL of APTES was previously coupled to 1 mg RBITC in DMSO (1 mL) used as solvent and then added to the colloidal solution. After 1 hour, 1,913 μL of a DEG solution (0.1 M of TEA, 10 M of water) was added. The whole coating procedure was repeated three more times (with no more addition of RBITC), every 24 hours. The final mixture was stirred for 48 hours at 40°C. The obtained solution could be stored at room temperature for weeks without alteration.

Coating of fluorescent nanohybrids with a Al(OH)₃ shell

A total of 2.5 mL of the colloidal solution was diluted by 2 to obtain a 5 mL solution in DEG. A total of 75 mg of aluminum nitrate nonahydrate was dissolved in 10 mL of water before addition to the colloidal solution. The resulting mixture was stirred for 5 minutes and 4 mL of a soda solution (0.2 M) was added before stirring for 1 hour.

Purification

Purification of Al-Rho was performed by tangential filtration through Vivaspin filtration membranes (MWCO = 10 kDa) purchased from Sartorius Stedim Biotech (Aubagne, France). The colloidal solution was introduced into 20 mL Vivaspin tubes and centrifuged at 4,100 rpm. This step was repeated several times, by filling the tubes with water and centrifuging again, until the desired purification rate was reached (≥100). The purified colloidal solution was freeze dried for storage in five pillboxes, using a Christ Alpha 1–2 lyophilisator. The compound contained 4 μg Al per μL of Al-Rho suspension. Control transmission electron microscopy showed non-fibrous particles about 10 nm in size, typical of aluminum hydroxyde (traditional precipitated alum). Similarly to vaccine alum, they formed agglomerates of submicronic/micronic size. The immunological properties of such traditional alum-protein precipitates are quite similar to those of the reference adjuvant

approved by the FDA (Al oxyhydroxyde: Alhydrogel[®], Invivogen, Toulouse France) and differ from other formulations not licensed for human use (18).

Peripheral injections of fluorescent nanomaterials

Two types of fluorescent nanomaterials were used: exploratory polychromatic fluorescent latex beads (FLBs) (500 nm fluorospheres, Polysciences, Warrington, PA, USA) and confirmatory Al-Rho nanohybrids constructed with a rhodamine containing core and an Al(OH)₃ shell. FLBs were used first because they offer several characteristics that facilitate their detection in tissues, including strong fluorescence, spheric appearance and homogeneous size. This allowed us to get a clear picture of what was happening in terms of biodistribution of these avidly phagocytosed particles. Al Rho particles were less fluorescent and more heterogeneous in shape and size than FLBs but better represented alum adjuvant surrogates. Almost all biodistribution experiments performed with FLBs in wild type mice were also done with Al-Rho. In contrast, FLBs and Al Rho were differentially used in mutated/genetically-modified mice: FLBs were preferred to study particle biodistribution in *mdx* mice with BBB alterations and when the GFP marker was used (that is, *CX3CR1*^{GFP/+} mice with fluorescent microglia, GFP + BMT studies); Al-Rho particles were preferred in gain/loss of CCL2/MCP-1 function studies designed on the basis of preliminary results on the CCL2 status of alum-intolerant humans.

FLB suspension diluted at 1:1 in PBS contained 1.8×10^{11} particles per mL. A total volume of 40 μ L (20 μ L in each TA muscle) was injected, corresponding to a total amount of 7.2×10^9 particles. The same volume of Al-Rho suspension was injected in TA muscles. PBS-injected mice were used as controls. Tissues, including popliteal and inguinal DLNs, spleen, brain and blood, were collected at various time points post injection. Three mice were included per group at each time point for both injected materials and their controls. Other administration routes were compared to the standard i.m. injection, including s.c. injection of 20 μ L FLBs in each hindlimb, and i.v. injection of 40 μ L FLBs in the tail vein.

Stereotactic cerebral injections

Mice were anaesthetized with ketamine and xylazine. Al-Rho suspension (0.5 μ L) was stereotactically injected in the striatum using a 1 μ L Hamilton syringe. Biodistribution of i.c. injected Al-Rho to cervical DLNs, assessed by serial sectioning of the whole cervical region, and spleen, was compared to biodistribution to the popliteal DLN and spleen of the same amount of Al-Rho injected in the TA muscle.

Pharmacological and physical migration blockade

The prostaglandin analog BW245C, an agonist of the PGD2 receptor, was used to inhibit APC migration as previously reported [20]. Since BW245C is active for two days after injection, BW245C (100 nM, Cat.no.12050, Cayman Chemical, Ann Arbor, MI, USA) was injected twice in the TA muscle: it was first co-injected with FLBs at d0 and a second time alone at d2, and DLNs were removed for examination at d4. Untreated FLB-injected mice were used as controls. In another set of experiments DLNs were surgically ablated and mice immediately injected with FLBs in the TA muscle.

Loss and gain of CCL2 function experiments

Exploratory analyses performed in MMF patients with ASIA [see Additional file 1: supplementary information section] yielded a CCL2 signal in the form of: (1) a selective increase of CCL2 in the serum of MMF patients compared to healthy controls; and (2) a given haplotype in the *CCL2* gene tending to be more frequent in MMF patients than in the general population. These results led us to use mouse models to explore the role of CCL2 in the biodisposition of particulate materials. Loss of CCL2 function studies were done using *CCL2*^{-/-} mice injected i.m. with 40 μ L Al-Rho. Gain of CCL2 function experiments consisted first of i.m. co-injection of 10 μ L murine rCCL2 (100 μ g/ml; R&D, Minneapolis, MN, USA) with 40 μ L Al-Rho. DLNs were removed at d4, spleen, brain and blood at d21. In other experiments murine rCCL2 was infused into the brain through a catheter stereotactically inserted into the striatum at d7 post-Al-Rho, fed by a subcutaneously implanted osmotic micropump fixed into the neck (0.25 μ L/hour Alzet brain infusion kit, Charles River, L'Arbresle, France). rCCL2 was infused for 14 days (diffusion rate 180 pg/day), with or without rCCL2 i.m. injection concurrent with Al-Rho injection. At d21 post Al-Rho injection, animals were sacrificed, and blood and tissues were collected. For controls, osmotic pumps filled with PBS were used.

Tissue preparation and particle counting

Mice under terminal anesthesia were transcardially perfused with PBS followed by ice-cold 4% paraformaldehyde (PFA) in 0.1 M phosphate buffer. Tissues and organs were removed, post-fixed in PFA for 4 hours at 4°C, immersed overnight at 4°C in a 30% sucrose solution, and quickly frozen. Whole brains were serially cut into coronal cryosections of 40 μ m, spleen and muscle into 20 μ m, and DLNs into 10 μ m, and stored at -20°C until particle counting or treatment. Brain sections were successively deposited on 10 different Superfrost[®] slides in order to obtain 10 identical series, thus allowing determination of total particle content by multiplying by

10 the number of particles found in one series. A similar approach was used for DLNs and spleen. Blood was collected by heart puncture and 100 μ L were smeared for particle counting.

Immunohistochemistry and Morin staining

Immunostaining was done using commercial primary antibodies routinely used in the lab, raised against CD11b (1/200, AbD Serotec, Oxford, UK), F4/80 (1/50, AbCam, Cambridge, UK), GFAP (1/200, DakoCytomation, Trappes, France), vimentin (1/500 DakoCytomation), collagen IV (1/100 Millipore, Temecula, CA, USA), NG2 (1/200, Millipore, Molsheim, France), MAP2 (1/100, Sigma-Aldrich, Lyon, France), and IL1 β (1/100, AbCam, Paris, France) or nonspecific mouse IgG (Jackson

ImmunoResearch, Suffolk, UK). Then, biotinylated anti-rat and anti-rabbit antibodies (1/200, Vector Laboratories, Paris, France) were used accordingly and were revealed using Alexa fluor 488-conjugated streptavidin (1/200 Invitrogen, Cergy-Pontoise, France). Neuron labeling was done using NeuroTrace[®] blue fluorescent Nissl Stain according to the manufacturer's instructions (Invitrogen). Al was stained with Morin (M4008-2 G, Sigma-Aldrich) used as 0.2 g dissolved in a solution consisting of 0.5% acetic acid in 85% ethanol [21]. Formation of a fluorescent complex with Al was detected under a 420 nm excitation wavelength as an intense green fluorescence with a characteristic 520 nm emission. Notably, nanohybrids (Gd₂O₃) core encapsulated by polysiloxane shell were not positively stained by

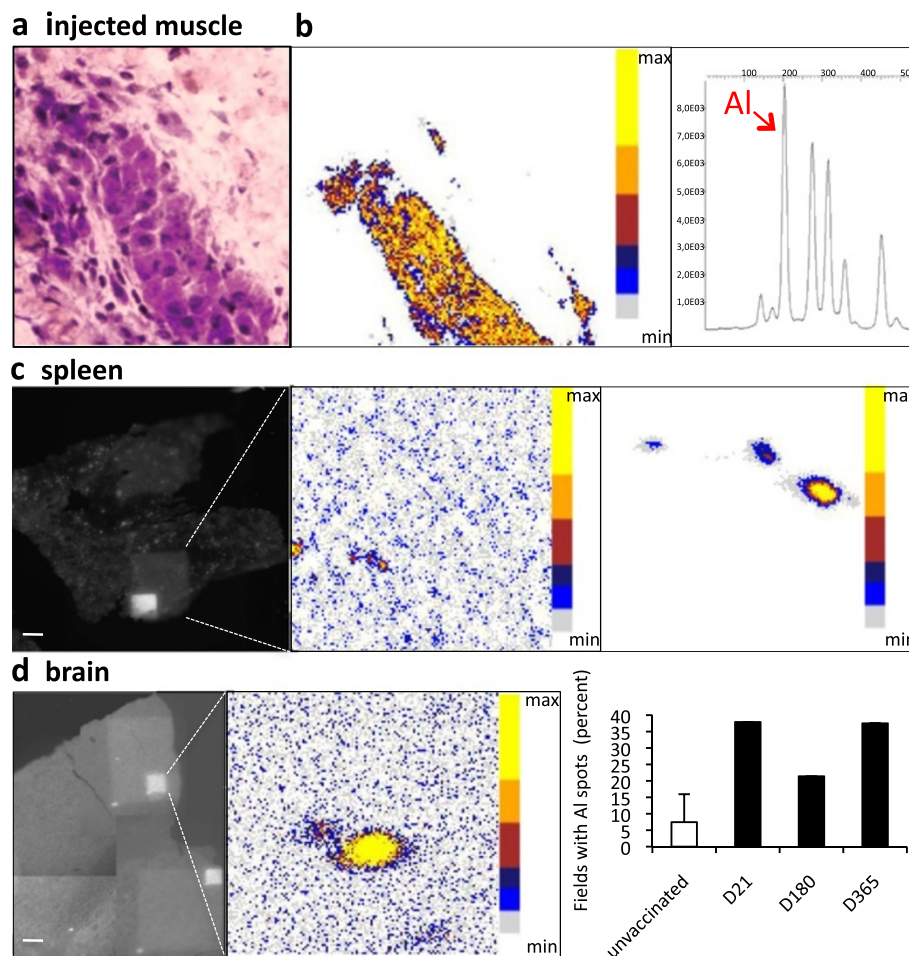


Figure 1 Aluminum deposits in tissues following injection of alum-containing vaccine in the TA muscle. a) Granuloma composed of PAST⁺ cells is formed in the injected muscle envelope; **b)** PIXE mapping shows muscle Al deposits in pseudocolors, with confirmatory Al emission spectrum (d21); **c)** Section of spleen tissue (left panel) displays the large 500 \times 500 μ m and restricted 100 \times 100 μ m protonized fields corresponding to the PIXE maps (middle and right panel, respectively) enclosing eligible Al spots (d21); **d)** Section of brain tissue (left left panel) displays the restricted 100 \times 100 μ m protonized field corresponding to the PIXE map (middle panel) enclosing eligible Al spot (d21); the number of fields containing one or more Al spots was increased at all tested time points compared to unvaccinated (right panel) mice. (bars: 100 μ m). d, day; PIXE, particle induced X-ray emission, TA tibialis anterior.

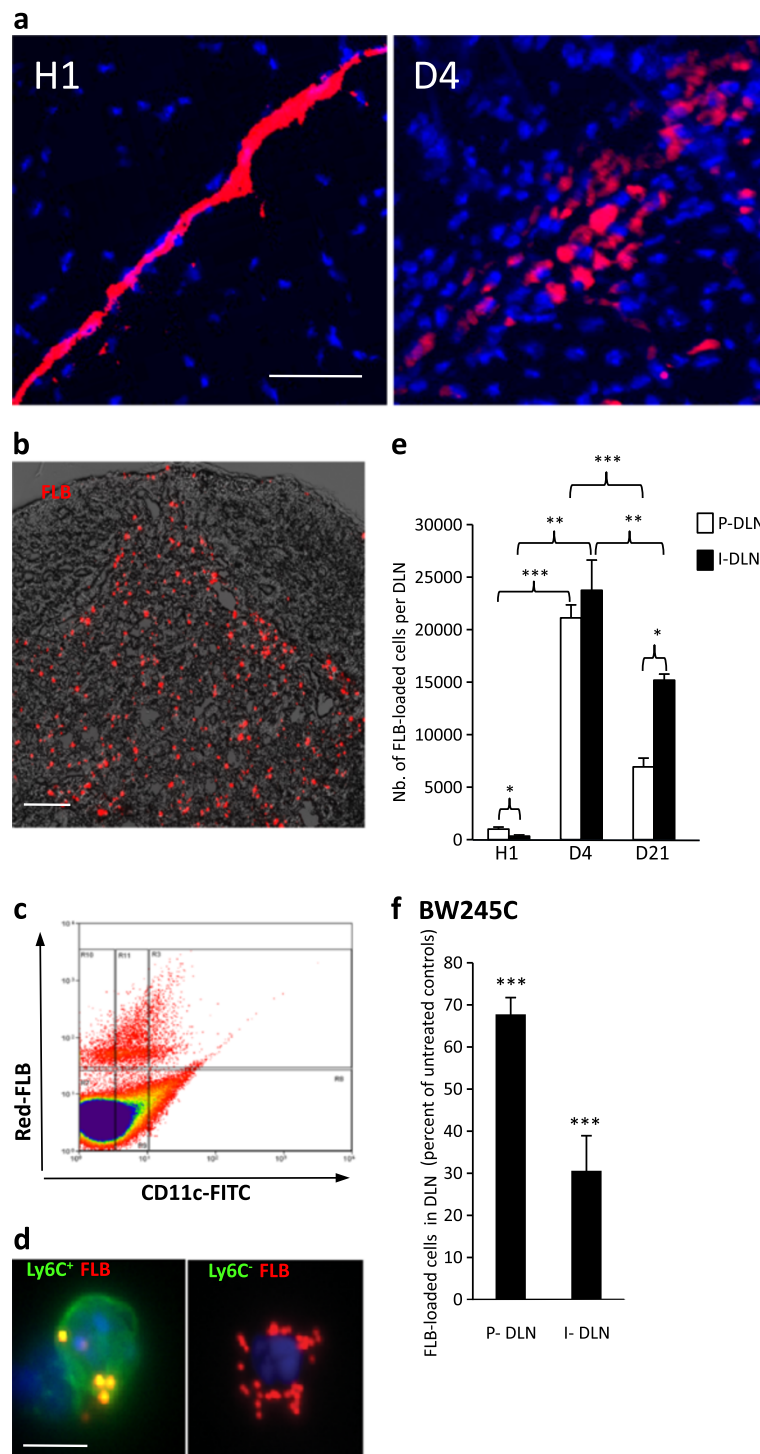
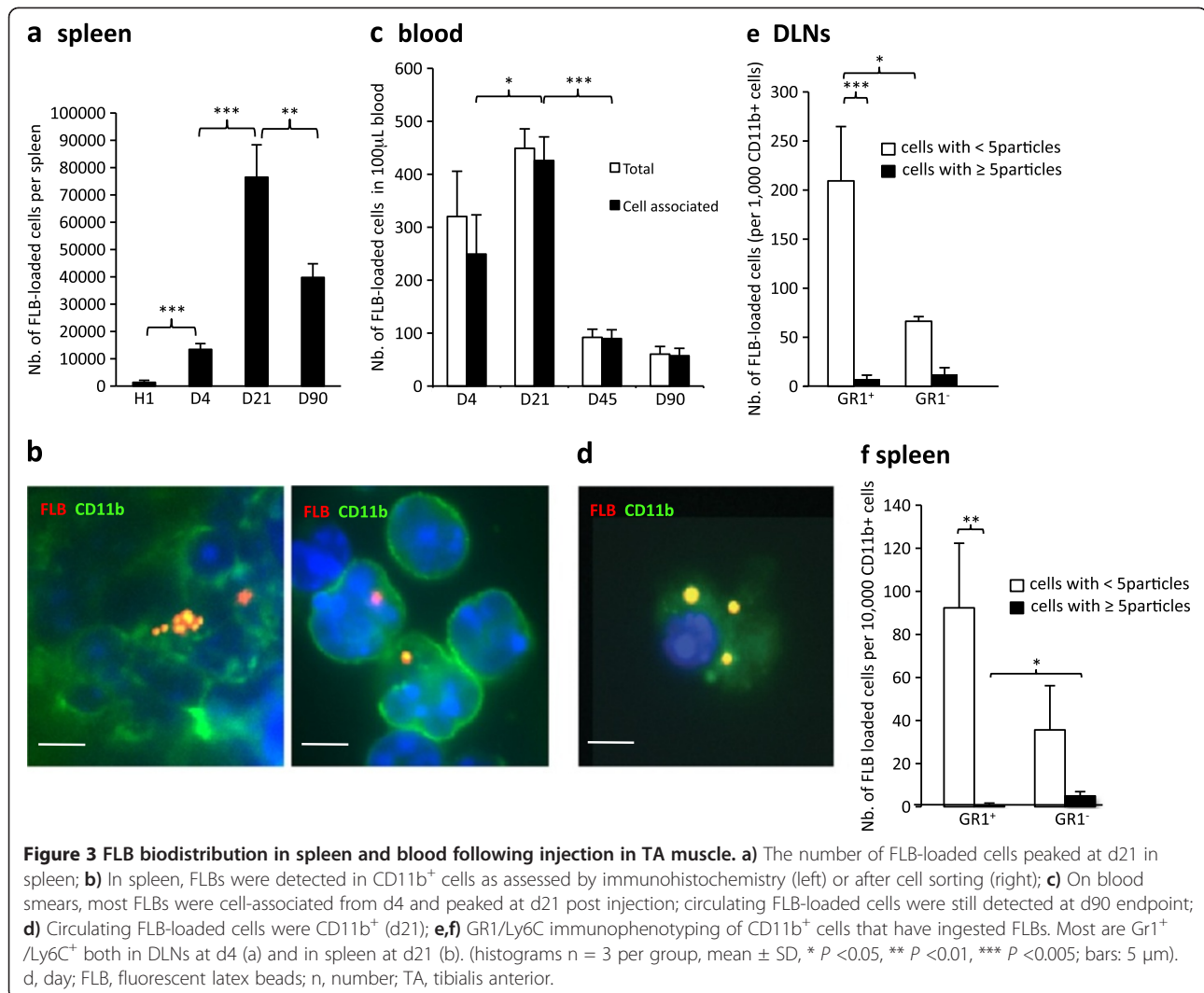


Figure 2 FLB translocation in DLN following injection in TA muscle. **a**) Marked translocation of FLBs in parafollicular areas of popliteal DLNs (d4); **b**) Flow cytometry showing that most FLB-loaded cells extracted from DLN express CD11c at either an intermediate or strong level (d4); **c**) Immunocytochemistry on CD11b⁺ cells extracted from DLNs were usually Gr1⁺/Ly6C⁺, especially when they had ingested a few particles (left), whereas heavily loaded ones were often Gr1⁻/Ly6C⁺ (right); **d**) The number of FLB-loaded cells peaked at d4 post-injection in both popliteal and inguinal DLNs; **e**) The migration inhibitor BW245C co-injected with FLBs in muscle markedly decreased the number of FLB-loaded cells detected in DLNs at d4 post-injection. The effect was more pronounced in the downstream inguinal DLN; **f**) The migration inhibitor BW245C co-injected with FLBs in muscle markedly decreased the number of FLB-loaded cells detected in DLNs at d4 post-injection. The effect was more pronounced in the downstream inguinal DLN; (histograms: n = 3 per group, mean + SD, * $P < 0.05$, ** $P < 0.01$, *** $P < 0.005$; bars: 100 μ m [a]; 5 μ m [c]). d, day; DLNs, draining lymph nodes; FLBs, fluorescent latex beads; TA, tibialis anterior.



Morin. In contrast, when coated with Al(OH)₃, these particles were strongly positive for Morin. Fluorescence microscopy and spectral analyses were done using Carl Zeiss light and confocal microscopes.

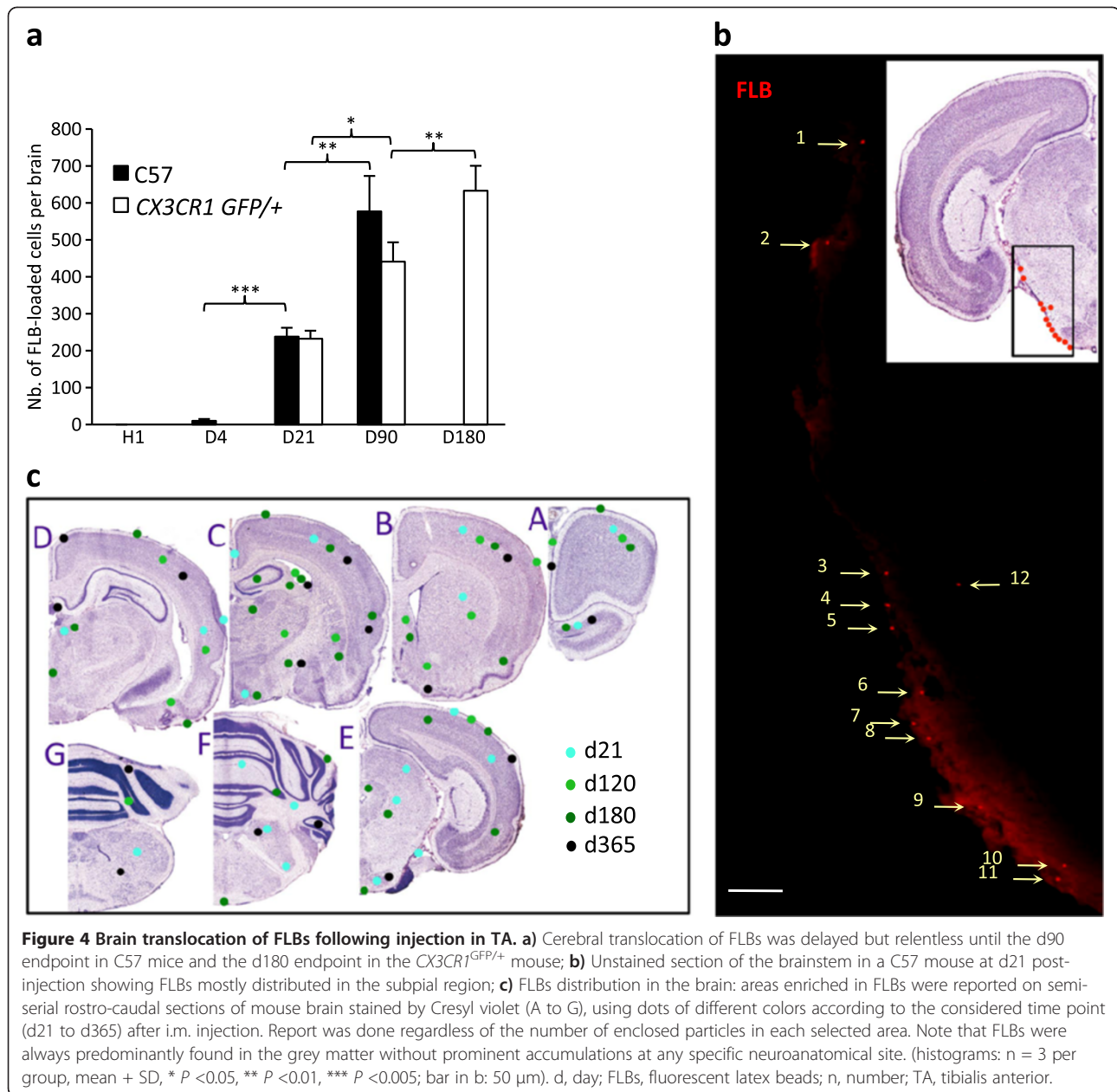
Cell isolation from blood and tissues and flow cytometry

For blood cell immunophenotyping, 100 µL blood was treated with ethylenediaminetetraacetic acid (EDTA) and stained with fluorescein isothiocyanate (FITC)-conjugated antibodies. Erythrocytes were lysed using hypotonic lysis solution, and then cells were washed with (D)MEM and sorted using a MoFlo cell sorter (Beckman Coulter, Villepinte, France). Cells were extracted from tissues of exsanguinated mice perfused with PBS. Tissues were removed and freshly dissociated in (D)MEM. DLNs and spleen were dissociated in (D)MEM containing 0.2% collagenase-B (Roche Diagnostics, Meylan, France) and 0.2% trypsin-EDTA at 37°C for 45 minutes twice.

Brain tissue was dissociated in 1% Trypsin-HBSS (Thermo Scientific HyClone, South Logan, UK) containing 100 U/mL DNase (Roche Diagnostics). Cell suspensions were filtered and counted. CD45⁺ or CD11b⁺ cells were isolated using magnetic cell sorting (MACS, Miltenyi Biotec, Paris, France) and stained with one of the following antibodies and their isotypes: FITC-conjugated anti-CD11b, FITC-conjugated anti-Ly-6C (GR1), FITC-conjugated anti-CD11c (BD-Pharmingen Bioscience, San Diego, CA, USA). Cells were sorted using a cell sorter. Populations presenting >90% purity were used. Sorted cells were cytopinned and stained with Hoechst-33342 for nucleus. Particle loaded cells were counted under a fluorescence microscope.

Bone marrow transplantation experiments

GFP⁺ bone marrow (BM) cells were obtained by flushing the femurs of adult CAG-GFP mice and were injected



retroorbitally (1×10^7 cells per mouse) to four-week-old C57BL/6 mice, as previously described [15]. Recipient mice were irradiated at 9.0 Gy on d1 before transplantation, and were treated with 10 mg/kg/day ciprofloxacin for 10 days. Blood chimerism of >90% was controlled at three to four weeks post-transplantation.

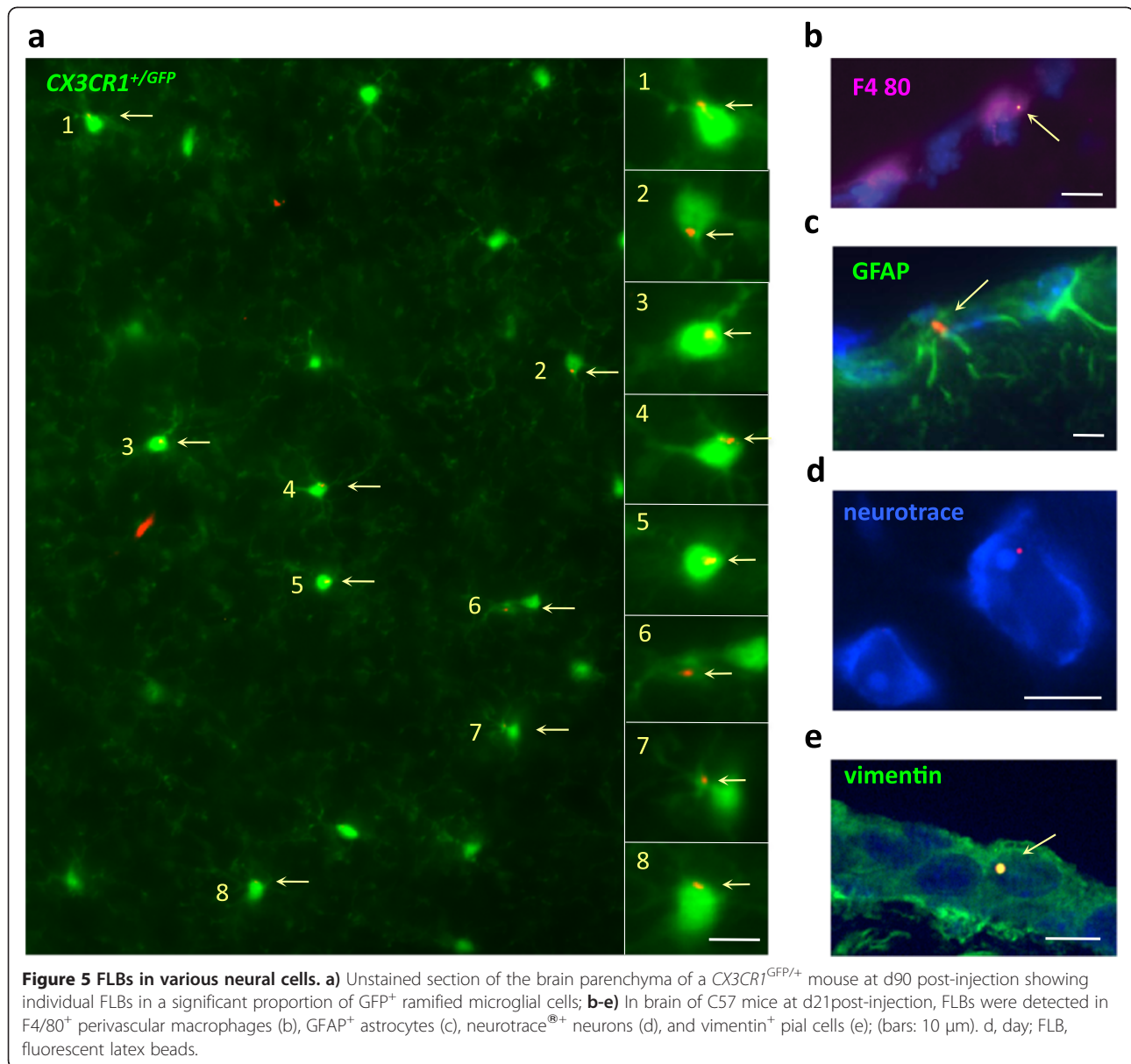
Statistical analyses

All experimental values are presented as means and standard deviation except when indicated. Statistical analyses used unpaired Student's *t*-test (genotypes); *P* < 0.05 was considered significant.

Results

Intramuscular alum-containing vaccine injection in mouse induces Al deposition in distant tissues

Alum-containing vaccine (36 μL corresponding to 18 μg Al) was first injected in the TA muscles of C57Bl6 mice. It induced an acute inflammatory reaction which stabilized after d4 in the form of collections of typical alum-loaded MPs with large hematoxylin⁺ and Periodic Acid Schiff⁺ cytoplasm in muscle envelopes (Figure 1a). In parallel, the local Al tissue concentration determined by atomic absorption spectrometry decreased by 50% from injection to d4 and then remained stable until d21



(2,342, 1,122, and 1,180 μg/g of dry muscle tissue, respectively). Al was additionally located in muscle and distant tissues by PIXE [19]. Random scanning of 20 μm thick sections, sampled and processed with careful protection against environmental Al, disclosed significant Al signals in muscle, spleen and brain (Figure 1b-c). In brain, Al spots accounted for 38, 21, and 37% of 500 × 500 μm tested fields at d21, and months 6 and 12 (mo6 and mo12) post-injection, respectively (mean = 31.5%; n = 73 fields, Figure 1d). The dip at month 6, was either due to inter-individual variations in aluminum handling or to sampling problems related to variable proportions of grey and white matter in the randomly scanned areas (see below). The spot size ranged from about 1 to 14 μm. By comparison, five unvaccinated mice showed only seven positive out of

94 tested fields (mean = 7.4%). These results confirmed that Al derived from alum can be translocated to, penetrate and persist in brain tissue [21-23]. Al depots detected in spleen and brain could have resulted from either physical translocation of alum particles, or *in situ* aggregation of soluble Al, or both.

Fluorospheres injected into mouse muscle undergo lymphatic and systemic biodistribution

To examine if particles translocate to distant sites, we next injected polychromatic FLBs. A size of 500 nm was chosen as an approximation of the average size of alum agglomerates observed *in vivo*, allowing FLB visualization as individual spheres by confocal and fluorescence microscopes (resolution >200 nm). After i.m. injection of 20 μL

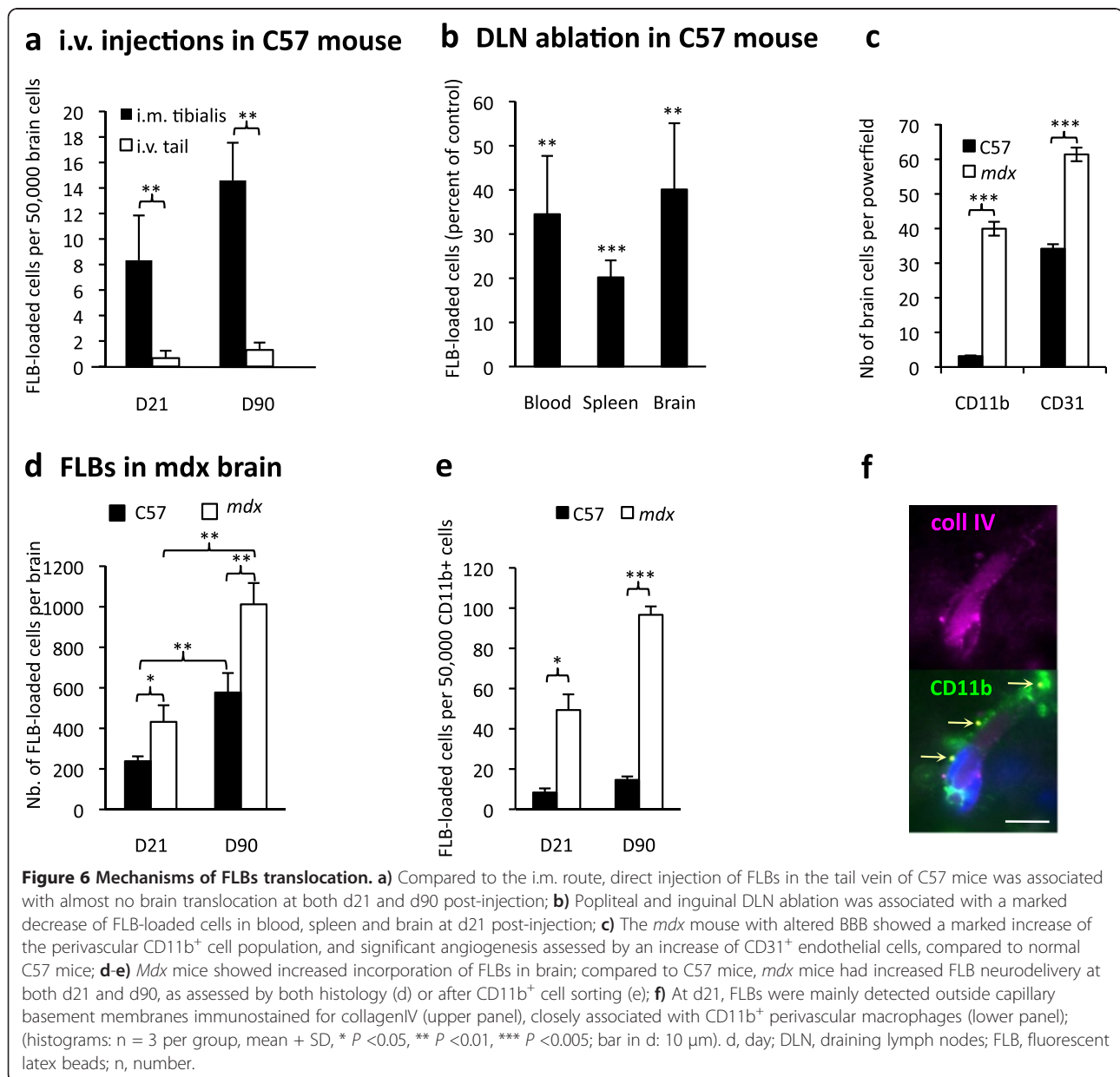
Table 1 Distribution of particles (percent of total) according to post-injection time

Time post-injection	D21	D90	D180	D365
Localization				
Choroid plexus	0%	5%	5%	3%
Leptomeninges	9%	5%	0%	3%
Parenchyma	91%	90%	95%	94%

suspensions, FLBs transiently peaked in free form in blood (1,200 + 400 FLBs per 100 μ L) at hour 1. As early as 1 hour post-injection, some FLBs had also reached DLNs. I. m. injection of GFP⁺CD45⁺ cells, either pre-loaded with FLBs or coinjected with FLBs, showed no GFP⁺ cells

translocation to DLNs at hour 1 (data not shown), indicating early cell-independent particle translocation to DLNs by lymphatic drainage of the muscle interstitial fluid [24]. In DLNs, however, most FLBs were cell-associated suggesting rapid capture by DLN resident cells. Within 24 hours, FLBs were phagocytosed by muscle CD11b⁺ MO/MPs. Phagocytes progressively cleared the particles away from the interstitium to form collections (Figure 2a), mainly located in muscle envelopes at d4.

At d4, FLBs had dramatically increased in DLNs, forming intracellular agglomerates in the interfollicular area (Figure 2b-e). Particle-loaded cells extracted from DLNs at d4 were CD45⁺, CD11b⁺, and more often GR1⁺/Ly6C⁺ (69% to 81%), and CD11c⁺, with either



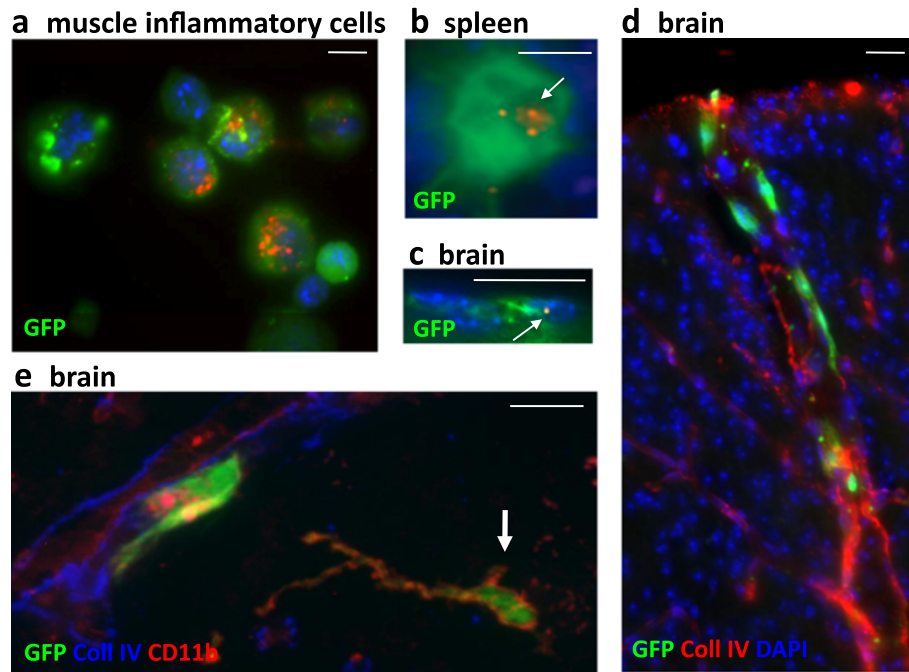


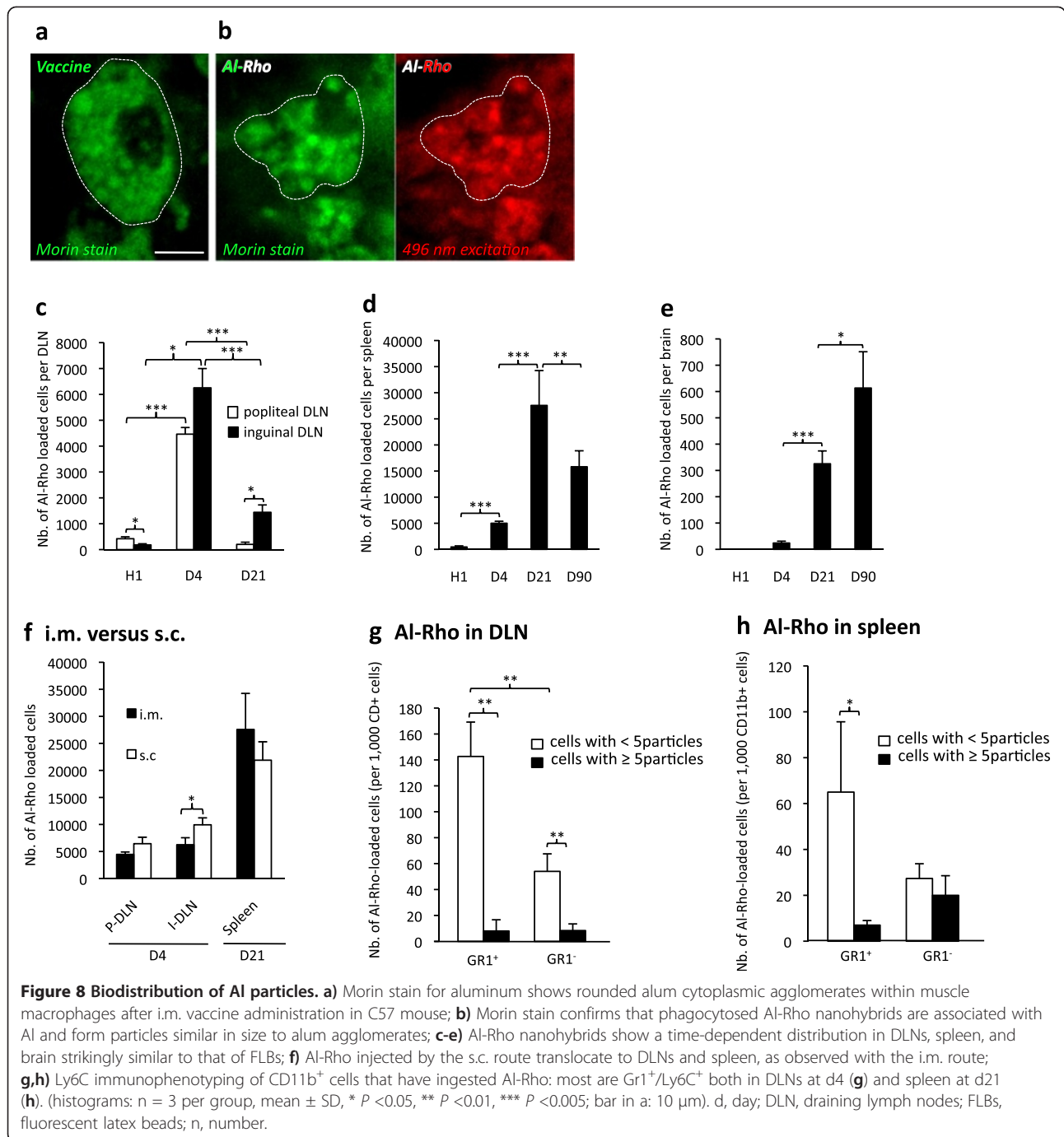
Figure 7 GFP⁺ BM chimeric mice. **a-c**) Chimeric mice injected intramuscularly with FLBs showed GFP⁺ BM-derived cells enclosing FLBs among inflammatory cells extracted from the injected muscle (a) at d4 after FLB injection, in spleen (b) and brain (c) at d33 after FLB injection. **d-e**) Chimeric mice showed incorporation of GFP⁺ cells in the brain, mainly in the form of perivascular cells in the cortex (d) and, occasionally, in more deeply located ramified CD11b⁺ cells (e, arrow) at d180 post-BM transplantation. (bars: 10 μ m). BM, bone marrow; d, day; FLB, fluorescent latex beads.

intermediate (46%) or high (22%) intensity (Figure 2a,c,d), thus corresponding to MO-derived inflammatory DCs and MPs [25]. Co-injection of FLBs with the synthetic prostaglandin analog BW245C, a compound known to inhibit DC migration [20], inhibited FLB translocation to DLNs at d4 by 32% in the popliteal and 69% in the inguinal DLNs, respectively (Figure 2f). This indicated prominent particle transport within phagocytic cells, at least downstream to popliteal DLN. At later time points, both the number of particle-loaded cells and the individual cell load markedly decreased in DLNs (Figure 2e). While decreasing in DLNs, FLBs dramatically increased in spleen from d4 to d21 (Figure 3a,b). As spleen is unplugged to lymphatic vessels, the particle transfer from DLNs to spleen implicated exit from the lymphatic system through the thoracic duct and circulation in the blood stream. Consistently, smears showed a similar d21 peak of FLB-loaded CD11b⁺ cells in the circulation (Figure 3c,d). From d4, circulating FLBs were cell-associated (Figure 3d). Most FLB-loaded cells in blood, DLNs and spleen exhibited a few particles and were GR1⁺/Ly6C⁺ (Figure 3e,f). However, 22% to 33% were GR1⁻/Ly6C⁻ in spleen and had frequently incorporated >5FLBs, suggesting phagocytosis-associated maturation of inflammatory MO-derived cells [20,25,26]. FLB-loaded cells had markedly decreased in

spleen at d90. Although declining after d21, FLB-loaded cells were still detected in blood at d45 and d90.

Fluorosphere incorporation into brain is delayed and depends on prior cell loading in peripheral and lymphoid tissues

Particles were detected in brain mainly from d21 post-injection. After d21 post-i.m. injection, FLBs gradually increased in brain until the d90 endpoint in the C57Bl6 mouse (Figure 4a,b) and until the d180 endpoint in the *CX3CR1*^{GFP/+} mouse conventionally used to study resident microglia (Figures 4a and 5a). FLBs were predominantly found in the grey matter (82% to 95%), regardless of the amount of injected FLBs (4, 10, 20 μ L), vaccine co-injection (36 μ L), or post-injection time from d21 to d365. Some FLBs were detected in leptomeninges (9%) and in the white matter (9%) at d21, but these locations became rare at later time points. FLBs were <5% in choroid plexus (Table 1). Comparative FLB distribution at month 3, month 6 and month 12 showed no prominent accumulations of particles at any neuroanatomical location (Figure 4c). FLBs were usually detected in brain as single particles located within or at the surface of cells; 37% to 62% of particles could be reliably assigned to a given cell subset by immunohistochemical screening. At d21,



particles were mainly associated with perivascular CD11b⁺ MPs, but at d90 they were also found in deep ramified CX3CR1⁺ microglia (Figure 5a). Particles were also detected in GFAP⁺ astrocytes, MAP2⁺ or Neurotrace-stained neurons, and vimentin⁺ leptomeningeal cells (Figure 5b-e), and in NG2⁺ oligodendroglial progenitors/pericytes (not shown). FLB incorporation into GFP⁺ resident ramified microglia of CX3CR1^{GFP/+} mice increased by up to 26-fold the d21 value at d180.

Importantly, compared to i.m. injection, the same FLB amount injected in the tail vein resulted in virtually no cerebral entry at d21 and d90 in C57Bl6 mice (Figure 6a). Moreover, ablation of popliteal and inguinal DLNs before FLB injection in TA muscle resulted in 60% to 80% reduction of FLB incorporation into blood, spleen and brain compartments at d21 (Figure 6b). Thus, cell uptake in muscle and DLNs, and subsequent cell traffic to blood crucially contributed to delayed particle translocation to

Table 2 Time of peak observation and peak value of particle loaded cells in studied organs (total number \pm SD)

Particle	Popliteal DLN		Inguinal DLN		Spleen		Blood		Brain	
	Peak	Number of loaded cells	Peak	Number of loaded cells	Peak	Number of loaded cells	Peak	Number of loaded cells	Endpoint	Number of loaded cells
FLB	D4	21,117 \pm 1,235	D4	23,746 \pm 2,880	D21	76,503 \pm 11,850	D21	9,878 \pm 792	D90	577 \pm 96
Al-Rho	D4	4,462 \pm 257	D4	6,253 \pm 745	D21	27,570 \pm 6,670	D21	7,546 \pm 1,034	D90	613 \pm 137

spleen and brain (Figure 6a-f). Consistently, by injecting FLBs into the muscle of GFP⁺BM chimeric mice obtained by transplanting GFP⁺BM-derived cells to irradiated syngenic C56Bl/6 mice [15], we detected FLB-loaded GFP⁺ cells in these organs (Figure 7a,b,c) and observed delayed incorporation of donor-derived cells in brain (Figure 7d,e).

This BM transplantation model is known to be associated with irradiation-induced BBB alteration. Dystrophin-deficient *mdx* mice also have chronically altered BBB [27]. As a corollary, compared to age-matched controls, they show significantly more CD31⁺ brain capillaries, and a dramatic increase of perivascular CD11b⁺ macrophages (Figure 6c) at the expense of deep ramified microglia. FLB injection in *mdx* mouse muscle resulted in increased brain incorporation of particles at both d21 and d90, as assessed by both histology and cytopins of CD45⁺/CD11b⁺ cells extracted from brain (Figure 6d,e,f). Thus, BBB alteration and/or the associated inflammatory/angiogenic response likely favors brain incorporation of circulating particle-loaded cells.

Fluorescent nanohybrids coated with Al(OH)₃ undergo CCL2-dependent systemic scattering and brain penetration

For confirmatory experiments we constructed fluorescent particles mimicking alum. Rhodamine nanohybrids [28] were covalently coated with a Al(OH)₃ shell. As assessed by the Morin stain for aluminum, these Al-Rho particles were avidly phagocytosed after i.m. injection and formed intracellular agglomerates similar in size to the vaccine adjuvant (Figure 8a,b). Biodistribution of the alum fluorescent surrogate injected into TA muscle was strikingly similar to that of FLB (Table 2), including d4 peak in DLNs, d21 peak in spleen, delayed entry in brain, and main association with GR1⁺/Ly6C⁺ MOs in tissues (Figure 8c-h). Compared to i.m. injection, s.c. injection of Al-Rho particles was associated with an even higher rate of diffusion to DLNs (Figure 8f), a finding consistent with the presence of abundant migratory DCs in skin.

On the grounds of a human SNP study, we performed CCL2 gain and loss of function experiments to investigate the role of CCL2-responsive cells in particle scattering and neurodelivery. Injection of Al-Rho particles into the TA muscle of CCL2-deficient mice decreased particle incorporation by 35% into popliteal DLN and by 76%

in inguinal DLN at d4, and by 71%, 85% and 82% in spleen, blood, and brain, respectively, at d21 (Figure 9a). Conversely, Al-Rho particle biodistribution increased in different gain of CCL2 function experiments (Figure 9b-d). I.m. co-injection of Al-Rho with murine recombinant CCL2 (rCCL2: 1 μ g) increased particle incorporation by 47% into popliteal and 163% into inguinal DLN (d4), and by 180% in spleen, 274% in blood, and 341% in brain (d21).

Moreover, slow intracerebral (i.c.) infusion of CCL2 by an osmotic pump (180 pg/day during 15 days starting at d7 after Al-Rho i.m. injection) increased particle incorporation into brain by 74% at d21 compared to PBS control. The combination of i.m. injection and i.c. infusion of rCCL2 increased particle incorporation into the brain by 539%. Despite important interindividual variations, a consistent trend of CCL2-dependent increase of Al brain levels was detected 21 days after i.m. injection of 40 μ L of alum-containing vaccine (Figure 9e). Taken together these results indicate that after i.m. injection, particles associated with inflammatory MOs can enter the brain using a CCL2-dependent mechanism, possibly through a Trojan horse mechanism. Importantly, Al-Rho particles gaining access to the brain after i.m. injection remained intact since they were still coated with Al(OH)₃ as assessed by both Morin stain (Figure 10a), and PIXE (Figure 10b). Their incorporation in neural cells was consistently associated with the expression of IL-1 β (Figure 10c), a reliable marker of particle-induced NALP3 inflammasome activation [29].

Fluorescent nanohybrids coated with Al(OH)₃ are retained in brain

An apparently irreversible accumulation of nanomaterials after i.m. injection was unique to brain tissue which lacks conventional lymphatic pathways and may retain immune cells [30]. We stereotactically injected 0.5 μ L Al-Rho in the striatum of C57Bl/6 mice, and counted particles in cervical LNs, blood, and spleen at d4 and d21. Compared to the same amount of Al-Rho injected in the TA muscle, i.c. injection was associated with almost no particle translocation to regional DLNs (Figure 10d), and the appearance of eight-fold fewer particles in spleen (Figure 10e). Since 25 free Al-Rho particles per 100 μ L were detected in blood at hour 1, it is likely that the rare particles subsequently detected in spleen reflected direct particle passage into

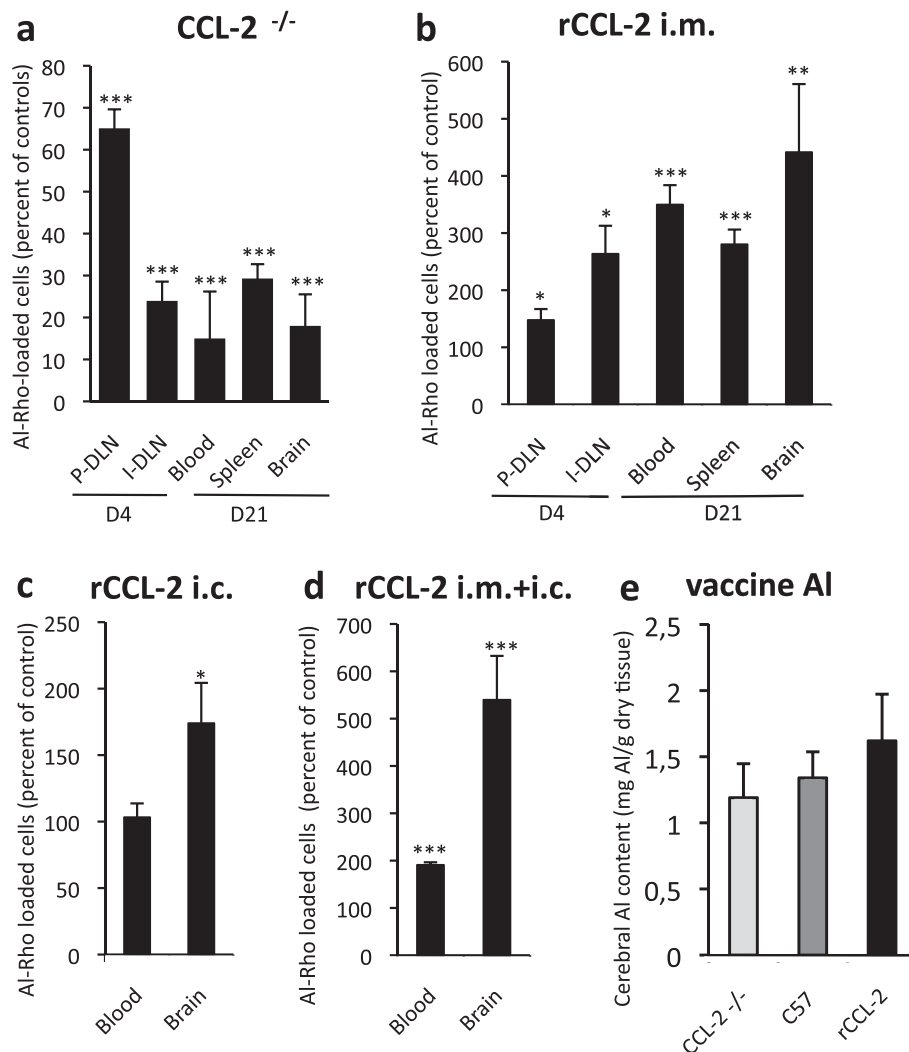


Figure 9 CCL2-dependent systemic translocation of Al-particles. **a**) CCL2 deficient mice show a dramatic decrease of Al-Rho translocation from the injected muscle to inguinal DLN, blood, spleen and brain, as compared to their respective controls (100%). Note that the difference is significant but less pronounced for popliteal DLN; **b**) rCCL-2 co-injection with Al-Rho is associated with a marked increase of Al-Rho translocation from the injected muscle to inguinal DLN, blood, spleen and brain, compared to their respective controls (100%). Note that the difference is significant but less pronounced for popliteal DLN; **c**) rCCL-2 infused by an osmotic micropump into the striatum for 15 days is associated with a significant increase of Al-Rho translocation from the injected muscle to brain; **d**) Combined i.m. and i.c. injection of rCCL2 is associated with a dramatic increase of FLB translocation from muscle to both blood and brain; **e**) Alum-containing vaccine injected into muscle of CCL-2-deficient, normal, and rCCL-2 mice was associated with a trend of CCL-2-dependent increase of Al concentration levels in brain; (histograms: n = 3 per group, mean ± SD, * P < 0.05, ** P < 0.01, *** P < 0.005, except [e]: n = 10 per group, mean ± SEM). Al-Rho, Al(OH)₃ rhodamine nanohybrid; DLN, draining lymph nodes; FLB, fluorescent latex beads; n, number; SEM, standard error of the mean.

blood during i.c. injection. It seems, therefore, that lack of recirculation likely contributed to progressive cerebral particle accumulation.

Discussion

Particles injected by the i.m. or s.c. route gained access to distant tissues. Latex and Al-Rho particles showed closely similar biodistribution, suggesting a shared basic scattering mechanism. Initial cell uptake in peripheral and DLN tissues and subsequent transport within inflammatory

MO-derived cells was critically involved, as indicated by immunophenotyping, cell migration blockade and DLN ablation. Cells were heavily loaded with particles soon after i.m. injection but usually contained only one to two particles after d4 and downstream the popliteal DLN, pointing to either dilution by cell division [31] or particle dispatching to other cells [32] within DLNs. Previous studies have reported particle cell transport from skin to DLNs [25] but downstream particle fate remained largely unexplored [33]. There is strong evidence that,

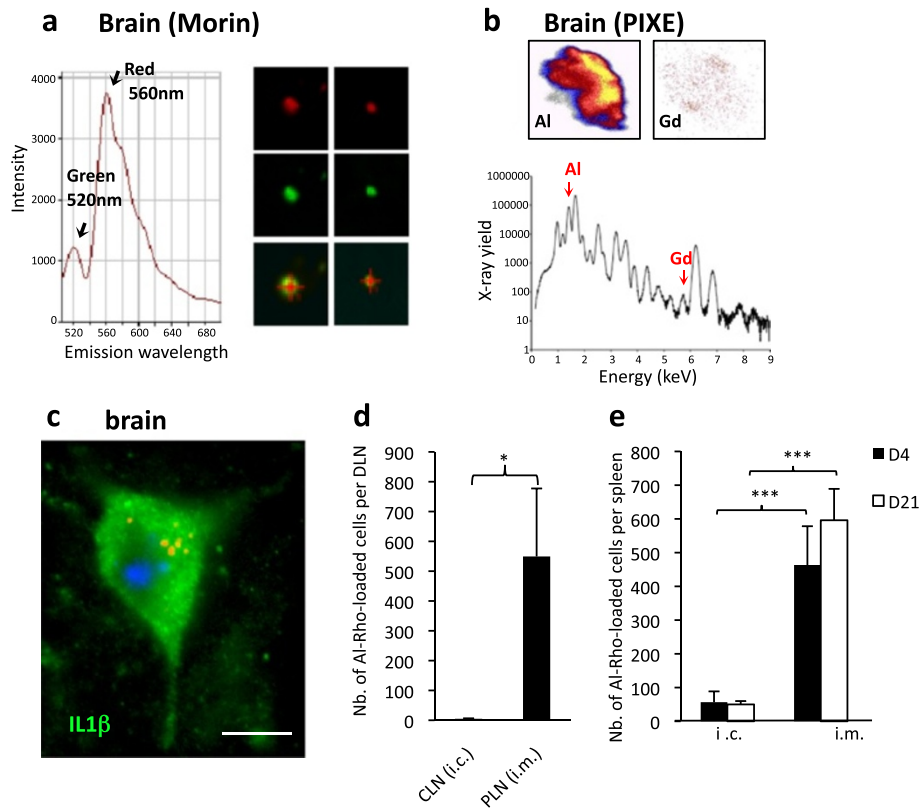


Figure 10 Al-Rho particles remain in brain and may induce inflammation. **a)** Al-Rho nanomaterial detected in brain by rhodamine fluorescence (upper row and emission spectrum at 560 nm) remains associated with Al as assessed by Morin stain (middle row and emission spectrum at 520 nm); **b)** Al-Rho nanomaterial detected in the brain by PIXE. Al coating colocalizing with Gd core assesses the integrity of Al-Rho nanohybrid after translocation; **c)** In mice with i.m. co-injection of Al-Rho and rCCL-2, particle incorporation into neural cells was associated with immunohistochemical expression of IL1beta; **d)** Stereotactic injection of Al-Rho into the striatum was associated with no translocation to cervical LNs (CLN) at d4, contrasting with conspicuous translocation to popliteal LNs (PLN) observed when the same particle amount was injected in TA muscle; **e)** Stereotactic injection of Al-Rho into the striatum, compared to similar injection into muscle, was associated with very little translocation to spleen at both d4 and d21. (histograms: n = 3 per group, mean ± SD, * P < 0.05, ** P < 0.01, *** P < 0.005; bar in c: 10 μm). Al(OH)₃ rhodamine nanohybrid; d, day; LN, lymph nodes; n, number; PIXE, particle induced X-ray emission; TA, tibialis anterior.

in inflammatory conditions, all DCs reaching DLNs do not die locally but may rather gain access to the blood through efferent lymphatics and the thoracic duct, and present antigens in spleen and bone marrow [33]. Ingested adjuvant particles boost this phenomenon which in turn likely favors their translocation from the injection point to distant sites as: (i) alum induces rapid differentiation of monocyte-lineage cells into APCs [34] and stimulates their migration to DLNs [35], (ii) beryllium hydroxide, a closely similar particulate adjuvant, strongly stimulates DC egress through efferent lymphatics [36]; and, as shown herein, (iii) Al deposits may be detected by PIXE in spleen and brain after i.m. injection of alum.

Delayed and slowly progressive particle accumulation occurred in intact brains. Experiments using the parabiosis model [37] or avoiding brain irradiation prior to BM transplantation [38] have shown that endogenous microglia are not replenished by the periphery under normal

central nervous system (CNS) conditions. Although low chimerism inherent in these experimental approaches may lead to some underestimation of slow microglia turnover from the periphery [39], a more likely explanation of our findings is that particles exert stimulatory effects on myeloid cell trafficking [36]. Both latex particles and aluminum hydroxide agglomerates promote inflammation [40,41] and non-specific immune stimulation can increase monocyte transendothelial migration by up to 20-fold in *in vitro* models of the BBB [42]. Consistently, i.m. injection of rCCL2 strongly increased particle incorporation into intact brain while CCL2-deficient mice had decreased neurodelivery. rCCL2 likely induced the exit of inflammatory MOs and hematopoietic stem and progenitor cells from BM [43], followed by their transmigration to the injected muscle and to DLNs [44], prior to particle loading and dissemination. Cerebral infusion of low doses of rCCL2, mimicking pathological states attracting inflammatory monocytes, also increased particle neurodelivery.

Intracerebral particles translocated with time from perivascular macrophages to the sentinel network of parenchymal microglia and to other resident neural cells and likely failed to recirculate, thus explaining their progressive cerebral accumulation.

Conclusions

Taken together, our results indicate that, similarly to intracellular bacteria [45], nanomaterials can be transported by MO-lineage cells to DLNs, blood and spleen, and, similarly to HIV [46] and other pathogens [47], may use CCL2-dependent MO transmigration across the BBB to enter the brain. This occurs at an extremely low rate in normal mice, the percentage of injected particles found in tissues being estimated at $1:10^5$ in d21 spleen and $1:10^7$ in d90 brain, consistent with the excellent tolerance of almost all individuals to limited doses of alum and other injected particles. Neurodelivery of nanomaterials significantly increased in mice with either a weak BBB or high tissue levels of CCL2, as previously suspected for pathogens in humans [48]. On the one hand, such a cerebral incorporation of nanomaterials injected into tissues should be regarded as an interesting characteristic in the setting of therapeutic strategies targeting the CNS. On the other hand, alum has high neurotoxic potential [49], and planning administration of continuously escalating doses of this poorly biodegradable adjuvant in the population should be carefully evaluated by regulatory agencies since the compound may be insidiously unsafe. It is likely that good tolerance to alum may be challenged by a variety of factors including overimmunization, BBB immaturity, individual susceptibility factors, and aging that may be associated with both subtle BBB alterations and a progressive increase of CCL2 production [50].

Additional file

Additional file 1: Appendix. Supplementary material.

Abbreviations

AI-Rho: Al(OH)₃ rhodamine nanohybrid; APC: antigen presenting cells; ASIA: autoimmune/inflammatory syndrome induced by adjuvant; BBB: blood brain barrier; BM: bone marrow; CCL2: chemokine (C-C motif) ligand 2; CNS: central nervous system; d: day; DC: dendritic cells; DEG: diethylene glycol; DLNS: draining lymph nodes; (D)MEM: (Dulbecco's) modified Eagle's medium; DMSO: dimethyl sulfoxide; EDTA: ethylenediaminetetraacetic acid; FITC: fluorescein isothiocyanate; FLB: fluorescent latex bead; GFAAS: graphite furnace atomic absorption spectrometry; IL: interleukin; *mdx*: dystrophin deficient mouse; MCP1: monocyte chemoattractive protein 1; MMF: macrophagic myofasciitis; MO: monocyte; mo: month; MP: macrophage; PBS: phosphate-buffered saline; PFA: paraformaldehyde; PIXE: proton induced X-ray emission; SNP: single nucleotide polymorphism; TA: *tibialis anterior* muscle; THGA: transversely heated graphite atomizer.

Competing interests

The authors declare they have no competing interests.

Authors' contributions

ZK carried out animal experiments and tissue processing and participated in data analysis; CC carried out molecular genetics studies; FJA contributed clinical data; VI processed tissue for PIXE and participated in their analysis; FL participated in surrogate particles production; CE carried out AI determination in tissues; MMY and PM participated in the PIXE analysis, XD carried out confocal analysis; OT conceived and contributed surrogate particles; RKG conceived and coordinated the study, analyzed data and drafted the manuscript; JC designed the study, performed animal experiments, analyzed data and prepared the figures, and participated in the manuscript writing. All authors read and approved the final manuscript.

Acknowledgements

This work has benefited from research funding from two patients associations: E3M (Entraide aux Malades de Myofasciite à Macrophages) "Neurodélivrance des particules injectées par voie intra musculaire et sécurité des adjuvants aluminiques", AFM (Association Française contre les Myopathies) "Etude des mécanismes de la myofasciite à macrophages" and Dwsokin Foundation (Nano in brain); from Région Ile-de-France through a programme PICRI (Partenariat Institutions-Citoyens pour la Recherche et l'Innovation) "Recherche de polymorphismes dans les gènes codant pour des facteurs inflammatoires (chimiokines) dans la myofasciite à macrophages", and through two post-doctoral positions from NeRF (Neuropole de Recherche Francilien) on the topic "The macrophage as a Trojan horse for brain delivery" and "Brain delivery of i.m. injected nanoparticles: relevance to safety of aluminum-containing adjuvants of vaccines"; and from the European Community's Seventh Framework Programme in the project ENDOSTEM "Activation of vasculature associated stem cells and muscle stem cells for the repair and maintenance of muscle tissue" (Grant agreement number 241440). We would like to thank for their most useful contributions: Dr Sophie Hue, Dr Fabrice Chrétien, Dr Madly Brigitte, Dr Anne Hulin, Lucie Poupel, Emilie House, Yasmine Baba-Amer, and Mathieu Surenaud.

Author details

¹Inserm, U955, 8 rue du Général Sarrail, Créteil 94010, France. ²Université Paris Est, Faculté de Médecine, 8 rue du Général Sarrail, Créteil 94010, France. ³Inserm, UMR-S 945, 91 Boulevard de l'Hôpital, Paris 75013, France. ⁴Université Pierre et Marie Curie, Faculté de Médecine, 11 Boulevard de l'Hôpital, Paris 75013, France. ⁵AP-HP, Groupe Hospitalier Pitié-Salpêtrière, Service d'Immunologie, 11 Boulevard de l'Hôpital, Paris 75013, France. ⁶AP-HP, Hôpital H. Mondor - A. Chenevier, Service d'Histologie, Centre de Référence Neuromusculaire GNMH, 51 Avenue du Maréchal de Lattre de Tassigny, Créteil 94000, France. ⁷CNRS UMR 5620, Laboratoire de Physico-Chimie des Matériaux Luminescents, 2 rue Victor Grignard, Villeurbanne 69622, France. ⁸Université Claude Bernard Lyon 1, 2 rue Victor Grignard, Villeurbanne 69622, France. ⁹The Birchall Centre, Lennard-Jones Laboratories, Keele University, Staffordshire ST5 5BG, UK. ¹⁰CNRS UMR 5797, Centre d'Etudes Nucléaires de Bordeaux Gradignan, Allée du haut Vignaud, Gradignan 33175, France. ¹¹Faculté des Sciences et Technologie, UPEC, 61 Avenue du Général de Gaulle, Créteil, France. ¹²IMRB Team 10, Faculté de Médecine, 8 rue du Général Sarrail, Créteil F-94010, France.

Received: 12 November 2012 Accepted: 7 March 2013

Published: 4 April 2013

References

1. *Committees on toxicity, mutagenicity and carcinogenicity of chemicals in food, consumer products and the environment (COT, COM, COC). Joint statement on nanomaterial toxicology.* 2005. Available at <http://cot.food.gov.uk/pdfs/cotstatements2005nanomats.pdf>.
2. Dobrovolskaia MA, Aggarwal P, Hall JB, McNeil SE: **Preclinical studies to understand nanoparticle interaction with the immune system and its potential effects on nanoparticle biodistribution.** *Mol Pharm* 2008, **5**:487–495.
3. Exley C, Siesjö P, Eriksson H: **The immunobiology of aluminium adjuvants: how do they really work?** *Trends Immunol* 2010, **31**:103–109.
4. Gherardi RK, Coquet M, Cherin P, Belec L, Moretto P, Dreyfus PA, Pelissier JF, Chariot P, Authier FJ: **Macrophagic myofasciitis lesions assess long-term persistence of vaccine-derived aluminium hydroxide in muscle.** *Brain* 2001, **124**:1821–1831.

5. Authier FJ, Cherin P, Creange A, Bonnotte B, Ferrer X, Abdelmoumni A, Ranoux D, Pelletier J, Figarella-Branger D, Granel B, Maisonobe T, Coquet M, Degos JD, Gherardi RK: **Central nervous system disease in patients with macrophagic myofasciitis.** *Brain* 2001, **124**:974–983.
6. Gherardi RK, Authier FJ: **Aluminum inclusion macrophagic myofasciitis: a recently identified condition.** *Immunol Allergy Clin North Am* 2003, **23**:699–712.
7. Shoenfeld Y, Agmon-Levin N: **'ASIA' - autoimmune/inflammatory syndrome induced by adjuvants.** *J Autoimmun* 2010, **36**:4–8.
8. Authier FJ, Sauvat S, Champey J, Drogou I, Coquet M, Gherardi RK: **Chronic fatigue syndrome in patients with macrophagic myofasciitis.** *Arthritis Rheum* 2003, **48**:569–570.
9. Couette M, Boisse MF, Maison P, Brugieres P, Cesaro P, Chevalier X, Gherardi RK, Bachoud-Levi AC, Authier FJ: **Long-term persistence of vaccine-derived aluminum hydroxide is associated with chronic cognitive dysfunction.** *J Inorg Biochem* 2009, **103**:1571–1578.
10. Flarend RE, Hem SL, White JL, Elmore D, Suckow MA, Rudy AC, Dandashli EA: **In vivo absorption of aluminum-containing vaccine adjuvants using 26Al.** *Vaccine* 1997, **15**:1314–1318.
11. Morefield GL, Sokolovska A, Jiang D, HogenEsch H, Robinson JP, Hem SL: **Role of aluminum-containing adjuvants in antigen internalization by dendritic cells in vitro.** *Vaccine* 2005, **23**:1588–1595.
12. Hamilton JA, Byrne R, Whitty G: **Particulate adjuvants can induce macrophage survival, DNA synthesis, and a synergistic, proliferative response to GM-CSF and CSF-1.** *J Leukoc Biol* 2000, **67**:226–232.
13. Verdier F, Burnett R, Michelet-Habchi C, Moretto P, Fievet-Groynne F, Sauzeat E: **Aluminium assay and evaluation of the local reaction at several time points after intramuscular administration of aluminium containing vaccines in the Cynomolgus monkey.** *Vaccine* 2005, **23**:1359–1367.
14. Authier FJ, Sauvat S, Christov C, Chariot P, Raisbeck G, Poron MF, Yiou F, Gherardi R: **AIOH3-adjuvanted vaccine-induced macrophagic myofasciitis in rats is influenced by the genetic background.** *Neuromuscul Disord* 2006, **16**:347–352.
15. Brigitte M, Schilte C, Plonquet A, Baba-Amer Y, Henri A, Charlier C, Tajbakhsh S, Albert M, Gherardi RK, Chretien F: **Muscle resident macrophages control the immune cell reaction in a mouse model of notexin-induced myoinjury.** *Arthritis Rheum* 2010, **62**:268–279.
16. Carbone FR, Belz GT, Heath WR: **Transfer of antigen between migrating and lymph node-resident DCs in peripheral T-cell tolerance and immunity.** *Trend Immunol* 2004, **25**:655–658.
17. Wang XY, Yao X, Wan YM, Wang B, Xu JQ, Wen YM: **Responses to multiple injections with alum alone compared to injections with alum adsorbed to proteins in mice.** *Immunol Lett* 2012, **149**:88–92.
18. Cain DW, Sanders SE, Cunningham MM, Kelson G: **Disparate adjuvant properties among three formulations of "alum".** *Vaccine* 2013, **31**:653–660.
19. Moretto P: **Nuclear microprobe: a microanalytical technique in biology.** *Cell Mol Biol* 1996, **42**:1–16.
20. Wen GY, Wisniewski HM: **Histochemical localization of aluminum in the rabbit CNS.** *Acta Neuropathol* 1985, **68**:175–184.
21. Redhead K, Quinlan GJ, Das RG, Gutteridge JM: **Aluminium-adjuvanted vaccines transiently increase aluminium levels in murine brain tissue.** *Pharmacol Toxicol* 1992, **70**:278–280.
22. Sahin G, Varol I, Temizer A, Benli K, Demirdamar R, Duru S: **Determination of aluminum levels in the kidney, liver, and brain of mice treated with aluminium hydroxide.** *Biol Trace Elem Res* 1994, **41**:129–135.
23. Kivela R, Silvennoinen M, Lehti M, Kainulainen H, Vihko V: **Effects of acute exercise, exercise training, and diabetes on the expression of lymphangiogenic growth factors and lymphatic vessels in skeletal muscle.** *Am J Physiol Heart Circ Physiol* 2007, **293**:H2573–H2590.
24. Randolph GJ, Inaba K, Robbiani DF, Steinman RM, Muller WA: **Differentiation of phagocytic monocytes into lymph node dendritic cells in vivo.** *Immunity* 1999, **11**:753–761.
25. Allan RS, Waithman J, Bedoui S, Jones CM, Villadangos JA, Zhan Y, Lew AM, Shortman K, Heath WR, Carbone FR: **Migratory dendritic cells transfer antigen to a lymph node-resident dendritic cell population for efficient CTL priming.** *Immunity* 2006, **25**:153–162.
26. Arnold L, Henry A, Poron F, Baba-Amer Y, van Rooijen N, Plonquet A, Gherardi RK, Chazaud B: **Inflammatory monocytes recruited after skeletal muscle injury switch into antiinflammatory macrophages to support myogenesis.** *J Exp Med* 2007, **204**:1057–1069.
27. Nico B, Frigeri A, Nicchia GP, Corsi P, Ribatti D, Quondamatteo F, Herken R, Girolamo F, Marzullo A, Svelto M, Roncali L: **Severe alterations of endothelial and glial cells in the blood-brain barrier of dystrophic mdx mice.** *Glia* 2003, **42**:235–251.
28. Fizet J, Riviere C, Bridot L, Charvet N, Louis C, Billotey C, Raccurt M, Morel G, Roux S, Perriat P, Tillement O: **Multi-luminescent hybrid gadolinium oxide nanoparticles as potential cell labeling.** *J Nanosci Nanotechnol* 2009, **9**:5717–5725.
29. Hornung V, Bauernfeind F, Halle A, Samstad EO, Kono H, Rock KL, Fitzgerald KA, Latz E: **Silica crystals and aluminum salts activate the NALP3 inflammasome through phagosomal destabilization.** *Nat Immunol* 2008, **9**:847–856.
30. Weller RO, Djuanda E, Yow HY, Carare RO: **Lymphatic drainage of the brain and the pathophysiology of neurological disease.** *Acta Neuropathol* 2009, **117**:1–14.
31. Kabashima K, Banks TA, Ansel KM, Lu TT, Ware CF, Cyster JG: **Intrinsic lymphotoxin-beta receptor requirement for homeostasis of lymphoid tissue dendritic cells.** *Immunity* 2005, **22**:439–450.
32. Angeli V, Ginhoux F, Llodrà J, Quemeneur L, Frenette PS, Skobe M, Jessberger R, Merad M, Randolph GJ: **B cell-driven lymphangiogenesis in inflamed lymph nodes enhances dendritic cell mobilization.** *Immunity* 2006, **24**:203–215.
33. Cavanagh LL, Bonasio R, Mazo IB, Halin C, Cheng G, van der Velden AW, Cariappa A, Chase C, Russell P, Stambach MN, Koni PA, Pillai S, Weninger W, von Andrian UH: **Activation of bone marrow-resident memory T cells by circulating antigen-bearing dendritic cells.** *Nat Immunol* 2005, **6**:1029–1037.
34. Rimioli AC, Gras G, Verdier F, Capel F, Grigoriev VB, Porcheray F, Sauzeat E, Fournier JG, Clayette P, Siegrist CA, Dormont D: **Aluminum hydroxide adjuvant induces macrophage differentiation towards a specialized antigen-presenting cell type.** *Vaccine* 2004, **22**:3127–3135.
35. Kool M, Soullie T, van Nimwegen M, Willart MA, Muskens F, Jung S, Hoogsteden HC, Hammad H, Lambrecht BN: **Alum adjuvant boosts adaptive immunity by inducing uric acid and activating inflammatory dendritic cells.** *J Exp Med* 2008, **205**:869–882.
36. Hall JG: **Studies on the adjuvant action of beryllium, I. Effects on individual lymph nodes.** *Immunology* 1998, **53**:105–113.
37. Ajami B, Bennett JL, Krieger C, Tetzlaff W, Rossi FM: **Local self-renewal can sustain CNS microglia maintenance and function throughout adult life.** *Nat Neurosci* 2007, **10**:1538–1543.
38. Mildner A, Schmidt H, Nitsche M, Merkler D, Hanisch UK, Mack M, Heikenwalder M, Brück W, Priller J, Prinz M: **Microglia in the adult brain arise from Ly-6C^{hi}CCR2⁺ monocytes only under defined conditions.** *Nat Neurosci* 2007, **10**:1544–1553.
39. Prinz M, Mildner A: **Microglia in the CNS: immigrants from another world.** *Glia* 2011, **59**:177–187.
40. Inoue K, Takano H, Yanagisawa R, Koike E, Shimada A: **Size effects of latex nanomaterials on lung inflammation in mice.** *Toxicol Appl Pharmacol* 2009, **234**:68–76.
41. Pauluhn J: **Pulmonary toxicity and fate of agglomerated 10 and 40 nm aluminium oxyhydroxides following 4-week inhalation exposure of rats: toxic effects are determined by agglomerated, not primary particle size.** *Toxicol Sci* 2009, **109**:152–167.
42. Persidsky Y, Stins M, Way D, Witte MH, Weinand M, Kim KS, Bock P, Gendelman HE, Fiala M: **A model for monocyte migration through the blood-brain barrier during HIV-1 encephalitis.** *J Immunol* 1997, **158**:3499–3510.
43. Si Y, Tsou CL, Croft K, Charo IF: **CCR2 mediates hematopoietic stem and progenitor cell trafficking to sites of inflammation in mice.** *J Clin Invest* 2010, **120**:1192–1203.
44. Palframan RT, Jung S, Cheng G, Weninger W, Luo Y, Dorf M, Littman DR, Rollins BJ, Zweerink H, Rot A, von Andrian UH: **Inflammatory chemokine transport and presentation in HEV: a remote control mechanism for monocyte recruitment to lymph nodes in inflamed tissues.** *J Exp Med* 2001, **5**:1361–1373.
45. Chackerian AA, Alt JM, Perera TV, Dascher CC, Behar SM: **Dissemination of Mycobacterium tuberculosis is influenced by host factors and precedes the initiation of T-cell immunity.** *Infect Immun* 2002, **70**:4501–4509.
46. Drevets DA, Dillon MJ, Schawang JS, Van Rooijen N, Ehrchen J, Sunderkotter C, Leenen PJ: **The Ly-6C^{high} monocyte subpopulation transports Listeria monocytogenes into the brain during systemic infection of mice.** *J Immunol* 2004, **172**:4418–4424.
47. Eugenin EA, Osiecki K, Lopez L, Goldstein H, Calderon TM, Berman JW: **CCL2/monocyte chemoattractant protein-1 mediates enhanced transmigration of human immunodeficiency virus (HIV)-infected**

leukocytes across the blood–brain barrier: a potential mechanism of HIV-CNS invasion and NeuroAIDS. *J Neurosci* 2006, **26**:1098–1106.

48. Gonzalez E, Rovin BH, Sen L, Cooke G, Dhanda R, Mummidi S, Kulkarni H, Bamshad MJ, Telles V, Anderson SA, Walter EA, Stephan KT, Deucher M, Mangano A, Bologna R, Ahuja SS, Dolan MJ, Ahuja SK: **HIV-1 infection and AIDS dementia are influenced by a mutant MCP-1 allele linked to increased monocyte infiltration of tissues and MCP-1 levels.** *Proc Natl Acad Sci U S A* 2002, **99**:13795–13800.
49. Shaw CA, Petrik MSJ: **Aluminum hydroxide injections lead to motor deficits and motor neuron degeneration.** *J Inorg Biochem* 2009, **103**:1555–1562.
50. Galimberti D, Fenoglio C, Lovati C, Venturelli E, Guidi I, Corra B, Scalabrini D, Clerici F, Mariani C, Bresolin N, Scarpini E: **Serum MCP-1 levels are increased in mild cognitive impairment and mild Alzheimer's disease.** *Neurobiol Aging* 2006, **27**:1763–1768.

doi:10.1186/1741-7015-11-99

Cite this article as: Khan *et al.*: Slow CCL2-dependent translocation of biopersistent particles from muscle to brain. *BMC Medicine* 2013 **11**:99.

**Submit your next manuscript to BioMed Central
and take full advantage of:**

- Convenient online submission
- Thorough peer review
- No space constraints or color figure charges
- Immediate publication on acceptance
- Inclusion in PubMed, CAS, Scopus and Google Scholar
- Research which is freely available for redistribution

Submit your manuscript at
www.biomedcentral.com/submit





Published in final edited form as:

J Inorg Biochem. 2009 November ; 103(11): 1555. doi:10.1016/j.jinorgbio.2009.05.019.

Aluminum hydroxide injections lead to motor deficits and motor neuron degeneration

Christopher A. Shaw^{a,b,c,*} and Michael S. Petrik^c

^a Departments of Ophthalmology and Visual Sciences, University of British Columbia, Vancouver, British Columbia, Canada

^b Experimental Medicine, University of British Columbia, Vancouver, British Columbia, Canada

^c Graduate Program in Neuroscience, University of British Columbia, Vancouver, British Columbia, Canada

Abstract

Gulf War Syndrome is a multi-system disorder afflicting many veterans of Western armies in the 1990–1991 Gulf War. A number of those afflicted may show neurological deficits including various cognitive dysfunctions and motor neuron disease, the latter expression virtually indistinguishable from classical amyotrophic lateral sclerosis (ALS) except for the age of onset. This ALS “cluster” represents the second such ALS cluster described in the literature to date. Possible causes of GWS include several of the adjuvants in the anthrax vaccine and others. The most likely culprit appears to be aluminum hydroxide. In an initial series of experiments, we examined the potential toxicity of aluminum hydroxide in male, outbred CD-1 mice injected subcutaneously in two equivalent-to-human doses. After sacrifice, spinal cord and motor cortex samples were examined by immunohistochemistry. Aluminum-treated mice showed significantly increased apoptosis of motor neurons and increases in reactive astrocytes and microglial proliferation within the spinal cord and cortex. Morin stain detected the presence of aluminum in the cytoplasm of motor neurons with some neurons also testing positive for the presence of hyper-phosphorylated tau protein, a pathological hallmark of various neurological diseases, including Alzheimer's disease and frontotemporal dementia. A second series of experiments was conducted on mice injected with six doses of aluminum hydroxide. Behavioural analyses in these mice revealed significant impairments in a number of motor functions as well as diminished spatial memory capacity. The demonstrated neurotoxicity of aluminum hydroxide and its relative ubiquity as an adjuvant suggest that greater scrutiny by the scientific community is warranted.

Keywords

Aluminum hydroxide; Adjuvant; Neurotoxicity; Gulf War Syndrome; Amyotrophic lateral sclerosis

* Corresponding author. Address: VGH Research Pavilion, 828 W10th Ave., Rm. 386, Vancouver, BC, Canada, V5Z 1L8. Tel.: +604 875 4111x68375; fax: +604 875 4376. cashawlab@gmail.com (C.A. Shaw).

Animal ethics approval: Protocols governing the use of animals were approved by review committees of the University of British Columbia and were in compliance with guidelines published by the Canadian Council on Animal Care and are in accordance with the international guidelines including the NIH Guide for the Care and Use of Laboratory Animals, as well as the EEC Council Directive.

Conflict of interest: None of the authors have received any grants or funding from Bioport, Chiron, Corixa, nor any other pharmaceutical companies named in this article.

1. Introduction

Various studies have established a correlation between Gulf War service (1990–1991) and a multi-system disorder commonly termed Gulf War Syndrome. Included in GWS are various neurological disorders, including an apparent cluster of cases of amyotrophic lateral sclerosis [1–4]. Haley [3] described classical ALS symptoms such as muscle weakness and wasting, impaired speech and swallowing, difficulty in breathing, and fasciculation in Gulf War veterans years after they first developed other symptoms of GWS. Seventeen of the 20 servicemen diagnosed with Gulf War illness and definite ALS were less than 45 years of age with the youngest of these 20 years old. All 20 of these patients presented with signs of upper (motor cortex or bulbar region) and lower (spinal cord) motor neuron degeneration. None of these patients had a family history of ALS or of other neurodegenerative disorders. Horner et al. [2] conducted a nationwide case study performed to identify incidence levels of ALS for the decade after August 1990 amongst active duty members of the military. One hundred and seven confirmed cases of ALS were identified from approximately 2.5 million eligible military personnel. When standardized to the average 1990 US general population, the average annual incidence of ALS among non-deployed military population was 1.4 per 100 000 persons per year compared to the generally accepted overall population incidence of 1.5 cases of ALS per 100 000. The incidence rate of ALS among the deployed military population was 3.6 per 100 000 persons/year. Weisskopf et al. [4] noted a general increase in ALS in US military populations going back a number of decades regardless of the conflict.

ALS–GWS is one of only two ALS disease clusters currently accepted as satisfying the definition of a cluster. The other is the Guamanian variant of ALS first described after World War 2 termed amyotrophic lateral sclerosis parkinsonism dementia complex (ALS–PDC). This spectrum of disorders, once present with an incidence levels hundreds of times higher than in the continental United States [5] (see Kurland, 1988, for review), expressed in one of two ways. The first was as a nearly classical form of ALS; the second was a form of parkinsonism associated with an Alzheimer's disease-like dementia (PDC). About 10% of the victims developed both disorders, with the ALS phenotype typically appearing first. Studies into potential etiologies focused on environmental factors with most attention eventually directed at the consumption of toxin-containing seeds of the local variety of cycad palm [6] and the presence of high aluminum in the soil on southern Guam [7].

In regard to the GWS-ALS AVA vaccine, attention has recently been directed at the anthrax vaccine adsorbed (AVA) and various vaccine ingredients, in particular the known and suspected adjuvants, aluminum hydroxide and squalene [8]. An adjuvant is a substance added during vaccine production designed to non-specifically increase the immune response to an antigen [9]. Aluminum compounds were first identified as adjuvants over 90 years ago. Currently aluminum, in various forms (aluminum hydroxide, aluminum phosphate and aluminum sulfate), is the most commonly licensed adjuvant whose use is generally regarded by both the pharmaceutical industry and the various governmental regulatory agencies as safe [10]. Various studies have found no adverse or long-term health effects due to aluminum adjuvants [11–13] and the Food and Drug Administration (FDA) has continued its longstanding approval for the use of aluminum in this fashion.

In spite of the long history of widespread use, the physicochemical interactions between aluminum compounds and antigens are relatively poorly understood and their underlying mechanisms remain relatively unstudied [14]. It also seems that there have been no rigorous animal studies of potential aluminum adjuvant toxicity. The absence of such studies is peculiar given the well known observation that aluminum in general can be neurotoxic under a number of conditions [15,16] and adjuvants in particular have previously been implicated in neurological disease [17–19]. Table 1 shows the results from previous studies that treated

animals with aluminum hydroxide, listing the resulting impacts on the nervous system. In context to the use of aluminum in vaccines, LD₅₀ values for aluminum hydroxide have not been published to date to the best of our knowledge (J.T. Baker Material Safety Data Sheets).

The potential for aluminum injections to induce macrophagic myofasciitis has also been noted in the literature [20–22].

A previous publication looked at the potential neurotoxicity of several known or suspected vaccine adjuvants [8]. In the current study, we will focus exclusively on the impact of aluminum hydroxide injections on motor and cognitive behaviours and on the expression of different forms of neuropathology in an *in vivo* mouse model.

2. Experimental procedures

2.1. Experimental animals

In our initial study [8], young adult (3 month old) CD-1 male mice were used (approx. 35 g at experiment onset). Younger animals were deliberately chosen to mimic the typical age of service during the Gulf War [3]. Four subcutaneous injection groups (two injections spaced 2 weeks apart) were used: control saline/phosphate buffered solution (PBS) ($n = 10$); aluminum hydroxide ($n = 11$); squalene ($n = 10$); and aluminum hydroxide and squalene ($n = 10$). The current study will report only on the aluminum treated and control groups from this experimental series. A second series of experiments was conducted on 9 month old CD-1 males that received six aluminum hydroxide injections over a 2 weeks period. These mice, along with controls and other treatment groups (to be reported elsewhere), were subjected to a more rigorous behavioural testing regime to be described below. Histological analyses of the spinal cords and brains of these mice are in progress.

All animals in both experiments were singly caged at the Jack Bell Research Centre animal care facility in Vancouver, B.C., Canada. An ambient temperature of 22 °C and a 12/12 h light cycle were maintained throughout the experiment. All mice were fed Purina® mouse chow and given access to both food and water *ad libitum*.

Mice from both studies were sacrificed with an overdose of halothane and transcardially perfused with 4% paraformaldehyde (PFA). CNS tissues were collected for histological examination. Fixed brains and spinal cords from all mice were transferred to a 30% sucrose/PBS solution overnight and then frozen and stored at –80 °C until sectioning. All brain/cord tissue blocks were mounted in Tissue-Tek optimum cutting temperature (O.C.T) compound (Sakura, Zoeterwoude, Netherlands), and then sectioned by cryostat into 30 µm coronal slices. Spinal cords were sectioned at 25 µm in the transverse plane. The sections were cryoprotected in 30% ethylene glycol–20% glycerol–dibasic and monobasic sodium phosphate solution and kept frozen at –20 °C until use.

2.2. Adjuvants

Alhydrogel®, an aluminum hydroxide (Al(OH)₃) gel suspension, was used as a source of aluminum hydroxide. Alhydrogel is manufactured by Superfos Biosector a/s (Denmark) and was purchased from SIGMA Canada.

2.2.1. Doses—To calculate approximate human dosages of aluminum hydroxide for our experiments, we used the following information: The AVA vaccine for human use is made by Bioport Corporation, of Lansing, Michigan. According to product data sheets from the Michigan Biologic Products Institute (MBPI, Lansing, Michigan, USA; Bioport's predecessor), a single dose of AVA vaccine contains 2.4 mg of aluminum hydroxide (equivalent to 0.83 mg aluminum). Based on an assumed average human body weight of 70–80 kg, the amount per

kg body weight would be approximately 30–34 $\mu\text{g}/\text{kg}$. Soldiers or civilians receiving the vaccine would have received between 30–34 $\mu\text{g}/\text{kg}$ (1 injection) and up to approx. 200 $\mu\text{g}/\text{kg}$ if six injections were received.

The adjuvant injections in the treated mice were calibrated based on average animal weight for both experiments. At 3-month-old male CD-1 mice weigh approx. 35 g; at 9 months, the weight is approx. 50 g. In Experiment 1, we performed two injections of a suspension of aluminum hydroxide of (50 $\mu\text{g}/\text{kg}$) in a total volume of 200 μL sterile PBS (0.9%) spaced 2 weeks apart. The mice in this experiment would therefore have received 100 $\mu\text{g}/\text{kg}$ versus a probable 68 $\mu\text{g}/\text{kg}$ in humans. In Experiment 2, mice received six injections for a total of 300 $\mu\text{g}/\text{kg}$ aluminum hydroxide over 2 weeks. Controls in both studies were injected with 200 μL PBS.

The injection site for human administration is typically subcutaneous over the deltoid muscle. For injections in mice we used a subcutaneous injection into the loose skin behind the neck (the “scruff”) to minimize discomfort and for ease of injection.

2.3. Behavioural tests

In the first study, mice were subjected at regular intervals to specific behavioral tests of motor and cognitive function, including wire mesh hang (2 \times /week), open field (1 \times /week), and water maze (1 \times /week) over a 6 months post injection period (see [22]). The order in which the animals were tested was randomized for each trial. In the second study, we conducted a more detailed behavioural examination based on the automated EthoVision system (Noldus Information Technology, Seattle, WA) employing a video camera and tracking software (Noldus EthoVision[®] 3.1). Individual movements of the mice were tracked for 5 min in an open field at weekly intervals. The software allowed for quantitative measurements of a variety of motor functions, including distance moved, percentage of time moving, velocity, and a variety of others. These latter experiments continued for 28 weeks following the last injections.

2.4. Histological measurements (Experiment 1)

2.4.1. NeuN and active caspase-3—As cited in Petrik et al. [8], five mice were used from each treatment group. In each, multiple brain ($n = 3$) and spinal cord ($n = 8$) sections at different levels were examined. Fluorescent intensity levels of NeuN and activated caspase-3 were used to identify neurons and cells dying by apoptosis, respectively. Regions of interest were defined using landmarks from mouse brain and spinal cord stereotaxic atlases [23,24]. All sections were counted in an unbiased manner under a 40 \times objective.

2.4.2. Choline acetyltransferase (ChAT) and Glial fibrillary acidic protein (GFAP)—As cited in Petrik et al. [8], the ChAT antibody was used to identify cholinergic motor neurons in the brain and spinal cord [25,26]. GFAP was used to label reactive astrocytes [27, 28].

2.4.3. Iba-1—A rabbit polyclonal antibody against the ionized calcium binding adapter molecule (Iba-1) (Wako, Richmond, VA, USA) was used to stain for activated microglia [29]. For Iba-1 fluorescent immunolabeling, staining followed the same protocol used for GFAP labeling except for the following modification: Sections were incubated with primary rabbit-anti-Iba-1 (in PBST with 1% NGS + 1% BSA; 1:1000 dilution) overnight at 4 $^{\circ}\text{C}$. Sections were then incubated in anti-rabbit AlexaFluor 546[™] secondary antibody for 2 h at room temperature (Molecular Probes; Eugene, OR, 1:200).

2.4.4. Morin (3,5,7,2',4'-pentahydroxyflavone, BDH)—Morin (M4008-2G, Sigma) is a fluorochrome which forms a fluorescent complex with aluminum fluorescing green (with an

excitation wavelength of 420 nm) [15,30] when it does so. The aluminum-Morin fluorescence assay was used for the visualization and detection of aluminum in lumbar spinal cord and other CNS tissues in the present experiments. The Morin stain was used as a 0.2% solution in 85% ethyl alcohol containing 0.5% acetic acid. All mounted sections were first washed with PBS twice for 5 min. Sections were then pretreated for 10 min in a 1% aqueous solution of hydrochloric acid, rinsed in double distilled water (ddH₂O) twice for 5 min, and immersed in 0.2% Morin stain for 10 min. The sections were then washed in ddH₂O twice for 5 min, dehydrated in 70%, 90%, and 100% ethyl alcohol (EtOH), and cleared with 100% xylene. All sections were then mounted using Vectashield mounting medium (Vector Laboratories), sealed with clear nail polish, and allowed to air dry.

2.4.5. Staining for hyper-phosphorylated tau protein—Hyper-phosphorylated tau (Anti-Human PHF-Tau, Pierce Biotechnology, Inc., Rockford, IL) labeling was determined using the non-fluorescent diaminobenzidine (DAB) method. Slides containing mounted sections of lumbar spinal cord were first rinsed twice PBS (2× 5 min) before performing antigen unmasking. Endogenous peroxidase activity was quenched using 0.3% hydrogen peroxide in methanol for 20 min. The sections were rinsed twice in PBS (2× 5 min) before blocking at room temperature for 1 h in M.O.M. blocking reagent (M.O.M. Kit – peroxidase, cat # PK 2200, Vector Laboratories, Inc., Burlingame CA) followed by a quick rinse in PBS and a 5 min incubation in M.O.M. diluent solution. The primary PHF-Tau antibody was diluted 100× in M.O.M. diluent solution and incubation was conducted at room temperature for 1 h. After the primary antibody incubation step, the slides were rinsed twice in PBS, and then incubated in the M.O.M. biotinylated anti-mouse IgG reagent for 10 min. The sections were rinsed in PBS before incubating with the secondary antibody (Vectastain ABC Elite Kit, cat # PK-6101) for 1 h at room temperature followed by incubation in the Vectorstain ABC Elite Reagents for another 30 min. The slides were rinsed again in 1× PBS. Color development was achieved using the Vector ImmPACT™ DAB solution (cat # SK-4105). When the desired color was achieved, the slides were rinsed in ddH₂O for 5 min and counter-stained in 0.1% methyl green for 5 min. After counter-staining, the slides were rinsed briefly in ddH₂O, two changes of 95% ethanol and two changes of 100% ethanol. The slides were allowed to dry before they were mounted in Permount® (Fisher Scientific, Fair Lawn, NJ).

2.5. Microscopy

Brain and spinal cord sections processed with fluorescent antibodies or DAB were viewed with a Zeiss Axiovert 200 M (Carl Zeiss Canada Limited, Toronto, ON, Canada) microscope at 40× and 100× (under oil) magnification. DAPI (blue fluorescence) was viewed with a 359/461 nm absorption/emission filter. Alexa Fluor 546™ (red), and rabbit IgG DuoLuX™ (red) were viewed with 556 557/572 573 nm filter. FITC was viewed with a 490 494/520 525 nm filter. Brain and lumbar spinal cord sections for histology were chosen randomly for each group. When counting using 40× magnification two images were captured per spinal cord section: ventral left, ventral right. 40× images were 350 × 275 μm and 100× images were 50 × 115 μm. Images were captured using AxioVision 4.3 software.

2.6. Criteria for determination and quantification of labeled cells

For quantification, only cells that were in focus and completely within the field of view were counted. To eliminate the likelihood that the same cell would be counted twice, slices for each histological experiment were drawn from only one well of the collection dish to ensure that sections were at least 250 μm apart. Regions of interest for cell counts were defined using landmarks and reference points from mouse spinal cord and brain stereotaxic atlases [39,40]. In the spinal cord, only cells which were anterior to the central canal and deep apex where the grey and white matters meet were considered as part of the ventral horns; conversely, only cells which were posterior to the central canal and the posterior deep apex were considered as

part of the dorsal horns. These criteria applied regardless of the spinal segments examined. In the brain, only cells found within the corresponding brain structures were counted. All sections were counted in an unbiased manner (a code key was assigned to the animals for tracking purposes, but did not reveal the identity of treatment the animal was prescribed).

2.7. Statistics

Values for each mouse on the individual tasks and in the cell counts were used to calculate mean \pm S.E.M. for each group and condition. Behavioral scores and cell counts were normalized to the mean value of controls. The means were compared using one- or two-way ANOVA (Statistica, Statsoft Inc., Tulsa, OK; GraphPad Prism, San Diego, CA).

3. Results

Unlike the Petrik et al. [8] study which showed a loss of ChAT positive motor neurons in the lumbar cord of aluminum hydroxide treated mice, there was no significant difference in ChAT labeling or motor neuron counts in either the cervical or thoracic spinal cord segments (Fig. 1A and B). However, the aluminum injected group showed a highly significant increase in the expression of GFAP positive astrocytes (70%) are the control group (listed as 100% for all graphs; Fig. 1C) in the cervical segment of spinal cord. These GFAP results mirrored the outcomes previously reported in lumbar cord.

Iba-1 labeling demonstrated significantly increased levels of activated microglia in the lumbar spinal cord of animals injected with aluminum (111%) compared to controls (Fig. 1E). Other levels of cord were not tested for microglia in the present study.

Only mice injected with aluminum hydroxide showed significantly increased Morin labeling of cells in lumbar spinal cord compared to the other groups (Fig. 2A–E). Similarly, only aluminum-injected mice showed the presence of abnormal tau protein in motor neurons in lumbar cord (Fig. 3). Other regions of the cord were not tested in the current studies for either Morin or tau protein.

The multiple aluminum hydroxide injections of experiment 2 showed profound effects on motor and other behaviours as shown in Figs. 4 and 5. Multiple aluminum injections produced significant behavioural outcomes including changes in locomotive behaviour, (Fig. 4) and induced memory deficits on water maze tasks (Fig. 5). Other behavioural measures including muscle strength and endurance as measured by the wire hang and motor coordination and balance as measured by rotarod were not significantly affected.

4. Discussion

The current results extend the preliminary results reported by Petrik et al. [8] by showing that microglial activation is part of the underlying pathology in the lumbar cord. These data add to those previously reported, i.e., the loss of motor and other neurons and the activation of reactive astrocytes. Taken together with the current data, the overall activation of a glial inflammatory response in lumbar cord suggests that this process is a key early stage of the pathological events leading to motor neuron death. This interpretation is supported by an absence of motor neuron loss and astrocyte activation in the other levels of the spinal cord observed in the present study. In ALS and in animal models of the disease, glial activation followed by motor neuron death often appears to proceed in sequential manner along the ventral neuraxis with the first signs of pathology appearing first in lumbar cord [31]. Given this, it seems possible that an examination of later time points would show pathological responses in the thoracic and cervical cord as well. Alternatively, the aluminum shown to be present in lumbar cord motor neurons may not

have reached these other spinal cord segments. Studies now in progress will determine if motor neurons in these other segments stain positively for aluminum.

The positive Morin staining in lumbar cord clearly demonstrates that post injection aluminum finds entry into this part of the nervous system. One possibility is that it does so by retrograde transport from muscles to motor neurons in particular segments. This seems unlikely given that our paradigm of injecting *subcutaneous* should not have targeted any particular spinal cord segment. Another possibility is that aluminum can enter the CNS in a systemic manner if it enters the circulatory system. Experiments in progress are designed to distinguish between these possibilities.

The presence of hyper-phosphorylated tau protein, one of the hallmarks of both Alzheimer's disease and ALS-PDC of Guam, in motor neurons in lumbar spinal cord clearly suggests that additional pathological processes associated with aluminum are occurring.

The behavioural outcomes in the second experiment reported here reinforce the pathological outcomes seen in the first studies. While the histological measurements from these studies are still pending, the extent of the behavioural deficits strongly suggests that we will observe widespread neuronal pathologies. The greater extent of the behavioural outcomes in this experiment may be related to the experimental paradigm that tripled the number of aluminum hydroxide injections.

Overall, the results reported here mirror previous work that has clearly demonstrated that aluminum, in both oral and injected forms, can be neurotoxic [15,16,32,33]. Potential toxic mechanisms of action for aluminum may include enhancement of inflammation (i.e., microgliosis) and the interference with cholinergic projections [34], reduced glucose utilization [33], defective phosphorylation-dephosphorylation reactions [35], altered rate of transmembrane diffusion and selective changes in saturable transport systems in the blood brain barrier (BBB) [36], and oxidative damage on cellular processes by the inhibition of the glutathione redox cycle [37].

Given the above, it is not surprising that aluminum has been widely proposed as a factor in neurodegenerative diseases and has been found in association with degenerating neurons in specific CNS regions [38–41]. In animal studies, aluminum has been linked to the accumulation of tau protein and amyloid-beta protein and observed to induce neuronal apoptosis *in vivo* as well as *in vitro*³⁰. Aluminum injected animals show severe anterograde degeneration of cholinergic terminals in cortex and hippocampus [42].

Aluminum in its adjuvant form can gain access to the CNS [42–44], however, oral administration of aluminum hydroxide gel does not appear to be neurotoxic in humans [45], although aluminum chloride is, in rats [46]. The route of exposure, and perhaps the form of aluminum, may be important factors that determine the potential for toxicity.

We speculate that the observed neurotoxic effects of aluminum hydroxide in the present study arise by both 'direct' and 'indirect' pathways, some of which are cited above. Direct toxicity refers to the physical presence (or close proximity) of aluminum and its potential for initiating cell death pathways. Accumulation of aluminum into the cytoplasm via cellular uptake mechanisms or diffusion could cause alterations in glutaminase and glutamine synthetase and easily alter the availability of the neurotransmitter glutamate [47]. Aluminum acting to induce abnormal tau protein accumulation could also increase neurofibrillary tangles and impair cellular transport mechanisms [48]. Outside the cell, aluminum could affect neurons by altering synapses. For example, aluminum has been shown to decrease the thickness of post-synaptic density, increase the width of the synaptic cleft, and increase the number of flat synapses [49]. Aluminum could also block voltage-activated calcium channels [50], augment the activity

of acetylcholinesterase [51], or interfere with synaptic transmission by merely accumulating in the synaptic cleft [52]. Aluminum can also induce apoptosis in astrocytes [53]. Since astrocytes are essential for maintaining neuronal health, any loss of astrocyte function could prove toxic to neurons. Indirect toxicity of aluminum could occur in various ways, including by activating various cytokines [54], releasing glutamate in an excitotoxic cascade, or by modifying various enzymatic pathways [55].

In addition to the above actions specifically on neural cells, aluminum might act indirectly by stimulating abnormal, generalized immune responses. This is, in fact, what adjuvants are placed in vaccines to do in the first place. Adjuvant neurotoxicity could thus be the result of an imbalanced immune response. Rook and Zumla [56] hypothesized that multiple vaccinations, stress, and the method of vaccination could lead to a shift in immune response [56,57]. Aluminum hydroxide has previously been shown to stimulate a Th2-cytokine response [9, 58].

While the current results and our previous study have demonstrated significant behavioural and neuropathological outcomes with aluminum hydroxide and some additionally significant outcomes due to a combination of adjuvants, it is important to recognize that these were achieved under *minimal* conditions. Table 1 summarizes aspects of human ALS and GWS symptoms compared with outcomes observed in aluminum-injected mice. The likelihood exists that a synergistic effect between adjuvants and other variables such as stress, multiple vaccinations, and exposure to other toxins likely occurs. A recent study examining some of these factors in combination showed that stress, vaccination, and pyridostigmine bromide (a carbamate anticholinesterase (AChE) inhibitor), may synergistically act on multiple stress-activated kinases in the brain to induce neurological impairments in GWS [59]. In addition, a genetic background in context to aluminum exposure may play a crucial role and may be an important area for future research.

The demonstration of neuropathological outcomes and behavioural deficits in aluminum hydroxide injected mice may provide some insight into the causes of not only GWS–ALS, but may open avenues of investigation into other neurological diseases.

Acknowledgments

This work was supported by grants from the Scottish Rite Charitable Foundation of Canada and the Natural Science and Engineering Research Council of Canada (to CAS). We thank Dr. Meryl Nass (Mount Desert Island Hospital, Maine, USA) and Lt. Col. John A. Richardson (USAFR, ret.) for their invaluable comments and advisory contributions to this project and manuscript.

References

1. Charatan F. *BMJ* 2002;324:65. [PubMed: 11786440]
2. Horner RD, Kamins KG, Feussner JR, Grambow SC, Hoff-Lindquist J, Harati Y, Mitsumoto H, Pascuzzi R, Spencer PS, Tim R, Howard D, Smith TC, Ryan MA, Coffman CJ, Kasarskis EJ. *Neurology* 2003;61:742–749. [PubMed: 14504315]
3. Haley RW. *Neurology* 2003;61:750–756. [PubMed: 14504316]
4. Weisskopf MG, O'Reilly EJ, McCullough ML, Calle EE, Thun MJ, Cudkovicz M, Ascherio A. *Neurology* 2005;64:32–37. [PubMed: 15642900]
5. Kurland LT. *Trends Neurosci* 1988;11:51–54. [PubMed: 2465598]
6. Whiting MG. *Econ Bot* 1963;17:271–302.
7. Garruto RM, Shankar SK, Yanagihara R, Salazar AM, Amyx HL, Gajdusek DC. *Acta Neuropathol Berl* 1989;78:210–219. [PubMed: 2750490]
8. Petrik MS, Wong MC, Tabata RC, Garry RF, Shaw CA. *Neuromol Med* 2007;9:83–100.

9. Brewer JM, Conacher M, Hunter CA, Mohrs M, Brombacher F, Alexander J. *J Immunol* 1999;163:6448–6454. [PubMed: 10586035]
10. Lindblad EB. *Vaccine* 2004;22:3658–3668. [PubMed: 15315845]
11. Baylor NW, Egan W, Richman P. *Vaccine* 2002;20(Suppl 3):S18–S23. [PubMed: 12184360]
12. Kanra G, Viviani S, Yurdakok K, Ozmert E, Anemona A, Yalcin S, Demiralp O, Bilgili N, Kara A, Cengiz AB, Mutlu B, Baldini A, Marchetti E, Podda A. *Pediatr Int* 2003;45:314–318. [PubMed: 12828588]
13. Jefferson T, Rudin M, Di Pietrantonj C. *Lancet Infect Dis* 2004;4:84–90. [PubMed: 14871632]
14. Lindblad EB. *Immunol Cell Biol* 2004;82:497–505. [PubMed: 15479435]
15. Crapper DR, Krishnan SS, Dalton AJ. *Science* 1973;180:511–513. [PubMed: 4735595]
16. Kawahara M, Kato M, Kuroda Y. *Brain Res Bull* 2001;55:211–217. [PubMed: 11470317]
17. Garruto RM, Yanagihara R, Gajdusek DC. *Neurology* 1985;35:193–198. [PubMed: 3969206]
18. Wagner-Recio M, Toews AD, Morell P. *J Neurochem* 1991;57:1891–1901. [PubMed: 1940905]
19. Bilkei-Gorzo A. *Food Chem Toxicol* 1993;31:357–361. [PubMed: 8505021]
20. Verdier F, Burnett R, Michelet-Habchi C, Moretto P, Fievet-Groyne F, Sauzet E. *Vaccine* 2005;23:1359–1367. [PubMed: 15661384]
21. Kalil RK, Monteiro A Jr, Lima MI, Silveira EB, Foltran FS, Martins CE, Rizzo IM. *Ultrastruct Pathol* 2007;31:45–50.
22. Exley C, Swarbrick L, Gherardi RK, Authier FJ. *Med Hypotheses* 2009;72:135–139. [PubMed: 19004564]
23. Sidman, RL.; Angevine, JB., Jr; Pierce, ET. *Atlas of the Mouse Brain and Spinal Cord*. Harvard University Press; Massachusetts: 1971.
24. Paxinos, G.; Franklin, KBJ. *The Mouse Brain in Stereotaxic Coordinates*. second. Academic Press; San Diego: 2001.
25. Wetts R, Vaughn JE. *Exp Neurol* 1996;141:248–255. [PubMed: 8812158]
26. Maatkamp A, Vlug A, Haasdijk E, Troost D, French PJ, Jaarsma D. *Eur J Neurosci* 2004;20:14–28. [PubMed: 15245475]
27. Lee VM, Page CD, Wu HL, Schlaepfer WW. *J Neurochem* 1984;42:25–32. [PubMed: 6358415]
28. Tohyama T, Lee VM, Rorke LB, Trojanowski JQ. *J Comp Neurol* 1991;310:285–299. [PubMed: 1787174]
29. Imai Y, Ibata I, Ito D, Ohsawa K, Kohsaka S. *Biochem Biophys Res Commun* 1996;224:855–862. [PubMed: 8713135]
30. De Boni U, Scott JW, Crapper DR. *Histochemistry* 1974;40:31–37. [PubMed: 4136834]
31. Tabata RC, Wilson JMB, Ly P, Zwieggers P, Kwok D, Van Kampen JM, Cashman N, Shaw CA. *Neuromol Med* 2008;10:24–39.
32. Banks WA, Kastin AJ. *Neurosci Biobehav Rev* 1989;13:47–53. [PubMed: 2671833]
33. Joshi JG. *Biofactors* 1990;2:163–169. [PubMed: 2198876]
34. Platt B, Fiddler G, Riedel G, Henderson Z. *Brain Res Bull* 2001;55:257–267. [PubMed: 11470325]
35. Cordeiro JM, Silva VS, Oliveira CR, Goncalves PP. *J Inorg Biochem* 2003;97:132–142. [PubMed: 14507469]
36. Kaya M, Kalayci R, Arican N, Kucuk M, Elmas I. *Biol Trace Elem Res* 2003;92:221–230. [PubMed: 12794274]
37. Murakami NJ. *J Neurol* 1999;256(Suppl 2):II16–II18. [PubMed: 10525998]
38. Perl DP, Gajdusek DC, Garruto RM, Yanagihara RT, Gibbs CJ. *Science* 1982;217:1053–1055. [PubMed: 7112111]
39. Perl DP, Penderbury WW. *Can J Neurol Sci* 1986;13:441–445. [PubMed: 3791060]
40. Rao JK, Katselos CD, Herman MM, Savory J. *Clin Lab Med* 1998;18:687–698. [PubMed: 9891607]
41. Savory J, Garruto RM. *Nutrition* 1998;14:313–314. [PubMed: 9583377]
42. Wen GY, Wisniewski HM. *Acta Neuropathol (Berl)* 1985;68:175–184. [PubMed: 2417440]
43. Redhead K, Quinlan GJ, Das RG, Gutteridge JM. *Pharmacol Toxicol* 1992;70:278–280. [PubMed: 1608913]

44. Sahin G, Varol I, Temizer A, Benli K, Demirdamar R, Duru S. *Biol Trace Elem Res* 1994;41:129–135. [PubMed: 7946900]
45. Rosati G, De Bastiani P, Gilli P, Paolino E. *J Neurol* 1980;223:251–257. [PubMed: 6157787]
46. Walton JR. *Neurosci Lett* 2007;412:29–33. [PubMed: 17156917]
47. Zielke HR, Jackson MJ, Tildon JT, Max SR. *Mol Chem Neuropathol* 1993;19:219–233. [PubMed: 8104402]
48. Bizzi A, Crane RC, Autilio-Gambetti L, Gambetti P. *J Neurosci* 1984;4:722–731. [PubMed: 6200578]
49. Jing Y, Wang Z, Song Y. *Synapse* 2004;15:292–298. [PubMed: 15103695]
50. Busseberg D, Platt B, Haas HL, Carpenter DO. *Brain Res* 1993;622:163–168. [PubMed: 8242354]
51. Zatta P, Ibn-Lkhatay-Idrissi M, Zambenedetti P, Kilyen M, Kiss T. *Brain Res Bull* 2002;59:41–45. [PubMed: 12372547]
52. Banin E, Meiri H. *Brain Res* 1987;423:359–363. [PubMed: 3676813]
53. Aremu DA, Meshitsuka S. *Brain Res* 2005;1031:284–296. [PubMed: 15649454]
54. Johnson VJ, Sharma RP. *Neurotoxicity* 2003;24:261–268.
55. Nayak P, Chatterjee AK. *Food Chem Toxicol* 2001;39:1285–1289. [PubMed: 11696403]
56. Rook GA, Zumla A. *Lancet* 1997;349:1831–1833. [PubMed: 9269228]
57. Rook GA, Zumla A. *Hosp Med* 1998;59:10–11. [PubMed: 9798557]
58. Valensi JP, Carlson JR, Van Nest GA. *J Immunol* 1994;153:4029–4039. [PubMed: 7930610]
59. Wang D, Perides G, Liu YF. *J Neurochem* 2005;93:1010–1020. [PubMed: 15857404]

Abbreviations

chE	Anticholinesterase
ALS–PDC	Amyotrophic lateral sclerosis- parkinsonism dementia complex
AVA	Anthrax vaccine adsorbed
BSA	Bovine serum albumin
GFAP	Glial fibrillary acidic protein
ChAT	Choline acetyltransferase
GWS	Gulf War Syndrome
NGS	normal goat serum
OCT	Optimum cutting temperature
PBST	Phosphate buffer saline – Tween 20
PFA	Paraformaldehyde

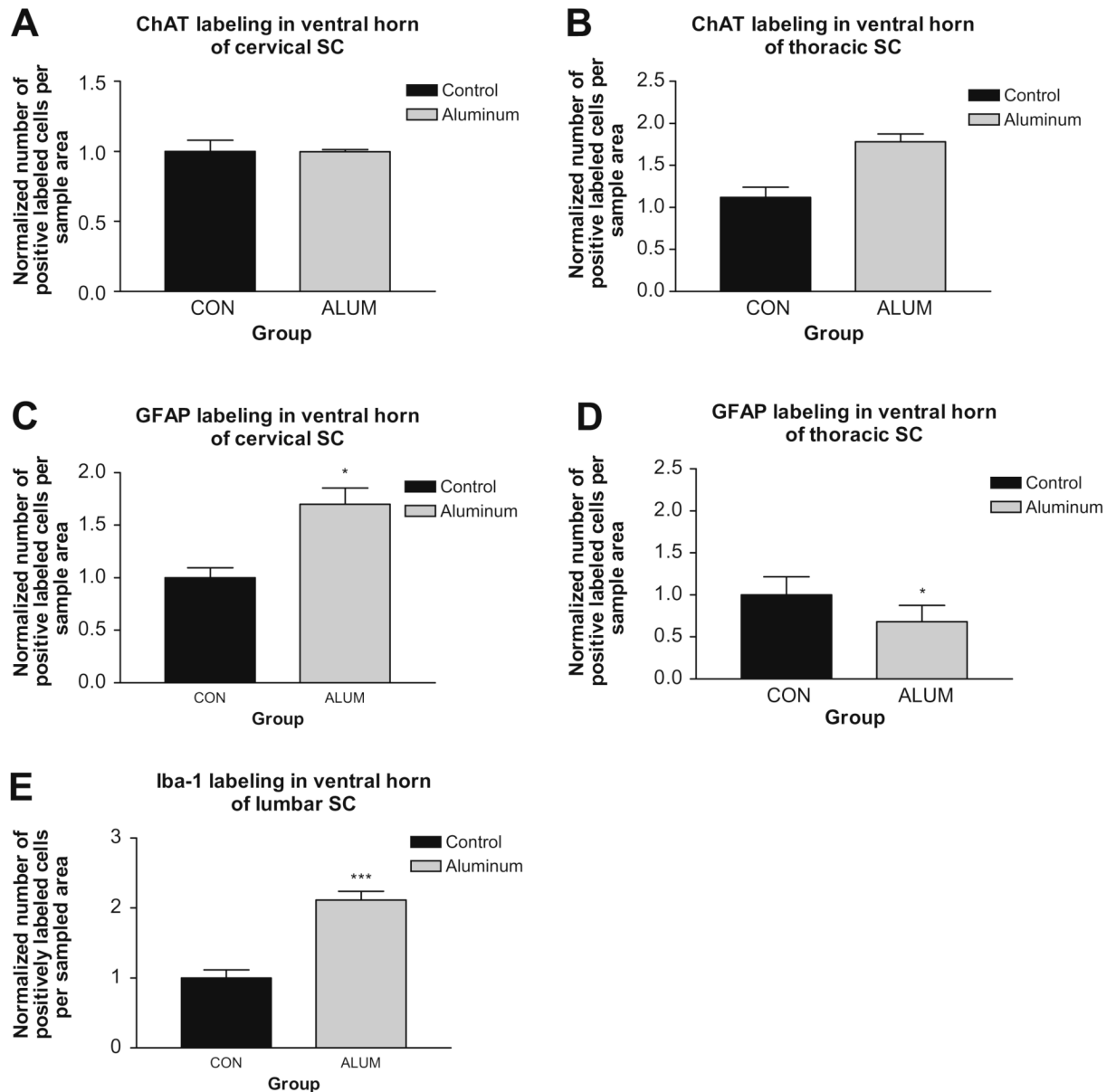


Fig. 1. Impact of aluminum hydroxide on different levels of spinal cord (SC). (A and B) ChAT labeling in cervical and thoracic cords, respectively. (C and D) Normalized cell counts for GFAP labeling of reactive astrocytes in cervical and thoracic spinal cord, respectively. In cervical cord, the aluminum hydroxide treated groups showed higher levels of GFAP labeling with the aluminum alone group achieving statistical significance. (E) Iba-1 fluorescent labeling in the ventral horn of mouse lumbar cord showed that aluminum-injected mice had significantly increased numbers of activated microglia. Data are means \pm S.E.M. *** $p < 0.001$, one-way ANOVA.

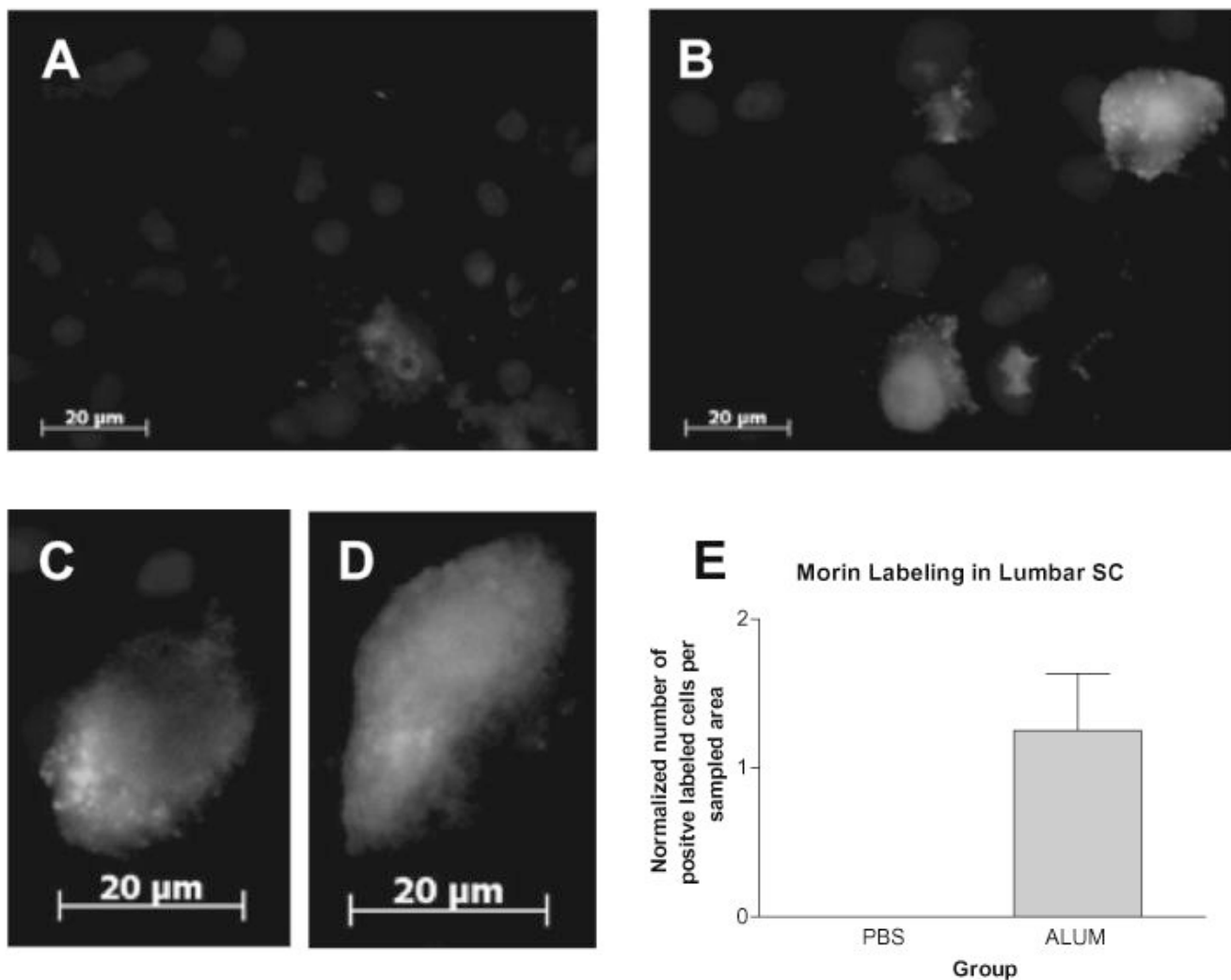


Fig. 2. Morin fluorescent labeling in ventral horn of mouse lumbar spinal cord. Sections from control (A) mice showed no Morin fluorescent labeling. Scale bar = 20 μm. (B) Morin-positive motor neurons in aluminum hydroxide treated mice. (C and D) Higher power of motor neurons in aluminum-injected mice showing show high levels of cytoplasmic Morin labeling. Scale bar = 20 μm. (E) Cell counts for Morin positive cells in the different treatment groups ($n = 4$ mice/group, four sections each). Data are mean \pm S.E.M. One-way ANOVA analysis revealed a significance level of $*p < 0.05$.

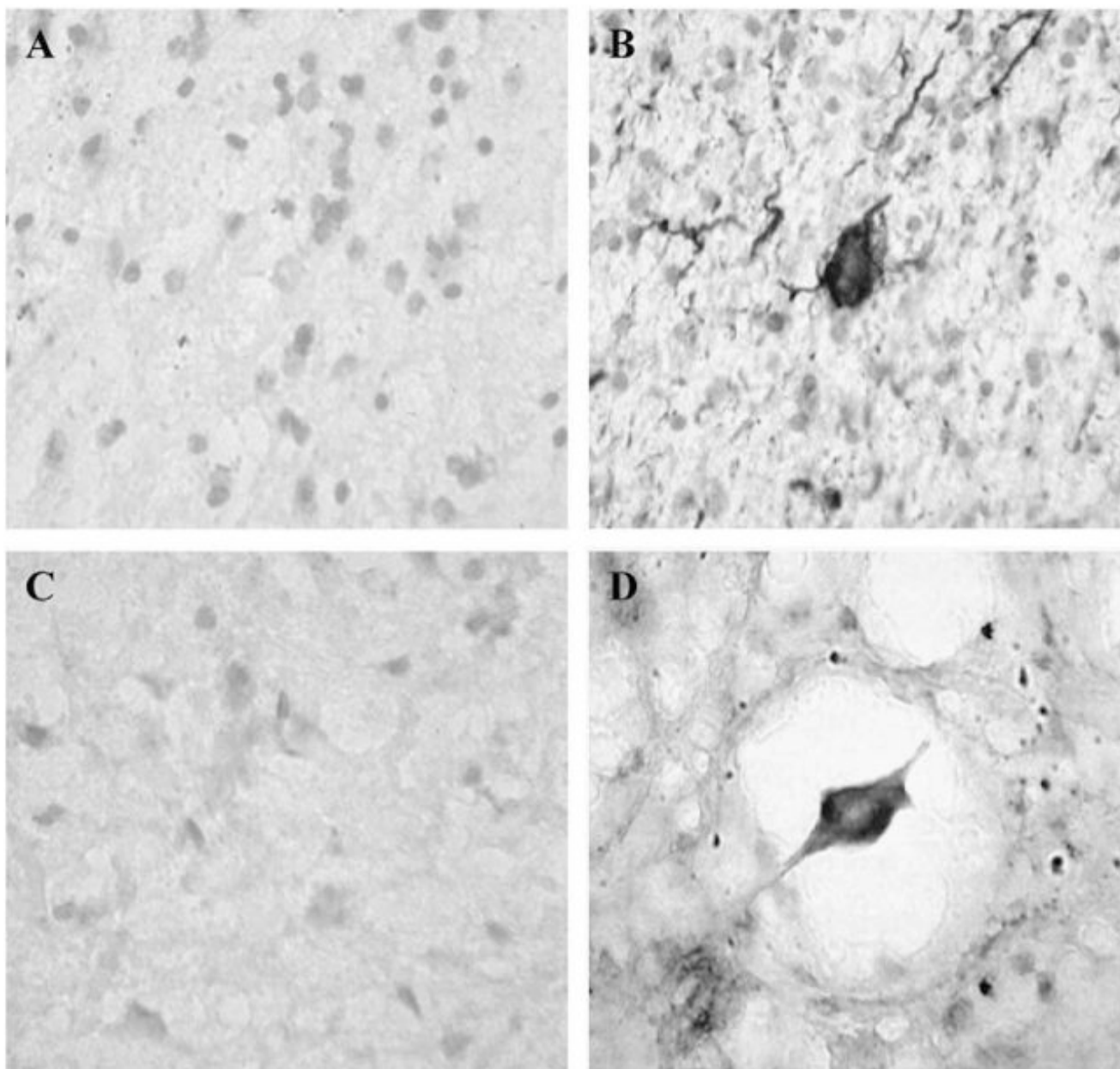


Fig. 3. Hyper-phosphorylated tau immunostaining in the ventral horn of mouse lumbar spinal cord compared to Alzheimer's disease. (A) A section of human entorhinal cortex from a control patient. (B) Human entorhinal cortex section from a patient with Alzheimer's disease (sections kindly provided courtesy of Dr. P. McGeer). (C) Lumbar spinal cord sample from a saline injected mouse. (D) Equivalent section from an aluminum hydroxide injected mouse. All pictures are 100× magnification.

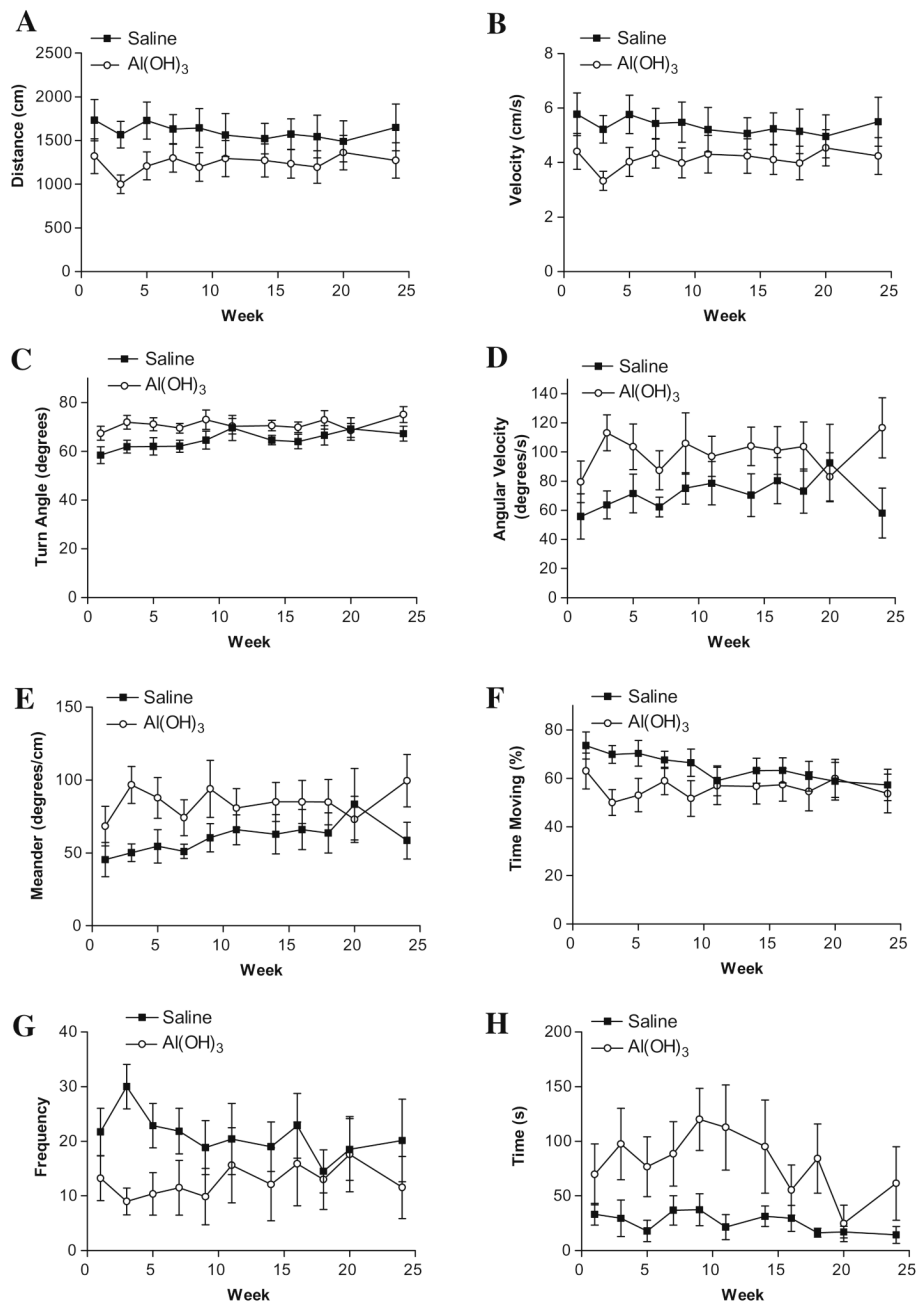


Fig. 4. Open field movement analysis as an assessment of spontaneous activity and anxiety in control mice vs. mice injected six times with aluminum hydroxide. Aluminum hydroxide injected mice showed the following behavioural changes: (A) Shorter distances moved ($***p < 0.0001$). (B) Slower movement ($***p < 0.0001$). (C) Greater mean turn angle ($***p < 0.0001$). (D) More rapid turning ($***p < 0.0001$). (E) Greater meander ($***p < 0.0001$). (F) Smaller percentage of time in overall movement ($**p = 0.0030$). (G) Fewer entries into the centre of the open field ($***p < 0.001$). Late entry into centre ($***p < 0.0001$). (All measures, two-way ANOVA).

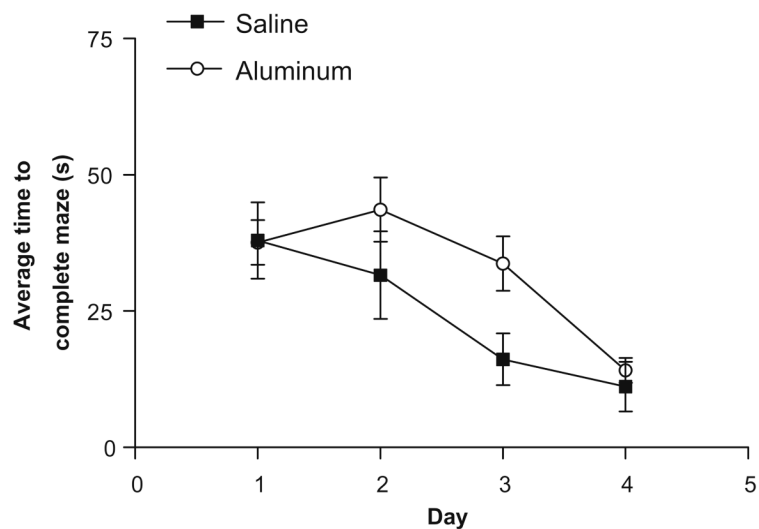


Fig. 5. Water maze test as an evaluation of learning and memory. Mice injected 6× with aluminum hydroxide on average took significantly longer to complete the maze compared to saline injected mice (two-way ANOVA. * $p = 0.0389$).

Table 1

Summary of human ALS and GWI symptoms compared with symptoms observed in aluminum-treated mice and rats. This table also outlines the similarities between human ALS and Gulf War illness.

Animal	Age	Dose	Injection type	Result	Reference
Female NIH mice	4 week	315–335 µg/kg	i.p.	Significantly elevated levels of Al in brain	Redhead et al., 1991
Male and female Long Evan rats	2 month	100 or 300 mg/kg/day	Oral	Significantly reduced learning ability and elevated levels of Al in brain	Bilkei-Gorzo, 1993
Male Swiss albino mice	Not stated	~20 µg/kg/day	Oral	Significantly elevated levels of Al in brain, kidney and liver.	Sahin et al., 1994
Pzh:SFIS mice	Not stated	1.0 mg every 2 weeks or 0.1 mg 5 days/week	i.p.	Significantly elevated levels of Al in liver and tibia (bone), but not in brain.	Fiejka et al., 1996



Administration of aluminium to neonatal mice in vaccine-relevant amounts is associated with adverse long term neurological outcomes



C.A. Shaw ^{a b c}  , Y. Li ^a, L. Tomljenovic ^a

Show more 

 Share  Cite

<https://doi.org/10.1016/j.jinorgbio.2013.07.022> ↗

[Get rights and content](#) ↗

Highlights

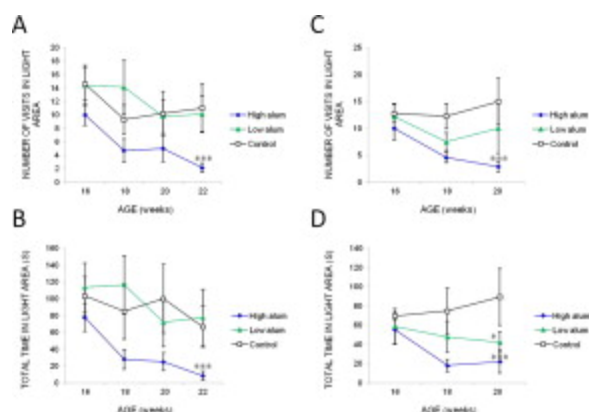
- Aluminium (Al) salts are the most widely used vaccine adjuvants today.
- Al adjuvants can persist in the body long-term and penetrate the blood-brain barrier.
- Al adjuvants can trigger adverse neurobehavioral outcomes in vaccine-relevant exposures.
- Efforts should be made to reduce Al exposure from vaccines.

Abstract

Our previous ecological studies of autism spectrum disorder (ASD) has demonstrated a correlation between increasing ASD rates and aluminium (Al) adjuvants in common use in paediatric vaccines in several Western countries. The correlation between ASD rate and Al adjuvant amounts appears to be dose-dependent and satisfies 8 of 9 Hill criteria for causality. We have now sought to provide an animal model to explore potential behavioural phenotypes and central nervous system (CNS) alterations using s.c. injections of Al hydroxide in early postnatal CD-1 mice of both sexes. Injections of a “high” and “low” Al adjuvant levels were designed to correlate to either the U.S. or Scandinavian paediatric vaccine schedules vs. control saline-injected mice. Both male and female mice in the “high Al” group showed significant weight gains following treatment up to sacrifice at 6 months of age. Male mice in the “high Al” group showed significant changes in light–dark box tests and in various measures of behaviour in an open field. Female mice showed significant changes in the light–dark box at both doses, but no significant changes in open field behaviours. These current data implicate Al injected in early postnatal life in some CNS alterations that may be relevant for a better understanding of the aetiology of ASD.

Graphical abstract

Repetitive administration of aluminium to neonatal mice in amounts comparable to those to children receive via routine vaccinations significantly increases anxiety and reduces exploratory behaviour and locomotor activities. The neurodisruptive effects of aluminium are long-lasting and persist for 6 months following injection.



[Download: Download full-size image](#)

Introduction

Aluminium (Al) is the most abundant metal and third most common element in the Earth's crust [1]. Normally chemically bound to other elements, Al is not typically bioavailable and indeed seems to play no role in any known biochemistry of plants, animals or humans. In the last 150 years, however, Al through human activities has become much more prevalent in the human environment. Notably, Al is widely used in industrial and material applications, is widely found in processed foods, is contained in various medicinal compounds, and can be used as a flocculant in water treatment. Because of such ubiquity, it is increasingly found in our bodies [2], [3], [4], [5]. Overall, we now live in what has been termed "The Aluminium Age" [6].

For all of its positive properties as a material, Al is also demonstrably toxic to biological systems [1], an observation that has been in the scientific literature for at least a century [7]. Although Al may deleteriously impact various organ systems, some of its worst impacts may be on the nervous system (for a review, see [2]). Some of the toxic actions of Al on the nervous system include: disruption of synaptic activity, misfolding of crucial proteins, promotion of oxidant stress, and increased permeability of the blood–brain barrier [2], [8], to mention only a few of the more egregious impacts. In particular, Al has been implicated in Alzheimer's disease [2], [4], [9], [10] and animal models of the disease clearly demonstrate Al-induced cognitive deficits and pathologies [11], [12], [13]. Al vaccine adjuvants, in use since the mid 1920s [14], have been shown to produce Lou Gehrig's-like motor phenotypes in mice and motor neuron degeneration [15], [16]. The neurotoxic effects of Al adjuvants have been discussed in previous publications by our group [17], [18], [19] and by others [20], [21], [22], [23]. Additionally, Al in vaccines has been linked to the induction of autoimmune diseases [24], [25], [26], [27].

Recently, we compared the amount of Al in various national paediatric vaccine schedules with increasing rates of autism spectrum disorder (ASD) and found a significant correlation that appeared to be dose-dependent [28]. These ecological data satisfied 8 or 9 so-called Hill criteria for causality [29]. Similar conclusions about a potential role of Al adjuvants in ASD have been discussed by other investigators [30], [31].

The above results led us to attempt to create an animal model of ASD based on early life administration of Al adjuvants by injection. The current manuscript describes the behavioural outcomes of this study. A future publication will address central nervous system (CNS) alterations.

Access through your organization

Check access to the full text by signing in through your organization.

Section snippets

Aluminium adjuvant

Alhydrogel®, an aluminium hydroxide (Al(OH)₃) gel suspension, was used as a source of aluminium hydroxide. Alhydrogel is manufactured by Superfos Biosector a/s (Denmark) and was purchased from SIGMA Canada. This formulation of the gel is presumed to be similar to that used in proprietary commercial vaccines, which may, however, differ in some chemical properties. ...

Dosage and administration

An example of the U.S. vaccination schedule is shown in Table 1 for reference. Previously, we estimated the amounts of Al per kg of ...

Overall mouse development

No significant mortality and no overt morbidity were observed in the groups of pups injected with either Al or saline control. There were however two cases of mortality recorded during the experimental period. One was a case of bilateral pyelonephritis with subsequent septicaemia in the group of male mice who received the “high Al” injection schedule. According to the necropsy report by the Animal Care Facility, the pyelonephritis may have been caused by bacterial infections (i.e., *E. coli* ...

Discussion

The present results demonstrate, to our knowledge for the first time, long-term alteration of behavioural responses in mice as a result of Al treatment by injection early in postnatal life. The administration of Al was meant to mimic the exposure of human infants to the standard paediatric schedules of various Western countries which we have previously linked to changing rates of ASD in these same countries [28].

In our experiment, mice of both sexes injected under the “high Al” schedule showed ...

Conclusions

Al salts are the most widely used adjuvants today and have been since the 1920s [14]. The fact that they can trigger pathological immunological responses and a cascade of unwanted health effects has been relatively under-appreciated to date [16], [17], [18], [19], [20], [21], [22], [23], [24], [25], [26], [27], [30], [45], [72], [73], [80], [84], [89]. Nevertheless, it is clear that the problem with vaccine-derived Al is three-fold: it can persist in the body, it can trigger pathological ...

Acknowledgements

The authors thank the Dwoskin Family Foundation and the Katlyn Fox Foundation for their financial support. We are also grateful to Agripina Suarez and other laboratory members for their assistance. ...

[Recommended articles](#)

References (89)

J.R. Walton

Neurotoxicology (2006)

W.A. Banks *et al.*

Neurosci. Biobehav. Rev. (1989)

C. Exley

J. Inorg. Biochem. (1999)

J.R. Walton *et al.*

J. Inorg. Biochem. (2009)

J.R. Walton

Neurotoxicology (2009)

J.R. Walton

J. Inorg. Biochem. (2007)

C.A. Shaw *et al.*

J. Inorg. Biochem. (2009)

E. Passeri *et al.*

J. Inorg. Biochem. (2011)

M. Couette *et al.*

J. Inorg. Biochem. (2009)

A. Batista-Duharte *et al.*

Toxicol. Lett. (2011)



View more references

Cited by (61)

Autism spectrum disorder: Trace elements imbalances and the pathogenesis and severity of autistic symptoms

2021, Neuroscience and Biobehavioral Reviews

Citation Excerpt :

...In most of these studies, patients' hair was used as study material, less often – the blood or urine. Further research into the relevance of Al in autism is motivated by the fact that the use of pediatric vaccines containing aluminum adjuvant directly correlates with the increase in the incidence of ASD (Tomljenovic and Shaw, 2011; Shaw et al., 2013). There exist numerous studies that describe disturbances in mineral levels in autistic children....

[Show abstract](#) ✓

Aluminium in brain tissue in autism

2018, Journal of Trace Elements in Medicine and Biology

[Show abstract](#) ✓

Autism genes are selectively targeted by environmental pollutants including pesticides, heavy metals, bisphenol A, phthalates and many others in food, cosmetics or household products

2016, Neurochemistry International

[Show abstract](#) ✓

Low levels of aluminum can lead to behavioral and morphological changes associated with Alzheimer's disease and age-related neurodegeneration

2016, NeuroToxicology

[Show abstract](#) 

Comparative Safety of Vaccine Adjuvants: A Summary of Current Evidence and Future Needs [↗](#)

2015, Drug Safety

Biopersistence and brain translocation of aluminum adjuvants of vaccines [↗](#)

2015, Frontiers in Neurology



[View all citing articles on Scopus](#) [↗](#)

[View full text](#)

Copyright © 2013 Elsevier Inc. All rights reserved.



All content on this site: Copyright © 2024 Elsevier B.V., its licensors, and contributors. All rights are reserved, including those for text and data mining, AI training, and similar technologies. For all open access content, the Creative Commons licensing terms apply.



FULL TEXT LINKS

[Comparative Study](#) > [Ann Neurol](#). 2005 Jan;57(1):67-81. doi: 10.1002/ana.20315.

Neuroglial activation and neuroinflammation in the brain of patients with autism

Diana L Vargas ¹, Caterina Nascimbene, Chitra Krishnan, Andrew W Zimmerman, Carlos A Pardo

Affiliations

PMID: 15546155 DOI: [10.1002/ana.20315](#)

Erratum in

[Ann Neurol](#). 2005 Feb;57(2):304

Abstract

Autism is a neurodevelopmental disorder characterized by impaired communication and social interaction and may be accompanied by mental retardation and epilepsy. Its cause remains unknown, despite evidence that genetic, environmental, and immunological factors may play a role in its pathogenesis. To investigate whether immune-mediated mechanisms are involved in the pathogenesis of autism, we used immunocytochemistry, cytokine protein arrays, and enzyme-linked immunosorbent assays to study brain tissues and cerebrospinal fluid (CSF) from autistic patients and determined the magnitude of neuroglial and inflammatory reactions and their cytokine expression profiles. Brain tissues from cerebellum, midfrontal, and cingulate gyrus obtained at autopsy from 11 patients with autism were used for morphological studies. Fresh-frozen tissues available from seven patients and CSF from six living autistic patients were used for cytokine protein profiling. We demonstrate an active neuroinflammatory process in the cerebral cortex, white matter, and notably in cerebellum of autistic patients. Immunocytochemical studies showed marked activation of microglia and astroglia, and cytokine profiling indicated that macrophage chemoattractant protein (MCP)-1 and tumor growth factor-beta1, derived from neuroglia, were the most prevalent cytokines in brain tissues. CSF showed a unique proinflammatory profile of cytokines, including a marked increase in MCP-1. Our findings indicate that innate neuroimmune reactions play a pathogenic role in an undefined proportion of autistic patients, suggesting that future therapies might involve modifying neuroglial responses in the brain.

[PubMed Disclaimer](#)

Related information

[Cited in Books](#)[MedGen](#)

LinkOut - more resources

Full Text Sources

[Wiley](#)

Other Literature Sources

[The Lens - Patent Citations Database](#)

Medical

[MedlinePlus Health Information](#)

Miscellaneous

[NCI CPTAC Assay Portal](#)



Distinct Cytokine and Chemokine Profiles in Autism Spectrum Disorders

Yvonne M. Y. Han¹, Winnie K. Y. Cheung², Chun Kwok Wong³, Sophia L. Sze^{2,4},
Timmy W. S. Cheng³, Michael K. Yeung² and Agnes S. Chan^{2,4*}

¹Department of Rehabilitation Sciences, The Hong Kong Polytechnic University, Hong Kong, China, ²Neuropsychology Laboratory, Department of Psychology, The Chinese University of Hong Kong, Hong Kong, China, ³Department of Chemical Pathology, Prince of Wales Hospital, The Chinese University of Hong Kong, Hong Kong, China, ⁴Chanwuyi Research Center for Neuropsychological Well-Being, The Chinese University of Hong Kong, Hong Kong, China

OPEN ACCESS

Edited by:

Fabrice Cognasse,
The Rhone-Alpes-Auvergne
Regional Branch of the French
National Blood System, France

Reviewed by:

Gabor Csanyi,
Georgia Regents Medical Center,
USA
Randall Davis,
Oklahoma State University Center for
Health Sciences, USA

*Correspondence:

Agnes S. Chan
aschan@psy.cuhk.edu.hk

Specialty section:

This article was submitted to
Inflammation,
a section of the journal
Frontiers in Immunology

Received: 13 October 2016

Accepted: 04 January 2017

Published: 23 January 2017

Citation:

Han YMY, Cheung WKY, Wong CK,
Sze SL, Cheng TWS, Yeung MK and
Chan AS (2017) Distinct Cytokine
and Chemokine Profiles in Autism
Spectrum Disorders.
Front. Immunol. 8:11.
doi: 10.3389/fimmu.2017.00011

Previous studies have shown that immunological factors are involved in the pathogenesis of autism spectrum disorders (ASDs). However, this research has been conducted almost exclusively in Western contexts, and only a handful of studies on immune measures have been conducted in Asian populations, such as Chinese populations. The present study examined whether immunological abnormalities are associated with cognitive deficits and problem behaviors in Chinese children with ASD and whether these children show different immunological profiles. Thirteen typically developing (TD) children and 22 children with ASD, aged 6–17 years, participated voluntarily in the study. Executive functions and short-term memory were measured using neuropsychological tests, and behavioral measures were assessed using parent ratings. The children were also assessed on immunological measures, specifically, the levels of cytokines and chemokines in the blood serum. Children with ASD showed greater deficits in cognitive functions, as well as altered levels of immunological measures, including CCL2, CCL5, and CXCL9 levels, compared to TD children, and the cognitive functions and associated behavioral deficits of children with ASD were significantly associated with different immunological measures. The children were further sub-classified into ASD with only autistic features (ASD-only) or ASD comorbid with attention deficit hyperactivity disorder (ASD + ADHD). The comorbidity results showed that there were no differences between the two groups of ASD children in any of the cognitive or behavioral measures. However, the results pertaining to immunological measures showed that the children with ASD-only and ASD + ADHD exhibited distinct cytokine and chemokine profiles and that abnormal immunologic function was associated with cognitive functions and inattention/hyperactivity symptoms. These results support the notion that altered immune functions may play a role in the selective cognitive and behavioral symptoms of ASD.

Keywords: immunologic function, autism, cognitive function, hyperactivity, comorbidity

INTRODUCTION

One essential finding in autism spectrum disorder (ASD) research has been the consistent immunological abnormality detected among autistic individuals. Although it is largely unknown how the immunologic factor specifically affects the neural networks in the brains of individuals with ASD, dysfunctional immune profiles involving inflammatory changes in the CNS have been documented in ASD. For example, increased levels of inflammatory cytokine transforming growth factor beta 1 [TGF β 1; (1)], chemokine macrophage chemoattractant CCL2 (1), and CXCL8 (2) were found in the brains of individuals with ASD. In addition to the elevated neuroinflammatory response in the autistic brain, altered levels of circulating cytokines and chemokine have also been reported. For example, higher levels of macrophage migration inhibitory factor (MIF) and CXCL8 were observed in plasma and cerebrospinal fluid (CSF) specimens from individuals with ASD compared with those from typically developing (TD) controls and subjects with other developmental disabilities (1, 3–5). In addition, elevated plasma CCL5 and CCL2 were observed in ASD, whereas increased CCL2 found newborn bloodspot specimens have been shown to be related to the risk of ASD (1, 6, 7). Similarly, altered levels of TGF β 1 have also been found in plasma and serum specimens of ASD compared with TD controls (8–10). These findings suggest that the increased inflammatory chemokine and cytokine production detected in the brain and peripheral blood of autistic individuals may produce a profoundly negative effect on proper neuronal development, migration, differentiation, and synapse formation and subsequently affect the behavior of individuals with ASD (1, 11, 12). Consistent with these findings, cytokine and chemokine levels have been shown to correlate with the severity of behavioral abnormalities in individuals with ASD. Increased plasma levels of MIF have been correlated with more severe social impairment and decreased imaginative play (4), whereas lower TGF β 1 levels have been associated with more stereotypy, irritability, hyperactivity, and other behavioral symptoms and fewer adaptive behaviors (8). Significant associations between increased plasma levels of CCL5 and CXCL8 and more frequent aberrant behaviors and fewer adaptive behaviors have also been found (3, 6).

Although the aforementioned studies have indicated plausible links between the severity of certain core behavioral symptoms and shifts in cytokine and chemokine levels in ASD, it is important to note that the exploration of neuroinflammatory mechanisms in ASD has been based predominantly on research conducted in Western populations, of which the expression of autistic traits does not necessarily extend to all populations. For example, ASD children from Western populations (United Kingdom and United States) showed significantly greater deficits in the domains of non-verbal communication/socialization and insistence on sameness/restricted interests than ASD children from Eastern populations (Israel and South Korea), as was demonstrated in a study conducted by Matson et al. (13). Therefore, it may be worth considering whether the immunological profiles in ASD differ according to ethnicity. Moreover, it will be interesting to determine whether the observed ethnic differences in the symptoms of ASD are reflected in their immunological profiles such that ethnic differences are

also observed in the levels of cytokine and chemokine production among autistic individuals from different ethnic backgrounds. Hence, our present study attempted to add new knowledge regarding the ethnic aspects of immunological dysfunctions in the peripheral blood of Chinese individuals with ASD.

Furthermore, although the relationship between the levels of cytokine and chemokine production and the severity of cognitive outcomes have been detected in ASD (3, 4, 6, 8), reports of peripheral chemokine levels have been inconsistent. For example, while higher levels of CCL2, CCL5, and CXCL10 were found in individuals with ASD than in TD controls in either plasma or CSF specimens (1, 6, 7), lower plasma levels of these three chemokines were detected in ASD subjects with fragile X syndrome (FXS, a single-gene disorder characterized by autistic symptoms) compared to TD controls (14). Similarly, several studies have reported decreased levels of TGF β 1 measured in plasma and serum (8–10), whereas the opposite trend has been observed in the brain tissue of individuals with ASD (1). Considering the discrepancies in the levels of cytokine and chemokine production reported in previous studies, it is questionable whether this relationship arises simply because chemokine and cytokine levels vary between different samples or because of the complexity of the clinical diagnosis of ASD, in which autism may be comorbid with symptoms associated with other neurological disorders, leading to the expression of different immunological profiles. Indeed, differing levels of chemokines were found between individuals with ASD + FXS and individuals with ASD-only, as well as between autistic individuals with regression and those with early onset of ASD (3, 14). Because there is a significant proportion of individuals with ASD comorbid with AD/HD symptoms (ASD + ADHD) who demonstrate a more severe profile of cognitive and behavioral impairment compared to individuals with only autistic features, this study also aimed to explore whether individuals with ASD and individuals with ASD + ADHD demonstrate different immunological profiles in terms of cytokine and chemokine production levels (15–19).

The purpose of the present study was therefore to (a) explore whether the patterns of the serum cytokine levels and chemokine production observed in individuals with ASD from Western populations would be replicated in ASD children from Eastern populations and (b) investigate whether the immunological measures of ASD would be associated with the severity of their behavioral and cognitive symptoms. To further highlight the relationship between altered immune functions and the diversity of autistic phenotypes, this study also aimed to (c) determine whether individuals diagnosed with ASD and co-diagnosed with ASD and ADHD would demonstrate different cytokine and chemokine profiles compared to their age- and IQ-matched TD counterparts. Drawing together the pieces of evidence linking ASD with altered immunologic function, we hypothesized that relative to TD children, Chinese children with ASD would show altered levels of inflammatory chemokine and cytokine in the blood serum. In addition, given that altered pro-inflammatory profile might be associated with neuronal damage which leads to the behavioral abnormalities in individuals with ASD, it was hypothesized that the specific panels of pro-inflammatory cytokines and chemokines would be associated with the severity of the cognitive dysfunction and behavioral problems in the

children with the disorder. Finally, considering the discrepancies in the levels of cytokine and chemokine production reported in previous studies, it was further hypothesized that the children with ASD would have a different cytokine and chemokine profile from those comorbid with ADHD.

MATERIALS AND METHODS

Participants

Participants in the study were recruited by posting advertisement on our websites and sending emails to parents in our existing database at the Neuropsychology Laboratory of the Chinese University of Hong Kong. Seventeen TD children and 23 children with ASD, aged 6–17 years, participated voluntarily in the study with their parents' written consent. All children with ASD were diagnosed by a clinical psychologist based on the diagnostic criteria of DSM-V (20), and the information collected from the Autism Diagnostic Interview-Revised [ADI-R; (21)]. Of the 23 children with ASD, 10 children also demonstrated prominent symptoms of attention deficit hyperactivity disorder (ADHD) that warranted a comorbid diagnosis of ASD and ADHD (ASD + ADHD) and 13 met the diagnostic criteria of ASD with no or only mild ADHD-like features that did not meet the diagnostic criteria of ADHD (ASD-only). The TD children had no history of delay in developmental milestones or any neurological or psychiatric disorders as reported by their parents; the children were screened for autism traits using the ADI-R and the Social Responsiveness Scale [SRS-2; (22)]. One ASD + ADHD child who was prescribed immunosuppressive drugs was excluded from the study, and four children from the TD group were also excluded because their scores were either above the cutoff scores of 10, 9, and 3 in the three subscales (reciprocal social interaction, communication, repetitive/restricted and stereotyped patterns of behaviors, respectively) of the ADI-R ($n = 3$), or of the total raw score of 70 in the SRS-2 ($n = 1$).

Tables 1 and 2 shows the demographic and clinical characteristics of the children. The ASD and TD groups were matched

on age, $t = 1.17$, $p = 0.26$, and intellectual functioning, $t = 1.80$, $p = 0.09$, as measured by the short form of the Chinese version of the Wechsler Intelligence Scale for Children-Fourth Edition (Hong Kong) [WISC-IV (HK)] (23). The ASD-only group contained significantly more males than the other two groups, likelihood ratio = 6.49, $p = 0.04$. The TD group demonstrated significantly fewer ASD or ADHD related symptoms than either ASD group (F ranges from 30.56 to 51.42, $p < 0.001$). Although the level of behavioral problems between the two ASD groups did not reach statistical significance, the ASD-only group demonstrated slightly more ASD-related features than the ASD + ADHD group.

Procedure

This study was conducted in accordance with the Helsinki Declaration of the World Medical Association Assembly.

TABLE 1 | Demographic and clinical characteristics of children with ASD ($n = 22$) and TD controls ($n = 13$).

	TD ($n = 13$)	ASD ($n = 22$)	t or χ^2	p
Age, years	10.92 (3.95)	9.50 (2.54)	1.17	0.26
Gender—male (%) ^a	69.23	90.91	2.62	0.11
IQ	106.69 (13.23)	99.36 (8.29)	1.80	0.09
ADI-R social interaction	3.85 (2.91)	18.55 (6.77)	8.89	<0.001**
ADI-R communication	1.31 (1.38)	13.64 (5.27)	10.39	<0.001**
ADI-R stereotyped behavior	0.23 (0.60)	5.18 (2.24)	9.80	<0.001**
SRS-2 total score	28.77 (10.29)	78.55 (25.94)	8.00	<0.001**

Data are presented as means (SD).

ADI-R, Autism Diagnostic Interview-Revised; IQ, intelligence quotient as assessed by the Chinese version of Wechsler Intelligence Scale for Children Forth Edition; SRS-2, Social Responsiveness Scale Second Edition; ASD, children with diagnosis of autism spectrum disorder; ASD-only, children with diagnosis of autism spectrum disorder only; ASD + ADHD, children with comorbid diagnosis of autism spectrum disorder and attention deficit hyperactivity disorder; TD, typically developing children.

^aLikelihood ratio Chi-square test were performed for distribution violating the sample size assumption of Chi-square test.

** $p < 0.01$.

TABLE 2 | Demographic and clinical characteristics of children with ASD only ($n = 13$), children with comorbid diagnosis of ASDs and attention deficit hyperactivity disorder ($n = 9$), and TD controls ($n = 13$).

	TD ($n = 13$)	ASD		F or χ^2	p	Post hoc results
		ASD-only ($n = 13$)	ASD + ADHD ($n = 9$)			
Age, years	10.92 (3.95)	9.38 (2.84)	9.67 (2.18)	0.84	0.44	
Gender—male (%) ^a	69.23	100.00	77.78	6.49	0.04*	
IQ	106.69 (13.23)	100.08 (9.30)	98.33 (6.98)	2.06	0.14	
ADI-R social interaction ^b	3.85 (2.91)	19.31 (7.18)	17.44 (6.37)	37.20	<0.001**	TD < ASD-only, ASD + ADHD
ADI-R communication ^b	1.31 (1.38)	13.77 (4.90)	13.44 (6.06)	51.42	<0.001**	TD < ASD-only, ASD + ADHD
ADI-R stereotyped behavior ^b	0.23 (0.60)	5.85 (2.19)	4.22 (2.05)	50.51	<0.001**	TD < ASD-only, ASD + ADHD
SRS-2 total score ^b	28.77 (10.29)	81.08 (28.68)	74.89 (22.51)	30.56	<0.001**	TD < ASD-only, ASD + ADHD

Data are presented as means (SD).

ADI-R, Autism Diagnostic Interview-Revised; IQ, intelligence quotient as assessed by the Chinese version of Wechsler Intelligence Scale for children Forth Edition; SRS-2, Social Responsiveness Scale Second Edition; ASD, children with diagnosis of autism spectrum disorder; ASD-only, children with diagnosis of autism spectrum disorder only; ASD + ADHD, children with comorbid diagnosis of autism spectrum disorder and attention deficit hyperactivity disorder; TD, typically developing children.

^aLikelihood ratio Chi-square test were performed for distribution violating the sample size assumption of Chi-square test.

^bWelch's test and Games-Howell post hoc test were performed for variables violating the homogeneity of variances assumption of ANOVA test.

* $p < 0.05$, ** $p < 0.01$.

The research protocol was approved by the Joint Chinese University of Hong Kong—New Territories East Cluster Clinical Research Ethics Committee (Ref. No. 2013.520). Prior to the assessment, all of the children and their parents were briefed on the procedure of the study, and informed consent was obtained from the parents. Peripheral blood samples and data on neuropsychological and behavioral measures were collected on separate days.

A registered nurse drew 3 ml of EDTA blood and 3 ml of clotted blood from each child using venipuncture at a medical clinic. Each blood sample was centrifuged at 3,000 rpm for 15 min, and the harvested serum was then stored at -80°C in a clinical laboratory until cytokine and chemokine levels were measured. Serum cytokine and chemokine concentrations were measured following the manufacturer's instructions. Blood sample processing and assay were performed by an experienced laboratory technician who was blind to the clinical characteristics and group assignments of the participants.

Neuropsychological assessments of the children and clinical interviews of the parents were administered on another day by well-trained research assistants. The neuropsychological assessment involved standardized tests on two cognitive domains (executive functioning and short-term memory) that are frequently found to be problematic in individuals with ASD (24, 25). In the clinical interview, information about the children's developmental and medical history, as well as past and present socio-emotional and behavioral characteristics, was collected from the parents through a structured interview and standardized questionnaires. The diagnosis of each child was confirmed by a clinical psychologist based on the DSM-V criteria and the ADI-R. The research assistants who conducted the assessment, the nurse who drew the blood, and the technician who performed the blood assays were blinded to the rationale of the study and the group assignment.

Measures

Immunological Measures

The concentrations of the cytokines TGF β 1 and MIF were measured using an enzyme-linked immunosorbent assay (R&D Systems, Inc., MN, USA) method, whereas those of the chemokines CCL2, CCL5, CXCL8, CXCL9, and CXCL10 were assessed using BDTM human chemokine cytometric bead array (CBA) reagent (Becton Dickinson Biosciences Pharmingen, CA, USA). Samples were analyzed on a multi-fluorescence BD FACSCaliburTM flow cytometer using BD CellQuestTM and BDTM CBA software.

Cognitive Measures

Executive Functioning

Four well-defined measures of executive functioning in planning and organization, cognitive flexibility, and generativity were used in the present study: (1) the Tower of London Test-Drexel Version (TOL^{DX}) (26), (2) completion time of the second trial of the Children's Color Trail Test [CCTT; (27)], (3) the total number of unique designs of the Five Point Test [FPT; (28)], and (4) the Copy trial of the Rey-Osterrieth Complex Figure Test

[Rey-O; (29)]. The TOL^{DX} requires movement of three colored beads on three vertical pegs to match a target arrangement while adhering to the test rules. The second trial of the CCTT requires connecting scattered numbers in ascending order and concurrently alternating between pink and yellow. The FPT requires the production of novel designs by connecting five points with straight lines within 5 min. The Rey-O Copy task involves copying a complex geometric figure and requires sufficient attention and concentration and the ability to organize the figure into a perceptual whole.

Short-term Memory

Short-term memory comprises two measures tapping the ability to temporarily store new information in memory: (1) total scores on Digit Span—Forward and Backward (DS) of the WISC-IV (HK) (23) and (2) the immediate recall trial of Rey-O. The Rey-O task requires drawing a complex figure from memory after copying the figure, and the DS requires the repetition of sequences of random numerals read aloud by the examiner.

Behavioral Measures

Social Communication/Interaction

This measure consists of three measures derived from two standardized questionnaires tapping core deficits in social functioning of ASD: (1) reciprocal social interaction, (2) communication subscale scores of the ADI-R, and (3) social communication/interaction total scores on the Social Responsiveness Scale, Second Edition [SRS-2; (22)].

Repetitive/Restricted Behavior

This measure consists of two behavioral measures tapping another set of core ASD symptoms in the repetitive, restricted behavior repertoire, interests or activities: (1) restricted, repetitive, and stereotyped patterns of behaviors subscale scores on the ADI-R and (2) repetitive/restricted behaviors subscale scores on the SRS-2.

Inattention/Hyperactivity

This measure involves three measures derived from standardized questionnaires tapping core AD/HD symptoms of inattention and hyperactivity/impulsivity: (1) cognitive problems/inattention, (2) hyperactivity, and (3) ADHD index subscale scores on the short version of Conners' Rating Scales-Revised [CRS-R; (30)].

Data Analyses

Cognitive functions and behavioral measures were compared and examined for differences between the ASD and TD groups. To reduce the number of statistical comparisons, two composite scores of the cognitive domain (*executive functioning, short-term memory*) and three composite scores of the behavioral domain (*social communication/interaction, repetitive/restricted behavior, inattention/hyperactivity*) were computed by summing and averaging the Z scores from the corresponding cognitive and behavioral measures of the different cognitive and behavioral domains. Low scores indicated poor performance in cognitive functioning and impaired behavior. To examine differences

between the ASD and TD groups of children, the two cognitive composite and the three behavioral composite scores were compared using the independent-samples *t*-test (independent *t*-test). For the immunological measures, the concentrations of the cytokines and chemokines were compared between the ASD and TD groups using independent *t*-tests.

To determine whether ASD and ASD + ADHD would demonstrate different cytokine and chemokine profiles compared to their TD counterparts, between-group comparisons on continuous variables were performed using multivariate analysis of variance (MANOVA) followed by separate univariate analysis of variance (ANOVA) and *post hoc* Tukey HSD tests. Between-group comparisons on categorical variables were analyzed using Chi-square tests. For distributions that had more than 20% of cells with an expected count of less than 5, the likelihood ratio was reported. Spearman's correlation was performed to analyze the association between two continuous variables. All statistical analyses were performed using the SPSS software (SPSS, Inc., Chicago, IL, USA). Given that specific hypotheses were tested, the alpha level was not adjusted to avoid reducing the power of the tests, and the corresponding effect sizes of different statistics were reported to determine the strength of association and degree of difference based on Cohen (31) and Hopkins (32) criteria.

RESULTS

Comparison of Cognitive and Behavioral Measurements between Children with ASD and TD Controls

Children with ASD showed significantly lower composite scores in all cognitive domains: executive functioning, $t(33) = 2.09, p = 0.04$, and short-term memory, $t(33) = 2.90, p = 0.007$; and in all behavioral domains: social communication/interaction, $t(33) = 11.93, p < 0.001$, repetitive/restricted behavior, $t(33) = 10.23, p < 0.001$, and inattention/hyperactivity, $t(33) = 6.01, p < 0.001$, compared to TD controls, indicating deficient cognitive and behavioral functioning in ASD (Table 3).

TABLE 3 | Comparison of mean composite scores in cognitive and behavioral domains in children with ASD ($n = 22$) and TD controls ($n = 13$).

	TD ($n = 13$)	ASD ($n = 22$)	<i>t</i>	<i>p</i>
Executive functioning	-0.30 (0.50)	-0.71 (0.60)	2.09	0.04*
Short-term memory	-0.08 (0.70)	-0.74 (0.62)	2.90	0.007**
Social communication/ interaction	3.10 (0.37)	-0.19 (1.20)	11.93	<0.001**
Repetitive/restricted behavior	1.53 (0.21)	-0.88 (1.07)	10.23	<0.001**
Inattention/hyperactivity	0.22 (0.51)	-1.48 (1.14)	6.01	<0.001**

Data are presented as means (SD).

ASD, children with diagnosis of autism spectrum disorder; ASD-only, children with diagnosis of autism spectrum disorder only; ASD + ADHD, children with comorbid diagnosis of autism spectrum disorder and attention deficit hyperactivity disorder; TD, typically developing children.

* $p < 0.05$, ** $p < 0.01$.

Comparison of Immunological Profiles between Children with ASD and TD Controls

Concentrations of CCL2 and CCL5 were significantly higher in children with ASD than in those with TD [CCL2: $t(33) = -2.27, p = 0.03$; CCL5: $t(33) = -3.07, p = 0.004$] (Table 4). Moreover, concentration of CXCL9 was approximately twofold lower in ASD children than in TD children, $t(33) = 4.02, p = 0.001$. No significant differences in the concentrations of MIF, TGF β 1, CXCL8, and CXCL10 were observed in children with ASD compared with those observed for TD children, $p > 0.05$. The results were consistent when only male participants in each group were compared. That is, significant between-group differences were found in CCL2, $t(27) = -1.93, p = 0.03$, CCL5, $t(27) = -2.28, p = 0.03$, and CXCL9, $t(27) = 3.69, p = 0.02$, suggesting that a gender difference was not a confounding factor that could account for differences in the immunological measures between the ASD and TD groups of children. Similarly, analysis of covariance was conducted to examine whether the differences between the TD and ASD groups could be attributed to age differences. Similar patterns of statistical significance were observed between the two groups after age adjustments were made, in which the level of CCL5 was significantly higher, $F(1, 32) = 5.33, p = 0.03$, and the CXCL9 level was significantly lower, $F(1, 32) = 23.09, p < 0.001$, in children with ASD than their TD counterparts. Nevertheless, although the level of CCL2 showed a higher trend in the ASD group after an adjustment was made for age, the difference between the ASD and TD groups did not reach statistical significance, $F(1, 32) = 3.23, p = 0.08$.

Associations between Concentrations of Cytokines and Chemokines with Cognitive and Behavioral Measures in the ASD and TD Groups

Spearman's rank-correlation analysis was performed to determine whether there were correlations between concentrations

TABLE 4 | Comparison of mean concentrations of cytokines and chemokines in children with ASD ($n = 22$) and TD controls ($n = 13$).

	TD ($n = 13$)	ASD ($n = 22$)	<i>t</i>	<i>p</i>
Cytokines				
Migration inhibitory factor (ng/mL)	17.25 (5.35)	20.89 (11.30)	-1.09	0.29
Transforming growth factor beta 1 (pg/mL)	31530.81 (5746.58)	32228.70 (8917.55)	-0.25	0.80
Chemokines				
CCL2 (pg/mL)	141.78 (38.89)	182.21 (66.61)	-2.27	0.03*
CCL5 (pg/mL)	32396.60 (8061.28)	45273.38 (16620.41)	-3.07	0.004**
CXCL8 (pg/mL)	79.87 (18.20)	78.83 (33.00)	0.12	0.91
CXCL9 (pg/mL)	522.64 (212.87)	270.19 (100.92)	4.02	0.001**
CXCL10 (pg/mL)	1155.78 (493.21)	999.70 (415.49)	1.00	0.32

Data are presented as means (SD).

ASD, children with diagnosis of autism spectrum disorder; TD, typically developing children.

* $p < 0.05$, ** $p < 0.01$.

of cytokines and chemokines and the cognitive and behavioral domains among ASD and TD participants. To reduce the number of statistical comparisons and thereby avoid inflation of Type I error, composite *Z* scores were computed for each of the two cognitive (executive functioning and short-term memory) and three behavioral (social communication/interaction, repetitive/restricted behavior and inattention/hyperactivity) domains. First, individual *Z* scores for each cognitive or behavioral measure were computed based on the mean and *SD* obtained from normative sample statistics. The composite *Z* score of each cognitive and behavioral domain was then calculated by taking the average of the individual *Z* scores for the cognitive or behavioral measures tapping the corresponding domain.

Table 5 shows the specific associations between concentrations of cytokines and chemokines with cognitive and behavioral domains assessed among all participants. Generally, fewer significant associations were observed between concentrations of chemokines and the cognitive domains than between those concentrations and the behavioral domains. For the cognitive domains, significant associations were found between MIF, CXCL10, and EF scores, such that lower EF scores were significantly correlated with increased concentrations of MIF, $r = -0.48$, $p = 0.003$, and reduced concentrations of CXCL10, $r = 0.49$, $p = 0.003$. For the behavioral domains, significant associations were found between increased CCL5 and lower composite scores in all of the behavioral domains, namely

social communication/interaction, $r = -0.39$, $p = 0.02$, repetitive/restricted behavior, $r = -0.39$, $p = 0.02$, and inattention/hyperactivity, $r = -0.70$, $p < 0.001$. Similarly, associations were also found between decreased concentrations of CXCL9 and poorer performance in all of the behavioral domains: social communication/interaction, $r = 0.49$, $p = 0.003$, repetitive/restricted behavior, $r = 0.49$, $p = 0.003$, except that a non-significant trend of association could only be detected in inattention/hyperactivity, $r = 0.30$, $p = 0.08$. Most of these associations between concentrations of cytokines and chemokines and the cognitive and behavioral domains showed moderate to large effect sizes, and the strongest association was found between increased CCL5 and lower composite scores for inattention/hyperactivity.

Associations between Concentrations of Cytokines and Chemokines with Cognitive and Behavioral Measures within the ASD Group

To determine whether there was specific relationship between measures of cytokines and chemokines and severity of cognitive and behavioral outcomes among children with ASD, a second correlation analysis was performed within the ASD group (as shown in **Table 6**). When the ASD group was analyzed alone, lower EF scores were found to be significantly correlated with increased

TABLE 5 | Whole-group association analysis of serum cytokines and chemokines with cognitive and behavioral domains in all participants enrolled in this study ($n = 35$) using Spearman's rank correlations.

	Migration inhibitory factor		Transforming growth factor beta 1		CCL2		CCL5		CXCL8		CXCL9		CXCL10	
	r_s	p	r_s	p	r_s	p	r_s	p	r_s	p	r_s	p	r_s	p
Executive functioning	-0.48	0.003**	0.01	0.97	0.24	0.16	-0.16	0.36	0.10	0.58	0.26	0.13	0.49	0.003**
Short-term memory	-0.30	0.08	-0.10	0.56	-0.10	0.55	-0.19	0.27	-0.06	0.72	0.07	0.70	0.10	0.58
Social communication/interaction	-0.20	0.25	0.04	0.83	-0.12	0.51	-0.39	0.02*	-0.04	0.84	0.49	0.003**	0.19	0.27
Repetitive/restricted behavior	-0.10	0.55	0.00	0.99	-0.09	0.62	-0.39	0.02*	0.03	0.88	0.49	0.003**	0.18	0.30
Inattention/hyperactivity	-0.19	0.26	-0.17	0.32	-0.19	0.26	-0.70	<0.001**	-0.07	0.69	0.30	0.08	0.08	0.67

* $p < 0.05$, ** $p < 0.01$.

TABLE 6 | ASD subgroup association analysis of serum cytokines and chemokines with cognitive and behavioral domains in participants with ASD ($n = 22$) using Spearman's rank correlations.

	Migration inhibitory factor		Transforming growth factor beta 1		CCL2		CCL5		CXCL8		CXCL9		CXCL10	
	r_s	p	r_s	p	r_s	p	r_s	p	r_s	p	r_s	p	r_s	p
Executive functioning	-0.57	0.005**	0.06	0.79	0.39	0.07	-0.14	0.53	0.26	0.24	-0.06	0.80	0.63	0.002**
Short-term memory	-0.28	0.21	-0.03	0.88	-0.15	0.51	-0.04	0.84	-0.03	0.88	-0.59	0.004**	-0.04	0.85
Social communication/interaction	-0.10	0.65	0.32	0.15	0.13	0.58	-0.13	0.58	-0.02	0.92	-0.05	0.83	0.28	0.20
Repetitive/restricted behavior	0.12	0.60	0.23	0.31	0.17	0.46	-0.05	0.82	0.16	0.47	-0.22	0.34	0.03	0.89
Inattention/hyperactivity	-0.37	0.09	-0.17	0.44	-0.16	0.49	-0.62	0.002**	-0.05	0.82	-0.36	0.10	-0.12	0.59

* $p < 0.05$, ** $p < 0.01$.

MIF, $r = -0.57$, $p = 0.005$, and decreased CXCL10, $r = 0.63$, $p = 0.002$. In addition, we found a significant correlation between concentration of CXCL9 and STM scores, such that as CXCL9 increased, STM performance decreased, $r = -0.59$, $p = 0.004$. Regarding the behavioral domains, the only association observed was that between the concentration of CCL5 and composite scores of inattention/hyperactivity at a large effect size, such that as the concentration of CCL5 increased, more inattention and hyperactive symptoms occurred, $r = -0.62$, $p = 0.002$. However, no other association was observed between the composite scores of social communication/interaction, repetitive/restricted behavior and concentrations of cytokines and chemokines.

Comparison of Cognitive and Behavioral Measurements between Children with ASD-Only and Children with ASD + ADHD

To examine the associated deficits and immunological profiles in ASDs comorbid with other disorders, the children with ASD in the present study were further divided into two groups: those who were diagnosed with ASD-only and those with a comorbid diagnosis of ASD and ADHD (ASD + ADHD). As shown in **Table 7**, no significant differences in any of the cognitive and behavioral domains were observed between children with ASD-only and those with ASD + ADHD. However, differences between the two ASD groups in the EF score were observed such that children with ASD + ADHD tended to perform poorer than children with ASD-only in the EF domain, $p = 0.07$. Children with ASD + ADHD also tended to show lower performance in the STM domain and had more features in the inattention/hyperactivity domain than did children with ASD-only. However, no significant between-group difference was detected, possibly because of the relatively small sample size in each of the ASD subgroups.

Comparison of Immunological Profiles among Children with ASD-Only and Those with ASD + ADHD

Two separate MANOVA tests were performed to compare, first, the concentrations of cytokines and, second, the concentrations

of chemokines among ASD-only, ASD + ADHD and TD controls, followed by *post hoc* Tukey HSD tests to examine the pair-wise group differences in concentrations of cytokines and chemokines. **Figure 1** shows the mean concentrations of cytokines and chemokines in each group. Results of MANOVA showed that there were significant between-group differences in both the profiles of cytokines, $F(4, 62) = 2.90$, $p = 0.03$, $\eta_p^2 = 0.16$, and the profiles of chemokines, $F(10, 56) = 3.66$, $p = 0.001$, $\eta_p^2 = 0.40$. Moreover, separate univariate ANOVAs on the dependent variables revealed that there were significant group differences in one cytokine [MIF: $F(2, 32) = 4.35$, $p = 0.02$, $\eta_p^2 = 0.21$], and four chemokines [CCL2: $F(2, 32) = 4.32$, $p = 0.02$, $\eta_p^2 = 0.21$; CCL5: $F(2, 32) = 3.40$, $p = 0.05$, $\eta_p^2 = 0.18$; CXCL8: $F(2, 32) = 4.52$, $p = 0.02$, $\eta_p^2 = 0.22$; CXCL9: $F(2, 32) = 11.52$, $p < 0.001$, $\eta_p^2 = 0.42$]. In contrast, there were no significant group differences with respect to the concentrations of TGF β 1, $F(2, 32) = 0.23$, $p = 0.80$, $\eta_p^2 = 0.01$, or CXCL10, $F(2, 32) = 0.80$, $p = 0.46$, $\eta_p^2 = 0.05$. Since the ASD-only group contained significantly more males than the TD and the ASD + ADHD groups, MANOVA tests were performed to examine whether there was gender difference in the cytokine and chemokine expressions within the ASD + ADHD and TD groups of children. Results showed that there was no significant gender difference in the profiles of cytokines or chemokines in the ASD + ADHD or TD groups, $ps > 0.30$. Moreover, results of separate univariate ANOVAs on the dependent variables also revealed that there was no significant group difference in any of the immunological measures between the males and females in the ASD + ADHD and TD groups, $ps > 0.05$. The results suggest that the females in the ASD + ADHD and TD groups exhibit similar cytokine and chemokine profiles as compared to their male counterparts and that the sex difference is not a confounding factor in the immunological measures between these groups.

Deviated Concentrations of Cytokines and Chemokines in ASD-Only Children

Regarding the deviated concentrations of cytokines and chemokines in ASD-only children, *post hoc* Tukey HSD tests showed that ASD-only children demonstrated significantly higher CCL2 concentrations, $p = 0.02$, and lower CXCL9 concentrations,

TABLE 7 | Comparison of mean composite scores in cognitive and behavioral domains between children with ASD only ($n = 13$), children with comorbid diagnosis of ASDs and attention deficit hyperactivity disorder ($n = 9$), and TD controls ($n = 13$).

	TD	ASD		F or α^2	p	Post hoc results
	($n = 13$)	ASD-only ($n = 13$)	ASD + ADHD ($n = 9$)			
Executive functioning	-0.30 (0.50)	-0.50 (0.59)	-1.02 (0.50)	5.06	0.01*	TD < ASD + ADHD
Short-term memory	-0.08 (0.70)	-0.61(0.67)	-0.94 (0.50)	4.96	0.01*	TD < ASD + ADHD
Social communication/interaction ^a	3.10 (0.37)	-0.29 (1.24)	-0.05 (1.21)	65.85	<0.001**	TD < ASD, ASD + ADHD
Repetitive/restricted behavior ^a	1.53 (0.21)	-1.08 (1.13)	-0.59 (0.97)	50.34	<0.001**	TD < ASD, ASD + ADHD
Inattention/hyperactivity ^a	0.22 (0.51)	-1.28 (1.20)	-1.75 (1.04)	18.89	<0.001**	TD < ASD, ASD + ADHD

Data are presented as means (SD).

ASD, children with diagnosis of autism spectrum disorder; ASD-only, children with diagnosis of autism spectrum disorder only; ASD + ADHD, children with comorbid diagnosis of autism spectrum disorder and attention deficit hyperactivity disorder; TD, typically developing children.

^aWelch's test and Games-Howell post hoc test were performed for variables violating the homogeneity of variances assumption of analysis of variance test.

* $p < 0.05$, ** $p < 0.01$.

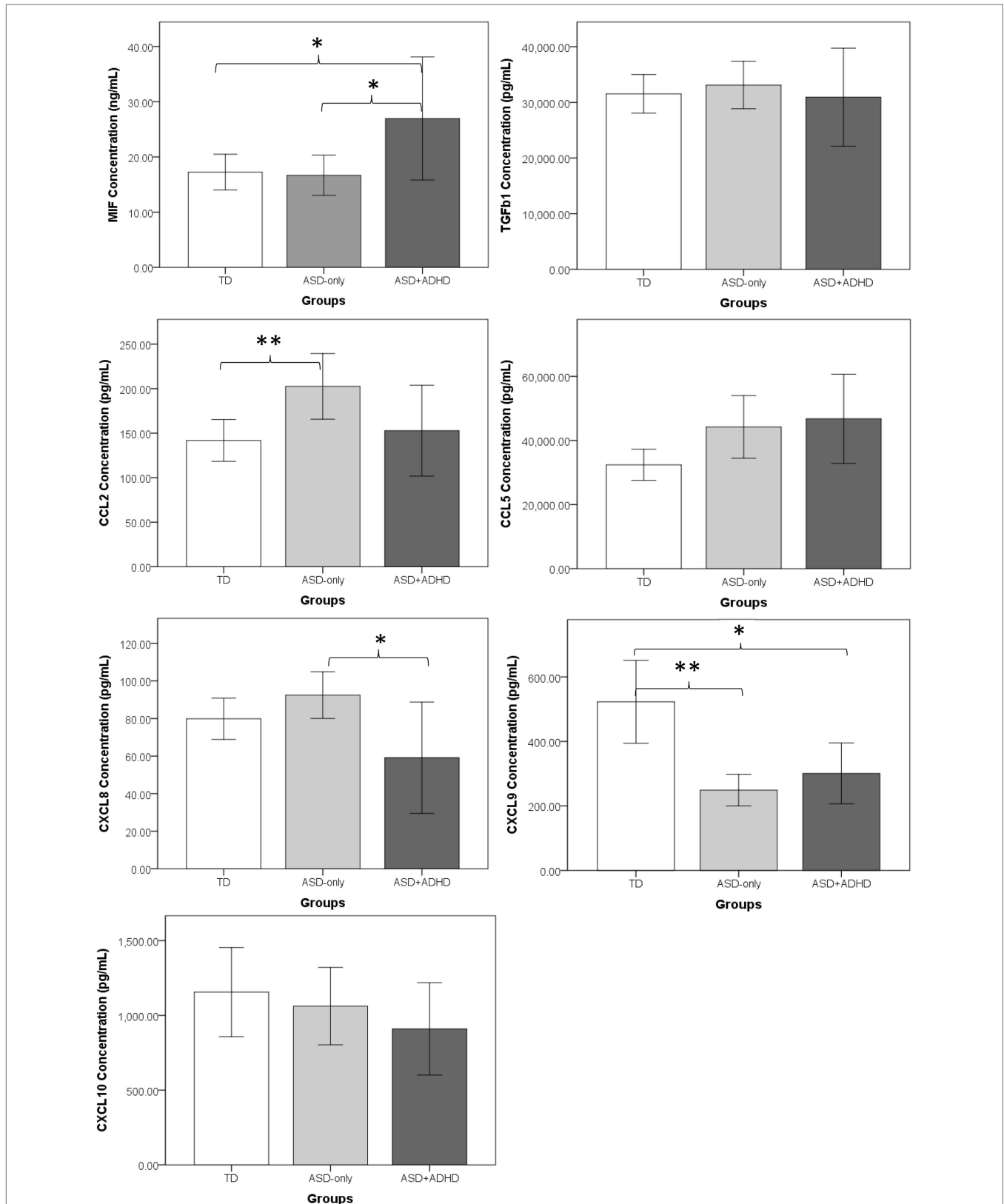


FIGURE 1 | Comparisons of mean concentrations of cytokines and chemokines between the ASD-only, ASD+ADHD, and TD groups. The error bars represent a 95% confidence interval around the mean. TD, typically developing children; ASD-only, children with diagnosis of autism spectrum disorder; ASD + ADHD, children with comorbid diagnosis of ASD and attention deficit hyperactivity disorder (ADHD). * $p < 0.05$, ** $p < 0.01$.

$p < 0.001$, than did the TD controls. In contrast, there were no significant differences between the ASD-only children and TD controls in the concentrations of two cytokines (MIF: $p = 0.99$; TGF β 1: $p = 0.87$) or three other chemokines (CCL5: $p = 0.10$; CXCL8: $p = 0.43$; CXCL10: $p = 0.86$) (Figure 1).

Deviated Concentrations of Cytokines and Chemokines in ASD Children Comorbid with ADHD

Post hoc Tukey HSD test results showed that ASD + ADHD children demonstrated a dissimilar immunological profile compared with that of ASD-only children (Figure 1). With respect to cytokine concentration, the ASD + ADHD group demonstrated a significantly higher MIF concentration than did the TD group, $p = 0.04$, but no such deviated concentration was observed for the ASD-only group. With respect to chemokine concentration, a significantly elevated CCL2 pattern was observed for the ASD-only group, $p = 0.02$, whereas no significant elevation of CCL2 concentrations was found in the ASD + ADHD group compared to the TD group, $p = 0.90$. In addition, when comparing the immunological profiles of the ASD-only and ASD + ADHD group, the ASD + ADHD group demonstrated significantly higher MIF, $p = 0.03$, and lower CXCL8, $p = 0.01$, concentrations than did the ASD-only group. Nevertheless, it is noted that a significantly lower concentration of CXCL9 was observed in both the ASD-only, $p < 0.001$, and ASD + ADHD groups, $p = 0.006$, compared with the TD controls. Moreover, a trend of elevated CCL5 was observed in both the ASD-only, $p = 0.10$, and ASD + ADHD groups, $p = 0.07$, when compared to the concentrations measured for the TD controls, suggesting a small degree of similarity between the immunological profiles of the ASD-only and ASD + ADHD groups.

DISCUSSION

The present study examined cognitive function deficits and behavioral problems among a group of children with ASD who were aged 6–17 years and whether these deficits were associated with altered pro-inflammatory cytokine and chemokine profiles. The findings of the present study showed deviated concentrations of serum cytokines and chemokines, with elevated macrophage/monocytes CCL2 and levels of the Th2-related chemokine CCL5 and reduced levels of the T helper type 1 (Th1)-related chemokine CXCL9 in children with ASD compared to TD controls. Consistent results were obtained from the subgroup analyses involving only male participants from each group and after controlling for age differences, suggesting that neither gender nor age could account for differences in the immunological profiles between the two groups of children. In addition, the deviations in CCL5 and CXCL9 were linked to impairments in the behavioral domains, with associations observed between more behavioral problems measured in the three behavioral domains, including social communication/interaction, repetitive/restricted behavior, and inattention/hyperactivity, and increased levels of CCL5 and decreased CXCL9, such that impairments in the behavioral domains were more pronounced in individuals with deviations in the concentrations of these two chemokines. The present results are in line with those of previous studies showing an increase in

plasma levels of CCL2 and CCL5 in individuals with ASD (1, 8). In what appears to be an important extension of previous studies, our findings are the first to show significantly reduced concentrations of CXCL9 in children with ASD compared to TD controls. The reduced levels of CXCL9 may be related to the slight decrease in the levels of the Th1-related chemokine CXCL10 in the ASD and ASD + ADHD groups, given that CXCL9 is a chemokine that is structurally and functionally related to CXCL10, which binds to a common inflammatory chemokine receptor, CXCR3, to coordinate inflammation in a variety of human diseases (9, 33). In fact, a positive correlation was found between levels of CXCL9 and CXCL10 in the present study, $r = 0.35$, $p = 0.04$, indicating that both of these chemokines may have important implications in the inflammatory mechanism in ASD, in that their levels of production show similar patterns. This finding may provide additional evidence of the involvement of CXCL9 in the pathophysiology of ASD for future research, given that CXCL9 has been relatively unexplored in previous studies. Furthermore, considering different cytokines/chemokines can be secreted by different T cell subsets, such as Th1, Th2, Th17, Th22, Th9, regulatory T cells, and follicular T helper cells; or leukocytes subsets including macrophages, dendritic cells, neutrophils, natural killers, and natural killer cells, it is reasonable to postulate that different cell number of the T cell subsets and leukocytes presented in ASD and the TD controls are responsible for the observed differences in cytokine/chemokine levels between the two groups of children.

However, in contrast to previous findings that have repeatedly indicated a significant reduction in TGF β 1 and a role for this reduction in the neuroinflammatory process of ASD (1, 4, 8–10), our results showed no difference in TGF β 1 between the TD and ASD groups. One possible reason could be related to the uniqueness of the genetic and environmental characteristics of different ethnic groups, varying immunological measures such as white blood cell counts and percentages of lymphocytes and granulocytes have been found to vary among different races (34, 35). For example, the association between decreased circulating concentrations of TGF β 1 and the severity of behavioral symptoms in ASD has been consistently reported in studies on Caucasians. In contrast, a study conducted on Japanese individuals with ASD did not demonstrate such an association between decreased serum levels of TGF β 1 and ASD symptoms (10). Another possible reason is the different biological samples analyzed. In most previous studies on peripheral levels of MIF and TGF β 1, samples were collected from plasma, whereas the samples used in the present study were collected from serum. It is still unknown whether the plasma level of cytokines directly reflects the serum level of the same cytokines (8, 10, 36–40). Nevertheless, given the relatively small sample size in the present study, further verification with a larger sample size is necessary before any firm conclusions can be drawn.

Furthermore, autism is a broad spectrum of disorders over which affected individuals demonstrate a broad range of symptoms in social and behavioral respects, with approximately 30–50% of ASD individuals showing prominent ADHD symptoms (15), and ASD children with or without ADHD have been found to exhibit distinct cognitive and behavioral profiles (15–19). For this reason, the present study also aimed to explore whether

different immune mechanisms are active in these children. Interestingly, findings from the present study have demonstrated a robustly increased level of CCL2 in the ASD group but not in the ASD + ADHD group. Specifically, robust between-group differences were observed in the elevated concentration of CCL2 between our samples of ASD-only and TD controls. On one hand, these results agree with the majority of findings reported in the literature indicating that substantially higher concentrations of CCL2 are observed across different biological samples, including plasma, CSF, astrocytes in the anterior cingulate gyrus, and even tissue from the cerebellum, where elevated concentrations of CCL2 appear to be relatively stable across a broad age range (from newborn to middle-aged adults) and across various levels of intellectual functioning (with or without mental disabilities) among individuals with ASD (1, 6, 7, 14). Given the critical role of CCL2 in the proinflammatory process and its implication in neuroinflammation underlying the pathogenesis of certain CNS diseases, e.g., Alzheimer's disease (41–45), it is postulated that the elevated CCL2 levels observed in the present study may indicate neuroinflammation in ASD. However, it should be noted that, in contrast to previous studies that showed associations between increased CCL2 and impairments in behavioral functions among individuals with ASD (6), the lack of between-group differences for the ASD + ADHD group and the absence of a significant association of CCL2 with any of the cognitive or behavioral measures considered in the present study warrants future work to delineate the role of CCL2 in the expression of autistic traits.

It is worth noting that although a non-significant trend of increased MIF and decreased CXCL10 was observed in children with ASD, significant associations were in fact detected between these deviations and poorer performance in the EF domain. Specifically, an increased MIF but reduced levels of the Th1-related chemokine CXCL10 were related to poorer executive performance. Furthermore, increased CXCL9 was associated with decreased short-term memory, and increased CCL5 was shown to be highly associated with more severe inattention/hyperactivity problems. Moreover, it is interesting to see that elevated MIF and decreased CXCL8 levels were found only in children with ASD comorbid with ADHD but not in children of the ASD-only group. Although the mechanism underlying the distinctive immunological profile of ASD and ASD + ADHD is unknown, this study provides important information indicating a potentially distinct cytokine/chemokine profile between different subtypes of autistic disorder. This notion is in agreement with previous studies that reported the opposite pattern of CCL5 concentrations between autistic individuals with and without FXS (14). In fact, our results seem to suggest that lumping ASD individuals with varying phenotypes into one group for analysis may in fact dilute the between-group difference relative to the control. Given the relaxed diagnostic criteria of the DSM-V that allows for the dual diagnosis of ASD and ADHD, it is worth further exploring the immunological difference between individuals with ASD-only and those with a co-diagnosis of ADHD in future studies. For example, it will be of interest to investigate the functional role of CCL5 in individuals with ADHD and to examine further whether CCR5 blockers will improve attention in animal models of ASD.

Although interesting associations that suggest the role of inflammatory chemokines and cytokines in the pathogenesis of ASD were observed in the present study, it should be noted that our findings of the association between concentrations of cytokines and chemokines and behavioral functions in ASD were not as strong as we hypothesized. A significant association was detected only between increased levels of the Th2-related chemokine CCL5 and more inattention/hyperactivity problems, which is in contrast with previous studies reporting a significant association between increased levels of CCL5 and greater impairments in social and communication skills in individuals with ASD (6). Nevertheless, the extent of all associations found in the present study had a larger effect size compared to that of the significant correlations detected by Ashwood et al. (6). Additionally, regarding the moderate degree of association between increased CXCL9 levels and deficits in short-term memory, the finding is a novel one in the neuro-immunological field of research on ASD. Although the underlying mechanism of aberrant serum levels of CXCL9 on the pathogenesis of ASD is not known, given its close association with CXCL10, it may also play a role in coordinating the inflammatory process in ASD (33, 46). Further investigation is needed to determine the link between decreased CXCL9 levels and better short-term memory performance in ASD patients. Moreover, our finding of the significant association between decreased serum levels of CXCL10 and poorer executive performance in ASD is in contrast to previous studies that showed an increased plasma level of CXCL10 was positively associated with disease progression and mental flexibility and inhibitory control in patients with Parkinson's disease (47). Thus, future research may be necessary to clarify whether the link between immunological abnormalities and cognitive functioning differ between diseases even if they both exhibit a neuroinflammatory profile.

Taken together, our results are in agreement with findings in previous studies showing that cytokines are involved in neurodevelopment and neuronal function and that cytokine imbalance and dysregulation can have long term neurological consequences (48). Furthermore, the fact that cytokine expression is dependent on genetic and environmental influences (49) may help explain our findings that showed distinct immunological profiles in children with ASD of Chinese ethnicity from previous studies conducted in Western populations. Specifically, cytokines may represent a biomarker for genetic or environmental factors in autism. Of which, an individual may be genetically predisposed to mount an inappropriate immune response, either too robustly or too weakly, against an infectious or toxic substance which in turn could cause associated damage to the brain and other body systems, including the immune system, for the development of ASD. Moreover, an individual may lack appropriate genetic machinery to excrete and eliminate toxins; thereby causing their accumulation in tissue or organ and subsequently lead to an amplification of the toxin's effects in a variety of body systems, including the brain and the immune system. Therefore, certain environmental challenge during a critical period of child development could have especially severe consequences, causing abnormal CNS function, altered immune phenotypes, and autism. Although findings from the present study may implicate potential areas where manipulation targeting individual cytokine-receptor

interactions may impact on the behavior and immunity in ASD, whether this manipulation of the immune response represents a therapeutic strategy in the treatment of ASD remains uncertain. The reason being that cytokines/chemokines are a complex immune network and individuals with ASD of different ethnicity may have different genetic backgrounds and expose to different environmental factors, therefore therapeutic strategy targeting on one or two cytokines/chemokines may not be sufficient for providing a general treatment of ASD.

Overall, the present study provides preliminary findings regarding immunological dysfunction in the peripheral blood of children with ASD in a Chinese population. To the best of our knowledge, there are no previous studies such as this one in Chinese population and only few in other Asian cohorts. Moreover, what appears to be an important extension of previous studies is that in the present study, it was found that individuals with ASD that do and do not have ADHD symptoms exhibit distinct pro-inflammatory profiles; and that cognitive function deficits, repetitive stereotyped behavior and inattention/hyperactivity exacerbated as a function of altered plasma levels of chemokines and cytokines between the two different subtypes of autistic disorder. The findings from the present study bring together several diverse areas of research on autism and establish a link between immunological alteration and cognitive and behavioral impairments in autistic children with different ethnic backgrounds. However, the following should be noted when interpreting the data. One of the main limitations of our study was the small sample size used, which may have led to the low statistical power detected in comparing the levels of chemokine and cytokine production between groups and the behavioral and cognitive correlations with the levels of chemokines and cytokines, although a moderate to large effect size was found. Moreover, a relatively weak relation between the concentrations of chemokines and cytokines and behavioral performance was observed in our study, which was likely because the level of behavioral impairment in our sample was not as severe as expected but showed a narrow spread around the mean. Therefore, it was rather difficult to determine whether our observations reflect a true picture of the relationship

between behavioral performance and immunological profiles in ASD among the general population. Further studies with a larger sample size will be required to verify the results before more conclusive interpretations can be made regarding the functional role of cytokines play in ASD. In addition, the number of detected cytokines/chemokines in the plasma is relatively low in the present study, and it may be argued that the correlations of cytokines/chemokines in different tissues are highly dependent on the types of studied inflammatory cytokines/chemokines. For example, circulating plasma levels of cytokines may have certain correlation with the local concentrations inside the brain or CSF such as TNF-alpha in ASD. But IL-6 was found to be present in CSF but not in plasma in ASD (50). Furthermore, the expression of some cytokines, e.g., IL-1, IL-2, TGF- β , and granulocyte-macrophage colony-stimulating factor, is actually controversial, and different studies have found various results in different tissues. Further investigations are therefore required to elucidate the correlations of cytokines in different sites such as plasma and the brain.

AUTHOR CONTRIBUTIONS

YH, WC, SS, TC, CW, MY, and AC contributed to the conceptualization of the study, subject recruitment, data collection and analysis, and drafting and revision of the manuscript. TC contributed to the analysis of blood samples.

ACKNOWLEDGMENTS

The authors especially thank the registered nurses who helped draw blood and all parents and children who participated in this study. Thanks are also extended to Debbie Yan, Lan He, Rex Wang, Carman Chu, Hannah Lee, and Thomas Lee, who assisted in data collection and management.

FUNDING

This study was supported by a donation from Mr. Li Sau Hung and Mr. Law Sau Wang to the Chinese University of Hong Kong.

REFERENCES

- Vargas DL, Nascimbene C, Krishnan C, Zimmerman AW, Pardo CA. Neuroglial activation and neuroinflammation in the brain of patients with autism. *Ann Neurol* (2005) 57(1):67–81. doi:10.1002/ana.20315
- Li X, Chauhan A, Sheikh AM, Patil S, Chauhan V, Li XM, et al. Elevated immune response in the brain of autistic patients. *J Neuroimmunol* (2009) 207(1):111–6. doi:10.1016/j.jneuroim.2008.12.002
- Ashwood P, Krakowiak P, Hertz-Picciotto I, Hansen R, Pessah I, Van de Water J. Elevated plasma cytokines in autism spectrum disorders provide evidence of immune dysfunction and are associated with impaired behavioral outcome. *Brain Behav Immun* (2011) 25(1):40–5. doi:10.1016/j.bbi.2010.08.003
- Grigorenko EL, Han SS, Yrigollen CM, Leng L, Mizue Y, Anderson GM, et al. Macrophage migration inhibitory factor and autism spectrum disorders. *Pediatrics* (2008) 122(2):438–45. doi:10.1542/peds.2007-3604
- Suzuki K, Matsuzaki H, Iwata K, Kamenno Y, Shimmura C, Kawai S, et al. Plasma cytokine profiles in subjects with high-functioning autism spectrum disorders. *PLoS One* (2011) 6(5):e20470. doi:10.1371/journal.pone.0020470
- Ashwood P, Krakowiak P, Hertz-Picciotto I, Hansen R, Pessah IN, Van de Water J. Associations of impaired behaviors with elevated plasma chemokines in autism spectrum disorders. *J Neuroimmunol* (2011) 232(1):196–9. doi:10.1016/j.jneuroim.2010.10.025
- Zerbo O, Yoshida C, Grether JK, Van de Water J, Ashwood P, Delorenze GN, et al. Neonatal cytokines and chemokines and risk of autism spectrum disorder: the early markers for autism (EMA) study: a case-control study. *J Neuroinflammation* (2014) 11:113. doi:10.1186/1742-2094-11-113
- Ashwood P, Enstrom A, Krakowiak P, Hertz-Picciotto I, Hansen RL, Croen LA, et al. Decreased transforming growth factor beta1 in autism: a potential link between immune dysregulation and impairment in clinical behavioral outcomes. *J Neuroimmunol* (2008) 204(1):149–53. doi:10.1016/j.jneuroim.2008.07.006
- Hashim H, Abdelrahman H, Mohammed D, Karam R. Association between plasma levels of transforming growth factor- β 1, IL-23 and IL-17 and the severity of autism in Egyptian children. *Res Autism Spectr Disord* (2013) 7(1):199–204. doi:10.1016/j.rasd.2012.08.007
- Okada K, Hashimoto K, Iwata Y, Nakamura K, Tsujii M, Tsuchiya KJ, et al. Decreased serum levels of transforming growth factor- β 1 in patients with

- autism. *Prog Neuropsychopharmacol Biol Psychiatry* (2007) 31(1):187–90. doi:10.1016/j.pnpbp.2006.08.020
11. Ashwood P, Van de Water J. Is autism an autoimmune disease? *Autoimmun Rev* (2004) 3(7):557–62. doi:10.1016/j.autrev.2004.07.036
 12. Goines P, Van de Water J. The immune system's role in the biology of autism. *Curr Opin Neurol* (2010) 23(2):111. doi:10.1097/WCO.0b013e3283373514
 13. Matson JL, Worley JA, Fodstad JC, Chung KM, Suh D, Jhin HK, et al. A multinational study examining the cross cultural differences in reported symptoms of autism spectrum disorders: Israel, South Korea, the United Kingdom, and the United States of America. *Res Autism Spectr Disord* (2011) 5(4):1598–604. doi:10.1016/j.rasd.2011.03.007
 14. Ashwood P, Nguyen DV, Hessel D, Hagerman RJ, Tassone F. Plasma cytokine profiles in Fragile X subjects: is there a role for cytokines in the pathogenesis? *Brain Behav Immun* (2010) 24(6):898–902. doi:10.1016/j.bbi.2010.01.008
 15. Davis NO, Kollins SH. Treatment for co-occurring attention deficit/hyperactivity disorder and autism spectrum disorder. *Neurotherapeutics* (2012) 9(3):518–30. doi:10.1007/s13311-012-0126-9
 16. Holtmann M, Bölte S, Poustka F. Attention deficit hyperactivity disorder symptoms in pervasive developmental disorders: association with autistic behavior domains and coexisting psychopathology. *Psychopathology* (2007) 40(3):172–7. doi:10.1159/000100007
 17. Rao PA, Landa RJ. Association between severity of behavioral phenotype and comorbid attention deficit hyperactivity disorder symptoms in children with autism spectrum disorders. *Autism* (2014) 18(3):272–80. doi:10.1177/1362361312470494
 18. Sikora DM, Vora P, Coury DL, Rosenberg D. Attention-deficit/hyperactivity disorder symptoms, adaptive functioning, and quality of life in children with autism spectrum disorder. *Pediatrics* (2012) 130(Suppl 2):S91–7. doi:10.1542/peds.2012-0900G
 19. Yerys BE, Wallace GL, Sokoloff JL, Shook DA, James JD, Kenworthy L. Attention deficit/hyperactivity disorder symptoms moderate cognition and behavior in children with autism spectrum disorders. *Autism Res* (2009) 2(6):322–33. doi:10.1002/aur.103
 20. American Psychiatric Association. *Diagnostic and Statistical Manual of Mental Disorders*. 5th ed. Arlington, VA: American Psychiatric Association (2013).
 21. Lord C, Rutter M, LeCouteur A. Autism diagnostic interview-revised: a revised version of a diagnostic interview for caregivers of individuals with possible pervasive developmental disorders. *J Autism Dev Disord* (1994) 24:659–85. doi:10.1007/BF02172145
 22. Constantino JN, Gruber CP. *The Social Responsiveness Scale Manual*. 2nd ed. Los Angeles, CA: Western Psychological Services (2012).
 23. Wechsler D. *Wechsler Intelligence Scale for Children*. 4th ed. Hong Kong, China: King-May Psychological Assessment (2010).
 24. Gilotty L, Kenworthy L, Sirian L, Black DO, Wagner AE. Adaptive skills and executive function in autism spectrum disorders. *Child Neuropsychol* (2002) 8(4):241–8. doi:10.1076/chin.8.4.241.13504
 25. Williams DL, Goldstein G, Minschew NJ. The profile of memory function in children with autism. *Neuropsychology* (2006) 20:21–9. doi:10.1037/0894-4105.20.1.21
 26. Culbertson WC, Zillmer EA. *The Tower of London DX Manual*. North Tonawanda, NY: Multi-Health Systems (2005).
 27. Williams J, Rickert V, Hogan J, Zolten AJ, Satz P, D'Elia LF, et al. Children's color trails. *Arch Clin Neuropsychol* (1995) 10(3):211–23. doi:10.1093/archclin/10.3.211
 28. Regard M, Strauss E, Knapp P. Children's production on verbal and non-verbal fluency tasks. *Percept Mot Skills* (1982) 55:839–44. doi:10.2466/pms.1982.55.3.839
 29. Bernstein JH, Waber DP. *Developmental Scoring System for the Rey-Osterrieth Complex Figure*. Odessa, FL: Psychological Assessment Resources (1996).
 30. Conners CK. *Conners' Rating Scales-Revised: Short Form*. North Tonawanda, NY: Multi-Health Systems (1997).
 31. Cohen J. *Statistical Power Analysis for the Behavioral Sciences*. 2nd ed. Hillsdale, NJ: Lawrence Erlbaum (1988).
 32. Hopkins WG. *New View of Statistics*. (1997). Available from: <http://www.sportsci.org/resource/stats/effectmag.html>
 33. Müller M, Carter S, Hofer MJ, Campbell IL. Review: the chemokine receptor CXCR3 and its ligands CXCL9, CXCL10 and CXCL11 in neuroimmunity—a tale of conflict and conundrum. *Neuropathol Appl Neurobiol* (2010) 36(5):368–87. doi:10.1111/j.1365-2990.2010.01089.x
 34. Bartlett JA, Goldklang AR, Schleifer SJ, Keller SE. Immune function in healthy inner-city children. *Clin Diagn Lab Immunol* (2001) 8(4):740–6. doi:10.1128/CDDI.8.4.740-746.2001
 35. Chen CL, Liu Q, Pui CH, Rivera GK, Sandlund JT, Ribeiro R, et al. Higher frequency of glutathione S-transferase deletions in black children with acute lymphoblastic leukemia. *Blood* (1997) 89(5):1701–7.
 36. Croonenberghs J, Bosmans E, Deboutte D, Kenis G, Maes M. Activation of the inflammatory response system in autism. *Neuropsychobiology* (2002) 45(1):1–6. doi:10.1159/000048665
 37. Enstrom A, Onore C, Hertz-Picciotto I, Hansen RL, Croen L, Van de Water JA, et al. Detection of IL-17 and IL-23 in plasma samples of children with autism. *Am J Biochem Biotechnol* (2008) 4(2):114–20. doi:10.3844/ajbbsp.2008.114.120
 38. Singh VK, Warren RB, Odell JD, Cole P. Changes of soluble interleukin-2, interleukin-2 receptor, T8 antigen, and interleukin-1 in the serum of autistic children. *Clin Immunol Immunopathol* (1991) 61(3):448–55. doi:10.1016/S0090-1229(05)80015-7
 39. Sweeten TL, Posey DJ, Shankar S, McDougle CJ. High nitric oxide production in autistic disorder: a possible role for interferon- γ . *Biol Psychiatry* (2004) 55(4):434–7. doi:10.1016/j.biopsych.2003.09.001
 40. Zimmerman AW, Jyonouchi H, Comi AM, Connors SL, Milstien S, Varsou A, et al. Cerebrospinal fluid and serum markers of inflammation in autism. *Pediatr Neurol* (2005) 33(3):195–201. doi:10.1016/j.pediatrneurol.2005.03.014
 41. Cartier L, Hartley O, Dubois-Dauphin M, Krause KH. Chemokine receptors in the central nervous system: role in brain inflammation and neurodegenerative diseases. *Brain Res Rev* (2005) 48(1):16–42. doi:10.1016/j.brainresrev.2004.07.021
 42. Galimberti D, Schoonenboom N, Scarpini E, Scheltens P. Chemokines in serum and cerebrospinal fluid of Alzheimer's disease patients. *Ann Neurol* (2003) 53(4):547–8. doi:10.1002/ana.10531
 43. Galimberti D, Schoonenboom N, Scheltens P, Fenoglio C, Bouwman F, Venturini E, et al. Intrathecal chemokine synthesis in mild cognitive impairment and Alzheimer disease. *Arch Neurol* (2006) 63(4):538–43. doi:10.1001/archneur.63.4.538
 44. Xia M, Qin S, McNamara M, Mackay C, Hyman BT. Interleukin-8 receptor B immunoreactivity in brain and neuritic plaques of Alzheimer's disease. *Am J Pathol* (1997) 150(4):1267.
 45. Westin K, Buchhave P, Nielsen H, Minthon L, Janciauskiene S, Hansson O. CCL2 is associated with a faster rate of cognitive decline during early stages of Alzheimer's disease. *PLoS One* (2012) 7(1):e30525. doi:10.1371/journal.pone.0030525
 46. Groom JR, Luster AD. CXCR3 ligands: redundant, collaborative and antagonistic functions. *Immunol Cell Biol* (2011) 89(2):207–15. doi:10.1038/icb.2010.158
 47. Rocha NP, Scalzo PL, Barbosa IG, Souza MS, Morato IB, Vieira ÉLM, et al. Cognitive status correlates with CXCL10/IP-10 levels in Parkinson's disease. *Parkinsons Dis* (2014) 2014:903796. doi:10.1155/2014/903796
 48. Onore C, Careaga M, Ashwood P. The role of immune dysfunction in the pathophysiology of autism. *Brain Behav Immun* (2012) 26(3):383–92. doi:10.1016/j.bbi.2011.08.007
 49. Goines PE, Ashwood P. Cytokine dysregulation in autism spectrum disorders (ASD): possible role of the environment. *Neurotoxicol Teratol* (2013) 36:67–81. doi:10.1016/j.ntt.2012.07.006
 50. Xu N, Li X, Zhong Y. Inflammatory cytokines: potential biomarkers of immunologic dysfunction in autism spectrum disorders. *Mediators Inflamm* (2015) 2015:531518. doi:10.1155/2015/531518
- Conflict of Interest Statement:** The authors declare that the research was conducted in the absence of any commercial or financial relationships that could be construed as a potential conflict of interest.
- Copyright © 2017 Han, Cheung, Wong, Sze, Cheng, Yeung and Chan. This is an open-access article distributed under the terms of the Creative Commons Attribution License (CC BY). The use, distribution or reproduction in other forums is permitted, provided the original author(s) or licensor are credited and that the original publication in this journal is cited, in accordance with accepted academic practice. No use, distribution or reproduction is permitted which does not comply with these terms.

RESEARCH

Open Access

Neonatal cytokines and chemokines and risk of Autism Spectrum Disorder: the Early Markers for Autism (EMA) study: a case-control study

Ousseny Zerbo^{1*}, Cathleen Yoshida¹, Judith K Grether^{1,2}, Judy Van de Water^{3,4}, Paul Ashwood^{4,5}, Gerald N Delorenze¹, Robin L Hansen^{4,6}, Marty Kharrazi² and Lisa A Croen¹

Abstract

Background: Biologic markers of infection and inflammation have been associated with Autism Spectrum Disorders (ASD) but prior studies have largely relied on specimens taken after clinical diagnosis. Research on potential biologic markers early in neurodevelopment is required to evaluate possible causal pathways and screening profiles.

Objective: To investigate levels of cytokines and chemokines in newborn blood specimens as possible early biologic markers for autism.

Methods: We conducted a population-based case-control study nested within the cohort of infants born from July 2000 to September 2001 to women who participated in the prenatal screening program in Orange County, California, USA. The study population included children ascertained from the California Department of Developmental Services with Autism Spectrum Disorder (ASD, n = 84), or developmental delay but not ASD (DD, n = 49), and general population controls randomly sampled from the birth certificate files and frequency matched to ASD cases on sex, birth month and birth year (GP, n = 159). Cytokine and chemokine concentrations were measured in archived neonatal blood specimens collected for routine newborn screening.

Results: Cytokines were not detected in the vast majority of newborn samples regardless of case or control status. However, the chemokine monocyte chemoattractant protein-1 (MCP-1) was elevated and the chemokine Regulated upon Activation Normal T-Cell Expressed and Secreted (RANTES) was decreased in ASD cases compared to GP controls. The chemokines macrophage inflammatory protein-1alpha (MIP-1α) and RANTES were decreased in children with DD compared to GP controls.

Conclusion: Measurement of immune system function in the first few days of life may aid in the early identification of abnormal neurodevelopment and shed light on the biologic mechanisms underlying normal neurodevelopment.

Keywords: Newborn, Cytokines, Chemokines, Autism spectrum disorders

Background

Recent epidemiologic studies estimate that 1 to 2% of children are affected by Autism Spectrum Disorder (ASD) [1-3]. Although autism was first described in 1943 [4], very little is known about the etiology of the vast majority of cases, and there are no definitive biological markers that clearly distinguish individuals with ASD from unaffected individuals.

Several epidemiological studies have reported immune dysregulation in children with ASD and their mothers, suggesting a role for the immune system in the pathophysiology of the disorder [5-9]. Several research groups have found that individuals with ASD have increased neuroinflammation in brain tissues [10-12], imbalances in immunoglobulins, including increased levels of plasma IgG4 [13], reduced levels of total IgG [14] or reduced levels of IgG and IgM [15,16], and imbalances in cytokine/chemokine levels [17,18]. However, the mechanisms through which immune dysfunction may contribute to the etiology of autism are not understood [19].

* Correspondence: ousseny.x.zerbo@kp.org

¹Division of Research, Kaiser Permanente Northern California, Oakland, CA 94612, USA

Full list of author information is available at the end of the article

Cytokines and chemokines are proteins involved in regulating hematopoiesis, inflammation, and immune cell proliferation and differentiation [20]. They also play an important role in normal neurodevelopment, including the processes of neuronal migration and synaptic plasticity [21,22]. These processes are tightly regulated and too much or too little of the signals mediated by cytokines can be detrimental to the developing fetus. For instance, in animal models, injection of the cytokine IL-6 or IL-2 into pregnant mice leads to neurodevelopmental abnormalities in the offspring including decreased prepulse inhibition and latent inhibition, attention, exploratory and social behaviors [23,24]. These findings suggest that reported associations between maternal infections or inflammation during pregnancy and ASD [25-31] could be mediated through a disruption in the balance of cytokine or chemokine levels.

The literature on cytokines/chemokines and ASD is expanding; however, results are sometimes inconsistent across studies [17,18,32-40]. The discrepancies are due to different research groups having utilized different types of bio-samples (serum, plasma, amniotic fluid), different age groups, different types of control groups (including siblings with likely inherited similarities with respect to ASD), non-standardized blood draws from differing seasons or times of day, and differences in length of time between biosample collection and ASD diagnosis (prenatal, newborn, post-ASD diagnosis). All of these factors may contribute to variability across studies in measured concentration of cytokines/chemokines and study findings [41]. Among the reported results on cytokines and chemokines in relation to autism, very few studies have so far utilized newborn samples.

The objective of this new study was to examine the potential association between cytokine and chemokine profiles measured at birth and risk of Autism Spectrum Disorders and developmental delays.

Methods

Study population

The study population has been previously described [42]. Briefly, the sample was derived from the Early Markers for Autism (EMA) study, a population-based, nested case-control study designed to evaluate biologic markers of susceptibility and exposure in archived maternal mid-pregnancy and neonatal blood specimens from the same mother-baby pairs. The EMA population was drawn from the cohort of children born in California from July 2000 to September 2001 to women who were pregnant in Orange County, California, USA, and who participated in the State's prenatal expanded alpha-fetoprotein screening program (XAFP). Three groups of children were identified: children with Autism Spectrum Disorder (ASD), children with developmental delay (DD) but not ASD, and general

population controls (GP). Children with ASD or DD were ascertained from the California Department of Developmental Services (DDS), which operates a system of 21 Regional Centers (RC) that coordinate services for persons with ASD, mental disability, and other developmental disabilities. GP controls were randomly sampled from the birth certificate files after excluding all past or current DDS/RC clients and were frequency matched to ASD cases by sex, birth month and birth year at a 2:1 ratio.

Diagnostic verification

After initial ascertainment of children with ASD or DD from records of the Regional Center of Orange County (RCOC), medical record abstractors compiled detailed diagnostic and clinical data from the RCOC records following a protocol initially developed by the Metropolitan Atlanta Developmental Disabilities Surveillance Program [43]. Expert clinical review of abstracted data was then conducted by a developmental pediatrician (RLH) to confirm the ASD or DD diagnoses for this study using the *Diagnostic and Statistical Manual of Mental Disorders, Fourth Edition (DSM-IV)* criteria. The final analytic sample consisted of 84 children with ASD, 49 children with DD but not ASD, and 159 GP controls.

Specimen collection

Neonatal blood specimens were retrieved from the newborn screening specimen archives maintained by the California Department of Public Health. The neonatal specimen archive contains dried bloodspots collected for screening purposes on nearly every infant born in California (approximately 500,000 per year) since 1980. All newborn blood specimens for children included in this study were obtained by the heel-stick method, usually within 24 to 48 hours of birth. The blood specimens were collected at the nursery on a special S&S filter paper, and allowed to dry at room temperature prior to transport to the regional laboratory for routine screening for metabolic and other disorders. During transport, usually by courier from the hospital to a regional screening laboratory, the temperature of the specimens was not controlled. Blood spots remaining after routine testing were catalogued and stored at -20°C .

Cytokine and chemokine measurements

Neonatal cytokine and chemokine concentrations were determined using a commercially available multiplex bead-based kit (BioSource Human Bead Kit; Invitrogen, Carlsbad, CA, USA). The following cytokines and chemokines were measured: IFN- γ , IL-2, IL-4, IL-5, IL-6, IL-1 β , IL-8, IL-10, IL-12p40, TNF- α , granulocyte macrophage colony-stimulating factor (GM-CSF), IFN- γ -induced protein 10 (IP-10), monocyte chemoattractant protein-1 (MCP-1), macrophage inflammatory protein-1 α and 1 β (MIP-1 α , MIP-1 β), Regulated upon Activation Normal T-Cell

Expressed and Secreted (RANTES), and C-C motif chemokine 11 (CCL 11 or eotaxin). The assays were carried out in accordance with the protocols provided by the manufacturer. Briefly, 50 μ L of serum was incubated with anti-cytokine-conjugated beads in a 96-well filter-bottomed plate on a plate shaker. After two hours, the beads were washed using a vacuum manifold, and biotin-conjugated detection antibodies were added for one-hour incubation. Following a repeat of the washing step, beads were incubated with streptavidin phycoerythrin for 30 minutes. The plates were then read on a Bio-Plex 100 system (Bio-Rad Laboratories, Hercules, CA, USA) and analyzed using Bio-Plex Manager Software (Bio-Rad Laboratories, Hercules, CA, USA) with a five-point standard curve. Reference samples were run on each plate to determine assay consistency. All laboratory assays were conducted blinded to case-control status.

Statistical analysis

Socio-demographic factors were compared between ASD, DD and GP groups using Chi-square test for categorical variables and *t*-test for continuous variables. For all values of analytes that were below the minimum detectable level (MDL) we assigned a value of MDL/2. Concentration of chemokines and cytokines were analyzed as untransformed, since natural log transformation of the values did not substantially change their distribution. All analyses were categorical and cut-points were based on the percent of study subjects with analyte values below the MDL. For analytes with < 25% sample below the MDL, we divided the observations into quartiles based on the distribution among the GP controls and used the lowest quartile as the reference. Values below the MDL were included in the lowest quartile. For analytes with 25 to 90% of the sample below the MDL, we created a binary variable and compared detected versus non-detected. Analytes with > 90% sample below the MDL were not considered for further analysis.

To investigate whether analyte concentrations at the extreme low or high end of the distribution predicted case status, we included two additional cut-points comparing values below the tenth percentile versus above the tenth percentile and values above the ninetieth percentile versus below the ninetieth, as was done in a previous study [32]. The 10th percentile cut-point was introduced when < 5% of GP samples were below the MDL. The 90th percentile cut-point was introduced when < 25% of the GP samples were below the MDL. We conducted crude and adjusted analyses using logistic regression to estimate the risk of ASD and DD associated with each analyte separately. Covariates considered for adjusted models were gender (male, female), child birth month (calendar month), birth year (2000, 2001), maternal ethnicity (Hispanic, non-Hispanic), maternal place of birth (US, Mexico, other), maternal age at child birth

(continuous in years), child age at blood draw (continuous in days), gestational age (<37 weeks, \geq 37 weeks). Covariates were considered confounders and retained in the final model if individually they changed the odds ratio by 10% or more. Frequency matching variables (sex, birth month, and birth year) were included in all logistic regression models comparing ASD to GP control. Since the specimens were spread out on different plates, we additionally adjusted for laboratory plate as a categorical variable. Odds ratios were estimated for exposure categories with a minimum cell count of 5.

The study was approved by the institutional review boards of the California Health and Human Services Agency and Kaiser Permanente of Northern California.

Results

There was no difference between ASD cases and GP controls in gestational age, age at newborn screening, or birth year. However, mothers of ASD cases were more likely to be non-Hispanic, born in the US, and to be slightly older compared to mothers of GP controls (Table 1). Children with DD were more likely than GP controls to be male, have their blood drawn slightly later and to be born in the year 2000 (Table 1).

For all cytokines and chemokines, the proportion of newborn specimens with analyte levels below the MDL was similar for children with ASD, children with DD, and GP controls (Table 2). IL-5, IL-8, IL-12p40, TNF- α , IP-10, MIP-1 β and GM-CSF were not considered for further analysis because they were detected in < 5% of specimens.

ASD versus GP controls

More than 50% of study subjects had levels of IFN- γ , IL-1 β , IL-2, IL-4, IL-6 and IL-10 below the MDL (Table 2). ASD status was not associated with the detection of these analytes in newborn bloodspots (Table 3). There was no significant difference between ASD and GP groups in the levels of MCP-1 when comparing quartiles in crude and adjusted analysis. However, ASD cases were more likely than GP controls to have levels of MCP-1 above the 90th percentile (adjusted odds ratio (OR_{adj}) = 3.24, 95% CI 1.41 to 7.47) (Table 3). We found no significant difference in levels of MIP-1 α between ASD cases and GP controls when comparing quartiles or extreme values. For RANTES, the proportion of ASD cases with concentration in the fourth quartile was lower than that of GP controls (OR_{adj} = 0.46, 95% CI 0.18 to 1.16). Moreover, a significantly higher proportion of ASD cases had concentrations of RANTES at or below the 10th percentile compared to GP controls (OR_{adj} = 2.42, 95% CI 1.05 to 5.55) (Table 3).

We found no significant association between levels of eotaxin and risk of ASD compared to GP controls in either crude or adjusted analyses (Table 3).

Table 1 Demographic characteristic of Autism Spectrum Disorder (ASD) cases, developmental delay (DD) and general population (GP) controls - the Early Markers for Autism study

Characteristics	ASD (n = 84) N (%)	GP (n = 159) N (%)	DD (n = 49) N (%)	Chi-square P-values	
				ASD versus GP	DD versus GP
Gender					
Male	73 (86.9)	139 (87.4)	29 (59.1)	0.89	< 0.01
Female	11 (13.1)	20 (12.6)	20 (40.8)		
Maternal ethnicity					
Hispanics	20 (23.8)	73 (45.9)	28 (57.1)		
Non-Hispanics	64 (76.2)	86 (54.1)	21 (42.9)	< 0.01	0.12
Maternal place of birth					
US	45 (53.6)	71 (44.7)	16 (32.7)	< 0.01	0.26
Mexico	9 (10.7)	58 (36.5)	22 (44.9)		
Other	30 (35.7)	30 (18.8)	11 (22.4)		
Maternal age (median and inter-quartile range)	31 (28 – 34)	28 (24 – 32)	29 (25 – 32)	< 0.01	0.68
Gestational age (GA in days)					
Preterm (GA < 260 days)	9 (10.7)	23 (14.5)	11 (22.5)	0.42	0.20
Term (GA ≥ 260 days)	75 (89.3)	136 (85.5)	38 (77.5)		
GA median and interquartile range	276 (269 – 280)	274 (267 – 279)	276 (265 – 282)	0.22	0.90
Child age (in days at newborn blood draw, median and inter- quartile range)	1.22 (1.02 – 1.76)	1.18 (1.03 – 1.56)	1.40 (1.05 – 2.27)	0.38	0.03
Birth year					
2000	23 (27.4)	31 (19.5)	26 (53)	0.15	< 0.01
2001	61 (72.6)	128 (80.5)	23 (47)		

Table 2 Working range and proportion below the minimal detection level (MDL) for each analyte measured in newborn dried blood by case-control status - the Early Markers for Autism study

Analytes	Working range (pg/ml)	ASD Cases (n =84) % below MDL	GP (n =159) % below MDL	DD (n = 49) % below MDL
MCP-1	13.03 – 9,160	19.0	18.0	26.3
MIP-1α	6.1 – 28,800	0.0	1.2	4.1
RANTES	22.36 – 19,100	0.0	0.6	2.0
Eotaxin	1.37 – 9,200	19.0	9.0	14.3
IFN-γ	0.58 – 11,370	77.4	73.0	86.0
IL-1β	2.5 – 5,470	77.4	76.8	79.6
IL-2	1.45 – 9,530	67.9	69.2	83.7
IL-4	2.21 – 14,470	77.4	74.2	86.0
IL-6	1.88 – 12,360	77.4	74.8	79.6
IL-10	3.4 – 22,350	53.6	54.1	51.0
IL-5	1.75 – 11,490	100	100	100
IL-8	6.23 – 13,630	97.6	98.7	98.0
IL-12p40	2.74 – 6,000	100	99.4	100
TNF-α	3.96 – 8,660	100	99.4	100
IP-10	2.01 – 1,420	100	100	100
MIP-1β	5.3 – 10,370	96.4	94.3	98.0
GM-CSF	0.88 – 5,760	98.8	99.4	97.9

ASD: Autism Spectrum Disorder; DD: developmental delay; GP: general population; MDL: minimal detection level.

Table 3 Crude and adjusted odds ratios with their 95% CIs Comparing levels of newborn blood spot cytokines/chemokines among children with Autism Spectrum Disorder (ASD), developmental delays (DD) and general population controls (GP) - the Early Markers for Autism study

Exposure	Exposure categories	Developmental category			ASD versus GP		DD versus GP	
		ASD (N = 84) n (%)	DD (N = 49) n (%)	TD (N = 159) n (%)	Crude OR (95% CI)	Adjusted OR ^a (95% CI)	Crude OR (95% CI)	Adjusted OR ^b (95% CI)
MCP-1	Q1	27 (32.14)	17 (34.69)	41 (25.79)	Reference	Reference	Reference	Reference
	Q2	13 (15.48)	14 (28.57)	39 (24.53)	0.50 (0.23 – 1.12)	0.49 (0.20 – 1.20)	0.86 (0.37 – 1.99)	0.52 (0.16 – 1.71)
	Q3	15 (17.86)	9 (18.37)	39 (24.53)	0.58 (0.27 – 1.26)	0.48 (0.20 – 1.14)	0.55 (0.22 – 1.39)	0.45 (0.13 – 1.54)
	Q4	29 (34.52)	9 (18.37)	40 (25.16)	1.10 (0.55 – 2.17)	0.93 (0.43 – 2.01)	0.54 (0.21 – 1.35)	0.55 (0.15 – 1.97)
	≤ 90%	66 (78.57)	45 (91.84)	143 (89.94)	Reference	Reference	Reference	Reference
	> 90%	18 (21.43)	4 (8.16)	16 (10.06)	2.43 (1.17 – 5.07)	3.24 (1.41 – 7.47)	-	-
MIP-1α	Q1	23 (27.38)	22 (44.90)	41 (25.79)	Reference	Reference	Reference	Reference
	Q2	20 (23.81)	7 (14.29)	39 (24.53)	0.91 (0.43 – 1.92)	0.86 (0.36 – 2.02)	0.33 (0.12 – 0.87)	0.21 (0.05 – 0.78)
	Q3	19 (22.62)	13 (26.53)	42 (26.42)	0.80 (0.38 – 1.69)	1.01 (0.37 – 2.70)	0.57 (0.25 – 1.29)	0.36 (0.10 – 1.23)
	Q4	22 (26.19)	7 (14.29)	37 (23.27)	1.06 (0.50 – 2.20)	1.53 (0.52 – 4.49)	0.35 (0.13 – 0.92)	0.29 (0.06 – 1.35)
	>10%	70 (83.33)	14 (28.57)	143 (89.94)	Reference	Reference	Reference	Reference
	≤ 10%	14 (16.67)	35 (71.43)	16 (10.06)	1.78 (0.82 – 3.86)	1.72 (0.71 – 4.14)	3.57 (1.59 – 8.01)	3.36 (1.16 – 9.69)^c
	≤ 90%	70 (83.33)	46 (93.88)	140 (88.05)	Reference	Reference	Reference	Reference
	> 90%	14 (16.67)	3 (6.12)	19 (11.95)	1.47 (0.69 – 3.11)	1.76 (0.70 – 4.39)	-	-
RANTES	Q1	26 (30.95)	21 (42.86)	40 (25.16)	Reference	Reference	Reference	Reference
	Q2	23 (27.38)	9 (18.37)	40 (25.16)	0.88 (0.43 – 1.80)	0.82 (0.37 – 1.81)	0.42 (0.17 – 1.04)	0.34 (0.10 – 1.15)
	Q3	20 (23.81)	14 (28.57)	40 (25.16)	0.76 (0.37 – 1.59)	0.63 (0.28 – 1.43)	0.66 (0.29 – 1.49)	0.55 (0.19 – 1.58)
	Q4	15 (17.86)	5 (10.20)	39 (24.53)	0.59 (0.27 – 1.28)	0.46 (0.18 – 1.16)	0.24 (0.08 – 0.71)	0.14 (0.03 – 0.62)
	> 10%	68 (80.95)	33 (67.35)	143 (89.94)	Reference	Reference	Reference	Reference
	≤ 10%	16 (19.05)	16 (32.65)	16 (10.06)	2.10 (0.99 – 4.45)	2.42 (1.05 – 5.55)	4.33 (1.96 – 9.54)	3.78 (1.29 – 11.03)
	≤ 90%	79 (94.05)	46 (93.88)	143 (89.94)	Reference	Reference	Reference	Reference
	> 90%	5 (5.95)	3 (6.12)	16 (10.06)	0.56 (0.20 – 1.60)	0.59 (0.18 – 1.89)	-	-
Eotaxin	Q1	25 (29.76)	17 (34.69)	41 (25.79)	Reference	Reference	Reference	Reference
	Q2	23 (27.38)	9 (18.37)	37 (23.27)	1.02 (0.49 – 2.09)	0.95 (0.42 – 2.14)	0.58 (0.23 – 1.47)	0.88 (0.27 – 2.85)
	Q3	19 (22.62)	12 (24.49)	42 (26.42)	0.74 (0.35 – 1.54)	0.58 (0.25 – 1.32)	0.68 (0.29 – 1.62)	0.62 (0.20 – 1.88)
	Q4	17 (20.24)	11 (22.45)	39 (24.53)	0.71 (0.33 – 1.52)	0.60 (0.20 – 1.79)	0.68 (0.28 – 1.63)	1.11 (0.27 – 4.58)
	≤ 90%	76 (90.48)	44 (89.80)	143 (89.94)	Reference	Reference	Reference	Reference
	> 90%	8 (9.52)	5 (10.20)	16 (10.06)	0.94 (0.38 – 2.29)	1.10 (0.36 – 3.34)	1.01 (0.35 – 2.93)	1.24 (0.34 – 4.42) ^c
IFN-γ	Non-detected	65 (77.38)	42 (85.71)	116 (72.96)	Reference	Reference	Reference	Reference
	Detected	19 (22.62)	7 (14.29)	43 (27.04)	0.78 (0.42 – 1.46)	0.91 (0.47 – 1.75)	0.45 (0.18 – 1.07)	0.64 (0.23 – 1.76) ^c
IL-1β	Non-detected	65 (77.38)	39 (79.59)	122 (76.73)	Reference	Reference	Reference	Reference

Table 3 Crude and adjusted odds ratios with their 95% CIs Comparing levels of newborn blood spot cytokines/chemokines among children with Autism Spectrum Disorder (ASD), developmental delays (DD) and general population controls (GP) - the Early Markers for Autism study (Continued)

IL-2	Detected	19 (22.62)	10 (20.41)	37 (23.27)	0.96 (0.51 – 1.80)	1.11(0.52 –2.35)	0.84 (0.38 – 1.85)	0.65 (0.19 – 2.23)
	Non-detected	57 (67.86)	41 (83.67)	110 (69.18)	Reference	Reference	Reference	Reference
IL-4	Detected	27 (32.14)	8 (16.33)	49 (30.82)	1.06 (0.60 – 1.87)	1.14 (0.38 – 3.43)	0.43 (0.19 – 1.00)	0.26 (0.01 – 8.76)
	Non-detected	65 (77.38)	42 (85.71)	118 (74.21)	Reference	Reference	Reference	Reference
IL-6	Detected	19 (22.62)	7 (14.29)	41 (25.79)	0.84 (0.45 – 1.56)	0.95 (0.49 – 1.85)	0.48 (0.20 – 1.15)	0.64 (0.23 – 1.80) ^c
	Non-detected	65 (77.38)	39 (79.59)	119 (74.84)	Reference	Reference	Reference	
IL-10	Detected	19 (22.62)	10 (20.41)	40 (25.16)	0.87 (0.46 – 1.62)	1.01 (0.52 – 1.96)	0.76 (0.34 – 1.66)	0.91 (0.35 – 2.35) ^c
	Non-detected	45 (53.57)	25 (51.02)	86 (54.09)	Reference	Reference	Reference	Reference
	Detected	39 (46.43)	24 (48.98)	73 (45.91)	1.02 (0.60 – 1.73)	0.17 (0.02 – 1.55)	1.13 (0.59 – 2.14)	1.53 (0.68 – 3.48) ^c

^aResults adjusted for maternal place of birth, child birth month, birth year, gender and specimen plate number.

^bResults adjusted for maternal place of birth, child year of birth, gender, specimen plate number and child age at blood draw.

^cResults adjusted for maternal place of birth, child year of birth, gender and child age at blood draw.

For MCP-1 and eotaxin, comparison between $\leq 10\%$ versus $> 10\%$ was not possible because more than 5% of the sample was below MDL.

DD versus GP controls

A higher proportion of children with DD had concentrations of MIP-1 α and RANTES at or below the 10th percentile compared to GP controls (for MIP-1 α , ORadj = 3.36, 95% CI 1.16 to 9.69; for RANTES, ORadj = 3.78, 95% CI 1.29 to 11.03) (Table 3).

We found no significant association between levels of MCP-1 or eotaxin and risk of DD compared to GP controls in either crude or adjusted analyses (Table 3).

Discussion

Children with ASD were more likely to have increased levels of MCP-1 and decreased levels of RANTES in newborn bloodspots compared to GP controls. Children with DD had decreased levels of MIP-1 α and RANTES compared to GP controls.

Our finding of increased levels of MCP-1 in ASD compared to GP controls contrasts with the study by Abdallah and colleagues [32], who reported no case-control differences in levels of MCP-1 measured in archived newborn blood samples from 359 ASD cases and 741 matched controls from Denmark. Our finding of no difference in concentration of MIP-1 α between ASD cases and controls is similar to those previously reported by Abdallah *et al.* (2012a). Like our study, they also found reduced levels of RANTES in ASD cases compared to controls. However, in our study, this finding was not specific to ASD cases, as we found that levels of RANTES were also reduced in newborn blood specimens of children with DD compared to GP controls.

In the present study, the vast majority of cytokines were not detected in newborn blood specimens, and detection was not associated with case-control status. Our results are in contrast with those reported by Abdallah *et al.* (2012) [35] who found decreased levels of IFN- γ , IL-2, IL-4, and IL-6 and increased levels of IL-8 and soluble IL-6 alpha (sIL-6 α) in newborn dried blood spots from ASD cases and controls. Differences in laboratory techniques, study populations, and length of time between sample collection and sample processing may have led to the observed differences in results. In the present study, samples were collected from children born in 2000 and 2001 compared to the wide range in year of birth of study participants of previous studies.

Alterations in chemokine and cytokine levels in other specimen types have been previously reported. In an analysis of chemokine levels in amniotic fluid Abdallah *et al.* (2012) reported elevated levels of MCP-1 for children who were later diagnosed with autism compared to controls [34]. Whether the chemokines were of maternal or fetal origin is not clear. Furthermore, increased levels of MCP-1 in blood specimens collected from children after the date of ASD diagnosis was reported in a study

of 2- to 5-year olds [17] that included 80 ASD cases and 37 typically developing controls.

MCP-1, RANTES and MIP-1 α play a role in neuron development. While often associated with inflammation, sufficient levels of these chemokines are needed for healthy neuronal migration. Therefore, changes in levels during critical windows of development could alter neurodevelopmental outcome leading to either ASD or DD, as suggested by our data. Cytokines and chemokines have overlapping biology and functions [44]. They are known to be redundant and pleiotropic [45] which makes the determination of the exact roles of specific chemokines during neurodevelopment challenging [17]. Increased concentration of MCP-1 in ASD cases versus controls may be suggestive of an increased immunological active state in newborns who are subsequently diagnosed with ASD.

The results of this study should be considered in light of the following limitations. We were unable to validate the diagnostic status of autism by systematic clinical evaluation. Instead, we relied on expert review of information recorded as part of diagnostic eligibility for developmental services from regional center records. In addition, we did not have any clinical information such as infection status of children at birth or their mothers. Despite these limitations, the study was strengthened by the measurement of a panel of chemokines and cytokines in newborn blood samples, prior to when ASD or DD diagnoses were made, so it gives us a window into what was going on biologically during a critical period of neurodevelopment. The inclusion of the DD group allowed us to evaluate the specificity of the findings. We were also able to adjust our results by including several covariates in the multivariate analysis. Finally, our comparison group was matched to the ASD group.

Conclusion

We found elevated levels of MCP-1 and decreased levels of RANTES in the newborn blood of children subsequently diagnosed with ASD. Levels of RANTES and MIP-1 α were also decreased in children later diagnosed with DD compared to GP controls. If replicated in future studies, these findings suggest that measurement of immune system function in the first few days of life may aid in the early identification of particular neurodevelopmental trajectories. Further research on early biologic markers will be useful in understanding the mechanisms underlying early abnormal neurodevelopment.

Abbreviations

ASD: Autism Spectrum Disorder; DD: developmental delay; DSM-IV: *Diagnostic Manual of Mental Disorders, Fourth Edition*; DDS: Department of Developmental Services; EMA: Early Markers for Autism; GA: gestational age; GM-CSF: granulocyte macrophage colony-stimulating factor; GP: general population; IFN: interferon; IL: interleukin; LOD: limit of detection; MDL: minimal detectable level;

MCP: monocyte chemotactic protein; MIP: macrophage inflammatory protein; ORadj: adjusted odds ratio; RANTES: Regulated upon Activation Normal T-cell Expressed and Secreted; RC: regional center; RCOC: Regional Center of Orange County; sIL-6 α : soluble IL-6 alpha; TNF: tumor necrosis factor; XAFP: expanded alpha-fetoprotein screening program.

Competing interests

The authors declare that they have no competing interests.

Authors' contributions

OZ contributed to the conception and design of the study, conducted statistical analyses, interpreted the data and was the primary writer of the manuscript. LAC contributed to the conception and design of the study, obtaining funding, acquiring data, interpreting the data, critical revision of the manuscript, and edited the manuscript. CKY managed the raw data. JKG contributed to the conception and design of the study, the interpretation of the data and critical revision of the manuscript. RLH contributed to the acquisition of data, the interpretation of the data and critical revision of the manuscript. PA contributed to the study design, the interpretation of data and critical revision of the manuscript. JvdW contributed to the design of the study, acquiring the data, the interpretation of data and edited the manuscript. GND contributed to the statistical analyses, interpretation of the data, and edited the manuscript. MK contributed to the conception and design of the study, obtaining funding, and acquiring data. All authors read and approved the final manuscript.

Acknowledgements

The study was supported by grants 3R01ES016669 from National Institute of Environmental Health Sciences; 5R01MH072565 from the National Institute of Mental Health.

Author details

¹Division of Research, Kaiser Permanente Northern California, Oakland, CA 94612, USA. ²(Retired) Environmental Health Investigations Branch, California Department of Public Health, Richmond, CA 94804, USA. ³Division of Rheumatology, Allergy and Clinical Immunology, University of California at Davis, 451 Health Sciences Drive, Suite 6510, Davis, CA 95616, USA. ⁴MIND Institute, 2825 50th Street, University of California at Davis, Sacramento, CA 95817, USA. ⁵Department of Medical Microbiology and Immunology, 1 Shields Avenue, University of California at Davis, Davis, CA 95616, USA. ⁶Department of Pediatrics, 2521 Stockton Boulevard, Suite 4100, Sacramento, CA 95817, USA.

Received: 14 February 2014 Accepted: 3 June 2014

Published: 20 June 2014

References

- Baio J: Prevalence of autism spectrum disorders - Autism and developmental disabilities monitoring network, 14 sites, United States, 2008. *MMWR Surveill Summ* 2012, **61**:1-19.
- Blumberg SJ, Bramlett MD, Kogan MD, Schieve LA, Jones JR, Lu MC: Changes in prevalence of parent-reported autism spectrum disorder in school-aged U.S. children: 2007 to 2011 to 2012 National health statistics reports. *Natl Center Health Stat* 2013, **2013**:65.
- Kim YS, Leventhal BL, Koh YJ, Fombonne E, Laska E, Lim EC, Cheon KA, Kim SJ, Kim YK, Lee H, Song DH, Grinker RR: Prevalence of Autism Spectrum Disorders in a Total Population Sample. *Am J Psychiatry*. 2011, **168**:904-912.
- Kanner L: Autistic disturbances of affective contact. *Acta Paedopsychiatr* 1968, **35**:100-136.
- Ashwood P, Wills S, Van de Water J: The immune response in autism: a new frontier for autism research. *J Leukoc Biol* 2006, **80**:1-15.
- Croen LA, Yoshida CK, Odouli R, Newman TB: Neonatal hyperbilirubinemia and risk of autism spectrum disorders. *Pediatrics* 2005, **115**:e135-e138.
- Goines PE, Ashwood P: Cytokine dysregulation in autism spectrum disorders (ASD): possible role of the environment. *Neurotoxicol Teratol* 2013, **36**:67-81.
- Goines PE, Croen LA, Braunschweig D, Yoshida CK, Grether J, Hansen R, Kharrazi M, Ashwood P, Van de Water J: Increased mid-gestational IFN-gamma, IL-4, and IL-5 in women giving birth to a child with autism: a case-control study. *Mol Autism* 2011, **2**:13.
- Jyonouchi H, Sun S, Le H: Proinflammatory and regulatory cytokine production associated with innate and adaptive immune responses in children with autism spectrum disorders and developmental regression. *J Neuroimmunol* 2001, **120**:170-179.
- Li X, Chauhan A, Sheikh AM, Patil S, Chauhan V, Li XM, Ji L, Brown T, Malik M: Elevated immune response in the brain of autistic patients. *J Neuroimmunol* 2009, **207**:111-116.
- Pardo CA, Vargas DL, Zimmerman AW: Immunity, neuroglia and neuroinflammation in autism. *Int Rev Psychiatry* 2005, **17**:485-495.
- Vargas DL, Nascimbene C, Krishnan C, Zimmerman AW, Pardo CA: Neuroglial activation and neuroinflammation in the brain of patients with autism. *Ann Neurol* 2005, **57**:67-81.
- Enstrom A, Krakowiak P, Onore C, Pessah IN, Hertz-Picciotto I, Hansen RL, Van de Water JA, Ashwood P: Increased IgG4 levels in children with autism disorder. *Brain Behav Immun* 2009, **23**:389-395.
- Grether JK, Croen LA, Anderson MC, Nelson KB, Yolken RH: Neonatally measured immunoglobulins and risk of autism. *Autism Res* 2010, **3**:323-332.
- Heuer L, Ashwood P, Schauer J, Goines P, Krakowiak P, Hertz-Picciotto I, Hansen R, Croen LA, Pessah IN, Van de Water J: Reduced levels of immunoglobulin in children with autism correlates with behavioral symptoms. *Autism Res* 2008, **1**:275-283.
- Heuer LS, Rose M, Ashwood P, Van de Water J: Decreased levels of total immunoglobulin in children with autism are not a result of B cell dysfunction. *J Neuroimmunol* 2012, **251**:94-102.
- Ashwood P, Krakowiak P, Hertz-Picciotto I, Hansen R, Pessah I, Van de Water J: Elevated plasma cytokines in autism spectrum disorders provide evidence of immune dysfunction and are associated with impaired behavioral outcome. *Brain Behav Immun* 2011, **25**:40-45.
- Suzuki K, Matsuzaki H, Iwata K, Kameno Y, Shimmura C, Kawai S, Yoshihara Y, Wakuda T, Takebayashi K, Takagai S, Matsumoto K, Tsuchiya KJ, Iwata Y, Nakamura K, Tsujii M, Sugiyama T, Mori N: Plasma cytokine profiles in subjects with high-functioning autism spectrum disorders. *PLoS One* 2011, **6**:e20470.
- Onore C, Careaga M, Ashwood P: The role of immune dysfunction in the pathophysiology of autism. *Brain Behav Immun* 2012, **26**:383-392.
- Dinarello CA: Proinflammatory cytokines. *Chest* 2000, **118**:503-508.
- Bauer S, Kerr BJ, Patterson PH: The neuropoietic cytokine family in development, plasticity, disease and injury. *Nat Rev Neurosci* 2007, **8**:221-232.
- Rostene W, Kitabgi P, Parsadaniantz SM: Chemokines: a new class of neuromodulator? *Nat Rev Neurosci* 2007, **8**:895-903.
- Ponzio NM, Servatius R, Beck K, Marzouk A, Kreider T: Cytokine levels during pregnancy influence immunological profiles and neurobehavioral patterns of the offspring. *Ann N Y Acad Sci* 2007, **1107**:118-128.
- Smith SE, Li J, Garbett K, Mirmics K, Patterson PH: Maternal immune activation alters fetal brain development through interleukin-6. *J Neurosci* 2007, **27**:10695-10702.
- Atladottir HO, Henriksen TB, Schendel DE, Parner ET: Autism after infection, febrile episodes, and antibiotic use during pregnancy: an exploratory study. *Pediatrics* 2012, **130**:e1447-e1454.
- Atladottir HO, Thorsen P, Ostergaard L, Schendel DE, Lemcke S, Abdallah M, Parner ET: Maternal infection requiring hospitalization during pregnancy and autism spectrum disorders. *J Autism Dev Disord* 2010, **40**:1423-1430.
- Brown AS, Sourander A, Hinkka-Yli-Salomaki S, McKeague IW, Sundvall J, Surcel HM: Elevated maternal C-reactive protein and autism in a national birth cohort. *Mol Psychiatry* 2014, **19**:259-264.
- Chess S: Autism in children with congenital rubella. *J Autism Child Schizophr* 1971, **1**:33-47.
- Deykin EY, MacMahon B: Viral exposure and autism. *Am J Epidemiol* 1979, **109**:628-638.
- Zerbo O, Iosif AM, Walker C, Ozonoff S, Hansen RL, Hertz-Picciotto I: Is maternal influenza or fever during pregnancy associated with autism or developmental delays? Results from the CHARGE (Childhood Autism Risks from Genetics and Environment) study. *J Autism Dev Disord* 2012, **43**:25-33.
- Zerbo O, Qian Y, Yoshida C, Grether JK, Van de Water J, Croen LA: Maternal infection during pregnancy and autism spectrum disorders. *J Autism Dev Disord* 2013, doi:10.1007/s10803-013-2016-3.
- Abdallah MW, Larsen N, Grove J, Bonefeld-Jorgensen EC, Norgaard-Pedersen B, Hougaard DM, Mortensen EL: Neonatal chemokine levels and risk of autism spectrum disorders: findings from a Danish historic birth cohort follow-up study. *Cytokine* 2013, **61**:370-376.

33. Abdallah MW, Larsen N, Grove J, Norgaard-Pedersen B, Thorsen P, Mortensen EL, Hougaard DM: **Amniotic fluid inflammatory cytokines: potential markers of immunologic dysfunction in autism spectrum disorders.** *World J Biol Psychiatry* 2013, **14**:528–538.
34. Abdallah MW, Larsen N, Grove J, Norgaard-Pedersen B, Thorsen P, Mortensen EL, Hougaard DM: **Amniotic fluid chemokines and autism spectrum disorders: an exploratory study utilizing a Danish historic birth cohort.** *Brain Behav Immun* 2012, **26**:170–176.
35. Abdallah MW, Larsen N, Mortensen EL, Atladottir HO, Norgaard-Pedersen B, Bonefeld-Jorgensen EC, Grove J, Hougaard DM: **Neonatal levels of cytokines and risk of autism spectrum disorders: an exploratory register-based historic birth cohort study utilizing the Danish Newborn Screening Biobank.** *J Neuroimmunol* 2012, **252**:75–82.
36. Al-Ayadhi LY, Mostafa GA: **Elevated serum levels of interleukin-17A in children with autism.** *J Neuroinflammation* 2012, **9**:158.
37. Ashwood P, Krakowiak P, Hertz-Picciotto I, Hansen R, Pessah IN, Van de Water J: **Associations of impaired behaviors with elevated plasma chemokines in autism spectrum disorders.** *J Neuroimmunol* 2011, **232**:196–199.
38. Ashwood P, Krakowiak P, Hertz-Picciotto I, Hansen R, Pessah IN, Van de Water J: **Altered T cell responses in children with autism.** *Brain Behav Immun* 2011, **25**:840–849.
39. Manzardo AM, Henkhaus R, Dhillon S, Butler MG: **Plasma cytokine levels in children with autistic disorder and unrelated siblings.** *Int J Dev Neurosci* 2012, **30**:121–127.
40. Nelson PG, Kuddo T, Song EY, Dambrosia JM, Kohler S, Satyanarayana G, Vandunk C, Grether JK, Nelson KB: **Selected neurotrophins, neuropeptides, and cytokines: developmental trajectory and concentrations in neonatal blood of children with autism or Down syndrome.** *Int J Dev Neurosci* 2006, **24**:73–80.
41. De Jager W, Bourcier K, Rijkers GT, Prakken BJ, Seyfert-Margolis V: **Prerequisites for cytokine measurements in clinical trials with multiplex immunoassays.** *BMC Immunol* 2009, **10**:52.
42. Croen LA, Goines P, Braunschweig D, Yolken R, Yoshida CK, Grether JK, Fireman B, Kharrazi M, Hansen RL, Van de Water J: **Brain-derived neurotrophic factor and autism: maternal and infant peripheral blood levels in the Early Markers for Autism (EMA) Study.** *Autism Res* 2008, **1**:130–137.
43. Yeargin-Allsopp M, Rice C, Karapurkar T, Doernberg N, Boyle C, Murphy C: **Prevalence of autism in a US metropolitan area.** *JAMA* 2003, **289**:49–55.
44. Dammann O, O'Shea TM: **Cytokines and perinatal brain damage.** *Clin Perinatol* 2008, **35**:643–663.
45. Rostene W, Guyon A, Kular L, Godefroy D, Barbieri F, Bajetto A, Banisadr G, Callewaere C, Conductier G, Rovere C, Melik-Parsadaniantz S, Florio T: **Chemokines and chemokine receptors: new actors in neuroendocrine regulations.** *Front Neuroendocrinol* 2011, **32**:10–24.

doi:10.1186/1742-2094-11-113

Cite this article as: Zerbo *et al.*: Neonatal cytokines and chemokines and risk of Autism Spectrum Disorder: the Early Markers for Autism (EMA) study: a case-control study. *Journal of Neuroinflammation* 2014 **11**:113.

Submit your next manuscript to BioMed Central and take full advantage of:

- Convenient online submission
- Thorough peer review
- No space constraints or color figure charges
- Immediate publication on acceptance
- Inclusion in PubMed, CAS, Scopus and Google Scholar
- Research which is freely available for redistribution

Submit your manuscript at
www.biomedcentral.com/submit



Immunity, neuroglia and neuroinflammation in autism

CARLOS A. PARDO^{1,2,3}, DIANA L. VARGAS^{1,2}, & ANDREW W. ZIMMERMAN^{1,4}

¹Department of Neurology, ²Division of Neuroimmunology and Infectious Disorders, ³Department of Pathology, Johns Hopkins University School of Medicine, Baltimore, and ⁴Kennedy Krieger Institute, Baltimore, Maryland, USA

Summary

Autism is a complex neurodevelopmental disorder of early onset that is highly variable in its clinical presentation. Although the causes of autism in most patients remain unknown, several lines of research support the view that both genetic and environmental factors influence the development of abnormal cortical circuitry that underlies autistic cognitive processes and behaviors. The role of the immune system in the development of autism is controversial. Several studies showing peripheral immune abnormalities support immune hypotheses, however until recently there have been no immune findings in the CNS. We recently demonstrated the presence of neuroglial and innate neuroimmune system activation in brain tissue and cerebrospinal fluid of patients with autism, findings that support the view that neuroimmune abnormalities occur in the brain of autistic patients and may contribute to the diversity of the autistic phenotypes. The role of neuroglial activation and neuroinflammation are still uncertain but could be critical in maintaining, if not also in initiating, some of the CNS abnormalities present in autism. A better understanding of the role of neuroinflammation in the pathogenesis of autism may have important clinical and therapeutic implications.

Introduction

Autism is the most severe and devastating condition in the broad spectrum of developmental disorders called ‘pervasive developmental disorders’ (Rapin, 1997). Autistic disorders are characterized by marked impairment in social skills, verbal communication, behavior, and cognitive function (Rapin, 1997; Lord et al., 2000). Abnormalities in language development, mental retardation, and epilepsy are frequent problems in the clinical profile of patients with autism (Rapin, 1997). The syndrome is clinically heterogeneous and can be associated in up to 10% of patients with well-described neurological and genetic disorders, such as tuberous sclerosis, fragile X, Rett and Down syndromes, although in most patients the causes are still unknown (Rapin & Katzman, 1998; Newschaffer et al., 2002; Cohen et al., 2005). The importance of autism as a public health problem has been recognized in recent years, as epidemiological studies have suggested that the age-adjusted incidence of research-identified autism has increased from 5.5 (95% confidence interval, 1.4–9.5) per 100 000 children in the period 1980–1983 to 44.9 (95% confidence interval, 32.9–56.9) in the period 1995–1997 (8.2-fold increase) (Barbarese et al., 2005) while the prevalence of autistic syndromes

has increased to 3–6 per 1000 children, with a male to female ratio of 3:1 (Fombonne, 2003; Yeargin-Allsopp et al., 2003). In addition to complex multigenic factors (Folstein & Rosen-Sheidley, 2001), several researchers have also hypothesized important roles for environmental factors, pre- or perinatal injuries, vaccines, mercury toxicity, or persistent viral infections (Wing & Potter, 2002; Larsson et al., 2005). These recent observations on the epidemiology of autism strongly suggest that an interplay between genetic and as yet undefined environmental factors may increase the risk of autism, to a level greater than one would expect from genetic causes alone.

Neurobiology of autism

Clinical and epidemiological aspects of autism

Although the neurobiological basis for autism remains poorly understood, several lines of research now support the view that genetic, environmental, neurological, and immunological factors contribute to its development (Rapin & Katzman, 1998; Newschaffer et al., 2002; Folstein & Rosen-Sheidley, 2001; Korvatska et al., 2002). Several different genetic factors and/or other risk factors may combine during development to produce complex

changes in CNS organization that translate into abnormalities of neuronal and cortical cytoarchitecture that are responsible for the complex language and behavioral problems that characterize the autistic phenotype. The core symptoms of autism include abnormal communication, social relatedness, behavior, and cognition (Rapin, 1997; Lord et al., 2000). The majority of children show abnormalities during infant development that may not become apparent until the second year of life. Approximately 30–50% of children undergo regression, with a loss of skills, including language, between 16 and 25 months of age (Lord et al., 2004). In the medical evaluation of autism, specific etiologies can be found in <10% of children, including fragile X, tuberous sclerosis, and other rare diseases (Cohen et al., 2005). Epilepsy occurs in up to 40% of patients, and epileptic discharges may occur on EEGs early in childhood, even in the absence of clinical seizures (Tuchman & Rapin, 2002). Although children with autism present with a wide spectrum of symptoms that vary in severity and clinical progression, it is possible to define these features in affected individuals and follow them over time (Aman et al., 2004).

Neuroanatomical abnormalities in autism

A wide range of anatomical and structural brain abnormalities have been observed in autistic patients by longitudinal clinical and magnetic resonance imaging studies. The most remarkable observation is that the clinical onset of autism appears to be preceded by two phases of brain growth abnormalities: a reduced head size at birth and a sudden and excessive increase in head size between 1–2 months and 6–14 months (Courchesne et al., 2004). These studies have also shown that the most abnormal pattern of brain overgrowth occurs in areas of the frontal lobe, cerebellum, and limbic structures between 2–4 years of age, a pattern that is followed by abnormal slowness and an arrest in brain growth (Courchesne et al., 2004; Courchesne & Pierce, 2005). Other studies of high-functioning autistic patients have shown an overall enlargement of brain volume associated with increased cerebral white matter and decrease in cerebral cortex and hippocampal-amygdala volumes (Herbert et al., 2003; Herbert et al., 2004). One of the most puzzling issues in the neuroanatomical observations in autism is the lack of an acceptable explanation for the cause of this dissociation or patterns of abnormal brain growth. However, it is likely that disruption of white matter tracts and disconnection between brain regions are present in autistic patients, as demonstrated by new techniques such as diffusion tensor imaging. This approach has demonstrated reduced fractional

anisotropy values in white matter adjacent to the ventromedial prefrontal cortices, anterior cingulate gyrus, and superior temporal regions, findings suggestive of the disruption in white matter tracts in brain regions involved in social functioning that has been described in autistic patients (Barnea-Goraly et al., 2004).

In addition to abnormal growth patterns of the brain, one of the most consistent findings of neuroimaging studies in autism is the presence of abnormalities in the cerebellum. Reduction in the size of cerebellar regions such as the vermis (Hashimoto et al., 1995; Kaufmann et al., 2003), an increase in white matter volume, and reduction in the gray/white matter ratio (Courchesne & Pierce, 2005) are the most prominent changes observed in the cerebellum. In one of these studies, the cerebellar changes appeared to be specific to autism, in contrast to other neurodevelopmental disorders such as Down syndrome, Down syndrome with autism, fragile X and fragile X with autism (Kaufmann et al., 2003). These observations concur with: (1) the findings from neuropathological studies describing abnormalities in the cerebellum, such as a decreased number of Purkinje cells (Kemper & Bauman, 1998; Bailey et al., 1998) and, most recently, (2) observation of increased microglial activation and astroglial reactions in both the granular cell and white matter layers and a reduction in Purkinje and granular cells (Vargas et al., 2005).

Neuropathology of autism

Cytoarchitectural organizational abnormalities of the cerebral cortex, cerebellum, and other subcortical structures appear to be the most prominent neuropathological changes in autism (Kemper & Bauman, 1998; Bailey et al., 1998). An unusual laminar cytoarchitecture with packed small neurons has been described in the classical neuropathological studies by Kemper and Bauman (1998), but no abnormalities in the external configuration of the cerebral cortex were noted. Cerebellar and brainstem pathology was prominent, with a loss and atrophy of Purkinje cells, predominantly in the posterolateral neocerebellar cortex. Kemper and Bauman (1998) have delineated at least three different types of pathological abnormalities in autism: (1) a curtailment of the normal development of neurons in the forebrain limbic system; (2) an apparent decrease in the cerebellar Purkinje cell population; and (3) age-related changes in neuronal size and number in the nucleus of the diagonal band of Broca, the cerebellar nuclei, and the inferior olive. These observations suggest that delays in neuronal maturation are important component in the spectrum of

neuropathological changes in autism (Kemper & Bauman, 1998). In addition to these cytoarchitectural abnormalities, the number of cortical minicolumns, the narrow chain of neurons that extend vertically across layers 2–6 to form anatomical and functional units, appeared to be more numerous, smaller, and less compact in their cellular configuration in the frontal and temporal regions of the brain of autistic patients, as compared with controls (Casanova et al., 2002). Pathological evidence of immunological reactions within the CNS, such as lymphocyte infiltration and microglial nodules, has been described in a few case reports (Bailey et al., 1998; Guerin et al., 1996).

Immunological factors associated with autism

Immunological abnormalities in autism

Reports of differences in systemic immune findings over the past 30 years have led to speculation that autism may represent, in some patients, an immune mediated or autoimmune disorder (Ashwood & de Water, 2004). Recent reviews of immune dysfunction in autism have sought to understand these findings in the clinical context of the syndrome (Korvatska et al., 2002; Ashwood & de Water, 2004; Zimmerman, 2005). Abnormalities of both humoral and cellular immune functions have been described in small studies of children with autism ($N = 10–36$), and include decreased production of immunoglobulins or B and T-cell dysfunction (Warren et al., 1986). Early studies suggested that prenatal viral infections might damage the immature immune system and induce viral tolerance (Stubbs & Crawford, 1977), while later studies showed altered T-cell subsets and activation, consistent with the possibility of an autoimmune pathogenesis (Gupta et al., 1998). Odell et al. (2005) recently confirmed earlier reports of a four-fold increase in the serum complement (C4B) null allele (i.e., no protein produced) in 85 children with autism, compared to controls.

Studies of peripheral blood have shown a range of abnormalities, including T-cell, B-cell, and NK-cell dysfunction; autoantibody production; and increased pro-inflammatory cytokines (Gupta et al., 1998; Singh et al., 1997; Singh et al., 2002; Vojdani et al., 2002; Jyonouchi et al., 2001). Shifts observed in Th1 to Th2 lymphocyte subsets and cytokines and associations with human leukocyte antigen (HLA)-DR4 have suggested the possibility that autoimmunity against brain antigens may contribute to the neuropathology of autism (van Gent et al., 1997). Decreases in immunoglobulin subsets and complement, the presence of auto-antibodies against CNS antigens, and an effect of maternal antibodies

have also been proposed as pathogenic factors (Dalton et al., 2003). In most of these studies, phenotyping was limited to descriptions of the subjects as ‘autistic’ based on criteria of the Diagnostic and Statistical Manual of the American Psychiatric Association. ‘Abnormal’ immune findings varied from 15–60% of children with autism. For some parameters, unaffected siblings showed intermediate values, and a background of such ‘abnormalities’ was noted in normal controls as well. In all studies, measurements have been reported at single time points and among subjects of different ages. Since these differences in systemic immune findings in autism have not been followed in the same patients over time, it is not clear whether they reflect true immune dysfunction or may represent dysmaturation that changes with age (Zimmermann, 2005). Also, no clinical immune deficiency states have been reported in association with unusual infections or reactions to immunizations, despite widespread interest in the possibility of such relationships (Halsey & Hyman, 2001).

Autoimmunity and autism

Circulating auto-antibodies directed against CNS antigens have been described in patients with autism, reacting to myelin basic protein (Singh, Lin, & Tang, 1998), frontal cortex (Todd et al., 1988), cerebral endothelial cells (Connolly et al., 1999), and neurofilament proteins (Singh et al., 1997). Autoreactivity to a human protein with molecular weight in the range (but distinct from) myelin basic protein has been reported (Silva et al., 2004). Recent findings suggest reactivity in sera from children with autism to a 73 Kd epitope in the cingulate gyrus and cerebellum. The significance of auto-antibodies in serum from patients with autism has been difficult to determine. Their presence might imply that autism is an autoimmune disorder. However, several criteria, including the necessity to demonstrate the autoimmune disease after passive transfer of antibodies into animals, would be necessary to establish the role of these auto-antibodies as pathogenic effectors (Rose & Bona, 1993), and this evidence is still lacking. Even though several antibodies in autism serum have been demonstrated to react against human brain tissue, their pathogenicity has not been demonstrated in autism postmortem brain tissue. Of equal interest to serum reactivity in the children, however, have been studies in maternal sera. Warren et al. (1990) demonstrated reactivity of mothers’ sera to their autistic children’s lymphocytes. Maternal serum has also been shown to cause antibody binding to fetal Purkinje cells when it was injected into pregnant mice (Dalton et al., 2003). Maternal antibodies may therefore be relevant

to prenatal brain development (Dalton et al., 2003), by interfering with cell signaling in the developing brain, and (perhaps) disturbing patterns of CNS organization.

Other autoimmune disorders, such as rheumatoid arthritis, lupus and thyroid disorders, have been found at increased rates in surveys of family members of children with autism, rather than in the children themselves, compared to controls. This was first observed in one family by Money (Money, Bobrow, & Clarke, 1971), and subsequently in three clinical surveys (Comi et al., 1999; Sweeten et al., 2003; Molloy CA, personal communication). However, these associations were not found in another study after review of medical records (Micali, Chakrabarti, & Fombonne, 2004). A recent study of mothers with autistic children reported an association with psoriasis but not other autoimmune disorders, and a two-fold increased risk of having an autistic child for those mothers with asthma and allergies during the second trimester (Croen et al., 2005). The meaning of these studies for autism is still not clear, but they suggest that maternal immunological effects might be important during gestation. They are also consistent with reported increases in frequencies of HLA DR4 and related alleles in children with autism and their mothers (Daniels et al., 1995; Torres et al., 2002).

Immunogenetics in autism

Some of the most promising studies that link the immune system to autism come from the study of the HLA genes, which are important genetic determinants of immune function within the major histocompatibility complex (MHC) and could reflect important antigenic differences between parents and their affected children. Other genetic loci associated with autoimmune and inflammatory disorders appear to cluster with those for autism (as well as Tourette's syndrome) and suggest a genetic relationship based on immune dysregulation (Becker, Freidlin, & Simon, 2003). In the case of HLA genes, the association of specific antigens/alleles with autoimmunity suggests that autistic patients may exhibit a similar pattern of association. Immunogenetic studies have shown an increased frequency of HLA-DR4 in children with autism and their mothers, a finding that is consistent with clinical observations of increased frequencies of autoimmune disorders in families with autism (although not in the children themselves) (Comi et al., 1999). These observations are important, as HLA-DR4, a class II antigen, has been identified as one of the susceptibility markers for certain autoimmune diseases, such as rheumatoid arthritis,

and is strongly associated with others such as hypothyroidism and autoimmune diabetes (Levin et al., 2004). These disorders have a higher incidence among families, especially mothers, of autistic children than of controls (Comi et al., 1999; Sweeten et al., 2003). These findings were further supported by a recent report that DR4 alleles occur in individuals with autism with higher frequency than in controls recruited from the National Marrow Donor Program (Torres et al., 2002). These observations have led researchers to investigate the possible expression of HLA-DR4 in the families of some children with autism. To confirm this possible association between HLA-DR4 and autism, we studied HLA-DR4 and its subtypes in single-birth and multiplex families with autism (Zimmerman, Tyler, & Matteson, 2001). Among 17 single-birth families with an autistic child in the East Tennessee region, the mothers were 4.62 times more likely (95% CI: 1.54, 14.34), and the children were 3.6 times more likely to have an HLA-DR4 haplotype than were controls (Lee et al., 2004).

Infections and autism

Infections have been associated with autism in small numbers of children, and include prenatal rubella (Chess, Fernandez, & Korn, 1978) and cytomegalovirus (Sweeten et al., 2003; Yamashita et al., 2003), and postnatal herpes encephalitis (DeLong, Bean, & Brown, 1981). Given the variety of viruses and their pathogenic effects that can be associated with autism, the location of the pathology and the neural networks affected appear to be more important than the specific types of viruses. For example, reversible symptoms of autism have been reported with bilateral temporal lobe involvement in herpes simplex virus encephalitis (DeLong, Bean, & Brown, 1981). Autism rarely results from known infectious causes, and the immune abnormalities or variants described in autism studies have not been consistent with typical immune deficiency states that would predispose to such infections. Furthermore, there have been no documented increased rates of infection in children with autism (Comi et al., 1999). And, although persistence of measles virus in the GI tract and peripheral mononuclear cells has been reported in children with autism (Kawashima et al., 2000), replication and further study of its possible relevance to autism in CSF and brain tissue are needed. Animal models of autism using prenatal infections (Patterson, 2002) lend credence to the importance of gestational effects on fetal brain development, as in the association of maternal influenza and the increased risk of schizophrenia (Shi et al., 2003). Autistic behaviors also have been

induced experimentally in a rat model using neonatal Borna disease virus (Carbone et al., 2002).

Neuroglia responses and neuroinflammation in autism

Neuroglia and CNS function

Neuroglial cells such as astrocytes and microglia, along with perivascular macrophages and endothelial cells, play important roles in neuronal function and homeostasis (Aloisi, 2001; Dong & Benveniste, 2001). Both microglia and astroglia are fundamentally involved in cortical organization, neuroaxonal guidance and synaptic plasticity (Fields & Stevens-Graham, 2002). Neuroglial cells contribute in a number of ways to the regulation of immune responses in the CNS. Astrocytes, for example, play an important role in the detoxification of excess excitatory amino acids (Nedergaard, Takano, & Hansen, 2002), maintenance of the integrity of the blood-brain barrier (Prat et al., 2001), and production of neurotrophic factors (Bauer, Rauschka, & Lassmann, 2001). In normal homeostatic conditions, astrocytes facilitate neuronal survival by producing growth factors and mediating uptake/removal of excitotoxic neurotransmitters, such as glutamate, from the synaptic microenvironment (Nedergaard, Takano, & Hansen, 2002).

However, during astroglial activation secondary to injury or in response to neuronal dysfunction, astrocytes can produce several factors that may modulate inflammatory responses; they secrete pro-inflammatory cytokines, chemokines, and metalloproteinases that can magnify immune reactions within the CNS (Bauer, Rauschka, & Lassmann, 2001; Rosenberg, 2002). Similarly, microglial activation is an important factor in the neuroglial responses to injury or dysfunction. Microglia are involved in synaptic stripping, cortical plasticity, and immune surveillance (Aloisi, 2001). Changes in astroglia and microglia can therefore produce marked neuronal and synaptic changes that are likely to contribute to CNS dysfunction or modify CNS homeostasis during disease processes. Neuronal dysfunction and abnormalities in cortical organization such as those seen in autism may also be responsible for pathophysiological responses that may lead to neuroglial activation, reactions that may subsequently increase the magnitude of neuronal dysfunction.

Neuroglia responses in autism

The role of neuroglia in autism has been ignored in the past several years and previous neuropathological studies did not show evidence of astrogliosis or

microglial reactions (Kemper & Bauman, 1998). Evidence of neuroglial activation and a role for neuroimmune responses mediated by innate immunity in the neuropathology of autism, recently has been demonstrated by our laboratory (Vargas et al., 2005). Based on neuropathological analysis of postmortem brain tissues from 11 autistic patients (age range 5–44 years), we have demonstrated the presence of an active and ongoing neuroinflammatory process in the cerebral cortex and white matter, and notably in the cerebellum. Immunocytochemical studies of brain tissues from these 11 autistic patients showed marked activation of microglia and astroglia as compared with controls. The neuroglial activation was particularly prominent in the granular cell layer and white matter of the cerebellum. An assessment of the magnitude of astrogliosis using immunocytochemistry for glial fibrillary acidic protein (GFAP) in the midfrontal (MFG) and anterior cingulate gyrus (ACG) and cerebellum (CBL) of the autistic brains revealed increased astroglial reactions characterized by an increase in the volume of perikarya and glial processes. In the brains of autistic patients, GFAP immunostaining of the cerebellum showed a marked reactivity of the Bergmann's astroglia in areas of neuronal loss within the Purkinje cell layer, as well as a marked astroglial reaction in the granular cell layer and cerebellar white matter. In the MFG and ACG, astroglial reactions were prominent in the subcortical white matter, and in some cases panlamina astroglia was observed. Quantitative assessment of astroglial immunoreactivity by fractional area methods showed a significant increase in GFAP immunoreactivity in the GCL ($P=0.000$) and white matter ($P=0.007$) compartments of the cerebellum. Further analysis by western blotting of GFAP expression in protein homogenates obtained from a subset of autistic ($n=7$) and control patients ($n=7$) from whom fresh-frozen brain tissue had been obtained, showed a significantly increased expression of GFAP in the cerebellum ($P=0.001$), MFG ($P=0.001$) and ACG ($P=0.038$) of autistic patients, as compared to controls, findings that demonstrate the presence of a marked astroglial reaction in autism.

The pattern of microglial activation in autistic brains was further characterized by immunocytochemical staining for MHC class II markers (HLA-DR). Marked microglial activation was observed in the cerebellum, cortical regions and white matter of autistic patients. The most prominent microglial reaction was observed in the cerebellum, where the immunoreactivity for HLA-DR showed a significantly higher fractional area of immunoreactivity in both the GCL ($P<0.0001$) and cerebellar white matter ($P<0.0001$) of autistic subjects than in controls

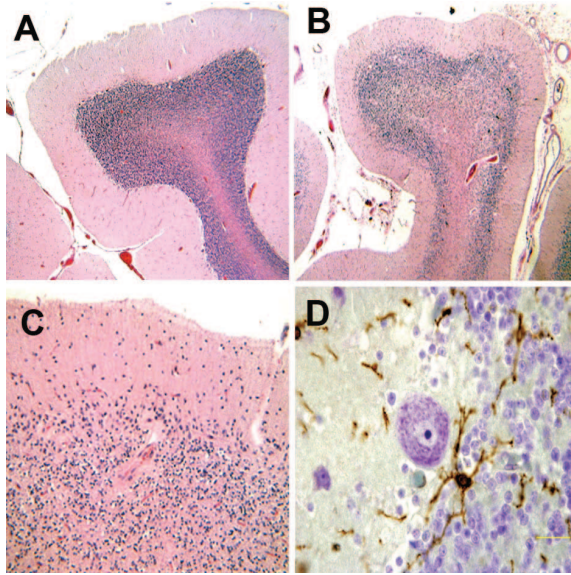


Figure 1. Neuropathology of cerebellum in autism. (A) Normal appearance of the cerebellum in a control patient; (B–C) atrophic folia and marked loss of Purkinje and granular cells in the cerebellum of an autistic patient (H&E stain); (D) microglia activation seen with anti-MHC class II immunostaining (from Vargas et al., 2005).

(Figure 1). At present, it is still unclear what the role of neuroglial responses in autism is or how these responses are involved in pathogenic mechanisms. The microglial and astroglial activation in the CNS may then have a dichotomous role in the inflammatory responses of the brain: as a direct effector of injury and on the other hand as neuroprotectant (Nguyen, Julien, & Rivest, 2002). It is unclear how and when microglia and astroglia become activated in the brain of autistic patients. Neuroglial activation in autism may be part of both primary (intrinsic) responses that result from disturbances of neuroglial function or neuronal–neuroglial interactions during brain development and secondary (extrinsic) effects, resulting from unknown factors that disturb prenatal or postnatal CNS development. It is possible that the presence of activated microglia in the brain in autism may reflect abnormal persistence of fetal patterns of development in response to genetic or environmental (e.g., intrauterine, maternal) factors. Our findings may indicate that at some point during cortical and neuronal organization, unknown factors influence both neuronal and neuroglial cell populations, disturbing neurodevelopment and producing the neurocytoarchitectural changes seen in autism as well as inducing CNS dysfunction that results in neuroinflammation. Another potential explanation is that extrinsic etiological factors (e.g., non-genetic, neurotoxic or environmental) involved in the pathogenesis of autism may produce neuronal and

cortical abnormalities, to which neuroglial reactions are only secondary responses.

Cytokine profile in the brain of autistic patients

Cytokines and chemokines play important roles as mediators of inflammatory reactions in the CNS and in processes of neuronal–neuroglial interactions that modulate the neuroimmune system. Cytokines may contribute to neuroinflammation as mediators of pro-inflammatory or anti-inflammatory responses within the CNS. Our laboratory has focused on studies to characterize the profiles of cytokines and chemokines in autistic brains by assessing the relative expression of these proteins in tissue homogenates from MFG, ACG, and CBL of autistic ($n=7$) and control ($n=7$) patients by using cytokine protein array methodology (Huang, 2004). A statistical analysis of the relative expression of cytokines in autistic and control tissues showed a consistent and significantly higher level of subsets of cytokines in the brains of autistic patients: the anti-inflammatory cytokine transforming growth factor $\beta 1$ (TGF- $\beta 1$) was increased in the MFG ($P=0.026$), ACG ($P=0.011$) and CBL ($P=0.035$) and the pro-inflammatory chemokines macrophage chemoattractant protein-1 (MCP-1) and thymus and activation-regulated chemokine (TARC), were increased in the ACG ($P=0.026$ and 0.035 , respectively) and CBL ($P=0.026$ and 0.035 , respectively). Interestingly, a larger spectrum of increases in pro-inflammatory and modulatory cytokines was seen in the ACG, an important cortical structure in autism, where there was a significant increase in pro-inflammatory cytokines such as interleukin-6 (IL-6), interleukin-10 (IL-10), macrophage chemoattractant protein-3 (MCP-3), eotaxin, eotaxin 2, macrophage-derived chemokine (MDC), chemokine- $\beta 8$ (Ck $\beta 8.1$), neutrophil activating peptide-2 (NAP-2), monokine induced by interferon- γ (MIG) and B-lymphocyte chemoattractant (BLC) (Figure 2).

The presence of MCP-1 is of particular interest, since it facilitates the infiltration and accumulation of monocytes and macrophages in inflammatory CNS disease (Mahad & Ransohoff, 2003). Chemoattractant protein-1 is produced by activated and reactive astrocytes, a finding that demonstrates the effector role of these cells in the disease process in autism. The increase in MCP-1 expression has relevance to the pathogenesis of autism as we believe its elevation in the brain is linked to pathways of microglial activation and perhaps to the recruitment of monocytes/macrophages to areas of neuronal–cortical abnormalities. Our observations resemble findings in other neurological disorders in

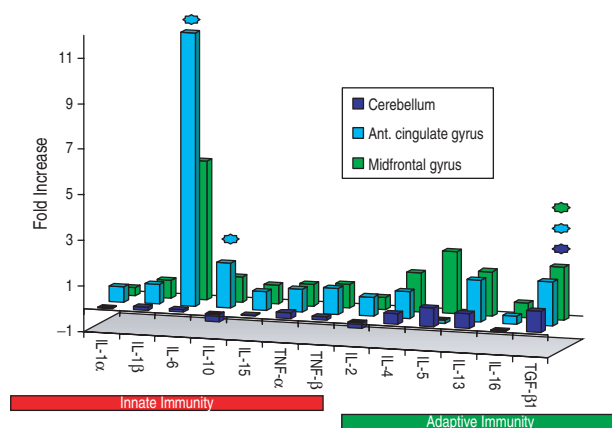


Figure 2. Pattern of increase of cytokines in brain regions of autistic patients (from Vargas et al., 2005).

which elevation of MCP-1 is associated with the pathogenesis of neuroinflammation and neuronal injury such as HIV dementia (Kelder et al., 1998), ALS (Henkel et al., 2004), and multiple sclerosis (Mahad & Ransohoff, 2003). It remains unclear whether MCP-1 plays a more pleiotropic role in the CNS or whether its presence is only associated with inflammatory conditions. The presence of increased TGF- β 1 in the cortex and cerebellum of autistic brains may have important implications for the neurobiology of autism. Transforming growth factor β 1 is a key anti-inflammatory cytokine and is involved in tissue remodeling following injury. It can suppress specific immune responses by inhibiting T-cell proliferation and maturation and down-regulates MHC class II expression (Letterio & Roberts, 1998). Importantly, cells undergoing cell death have been shown to secrete TGF- β 1, possibly to reduce local inflammation and prevent degeneration of additional surrounding cells (Chen et al., 2001). Transforming growth factor β 1 is produced mostly by reactive astrocytes and neurons. The elevation of TGF- β 1 suggests that the elevation of this cytokine in autism may reflect an attempt to modulate neuroinflammation or remodel and repair injured tissue. A remarkable profile of cytokine up-regulation was observed in the ACG, a region in which several cytokines, chemokines, and growth factors were markedly elevated when compared to controls. Pro-inflammatory cytokines (e.g., IL-6) and anti-inflammatory cytokines (e.g., IL-10) as well as subsets of chemokines were markedly elevated in the ACG, an important cortical region involved in dysfunctional brain activity in autism. These findings support the conclusion that an active, ongoing immunological process was present in multiple areas of the brain but at different levels of expression in each area.

Cerebrospinal fluid and neuroinflammation in autism

Despite these indications of multiple peripheral immune system abnormalities, there has been no consistent demonstration of inflammatory changes in cerebrospinal fluid (CSF) studies, and there has been no evidence of inflammation as indicated by standard cell counts, protein electrophoresis, protein concentration, increase of IgG index, or presence of oligoclonal bands (Zimmerman et al., 2005). We have recently studied the profile of cytokines and chemokines in the CSF of autistic patients as an approach to evaluate proteins involved in innate and adaptive immune pathways (Vargas et al., 2005). Cytokine protein arrays were used to compare the cytokine profiles of CSF from six autistic patients to that of CSF from a pool of donors without CNS pathology or inflammatory disorders (e.g., pseudotumor cerebri or headaches). We observed a marked increase in subsets of cytokines and chemokines involved in innate immune responses. As we had observed in brain tissues, CSF from autistic patients showed a significant increase in MCP-1 (12-fold increase) when compared to controls. Other pro-inflammatory such as IL-6, IFN- γ , IL-8, macrophage inflammatory protein-1 β (MIP1 β), NAP-2, interferon- γ inducing protein-10 (IP-10) and angiogenin were all significantly increased when compared to control CSF (Figure 3). These cytokines play important roles in immune-mediated processes and their presence in the CSF in autistic patients may reflect an ongoing stage of inflammatory reactions likely associated with neuroglial activation and/or neuronal injury. Reasons for the relatively greater increases in these cytokines in CSF compared to brain are unknown. The differences we observed in cytokines in CSF compared to brain could result from other sources of production, such the leptomeninges or choroid plexus or might represent a persistent elevation of cytokines as result of a stage of neurodevelopmental arrest as some of the cytokines are normally elevated during phases of neurodevelopment. Since the CSF is easily accessible for clinical studies, CSF cytokine profiling may be useful in the future to diagnose, characterize and follow the clinical course of autistic disorders.

Clinical and therapeutic implications of neuroinflammation in autism

Evaluation of neuroinflammation in autistic patients and its use in clinical assessment raises an important challenge. The classical techniques in the evaluation of CSF in autistic patients have failed in providing information about the presence of

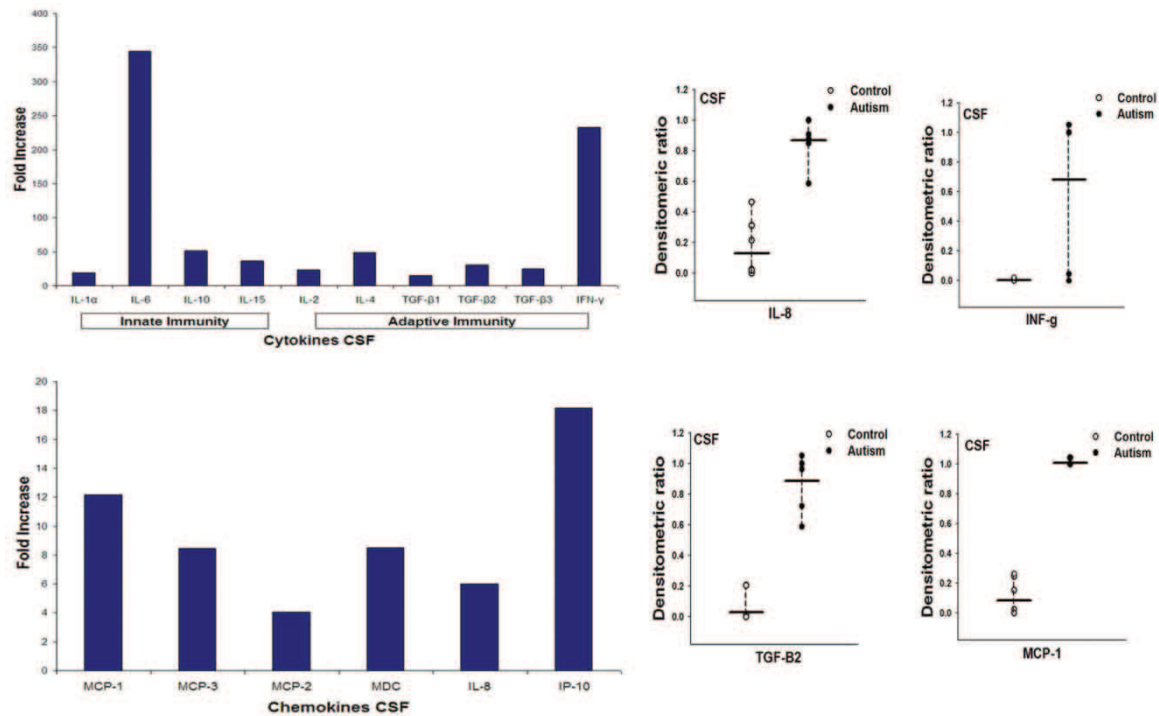


Figure 3. Pattern of increase in cytokines and chemokines in the CSF of autistic patients (from Vargas et al., 2005).

inflammatory changes as there is not evidence of either pleocytosis, cellular reactions or humoral responses such as increase in immunoglobulin index or oligoclonal bands. Recent studies using detection of products of macrophage and immune reactions such as neopterin, quinolinic acid or biopterin were shown to be unhelpful in the detection of neuroinflammation in autistic patients (Zimmerman et al., 2005). Our observations that subsets of cytokines and chemokines such as IL-6, IFN- γ and MCP-1 are elevated in patients with autism suggest that assessment of cytokine profiles are a potential approach to identify and evaluate the magnitude of inflammatory responses in these patients. It remains unknown whether these profiles correlate with the clinical spectrum of autism and further studies are required to understand the role of these cytokines and chemokines in the disease process. Another approach that may become practical in the future is the use of novel neuroimaging techniques such as brain imaging using PK11195, a ligand to the benzodiazepine receptor as a marker of microglial activation *in vivo* to determine the magnitude and extension of neuroglial reactions (Versijpt et al., 2003).

Another issue that is extremely important is to determine whether neuro-inflammation and neuroglial activation may be a target for treatment in autism. This issue requires a more detailed evaluation as the precise role of neuroinflammation in the pathogenesis and natural history of autism

is still uncertain. Studies in animal models and other neurological disorders suggest that microglial activation and neuroinflammation may play a role in processes of injury as there is increased oxidative stress and tissue injury, however, there is also recent evidence that neuroinflammation may be associated with repair processes and regeneration (Neuhaus, Archelos, & Hartung, 2003). Further studies are required in autism to help in the clarification of these issues. So, at this moment, we consider premature the use of any immunomodulatory intervention to modify the neuroglial activation and neuroinflammation. Furthermore, current treatment approaches to modify neuroimmune responses are very nonspecific and may bring more potential problems than benefits. The use of steroids or other immunotherapies such as immunoglobulin infusion and use of cytotoxic drugs may bring potential risks as these medications act mostly in cellular and humoral responses that are part of the adaptive immune system rather than neuroglial activation or innate immune responses.

Future directions

Several important questions regarding the role of neuroimmunity in autism remain unanswered, including: (1) Whether the neuroglial and neuroimmune responses associated with autism are part of the primary reactions that contribute to CNS dysfunction in this disorder or are epiphenomena

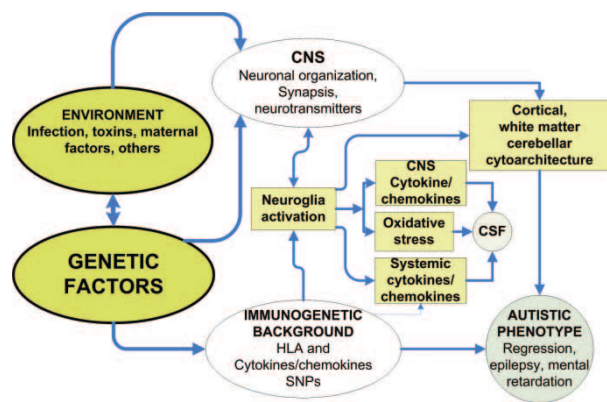


Figure 4. Hypothetical interactions of environmental and genetic factors that influence neuroglia activation, CNS organization and the presence of autism.

resulting from reactions to CNS dysfunction; (2) the nature of the relationship of cytokines and chemokines to immune and neurobiological processes in the brain of autistic patients; (3) whether the cerebellar pathology in autism is primarily the result of neuroimmune processes or primary abnormalities in neuronal function; (4) how analysis of CSF may help us identify markers of immune reactions within the CNS; and (5) whether the immunogenetic background of the host influences the development of neuroimmune reactions or determines patterns of susceptibility to autism.

Conclusions

Autism is a complex neurobehavioral disorder of early life onset influenced by the interaction of different risk factors. We hypothesize that environmental factors (e.g., neurotoxins, infections, maternal infections) in presence of genetic susceptibility and the immunogenetic background of the host influence the development of abnormalities in cortical organization and neuronal circuitry and neuroinflammatory changes responsible for the generation of the autistic symptoms (Figure 4). Our neuroimmunopathological studies strongly suggests that innate rather than adaptive neuroimmune responses are part of the immunopathogenic mechanisms associated with autism, but we cannot exclude the possibility that specific immune reactions, cellular or humoral, may occur at early stages of the disease, during prenatal or postnatal stages of brain development. The roles of neuroglial activation and neuroinflammation in the pathogenesis of autism are still uncertain but could be critical in maintaining, if not also in initiating, some of the CNS abnormalities present in this neurodevelopmental disorder. Neuroglial and neuroinflammatory responses likely have polygenic

and environmental bases and may have important clinical and therapeutic implications in autism.

Acknowledgements

The authors are grateful for the support received from the Cure Autism Now Foundation (CAN), by Dr. Barry and Mrs. Renee Gordon, Dr. Jane Pickett and the Autism Tissue Program. Dr. Pardo is supported by a grant from NIH-NIDA (K08-DA 16160-01a1).

References

- Aloisi, F. (2001). Immune function of microglia. *Glia*, 36, 165–179.
- Aman, M. G., Novotny, S., Samango-Sprouse, C., Lecavalier, L., Leonard, E., Gadow, K. D., et al. (2004). Outcome measures for clinical drug trials in autism. *CNS Spectrums*, 9, 36–47.
- Ashwood, P., & Van de Water, J. (2004). Is autism an autoimmune disease? *Autoimmunity Reviews*, 3, 557–562.
- Bailey, A., Luthert, P., Dean, A., Harding, B., Janota, I., Montgomery, M., et al. (1998). A clinicopathological study of autism. *Brain*, 121(Pt 5), 889–905.
- Barbaresi, W. J., Katusic, S. K., Colligan, R. C., Weaver, A. L., & Jacobsen, S. J. (2005). The incidence of autism in Olmsted County, Minnesota, 1976–1997: Results from a population-based study. *Archives of Pediatric & Adolescent Medicine*, 159, 37–44.
- Barnea-Goraly, N., Kwon, H., Menon, V., Eliez, S., Lotspeich, L., & Reiss, A. L. (2004). White matter structure in autism: Preliminary evidence from diffusion tensor imaging. *Biological Psychiatry*, 55, 323–326.
- Bauer, J., Rauschka, H., & Lassmann, H. (2001). Inflammation in the nervous system: The human perspective. *Glia*, 36, 235–243.
- Becker, K. G., Freidlin, B., & Simon, R. M. (2003). Comparative genomics of autism, Tourette syndrome and autoimmune/inflammatory disorders. www.grc.nia.nih.gov/branches/trrb/dna/pubs/cgoatad.pdf.
- Carbone, K. M., Rubin, S. A., & Pletnikov, M. (2002). Borna disease virus (BDV)-induced model of autism: Application to vaccine safety test design. *Molecular Psychiatry*, 7 (Suppl. 2), S36–S37.
- Casanova, M. F., Buxhoeveden, D. P., Switala, A. E., & Roy, E. (2002). Minicolumnar pathology in autism. *Neurology*, 58, 428–432.
- Chen, W., Frank, M. E., Jin, W., & Wahl, S. M. (2001). TGF-beta released by apoptotic T cells contributes to an immunosuppressive milieu. *Immunity*, 14, 715–725.
- Chess, S., Fernandez, P., & Korn, S. (1978). Behavioral consequences of congenital rubella. *Journal of Pediatrics*, 93, 699–703.
- Cohen, D., Pichard, N., Tordjman, S., Baumann, C., Burglen, L., Excoffier, E., et al. (2005). Specific genetic disorders and autism: Clinical contribution towards their identification. *Journal of Autism & Developmental Disorders*, 35, 103–116.
- Comi, A. M., Zimmerman, A. W., Frye, V. H., Law, P. A., & Peeden, J. N. (1999). Familial clustering of autoimmune disorders and evaluation of medical risk factors in autism. *Journal of Child Neurology*, 14, 388–394.
- Connolly, A. M., Chez, M. G., Pestronk, A., Arnold, S. T., Mehta, S., & Deuel, R. K. (1999). Serum autoantibodies to

- brain in Landau-Kleffner variant, autism, and other neurologic disorders. *Journal of Pediatrics*, 134, 607–613.
- Courchesne, E., & Pierce, K. (2005). Brain overgrowth in autism during a critical time in development: Implications for frontal pyramidal neuron and interneuron development and connectivity. *International Journal of Developmental Neuroscience*, 23, 153–170.
- Courchesne, E., Redcay, E., & Kennedy, D. P. (2004). The autistic brain: Birth through adulthood. *Current Opinions in Neurology*, 17, 489–496.
- Croen, L. A., Grether, J. K., Yoshida, C. K., Odouli, R., & Van de, W. J. (2005). Maternal autoimmune diseases, asthma and allergies, and childhood autism spectrum disorders: A case-control study. *Archives in Pediatric & Adolescent Medicine*, 159, 151–157.
- Dalton, P., Deacon, R., Blamire, A., Pike, M., McKinlay, I., Stein, J., et al. (2003). Maternal neuronal antibodies associated with autism and a language disorder. *Annals of Neurology*, 53, 533–537.
- Daniels, W. W., Warren, R. P., Odell, J. D., Maciulis, A., Burger, R. A., Warren, W. L., et al. (1995). Increased frequency of the extended or ancestral haplotype B44-SC30-DR4 in autism. *Neuropsychobiology*, 32, 120–123.
- DeLong, G. R., Bean, S. C., & Brown, F. R. III. (1981). Acquired reversible autistic syndrome in acute encephalopathic illness in children. *Archives in Neurology*, 38, 191–194.
- Dong, Y., & Benveniste, E. N. (2001). Immune function of astrocytes. *Glia*, 36, 180–190.
- Fields, R. D., & Stevens-Graham, B. (2002). New insights into neuron-glia communication. *Science*, 298, 556–562.
- Folstein, S. E., & Rosen-Sheidley, B. (2001). Genetics of autism: Complex aetiology for a heterogeneous disorder. *Nature Reviews Genetics*, 2, 943–955.
- Fombonne, E. (2003). Epidemiological surveys of autism and other pervasive developmental disorders: An update. *Journal of Autism & Developmental Disorders*, 33, 365–382.
- Guerin, P., Lyon, G., Barthelemy, C., Sostak, E., Chevrollier, V., Garreau, B., et al. (1996). Neuropathological study of a case of autistic syndrome with severe mental retardation. *Developmental Medicine & Child Neurology*, 38, 203–211.
- Gupta, S., Aggarwal, S., Roshanravan, B., & Lee, T. (1998). Th1- and Th2-like cytokines in CD4+ and CD8+ T cells in autism. *Journal of Neuroimmunology*, 85, 106–109.
- Halsey, N. A., & Hyman, S. L. (2001). Measles-mumps-rubella vaccine and autistic spectrum disorder: Report from the New Challenges in Childhood Immunizations Conference convened in Oak Brook, Illinois, June 12–13, 2000. *Pediatrics*, 107, E84.
- Hashimoto, T., Tayama, M., Murakawa, K., Yoshimoto, T., Miyazaki, M., Harada, M., et al. (1995). Development of the brainstem and cerebellum in autistic patients. *Journal of Autism & Developmental Disorders*, 25, 1–18.
- Henkel, J. S., Engelhardt, J. I., Siklos, L., Simpson, E. P., Kim, S. H., Pan, T., et al. (2004). Presence of dendritic cells, MCP-1, and activated microglia/macrophages in amyotrophic lateral sclerosis spinal cord tissue. *Annals of Neurology*, 55, 221–235.
- Herbert, M. R., Ziegler, D. A., Deutsch, C. K., O'Brien, L. M., Lange, N., Bakardjiev, A., et al. (2003). Dissociations of cerebral cortex, subcortical and cerebral white matter volumes in autistic boys. *Brain*, 126, 1182–1192.
- Herbert, M. R., Ziegler, D. A., Makris, N., Filipek, P. A., Kemper, T. L., Normandin, J. J., et al. (2004). Localization of white matter volume increase in autism and developmental language disorder. *Annals of Neurology*, 55, 530–540.
- Huang, R. P. (2004). Cytokine protein arrays. *Methods in Molecular Biology*, 278, 215–232.
- Jyonouchi, H., Sun, S., & Le, H. (2001). Pro-inflammatory and regulatory cytokine production associated with innate and adaptive immune responses in children with autism spectrum disorders and developmental regression. *Journal of Neuroimmunology*, 120, 170–179.
- Kaufmann, W. E., Cooper, K. L., Mostofsky, S. H., Capone, G. T., Kates, W. R., Newschaffer, C. J., et al. (2003). Specificity of cerebellar vermian abnormalities in autism: A quantitative magnetic resonance imaging study. *Journal of Child Neurology*, 18, 463–470.
- Kawashima, H., Mori, T., Kashiwagi, Y., Takekuma, K., Hoshika, A., & Wakefield, A. (2000). Detection and sequencing of measles virus from peripheral mononuclear cells from patients with inflammatory bowel disease and autism. *Digestive Diseases & Science*, 45, 723–729.
- Kelder, W., McArthur, J. C., Nance-Sproson, T., McClernon, D., & Griffin, D. E. (1998). Beta-chemokines MCP-1 and RANTES are selectively increased in cerebrospinal fluid of patients with human immunodeficiency virus-associated dementia. *Annals of Neurology*, 44, 831–835.
- Kemper, T. L., & Bauman, M. (1998). Neuropathology of infantile autism. *Journal of Neuropathology & Experimental Neurology*, 57, 645–652.
- Korvatska, E., Van de, W. J., Anders, T. F., & Gershwin, M. E. (2002). Genetic and immunologic considerations in autism. *Neurobiology of Disease*, 9, 107–125.
- Larsson, H. J., Eaton, W. W., Madsen, K. M., Vestergaard, M., Olesen, A. V., Agerbo, E., et al. (2005). Risk factors for autism: Perinatal factors, parental psychiatric history, and socioeconomic status. *American Journal of Epidemiology*, 161, 916–925.
- Lee, L.-C., Zachary, A. A., Leffell, M. S., Newschaffer, C. J., Matteson, K. J., Tyler, J. D., et al. (2004). Increased incidence of maternal HLA-DR4 in single-birth, but not multiplex families with autism. International Meeting for Autism Research, Sacramento, CA. May 2004 (abstr).
- Letterio, J. J., & Roberts, A. B. (1998). Regulation of immune responses by TGF-beta. *Annual Review of Immunology*, 16, 137–161.
- Levin, L., Ban, Y., Concepcion, E., Davies, T. F., Greenberg, D. A., & Tomer, Y. (2004). Analysis of HLA genes in families with autoimmune diabetes and thyroiditis. *Human Immunology*, 65, 640–647.
- Lord, C., Cook, E. H., Leventhal, B. L., & Amaral, D. G. (2000). Autism spectrum disorders. *Neuron*, 28, 355–363.
- Lord, C., Shulman, C., & DiLavore, P. (2004). Regression and word loss in autistic spectrum disorders. *Journal of Child Psychology & Psychiatry*, 45, 936–955.
- Mahad, D. J., & Ransohoff, R. M. (2003). The role of MCP-1 (CCL2) and CCR2 in multiple sclerosis and experimental autoimmune encephalomyelitis (EAE). *Seminars in Immunology*, 15, 23–32.
- Micali, N., Chakrabarti, S., & Fombonne, E. (2004). The broad autism phenotype: Findings from an epidemiological survey. *Autism*, 8, 21–37.
- Money, J., Bobrow, N. A., & Clarke, F. C. (1971). Autism and autoimmune disease: A family study. *Journal of Autism & Child Schizophrenia*, 1, 146–160.
- Nedergaard, M., Takano, T., & Hansen, A. J. (2002). Beyond the role of glutamate as a neurotransmitter. *Nature Reviews Neuroscience*, 3, 748–755.
- Neuhaus, O., Archelos, J. J., & Hartung, H. P. (2003). Immunomodulation in multiple sclerosis: From immunosuppression to neuroprotection. *Trends in Pharmacological Science*, 24, 131–138.
- Newschaffer, C. J., Fallin, D., & Lee, N. L. (2002). Heritable and non-heritable risk factors for autism spectrum disorders. *Epidemiology Reviews*, 24, 137–153.
- Nguyen, M. D., Julien, J. P., & Rivest, S. (2002). Innate immunity: The missing link in neuroprotection and neurodegeneration? *Nature Reviews Neuroscience*, 3, 216–227.

- Odell, D., Maciulis, A., Cutler, A., Warren, L., McMahon, W. M., Coon, H., et al. (2005). Confirmation of the association of the C4B null allele in autism. *Human Immunology*, *66*, 140–145.
- Patterson, P. H. (2002). Maternal infection: Window on neuroimmune interactions in fetal brain development and mental illness. *Current Opinions in Neurobiology*, *12*, 115–118.
- Prat, A., Biernacki, K., Wosik, K., & Antel, J. P. (2001). Glial cell influence on the human blood-brain barrier. *Glia*, *36*, 145–155.
- Rapin, I. (1997). Autism. *New England Journal of Medicine*, *337*, 97–104.
- Rapin, I., & Katzman, R. (1998). Neurobiology of autism. *Annals of Neurology*, *43*, 7–14.
- Rose, N. R., & Bona, C. (1993). Defining criteria for autoimmune diseases (Witebsky's postulates revisited). *Immunology Today*, *14*, 426–430.
- Rosenberg, G. A. (2002). Matrix metalloproteinases in neuroinflammation. *Glia*, *39*, 279–291.
- Shi, L., Fatemi, S. H., Sidwell, R. W., & Patterson, P. H. (2003). Maternal influenza infection causes marked behavioral and pharmacological changes in the offspring. *Journal of Neuroscience*, *23*, 297–302.
- Silva, S. C., Correia, C., Fesel, C., Barreto, M., Coutinho, A. M., Marques, C., et al. (2004). Autoantibody repertoires to brain tissue in autism nuclear families. *Journal of Neuroimmunology*, *152*, 176–182.
- Singh, V. K., Lin, S. X., Newell, E., & Nelson, C. (2002). Abnormal measles-mumps-rubella antibodies and CNS autoimmunity in children with autism. *Journal of Biomedical Science*, *9*, 359–364.
- Singh, V. K., Lin, S. X., & Yang, V. C. (1998). Serological association of measles virus and human herpesvirus-6 with brain auto-antibodies in autism. *Clinical Immunology & Immunopathology*, *89*, 105–108.
- Singh, V. K., Warren, R., Averett, R., & Ghaziuddin, M. (1997). Circulating autoantibodies to neuronal and glial filament proteins in autism. *Pediatric Neurology*, *17*, 88–90.
- Stubbs, E. G., & Crawford, M. L. (1977). Depressed lymphocyte responsiveness in autistic children. *Journal of Autism & Child Schizophrenia*, *7*, 49–55.
- Sweeten, T. L., Bowyer, S. L., Posey, D. J., Halberstadt, G. M., & McDougle, C. J. (2003). Increased prevalence of familial autoimmunity in probands with pervasive developmental disorders. *Pediatrics*, *112*, e420.
- Todd, R. D., Hickok, J. M., Anderson, G. M., & Cohen, D. J. (1988). Antibrain antibodies in infantile autism. *Biological Psychiatry*, *23*, 644–647.
- Torres, A. R., Maciulis, A., Stubbs, E. G., Cutler, A., & Odell, D. (2002). The transmission disequilibrium test suggests that HLA-DR4 and DR13 are linked to autism spectrum disorder. *Human Immunology*, *63*, 311–316.
- Tuchman, R., & Rapin, I. (2002). Epilepsy in autism. *Lancet Neurology*, *1*, 352–358.
- van Gent, T., Heijnen, C. J., & Treffers, P. D. (1997). Autism and the immune system. *Journal of Child Psychology & Psychiatry*, *38*, 337–349.
- Vargas, D. L., Nascimbene, C., Krishnan, C., Zimmerman, A. W., & Pardo, C. A. (2005). Neuroglial activation and neuroinflammation in the brain of patients with autism. *Annals of Neurology*, *57*, 67–81.
- Versijpt, J. J., Dumont, F., Van Laere, K. J., Decoo, D., Santens, P., Audenaert, K., et al. (2003). Assessment of neuroinflammation and microglial activation in Alzheimer's disease with radiolabelled PK11195 and single photon emission computed tomography. A pilot study. *European Journal of Neurology*, *50*, 39–47.
- Vojdani, A., Campbell, A. W., Anyanwu, E., Kashanian, A., Bock, K., & Vojdani, E. (2002). Antibodies to neuron-specific antigens in children with autism: Possible cross-reaction with encephalitogenic proteins from milk, Chlamydia pneumoniae and Streptococcus group A. *Journal of Neuroimmunology*, *129*, 168–177.
- Warren, R. P., Cole, P., Odell, J. D., Pingree, C. B., Warren, W. L., White, E., et al. (1990). Detection of maternal antibodies in infantile autism. *Journal of the American Academy of Child & Adolescent Psychiatry*, *29*, 873–877.
- Warren, R. P., Margaretten, N. C., Pace, N. C., & Foster, A. (1986). Immune abnormalities in patients with autism. *Journal of Autism & Developmental Disorders*, *16*, 189–197.
- Wing, L., & Potter, D. (2002). The epidemiology of autistic spectrum disorders: Is the prevalence rising? *Mental Retardation & Developmental Disabilities Research Reviews*, *8*, 151–161.
- Yamashita, Y., Fujimoto, C., Nakajima, E., Isagai, T., & Matsuiishi, T. (2003). Possible association between congenital cytomegalovirus infection and autistic disorder. *Journal of Autism & Developmental Disorders*, *33*, 455–459.
- Yeargin-Allsopp, M., Rice, C., Karapurkar, T., Doernberg, N., Boyle, C., & Murphy, C. (2003). Prevalence of autism in a US metropolitan area. *Journal of the American Medical Association*, *289*, 49–55.
- Zimmerman, A. W., Jyonouchi, H., Comi, A. M., Connors, S. L., Milstien, S., Varsou, A., et al. (2005). Cerebrospinal fluid and serum markers of inflammation in autism. *Pediatric Neurology*, *33*, 195–201.
- Zimmerman, A. W., Tyler, J. D., & Matteson, K. J. (2001). Increased incidence of HLA-B60 and maternal DR4 in autism. *Annals of Neurology*, *50*, S122–S123.
- Zimmerman, A. W. (2005). The immune system. In M. Bauman & T. L. Kemper (Eds.), *The neurobiology of autism* (pp. 371–386). Baltimore: The Johns Hopkins University Press.